

Underwater Acoustic Modeling and Simulation

Third edition

Paul C. Etter

 Spon Press
Taylor & Francis Group
LONDON AND NEW YORK

**Also available as a printed book
see title verso for ISBN details**

Underwater Acoustic Modeling and Simulation

Third edition

Underwater Acoustic Modeling and Simulation

Third edition

Paul C. Etter



Spon Press
Taylor & Francis Group

LONDON AND NEW YORK

First published 2003
by Spon Press
11 New Fetter Lane, London EC4P 4EE

Simultaneously published in the USA and Canada
by Spon Press
29 West 35th Street, New York, NY 10001

This edition published in the Taylor & Francis e-Library, 2003.

Spon Press is an imprint of the Taylor & Francis Group

© 2003 Paul C. Etter

All rights reserved. No part of this book may be reprinted or reproduced or utilised in any form or by any electronic, mechanical, or other means, now known or hereafter invented, including photocopying and recording, or in any information storage or retrieval system, without permission in writing from the publishers.

The publisher makes no representation, express or implied, with regard to the accuracy of the information contained in this book and cannot accept any legal responsibility or liability for any errors or omissions that may be made.

British Library Cataloguing in Publication Data

A catalogue record for this book is available from the British Library

Library of Congress Cataloging in Publication Data

A catalog record for this book has been requested

ISBN 0-203-41765-8 Master e-book ISBN

ISBN 0-203-41910-3 (Adobe eReader Format)

ISBN 0-419-26220-2 (Print Edition)

To my wife Alice and my sons Gregory and Andrew

Contents

<i>Preface</i>	xv
<i>Preface to the second edition</i>	xvii
<i>Preface to the first edition</i>	xix
<i>Acknowledgments</i>	xxi
1 Introduction	1
1.1 <i>Background</i>	1
1.1.1 <i>Setting</i>	1
1.1.2 <i>Framework</i>	2
1.2 <i>Measurements and prediction</i>	4
1.3 <i>Developments in modeling</i>	6
1.4 <i>Advances in simulation</i>	9
1.5 <i>Operational challenges</i>	10
1.5.1 <i>Naval operations</i>	11
1.5.2 <i>Offshore industries</i>	13
1.5.3 <i>Operational oceanography</i>	14
1.6 <i>Inverse acoustic sensing of the oceans</i>	15
1.7 <i>Standard definitions</i>	17
2 Acoustical oceanography	19
2.1 <i>Background</i>	19
2.2 <i>Physical and chemical properties</i>	19
2.2.1 <i>Temperature distribution</i>	21
2.2.2 <i>Salinity distribution</i>	22
2.2.3 <i>Water masses</i>	22
2.3 <i>Sound speed</i>	25
2.3.1 <i>Calculation and measurements</i>	25
2.3.2 <i>Sound-speed distribution</i>	28
2.4 <i>Boundaries</i>	35
2.4.1 <i>Sea surface</i>	35
2.4.2 <i>Ice cover</i>	38
2.4.3 <i>Sea floor</i>	39

2.5	<i>Dynamic features</i>	43
2.5.1	<i>Large-scale features</i>	43
2.5.2	<i>Mesoscale features</i>	44
2.5.3	<i>Fine-scale features</i>	54
2.6	<i>Biologics</i>	55
3	Propagation I: observations and physical models	57
3.1	<i>Background</i>	57
3.2	<i>Nature of measurements</i>	58
3.3	<i>Basic concepts</i>	59
3.4	<i>Sea-surface boundary</i>	65
3.4.1	<i>Forward scattering and reflection loss</i>	66
3.4.2	<i>Image interference and frequency effects</i>	67
3.4.3	<i>Turbidity and bubbles</i>	69
3.4.4	<i>Ice interaction</i>	70
3.4.5	<i>Measurements</i>	72
3.5	<i>Sea-floor boundary</i>	72
3.5.1	<i>Forward scattering and reflection loss</i>	73
3.5.2	<i>Interference and frequency effects</i>	78
3.5.3	<i>Attenuation by sediments</i>	78
3.5.4	<i>Measurements</i>	79
3.6	<i>Attenuation and absorption in sea water</i>	80
3.7	<i>Surface ducts</i>	82
3.7.1	<i>Mixed-layer distribution</i>	82
3.7.2	<i>General propagation features</i>	85
3.7.3	<i>Low-frequency cutoff</i>	88
3.8	<i>Deep-sound channel</i>	91
3.9	<i>Convergence zones</i>	93
3.10	<i>Reliable acoustic path</i>	94
3.11	<i>Shallow-water ducts</i>	94
3.12	<i>Arctic half-channel</i>	95
3.13	<i>Coherence</i>	97
4	Propagation II: mathematical models (Part One)	99
4.1	<i>Background</i>	99
4.2	<i>Theoretical basis for propagation modeling</i>	100
4.2.1	<i>Wave equation</i>	100
4.2.2	<i>Classification of modeling techniques</i>	102
4.3	<i>Ray-theory models</i>	103
4.3.1	<i>Basic theory</i>	103
4.3.2	<i>Caustics</i>	106

4.3.3	<i>Gaussian beam tracing</i>	107
4.3.4	<i>Range dependence</i>	107
4.3.5	<i>Arrival structure</i>	109
4.3.6	<i>Beam displacement</i>	111
4.4	<i>Normal-mode models</i>	113
4.4.1	<i>Basic theory</i>	113
4.4.2	<i>Normal-mode solution</i>	114
4.4.3	<i>Dispersion effects</i>	116
4.4.4	<i>Experimental measurements</i>	117
4.4.5	<i>Range dependence</i>	118
4.4.6	<i>High-frequency adaptations</i>	120
4.4.7	<i>Wedge modes</i>	120
4.5	<i>Multipath expansion models</i>	121
4.6	<i>Fast-field models</i>	122
4.7	<i>Parabolic equation models</i>	123
4.7.1	<i>Basic theory</i>	124
4.7.2	<i>Numerical techniques</i>	126
4.7.3	<i>Wide-angle and 3D adaptations</i>	129
4.7.4	<i>Range-refraction corrections</i>	129
4.7.5	<i>High-frequency adaptations</i>	130
4.7.6	<i>Time-domain applications</i>	130
4.8	<i>The RAYMODE model – a specific example</i>	131
4.9	<i>Numerical model summaries</i>	135
5	Propagation II: mathematical models (Part Two)	152
5.1	<i>Background</i>	152
5.2	<i>Surface duct models</i>	152
5.2.1	<i>Ray-theory models</i>	152
5.2.2	<i>Wave-theory models</i>	154
5.2.3	<i>Oceanographic mixed-layer models</i>	155
5.3	<i>Shallow-water duct models</i>	158
5.3.1	<i>Shallow-water propagation characteristics</i>	158
5.3.2	<i>Optimum frequency of propagation</i>	159
5.3.3	<i>Numerical models</i>	162
5.3.4	<i>Empirical models</i>	167
5.4	<i>Arctic models</i>	172
5.4.1	<i>Arctic environmental models</i>	172
5.4.2	<i>Arctic propagation models</i>	172
5.4.3	<i>Numerical models</i>	173
5.4.4	<i>Empirical models</i>	174

5.5	<i>Data support requirements</i>	176
5.5.1	<i>Sound-speed profile synthesis</i>	177
5.5.2	<i>Earth curvature corrections</i>	179
5.5.3	<i>Merging techniques</i>	180
5.6	<i>Special applications and inverse techniques</i>	180
5.6.1	<i>Stochastic modeling</i>	181
5.6.2	<i>Broadband modeling</i>	182
5.6.3	<i>Matched field processing</i>	183
5.6.4	<i>Transmutation approaches</i>	185
5.6.5	<i>Chaos</i>	186
5.6.6	<i>Three-dimensional modeling</i>	187
5.6.7	<i>Ocean fronts, eddies and internal waves</i>	188
5.6.8	<i>Coupled ocean–acoustic modeling</i>	193
5.6.9	<i>Acoustic tomography</i>	194
5.6.10	<i>Phase conjugation and time-reversal mirrors</i>	198
5.6.11	<i>Deductive geoacoustic inversion</i>	198
6	Noise I: observations and physical models	200
6.1	<i>Background</i>	200
6.2	<i>Noise sources and spectra</i>	200
6.2.1	<i>Seismo-acoustic noise</i>	202
6.2.2	<i>Shipping noise</i>	203
6.2.3	<i>Bioacoustic noise</i>	205
6.2.4	<i>Wind and rain noise</i>	205
6.3	<i>Depth dependence</i>	209
6.4	<i>Directionality</i>	209
6.5	<i>Arctic ambient noise</i>	210
6.6	<i>Acoustic daylight</i>	211
6.7	<i>Geoacoustic inversion</i>	212
7	Noise II: mathematical models	214
7.1	<i>Background</i>	214
7.2	<i>Theoretical basis for noise modeling</i>	214
7.3	<i>Ambient-noise models</i>	216
7.4	<i>The RANDI model – a specific example</i>	219
7.4.1	<i>Transmission loss</i>	219
7.4.2	<i>Noise sources and spectra</i>	219
7.4.3	<i>Directionality</i>	219
7.4.4	<i>Recent developments</i>	221
7.5	<i>The noise notch</i>	222

7.6	<i>Beam-noise statistics models</i>	225
7.7	<i>Data support requirements</i>	226
7.8	<i>Numerical model summaries</i>	229
8	Reverberation I: observations and physical models	232
8.1	<i>Background</i>	232
8.2	<i>Volume reverberation</i>	233
8.2.1	<i>Deep scattering layer</i>	234
8.2.2	<i>Column or integrated scattering strength</i>	234
8.2.3	<i>Vertical-scattering plumes</i>	235
8.3	<i>Boundary reverberation</i>	236
8.3.1	<i>Sea-surface reverberation</i>	236
8.3.2	<i>Under-ice reverberation</i>	240
8.3.3	<i>Sea-floor reverberation</i>	240
8.4	<i>Inversion techniques</i>	243
9	Reverberation II: mathematical models	244
9.1	<i>Background</i>	244
9.2	<i>Theoretical basis for reverberation modeling</i>	244
9.2.1	<i>Basic approaches</i>	244
9.2.2	<i>Advanced developments</i>	247
9.3	<i>Cell-scattering models</i>	248
9.3.1	<i>Volume-reverberation theory</i>	248
9.3.2	<i>Boundary-reverberation theory</i>	250
9.4	<i>The REVMOD model – a specific example</i>	251
9.5	<i>Bistatic reverberation</i>	255
9.5.1	<i>Computational considerations</i>	255
9.5.2	<i>The bistatic acoustic model – a specific example</i>	257
9.6	<i>Point-scattering models</i>	259
9.6.1	<i>Computational considerations</i>	259
9.6.2	<i>The under-ice reverberation simulation model – a specific example</i>	260
9.7	<i>Numerical model summaries</i>	261
10	Sonar performance models	264
10.1	<i>Background</i>	264
10.2	<i>Sonar equations</i>	265
10.3	<i>The NISSM model – a specific example</i>	270
10.3.1	<i>Propagation</i>	271
10.3.2	<i>Reverberation</i>	273

10.3.3	<i>Target echo</i>	275
10.3.4	<i>Noise</i>	275
10.3.5	<i>Signal-to-noise ratio</i>	276
10.3.6	<i>Probability of detection</i>	277
10.3.7	<i>Model outputs</i>	277
10.4	<i>Model operating systems</i>	281
10.4.1	<i>System architecture</i>	282
10.4.2	<i>Sonar modeling functions</i>	283
10.4.3	<i>System usage</i>	286
10.4.4	<i>The generic sonar model – a specific example</i>	286
10.4.5	<i>The comprehensive acoustic system simulation – a specific example</i>	287
10.5	<i>Data sources and availability</i>	288
10.6	<i>Numerical model summaries</i>	292
11	Model evaluation	296
11.1	<i>Background</i>	296
11.2	<i>Past evaluation efforts</i>	297
11.3	<i>Analytical benchmark solutions</i>	298
11.4	<i>Quantitative accuracy assessments</i>	301
11.5	<i>The POSSM experience – a specific example</i>	302
11.6	<i>Evaluation guidelines</i>	305
11.6.1	<i>Documentation</i>	305
11.6.2	<i>Verification</i>	307
11.6.3	<i>Validity</i>	308
11.6.4	<i>Maintainability</i>	308
11.6.5	<i>Usability</i>	309
11.7	<i>Documentation standards</i>	309
12	Simulation	313
12.1	<i>Background</i>	313
12.2	<i>Hierarchical levels</i>	314
12.2.1	<i>Engineering</i>	315
12.2.2	<i>Engagement</i>	315
12.2.3	<i>Mission</i>	316
12.2.4	<i>Theater</i>	316
12.3	<i>Simulation infrastructure</i>	316
12.4	<i>High-level architecture</i>	317
12.5	<i>Testbeds</i>	318

12.6	<i>Applications</i>	319
12.6.1	<i>Systems engineering</i>	320
12.6.2	<i>Simulation-based acquisition</i>	320
12.6.3	<i>Operations analysis</i>	325
12.6.4	<i>Training</i>	326
Appendix A	Abbreviations and acronyms	328
Appendix B	Glossary of terms	342
Appendix C	Websites	351
References		354
	<i>Author index</i>	403
	<i>Subject index</i>	415

Preface

Broadly defined, modeling is a method for organizing knowledge accumulated through observation or deduced from underlying principles while simulation refers to a method for implementing a model over time. The field of underwater acoustic modeling and simulation translates our physical understanding of sound in the sea into mathematical models that can simulate the performance of complex acoustic systems operating in the undersea environment.

This book discusses the fundamental processes involved in simulating underwater-acoustic systems and emphasizes the importance of applying the proper modeling resources to simulate the behavior of sound in virtual ocean environments. Summary tables identify available propagation, noise, reverberation and sonar performance models. Guidelines for selecting and using these various models are highlighted. Specific examples of each type of model are discussed to illustrate model formulations, assumptions and algorithm efficiency. Instructive case studies in simulation are reviewed to demonstrate practical applications.

Over the past decade, rapid changes in the world situation have opened new avenues for international collaboration in modeling and simulation. Concurrent advances in electronic communications have greatly facilitated the transfer of modeling and simulation technologies among members of the international community. The Internet now provides unprecedented access to models and databases around the world. Where appropriate, references to pertinent websites are incorporated in this edition.

The level of technical detail presented in this book is appropriate for a broad spectrum of practitioners and students in sonar technology, acoustical oceanography, naval operations analysis, systems engineering and applied mathematics. The material is organized into 12 chapters. The order of presentation of the first ten chapters follows the structure suggested by a hierarchical method of sonar model construction. Chapter 1 introduces the types of underwater acoustic models, provides a framework for the consistent classification of modeling techniques and defines the terminology common to modeling and simulation. Aspects of oceanography essential to an understanding of acoustic phenomena are presented in Chapter 2.

Chapters 3 through 9 address the observations and models dealing with propagation, noise and reverberation in the sea. In Chapter 10, the information from Chapters 3–9 is integrated into sonar performance models. Chapter 11 describes the process of model evaluation. Chapter 12, which is new to this edition, discusses the application of simulation in underwater acoustics. Since simulation is a method for implementing a model over time, it is fitting that this topic is addressed only after a firm foundation of modeling and evaluation has been established. The title of this edition has been changed to *Underwater Acoustic Modeling and Simulation* to reflect the inclusion of material on simulation.

Rather than purging older material from the third edition, I have intentionally retained descriptions of earlier developments (including the older models) to provide a historical account of the progress that has been achieved over the cumulative period of record covered by these three editions. I trust that this new edition will continue to serve as a useful source of information for all those engaged in modeling and simulation in underwater acoustics.

Paul C. Etter
Rockville, Maryland
USA

Preface to the second edition

The subject of underwater acoustic modeling deals with the translation of our physical understanding of sound in the sea into mathematical formulae solvable by computers. This book divides the subject of underwater acoustic modeling into three fundamental aspects: the physical *principles* used to formulate underwater acoustic models; the mathematical *techniques* used to translate these principles into computer models and modeling *applications* in sonar technology and oceanographic research.

The material presented here emphasizes aspects of the ocean as an acoustic medium. It shows mathematicians and physical scientists how to use this information to model the behavior of sound in a spatially complex and temporally variable ocean. This approach diminishes the need for discussions of engineering issues such as transducers, arrays and targets. Aspects of hardware design and modeling in underwater acoustics are discussed in other excellent texts.

Recent developments in underwater acoustic modeling have been influenced by changes in global geopolitics. These changes are evidenced by strategic shifts in military priorities as well as by efforts to transfer defense technologies to non-defense applications.

The strategic shift in emphasis from deep-water to shallow-water naval operations has focused attention on improving sonar performance in coastal regions. These near-shore regions, which are sometimes referred to as the littoral zone, are characterized by complicated and highly variable acoustic environments. Such difficult environments challenge the abilities of those sonar models intended for use in deep-water scenarios. This situation has prompted further development of underwater acoustic models suitable for forecasting and analyzing sonar performance in shallow-water areas.

The policy of defense conversion has encouraged the transfer of sonar modeling technology to non-defense applications. Much of this transfer has benefited the growing field of environmental acoustics, which seeks to expand exploration of the oceans through acoustic sensing. Such technology conversion is exemplified by the utilization of naval underwater acoustic models as both prognostic and diagnostic tools in sophisticated experiments employing inverse acoustic sensing of the oceans.

These rapid developments in modeling have created a need for a second edition. The intent is to update recent advances in underwater acoustic modeling and to emphasize new applications in oceanographic research. This edition also reflects a broader international interest in the development and application of underwater acoustic models. The coming years promise to be challenging in terms of defining research directions, whether for defense or industry, and this edition should provide technology planners with a useful baseline.

The original organization of material into 11 chapters has served well and therefore remains unchanged. When required, new material has been arranged into additional subsections.

Comments from users of the first edition have evidenced appeal from acousticians, as well as oceanographers, who have enthusiastically endorsed this book as both a practical tool and an instructional aid. In this latter regard, several academic institutions have utilized this book as an adjunct text for graduate-level courses in applied mathematics and ocean sciences.

This edition has benefited from a continuation of my short courses which, since 1993, have been offered through the Applied Technology Institute of Clarksville, Maryland (USA). Continued exposure to the insightful questions posed by my students has provided me with the opportunity to further refine my presentation.

Despite the appearance of several new books in the field of ocean acoustics, this book remains unique in its treatment and coverage of underwater acoustic modeling. It is a pleasure to note that the first edition has been recognized as an authoritative compendium of state-of-the-art models and is often cited as the standard reference.

Paul C. Etter
Rockville, Maryland
USA

Preface to the first edition

The subject of underwater acoustic modeling deals with the translation of our physical understanding of sound in the sea into mathematical formulae solvable by computers. These models are useful in a variety of research and operational applications including undersea defense and marine seismology. There has been a phenomenal growth in both the number and types of models developed over the past several decades. This growth reflects the widespread use of models for the solution of practical problems as well as the considerable advances made in our computational abilities.

The primary motivation for the development of underwater acoustic models is defense related. Researchers involved in Anti-Submarine Warfare (ASW) and associated undersea defense disciplines use models to interpret and forecast acoustic conditions in the sea in support of sonar design and sonar operation. Consequently, the emphasis in this book is placed on those models that are particularly useful in solving sonar performance problems.

Users and potential users of models are commonly ill acquainted with model formulations. As a result, the capabilities and limitations of the models are poorly understood and the models are often improperly used. Moreover, the sheer number of available models complicates the process of model selection.

This book is intended for those who have a fundamental understanding of underwater acoustics but who are not familiar with the various aspects of modeling. Sufficient mathematical derivations are included to demonstrate model formulations, and guidelines are provided to assist in the selection and proper application of these models. Comprehensive summaries identify the available models and associated documentation.

The material is organized into 11 chapters. The order of presentation follows the structure suggested by a hierarchical method of sonar model construction. Chapter 1 introduces the types of underwater acoustic models, provides a framework for the consistent classification of modeling techniques and defines the terminology common to modeling work. Aspects of oceanography essential to an understanding of acoustic phenomena are presented in Chapter 2. Chapters 3 through 9 address the observations and models dealing with propagation, noise and reverberation in the sea. In Chapter 10,

the information from Chapters 3–9 is integrated into sonar performance models. Finally, Chapter 11 describes the process of model evaluation.

Since 1982, I have developed and taught a series of intensive short courses for the Technology Service Corporation of Silver Spring, Maryland (USA). Earlier versions of this course were taught in collaboration with Professor Robert J. Urick of the Catholic University of America. Professor Urick would discuss underwater acoustic measurements while I would review the related modeling techniques. As the course evolved into one in which I became the sole instructor, I borrowed heavily from Professor Urick's several books (with permission) in order to preserve the continuity of the course material. The success of this course encouraged me to publish my class notes as a book.

Many notable books have been published in the field of underwater acoustics. None, however, has dealt exclusively with modern developments in modeling, although some have addressed aspects of propagation modeling. This book is unique in that it treats the entire spectrum of underwater acoustic modeling including environmental, propagation, noise, reverberation and sonar performance models.

I have intentionally preserved the notation, terminology and formalism used by those researchers whose work I have cited. I have also intentionally emphasized aspects of oceanography since my experience has indicated that many acousticians have little appreciation for the complex role played by the ocean as an acoustic medium. Conversely, oceanographers frequently fail to appreciate the great potential of underwater acoustics as a remote sensing technique.

Paul C. Etter

Acknowledgments

The students who have attended my short courses over the past 20 years have provided both a receptive and critical audience for much of the material contained in this book. Many of my colleagues have provided useful insights and suggestions. In particular, I want to recognize Dr Michael A. Ainslie, Dr Aubrey L. Anderson, Dr Stanley A. Chin-Bing, Dr Richard B. Evans, Dr Robert W. Farwell, Dr Richard P. Flanagan, Dr Robert L. Martin¹, Dr Peter M. Ogden, Dr Frederick D. Tappert and Dr Henry Weinberg. Robert S. Winokur provided administrative guidance in the early stages of my work in underwater acoustic modeling.

Professor Robert J. Urick¹ provided much encouragement and graciously allowed me to liberally borrow material from his several books. Professor John D. Cochran¹ of Texas A&M University inspired the scholarly discipline that facilitated creation of this book.

¹ Deceased.

1 Introduction

1.1 Background

1.1.1 *Setting*

Underwater acoustics entails the development and employment of acoustical methods to image underwater features, to communicate information via the oceanic waveguide or to measure oceanic properties. In its most fundamental sense, *modeling* is a method for organizing knowledge accumulated through observation or deduced from underlying principles. *Simulation* refers to a method for implementing a model over time.

Historically, sonar technologists initiated the development of underwater acoustic modeling to improve sonar system design and evaluation efforts, principally in support of naval operations. Moreover, these models were used to train sonar operators, assess fleet requirements, predict sonar performance and develop new tactics. Despite the restrictiveness of military security, an extensive body of relevant research accumulated in the open literature, and much of this literature addressed the development and refinement of numerical codes that modeled the ocean as an acoustic medium. This situation stimulated the formation of a new sub-discipline known as *computational ocean acoustics*. Representative developments in computational ocean acoustics have been documented by Merklinger (1987), Lee *et al.* (1990a–c, 1993) and Lau *et al.* (1993).

As these modeling technologies matured and migrated into the public domain, the private industry was able to apply many aspects of this pioneering work. Subsequently, there has been much cross-fertilization between the geophysical-exploration and the sonar-technology fields as the operating frequencies of both fields began to converge. Recently, acoustical oceanographers have employed underwater acoustic models as adjunct tools for inverse-sensing techniques (see Section 1.6) that can be used to obtain synoptic portraits of large ocean areas or to monitor long-term variations in the ocean.

Underwater acoustic models are now routinely used to forecast acoustic conditions for planning at-sea experiments, designing optimized sonar

2 Introduction

systems and predicting sonar performance at sea. Modeling has become the chief mechanism by which researchers and analysts can simulate sonar performance under laboratory conditions. Modeling provides an efficient means by which to parametrically investigate the performance of hypothetical sonar designs under varied environmental conditions as well as to estimate the performance of existing sonars in different ocean areas and seasons.

1.1.2 Framework

A distinction is made between physical (or “physics-based”) models and mathematical models, both of which are addressed in this book. Physical models pertain to theoretical or conceptual representations of the physical processes occurring within the ocean; the term “analytical model” is sometimes used synonymously. Mathematical models include both empirical models (those based on observations) and numerical models (those based on mathematical representations of the governing physics). The subject of analog modeling, which is defined here as controlled acoustic experimentation in water tanks employing appropriate oceanic scaling factors, is not addressed in this book. Barkhatov (1968) and Zornig (1979) have presented detailed reviews of acoustic analog modeling.

The physical models underlying the numerical models have been well known for some time. Nevertheless, the transition to operational computer models has been hampered by several factors: limitations in computer capabilities, inefficient mathematical methods and inadequate oceanographic and acoustic data with which to initialize and evaluate models. Despite continuing advances in computational power, the development of more efficient mathematical methods and the dramatic growth in databases, the emergence of increasingly sophisticated models continues to challenge available resources.

This book addresses three broad types of underwater acoustic models: *environmental models*, *basic acoustic models* and *sonar performance models*.

The first category – environmental models – includes empirical algorithms that are used to quantify the boundary conditions (surface and bottom) and volumetric effects of the ocean environment. Such models include, for example, sound speed, absorption coefficients, surface and bottom reflection losses and surface, bottom and volume backscattering strengths.

The second category – basic acoustic models – comprises propagation (transmission loss), noise and reverberation models. This category is the primary focus of attention in this book.

The third category – sonar performance models – is composed of environmental models, basic acoustic models and appropriate signal processing models. Sonar performance models are organized to solve specific sonar-applications problems such as submarine detection, mine hunting, torpedo homing and bathymetric sounding.

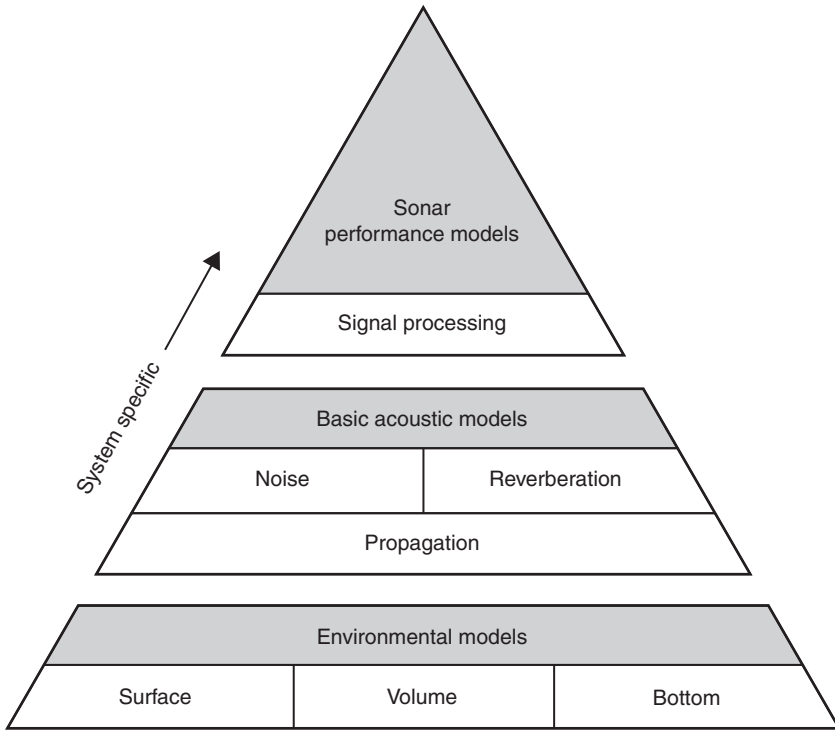


Figure 1.1 Generalized relationships among environmental models, basic acoustic models and sonar performance models.

Figure 1.1 illustrates the relationships among these three broad categories of models. As the applications become more and more system specific (i.e. as one progresses from environmental models toward sonar performance models), the respective models become less universal in application. This is a consequence of the fact that system-specific characteristics embedded in the higher-level models (e.g. signal processing models) restrict their utility to particular sonar systems. Thus, while one propagation model may enjoy a wide variety of applications, any particular sonar performance model is, by design, limited to a relatively small class of well-defined sonar problems.

The wide breadth of material covered in this book precludes exhaustive discussions of all existing underwater acoustic models. Accordingly, only selected models, considered to be representative of each of the three broad categories, will be explored in greater detail. However, comprehensive summary tables identify all known basic acoustic models and sonar performance models. These tables also contain brief technical descriptions of each model together with pertinent references to the literature. Notable

4 *Introduction*

environmental models are identified and discussed in appropriate sections throughout this book.

Modeling applications will generally fall into one of two basic areas: research or operational. Research-oriented applications are conducted in laboratory environments where accuracy is important and computer time is not a critical factor. Examples of research applications include sonar system design and field experiment planning. Operationally oriented applications are conducted as field activities, including fleet operations at sea and sonar system training ashore. Operational applications generally require rapid execution, often under demanding conditions; moreover, modeling accuracy may be subordinate to processing speed.

1.2 **Measurements and prediction**

The scientific discipline of underwater acoustics has been undergoing a long transition from an observation phase to a phase of understanding and prediction. This transition has not always been smooth – direct observations have traditionally been limited, the resulting prediction tools (models) were not always perfected and much refinement remains to be completed.

Experimental measurements in the physical sciences are generally expensive due to instrumentation and facility-operation costs. In the case of oceanographic and underwater acoustic data collection, this is particularly true because of the high costs of platform operation (ships, aircraft, submarines). Acoustic datasets obtained at sea are limited by their inherent spatial, temporal and spectral dimensions. Consequently, in the field of underwater acoustics, much use is made of what field measurements already exist. Notable large-scale field programs that have been conducted successfully in the past include AMOS (Acoustic, Meteorological and Oceanographic Survey) and LRAPP (Long Range Acoustic Propagation Project). More recent examples include ATOC (Acoustic Thermometry of Ocean Climate) and other basin-scale tomographic experiments.

Modeling has been used extensively to advance scientific understanding without expending scarce resources on additional field observations. The balance between observations and modeling, however, is very delicate. Experimenters agree that modeling may help to build intuition or refine calculations, but they argue further that only field observations give rise to genuine discovery. Accordingly, many researchers find mathematical models most useful once the available observations have been analyzed on the basis of simple physical models.

The relationship between experimentation and modeling (in the furtherance of understanding and prediction) is depicted schematically in Figure 1.2. Here, physical models form the basis for numerical models while experimental observations form the basis for empirical models. Moreover, analog modeling is represented as a form of laboratory (versus field) experimentation.

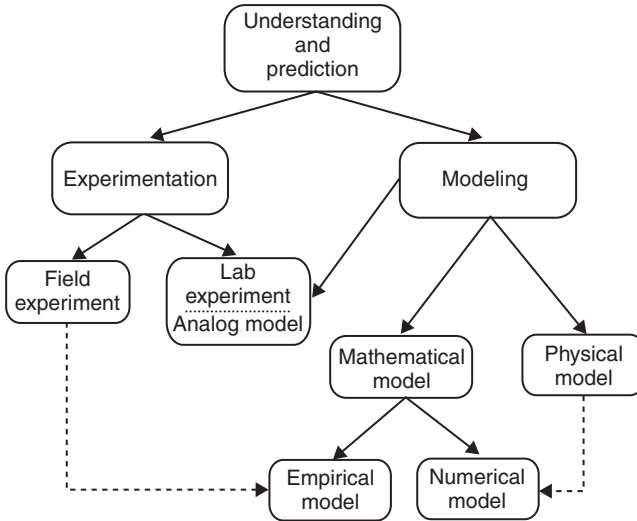


Figure 1.2 Schematic relationship between experimentation and modeling.

Scientists are becoming more aware of the connection between physical processes and computation, and many now find it useful to view the world in computational terms. Consequently, computer simulation is sometimes viewed as a third form of science, midway between theory and experiment. Furthermore, understanding can be enhanced through the use of advanced computer graphics to convert large volumes of data into vivid and comprehensible patterns.

Because of national security concerns, some existing datasets are limited in accessibility. Also, because of the wide range of acoustic frequencies, ocean areas and geometries of interest to researchers, it is virtually impossible to accommodate all potential observational requirements within normal fiscal constraints. To make matters worse, acoustic data are sometimes collected at sea without the supporting oceanographic data. Thus, models cannot always replicate the observed acoustic results because they lack the necessary input parameters for initialization. This situation has been improving with the advent of modern, multidisciplinary research that necessitates the inclusion of oceanographers in the planning and execution of complex field experiments.

Satellites, together with other remote-sensing techniques, provide a useful adjunct to the prediction of underwater acoustic conditions. Specifically, many dynamic features of the ocean affect the behavior of sound in the sea. Knowledge of the location and size of such dynamic features can improve the prediction of sonar performance. Although satellite-borne sensors detect only surface (or near-surface) features of the ocean, such as

6 Introduction

thermal contrast, color or surface roughness, these “surface expressions” can generally be associated with dynamic oceanographic features below the surface, particularly when comprehensive climatological databases already exist with which to establish such associations. Thus, for example, satellite imagery can be used to provide timely and accurate position information on variable ocean features such as fronts and eddies – features that are known to have a significant impact on the propagation of acoustic signals in the sea.

Tactical oceanographic data collection in support of naval operations has been augmented by drifting buoys, which use satellite relays to transmit data to mobile or stationary receiving stations, and by autonomous underwater vehicles (AUVs) to access remote ocean areas such as shallow-water and under-ice regions (Brutzman *et al.*, 1992; Dantzer *et al.*, 1993; Selsor, 1993; Etter, 2001b).

The problem of operational sonar prediction embraces many disciplines, one of which is modeling. Such modern operational applications involve not only underwater acoustic models but also oceanographic models (Etter, 1989). The coupling of these two types of models provides a valuable set of prediction tools to naval force commanders by enabling them to respond to the changing environmental conditions that affect their sonar performance. The remote-sensing data now available to naval forces afloat can be used in conjunction with oceanographic models to accurately forecast the locations and characteristics of dynamic ocean features (Robinson, 1992). This information can then be input to the appropriate acoustic models to assess the resultant impact on sonar performance. These sonar systems can then be optimized for performance in each region of operation at any given time of the year.

Advances in sonar technologies have rendered modern sonar systems useful for *in situ* measurements of the ambient marine environment. For example, through-the-sensor measurements of the ocean impulse response (Smith, 1997) have enabled modern sonars to perform collateral functions as “tactical environmental processors.”

1.3 Developments in modeling

A goal of science is to develop the means for reliable prediction to guide decision and action (Ziman, 1978). This is accomplished by finding algorithmic compressions of observations and physical laws. Physical laws are statements about classes of phenomena, and initial conditions are statements about particular systems. Thus, it is the solutions to the equations, and not the equations themselves, that provide a mathematical description of the physical phenomena. In constructing and refining mathematical theories, we rely heavily on models. At its conception, a model provides the framework for a mathematical interpretation of new phenomena.

In its most elemental form, a model is intended to generalize and to abstract. A perfect model is one that perfectly represents reality. In practice,

however, such a perfect model would defeat its purpose: it would be as complex as the problem it is attempting to represent. Thus, modeling in the physical sciences is normally reduced to many, more easily managed, components. Oreskes *et al.* (1994) argued that the primary value of models in the earth sciences is heuristic (i.e. an aid to learning, as through trial-and-error methods) and that the demonstration of agreement between observation and prediction is inherently partial since natural systems are never closed. The ocean is a natural system and, as an acoustic medium, it is not a closed (or deterministic) system. As will be demonstrated, most underwater acoustic models treat the ocean as a deterministic system. This can create problems when evaluating models against field data that are, by nature, non-deterministic (i.e. stochastic or chaotic). Thus, evaluation is an important aspect of any discussion of modeling. Frequently, models become data limited. This means that observational data are lacking in sufficient quantity or quality with which to support model initialization and model evaluation.

With the advent of digital computers, modeling in the physical sciences advanced dramatically. Improvements in computer capabilities over the past several decades have permitted researchers to incorporate more complexity into their models, sometimes with little or no penalty in run time or computer costs (e.g. Hodges, 1987; Runyan, 1991). Although computational capabilities have increased dramatically over the past several decades, so too have the expectations placed on software performance. Consequently, software efficiency still remains a very critical issue – we cannot look to unlimited computing power as a panacea for inefficient software. Furthermore, with the dramatic increase in autonomous, self-guided systems such as AUVs and unmanned undersea vehicles (UUVs) (National Research Council, 1996, 1997), many of which use self-contained modeling and simulation technologies, issues of verification, validation and accreditation (VV&A) will assume even greater importance in maintaining and improving system reliability.

As modeling techniques continue to proliferate within the underwater acoustics community, it becomes increasingly difficult to take stock of the various models already in existence before launching a new effort to develop yet more models. Moreover, analysts confronted with sonar performance problems have difficulty in determining what models exist and, of those, which are best for their particular situation. This book had its genesis in just such a dilemma. The US Navy sponsored a small study in 1978 (Etter and Flum, 1978) to review the availability of numerical models of underwater acoustic propagation, noise and reverberation as well as the availability of databases with which to support model development and operation. Results of this work, and extensions thereto (Etter and Flum, 1980; Etter *et al.*, 1984), have subsequently been presented at meetings of the Acoustical Society of America (Etter and Flum, 1979; Etter, 1987b, 1995, 1999). Moreover, progress has been documented in periodic literature review articles (Etter, 1981, 1984, 1987a, 1990, 1993, 2001a). An enhanced

8 Introduction

version of the first review article (Etter, 1981) was included as chapter 3 in a book by Urick (1982). Collectively, this work later evolved into a series of lectures and culminated in the first edition of this book (Etter, 1991). A second edition (Etter, 1996) was prepared to address the rapid advances unfolding in this area. The present edition continues this review work.

As new models have been developed and older models have fallen into disuse, it is fair to ask why the older material has not been purged from the newer editions. Simply stated, this book serves two purposes. First, this book introduces a complicated topic to people of varied backgrounds, including those who do not routinely work in the field of underwater acoustic modeling and simulation. In this sense, the older material provides an historical perspective and identifies the pioneering names that are taken for granted by the seasoned professionals in the field. Second, for those who routinely work in this field, retention of the older material provides an inverted roadmap of past exploration.

The technical literature cited in this book includes many unpublished reports (so-called “gray” literature) since no other sources of documented technical information were available. Unpublished reports comprised nearly 40 percent of the literature cited in the first edition. In the present edition, reliance on unpublished reports decreased to about 30 percent. This trend is attributed, in part, to the maturing of underwater acoustic modeling and simulation technologies and their subsequent migration into the academic literature. Approximately 34 percent of the literature cited in all three editions was drawn from the *Journal of the Acoustical Society of America*; evidencing the role of this journal in communicating progress in the field of underwater acoustic modeling and simulation. As work has advanced in simulation, progress has been reported in related academic journals as well. References to Internet websites are now included as sources of information, and specific sites of interest are indicated in Appendix C. While websites are useful sources of information, they are problematic as references since the addresses for these websites sometimes change or disappear entirely.

Other researchers have conducted reviews of modeling that provide useful sources of information. These reviews have tended to be more in-depth but more narrowly focused than the work presented in this book. Weston and Rowlands (1979) reviewed the development of models with application to underwater acoustic propagation over the period 1963–78. DiNapoli and Deavenport (1979) provided a highly mathematical examination of a select number of propagation models. Brekhovskikh and Lysanov (1982) presented a comprehensive Russian perspective on underwater acoustics with a limited treatment of modeling. Piskarev (1992) provided an account of state-of-the-art Soviet research in underwater acoustic propagation modeling up to 1989. Finally, Jensen *et al.* (1994) provided a lucid and comprehensive review of recent theoretical developments in ocean acoustic propagation modeling.

1.4 Advances in simulation

Broadly defined, simulation refers to a method for implementing a model over time. The term “modeling and simulation” (M&S) will refer collectively to those techniques that can predict or diagnose the performance of complex systems operating in the undersea environment.

The functions of M&S can be categorized as either prognostic or diagnostic. Prognostic functions include prediction and forecasting, where future oceanic conditions or acoustic sensor performance must be anticipated. Diagnostic functions include systems design and analyses, which are typically encountered in engineering tradeoff studies.

In the context of naval operations, simulations can be decomposed into four fundamental levels: engineering, engagement, mission and theater (National Research Council, 1997). Engineering-level simulation comprises environmental, propagation, noise, reverberation and sonar performance models. Engagement-level simulation executes engineering-level models to generate estimates of system performance in a particular spatial and temporal ocean environment when operating against (engaging) a particular target. Mission-level simulation aggregates multiple engagements to generate statistics useful in evaluating system concepts within the context of well-defined mission scenarios. Finally, theater-level simulation aggregates mission-level components to analyze alternative system employment strategies. Figure 1.3 illustrates the hierarchical relationship between engineering-level simulations and underwater acoustic models. Aspects of simulation will be discussed in greater detail in Chapter 12.

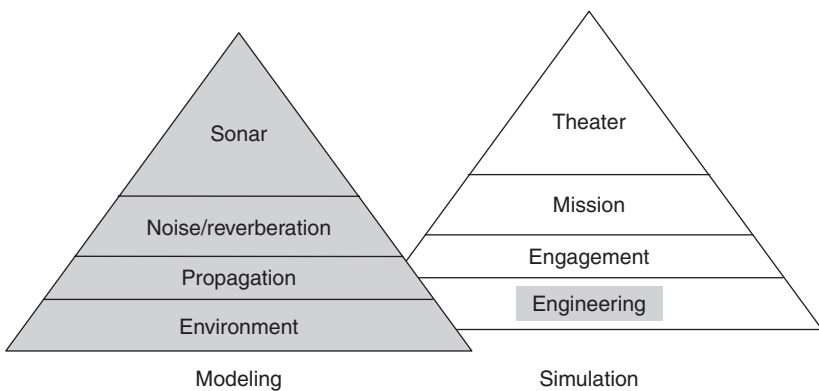


Figure 1.3 Modeling and simulation hierarchies illustrating the relationship between underwater acoustic models (left) and simulations (right). In this context, engineering-level simulations comprise environmental, propagation, noise, reverberation and sonar performance models (Etter, 2001a).

1.5 Operational challenges

Modeling and simulation products aid the development and employment of acoustical techniques used to image underwater features, communicate information via the oceanic waveguide or measure oceanic properties (Etter, 2000). Representative applications of these techniques are summarized in Table 1.1.

Technology investment strategies driven by the geopolitical realities of the past decade have greatly influenced the direction of research and development (R&D) in general, and of M&S in particular. These investment strategies have adversely impacted government and academia by diminishing budgets for undersea research, reducing the number of field experiments, reducing at-sea training time and limiting asset modernization. Other economic factors have adversely affected the offshore industries. This situation creates new opportunities and challenges for M&S. As will be discussed below, M&S can be leveraged as enabling technologies to meet the technical and programmatic challenges in naval operations, offshore industries and oceanographic research.

Underwater acoustics also plays a role in the international monitoring system (IMS), which comprises a network of stations that monitor Earth for evidence of nuclear explosions in all environments to ensure compliance with the comprehensive nuclear-test-ban treaty (CTBT). The system employs seismic, hydroacoustic and infrasound stations to monitor the underground, underwater and atmosphere environments, respectively.

Table 1.1 Summary of acoustical techniques and representative applications

<i>Acoustical technique</i>	<i>Applications</i>
Image underwater features	Detection, classification and localization of objects in the water column and in the sediments using monostatic or bistatic sonars Obstacle avoidance using forward-looking sonars Navigation using echo sounders or sidescan sonars to recognize sea-floor topographic reference features
Communicate information via the oceanic waveguide	Acoustic transmission and reception of voice or data signals in the oceanic waveguide Navigation and docking guided by acoustic transponders Release of moored instrumentation packages using acoustically activated mechanisms
Measure oceanic properties	Measurement of ocean volume and boundaries using either direct or indirect acoustical methods Acoustical monitoring of the marine environment for regulatory compliance Acoustical surveying of organic and inorganic marine resources

Bedard and Georges (2000) reviewed the application of atmospheric infrasound for such monitoring. Newton and Galindo (2001) described aspects of the hydroacoustic monitoring network. Moreover, Farrell and LePage (1996) described the development of a model to predict the detection and localization performance of this hydroacoustic monitoring network.

Whitman (1994) reviewed defense conversion opportunities in marine technology and made a distinction between dual use and conversion. Dual use suggests the deliberate pursuit of new research, development or economic activity that is applicable within both military and civilian domains. Conversion implies seeking new uses for existing defense resources. An example of conversion is the utilization of existing undersea surveillance assets as a National Acoustic Observatory. Research uses include stock and migration monitoring of large marine mammals, remote ocean observations, seismic and volcanic monitoring, acoustic telemetry and fisheries enforcement (Amato, 1993; Carlson, 1994).

1.5.1 *Naval operations*

Over the past decade, naval mission requirements have shifted from open-ocean operations to littoral (or shallow-water) scenarios. This has not been an easy transition for sonar technologists since sonar systems that were originally designed for operation in deep water seldom work optimally in coastal regions. This has also held true for modeling and simulation technologies, which have undergone a redefinition and refocusing to support a new generation of multistatic naval systems that are intended to operate efficiently in littoral regions while still retaining a deep-water capability. A corresponding shift has been reflected in the research directions of the supporting scientific community as technical priorities have been realigned.

Shallow-water geometries increase the importance of boundary interactions, which diminish acoustic energy through scattering and also complicate the detection and localization of submerged objects due to multipath propagation. Moreover, the higher levels of interfering noises encountered in coastal regions combine with higher levels of boundary reverberation to mask signals of interest.

Naval operations in littoral regions often rely on multistatic acoustic sensors, thus increasing the technical challenges associated with the field-intensive experiments necessary to test multistatic geometries. Acoustical oceanographers have conducted supporting research using traditional direct-sensing methods in addition to more sophisticated inverse-sensing techniques such as acoustic tomography, full-field processing and ambient-noise imaging (see Section 1.6). Due to an increased awareness of the potential technological impacts on marine life, naval commanders and acoustical oceanographers must now comply with new environmental regulations governing the acoustic emissions of their sonar systems.

12 Introduction

Modeling and simulation can mitigate these technical and programmatic challenges in four ways. First, reduced at-sea training opportunities can be offset through the use of computer-based training (CBT). Second, simulation *testbeds* can facilitate system-design efforts aimed at maximizing returns on diminished asset-modernization expenditures. Third, the operation of existing systems can be optimized through the application of high-fidelity modeling and simulation products. Fourth, system-design tradeoffs can be evaluated using modeling and simulation products as metrics. Such efforts are important components of so-called simulation-based acquisition (SBA). Simulation-based acquisition comprises product representations, analysis tools (for design optimization and cost estimation) and an infrastructure that allows the product representations and analysis tools to interact with one another. These issues will be addressed in Chapter 12.

In advance of naval operations, it is necessary to collect meteorological and oceanographic (Met/Ocean) data from remote or hostile coastal environments in order to forecast acoustic sensor performance. Coupled atmosphere–ocean–acoustic models could reduce the need for hazardous *in situ* data collection by numerically computing initial states for the embedded acoustic models.

Specific solutions may include integration of M&S technologies in AUVs or UUVs to create an advanced generation of environmentally adaptive acoustic-sensor systems for naval operations and for oceanographic research. This environmental adaptation is accomplished by making *in situ*, through-the-sensor measurements of environmental conditions in conjunction with a sonar controller using an environmental feedback loop.

It may also be possible to leverage M&S technologies to enhance evolving network-centric data fusion and sensor-integration functions (Morgan, 1998), as has already been demonstrated in model-based signal-processing approaches (Candy and Sullivan, 1992). A network-centric operation derives its power from the strong networking of well-informed but geographically dispersed entities. The networked platforms can include AUVs, surface ships, submarines, aircraft or satellites. The elements that enable network centrality include distributed sensor networks, a high-performance information grid, access to pertinent information sources (*in situ* and archival), precision and speed of response and command and control processes. Network centrality fuses common tactical and environmental pictures, thus reducing uncertainties in measurements and modeling. Simulated volumetric (3D) visualizations of the undersea battlespace derived from M&S technologies could further enhance the efficient management and deployment of critical resources.

High-fidelity, multistatic sonar performance models can also be used to gauge compliance with environmental noise regulations concerning marine mammal protection. Moreover, controlling underwater radiated noise and sonar self-noise on naval vessels is critically important, and simulation can be used to predict the noise environments on surface ships and submarines.

1.5.2 Offshore industries

In the commercial sector, acoustic sensing methods have found numerous applications including acoustic Doppler current profilers (ADCPs) for measuring currents, compact sonars for obstacle location and avoidance by AUVs (e.g. Brutzman *et al.*, 1992), fish-finding devices, underwater communications systems for divers, fathometers for bathymetric sounding and navigation and side-scanning sonars for topographic mapping of the sea-floor relief. Some point-source and non-point-source pollution studies now use acoustic backscatter measurements to monitor the marine environment.

Offshore industries, particularly oil and gas, have undergone profound changes over the past decade in response to global economic factors. Specifically, the contribution of offshore oil production to the total non-OPEC supply increased from about 25 percent in 1990 to about 30 percent in 1995. Approximately 80 percent of the significant growth in non-OPEC supply up to 2000 was offshore. An appreciable contribution to the growth in offshore production was made by new technologies such as 3D seismic evaluations, horizontal drilling, sub-sea completions, multi-phase pipelines and floating production, storage and off-loading (FPSO) vessels (International Energy Agency, 1996).

As the exploitation of offshore oil reserves has increased, exploration and production (E&P) operations have expanded into deeper waters. For example, recent Angolan oil-exploration concession areas comprised three water-depth bands: shallow blocks (<500 m), deep blocks (500–1,500 m) and ultra-deep blocks (1,500–2,500 m). In comparison, significant sub-sea oil production in the Gulf of Mexico has typically occurred in water depths approaching 1,200 m. At such depths, it is not possible to build fixed oil rigs. Instead, floating platforms are anchored to the seabed. Since the equipment needed to operate each well is too heavy to install on the floating platforms, the equipment is placed on the sea floor where it is maintained by remotely operated vehicles (ROVs) deployed from the floating platforms.

Because these formerly topside systems were designed for direct (human) intervention rather than for remote intervention, the tasks necessary to install and maintain these systems are difficult (if not impossible) to perform with traditional ROV-based tools and techniques. Automation of remote-intervention tasks can make use of commercial-off-the-shelf (COTS) technologies such as acoustic positioning, acoustic imaging and enhanced user interfaces integrated into a single system (Schilling, 1998). These technologies can also be used for inspection, maintenance and repair (IMR) operations.

Pipeline routes are planned to be as short as possible to reduce costs. Moreover, bottom slopes that could put stress on unsupported pipes are avoided, seabed sediments are mapped to identify unstable areas and pipe-burial options are assessed. Surveys of potential pipeline routes commonly utilize data derived from sidescan sonars.

Met/Ocean data collection efforts in support of offshore operations often employ ADCP sensors to measure surface and sub-surface ocean currents. These data are required to determine the vertical and horizontal current shears that can impact the siting and placement of offshore structures.

Employing volumetric (acoustic) plume detection to identify hydrocarbon seepages of natural or man-made origins can fulfill environmental monitoring mandates. Oil-spill tracking, prediction and containment operations, as well as disposal monitoring, can also employ volumetric acoustic methods.

Offshore work in marginal ice zones (MIZ) requires knowledge of ice thickness and under-ice features (especially keels). Information on under-ice features can be obtained from AUVs or ROVs equipped with upward-looking (acoustic) echo sounders. This information can complement independent surface (altimeter) measurements of ice ridges to obtain estimates of total ice thickness.

Acoustic systems are used widely in the offshore industry for ROV tracking, seismic-towfish tracking and drilling operations. These systems must perform in noisy, shallow-water environments. Acoustic transponders function as navigational beacons and as remote-control release mechanisms in the deployment and recovery of instrumentation packages. Moreover, sub-sea drilling-rig supply operations employ acoustic beacons for navigation and docking evolutions. Similarly, divers often rely on portable acoustic devices for communication and navigation.

Noise-control design of planned facilities and noise-control retrofit of existing plants entail environmental noise monitoring, modeling and simulation, and development of noise-control procurement specifications.

Offshore industries can benefit most from recent advances in modeling and simulation by integrating such technologies directly into ROV/AUV control software in order to improve responsiveness to changing environmental conditions. Furthermore, increasing the use of M&S in system design and operator-training functions may derive additional technical and economic benefits.

1.5.3 Operational oceanography

The term “operational oceanography” has become a topic of frequent discussion in the contemporary trade literature, although the activities normally associated with this term have been in existence for some time. The three principal attributes that characterize operational oceanography are: (1) routine and systematic measurements of the oceans and atmosphere; (2) modeling, simulation, analysis and interpretation of these measurements to generate useful information products; and (3) rapid dissemination of these products to the user communities. The user communities typically comprise government, industry, regulatory authorities, research institutions and the general public.

In data assimilation centers, numerical forecasting models process the data and generate information products. The utility of these simulated products is further enhanced (value engineered) by subject matter experts in such disciplines as marine transportation, marine construction, public health and seawater quality. Different applications require different products. This implies that an array of information products must be tailored to satisfy the needs of specific user communities, who have been identified in advance through socio-economic or cost-benefit analyses.

Civil applications of operational oceanography in coastal regions are the most visible and include warnings against such hazards as coastal floods, waves, coastal erosion and effluent contamination. Commercial applications in the open ocean include guidance on optimal ship routing. Defense applications of operational oceanography, as defined by the US Department of the Navy (2000b), include the development of oceanic and atmospheric observations and models to provide on-scene commanders with predictive capabilities, especially in the littoral zone. The US Navy's Geophysics Fleet Mission Program Library (GF MPL) contains meteorological, oceanographic, electromagnetic and acoustic software for use as aids in planning naval operations in the open ocean as well as in the littoral zone. Clancy (1999) and Clancy and Johnson (1997) provided useful overviews of naval operational ocean modeling products and applications.

1.6 Inverse acoustic sensing of the oceans

Useful information about the ocean can be derived from both forward and inverse applications of underwater sound. Direct methods include traditional sonar applications. Inverse methods extract information from direct measurements of the physical properties of the ocean. These inverse methods combine direct physical measurements with theoretical models of underwater acoustics. The objective is to estimate detailed underwater acoustic fields from sparse physical measurements using the theoretical models as guides.

Inverse sensing techniques that employ acoustics have been used in several sub-disciplines of geophysics including seismology, meteorology and oceanography. Seismologists have used tomographic techniques to infer the bulk properties of the lithosphere (e.g. Menke, 1989). Atmospheric scientists have employed naturally generated, low-frequency sound (microbaroms) to probe the upper layers of the atmosphere in an inverse fashion (Donn and Rind, 1971); Coulter and Kallistratova (1999) discussed acoustic remote sensing of the lower atmosphere. In oceanography, inverse acoustic data provide estimates of spatially integrated and temporally averaged oceanic conditions that are not readily available from a traditional constellation of point sensors (e.g. Bennett, 1992). Collins and Kuperman (1994b) presented a broad discussion of inverse problems in ocean acoustics and methods for solving them. Parameters of interest included sound speed in the water

column, sediment properties and boundary roughness. The importance of forward models in solving inverse problems was stressed.

Diachok *et al.* (1995) documented the proceedings of a conference on full-field inversion methods in ocean and seismo-acoustics, which was sponsored by the NATO SACLANT Undersea Research Centre in Italy in June 1994. At this conference, it was demonstrated that inversion methods could exploit the amplitude and phase information detected on hydrophone arrays or geophone arrays to infer environmental information about the ocean. Furthermore, proceedings of an international workshop on *Tomography and Acoustics: Recent Developments and Methods* (University of Leipzig, March 2001) were documented in a special issue of the Journal of the European Acoustics Association (*ACUSTICA acta acustica*, Vol. 87, No. 6, 2001). This two-day workshop addressed tomography, acoustics, atmosphere applications and ocean applications.

Inverse acoustic sensing of the oceans utilizes one of three natural phenomena: propagation, noise or reverberation. Table 1.2 summarizes selected inverse ocean acoustic sensing techniques according to the natural phenomenon utilized. The specific techniques identified in Table 1.2 will be discussed below and in appropriate sections throughout this book.

Acoustic propagation characteristics in the deep oceans are determined largely by the refractive properties of the water column and, to a lesser extent, by the surface and bottom boundary conditions. Propagation measurements can be used to infer bulk properties of the water column such as temperature, sound speed, density and currents. In shallow ocean areas, where propagation characteristics can be strongly affected by the bottom boundary, propagation measurements can be used to infer properties of the sea floor such as composition and scattering characteristics. Caiti *et al.* (2000) reviewed recent progress in experimental acoustic inversion methods for use in shallow-water environments based on papers presented at a workshop sponsored by the Portuguese Foundation for Science and Technology in March 1999. Taroudakis and Makrakis (2001) edited a collection of papers

Table 1.2 Summary of inverse ocean acoustic sensing techniques

<i>Propagation</i>	<i>Noise</i>	<i>Reverberation</i>
Matched field processing <ul style="list-style-type: none"> ● source localization ● marine environment characterization 	Field inversion <ul style="list-style-type: none"> ● wind speeds ● rainfall rates 	Field inversion <ul style="list-style-type: none"> ● sea-floor imaging
Ocean acoustic tomography <ul style="list-style-type: none"> ● density field (eddies, currents) ● temperature (climate monitoring) 	Acoustic daylight <ul style="list-style-type: none"> ● object imaging 	
Deductive geoacoustic inversion <ul style="list-style-type: none"> ● sediment parameters ● sea-floor scattering characteristics 	Geoacoustic inversion <ul style="list-style-type: none"> ● seabed acoustics 	

that addressed a wide spectrum of inverse problems in underwater acoustics including estimation of geoacoustic parameters, acoustic thermometry and shallow-water characterization. Inverse acoustic sensing methods utilizing the propagation characteristics of the oceans include matched field processing, ocean acoustic tomography and deductive geoacoustic inversion (see Chapter 5).

The ambient noise field in the oceans is described by the spectral, spatial and temporal characteristics of sound generated by both natural and industrial sources. Measurements of these characteristics can provide useful information regarding the nature of the noise sources themselves as well as physical features within the oceans. Examples of inverse applications of the noise field include wind speed determination, rainfall measurements, object imaging (“acoustic daylight”) and geoacoustic inversion (see Chapter 6).

The reverberation field in the oceans is the product of acoustic scattering by the surface and bottom boundaries, and by inhomogeneities within the oceans. The utility of the reverberation field as an inverse sensing technique is analogous to that of the ambient noise field. For example, the reverberation field can be inverted to image the sea floor (see Chapter 8).

Inverse acoustic sensing techniques presently constitute adjuncts to direct measurement methods. However, the application of inverse acoustic sensing techniques to dynamical studies of the oceans’ boundaries and interior show great promise for three reasons. First, such data can be used to establish comparative baselines for other remote sensors, such as satellites, by providing synoptic portraits of the interior oceans together with concurrent groundtruth data at the sea surface. Second, inverse acoustic techniques often afford useful insights into a broad class of oceanic phenomena since their successful employment relies heavily on the use of numerical models first to understand the role of the oceans as an acoustic medium. Third, inverse data provide estimates of spatially integrated and temporally averaged oceanic conditions that are not readily available from traditional oceanographic sensors.

1.7 Standard definitions

A consistent vocabulary and standard system of units is essential for work in any scientific discipline. Such a system facilitates efficient and unambiguous communication among members of the community. The underwater acoustics community has struggled with a common vocabulary and standard system of units for quite some time. This situation derives, in part, from the fact that many of the participants in this community have been trained in other disciplines and later migrated into this field.

A number of investigators have introduced suggestions for a standard system of units to satisfy the requirements that are unique to the underwater acoustics community. Recently, for example, Carey (1995) clarified the use of SI metric units for measurements and calculations used in

underwater acoustics and bioacoustics, while Hall (1995) re-examined the dimensions of units for source strength, transmission loss, target strength, surface-scattering strength and volume-scattering strength. In addition, technical dictionaries (e.g. Morfey, 2000) provide useful guidance on proper terminology and usage.

Work in modeling and simulation also requires a consistent vocabulary. In this regard, the Institute of Electrical and Electronics Engineers (1989) published a glossary of definitions for modeling and simulation terms. The US Defense Modeling and Simulation Office (DMSO) assembled the *DOD Modeling and Simulation Glossary*, which prescribes a uniform M&S terminology, particularly for use throughout the Department of Defense. In addition to the main glossary of terms, this highly useful manual includes a list of M&S-related abbreviations, acronyms and initials commonly used within the Department of Defense (refer to Appendix C for the DMSO website).

Recent communications in the forum of the *Journal of the Acoustical Society of America* (Clay, 1999; Hickling, 1999; Chapman, 2000) highlight confusion over use of the decibel (dB). In Chapter 3, the use of the decibel in underwater acoustics will be explained in greater detail. Confusion over the use of decibel has created significant technical and legal problems for those acoustical oceanographers and sonar technologists who must interact with their counterparts in aeroacoustics and bioacoustics. In air acoustics, a reference sound pressure of $20 \mu\text{Pa}$ is used while the current choice in underwater acoustics is $1 \mu\text{Pa}$. Part of the confusion arises from the use of decibels to represent ratios of dimensionless quantities as well as ratios of absolute quantities having physical dimensions. When reporting ratios of dimensionless quantities (such as reflection losses), decibels can be used without further qualification. However, when decibels are used to represent ratios of absolute quantities having physical dimensions (such as radiated noise levels), the reference quantities (pressure and distance) must be clearly stated. Since acoustical measurements are first made in SI units (sound pressure in pascals and radiated source power in watts) and then converted to decibels, some researchers have argued that confusion caused by the decibel could be removed by reporting acoustical measurements in SI units.

2 Acoustical oceanography

2.1 Background

Acoustical oceanography describes the role of the ocean as an acoustic medium. It relates oceanic properties to the behavior of underwater acoustic propagation, noise and reverberation. Acoustical oceanography crosses four other branches of oceanography: physical, chemical, geological and biological oceanography.

The single most important acoustical variable in the ocean is sound speed. The distribution of sound speed in the ocean influences all other acoustic phenomena. The sound speed field, in turn, is determined by the density (or temperature and salinity) distribution in the ocean. Advection of the underwater sound field by water currents is also important. Refraction of sound by fronts, eddies and other dynamic features can distort the propagation of acoustic signals. Knowledge of the state of the sea surface as well as the composition and topography of the sea floor is important for specification of boundary conditions. Bathymetric features can block the propagation of sound. Biological organisms contribute to the noise field and also scatter underwater sound signals. The balance of this chapter will address physical and chemical properties, sound speed, boundaries, dynamic features and biologics.

A number of books and published papers already exist on these subjects and appropriate citations will be made to them. Notable text and reference books of a general nature include those by Sverdrup *et al.* (1942), Neumann and Pierson (1966), Gill (1982), Apel (1987), Pickard and Emery (1990), Peixoto and Oort (1992) and Medwin and Clay (1998).

2.2 Physical and chemical properties

Temperature is basic to any physical description of the oceans. It is the easiest and therefore the most common type of oceanographic measurement made. The exchange of heat between the ocean and the atmosphere depends strongly on temperature. The density field and resulting stratification of the ocean depend largely on temperature. The speed of sound in the upper layers

of the ocean is most strongly dependent on temperature. Temperature further influences the kinds and rates of chemical reactions occurring in the ocean. The distribution of nutrients and other biologically important substances depends on temperature and the resulting density stratification.

Sea water is a binary fluid in that it consists of various salts in water. The presence of salts affects a number of oceanic parameters, including compressibility, sound speed, refractive index, thermal expansion, freezing point and temperature of maximum density. Salinity is a term used to measure the quantity of salts dissolved in sea water and is expressed in units of parts per thousand (‰ or ppt). The precise definition of salinity is complicated. Fofonoff (1985) reviewed the development of the modern salinity scale and the equation of state for sea water. The Practical Salinity Scale 1978 was introduced to rectify shortcomings associated with the traditional chlorinity–conductivity relationship used to establish salinity (Lewis, 1980; Perkin and Lewis, 1980; Culkin and Ridout, 1989). In the new scale, the existing link between chlorinity and salinity was broken in favor of a definitive salinity–conductivity relationship. The new practical standard is IAPSO (International Association for the Physical Sciences of the Ocean) Standard Seawater, produced and calibrated by the IAPSO Standard Seawater Service. Salinity is now a dimensionless quantity (psu or practical salinity unit) because the algorithms in the new scale were adjusted to eliminate the ‰ (or ppt) used in previous scales.

The density of sea water is related to temperature, salinity and pressure (which is nearly proportional to depth) through the equation of state (e.g. Fofonoff, 1985). Density provides a measure of the hydrostatic stability in the ocean. Specifically, a stable water column is one in which density increases monotonically with increasing depth. Sea water is compressible, although less so than pure water. The compressibility of sea water can be expressed by the coefficient of compressibility, which relates fractional changes in water volume to the corresponding changes in pressure (e.g. Apel, 1987).

Compressibility of sea water is an important factor in several applications: the precise determination of the density of sea water, particularly at great depths; the computation of adiabatic temperature changes in the ocean (in an adiabatic process, compression results in warming, while expansion results in cooling); and most importantly, the computation of sound speed in sea water.

The speed of sound (c) in sea water is related to the isothermal compressibility (K) as

$$c = \sqrt{\frac{\gamma}{K\rho}} \quad (2.1)$$

where γ is the ratio of specific heats of sea water at constant pressure and constant volume and ρ the density of sea water. The isothermal compressibility is easier to measure experimentally than is the adiabatic compressibility.

2.2.1 Temperature distribution

The distribution of temperature at the surface of the oceans is zonal in nature, with isotherms (lines of constant temperature) oriented in an east-west pattern. The annual mean temperature distribution shown in Figure 2.1 illustrates this general zonal gradation. This pattern is due largely to the zonal distribution of the solar energy received at the sea surface. Specific exceptions to this pattern occur in regions of upwelling (where colder water from below is brought to the surface through the action of the winds), and in the vicinity of major (baroclinic) current systems such as the Gulf Stream (where the temperature field is distorted). The relatively low equatorial and tropical sea-surface temperatures in the eastern Pacific and Atlantic oceans are generally ascribed to the effects of upwelling. The more meridional trend of the isotherms off the northeast coast of the United States, for example, is evidence of the Gulf Stream current system. Examining only annual averages, however, can sometimes be misleading. The monsoon circulation in the Indian Ocean, for example, makes interpretation of an annual mean temperature field questionable.

The temperature field in the ocean exhibits a high degree of stratification with depth. Since the isotherms are nearly parallel to the horizontal plane, this type of structure is referred to as horizontal stratification. This is evidenced in Figure 2.2, which presents zonal (annual) averages of temperature in the Atlantic Ocean by 1° latitude belts. These zonal averages do not include the Mediterranean Sea, the Baltic Sea or the Hudson Bay.

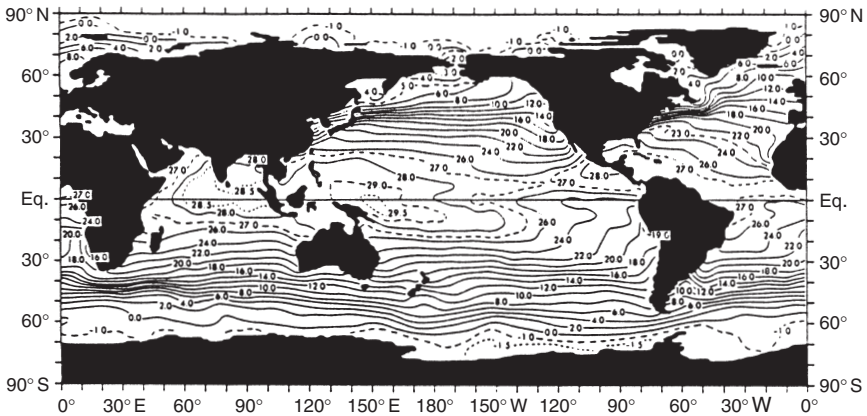


Figure 2.1 Annual mean temperature ($^\circ\text{C}$) at the sea surface. The distribution of surface temperatures shows a strong latitudinal dependence due largely to the zonal distribution of solar energy received at the sea surface (Levitus, 1982).

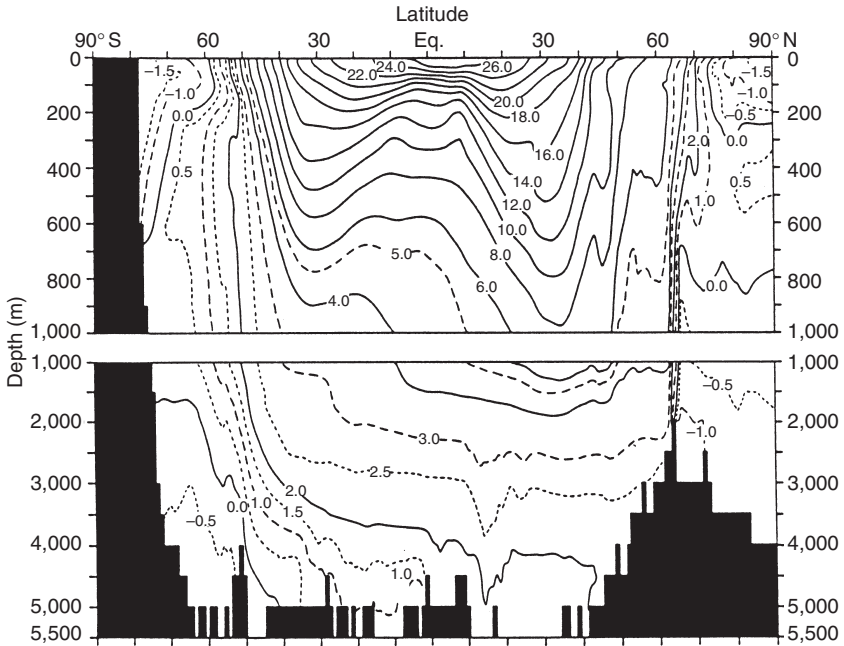


Figure 2.2 Annual mean Atlantic Ocean zonal average (by 1° squares) of temperature ($^\circ\text{C}$) as a function of depth. Note the break in the depth scale at 1000 m (Levitus, 1982).

2.2.2 Salinity distribution

The distribution of salinity at the surface of the ocean is shown in Figure 2.3, and notable features have been summarized by Levitus (1982). Specifically, subtropical salinity maxima associated with the excess of evaporation (E) over precipitation (P) appear in all the individual oceans (regions where $E - P > 0$). Subpolar regions exhibit low salinities associated with the excess of precipitation over evaporation (regions where $E - P < 0$). Low-salinity tongues associated with runoff from major river systems, such as the Amazon, are also apparent.

Unlike the temperature fields, salinity does not exhibit a consistent stratification with depth, as for example in the Atlantic Ocean (Figure 2.4). These patterns reflect the complex movements of water throughout the oceans.

2.2.3 Water masses

Using the concept of water masses facilitates descriptions of sea-water characteristics and motions. This concept is analogous to that employed by meteorologists to describe air masses in weather patterns. Air masses are

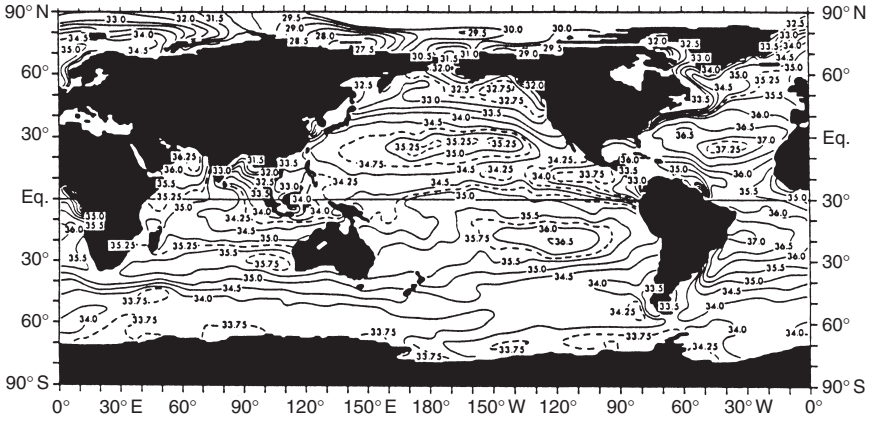


Figure 2.3 Annual mean salinity (ppt) at the sea surface (Levitus, 1982).

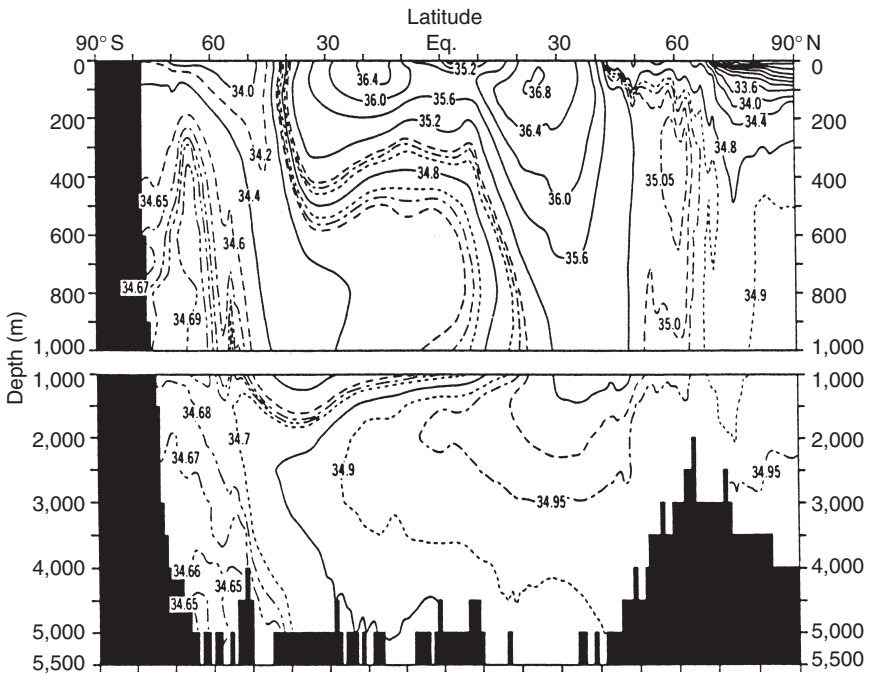


Figure 2.4 Annual mean Atlantic Ocean zonal average (by 1° squares) of salinity (ppt) as a function of depth. Note the break in the depth scale at 1,000 m (Levitus, 1982).

identified by characteristic combinations of air temperature and moisture content (humidity). These characteristics allow meteorologists to identify the history (or source regions) of the various air masses. Examples of common air masses include continental polar (cold, dry air formed over high-latitude land areas) and maritime tropical (warm, moist air formed over equatorial ocean areas).

Oceanographers (e.g. Sverdrup *et al.*, 1942) have convincingly demonstrated that certain characteristic combinations of water temperature and salinity are associated with water masses formed in particular regions of the world's oceans. After formation, these water masses spread both vertically and laterally to occupy depth ranges of the water column consistent with their density. Moreover, these water masses are distinguishable from one another when plotted on a graph of temperature-versus-salinity, referred to as a *T-S* diagram. The *T-S* relations of the principal water masses of the Atlantic Ocean are presented in Figure 2.5 (Naval Oceanographic Office, 1972). The names of these water masses suggest their relative positions in the water column (e.g. central, intermediate, deep and bottom). From Figure 2.5, for example, one can conclude that the waters of the South Atlantic Ocean are fresher (i.e. less saline) than those of the north Atlantic.

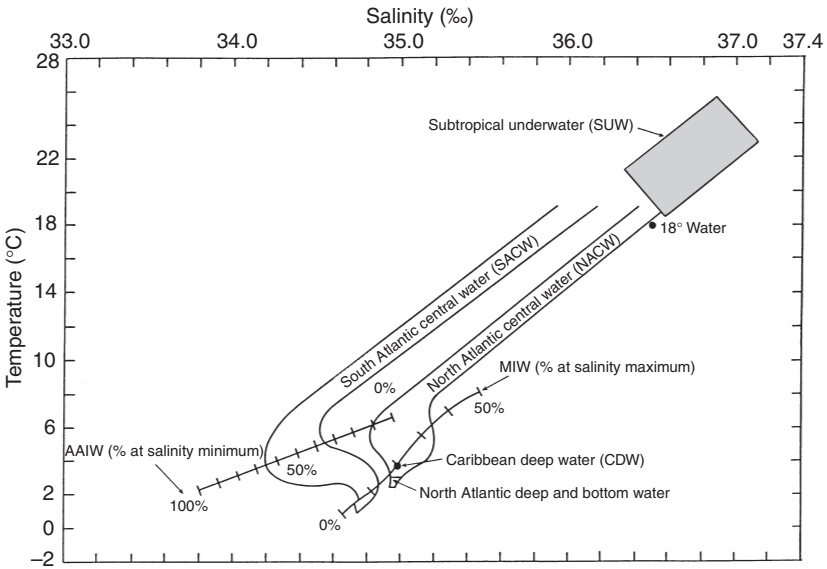


Figure 2.5 Temperature-salinity (*T-S*) diagrams of the major water masses of the Atlantic Ocean (Naval Oceanographic Office, 1972).

- Notes
 AAIW Antarctic Intermediate Water.
 MIW Mediterranean Intermediate Water.

Emery and Meincke (1986) provided an updated review and summary of the global water masses.

The movement of Antarctic intermediate water (AAIW), for example, can now be identified in the distribution of salinity illustrated previously in Figure 2.4. Specifically, the movement of AAIW is evidenced by a low-salinity tongue ($\sim 34.0\text{--}34.6$ ppt) extending downward from the surface in the latitude belt $60\text{--}70^\circ$ S, then northward at a depth of about 700–800 m and finally upward near the equator.

The distribution of sound speed in the ocean can be related to the local water-mass structure. Knowledge of the water-mass structure, then, can greatly enhance understanding of the large-scale spatial and temporal variability of the sound-speed field in the ocean.

2.3 Sound speed

The speed of sound in sea water is a fundamental oceanographic variable that determines the behavior of sound propagation in the ocean. Equation (2.1) defined the speed of sound in sea water as a function of the isothermal compressibility, the ratio of specific heats of sea water at constant pressure and constant volume, and the density of sea water.

The term “sound velocity” is sometimes used synonymously with “sound speed.” The symbol c , which is commonly used to indicate sound speed, is derived from the word “celerity.”

Since Equation (2.1) is difficult to compute in practice, considerable work has been devoted to expressing the speed of sound in sea water in terms of more commonly observed oceanographic parameters. Specifically, it is known empirically that sound speed varies as a function of water temperature, salinity and pressure (or depth). Moreover, the speed of sound in sea water increases with an increase in any of these three parameters.

2.3.1 *Calculation and measurements*

Many empirical relationships have been developed over the years for calculating sound speed using values of water temperature, salinity and pressure (or depth). Frequently used formulas include those of Wilson (1960), Leroy (1969), Frye and Pugh (1971), Del Grosso (1974), Medwin (1975), Chen and Millero (1977), Lovett (1978), Coppens (1981) and Mackenzie (1981). As summarized in Table 2.1, each formula has its own ranges of temperature, salinity and pressure (or depth). Collectively, these ranges are referred to as “domains of applicability.” Calculations outside of the specified domains may lead to errors. The individual equations are not reported in Table 2.1. However, the number of terms comprising each equation is indicated in the far-right column. The simplest equation (Medwin, 1975) contains six terms while the most complicated equation (Wilson, 1960) contains 23 terms.

Table 2.1 Summary of sound-speed algorithm parameter ranges

Reference	Temperature range (°C)	Salinity range (ppt)	Pressure or depth range ^a	Standard error (m s ⁻¹)	Number of terms
Wilson (1960)	-4-30	0-37	1-1,000 kg cm ⁻²	0.30	23 terms
Leroy (1969)	-2-34	20-42	0-8,000 m	0.2	13 terms [complete (1st formula)]
Frye and Pugh (1971)	-3-30	33.1-36.6	1.033-984.3 kg cm ⁻²	0.10	12 terms
Del Grosso (1974)	0-35	29-43	0-1,000 kg cm ⁻²	0.05	19 terms
Medwin (1975)	0-35	0-45	0-1,000 m	~0.2	6 terms [simple formula]
Chen and Millero (1977)	0-40	5-40	0-1,000 bar	0.19	15 terms [requires correction at low temperature and high pressure (Millero and Li, 1994)]
Lovett (1978)	0-30	30-37	0-10,000 dbar	0.063	13 terms [3rd equation]
Coppens (1981)	-2-35	0-42	0-4,000 m	0.1	8 terms [Lovett's 3rd equation simplified]
Mackenzie (1981)	-2-30	25-40	0-8,000 m	0.07	9 terms

Note

^a For each 10 m increase in water depth, pressure increases by approximately 10 dbar, 1 bar or 1 kg cm⁻². Refer to Mackenzie (1981) or Leroy and Parthiot (1998) for algorithms useful in converting pressure to depth.

For convenience, the nine-term algorithm developed by Mackenzie (1981) is presented here:

$$\begin{aligned}
 c = & 1448.96 + 4.591T - 5.304 \times 10^{-2}T^2 + 2.374 \times 10^{-4}T^3 \\
 & + 1.340(S - 35) + 1.630 \times 10^{-2}D + 1.675 \times 10^{-7}D^2 \\
 & - 1.025 \times 10^{-2}T(S - 35) - 7.139 \times 10^{-13}TD^3
 \end{aligned} \quad (2.2)$$

where c is the speed of sound in sea water (m s^{-1}), T the water temperature ($^{\circ}\text{C}$), S the salinity (‰ or psu) and D the depth (m). Mackenzie (1981) also discussed the mathematical relationship between pressure and depth in the ocean. In related work, Leroy and Parthiot (1998) developed convenient equations for converting pressure to depth and *vice versa*.

Recent tomographic measurements of sound speed in the oceans (Chapter 5, Section 5.6.9) have implications for very-long-range ducted propagation (Spiesberger and Metzger, 1991b). Specifically, previous algorithms derived from laboratory measurements have been found to overpredict sound speeds due to pressure effects at great depths (Dushaw *et al.*, 1993). This matter is still the subject of investigation. Millero and Li (1994) corrected the earlier Chen and Millero (1977) sound-speed formula to improve its applicability to low temperatures and high pressures. This correction is especially important for tomographic applications.

Two practical devices that are commonly used to measure sound speed as a function of depth in the ocean are the bathythermograph (BT) and the velocimeter. Expendable versions of the bathythermograph, designated XBT, actually measure temperature (using a thermistor) as a function of depth (through a known fall rate). Sound speed can then be calculated using one of the algorithms identified in Table 2.1, often on the assumption that salinity is constant, or nearly so. This assumption is justified by the observation that the typical range of salinities in the open ocean is usually small and that the corresponding impact on sound speed is negligible from a practical standpoint. In coastal areas, and near rivers or ice, this assumption is not generally valid and a velocimeter, which measures sound speed directly in terms of the travel time of sound over a fixed (constant-length) path, would be preferable. An expendable version of this instrument is also available (often designated XSV).

The velocimeter would seem to be the preferred instrument for obtaining measurements of sound speed in support of naval operations. From a broader scientific perspective, however, information on the temperature distribution in the ocean directly supports many other naval applications, including ocean dynamics modeling, air-sea interaction studies and various marine biological investigations, to name a few. The demonstrated accuracy of the various algorithms (when used within the specified domains of applicability) is sufficient for most operational applications. In terms of expendable sensors, measurements of temperature represent a better scientific investment than

do measurements of sound speed. Nevertheless, naval operations in coastal area or in ice-covered regions may be better supported by the velocimeter. Increasing emphasis on naval operations in the littoral zone has placed greater importance on measuring, in real time, coastal processes that are characterized by extreme temporal and spatial variability. Precise scientific measurements are normally accomplished using expensive, but recoverable, instrumentation. Such instruments are typically deployed from surface ships that maintain station while the instrument package is lowered and then raised in what is termed a hydrographic cast. The instrument package can contain an assortment of sensors for measuring water temperature, salinity (or conductivity), pressure, sound speed, currents and dissolved oxygen, among others.

2.3.2 *Sound-speed distribution*

Typical North Atlantic winter and summer profiles of sound speed versus depth are shown in Figure 2.6. These profiles represent a region of the North Atlantic Ocean located near 23° N and 70° W (Naval Oceanographic Office, 1972). Temperature–salinity (T – S) diagrams for winter and summer seasons, based on actual measurements, are also presented to show their relationships with the sound-speed profiles. Since the T – S diagrams indicate the ocean depths corresponding to the measured T – S pairs, the individual temperature and salinity profiles for both winter and summer can be reconstructed. Principal water masses are also noted on the sound speed profiles. The so-called 18° water (refer back to Figure 2.5) marks a change in the sound-speed gradient at a depth of about 300 m, and Mediterranean intermediate water (MIW) occupies the region of the water column near the sound-speed minimum (at about 1,200 m).

The sound-speed profiles in Figure 2.6 are representative of those encountered in many tropical and sub-tropical deep-ocean areas. Such profiles may be divided into arbitrary layers, each having different characteristics and occurrence (Figure 2.7). Just below the sea surface is the sonic layer where the speed of sound is influenced by local changes in heating, cooling and wind action. The base of the sonic layer is defined as the sonic layer depth (SLD), which is associated with the near-surface maximum in sound speed. This surface layer is usually associated with a well-mixed layer of near-isothermal water. Oceanographers refer to this well-mixed region as the mixed layer. The base of this layer is then termed the mixed layer depth (MLD).

Below the mixed layer lies the thermocline, a region of the water column where the temperature decreases rapidly with increasing depth. This region is characterized by a negative sound-speed gradient (i.e. sound speed decreases with increasing depth).

Below the thermocline, and extending to the sea floor, is the deep isothermal layer. This layer has a nearly constant temperature in which the speed of sound increases with depth due to the effects of pressure (pressure

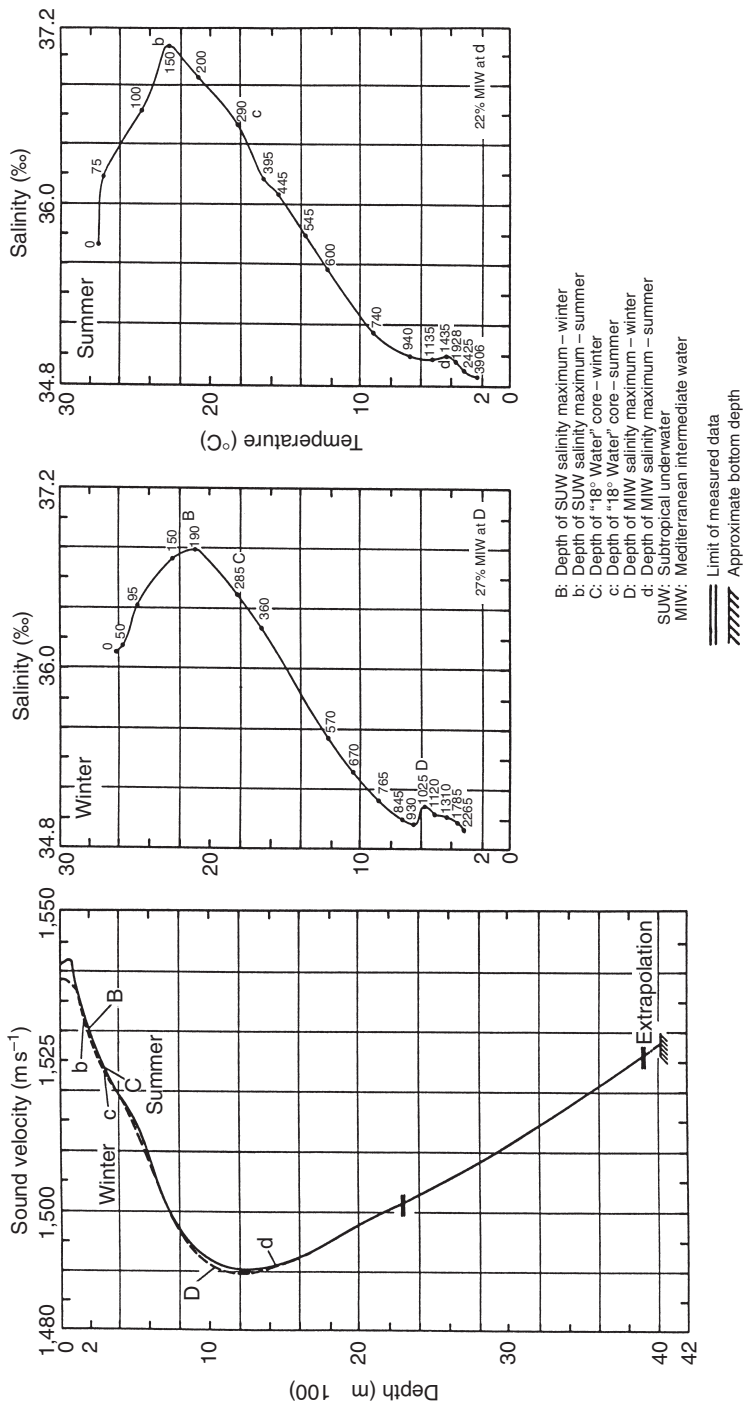


Figure 2.6 Sound speed profiles (winter and summer) and T-S comparisons for the North Atlantic Ocean near 23° N, 70° W (Naval Oceanographic Office, 1972).

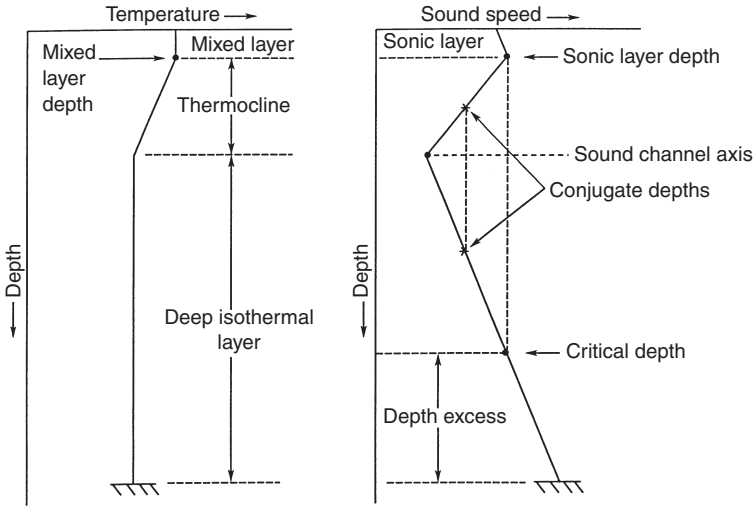


Figure 2.7 Schematic relationship between temperature and sound-speed profiles in the deep ocean.

increases with increasing depth). In this region of the water column, the sound-speed profile becomes nearly linear with a positive gradient of about $0.017 \text{ (m s}^{-1}\text{) m}^{-1}$ or 0.017 s^{-1} . Between the negative sound speed gradient of the thermocline and the positive sound speed gradient of the deep isothermal layer is a sound-speed minimum. The depth corresponding to this sound-speed minimum is referred to as the sound channel axis. At high latitudes, the deep isothermal layer extends nearly to the sea surface. That is, the sound channel axis shoals as one approaches the polar regions. This behavior is vividly demonstrated in Figure 2.8. The top panel presents contours of the depth of the minimum sound speed (m) and the bottom panel presents the sound speed (m s^{-1}) on this axial surface (Munk and Forbes, 1989). At low latitudes, the depth of the sound channel axis is typically near 1,000 m. At high latitudes, the axis is located near the sea surface. The associated sound speeds on this axial surface generally decrease away from the equatorial regions.

In profiles containing a sound channel axis, a critical depth can be defined as that depth below the axis at which the sound speed equals the near-surface maximum value. (The near-surface maximum value of sound speed is usually located at the SLD.) The vertical distance between the critical depth and the sea floor is referred to as the depth excess. Other pairs of points can be identified on the sound-speed profile that have the same value of sound speed but which lie on opposite sides of the sound channel axis. Such pairs are referred to as conjugate depths. In Figure 2.7, the critical depth is actually a conjugate of the SLD.

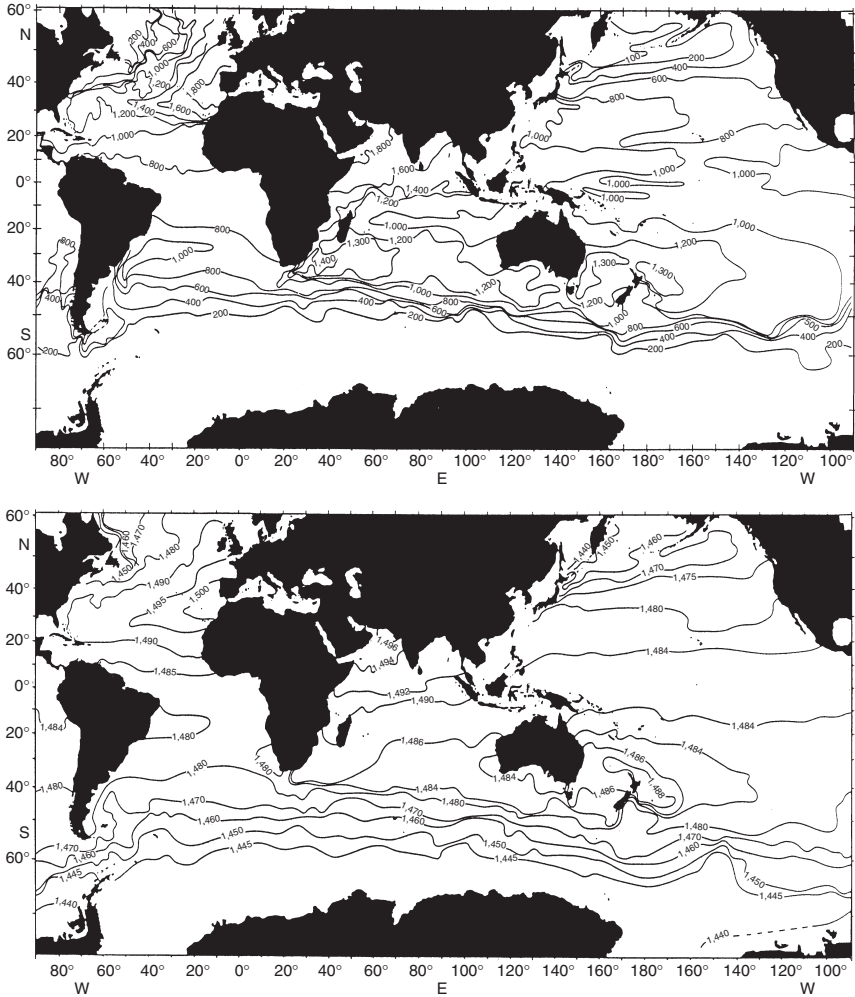


Figure 2.8 Global maps of the sound channel axis. Upper panel: channel depth (m). Bottom panel: channel speed (m s^{-1}). (Munk and Forbes, 1989; *J. Phys. Oceanogr.*, 19, 1765–78; copyright by the American Meteorological Society.)

It is convenient at this juncture to discuss additional points of morphology relating to the sound-speed profile illustrated in Figure 2.7. These points will be useful in later discussions concerning full channels, half-channels and ducts. A full channel is formed around the sound channel axis and, for purposes of discussion, is limited above the axis by the SLD and below the axis by the sea floor. Either the upper portion or the lower

portion of the full channel represents a half-channel. The upper half-channel is characterized by a negative sound-speed gradient (as is found in some shallow-water regions) while the lower half channel is characterized by a positive sound-speed gradient (as is found in the Arctic or in some shallow-water regions). In Figure 2.7, the sea surface and the SLD define, respectively, the upper and lower boundaries of a duct. The properties of acoustic propagation in a full channel, half-channel and duct will be discussed in Chapter 3.

Additional sound-speed profiles typical of the winter season in different ocean areas of the world are presented in Figure 2.9. These additional profiles demonstrate that the simple model described above (specifically in Figure 2.7), which is representative of many tropical and sub-tropical deep-ocean areas, is not applicable to high-latitude ocean areas or to some smaller water bodies.

The depth dependence of sound speed in the ocean poses a particular problem for echo sounders, which use near-vertical acoustic paths to measure the depth of the sea floor based on the two-way travel time of the signal. Echo sounders are set to read the depth directly by assuming a constant speed of sound in the water column, usually $1,463$ or $1,500 \text{ m s}^{-1}$. When the actual depth-integrated (or mean) sound speed departs from the assumed value, a correction must be applied to the observed readings. Bialek (1966: 63), for example, tabulated such corrections according to ocean area. Depending on the particular ocean area and water depth, these corrections can be on the order of several percent of the true water depth. It is important to check navigational charts to see if any such correction has been applied to the soundings. If no corrections have been made, then care should be exercised in ascertaining the true bottom depth before undertaking any deep-water operations in proximity to the sea floor.

Underwater acoustic propagation problems involving long ranges may not be able to ignore horizontal variations in either the sound speed or bathymetry. Modeling developments, therefore, generally distinguish between range-independent (1D, where the ocean varies only as a function of depth) and range-dependent (2D, where the ocean varies as a function of both depth and range) problems. Parameters other than sound speed and water depth may also be considered in range-dependent problems such as surface losses, bottom losses and absorption. If, in addition to the 2D problem, there are azimuthal variations, then the problem is considered to be 3D.

An east-west cross-section of the North Atlantic Ocean between 23 and 24° N is presented in Figure 2.10 to illustrate the variability of both sound speed and bathymetry over moderate range scales. Also noteworthy are changes in the depth of the sound channel axis and the absence of a critical (or limiting) depth in some basins. The sound-speed profiles presented previously in Figure 2.6 are consistent with the data of Figure 2.10 at a longitude of about 70° W .

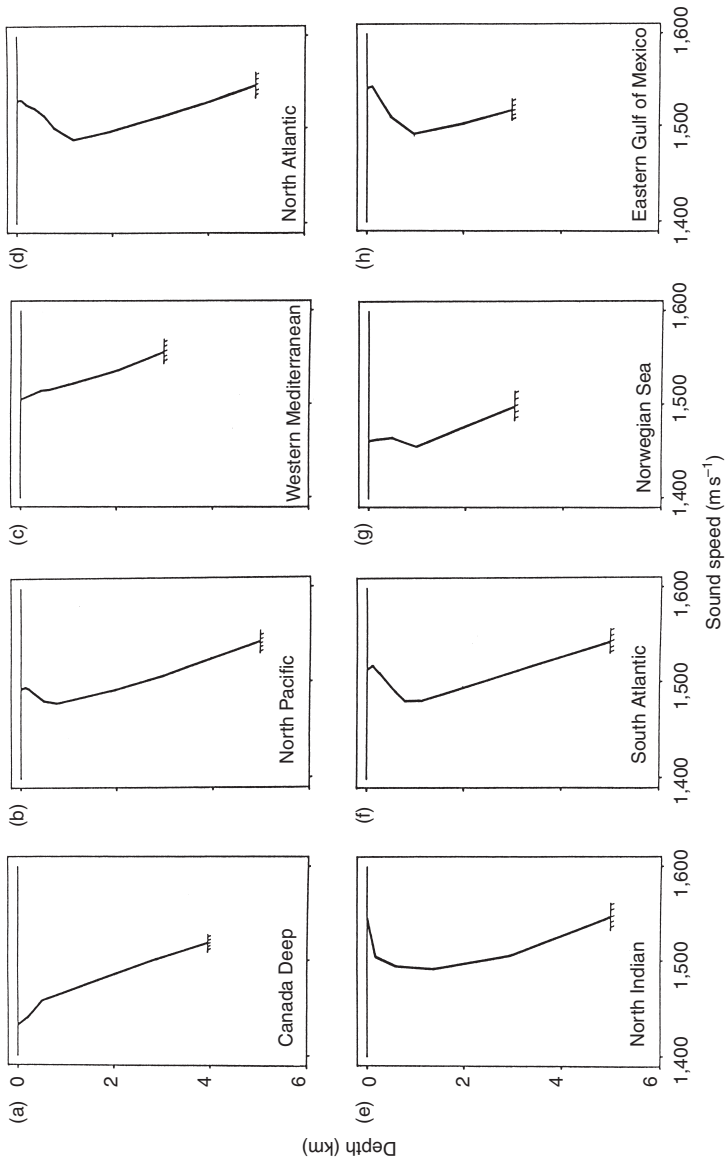


Figure 2.9 Characteristic winter sound-speed profiles for selected deep-ocean areas of the world.

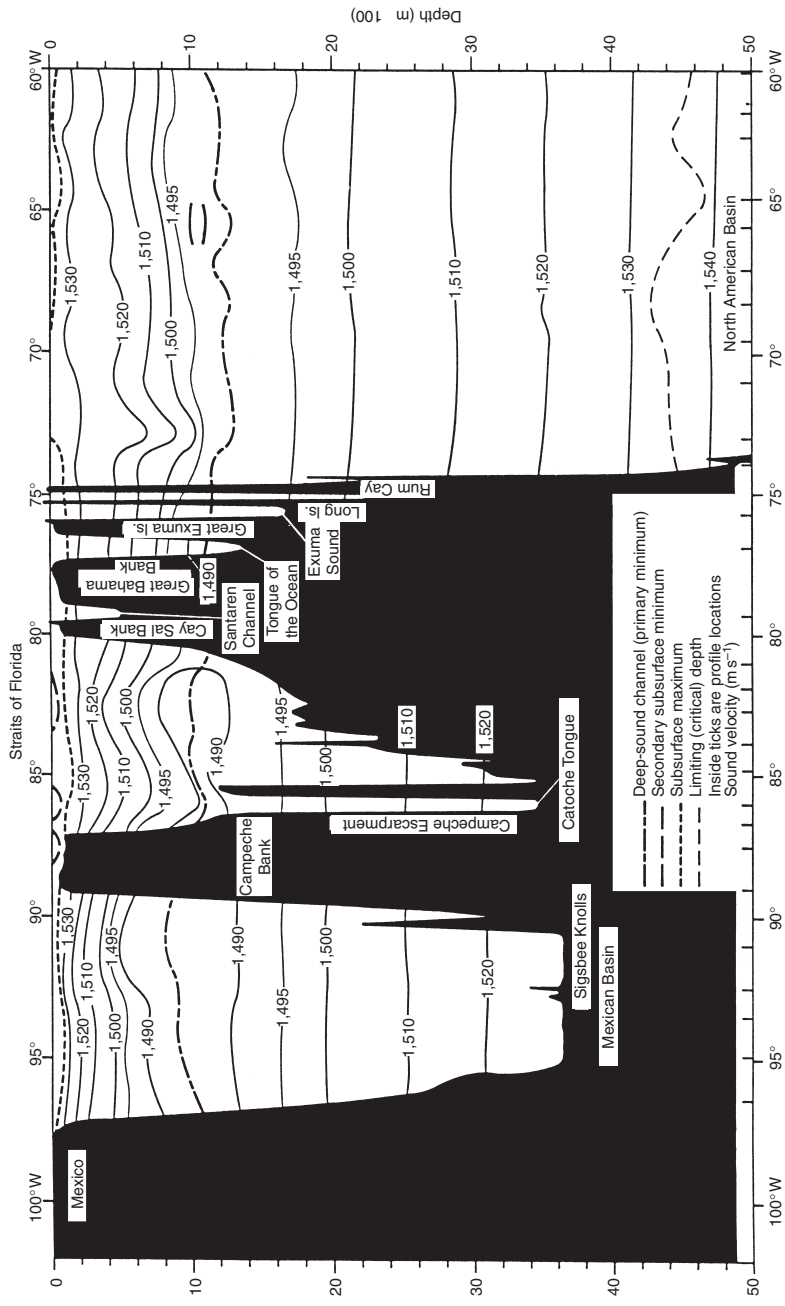


Figure 2.10 East-west sound-speed cross-section between 23° and 24° N and between 60° and 100° W for the period February–April (Naval Oceanographic Office, 1972).

2.4 Boundaries

The boundaries of the water column – the sea surface and the sea floor – can exert a profound influence on the propagation of acoustic energy through the actions of reflection, scattering and absorption.

2.4.1 Sea surface

The surface of the sea is both a reflector and a scatterer of sound. If the sea surface were perfectly smooth, it would form an almost perfect reflector of sound due to the acoustic impedance mismatch at the air–water interface. As the sea surface becomes rough, as it does under the influence of wind (refer to Table 2.2), reflection losses are no longer near zero.

Sea-surface roughness is typically specified in terms of wave height. At sea, however, weather observers generally record wind speed and not wave height as a description of sea state (Bowditch, 1977). A number of statistical relationships exist with which to quantitatively associate these two parameters (e.g. Earle and Bishop, 1984). These relationships are very precise as to the height above sea level at which the wind speed is measured and the type of statistical wave height that is considered. Also factored in are the duration of the wind and the fetch (i.e. the distance along open water over which the wind acts from the same direction). Based on the Pierson–Moskowitz spectrum (Moskowitz, 1964; Pierson and Moskowitz, 1964; Pierson, 1964, 1991), a fully developed significant wave height can be calculated from the observed wind speed as:

$$H_{1/3} = 0.566 \times 10^{-2} V^2 \quad (2.3)$$

where V is the wind speed (knots), measured at a height of 19.5 m, and $H_{1/3}$ the average height (m) of the one-third highest waves.

Two other commonly used wave-height descriptors are the rms wave height (H_{rms}) and the one-tenth significant wave height ($H_{1/10}$). These are related to the one-third significant wave height as (Earle and Bishop, 1984):

$$H_{\text{rms}} = 0.704 H_{1/3} \quad (2.4)$$

and

$$H_{1/10} = 1.80 H_{\text{rms}} \quad (2.5)$$

The average wave height (H_{avg}) can be related to the significant wave height ($H_{1/3}$) as

$$H_{\text{avg}} = \frac{\sqrt{\pi}}{2} H_{\text{rms}} = 0.886 H_{1/3} \quad (2.6)$$

These relationships can be compared with those presented in Table 2.2, which closely follow the values of H_{avg} .

Table 2.2 Beaufort wind scale with corresponding sea state codes (Bowditch, 1977)

Beaufort number of force	Wind speed			World Meteorological Organization (1964)	Estimating wind speed		Sea state			
	Knots	Miles per hour	Meters per second		Kilometers per hour	Effects observed from land		Effects observed near coast	Term and height of waves (m)	
0	Under 1	Under 1	0.0-0.2	Under 1	Calm	Sea like mirror	Calm	Calm; smoke rises vertically	Calm, glassy (0)	0
1	1-3	1-3	0.3-1.5	1-5	Light air	Ripples with appearance of scales; no foam crests	Fishing smack just has steerage way	Smoke drift indicates wind direction; vanes do not move	Calm, rippled (0-0.1)	1
2	4-6	4-7	1.6-3.3	6-11	Light breeze	Small wavelets; crests of glassy appearance, not breaking	Wind fills the sails of smacks, which then travel at about 1-2 mph	Wind felt on face; leaves rustle; vanes begin to move	Smooth, wavelets (0.1-0.5)	2
3	7-10	8-12	3.4-5.4	12-19	Gentle breeze	Large wavelets; crests begin to break; scattered whitecaps	Smacks begin to careen and travel about 3-4 mph	Leaves, small twigs in constant motion; light flags extended	Slight (0.5-1.25)	3
4	11-16	13-18	5.5-7.9	20-28	Moderate breeze	Small waves, becoming longer; numerous whitecaps	Good working breeze, smacks carry all canvas with good list	Dust, leaves and loose paper raised up; small branches move	Moderate (1.25-2.5)	4
5	17-21	19-24	8.0-10.7	29-38	Fresh breeze	Moderate waves, taking longer form; many whitecaps; some spray	Smacks shorten sail	Small trees in leaf begin to sway		
6	22-27	25-31	10.8-13.8	39-49	Strong breeze	Larger waves forming; whitecaps everywhere; more spray	Smacks have doubled reef in mainsail; care required when fishing	Larger branches of trees in motion; whistling heard in wires	Rough (2.5-4)	5

7	28-33	32-38	13.9-17.1	50-61	Near gale	Sea heaps up; white foam from breaking waves begins to be blown in streaks	Smacks remain in harbor and those at sea lie-to	Whole trees in motion; resistance felt in walking against wind	Very rough (4-6)	6
8	34-40	39-46	17.2-20.7	62-74	Gale	Moderately high waves of greater length; edges of crests begin to break into spindrift; foam is blown in well-marked streaks	All smacks make for harbor, if near	Twigs and small branches broken off trees; progress generally impeded		
9	41-47	47-54	20.8-24.4	75-88	Strong gale	High waves; sea begins to roll; dense streaks of foam; spray may reduce visibility		Slight structural damage occurs; slate blown from roofs		
10	48-55	55-63	24.5-28.4	89-102	Storm	Very high waves with overhanging crests; sea takes white appearance as foam is blown in very dense streaks; rolling is heavy and visibility is reduced		Seldom experienced on land; trees broken or uprooted; considerable structural damage occurs	High (6-9)	7
11	56-63	64-72	28.5-32.6	103-117	Violent storm	Exceptionally high waves; sea covered with white foam patches; visibility still more reduced		Very rarely experienced on land; usually accompanied by widespread damage	Very high (9-14)	8
12	64 and over	73 and over	32.7 and over	118 and over	Hurricane	Air filled with foam; sea completely white with driving spray; visibility greatly reduced			Phenomenal (over 14)	9

This aspect is important since many underwater acoustic propagation models require an input of wind speed or wave height (and sometimes both) for specification of sea-surface roughness. This input is used to initialize an internal sub-model that generates surface losses. If the wrong statistical relationship is used for the wave heights, then errors can be introduced into the computed solution due to an improper characterization of surface roughness. It is therefore important to understand what type of statistical wave height is expected as an input by the propagation model being used.

Wind-wave generation in coastal regions may be limited by the geometry of the water body, which is often irregular. Therefore, it may be necessary to consider the effects of fetch shape (both distance and width) in order to estimate wave spectra in coastal environments, especially when sea conditions are not fully developed. The Pierson–Moskowitz spectrum, which was discussed earlier for open-ocean applications, assumed that sea conditions were fully developed.

Air bubbles are produced by the breaking of waves and are carried beneath the surface by turbulence. They are also generated in the wakes of ships where they can persist for long periods of time. Free air bubbles in the sea are quite small since the larger bubbles tend to rise quickly to the surface. Bubbles only form a very small volumetric percentage of the sea. However, because air has a markedly different density and compressibility from that of sea water and because of the resonant characteristics of bubbles (e.g. Leighton, 1994), the suspended air content of sea water has a profound effect upon underwater sound. Urick (1983: 249–54) summarized these effects, which include resonance and changes in the effective sound speed. Norton *et al.* (1998) developed a numerical procedure to parameterize bubble clouds in terms of an effective complex index of refraction for use in high-fidelity models of forward propagation.

Aside from reflection losses, there are other acoustic effects associated with interactions with the sea surface. A moving sea surface produces frequency-smearing and shifting effects on constant-frequency signals. Large and rapid fluctuations in amplitude or intensity are also produced by reflection at the sea surface. Furthermore, Lloyd mirror (or image-interference) effects produce a pattern of constructive and destructive interference between direct and surface-reflected signals. This effect is diminished when the sea surface is roughened by wind.

2.4.2 *Ice cover*

When the sea surface is covered by an ice canopy, as in the polar regions (see Figures 2.11 and 2.12), acoustic interaction with the surface is further complicated by an irregular under-ice surface. The Arctic environment can be segregated into three distinct regions according to the type of ice cover: (1) pack ice; (2) MIZ; and (3) open ocean. Field measurements have shown that forward scatter from a rough anisotropic ice canopy is a function

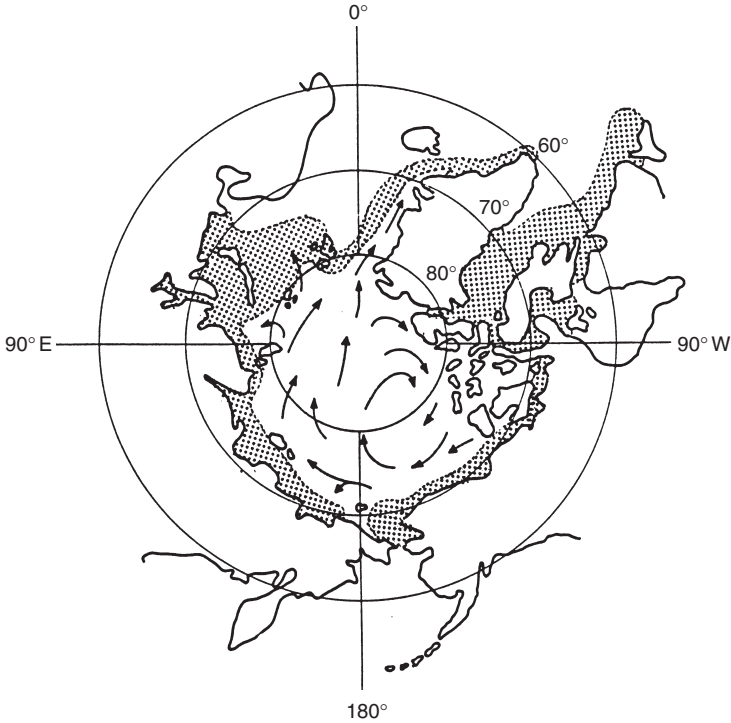


Figure 2.11 Average boundaries of sea ice (coverage at least five- to eight-tenths) in autumn and spring in the Arctic. Arrows indicate the general drift pattern. The width of the stippled area indicates the range of ice limits between autumn and spring (Untersteiner, 1966).

of acoustic frequency, geometry and the statistical (spatial correlation) properties of the under-ice surface.

2.4.3 Sea floor

The sea floor is a reflecting and scattering boundary having a number of characteristics similar in nature to those of the sea surface. Its effects, however, are more complicated than those of the sea surface because of its diverse and multilayered composition. Specifically, the sea floor is often layered, with a density and sound speed that may change gradually or abruptly with depth or even over short ranges. Furthermore, the sea floor is more variable in its acoustic properties since its composition may vary from hard rock to soft mud. One feature that is distinct from the sea surface is that the bottom characteristics can be considered to be constant over time, whereas the configuration of the sea surface is statistically in a state of change as the wind velocity changes.

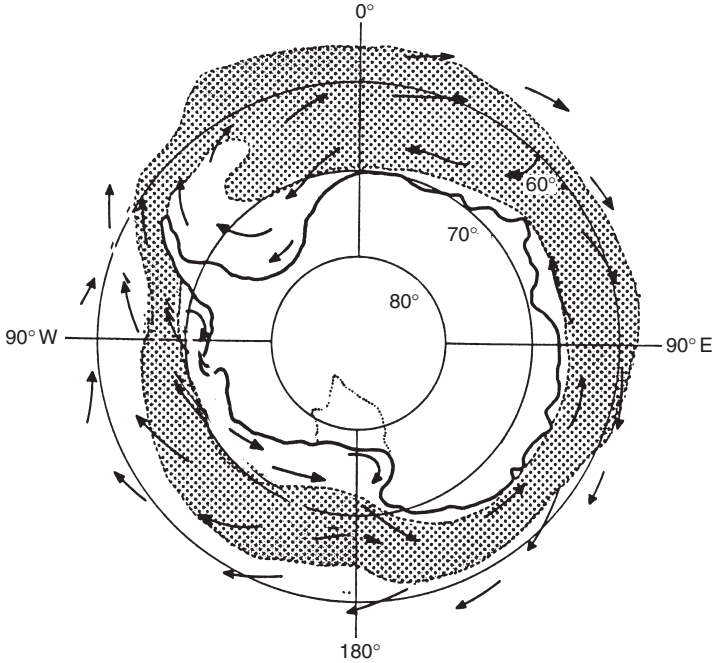


Figure 2.12 Average boundaries of sea ice (coverage at least five- to eight-tenths) in autumn and spring in the Antarctic. Arrows indicate the general drift pattern. The width of the stippled area indicates the range of ice limits between autumn and spring (Untersteiner, 1966).

Because of the variable stratification of the bottom sediments in many areas, sound is often transmitted into the bottom where it is refracted or internally reflected. Thus, the bottom often becomes a complicated propagating medium that is characterized by both shear and compressional sound speeds.

The topography of the sea floor exhibits a diversity of features not unlike those of the continental landmasses. Figure 2.13 presents an artist's conception of common ocean basin features. The undersea features noted in Figure 2.13 are defined in the Glossary (Appendix B).

Underwater ridges and seamounts can effectively block the propagation of sound, an occurrence that is referred to as bathymetric blockage. Moreover, when actively ensonified, seamounts can mask targets of interest by either providing false targets or by shadowing targets of interest.

Marine seismic studies have greatly improved our understanding of the crustal structure of that part of Earth covered by the oceans (Bryan, 1967). A typical bottom-structure section is presented in Figure 2.14. This typical section consists of 5–6 km of water, about 0.5 km of unconsolidated



Figure 2.13 Common sea-floor features (Bowditch, 1977).

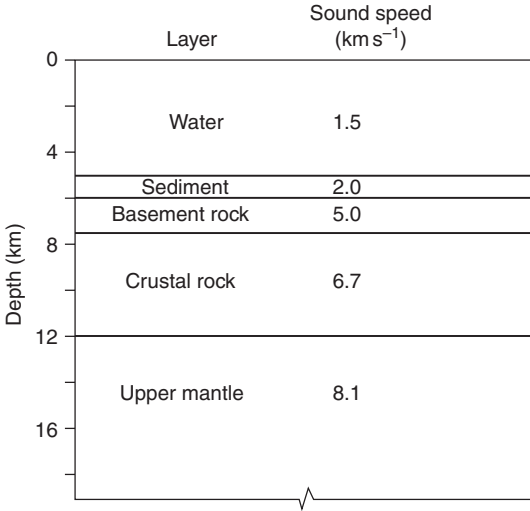


Figure 2.14 Typical oceanic section with associated depths and sound speeds in the water column and subbottom layers (Bryan, 1967).

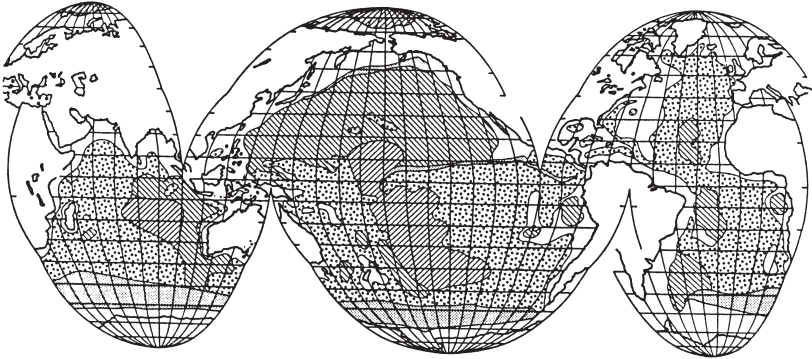


Figure 2.15 Idealized distribution of marine sediments. Hatched areas indicate inorganic pelagic and terrigenous sediments. Stippled areas denote organic pelagic sediments comprising calcareous and silicious oozes. (Adapted from Arrhenius, 1963; *The Sea*, Vol. 3, pp. 655–727; reprinted by permission of John Wiley & Sons, Inc., all rights reserved.)

sediments, 1–2 km of basement rock and 4–6 km of crustal rock overlying the upper mantle.

Major portions of the sea floor are covered with unconsolidated sediments with an average thickness of approximately 500 m. Sediments can be classified according to their origin as either terrigenous or pelagic, although no single classification scheme has universal approval. The general distribution of sediments according to Arrhenius (1963) is presented in Figure 2.15.

Terrigenous sediments are derived from land and are particularly prominent near the mouths of large rivers. These sediments are generally classified as silt, sand and mud. Pelagic sediments are derived from either organic or inorganic sources. Organic pelagic sediments comprise the remains of dead organisms and are further classified as either calcareous or siliceous oozes. Inorganic pelagic sediments are derived from materials suspended in the atmosphere and are generally classified as clay.

2.5 Dynamic features

It is convenient to categorize dynamic features of the ocean according to characteristic time and space scales. While no precise terminology is universally accepted, it is common to recognize space scales as large (>100 km), meso (100 m–100 km) and fine (<100 m). Time scales are less precise, but generally distinguish among seasonal, monthly, inertial, tidal and other feature-specific time scales appropriate to currents, eddies, waves (both surface and internal) and turbulence, among others.

2.5.1 *Large-scale features*

The large-scale circulation of the ocean can be classified either as wind-driven or thermohaline. The former is due to wind stress acting on the sea surface, while the latter is due, in part, to density changes arising from variations in temperature and salinity (e.g. Pickard, 1963).

The wind-driven component of circulation is usually horizontal in nature and is restricted primarily to the upper few hundred meters of the ocean. In the case of upwelling or downwelling near coasts, the original horizontal flow is forced to become vertical due to the basin geometry. In the open ocean, bands of upwelling and downwelling can be created by divergence and convergence, respectively, of wind-generated surface currents. Such currents are commonly referred to as Ekman drift currents.

The thermohaline component normally originates as a vertical flow arising from imbalances in the heat or freshwater (salt) fluxes near the sea surface. These vertical flows eventually become horizontal at a depth that is consistent with the density of the newly formed water.

The circulation of the surface waters corresponds closely to the prevailing wind patterns. The water currents set in motion by the winds would encircle the globe in the absence of land masses. The land masses, however, obstruct the flow and force the water along the coasts, thus forming completed loops (or gyres) in the Pacific (Figure 2.16) and Atlantic oceans (Figure 2.17). The effect of changing wind patterns due to monsoons is evident in the Indian Ocean (Figure 2.18). Only in the Antarctic Ocean does the absence of land masses permit true circumpolar flow at a latitude of about 60° S (Figures 2.16–2.18).

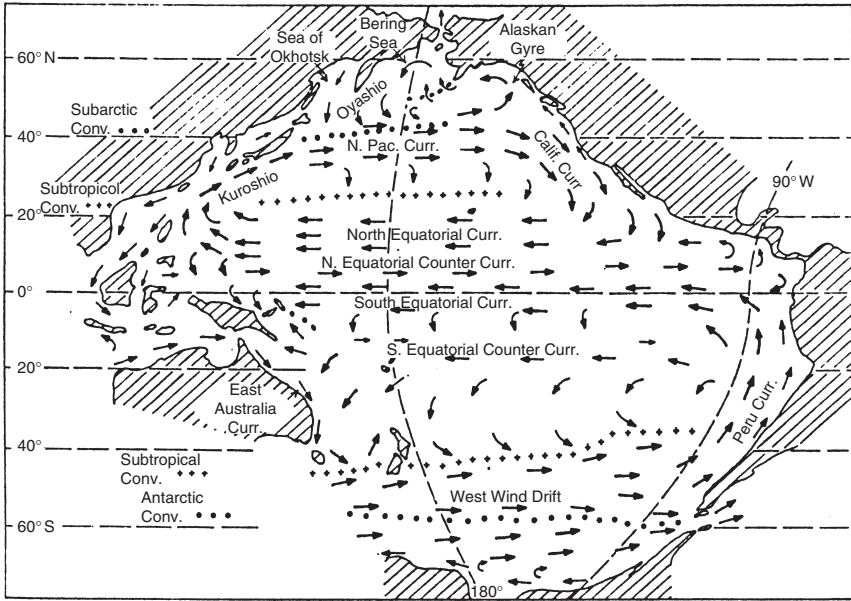


Figure 2.16 Surface circulation of the Pacific Ocean. (Reprinted with permission from Pickard, 1963; *Descriptive Physical Oceanography*, copyright by Pergamon Press Plc.)

2.5.2 *Mesoscale features*

Mesoscale oceanic features of importance to underwater acoustics include fronts, eddies (or rings) and internal waves.

2.5.2.1 *Fronts and eddies*

Ocean frontal features are frequently associated with major ocean currents or with vertical circulation patterns in areas of upwelling or downwelling. An example of ocean fronts associated with major ocean currents is shown in Figure 2.19 (Naval Oceanographic Office, 1967). This figure represents a range-depth section crossing the North Atlantic Ocean between Newfoundland (left) and Senegal (right). The hydrographic station numbers used in creating this section are shown at the top. Between stations 6 and 23, the isotherms are relatively horizontal. Two adjacent frontal features are evidenced by the vertically oriented isotherms between stations 3 and 6. These features correspond to the cold, southward-flowing Labrador Current (centered at station 4) and the warm, northward-flowing Gulf Stream (centered at station 5). The effects of the Gulf Stream frontal system are evident at depths exceeding 1,000 m.

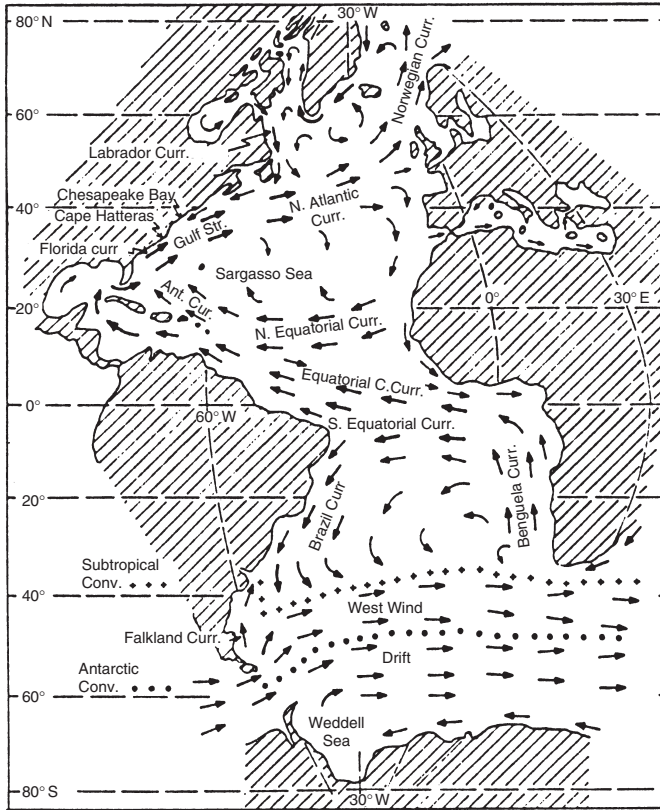


Figure 2.17 Surface circulation of the Atlantic Ocean. (Reprinted with permission from Pickard, 1963; *Descriptive Physical Oceanography*, copyright by Pergamon Press Plc.)

Different water masses are commonly separated by a transition zone referred to as an ocean front. The degree of abruptness in the change of water-mass characteristics (particularly temperature and salinity, and thus sound speed) determines whether the front is classified as a strong or a weak front. Ocean fronts are similar in concept to the more familiar fronts encountered in meteorology that separate different air masses.

Cheney and Winfrey (1976) summarized the classification and distribution of ocean fronts. For underwater acoustic applications, they recommended the following definition of an ocean front: a front is any discontinuity in the ocean that significantly alters the pattern of sound propagation and transmission loss. Thus, a rapid change in the depth of the sound channel, a difference in SLD or a temperature inversion would denote the presence of a front.

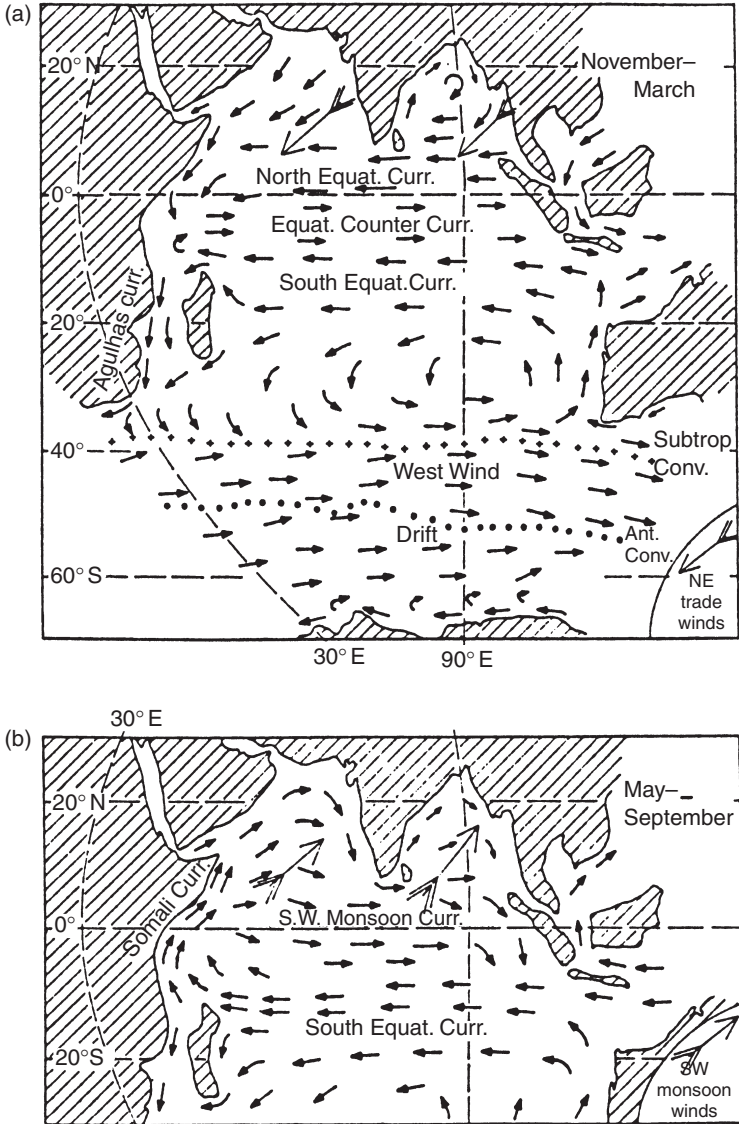


Figure 2.18 Surface circulation of the Indian Ocean showing effects of the monsoon seasons: (a) NE trade winds and (b) SW monsoon winds. (Reprinted with permission from Pickard, 1963; *Descriptive Physical Oceanography*, copyright by Pergamon Press Plc.)

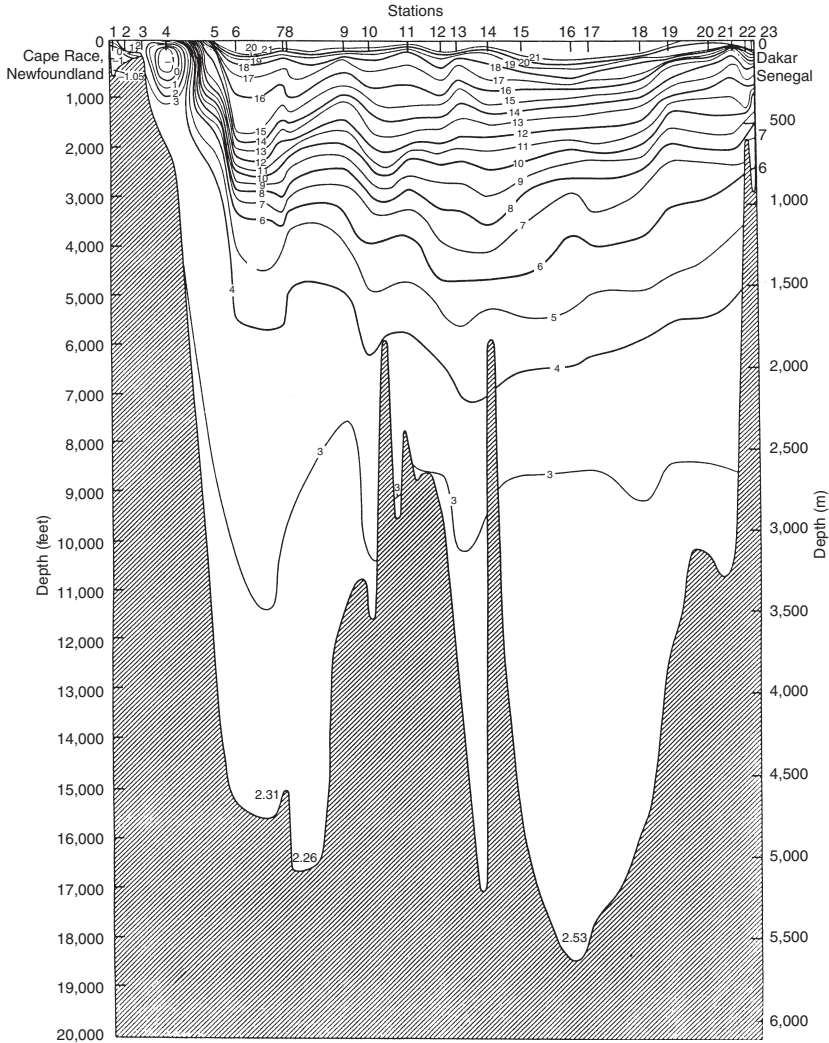


Figure 2.19 Vertical section of water temperature ($^{\circ}\text{C}$) for the transect between Cape Race, Newfoundland (left), and Dakar, Senegal (right) (Naval Oceanographic Office, 1967).

In terms of acoustics, Cheney and Winfrey (1976) identified the following significant effects:

- 1 Surface sound speed can change by as much as 30 m s^{-1} . Although this is due to the combined effect of changing temperature and salinity, temperature is usually the dominant factor.

- 2 Differences in SLD on the order of 300 m can exist on opposite sides of a front during certain seasons.
- 3 A change in in-layer and below-layer gradient usually accompanies a change in surface sound speed and SLD.
- 4 Depth of the sound channel axis can change by 750 m when crossing from one water mass to the next.
- 5 Increased biological activity generally found along a front will increase ambient noise and reverberation levels.
- 6 Enhanced air-sea interaction along a frontal zone can cause a dramatic change in sea state and thus increase ambient noise levels and surface roughness.
- 7 Refraction of sound rays as they pass through a front at an oblique angle can cause bearing errors in sonar systems.

A summary of the positions of prominent fronts is presented in Figure 2.20 (accompanied by Table 2.3). Each front is characterized as strong, moderate or weak depending upon representative values for: (1) the maximum change in sound speed across a front; (2) change of SLD; (3) depth to which the front extends; and (4) persistence. Detached eddies, such as are found in the Atlantic Ocean near the Gulf Stream and in the Pacific Ocean near the Kuroshio Current, represent another class of ocean fronts since they are

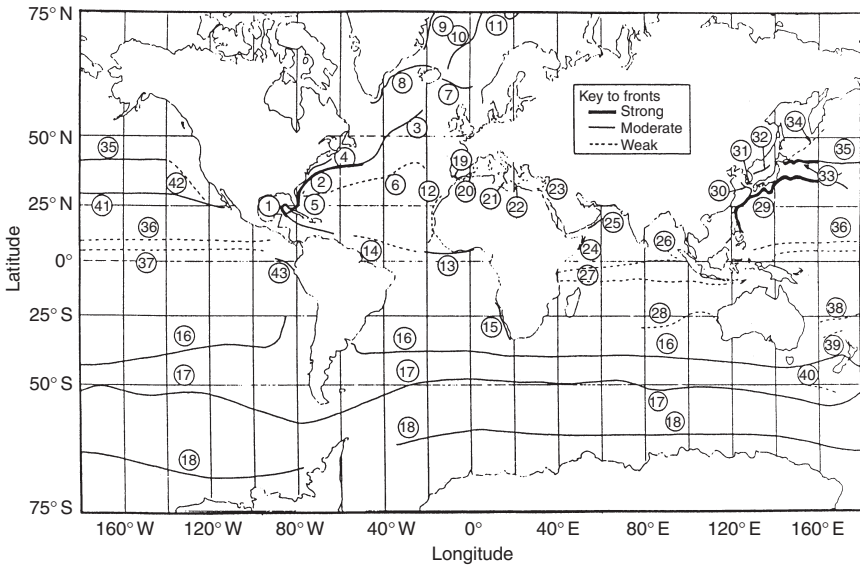


Figure 2.20 Global distribution of ocean fronts. Numbers correspond to the generally accepted names, as listed in Table 2.3. Only the mean positions are presented. Due to seasonal variability, frontal locations can shift by as much as 200 km (Cheney and Winfrey, 1976).

Table 2.3 Names of ocean fronts shown in Figure 2.20

Atlantic Ocean fronts

1	Loop Current (Gulf of Mexico)
2	Gulf Stream
3	North Atlantic Current (north polar front)
4	Slope front
5	Sargasso Sea front
6	Subtropical convergence
7	Iceland-Faeroe Islands front
8	Denmark Strait front
9	East Greenland polar front
10	Greenland-Norwegian Sea front
11	Bear Island front
12	Northwest African upwelling
13	Gulf of Guinea front
14	Guiana Current
15	Benguela upwelling
16	Subtropical convergence
17	Antarctic convergence (south polar front)
18	Antarctic divergence

Mediterranean Sea fronts

19	Huelva front
20	Alboran Sea front
21	Maltese front
22	Ionian Sea front
23	Levantine Basin front

Indian Ocean fronts

24	Somali upwelling
25	Arabian upwelling
26	Indian Ocean salinity front
27	Equatorial Countercurrent fronts
28	West Australian front

Pacific Ocean fronts

29	Kuroshio front
30	Yellow Sea Warm Current
31	Korean coastal front
32	Tsushima Current
33	Oyashio front
34	Kuril front
35	Subarctic front
36	North Doldrum salinity front
37	South Doldrum salinity front
38	Tropical convergence
39	Mid Tasman convergence
40	Australian Subarctic front
41	Subtropical front
42	California front
43	East Pacific equatorial front

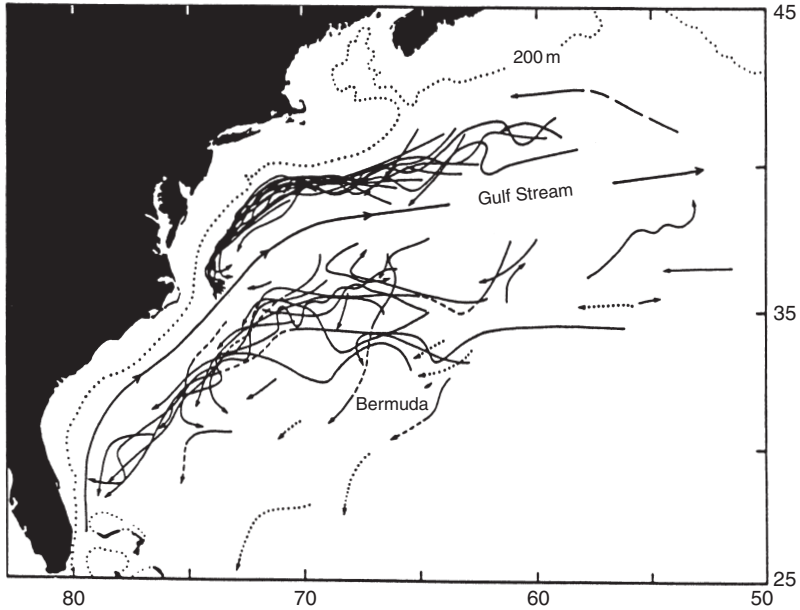


Figure 2.21 Trajectories of Gulf Stream rings. Cold rings south of the stream: unbroken lines represent inferred ring time series; dashed and dotted lines indicate estimated trajectories of rings based on incomplete data. Warm rings north of the stream: trajectories are confined between the continental slope and the Gulf Stream. (Lai and Richardson, 1977; *J. Phys. Oceanogr.*, 7, 670–83; copyright by the American Meteorological Society.)

separate water-mass entities contained within their own enclosed circulation and surrounded by water having different characteristics (Kerr, 1977).

Cold-core Gulf Stream rings form on the south side of the Gulf Stream. These rings are typically 100–300 km in diameter and rotate cyclonically (i.e. counterclockwise in the northern hemisphere) at speeds up to 3 knots at the surface (The Ring Group, 1981). These rings generally drift in a southwestward direction in the Sargasso Sea and can persist for up to a year before losing their identity or being reabsorbed into the Gulf Stream (Figure 2.21). It has been estimated that five to eight cold-core rings form each year (Lai and Richardson, 1977). These rings have cold cores of slope water encircled by warm Sargasso Sea waters, as illustrated in the temperature section of Figure 2.22. Therefore, these rings represent strong thermal anomalies.

Warm-core Gulf Stream rings form on the north side of the Gulf Stream, trapping pockets of warm Sargasso Sea water in the cold slope water (Figure 2.21). The resulting circulation is anticyclonic (i.e. clockwise in

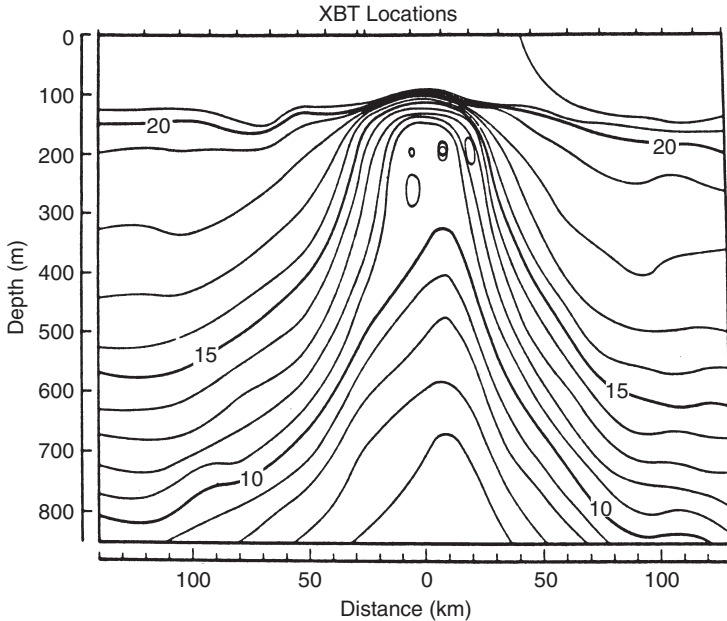


Figure 2.22 Temperature ($^{\circ}\text{C}$) section through a cyclonic (cold-core) Gulf Stream ring as observed during December 1975 near 36°N , 58°W . This cross-section, which is oriented southwest to northeast, shows that the central core of the ring contains cold, low-saline slope water with isotherms rising about 500 m above the normal depth in the surrounding Sargasso Sea water. The overall size of the ring is approximately 200 km. (Lai and Richardson, 1977; *J. Phys. Oceanogr.*, 7, 670–83; copyright by the American Meteorological Society.)

the northern hemisphere). An average of 22 warm-core rings are formed annually between 75° and 44°W (Auer, 1987).

Another example of rings is provided by Goni and Johns (2001), who conducted a census of anticyclonic rings shed by the North Brazil Current in the western tropical Atlantic off the northeast coast of South America near 8°N latitude. The North Brazil Current is separate from the Guiana Current, which is noted on the ocean frontal chart of Figure 2.20. These rings were tracked over the period of October 1992–December 1998 using sea height anomaly data derived from TOPEX/Poseidon satellite radar altimeters. On an average, five rings were formed each year with estimated translation speeds of 14 km day^{-1} . One in six of these rings penetrated into the Caribbean Sea through the southern Lesser Antilles while the rest followed a northern trajectory past Barbados. Available data suggest that the

vertical structures of these rings can vary widely. Some rings may have intense subsurface structure but weak surface signatures, which would make them difficult to detect from satellites.

The acoustic impacts of ocean fronts and eddies will be further explored in Chapter 5 (Section 5.6.7).

2.5.2.2 *Internal waves*

Internal waves are sub-surface waves that propagate along interfaces separating fluid layers of different densities. They can also exist within fluid layers where vertical density gradients are present. These waves can be generated by a number of mechanisms including surface waves, wind forcing, submarine earthquakes, submarine landslides, air pressure changes and current shears, among others.

In the open ocean, internal waves appear to take the form of progressive waves. In partially closed water bodies, standing internal waves are generally found. Internal waves are commonly observed over continental shelves. Such waves are probably generated by the scattering of the barotropic tide into baroclinic modes at the edge of the shelf, and then propagate shoreward on the shelf where they are absorbed and reflected as they break on the sloping bottom. Evidence suggests that such internal waves may have lifetimes of several days on the shelf. Over the shelf, internal waves may be manifested as solitary wave packets (or solitons).

The distribution of internal wave amplitudes as a function of depth is influenced by the vertical density distribution. Specifically, as the density boundary weakens the amplitudes become larger. Internal waves will normally have amplitudes several times greater than surface waves. Crest-to-trough wave heights for internal waves can be on the order of 10 m. Wavelengths can range from a few hundred meters to many kilometers. At the long-wavelength end of the internal wave spectrum are internal tides.

In theory, free internal waves can only exist in the frequency range bounded at the lower limit by the inertial frequency (which is a function of latitude) and at the upper limit by the buoyancy frequency (which is a function of depth). The inertial frequency (ω_i) is equivalent to the Coriolis parameter (f). Specifically, $\omega_i = f = (2\pi \sin L)/12 \text{ rad h}^{-1}$, where L is the latitude (in degrees). The associated period (T) is $12 \text{ h}/\sin L$. At latitude 30° N , the inertial period is 24 h. The buoyancy frequency (N), also referred to as the Brunt-Väisälä frequency, is related to water density (ρ), depth (z), gravitational acceleration (g) and sound speed (c) by:

$$N = \sqrt{-g \left(\frac{1}{\rho} \frac{d\rho}{dz} + \frac{g}{c^2} \right)} \text{ rad s}^{-1} \quad (2.7)$$

where water depth (z) is measured in the negative (downward) direction (Apel, 1987: 169–70). The buoyancy frequency measures the stability of the

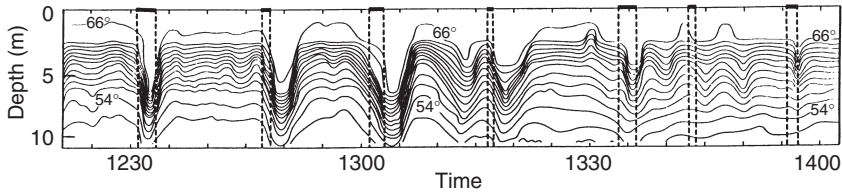


Figure 2.23 Passage of internal waves observed at a stationary observation point. The internal waves are evidenced by temporal fluctuations in the isotherm patterns ($^{\circ}\text{F}$). Vertical dashed lines indicate the relationship between the internal wave structure and the location of sea-surface slicks. (LaFond, 1962; *The Sea*, Vol. 1, pp. 731–51; reprinted by permission of John Wiley & Sons, Inc., all rights reserved.)

water column against small vertical perturbations: when N is real (a stable water column), buoyant oscillations are initiated; when N is imaginary (an unstable water column), rising or sinking motions are initiated. In a typical stable water column, the buoyancy frequency decreases approximately exponentially with depth with a maximum value ($N/2\pi$) of about 10 cycles per hour near the surface and an e-folding depth of about 1.5 km (Spindel, 1985).

When present, internal waves can be detected by making continuous temperature measurements at one location (as with a fixed vertical array of thermistors) over a given period of time. Their presence is evidenced by oscillations in the temperature record with periods consistent with those of internal waves. Figure 2.23 shows the passage of internal waves as recorded in the changed depths of the isotherms.

One problem in testing theories of acoustic propagation in inhomogeneous media is the inability to determine accurately the spatial and temporal scales associated with fluctuations in the index of refraction. These fluctuations can be caused by tides, internal waves and fine-scale features. Ewart and Reynolds (1984) reported results from the mid-ocean acoustic transmission experiment (MATE). This experiment was designed to measure phase and intensity fluctuations in sound pulses transmitted at 2, 4, 8 and 13 kHz over a wholly refracted path (i.e. no boundary interactions). Two receiver towers were placed on Cobb Seamount (in the northeastern portion of the North Pacific Ocean). A sister tower located 20 km to the southwest was used for placement of the acoustic transmitter. This geometry minimized transducer motion and also assured the presence of wholly refracted paths between source and receiver. The environmental program conducted in support of MATE was specifically designed to oversample the internal-wave variability within the context of the Garrett–Munk model (Garrett and Munk, 1979). This archive of environmental measurements contains sufficient data with which to test existing internal-wave models as well as test future models of internal-wave variability. In related work, Macaskill and

Ewart (1996) refined numerical solutions of the fourth-moment equation for acoustic intensity correlations, particularly the temporal cross-correlation between acoustic signals of different frequencies propagating through the same medium.

Internal waves are considered to be a limiting factor in the propagation of acoustic energy, particularly in the frequency range of 50 Hz–20 kHz. The effects are manifested as amplitude and phase variations. Internal waves may also limit both the temporal and spatial stability of acoustic paths (Flatté, 1979). Below 50 Hz, the relatively long acoustic wavelengths (>30 m) are less likely to be affected by internal waves. Above 20 kHz (with acoustic wavelengths less than a few centimeters), the effects of fine-scale features are probably more important. The acoustic impacts of internal waves will be further explored in Chapter 5 (Section 5.6.7).

2.5.3 *Fine-scale features*

One type of fine-scale oceanic feature is the “thermohaline staircase.” These staircases are generally found in the main thermocline and are evidenced by layers of uniform temperature and salinity on the order of 10 m in thickness separated by thin, high-gradient interfaces on the order of a few meters in thickness (Figure 2.24). The incidence of well-developed staircases appears to be limited to less than 10 percent of the available high-resolution profiles taken in the North Atlantic Ocean (Schmitt, 1987; Schmitt *et al.*, 1987).

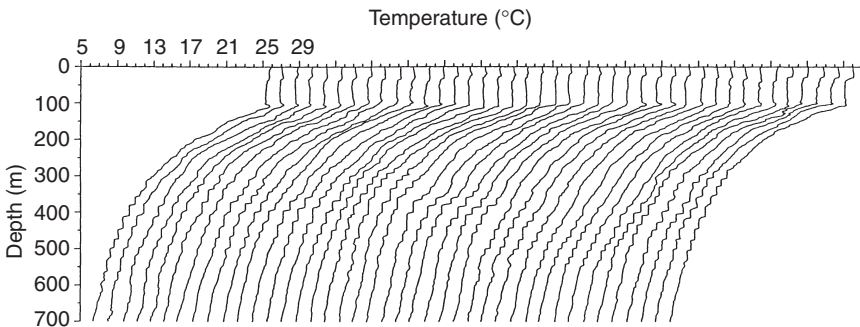


Figure 2.24 Series of expendable bathythermograph (XBT) temperature profiles taken from an east–west section east of Barbados in the Atlantic Ocean. The profiles are separated by a distance of 5.5 km; the total distance covered is 220 km. The temperature scale is correct for the profile at the extreme left (west), and each subsequent profile is offset by 1.6°C. Undulations of the thermocline caused by internal waves and mesoscale eddies can also be seen. (Schmitt, 1987; *EOS, Trans. Amer. Geophys. Union*, 68, 57–60; copyright by the American Geophysical Union.)

Staircase structures are most frequently associated with a strongly destabilizing vertical gradient of salinity (caused by the confluence of fresh- and saline-water masses). These features have been observed northeast of South America in the tropical Atlantic Ocean just outside the Caribbean Sea, and also in the eastern Atlantic Ocean outside the Mediterranean Sea. Before the dynamics of thermohaline staircases were understood, these features were sometimes dismissed as malfunctions in the oceanographic sensors that recorded them.

Research is not conclusive as to what effect these staircase features might have on underwater acoustic propagation. Chin-Bing *et al.* (1994) studied the effects of thermohaline staircases on low-frequency (50 Hz) sound propagation. Several propagation models were used to generate transmission loss as a function of range from source to receiver based on a sound-speed profile containing staircase features. A source was placed (in depth) at the center of the staircase features while receivers were placed above, below and at the center of the features. These results were then compared to baseline (control) simulations based on a profile in which the effects of the staircase features were effectively averaged out. The greatest effects were observed when both the source and the receiver were placed at the center of the features. These effects were attributed to a redistribution of intensity caused by the staircase features. Chin-Bing *et al.* (1994) also noted that backscatter can occur when the step-structured discontinuities of the thermohaline staircase are on the order of an acoustic wavelength. Thus, at frequencies greater than about 3 kHz, backscatter from the thermohaline steps could become significant.

2.6 Biologics

Marine organisms can be segregated into four major categories: plankton, nekton, benthos and algae. Plankton (or floaters) include both plants (phytoplankton) and animals (zooplankton). The zooplankton have little or no swimming ability and thus drift with the currents. Phytoplankton are typically smaller than 0.5 mm while zooplankton are smaller than 1 cm.

Nekton (or free swimmers) are animals that are capable of swimming purposefully. Nekton include fish and mammals and occur over the entire depth range of the ocean. Benthos are dwellers on, in or near the bottom of the ocean. Fouling organisms such as barnacles would also be included in this category. Algae include marine plant life, such as seaweed.

Biological organisms can affect underwater sound through noise production, attenuation and scattering of signals, presentation of false targets and fouling of sonar transducers. Certain marine animals, many of which are found over the continental shelves, produce sounds that increase the background noise levels. These include snapping shrimp, whales, porpoises and various fish such as croakers and drum fish. Organisms that may cause attenuation are schools of fish, dense populations of plankton and floating kelp,

for example. False targets are commonly presented to active sonars by whales or large schools of fish or porpoises.

While fouling organisms such as barnacles do not directly affect sound, indirectly they can degrade sonar performance by fouling sonar domes and transducer faces. Furthermore, such organisms can contribute to an increase in hull noise of ships and submarines through the generation of turbulence as the vessels move through the water. This effect is also referred to as self noise, as distinguished from ambient noise.

Perhaps the most notable impact of marine organisms on active sonars (particularly those operating at frequencies near 10 kHz) is known as the deep scattering layer (DSL). The DSL is a dense accumulation of marine organisms at depth below the sea surface. The strong scattering nature of the DSL is attributed primarily to fish and other marine animals with swim bladders and gas floats, although plankton and nekton are also present. The DSL is typically encountered in temperate regions. Moreover, the DSL exhibits a diurnal migration in depth, being shallower at night and deeper during the day. The DSL will be further discussed in Chapter 8 (Section 8.2.1).

3 Propagation I

Observations and physical models

3.1 Background

The propagation of sound in the sea has been studied intensely since the beginning of Second World War when it was recognized that an understanding of this phenomenon was essential to the successful conduct of anti-submarine warfare (ASW) operations. These early measurements were quickly transformed into effective, albeit primitive, prediction tools. Naval requirements continue to motivate advances in all aspects of underwater acoustic modeling, particularly propagation modeling.

The study of sound propagation in the sea is fundamental to the understanding and prediction of all other underwater acoustic phenomena. The essentiality of propagation models is inherent in the hierarchy of acoustic models illustrated previously in Figure 1.1.

Advances in propagation modeling have been achieved by both marine seismologists and underwater acousticians, although the motivating factors have been quite different. Marine seismologists have traditionally used earth-borne propagation of elastic waves to study the solid earth beneath the oceans. Underwater acousticians have concentrated on the study of water-borne, compressional-wave propagation phenomena in the ocean as well as in the shallow sub-bottom layers (Akal and Berkson, 1986). As research in underwater acoustics has extended to frequencies below several hundred hertz, it has overlapped with the spectral domain of marine seismologists. Moreover, marine seismologists have become more interested in exploring the velocity–depth structure of the uppermost layers of the sea floor using higher frequencies. This area of overlapping interests has been recognized as a sub-discipline of both communities and is referred to as “ocean seismo-acoustics.”

The emphasis in this chapter is focused on applications in underwater acoustics. Developments in marine seismology will be discussed when the applications to sonar modeling are clearly evident. Much research has been performed in the marine seismology community that is theoretically and conceptually applicable to underwater acoustics. Such practical research

includes the development of sophisticated, yet robust, mathematical methods.

Propagation models have continued to be used for the prediction of sonar performance. They have also found great utility in analyzing field measurements, in designing improved sonar systems and in designing complicated inverse-acoustic field experiments.

As modeling has continued to grow in prominence in many aspects of underwater acoustics, it is prudent to reassess the state-of-the-art in modeling techniques and the relationship to available measurements. Ideally, such an assessment should identify those areas requiring further measurement support as well as those that are firmly understood and hence properly modeled.

This chapter addresses the observations that have been made in the field and the physical (i.e. physics-based) models that have been developed. Aspects of propagation phenomena including ducts and channels, boundary interactions, volumetric effects and coherence are described. Chapter 4 addresses the mathematical models that have been developed for underwater acoustic propagation. Specialized aspects of surface ducts, shallow-water areas and Arctic regions are discussed in Chapter 5.

3.2 Nature of measurements

Field measurement programs are usually quite complex and typically involve multiple platforms (e.g. ships, buoys, towers, aircraft, submarines or satellites).

A wide variety of experimental field techniques have been used in underwater acoustic propagation studies. Some of the more typical types of measurement platforms and experimental geometries that have been utilized include (Urick, 1982: chapter 1):

- 1 Two ships – one a source ship and the other a receiving ship. The range between them is changed as transmission runs are made in order to yield level versus range.
- 2 Single ship – using a suspended transmitter and either sonobuoys or a hydrophone array for reception.
- 3 Ship and aircraft – where the aircraft drops explosive sound sources while flying toward or away from the ship.
- 4 Single aircraft – using sonobuoys for reception and recording on board the aircraft.
- 5 Bottomed hydrophone array – with a cable connected to shore, receives signals transmitted from a ship or the explosive shots dropped by an aircraft.
- 6 Two bottomed transducers – one acting as a source and the other as a receiver. This geometry is typically used in studies of the fluctuation of sound transmission between two fixed points in the sea.

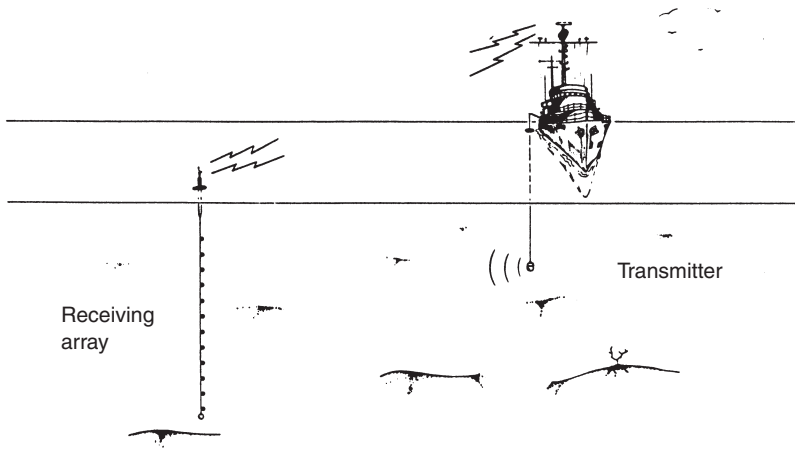


Figure 3.1 Example of a simple experimental geometry (adapted from Ingenito *et al.*, 1978).

A simple experimental geometry illustrating method (2) above is presented in Figure 3.1. Here, the transmitting ship is receiving signals via radio directly from the array. Fully integrated oceanographic and acoustic field experiments are required in order to obtain a comprehensive portraiture of the temporal, spatial and spectral scales necessary to characterize the marine environment for a full understanding of the governing acoustic phenomena.

3.3 Basic concepts

The standard unit of measure of underwater acoustic propagation is acoustic intensity (I), which is sound pressure flow (power) per unit area (reported in units of watts per square meter):

$$I = \frac{p^2}{\rho c} \quad (3.1)$$

where p is the instantaneous pressure amplitude of a plane wave, ρ the density of sea water and c the speed of sound in sea water. Sound intensity is actually a vector quantity, but in the far-field approximation it is represented as a scalar quantity based on sound pressure squared. The product ρc is commonly referred to as the characteristic acoustic impedance.

Transmission loss (TL) is defined as 10 times the log (base 10) of the ratio of the reference intensity (I_{ref}), measured at a point 1 m from the source, to the intensity (I), measured at a distant point, and is expressed in units of decibels (dB):

$$\text{TL} = 10 \log_{10} \frac{I_{\text{ref}}}{I} \quad (3.2)$$

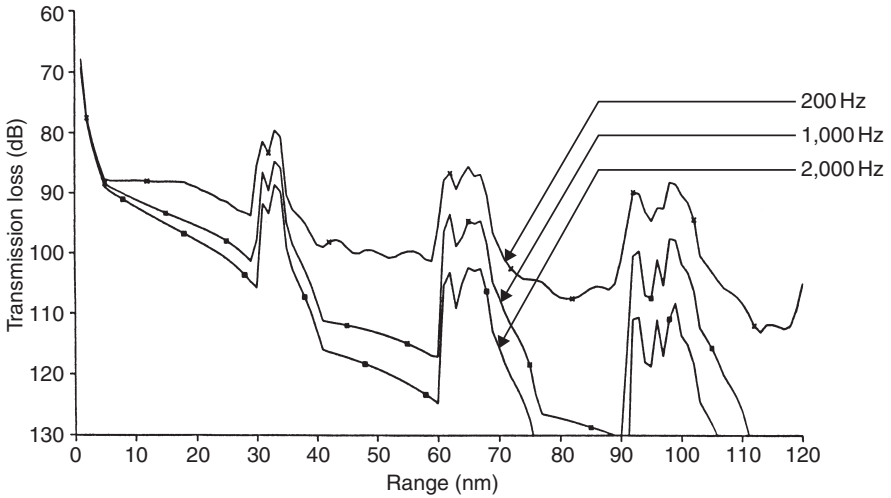


Figure 3.2 Example of standard TL curves generated by the FACT model for each combination of frequency, source depth and receiver depth. Here, the source and receiver depths are fixed at 150 and 90 m, respectively. The peaks (minimum TL values) correspond to convergence zones. Note the increase in TL with increasing frequency due to absorption.

The standard metric unit for pressure (force per unit area) is $1 \mu\text{Pa}$, which is equivalent to 10^{-6} N m^{-2} .

Transmission loss has conventionally been plotted for each frequency, source depth and receiver depth as a function of range, as illustrated in Figure 3.2. This type of display is easily generated by all propagation models. Certain types of propagation models can also generate and display acoustic TL in the entire range–depth plane for all receiver depths and ranges, given a fixed source depth (Figure 3.3).

Sonar performance is commonly described in terms of a figure of merit (FOM). The FOM is a quantitative measure of sonar performance. Specifically, the larger the FOM value, the greater the performance potential of the sonar. Numerically, the FOM is equal to the allowable one-way TL in passive sonars. The FOM is further described in Chapter 10 within the context of the sonar equations.

The display method illustrated in Figure 3.2 is very useful in evaluating passive sonar performance. Specifically, once an FOM has been calculated for a particular sonar operating in a particular ocean environment against a particular target, a horizontal line can be drawn on the plot equating the numerical value of the FOM to TL. Then, any area below the TL curve, but above the FOM line, represents a sonar detection area. Figure 3.4 shows

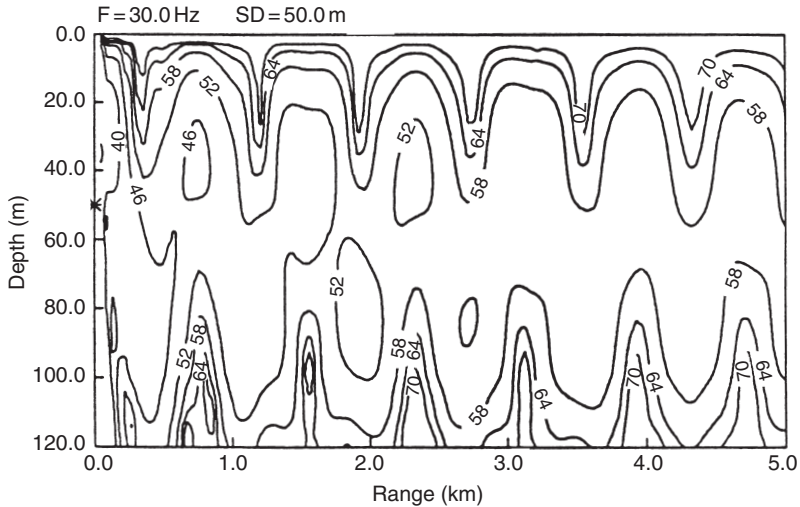


Figure 3.3 Example showing contours of TL plotted in the range–depth plane. This plot is valid for one frequency (30 Hz) and one source depth (50 m), but can be used to determine the TL at any receiver location in the range–depth plane. The contour interval is 6 dB (Schmidt, 1988).

a hypothetical relationship between the FOM and the sonar detection areas (upper panel), and the correspondence between the TL curve and the ray paths as propagated in the water column (lower panel). These ray paths are consistent with those resulting from a shallow source (target) and shallow receiver (sonar) positioned in a water column characterized by the sound-speed profile shown on the left side of the lower panel of Figure 3.4.

Sound propagates in the sea by way of a variety of paths. The particular paths traveled depend upon the sound-speed structure in the water column and the source–receiver geometry. The six basic paths include direct path, surface duct, bottom bounce, convergence zone, deep-sound channel and reliable acoustic path. These six paths are illustrated in Figure 3.5. Depending upon the ocean environment, propagation over combinations of paths may be possible for any given source–receiver geometry; this situation is referred to as multipath propagation. Four of these paths (surface duct, deep sound channel, convergence zone and reliable acoustic path) are strongly affected by the sound-speed structure in the water column and will be discussed in detail in Sections 3.7, 3.8, 3.9 and 3.10, respectively. The remaining two paths (direct path and bottom bounce) are relatively unaffected by the refractive properties of the sound-speed structure: direct paths span relatively short distances and bottom-bounce paths penetrate the refractive layers at steep angles.

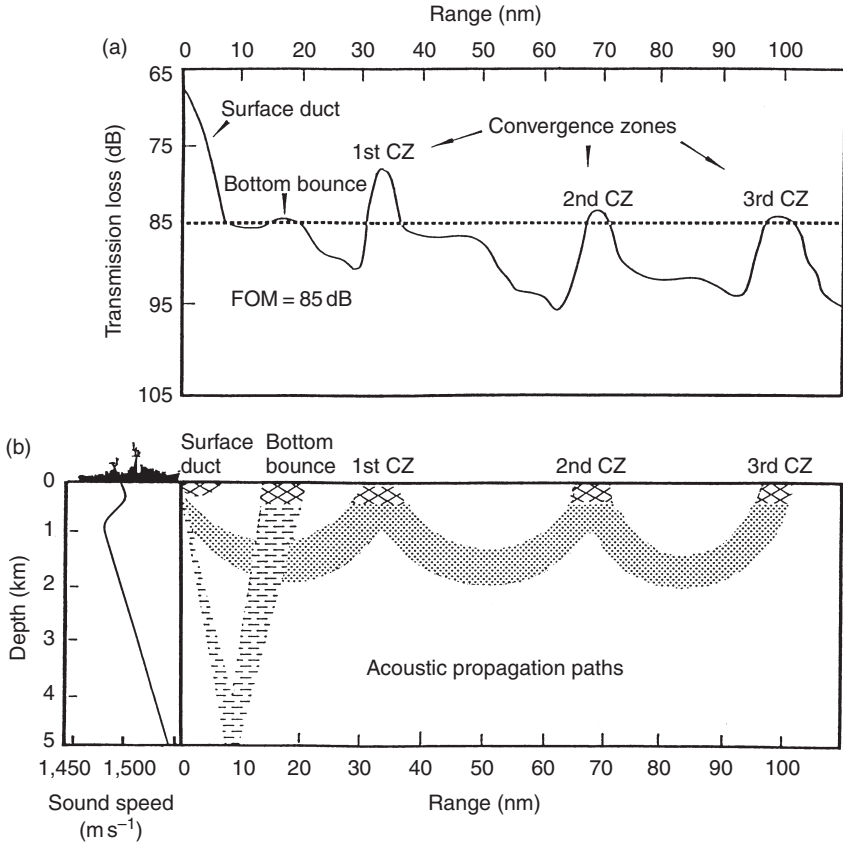


Figure 3.4 Hypothetical relationship between (a) TL curve and (b) the corresponding propagation paths and detection zones (cross-hatched areas near the sea surface) associated with a FOM of 85 dB. A plausible sound-speed profile is shown at the left side of panel (b). Both the source (target) and receiver (ship's sonar) are positioned near the surface.

In basic ray tracing, Snell's law is used in one form or another. This law describes the refraction of sound rays in a medium in which sound speed varies as a function of depth, but is constant within discrete horizontal layers of the water column. Consider Figure 3.6 where a ray (which is normal to the acoustic wavefronts) is traveling from medium 1 (with sound speed c_1) into medium 2 (with sound speed c_2), where $c_1 \neq c_2$. Let λ_1 be the distance between successive wavefronts (i.e. the wavelength) in medium 1 and λ_2 the corresponding value in medium 2. Then, as defined in Figure 3.6:

$$\lambda_1 = \Delta x \sin \phi_1 = c_1 \Delta t \quad \text{and} \quad \lambda_2 = \Delta x \sin \phi_2 = c_2 \Delta t$$

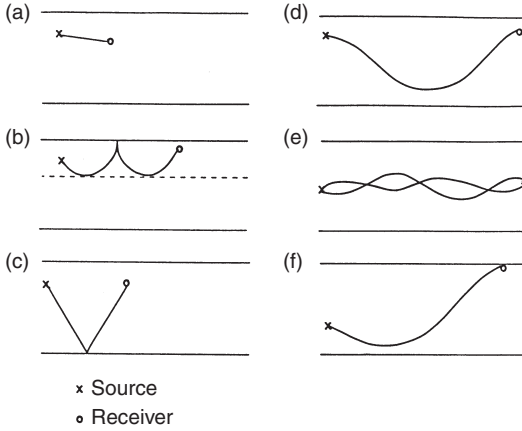


Figure 3.5 Six basic propagation paths in the sea: (a) direct path (DP); (b) surface duct (SD); (c) bottom bounce (BB); (d) convergence zone (CZ); (e) deep-sound channel (DSC); and (f) reliable acoustic path (RAP).

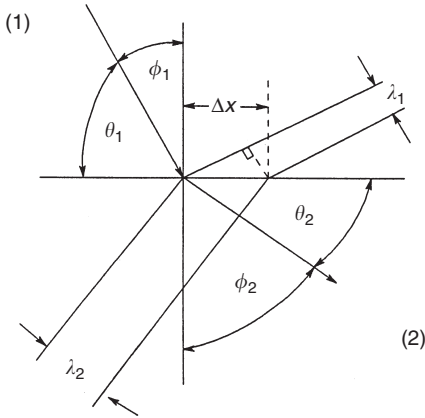


Figure 3.6 Geometry for Snell's law.

where Δt is an increment of time. Rearranging terms, we obtain the familiar relationship:

$$\frac{\sin \phi_1}{c_1} = \frac{\sin \phi_2}{c_2} \tag{3.3a}$$

or, equivalently from Figure 3.6:

$$\frac{\cos \theta_1}{c_1} = \frac{\cos \theta_2}{c_2} \tag{3.3b}$$

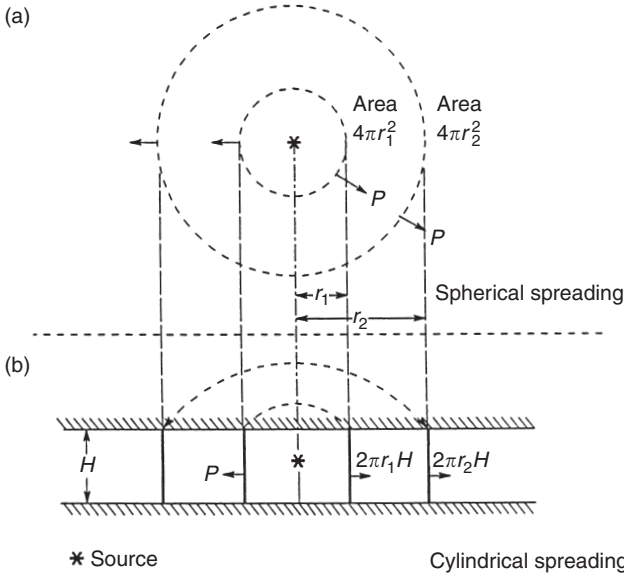


Figure 3.7 Geometry for (a) spherical spreading and (b) cylindrical spreading. (Urick, 1983; *Principles of Underwater Sound*, 3rd edn; reproduced with permission of McGraw-Hill Publishing Company.)

As a matter of convention, ϕ is referred to as the incidence angle while θ is referred to as the grazing angle.

In a homogeneous medium, acoustic TL varies as the inverse of the range squared. This relationship is easily derived, as demonstrated below.

Let I = intensity, P = power and A = area, then:

$$I = \frac{P}{A}$$

For spherical spreading (see Figure 3.7(a)):

$$I_1 A_1 = I_1 (4\pi \cdot r_1^2) \quad I_2 A_2 = I_2 (4\pi \cdot r_2^2)$$

where r_1 and r_2 are the radii of concentric spherical sections.

Power (P) is conserved; therefore, $P_1 = I_1 A_1 = I_2 A_2$ and:

$$I_2 = I_1 \left(\frac{r_1^2}{r_2^2} \right)$$

but r_1 represents a unit reference distance and thus:

$$I_2 = \frac{I_1}{r_2^2}$$

Since intensity is power per unit area, and since the area of a sphere increases as the square of its radius, the intensity falls off as the inverse square of the radius (or range) in order that power remains constant.

The corresponding TL is defined as:

$$TL = 10 \log_{10} \frac{I_1}{I_2} = 10 \log_{10} r_2^2 = 20 \log_{10} r_2 \quad (3.4)$$

This relationship is valid for an isotropic deep ocean with no absorption effects.

An analogous expression can be derived for cylindrical spreading. This spreading law would be appropriate for a duct, or in shallow water, where the water is homogeneous and the boundaries are perfect reflectors. Then, referring to Figure 3.7(b):

$$I_1 A_1 = I_1 (2\pi \cdot r_1 H) \quad I_2 A_2 = I_2 (2\pi \cdot r_2 H)$$

where H is the depth of the duct or of the water column. Since power is conserved, $P_1 = I_1 A_1 = I_2 A_2$ and:

$$I_2 = I_1 \frac{r_1}{r_2}$$

For unit radius r_1

$$I_2 = \frac{I_1}{r_2}$$

Thus, the intensity falls off as the inverse of the radius (or range). The corresponding TL is defined as:

$$TL = 10 \log_{10} \frac{I_1}{I_2} = 10 \log_{10} r_2 \quad (3.5)$$

This relationship is valid in an isotropic ocean with no absorption effects.

3.4 Sea-surface boundary

The sea surface affects underwater sound by providing a mechanism for:

- 1 forward scattering and reflection loss;
- 2 image interference and frequency effects;
- 3 attenuation by turbidity and bubbles;
- 4 noise generation at higher frequencies due to surface weather; and
- 5 backscattering and surface reverberation.

Urlick (1982: chapter 10) provided a comprehensive summary of sound reflection and scattering by the sea surface. Items (1)–(3) will be discussed

below. Item (4) will be addressed in Chapter 6 and item (5) will be discussed in Chapter 8.

The mechanisms operating at the sea surface can be incorporated into mathematical models through the specification of appropriate “boundary conditions.” These boundary conditions can range from simplistic to complex depending upon the sophistication of the model and the availability of information concerning the state of the sea surface.

3.4.1 *Forward scattering and reflection loss*

When a plane sound wave in water strikes a perfectly smooth surface, nearly all of the energy is reflected at the boundary in the forward (or specular) direction as a coherent plane wave. As the sea surface roughens under the influence of wind, sound is also scattered in the backward and out-of-plane directions, and the intensity of sound reflected in the forward direction is accordingly reduced. The backward-directed (backscattered) energy gives rise to surface reverberation (see Chapter 8). Eckart (1953) developed a theoretical treatment of scattering by a sinusoidal boundary as a way to approximate reflection from a wind-roughened sea surface. Marsh *et al.* (1961) developed simple formulae to express scattering losses at the sea surface. Eller (1984a) reviewed the availability of simple surface loss algorithms appropriate for incorporation into propagation models.

The sea surface is most commonly modeled as a pressure release surface (see Kinsler *et al.*, 1982: 126–7). This is a condition in which the acoustic pressure at the air–water interface is nearly zero, the amplitude of the reflected wave (in water) is almost equal to that of the incident wave, and there is a 180° phase shift. This is also known as the Dirichlet boundary condition (Frisk, 1994: 32).

It is also common practice to use the term “reflection coefficient” to express the amount of acoustic energy reflected from a surface or from a boundary between two media. This coefficient depends upon the grazing angle and the difference in the acoustic impedance between the two media. A reflection loss is then defined as $10 \log_{10}$ (reflection coefficient). This reflection loss is referred to as “surface loss” when describing the reflection of sound from the sea surface or “bottom loss” when describing the reflection of sound from the sea floor.

A measure of the acoustic roughness of the sea surface is provided by the Rayleigh parameter R through the relationship:

$$R = 2ka \sin \theta \quad (3.6)$$

where $k = 2\pi/\lambda$ is the acoustic wavenumber, λ the acoustic wavelength, a the root-mean-square (rms) amplitude of the surface waves [$2a$ is the crest-to-trough rms wave height (or H_{rms}): refer back to Equation (2.4) in Chapter 2] and θ the grazing angle (measured relative to the horizontal plane). When

$R \ll 1$, the sea surface is considered to be acoustically smooth; when $R \gg 1$, the sea surface is acoustically rough.

Sea-surface wave spectra can be generated numerically by executing available spectral ocean wave models in the hindcast mode. Hindcasting is usually the only means available for obtaining sufficiently long record lengths from which to generate reliable statistics. A statistical analysis of these hindcast data produces probability distributions of critical parameters for use in estimating future sea-surface conditions.

Kuo (1988) reviewed and clarified earlier formulations of sea-surface scattering losses based on perturbation methods and also presented new predictions based on numerical integration in a complex domain.

3.4.2 Image interference and frequency effects

When the surface is smooth, an interference pattern is produced between direct-path sound and sound reflected from the sea surface. The sound reflected from the sea surface may be considered to originate from an image source located on the opposite (mirror image) side of the surface (Figure 3.8). This image signal will have an amplitude nearly equal to that of the incident signal, but will be out of phase. The resulting sound field can be divided into three parts (Figure 3.9): (1) the near field close to the source in which the image source is too far away, and the reflected sound is too weak to produce appreciable interference; (2) an interference field in which there are strong peaks and nulls in the received signal as range increases; and (3) the far field in which there is an increasingly out-of-phase condition between the source and image, and the intensity falls off as the inverse fourth power of range.

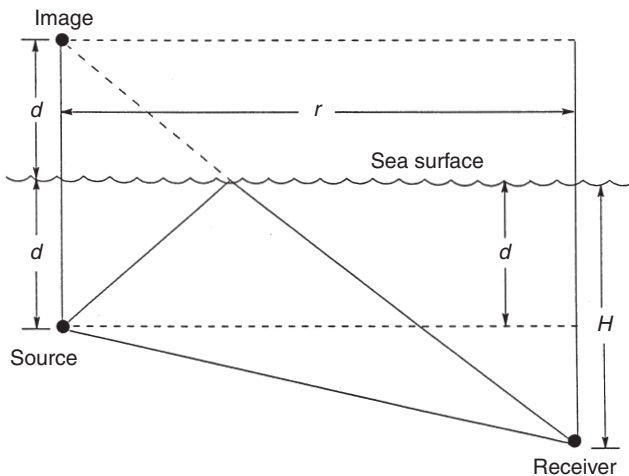


Figure 3.8 Geometry for image interference effect.

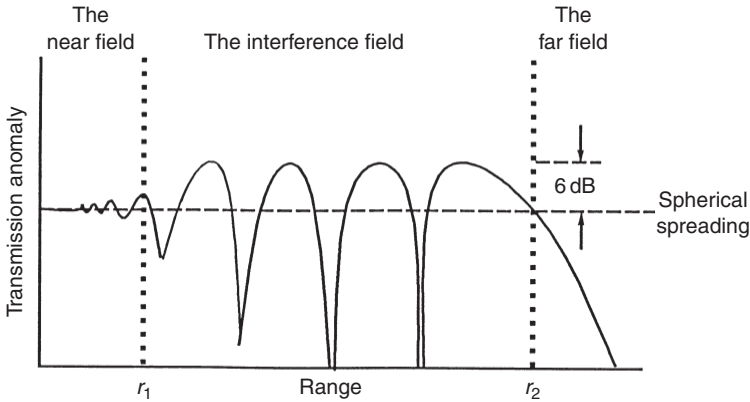


Figure 3.9 Illustration of image interference effects. The transmission anomaly (TA) represents the difference between the observed TL and losses due to the effects of spherical spreading ($TA = 20 \log_{10}(r) - TL$, where the range (r) is measured in meters (adapted from Urick, 1979).

This phenomenon, also known as the Lloyd Mirror effect, diminishes with increasing surface roughness.

Assuming an acoustically smooth sea surface ($R \ll 1$) and a shallow source depth (d) in deep water, the ranges r_1 and r_2 in Figure 3.9 can be approximated as (Urick, 1982, 1983):

$$r_1 \approx 2\sqrt{dH} \quad r_2 \approx \frac{4\pi \cdot dH}{\lambda}$$

where λ is the acoustic wavelength and H the receiver depth.

The image effect can be used to estimate the depth of a submerged object at short ranges. In Figure 3.8, if the source is replaced by a submerged object that has been ensonified by a single, short pulse, then the depth (d) of the object is approximated by:

$$d \approx \frac{rc\Delta t}{2H} \tag{3.7}$$

where c is the speed of sound and Δt the difference in time between receipt of the direct and the surface-reflected pulses (Albers, 1965: 50–1).

The concept of surface interference can also be used to solve relatively simple propagation problems. The approach is called the “method of images” and is valid for all frequencies. The solution is normally expressed as a sum of contributions from all images within a multilayered space. Although this method is usually cumbersome, it is commonly employed as a physical model against which to check the results of more elaborate mathematical models (to be discussed in Chapter 4). Kinsler *et al.* (1982: 427–30) provided a detailed

discussion of this method together with several examples of its application. Tolstoy and Clay (1966: 33–6) discussed solutions in waveguides.

When the sea surface is rough, the vertical motion of the surface modulates the amplitude of the incident wave and superposes its own spectrum as upper and lower sidebands on the spectrum of the incident sound. Moreover, when there is a surface current, the horizontal motion will appear in the scattered sound and cause a Doppler-shifted and Doppler-smearred spectrum.

3.4.3 *Turbidity and bubbles*

3.4.3.1 *Open ocean*

The presence of bubble layers near the sea surface further complicates the reflection and scattering of sound as a result of the change in sound speed, the resonant characteristics of bubbles and the scattering by bubbly layers (e.g. Leighton, 1994).

Hall (1989) developed a comprehensive model of wind-generated bubbles in the ocean. The effects on the transmission of short pulses in the frequency range 1.25–40 kHz were also examined. For long-range propagation, Hall concluded that the decrease in the near-surface sound speed due to bubbles does not significantly affect the intensity of the surface-reflected rays.

3.4.3.2 *Coastal ocean*

Coastal waters are often characterized by suspensions of solid mineral particles that are agitated by waves, currents or river outflows, in addition to microbubbles that are generated at the sea surface by wind and wave action or at the sea floor by biochemical processes (Richards and Leighton, 2001a,b). Suspended solid particles and microbubbles jointly modify the complex acoustic wavenumber, thus influencing the acoustic properties of the medium and thereby affecting the performance of acoustic sensors operating in such turbid and bubbly environments.

Consequently, the acoustic attenuation coefficient (Section 3.6) in shallow coastal waters is of interest to designers and operators of Doppler-current profiles, sidescan-surveying sonars and naval mine-hunting sonars operating in the frequency range from tens of kilohertz to several hundred kilohertz and possibly up to 1 MHz. At these frequencies, attenuation due to suspended particulate matter is an important contribution to the total attenuation coefficient (Richards, 1998). Typical suspensions contain particles in the size range 1–100 μm , where a variety of shapes and concentrations from 0.1 to 4 kg m^{-3} are possible (Brown *et al.*, 1998). Microbubbles with radii in the range 10–60 μm will be resonant in the frequency interval 50–300 kHz. Preliminary calculations using viscous-damping theory suggest that particulate concentrations on the order of 0.1 kg m^{-3} may be important, even possibly reducing the detection range of sonars by a factor of two relative to

clear water at a frequency of 100 kHz. Observations have shown that concentrations of this level, or greater, often occur in coastal waters and have been detected several tens of kilometers offshore of the Amazon river, in the Yellow Sea and in the East China Sea offshore of the Yangtze and Yellow rivers (Richards *et al.*, 1996).

The presence of microbubbles increases acoustic attenuation through the effects of thermal and viscous absorption and scattering. Unlike particles, however, the resonant scattering of bubbles can be important – the scattering cross-section of a bubble near resonance can be much larger than its geometric cross-section. Moreover, bubbles cause the compressibility of the medium to be complex, thereby resulting in dispersion. The effect of bubbles on the phase speed should be used to modify the sound-speed profile when computing ray paths in bubbly layers. A numerical procedure was developed by Norton *et al.* (1998) to parameterize bubble clouds in terms of an effective complex index of refraction for use in high-fidelity models of forward propagation.

The effective attenuation coefficient in turbid and bubbly environments can be expressed as (Richards and Leighton, 2001a):

$$\alpha = \alpha_w + \alpha_p + \alpha_b$$

and

$$\alpha_p = \alpha_v + \alpha_s$$

where α is the total volume attenuation coefficient of sea water containing suspended particles and microbubbles, α_w the physico-chemical absorption by clear sea water (see Section 3.6), α_p the plane-wave attenuation coefficient due to a suspension of solid particles (neglecting thermal absorption) and α_b the attenuation coefficient for a bubbly liquid. Furthermore, α_p is composed of two terms: α_v is the attenuation coefficient associated with the visco-inertial absorption by suspended particles and α_s the attenuation coefficient associated with scattering by suspended particles.

3.4.4 *Ice interaction*

Acoustic interaction with an ice canopy is governed by the shape of the under-ice surface and by the compressional wavespeeds (typically 1,300–3,900 m s⁻¹) and shear wavespeeds (typically, 1,400–1,900 m s⁻¹) (see Untersteiner, 1966; Medwin *et al.*, 1988).

McCammom and McDaniel (1985) examined the reflectivity of ice due to the absorption of shear and compressional waves. They found that shear wave attenuation is the most important loss mechanism from 20° to 60° incidence for smooth ice at low frequencies (≤ 2 kHz).

In Arctic regions, the presence of a positive-gradient sound-speed profile and a rough under-ice surface (with a distribution of large keels) may lead

to significant out-of-plane scattering. The acoustic impacts of this scattering are twofold. First, significant beam widening may result from the multiple interactions with the randomly rough under-ice surface. Second, the presence of ice keels in the vicinity of the receiver leads to multiple source images or beam-steering errors arising from interactions of the acoustic signal with the facets of the local under-ice surface.

Because of the overwhelming effect of ice on the propagation of sound in the Arctic, the magnitude of the excess attenuation observed under the ice should be determined by the statistics of the under-ice surface. Available ice-ridge models can be used to generate such statistics. These models can be categorized according to two classes: discrete models and continuous statistical models. These two classes of ice-ridge models are briefly described below.

Discrete ice-ridge models prescribe a representative ridge shape, or an ensemble of ridge shapes, to calculate the statistics of the surface from the discrete statistics of the known ice structure. Continuous statistical ice-ridge models treat the under-ice surface as a stochastic process. This process is then analyzed using the techniques of time-series analysis in which the under-ice surface can be characterized by its autocorrelation function. Continuous statistical models can give a more complete description of the under-ice roughness than can the discrete models; however, they are limited in application to those surfaces that can be completely specified by a Gaussian depth distribution.

The model developed by Diachok (1976) will be described since it is considered to be representative of the class of discrete ice-ridge models known to exist and because of its intuitive appeal. The discrete models are also more robust (i.e. require less knowledge of the under-ice surface) than the continuous statistical models. Furthermore, Diachok's model has been incorporated into existing propagation models with some success.

According to Diachok's model, sea ice may be described as consisting of floating plates, or floes, about 3 m thick, occasionally interrupted by ridges, which are rubble piles formed by collisions and shear interactions between adjacent floes. Ridge dimensions vary widely, but are nominally about 1 m high, 4 m deep and 12 m wide, with the ridge lengths generally being much greater than the depths or widths. A representative average spacing between ridges (the spacing is random) is about 100 m. Ice-ridge orientation is commonly assumed to be directionally isotropic, although limited empirical data suggest that, at least locally, there may be a preferred orientation. The physical model of reflection developed by Twersky (1957) was used.

A comparison between measured contours and simple geometrical shapes suggests that ridge keel contours may reasonably be represented by a half-ellipse (as in Figure 3.10) and that ridge sail contours may be described using a Gaussian distribution function. The relative dimensions of this geometrical model are indicated in Figure 3.10. The exact solution of under-ice scattering off a flat surface with a single semi-elliptical cylindrical boss of infinite extent was developed by Rubenstein and Greene (1991).

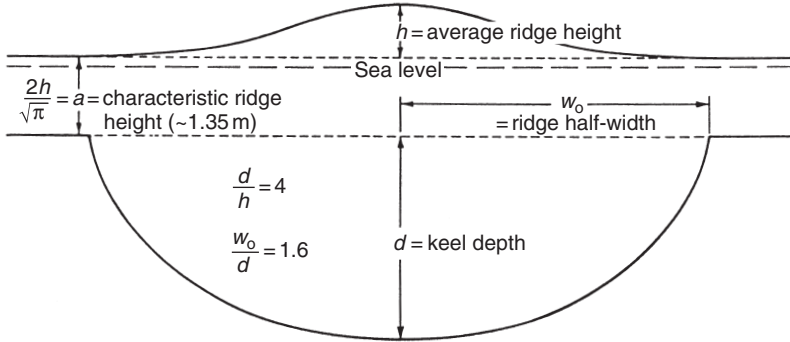


Figure 3.10 Geometrical model of sea-ice ridges (Diachok, 1976).

LePage and Schmidt (1994) extended the applicability of perturbation theory to under-ice scattering at low frequencies (10–100 Hz) by including the scattering of incident acoustic energy into elastic modes, which then propagate through the ice. Kapoor and Schmidt (1997) developed a canonical model in which the under-ice scattering surface was represented as an infinite elastic plate with protuberances.

3.4.5 Measurements

Three basic experimental techniques have been employed to measure forward reflection losses at the sea surface:

- 1 comparing the amplitude or energy of pulses returned from the surface with that of the direct arrival;
- 2 using the Lloyd mirror effect and observing the depth of the minima as the frequency is varied; and
- 3 measuring the attenuation in the surface duct.

Based on a compilation of results in the literature by Urlick (1982: chapter 10), it appears that surface losses are less than 1 dB (per bounce) at frequencies below 1 kHz, and rise to about 3 dB (per bounce) at frequencies above 25 kHz.

3.5 Sea-floor boundary

The sea floor affects underwater sound by providing a mechanism for:

- 1 forward scattering and reflection loss (but is complicated by refraction in the bottom);
- 2 interference and frequency effects;
- 3 attenuation by sediments;

- 4 noise generation at lower frequencies due to seismic activity; and
- 5 backscattering and bottom reverberation.

Items (1)–(3) will be discussed below. Item (4) will be discussed in Chapter 6 and item (5) in Chapter 8. Urick (1982: chapter 11) provided a comprehensive summary of sound reflection and scattering by the sea floor. The single most important physical property that determines the acoustic characteristics of sediments is their porosity.

The return of sound from the sea floor is more complex than from the sea surface for several reasons: (1) the bottom is more variable in composition; (2) the bottom is often stratified (layered) with density and sound speeds (both shear and compressional) varying gradually or abruptly with depth; (3) bottom characteristics (composition and roughness) can vary over relatively short horizontal distances; and (4) sound can propagate through a sedimentary layer and either be reflected back into the water by sub-bottom layers or be refracted back by the large sound-speed gradients in the sediments.

These mechanisms can be incorporated into mathematical models through the specification of appropriate “boundary conditions.” The complexity of these boundary conditions will depend upon the level of known detail concerning the composition and structure of the sea floor, and also to some degree on the sophistication of the mathematical model being used.

The specification of boundary conditions at the sea floor has assumed greater importance due to increased interest in the modeling of sound propagation in shallow-water areas. Such propagation, by definition, is characterized by repeated interactions with the bottom boundary. Acoustic interactions with highly variable sea-floor topographies and bottom compositions often necessitate the inclusion of both compressional- and shear-wave effects, particularly at lower frequencies. A fluid, by definition, cannot support shear stresses. Therefore, in modeling acoustic propagation in an ideal (boundless) fluid layer, only compressional-wave effects need be considered. As an approximation, saturated sediments are sometimes modeled as a fluid layer in which the sound speed is slightly higher than that of the overlying water column. The basement, however, can support both compressional and shear waves, and rigorous modeling of acoustic waves that interact with and propagate through such media must consider both types of wave effects. As an approximation, shear-wave effects are sometimes included in the form of modified attenuation coefficients.

3.5.1 Forward scattering and reflection loss

3.5.1.1 Acoustic interaction with the sea floor

Westwood and Vidmar (1987) summarized pertinent developments in the modeling of acoustic interaction with the sea floor. It is convenient to partition the discussion according to low-frequency and high-frequency

bottom interaction. The transition between low and high frequencies is imprecise but can be considered to occur near 200 Hz.

At low frequencies and low grazing angles, acoustic interaction with the sea floor in deep ocean basins is simple and well understood. The relatively long acoustic wavelengths are insensitive to details of small-scale layering in the sediments. Moreover, for low grazing angles, there is little interaction with the potentially rough substrate interface. Accordingly, the sea floor can be accurately approximated as a horizontally stratified and depth-dependent fluid medium. The major acoustical processes affecting interaction with the sea floor are: (1) reflection and transmission of energy at the water–sediment interface; (2) refraction of energy by the positive sound-speed gradient in the sediments; and (3) attenuation within the sediments. Modeling of this interaction is further enhanced by the availability of established methods for estimating the geoacoustic profile (i.e. sound speed, density and attenuation as functions of depth) of deep-sea sediments, given the sediment type and physiographic province.

In contrast, bottom interaction at high frequencies is not well understood. The relatively short wavelengths are more sensitive to the small-scale sediment layering. These layers are reported to have an important effect on the magnitude and phase of the plane-wave reflection coefficient. Stochastic techniques with which to analyze the effects of the near-surface sediment layering are being developed, but they do not yet incorporate potentially important acoustical processes such as refraction and shear-wave generation. Modeling at high frequencies is further frustrated by the high spatial variability of sediment layering.

The concept of “hidden depths” (Williams, 1976) states that the deep ocean sediment structure well below the ray turning point has no acoustical effect. This concept is important because it focuses attention on those low-frequency processes occurring in the upper regions of the sediments (see Knobles and Vidmar, 1986).

3.5.1.2 *Boundary conditions and modeling*

The ideal forward reflection loss of sound incident on a plane boundary separating two fluids characterized only by sound speed and density was originally developed by Rayleigh (1945: Vol. II, 78). This model is commonly referred to as Rayleigh’s law. In the simplest model incorporating absorption, the bottom can be taken to be a homogeneous absorptive fluid with a plane interface characterized by its density, sound speed and attenuation coefficient. In the case of sedimentary materials, all three of these parameters are affected by the porosity of the sediments.

In underwater acoustics, a common idealized model for the interaction of a point-source field with the sea floor is the so-called Sommerfeld model (after A.N. Sommerfeld). This model consists of an isospeed half-space water column overlying an isospeed half-space bottom. The bottom has a higher

sound speed than the water. Thus, a critical angle exists in the plane-wave reflection coefficient. For large grazing angles, energy is partially reflected and partially transmitted at the water–bottom interface. For small grazing angles, energy is totally reflected back into the water column. Energy incident near the critical angle produces a complex phenomenon known as the lateral, or head, wave (Chin-Bing *et al.*, 1982, 1986; Westwood, 1989a; see also the discussions by Clay and Medwin, 1977: 262–3; Frisk, 1994: 32). This boundary condition is referred to as an “impedance (or Cauchy) boundary.”

Another commonly assumed boundary condition for the sea floor is the homogeneous Neumann bottom-boundary condition. Here, the derivative of the pressure normal to the boundary vanishes (Frisk, 1994: 32–3). There is no phase shift in the reflected wave. For harmonic time dependence and constant density, this condition is also termed a “rigid boundary.”

Hall and Watson (1967) developed an empirical bottom reflection loss expression based largely on the results of Acoustic Meteorological and Oceanographic Survey (AMOS) (Marsh and Schulkin, 1955). Ainslie (1999) demonstrated that much of the complexity of bottom interaction could be represented in simple equations for the reflection coefficient when expressed in the form of a geometric series. Such simplifications can be useful in modeling acoustic propagation in shallow water where repeated interactions with the seabed are expected. Moreover, Ainslie *et al.* (1998b) presented benchmarks for bottom reflection loss versus angle at 1.5, 15 and 150 Hz for four different bottom types, each comprising a layered fluid sediment (representing sand or mud) overlying a uniform solid substrate (representing limestone or basalt). These benchmarks provide ground-truth reference solutions against which the accuracy of other models can be assessed. The benchmarks are calculated using exact analytical solutions where available (primary benchmarks) or they are calculated using a numerical model (secondary benchmark). While the secondary benchmarks are approximate, they provide useful diagnostic information. Robins (1991) developed a FORTRAN program called PARSIFAL to compute plane-wave reflection coefficients from a sediment layer modeled as an inhomogeneous fluid overlying a uniform substrate.

Tindle and Zhang (1992) demonstrated that the acoustic-reflection coefficient for a homogeneous fluid overlying a homogeneous solid with a low shear speed could be approximated by replacing the solid with a fluid having different parameters. Zhang and Tindle (1995) subsequently simplified these expressions by approximating the acoustic-reflection coefficients of solid layers with a fluid described by suitably chosen (proxy) parameters.

Westwood and Vidmar (1987) developed a ray-theoretical approach called CAPARAY for simulating the propagation of broadband signals interacting with a layered ocean bottom. CAPARAY can simulate a time series at a receiver due to an arbitrary source waveform by constructing a frequency domain transfer function from the eigenray characteristics.

3.5.1.3 *Geoacoustic models*

Geoacoustic models of the sea floor more properly account for the propagation of sound in sediments (Anderson and Hampton, 1980a,b; Hamilton, 1980). As summarized by Holland and Brunson (1988), geoacoustic models of marine sediments can be formulated in one of three ways: (1) by empirically relating geoacoustic and geophysical properties of the sediments (e.g. Hamilton, 1980); (2) by using the Biot–Stoll model to relate sediment geoacoustic properties to geophysical properties on the basis of physical principles (Biot, 1956a,b; Stoll, 1974, 1980, 1989); and (3) by using an inversion technique to generate sediment geophysical parameters from bottom loss measurements (e.g. Hovem *et al.*, 1991 (see especially section 3, Modelling and inversion techniques); McCammon, 1991; Rajan, 1992; Dosso *et al.*, 1993; Hovem, 1993; Frisk, 1994).

The Biot–Stoll model (Biot, 1956a,b; Stoll, 1974, 1980, 1989) provides a comprehensive description of the acoustic response of linear, porous materials containing a compressible pore fluid. The model predicts two types of compressional waves and one shear wave. Recent applications in underwater acoustics with references to the key historical literature were provided by Beebe *et al.* (1982) and by Holland and Brunson (1988). Routine operational employment of this model is complicated by the input of more than a dozen geophysical parameters, some of which are difficult to obtain even in laboratory environments.

McCammon (1988) described the development of a geoacoustic approach to bottom interaction, called the thin layer model. This model, which is based on an inversion technique, contains a thin surficial layer, a fluid sediment layer and a reflecting sub-bottom half-space. There are 10 input parameters to this model: sediment density, thickness, sound-speed gradient and curvature, attenuation and attenuation gradient, thin-layer density and thickness, basement reflectivity and water–sediment velocity ratio (Figure 3.11). The model generates bottom-loss curves as a function of grazing angle over the frequency range 50–1,500 Hz. The model makes several assumptions: it relies upon the “hidden depths” concept of Williams (1976), the sediments are isotropic, the roughness of the sediment and basement interfaces and multiple scattering within the layers are neglected and shear wave propagation is ignored.

Sample outputs from this thin layer model are presented in Figure 3.12. A ratio (c_s/c_w) > 1 (where c_s is the sound speed in the upper sediment and c_w is the sound speed at the base of the water column) predicts a critical angle $\theta_c = \cos^{-1}(c_w/c_s)$, below which most of the incident energy is reflected; that is, the bottom loss is nearly zero. By comparison, a ratio (c_s/c_w) < 1 would refract the incident energy into the sediments and result in greater losses at small angles.

A qualitative comparison of bottom loss versus grazing angle for (c_s/c_w) ≥ 1 and (c_s/c_w) < 1 is presented in Figure 3.13. It has been

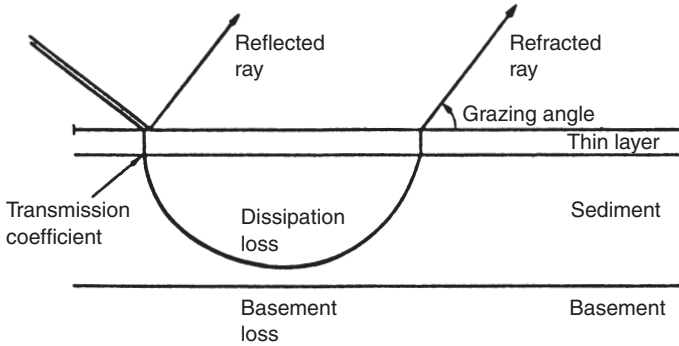


Figure 3.11 Thin layer model for sediment reflected and refracted paths. (McCammon, 1988; *J. Geophys. Res.*, **93**, 2363–9; published by the American Geophysical Union.)

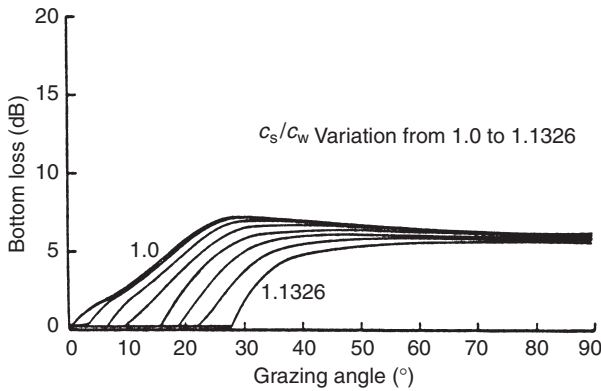


Figure 3.12 Variation of bottom loss (dB) as a function of grazing angle for a frequency of 1,000 Hz. Curves are presented for various values of the ratio of the upper sediment sound speed (c_s) to the sound speed at the base of the water column (c_w). (McCammon, 1988; *J. Geophys. Res.*, **93**, 2363–9; published by the American Geophysical Union.)

demonstrated that high-porosity sediments (e.g. mud and silt) have sound speeds less than that of the overlying water (Urick, 1983: 138–9; Apel, 1987: 386). Qualitatively, then, the comparison presented in Figure 3.13 contrasts the effects of high-porosity [$(c_s/c_w) < 1$] and low-porosity sediments [$(c_s/c_w) \geq 1$].

The bottom loss upgrade (BLUG) model, which was a modular upgrade designed for incorporation into existing propagation models to treat bottom

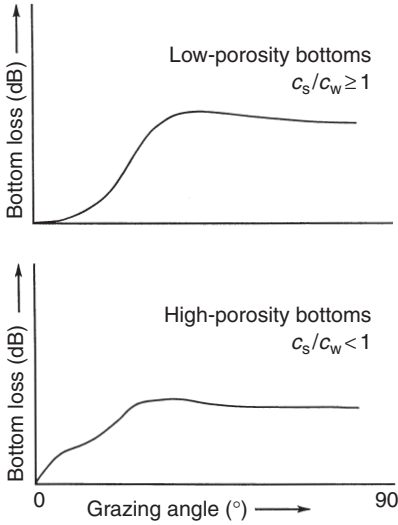


Figure 3.13 Qualitative illustration of bottom loss versus grazing angle for low-porosity and high-porosity bottoms.

loss, was based on a geoacoustic (or inverse) approach. The low-frequency bottom loss (LFBL) model has subsequently replaced the BLUG model.

3.5.2 Interference and frequency effects

Stratification and attendant scattering within the bottom produce pulse distortion, as does reflection at grazing angles less than the critical angle. Zabal *et al.* (1986) developed a simple geometric-acoustic model to predict frequency and angle spreads as well as coherence losses to sonar systems. The sea floor was modeled by homogeneous and isotropic slope statistics. The facets are planar and reflect specularly, thus giving rise to the name “broken mirror” model.

3.5.3 Attenuation by sediments

Sound that propagates within sediment layers is subject to the effects of attenuation. A variety of sediment attenuation units are commonly used in the underwater acoustic and marine seismology communities. The relationships among these units can become very confusing when attempting to enter values into propagation models.

Mathematically, acoustic attenuation (α) is expressed in the exponential form as $e^{-\alpha x}$ using the units of nepers (Np) per unit distance for α . The acoustic attenuation can be converted to the units of decibels per meter

using the relationship:

$$\begin{aligned}\alpha(\text{dB m}^{-1}) &= 20 (\log_{10} e)\alpha(\text{Np m}^{-1}) \\ &= 8.6859\alpha(\text{Np m}^{-1})\end{aligned}$$

Some propagation models require that the attenuation be specified in units of decibels per wavelength (λ):

$$\alpha(\text{dB } \lambda^{-1}) = \lambda(\text{m})\alpha(\text{dB m}^{-1})$$

Another term commonly encountered in underwater acoustic modeling is the attenuation coefficient (k), which is based on the concept that attenuation (α) and frequency (f) are related by a power law:

$$\alpha(\text{dB m}^{-1}) = kf^n$$

where f is measured in kilohertz and n is typically assumed to be unity. Over the frequency range of interest to underwater acousticians, attenuation is approximately linearly proportional to frequency.

A compilation of sediment attenuation measurements made by Hamilton (1980) over a wide frequency range showed that the attenuation in natural, saturated sediments is approximately equal to $0.25f$ (dB m^{-1}) when f is in kilohertz. There was a tendency for the more dense sediments (such as sand) to have a higher attenuation than the less dense, higher-porosity sediments (such as mud). The attenuation in sediments is several orders of magnitude higher than in pure water.

In the Arctic, acoustical parameters of the sea floor and sub-bottom are poorly known. Difficulties in obtaining direct core samples to great depths limit the database from which to extract the parameters needed to determine many of the major acoustical processes in bottom interaction. Estimating these geoacoustical parameters based on data from contiguous areas may not be meaningful since the basic processes of sedimentation at work under the pack ice are unique to that environment. Sedimentation rates are very low, being dominated by material carried by the ice rather than by material of biologic origin, as is the case in more temperate areas. The ice pack may also carry large boulders of glacial origin and deposit them in the Arctic Ocean. The low sedimentation rate leaves the boulders exposed as potential scatterers for acoustic energy over a wide range of frequencies.

3.5.4 Measurements

The standard method for measuring bottom loss is to use pings or explosive pulses and to compare the amplitude, intensity or energy density (integrated intensity) of the bottom pulse with that of the observed or computed pulse traveling via a direct path.

Bottom loss data typically show a loss increasing with angle at low angles, followed by a nearly constant loss extending over a wide range of higher angles (refer back to Figure 3.13). High-porosity bottoms (having a sound speed less than that of the overlying water) tend to have a maximum loss at an angle between 10° and 20° where an angle of intromission (i.e. no reflection, but complete transmission into the bottom) would be expected to occur in the absence of attenuation in the bottom. When narrowband pulses are used, measured losses are often irregular and variable, showing peaks and troughs due to the interference effects of layering in the bottom. Measured data rarely show a sharp critical angle (as would be inferred from the Rayleigh reflection model) because of the existence of attenuation in the bottom (Urlick, 1983: chapter 5).

3.6 Attenuation and absorption in sea water

Sound losses in the ocean can be categorized according to spreading loss and attenuation loss. Spreading loss includes spherical and cylindrical spreading losses in addition to focusing effects. Attenuation loss includes losses due to absorption, leakage out of ducts, scattering and diffraction. Urlick (1982: chapter 5) summarized the relevant literature pertaining to this subject.

Absorption describes those effects in the ocean in which a portion of the sound intensity is lost through conversion to heat. Field measurements of the absorption coefficient (α), typically expressed in units of decibels per kilometer, span the frequency range 20 Hz to 60 kHz. In practice, absorption loss (in dB) is computed as the product of α and range (r) using self-consistent units for range.

The dependence of α on frequency is complicated, reflecting the effects of different processes or mechanisms operating over different frequency ranges. The equation developed by Thorp (1967) is probably the best known and is valid at frequencies below 50 kHz:

$$\alpha = 1.0936 \left[\frac{0.1f^2}{1+f^2} + \frac{40f^2}{4100+f^2} \right] \quad (3.8)$$

where α is the absorption coefficient (dB km^{-1}) and f the frequency (kHz). The factor 1.0936 converts the original formula from units of dB kyd^{-1} to dB km^{-1} . More recent formulae for the absorption coefficient have been described by Fisher and Simmons (1977) and by Francois and Garrison (1982a,b). Ainslie and McColm (1998) simplified a version of the Francois–Garrison equations for viscous and chemical absorption in sea water by making explicit the relationships among acoustic frequency, depth, sea-water absorption, pH, temperature and salinity. An older dataset that has received renewed attention is that reported by Skretting and Leroy (1971), which included measurements of sound attenuation in the western Mediterranean Sea.

In practice, the effects of absorption and attenuation are considered jointly. Then, the frequency dependence can conveniently be segregated into four distinct frequency regions over which the controlling mechanisms can be readily identified. These regions are (in order of ascending frequency): (1) large-scale scattering or leakage; (2) boric acid relaxation; (3) magnesium sulfate relaxation; and (4) viscosity. Fisher and Simmons (1977) summarized these effects graphically (Figure 3.14). Research conducted by

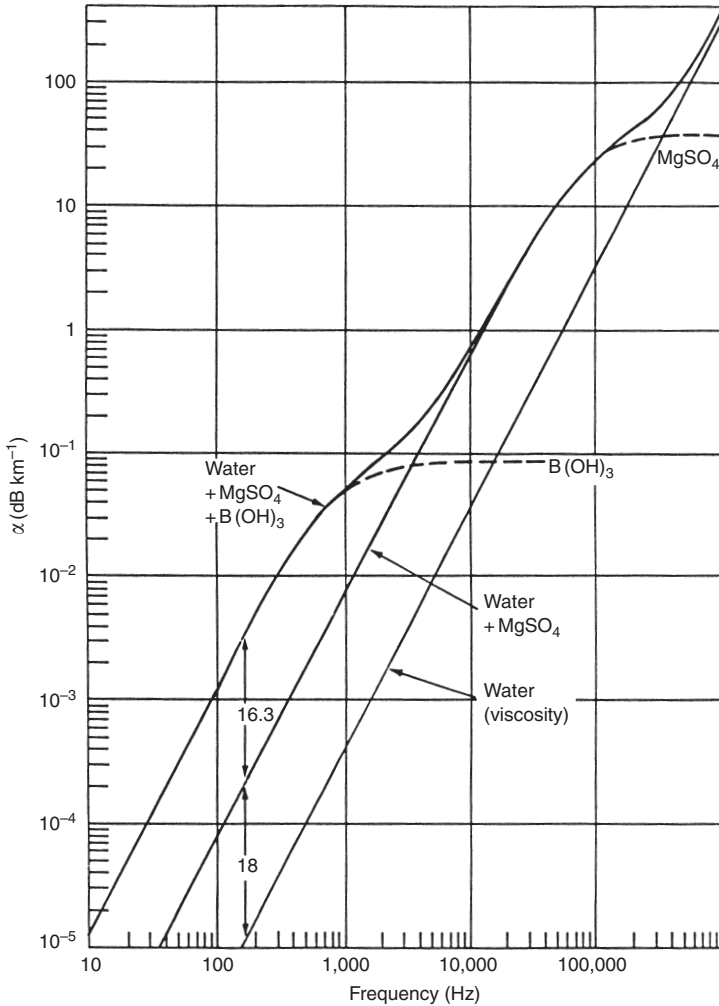


Figure 3.14 Absorption coefficients for sea water at a temperature of 4°C at the sea surface. Dashed lines indicate contributing absorption rates due to relaxation processes (Fisher and Simmons, 1977).

other investigators provides regional formulae for absorption and attenuation (Skretting and Leroy, 1971; Kibblewhite *et al.*, 1976; Mellen *et al.*, 1987a–c; Richards, 1998). Absorption is regionally dependent mainly due to the pH dependence of the boric acid relaxation. Attenuation due to turbidity and bubbles was discussed in Section 3.4.3.

The Applied Physics Laboratory, University of Washington (1994), documented high-frequency (approximately 10–100 kHz) acoustic models with potential application to sonar simulation and sonar system design efforts. These models treat volumetric sound speed, absorption and backscattering; boundary backscatter and forward loss for the sea surface and the sea floor; ambient-noise sources and levels and Arctic attenuation and under-ice losses.

3.7 Surface ducts

Sound travels to long distances in the ocean by various forms of ducted propagation. When sound travels in a duct, it is prevented from spreading in depth and remains confined between the boundaries of the duct. The surface duct is a zone bounded above by the sea surface and below by the SLD. Within the surface duct, sound rays are alternatively refracted and reflected. A surface duct exists when the negative temperature gradient within it does not exceed a value determined by the effect of pressure on sound speed (refer to Chapter 2). Specifically, the surface duct is characterized by a positive sound-speed gradient. For example, in isothermal water (and ignoring the effects of salinity), the pressure effect will produce a positive sound-speed gradient of 0.017 s^{-1} .

The surface duct is the acoustical equivalent of the oceanographic mixed layer, although they are defined differently. While the SLD is normally defined in terms of the sound-speed gradient, the MLD is defined in terms of temperature, or more precisely, in terms of density (which is a function of temperature, salinity and pressure). The mixed layer is a quasi-isothermal layer of water created by wind-wave action and thermohaline convection. Algorithms for the prediction of surface duct propagation will be discussed in Chapter 5. These algorithms use the depth of the mixed layer as an input variable.

3.7.1 *Mixed-layer distribution*

Oceanographers have extensively studied the dynamics of the mixed layer. Variations in the temperature and depth of the mixed layer are closely related to the exchange of heat and mass across the air–sea interface and are thus of interest to scientists engaged in studies of the global climate. Lamb (1984) presented bimonthly charts of the mean mixed layer depths for the North and tropical Atlantic oceans. Bathen (1972) presented monthly charts of MLDs for the North Pacific Ocean.

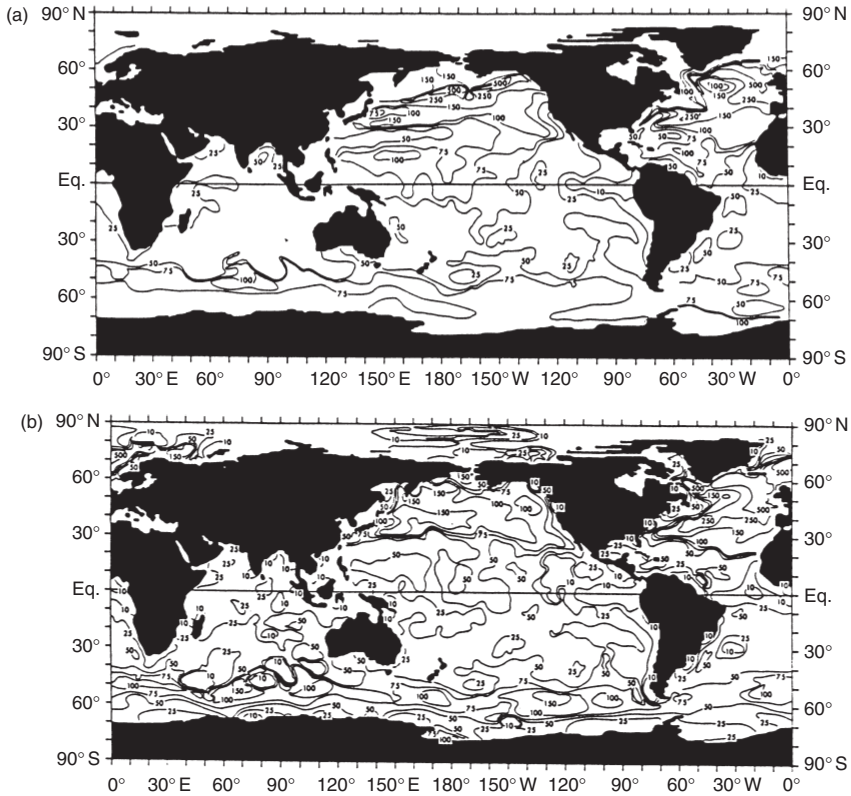


Figure 3.15 Mixed layer depths (m) for March based on (a) a temperature criterion of 0.5°C and (b) a density criterion of $0.125 \times 10^{-3} \text{ g cm}^{-3}$ (Levitus, 1982).

Levitus (1982) presented charts of MLDs on a global basis. Distributions of MLDs were calculated using both a temperature criterion and a density criterion. The temperature criterion was based on a temperature difference of 0.5°C between the surface and the depth referred to as the MLD. The density criterion was based on a difference of $0.125 \times 10^{-3} \text{ g cm}^{-3}$ between the surface and the depth of the mixed layer. The use of the density criterion recognized the importance of salinity in determining the stability of the mixed layer and hence, from an acoustics viewpoint, the true depth of the sonic layer. For example, in sub-arctic regions, isothermal conditions (or even temperature profiles with inversions) combine with a salinity profile that stabilizes the water column to control the depth of mixing. Mixed layer depths for the months of March and September are presented in Figures 3.15 and 3.16, respectively, comparing the global distributions resulting from both the temperature and the density criteria.

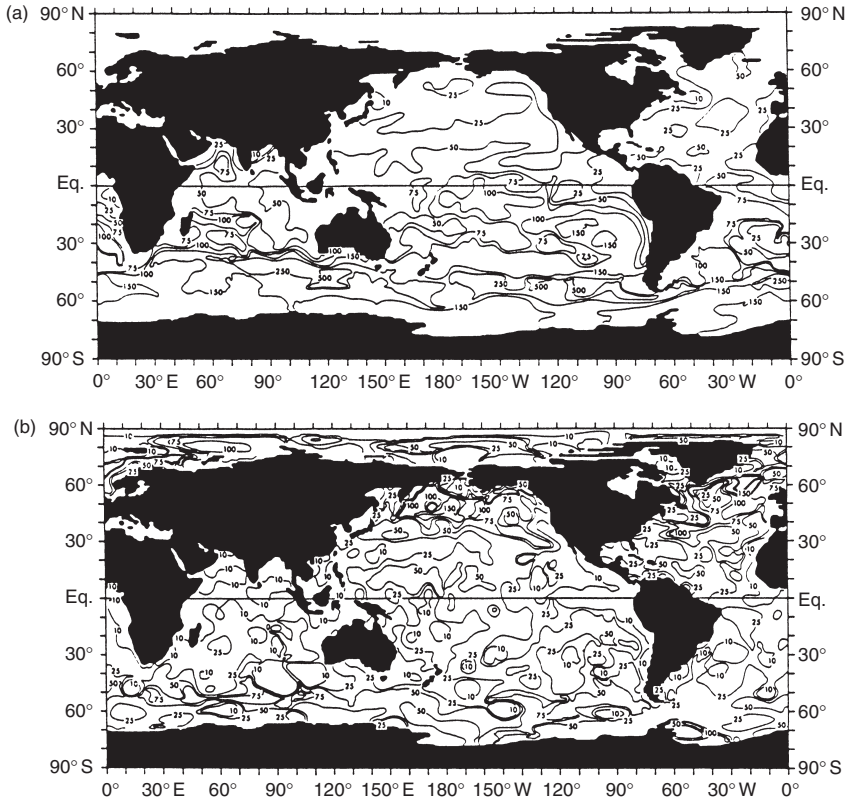


Figure 3.16 Mixed layer depths (m) for September based on (a) a temperature criterion of 0.5°C and (b) a density criterion of $0.125 \times 10^{-3} \text{ g cm}^{-3}$ (Levitus, 1982).

Traditionally, it has been assumed that the mixed layer is the vertical extent of the turbulent boundary layer. Peters and Gregg (1987) have pointed out that the turbulence initiated by the exchanges of energy, buoyancy or momentum across the air–sea interface may actually penetrate the lower boundary of the mixed layer as defined by the previous criteria. Thus, precise discussions of the mixed layer are often frustrated by imprecise terminology.

Some regional examples will serve to clarify features of the mixed layer as evidenced by the thermal structure of the water column. For these examples, the continental shelf region off the Texas–Louisiana coast in the Gulf of Mexico (Etter and Cochrane, 1975) will be explored. Figure 3.17 presents the annual variation of water temperature down to 225 m. In this graphical representation, the seasonal variation of the depth of the mixed layer is portrayed as a uniform layer of temperature versus depth. In January,

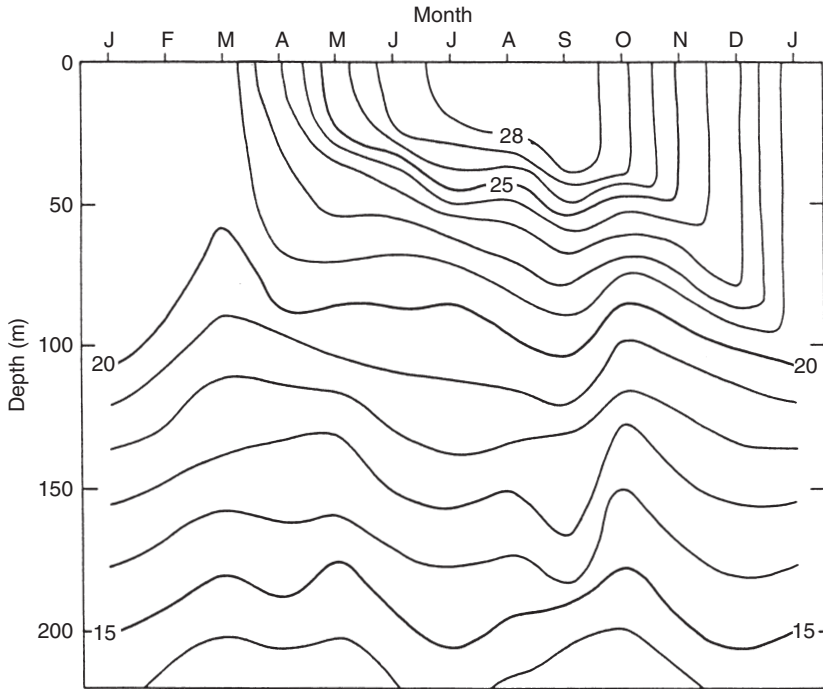


Figure 3.17 Temperature contours ($^{\circ}\text{C}$) for a region of the Texas–Louisiana continental shelf in the Gulf of Mexico (Etter and Cochrane, 1975).

for example, the mixed layer is approximately 100 m deep while in August the MLD is seen to be shallow, about 25 m. These variations are further illustrated in Figures 3.18 and 3.19, which are vertical sections across the shelf. In winter (February), for example, the isotherms tend to be vertically oriented, evidencing strong mixing and vertical (versus the more typical horizontal) stratification. In summer (July), however, the isotherms tend to be more horizontal, the result of weak mixing, with attendant horizontal stratification.

3.7.2 General propagation features

A computer-generated ray diagram for a source in a typical mixed layer is shown in Figure 3.20. Under the conditions for which the diagram was drawn, the ray leaving the source at an angle of 1.76° becomes horizontal at the base of the mixed layer. Rays leaving the source at shallower angles remain in the layer, and rays leaving the source at steeper angles are refracted downward to greater depths. A shadow zone is produced beneath the layer at ranges beyond the immediate sound field. The shadow zone is not completely

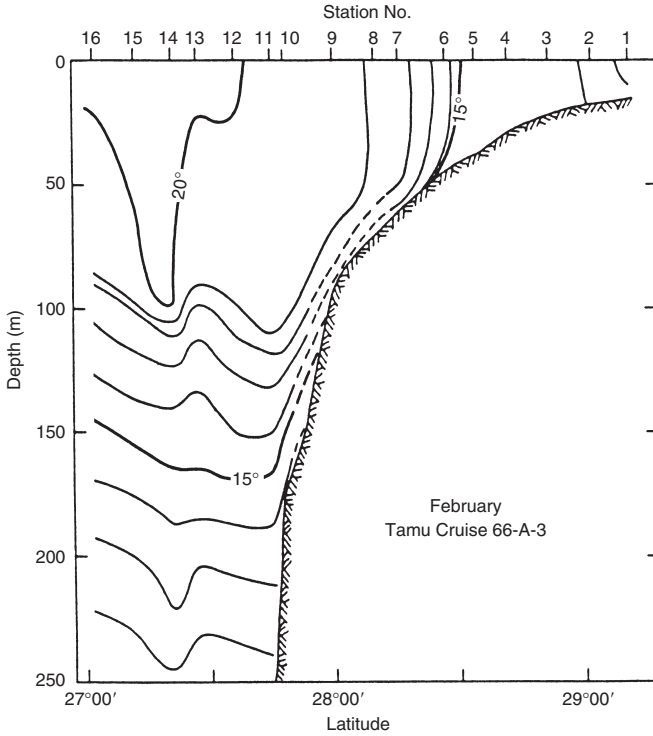


Figure 3.18 Vertical section of water temperatures ($^{\circ}\text{C}$) over the Texas-Louisiana continental shelf in the Gulf of Mexico in February (Etter and Cochrane, 1975).

devoid of acoustic energy since it is insonified by diffraction and by sound scattered from the sea surface. The rate of sound leakage out of the surface duct can be quantified in terms of an empirical leakage coefficient (α_L), which expresses the attenuation (dB km^{-1}) of sound trapped within the duct. This leakage coefficient varies with the surface roughness (wave height), duct thickness (SLD or MLD), sound-speed gradient below the layer and acoustic frequency (Urlick, 1983: 153–4).

Over short distances, or even at a fixed location over time, the thickness of the mixed layer may vary because of internal waves. These waves propagate along the density discontinuity at the base of the mixed layer (Figure 3.21). Internal waves complicate the propagation of underwater sound by causing variations in TL over short distances. Fluctuations of echoes between a source and receiver separated by the MLD or SLD are attributable in part to the existence of internal waves.

Urlick (1982: chapter 6) reviewed the available open-literature algorithms for estimating TL in the surface duct. In particular, an analysis of the

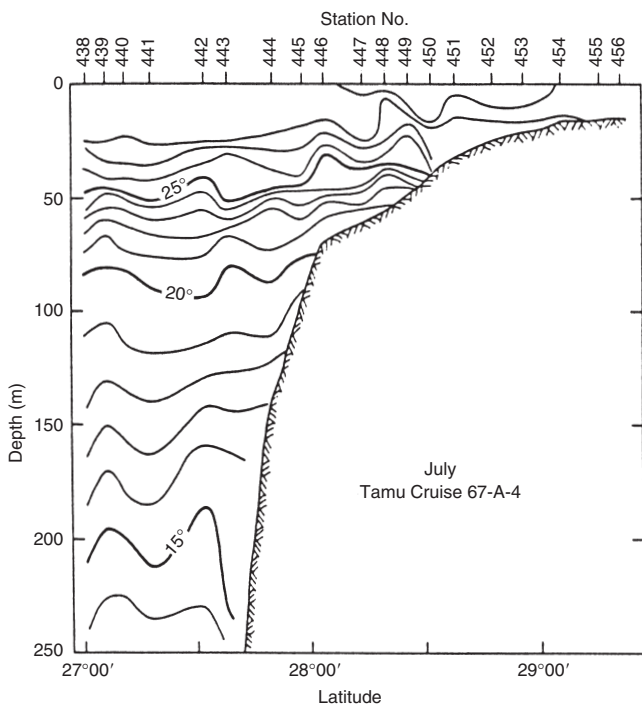


Figure 3.19 Vertical section of water temperatures ($^{\circ}\text{C}$) over the Texas-Louisiana continental shelf in the Gulf of Mexico in July (Etter and Cochrane, 1975).

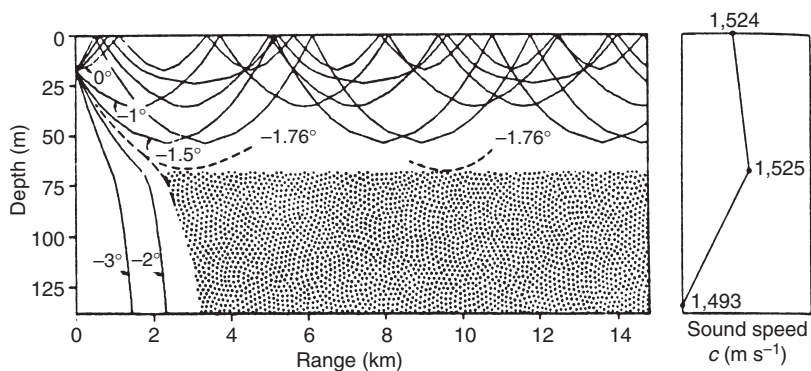


Figure 3.20 Ray diagram for a sound source located at a depth of 16 m, showing propagation and trapping of energy in the surface duct, with a shadow zone below 60 m, for the sound-speed profile shown at the right. (Urlick, 1983; *Principles of Underwater Sound*, 3rd edn; reproduced with permission of McGraw-Hill Publishing Company.)

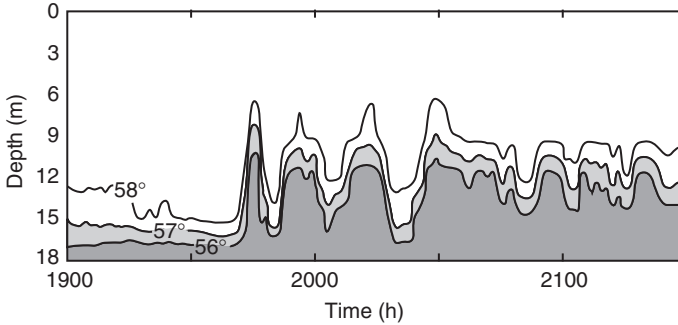


Figure 3.21 Fluctuations in the depth of the mixed layer caused by the passage of internal waves. Water temperature is measured in °F. The MLD is defined by the 58°F isotherm. (LaFond, 1962; *The Sea*, Vol. 1, 731–51; reprinted by permission of John Wiley & Sons, Inc., all rights reserved.)

extensive data set collected during the AMOS program (Marsh and Schulkin, 1955) has been used to characterize TL in the surface duct in the frequency range 2–8 kHz. Graphical results derived from Condron *et al.* (1955) are summarized in Figures 3.22 and 3.23. These figures demonstrate the importance of source–receiver geometry (relative depths) in surface duct propagation, particularly in those cases where the source and receiver are situated on opposite sides of the layer depth (referred to as cross-layer geometries).

3.7.3 Low-frequency cutoff

At very low frequencies, sound ceases to be trapped in the surface duct. The maximum wavelength for duct transmission may be derived from the theory of radio propagation in ground-based radio ducts to be (Kerr, 1951: 20)

$$\lambda_{\max} = \frac{8\sqrt{2}}{3} \int_0^H \sqrt{n(z) - n(H)} dz \quad (3.9)$$

where $n(z)$ is the index of refraction at any depth z in the duct and $n(H)$ the index of refraction at the base of the duct. Using values of sound speed and sound-speed gradient appropriate for sound propagation in the mixed layer, Equation (3.9) reduces to

$$\lambda_{\max} = 8.51 \times 10^{-3} H^{3/2} \quad (3.10)$$

for the maximum wavelength (λ_{\max}) in meters trapped in a mixed-layer duct of depth H in meters. For example, a mixed layer 30 m thick would trap a maximum wavelength of 1.4 m, corresponding to a frequency of

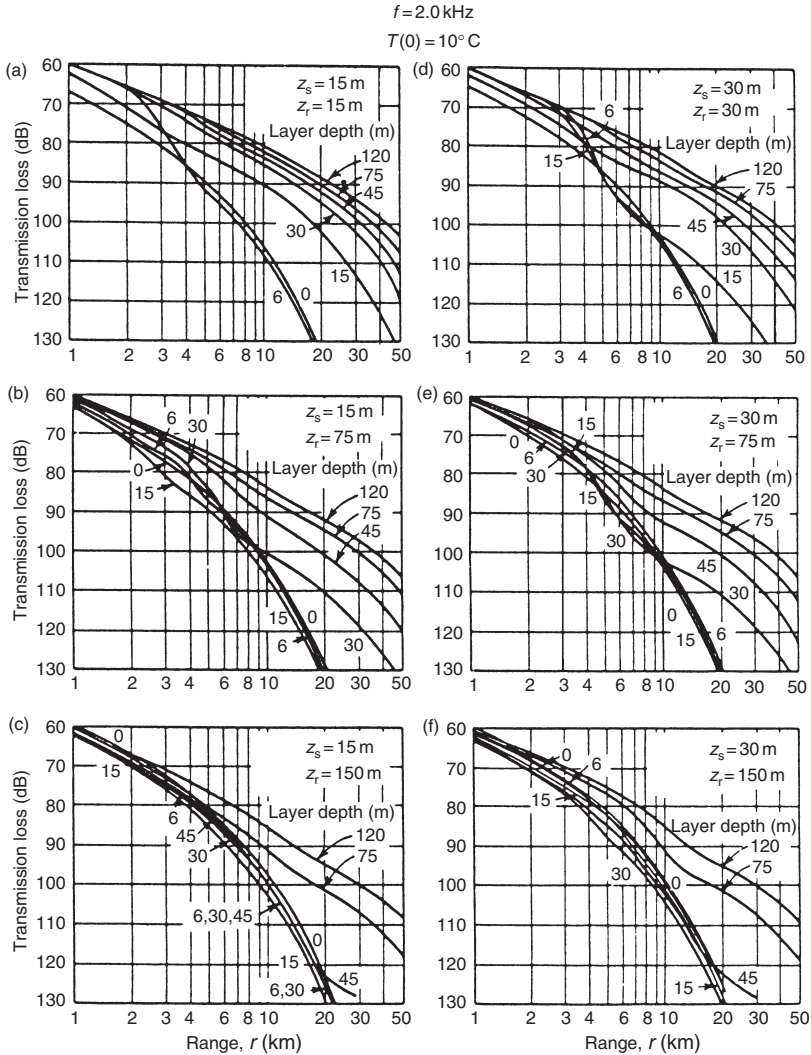


Figure 3.22 Surface duct TL estimates generated from the AMOS empirical relationships at a frequency of 2 kHz for various combinations of mixed layer depths, source depths (z_s) and receiver depths (z_r) (adapted from Condron *et al.*, 1955, by Apel, 1987).

approximately 1,070 Hz (assuming that the sound speed is $1,500 \text{ m s}^{-1}$). This relationship is illustrated in Figure 3.24 under the assumption that the speed of sound is fixed at $1,500 \text{ m s}^{-1}$. Although this does not represent a sharp cutoff, wavelengths much longer (or frequencies much lower)

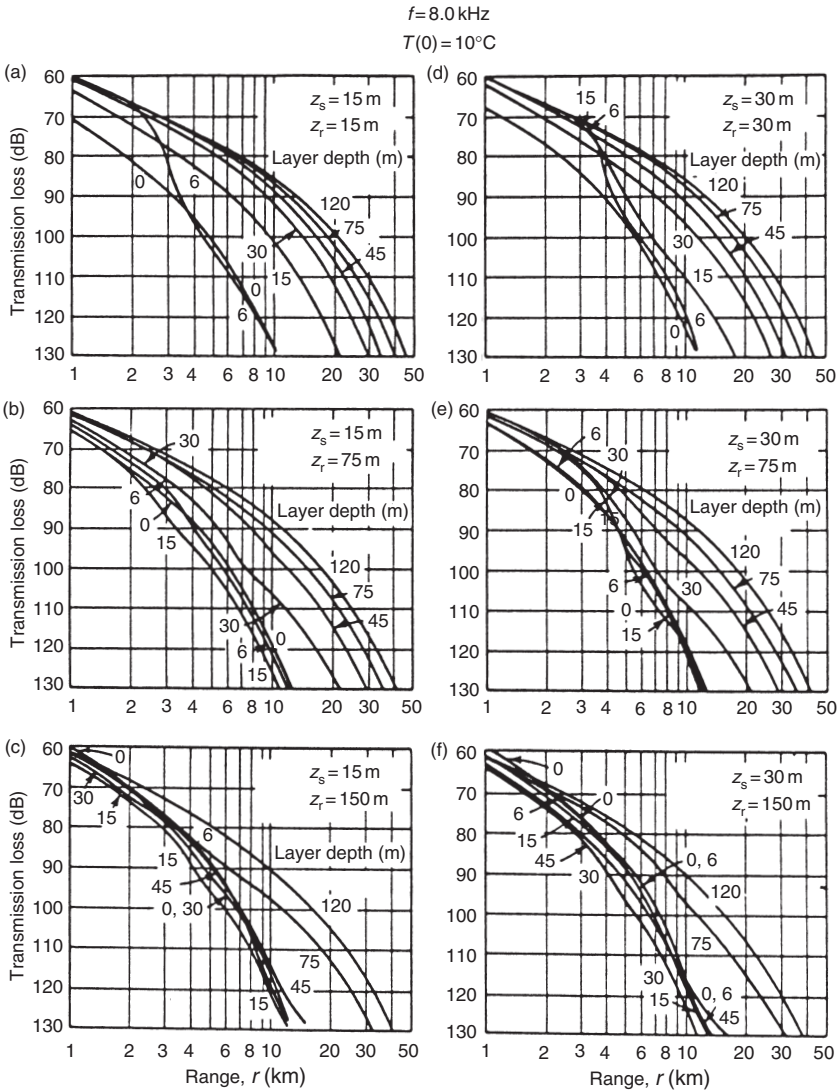


Figure 3.23 As in Figure 3.22, except at a frequency of 8 kHz (adapted from Condron *et al.*, 1955 by Apel, 1987).

than this are strongly attenuated. Conversely, wavelengths much shorter (or frequencies much higher) suffer losses due to absorption and leakage. Thus, for a mixed layer of a given thickness, it follows that there is an optimum frequency for propagation at which the loss of sound is a minimum (Figure 3.25).

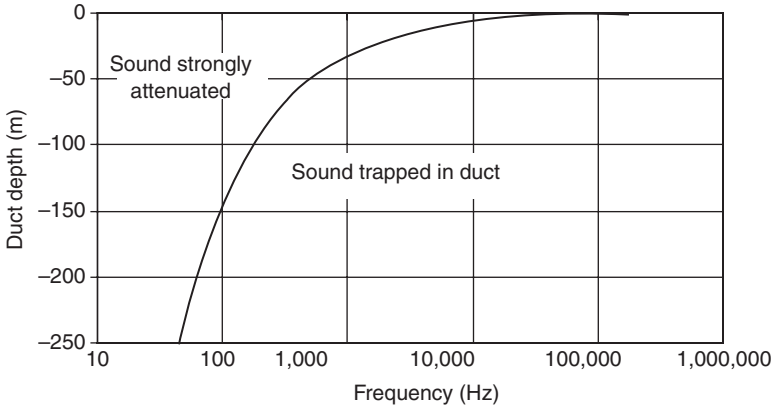


Figure 3.24 Cutoff frequency calculated according to Equation (3.10) assuming a sound speed of $1,500 \text{ m s}^{-1}$.

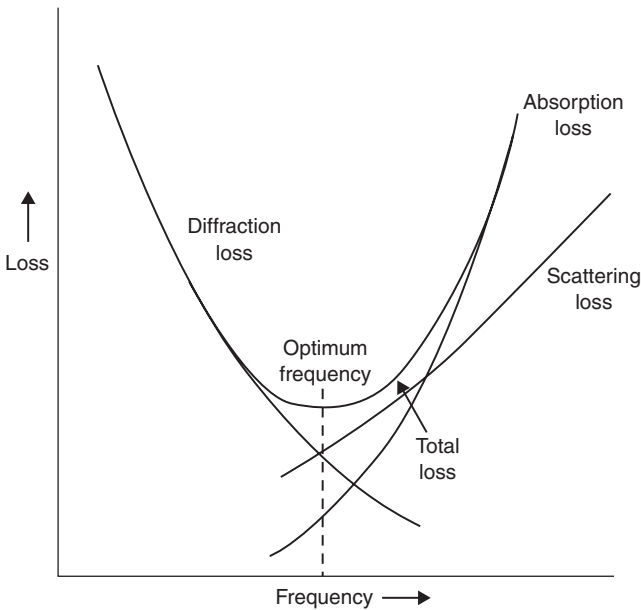


Figure 3.25 Loss to a fixed range in a surface duct. The optimum frequency is that at which the total loss is a minimum (Urick, 1979).

3.8 Deep-sound channel

The deep-sound channel, sometimes referred to as the sound fixing and ranging (SOFAR) channel, is a consequence of the sound-speed profile

characteristic of the deep ocean (see Section 2.3). This profile has a sound-speed minimum at a depth that varies from about 1,000 m at mid-latitudes to near the surface in polar regions. This sound-speed minimum causes the ocean to act like a lens: above and below the minimum, the sound-speed gradient continually refracts the sound rays back toward the depth of minimum sound speed. This depth is termed the axis of the sound channel (refer back to Figure 2.7). A portion of the acoustic energy originating in the deep-sound channel thus remains within the channel and encounters no losses by reflection from the sea surface or the sea floor. Sound in this channel will be diminished by the effects of absorption. The properties of the deep-sound channel were first investigated by Ewing and Worzel (1948). The exceptional ducting characteristics of this channel have been used to advantage by oceanographers in the design and conduct of acoustic tomography experiments (see Section 5.6.9).

In terms of the sound-speed profile, the upper and lower limits of the channel are defined by the two (conjugate) depths of equal maximum sound speed in the profile between which a minimum exists. In Figure 3.26, these limits of the deep-sound channel are the depths A and A' ; the depth A' is

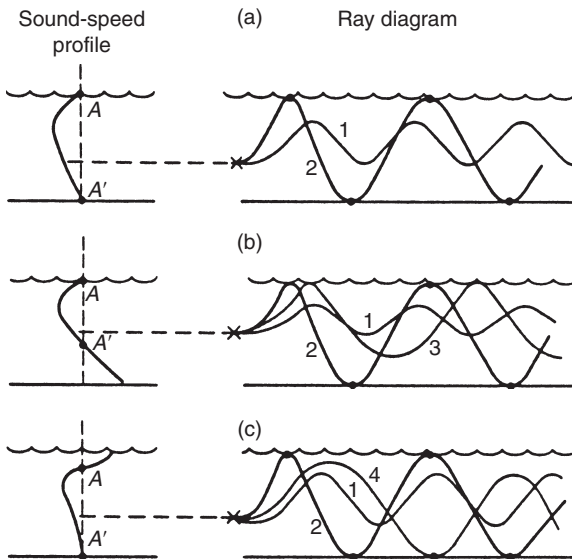


Figure 3.26 Ray paths for a source in the deep-sound channel. In (a), the channel extends between the sea surface and the sea floor. It is cut off by the sea surface in (b) and by the sea floor in (c). The depth A' is referred to as the critical depth. (Urlick, 1983; *Principles of Underwater Sound*, 3rd edn; reproduced with permission of McGraw-Hill Publishing Company.)

referred to as the critical (or conjugate) depth. Different ray paths from a source in the channel exist depending on whether or not the channel extends to the sea surface or to the sea floor. In Figure 3.26(a), the sound speeds at the sea surface and sea floor are the same. All depths in the water column then lie within the channel, and sound is propagated via paths that are either refracted (path 1) or reflected (path 2). In Figure 3.26(b), the upper limit of the deep-sound channel lies at the sea surface (which may happen at high latitudes). Here, in addition to paths 1 and 2, refracted–surface-reflected (RSR) paths occur (path 3) involving losses at levels intermediate to those suffered by paths 1 and 2. In Figure 3.26(c), the channel is cut off by the sea floor and refracted–bottom-reflected (RBR) paths exist (path 4). The entirely refracted paths and the low TLs associated with these paths do not exist when the source or the receiver is outside the depth limits A and A' of the channel.

3.9 Convergence zones

Urick (1983: 163–8) described the formation of convergence zones in the ocean (Figure 3.26). Specifically, there must exist a refracted ray that leaves the source horizontally. If this ray is reflected at either the sea surface or the sea floor (ray types 2 or 4 in Figure 3.26), then the required caustic pattern is destroyed and no convergence is possible. Another requirement for convergence is that the water depth must be greater than the critical depth (depth A' in Figure 3.26) in order to allow the rays traveling downward to refract without striking the bottom and to later converge downrange (ray type 3). There must also be a depth excess (i.e. a vertical separation between the critical depth and the bottom) on the order of a few hundred meters. For water depths less than critical (Figure 3.26(a) and (c)), the rays that would converge if the water were deeper are cut off by the bottom and become bottom-reflected without convergence.

Because the deep waters of the ocean are of a fairly uniform low temperature (near 1°C), the speed of sound at great depths is largely a function of pressure only. Near the surface, however, the speed of sound is determined largely by the water temperature. Thus, water temperature near the sea surface and the water depth in any particular area will largely determine whether sufficient depth excess exists and therefore whether or not a CZ will occur. Charts of surface temperature and water depth can then be used as basic prediction tools for ascertaining the existence of CZs. A convergence-zone-range slide rule (TACAID 6–10) was developed in 1973 by the Naval Underwater Systems Center based on an analysis of oceanographic data performed by E.M. Podeszwa. This slide rule could be used in the North Atlantic and North Pacific oceans, and the Mediterranean, Norwegian and Caribbean seas to determine CZ ranges.

In the North Atlantic Ocean, CZs are seen to appear at intervals of approximately 35 nm (65 km), with zone widths of about 2 nm (4 km). TL

is significantly lower than spherical spreading within the zones, but significantly higher than spherical spreading between zones. Successive CZs get wider with increasing range until, at a range beyond a few hundred nautical miles, they coalesce. Beyond this range, TL increases smoothly with range and is characterized by cylindrical spreading plus attenuation.

3.10 Reliable acoustic path

When a source is located at the critical depth (depth A' in Figure 3.26), and provided sufficient depth excess exists, propagation to moderate ranges can take place via the so-called reliable acoustic path (RAP), as illustrated in Figure 3.5(f). Such paths are termed “reliable” because they are sensitive neither to near-surface effects nor to bottom interaction.

3.11 Shallow-water ducts

There are two definitions of shallow water: hypsometric and acoustic. The hypsometric definition is based on the fact that most continents have continental shelves bordered by the 200 m bathymetric contour, beyond which the bottom generally falls off rapidly into deep water. Therefore, shallow water is often taken to mean continental shelf waters shallower than 200 m. Using this definition, shallow water represents about 7.5 percent of the total ocean area.

Acoustically, shallow-water conditions exist whenever the propagation is characterized by numerous encounters with both the sea surface and the sea floor. By this definition, some hypsometrically shallow-water areas are acoustically deep. Alternatively, the deep ocean may be considered shallow when low-frequency, long-range propagation conditions are achieved through repeated interactions with the sea surface and the sea floor.

Shallow-water regions are distinguished from deep-water regions by the relatively greater role played in shallow water by the reflecting and scattering boundaries. Also, differences from one shallow-water region to another are primarily driven by differences in the structure and composition of the sea floor. Thus, aside from water depth, the sea floor is perhaps the most important part of the marine environment that distinguishes shallow-water propagation from deep-water propagation.

The most common shallow-water bottom sediments are sand, silt and mud (see Chapter 2), with compressional sound speeds greater than that of the overlying water. Sediments are also characterized by shear waves, which are not present in the water column. Acoustic energy that strikes the sea floor at sufficiently small grazing angles is nearly totally reflected back into the water column. This results in a slightly lossy duct with TL approximately characterized by cylindrical spreading within the frequency range 100–1,500 Hz. At low frequencies, the acoustic field can extend into

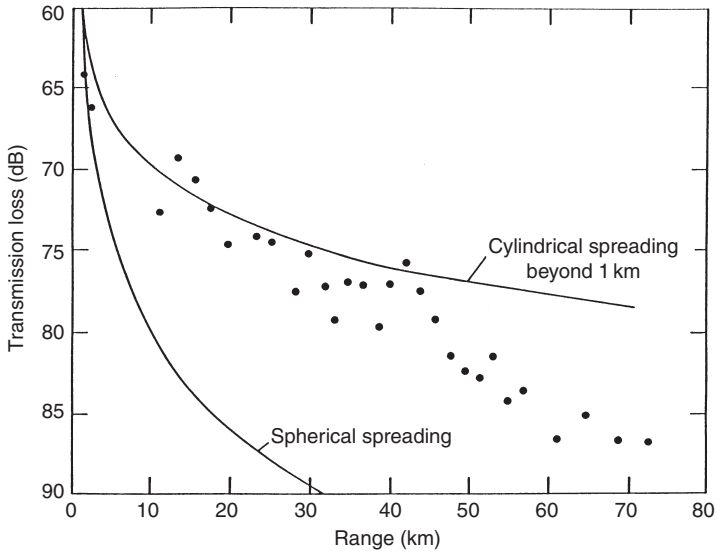


Figure 3.27 Example of TL data in shallow water illustrating the cylindrical spreading associated with energy trapping by the waveguide. Data are for the one-third-octave band centered at 200 Hz (Eller, 1984b).

the bottom with sound being returned to the water by subbottom reflection or refraction (Eller, 1984b).

The tendency toward cylindrical spreading is illustrated in Figure 3.27, which shows one-third-octave-band TL data at a center frequency of 200 Hz as a function of range. An omnidirectional hydrophone was located at a depth of 91 m in water approximately 210 m deep. The sources were set at a depth of 91 m on a track along which the water depth increased gradually from about 220 to about 300 m. The sound-speed profile was nearly constant along the track, and the bottom sediments were reported to be silty-sand near the beginning range and sand-silt-clay at greater ranges. Figure 3.27 also presents reference curves depicting spherical and cylindrical spreading (beyond 1 km). The acoustic energy is effectively trapped in the shallow-water duct at ranges less than about 40 km, beyond which the TL drops below the reference curve for cylindrical spreading.

3.12 Arctic half-channel

The acoustic waveguide in the Arctic is determined by the geometry of the ocean (type of ice cover and water depth) and by a positive-gradient sound-speed profile (sound speed increases with increasing depth). This waveguide forms a half-channel, that is, the lower half of the deep-sound channel, with the axis of the sound channel located at the sea surface.

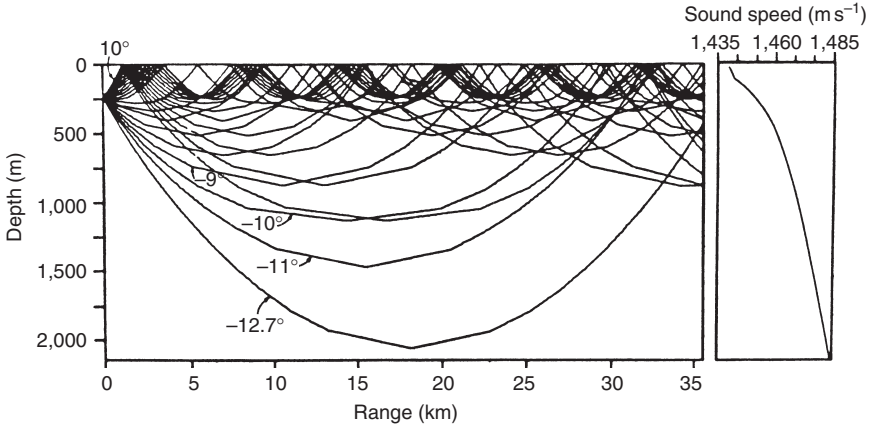


Figure 3.28 Typical sound-speed profile and corresponding ray diagram for sound propagation in the Arctic region (Urlick, 1979).

The continuously upward-refracting propagation conditions that generally prevail in Arctic waters (as demonstrated by the ray trace in Figure 3.28) cause repeated interactions with the ice canopy and tend to create a low-pass filter, favoring the propagation of low-frequency (<300 Hz) signals. The situation is further complicated when the geometry of the sea floor and the acoustic wavelength combine to yield shallow-water conditions with the attendant increase in bottom interaction opportunities.

Measurements of TL in the Arctic are limited since access to this region has historically been restricted to the spring season when conditions are favorable for manned camps. Consequently, there is a relatively poor understanding of the seasonal variability based on historical data. This situation has gradually improved with the introduction of autonomous sensors that can be deployed through the ice from aircraft throughout the year.

One of the principal characteristics of acoustic propagation measurements under an ice cover is the rapid increase in TL with range at frequencies above about 30 Hz (the low-pass filter effect). The loss mechanism has been attributed primarily to scattering at the ice–water interface. Other possible mechanisms include dissipative processes in the ice canopy, conversion of waterborne energy into energy traveling in and confined to the ice canopy and increased absorption in the water column.

Buck (1968) summarized available Arctic TL data (Figure 3.29). These curves give the average measured TL in the Arctic Ocean at a number of frequencies. The standard deviation of the various data points from the smooth curve is stated for each frequency. The dashed line shows spherical spreading ($TL = 20 \log_{10} r$, where r is the range measured in meters). It is

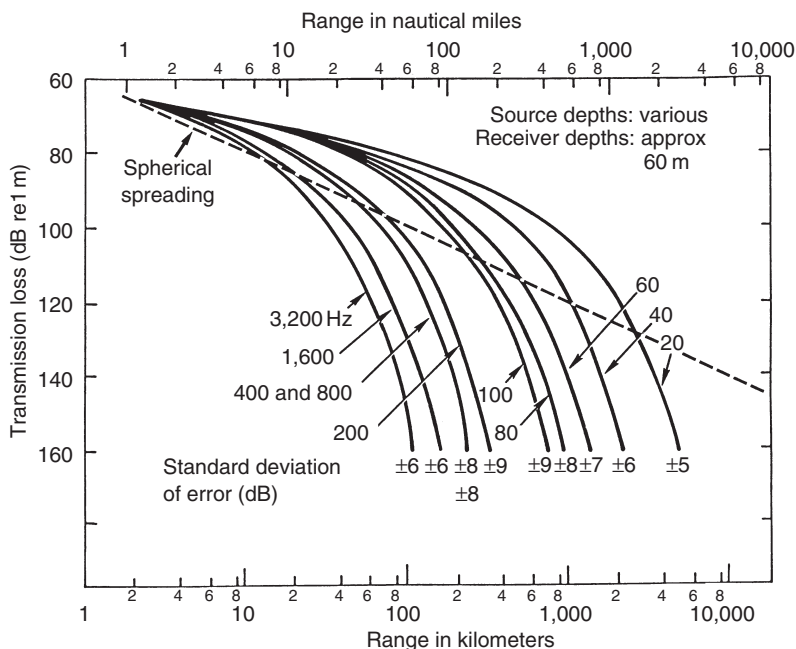


Figure 3.29 Average curves of Arctic TL versus range based on measured data. Note that range is plotted on a log scale (Buck, 1968).

evident that sound propagation in the Arctic degrades rapidly with increasing frequency, particularly above about 30 Hz. At short-to-moderate ranges, ducting improves propagation relative to spherical spreading. At long ranges, repeated encounters with the under-ice surface degrade propagation.

3.13 Coherence

Coherence is defined as a measure of the phase and amplitude relationships between sets of acoustic waves. In the ocean, which is characterized by both temporal and spatial variations, the effects of the medium on small-amplitude wave propagation can be described in terms of coherence time, coherence bandwidth, spatial coherence and angular coherence. As described by Ziomek (1985: chapter 7), for example, this information can be obtained from the generalized coherence (or autocorrelation) function.

Temporal coherence (fluctuations) refers to changes in a received signal (relative to a steady signal) over a period of time. Spatial coherence refers to the changes in the signals received at different locations in the ocean at a given time. Urick (1982: chapters 12 and 13) discussed additional aspects of temporal and spatial coherence.

98 *Propagation I: observations and physical models*

Signal fluctuations can be caused by a number of physical processes including:

- 1 source or receiver motion;
- 2 oceanic fine-scale features;
- 3 sea-surface motion (waves and tides);
- 4 scatterers;
- 5 internal waves and internal tides; and
- 6 ocean currents and eddies.

4 Propagation II

Mathematical models (Part One)

4.1 Background

Chapter 1 described a framework within which all underwater acoustic models could be categorized. It was shown that propagation models formed the foundation for the category of models classified as basic acoustic models. In turn, basic acoustic models supported the more specialized category of sonar performance models. Propagation models are the most common (and thus the most numerous) type of underwater acoustic models in use. Their application is fundamental to the solution of all types of sonar performance problems.

Chapter 3 described the observations and physical (physics-based) models that are available to support the mathematical modeling of sound in the sea. Conceptually, it was convenient to separate propagation phenomena into the categories of boundary interactions, volumetric effects and propagation paths. A similar approach will be adopted here in the description of the mathematical models.

The mathematical models will first be distinguished on the basis of their theoretical treatment of volumetric propagation. Then, as appropriate, further distinctions will be made according to specification of boundary conditions and the treatment of secondary volumetric effects such as attenuation due to absorption, turbidity and bubbles. These secondary effects are generally accommodated by using the physical models described in Chapter 3. Special propagation paths such as surface ducts, shallow water and Arctic half-channels will be discussed in Chapter 5.

The various physical and mathematical models all have inherent limitations in their applicability. These limitations are usually manifested as restrictions in the frequency range or in specification of the problem geometry. Such limitations are collectively referred to as “domains of applicability,” and vary from model to model. Most problems encountered in model usage involve some violation of these domains. In other words, the models are misapplied in practice. Therefore, considerable emphasis is placed on these restrictions and on the assumptions that ultimately give rise to them. Finally, model selection criteria are provided to guide potential

users to those models most appropriate to their needs. Comprehensive summaries identify the available models and associated documentation. Brief descriptions have been provided for each model.

The emphasis in this chapter, as throughout the book, is placed on sonar (versus seismic) applications. Reviews of mathematical models of seismo-acoustic propagation in the ocean have been provided by Tango (1988) and by Schmidt (1991). Tango (1988) placed particular emphasis on the very-low-frequency (VLF) band.

4.2 Theoretical basis for propagation modeling

The theoretical basis underlying all mathematical models of acoustic propagation is the wave equation. The earliest attempts at modeling sound propagation in the sea were motivated by practical problems in predicting sonar performance in support of anti-submarine warfare (ASW) operations during the Second World War. These early models used ray-tracing techniques derived from the wave equation to map those rays defining the major propagation paths supported by the prevailing marine environment. These paths could then be used to predict the corresponding sonar detection zones. This approach was a forerunner to the family of techniques now referred to as ray-theoretical solutions.

An alternative approach, referred to as wave-theoretical solutions, was first reported by Pekeris (1948), who used the normal-mode solution of the wave equation to explain the propagation of explosively generated sound in shallow water.

As modeling technology matured over the intervening decades, the attendant sophistication has complicated the simple categorization of ray versus wave models. The terminology is still useful in distinguishing those models based principally on ray-tracing techniques from those using some form of numerical integration of the wave equation. Occasionally, a mixture of these two approaches is used to capitalize on the strengths and merits of each and to minimize weaknesses. Such combined techniques are referred to as hybrid approaches. Related developments in propagation modeling have been reviewed by Harrison (1989), McCammon (1991), Buckingham (1992), Porter (1993) and Dozier and Cavanagh (1993). Finite-element methods have also been used in underwater acoustics to treat problems requiring high accuracy [see Kalinowski (1979) for a good introduction to applications in underwater acoustics]. Developments in finite-element modeling will be discussed in appropriate sections throughout this book.

4.2.1 *Wave equation*

The wave equation is itself derived from the more fundamental equations of state, continuity and motion. Rigorous derivations have been carried out

in numerous basic texts in physics. Kinsler *et al.* (1982: Chapter 5) presented a particularly lucid derivation. DeSanto (1979) derived a more general form of the wave equation that included gravitational and rotational effects. Accordingly, the derivation will not be repeated here. Rather, the mathematical developments described in this book will build directly upon the wave equation.

Formulations of acoustic propagation models generally begin with the three-dimensional, time-dependent wave equation. Depending upon the governing assumptions and intended applications, the exact form of the wave equation can vary considerably (DeSanto, 1979; Goodman and Farwell, 1979). For most applications, a simplified linear, hyperbolic, second-order, time-dependent partial differential equation is used:

$$\nabla^2 \Phi = \frac{1}{c^2} \frac{\partial^2 \Phi}{\partial t^2} \quad (4.1)$$

where ∇^2 is the Laplacian operator [= $(\partial^2/\partial x^2) + (\partial^2/\partial y^2) + (\partial^2/\partial z^2)$], Φ the potential function, c the speed of sound and t the time.

Subsequent simplifications incorporate a harmonic (single-frequency, continuous wave) solution in order to obtain the time-independent Helmholtz equation. Specifically, a harmonic solution is assumed for the potential function Φ :

$$\Phi = \phi e^{-i\omega t} \quad (4.2)$$

where ϕ is the time-independent potential function, ω is the source frequency ($2\pi f$) and f the acoustic frequency. Then the wave equation (4.1) reduces to the Helmholtz equation:

$$\nabla^2 \phi + k^2 \phi = 0 \quad (4.3a)$$

where $k = (\omega/c) = (2\pi/\lambda)$ is the wavenumber and λ the wavelength. In cylindrical coordinates, Equation (4.3a) becomes:

$$\frac{\partial^2 \phi}{\partial r^2} + \frac{1}{r} \frac{\partial \phi}{\partial r} + \frac{\partial^2 \phi}{\partial z^2} + k^2(z) \phi = 0 \quad (4.3b)$$

Equation (4.3a) is referred to as the time-independent (or frequency-domain) wave equation. Equation (4.3b), in cylindrical coordinates, is commonly referred to as the elliptic-reduced wave equation.

Various theoretical approaches are applicable to the Helmholtz equation. The approach used depends upon the specific geometrical assumptions made for the environment and the type of solution chosen for ϕ , as will be discussed in the following sections. To describe the different approaches effectively, it is useful to first develop a classification scheme, with associated taxonomy, based on five canonical solutions to the wave equation: ray

theory, normal mode, multipath expansion, fast field and parabolic equation techniques.

Throughout the theoretical development of these five techniques, the potential function ϕ normally represents the acoustic field pressure. When this is the case, the transmission loss (TL) can easily be calculated as:

$$TL = 10 \log_{10}[\phi^2]^{-1} = -20 \log_{10} |\phi|$$

This relationship necessarily follows from Equations (3.1) and (3.2). If phases are considered, the resulting TL is referred to as coherent. Otherwise, phase differences are ignored and the TL is termed incoherent.

4.2.2 *Classification of modeling techniques*

Although acoustic propagation models can be classified according to the theoretical approach employed, the cross-connections that exist among the various approaches complicate a strict classification, or taxonomic, scheme. Consequently, as the schemes become more detailed, more cross-connections will appear. A generalized classification scheme has been constructed using five categories corresponding to the five canonical solutions of the wave equation (also see Jensen and Krol, 1975; DiNapoli and Deavenport, 1979; Weston and Rowlands, 1979).

Within these five categories, a further subdivision can be made according to range-independent and range-dependent models. Range independence means that the model assumes a horizontally stratified ocean in which properties vary only as a function of depth. Range dependence indicates that some properties of the ocean medium are allowed to vary as a function of range (r) and azimuth (θ) from the receiver, in addition to a depth (z) dependence. Such range-varying properties commonly include sound speed and bathymetry, although other parameters such as sea state, absorption and bottom composition may also vary. Range dependence can further be regarded as two dimensional (2D) for range and depth variations or three dimensional (3D) for range, depth and azimuthal variations.

In order to illustrate the relationships among the five approaches used to solve the wave equation, the rather elegant scheme developed by Jensen and Krol (1975) will be adopted with slight modifications (Figure 4.1). According to this classification scheme, there are three avenues that connect the five basic approaches applicable to underwater acoustic propagation modeling. These five categories of propagation models will be described in detail in the following sections, and Figure 4.1 will serve as a useful road map. For convenience, the general functions and equations represented in Figure 4.1 have been identified with the letters F and G . In the discussions that follow, different symbols will be substituted to facilitate identification with relevant physical properties or with other well-known mathematical functions.

Equation (4.4) contains the real terms and defines the geometry of the rays. Equation (4.5), also known as the transport equation, contains the imaginary terms and determines the wave amplitudes. The separation of functions is performed under the assumption that the amplitude varies more slowly with position than does the phase (geometrical acoustics approximation). The geometrical acoustics approximation is a condition in which the fractional change in the sound-speed gradient over a wavelength is small compared to the gradient c/λ , where c is the speed of sound and λ is the acoustic wavelength. Specifically

$$\frac{1}{A} \nabla^2 A \ll k^2 \quad (4.6)$$

In other words, the sound speed must not change much over one wavelength. Under this approximation, Equation (4.4) reduces to

$$[\nabla P]^2 = k^2 \quad (4.7)$$

Equation (4.7) is referred to as the eikonal equation. Surfaces of constant phase ($P = \text{constant}$) are the wavefronts, and the normals to these wavefronts are the rays. Eikonal refers to the acoustic path length as a function of the path endpoints. Such rays are referred to as eigenrays when the endpoints are the source and receiver positions. Differential ray equations can then be derived from the eikonal equation. Typically, four sets of eigenrays are considered (Figure 4.2): direct path (DP), RSR, RBR and refracted–surface–reflected–bottom–reflected (RSRBR). The physical models described in Chapter 3 are generally incorporated into ray models to account for boundary interaction and volumetric effects.

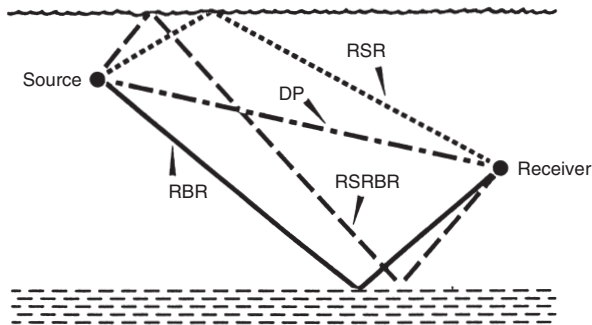


Figure 4.2 Four basic types of eigenrays: DP, direct path; RSR, refracted–surface–reflected; RBR, refracted–bottom–reflected; RSRBR, refracted–surface–reflected–bottom–reflected.

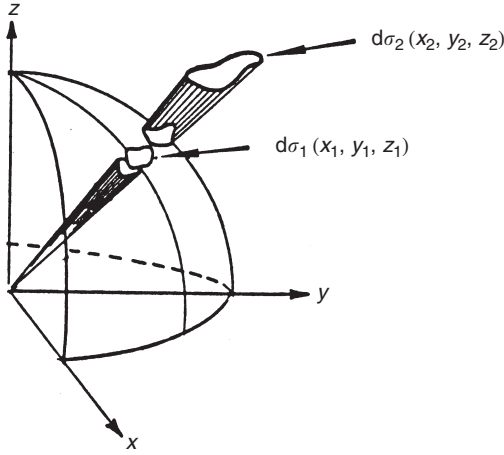


Figure 4.3 Geometry of a ray bundle.

The geometrical acoustics approximation effectively limits the ray-theoretical approach to the high-frequency domain. An approximate guideline for defining high frequency is provided by the relation

$$f > 10 \frac{c}{H} \quad (4.8)$$

where f is the frequency, H the duct depth and c the speed of sound.

The computation of the pressure amplitude can be accomplished using the transport equation (4.5) and by invoking the principle of conservation of energy flux for a ray bundle (Figure 4.3). Assuming constant density (Tolstoy and Clay, 1966: 57)

$$A_2 = \left[\frac{c_2 d\sigma_1}{c_1 d\sigma_2} \right]^{1/2} A_1 \quad (4.9)$$

where

$$A_2 = A(x_2, y_2, z_2) \quad A_1 = A(x_1, y_1, z_1)$$

are the signal amplitudes,

$$c_2 = c(x_2, y_2, z_2) \quad c_1 = c(x_1, y_1, z_1)$$

are the sound speeds and $d\sigma_1$ is the ray bundle cross-section at x_1, y_1, z_1 and $d\sigma_2$ is the ray bundle cross-section at x_2, y_2, z_2 .

As $d\sigma_2$ approaches zero, A_2 approaches infinity. Thus, ray theory does not hold in the vicinity of focal surfaces (caustics) and focal points.

4.3.2 Caustics

Focal surfaces, or caustics, are formed when the refractive properties of the ocean environment focus a number of adjacent rays into close proximity. There are two types of caustics: smooth and cusped. A cusp is actually the intersection of two smooth caustics. Examples of smooth and cusped caustics are presented in Figure 4.4.

In the vicinity of caustics, a higher-order approximation can be used to yield predictions on the caustic itself, and also in the nearby shadow zone. One theory, developed by Sachs and Silbiger (1971), is essentially an approximate asymptotic method that predicts a spatially oscillating field amplitude on the illuminated side of the caustic. In the shadow zone, the field is damped with increasing distance from the caustic boundary. Boyles (1984: Chapter 5) provided a lucid description of caustic formation together with appropriate corrections to ray theory. With appropriate frequency-dependent (diffraction) corrections and proper evaluation of caustics, ray theory can be extended to frequencies lower than those normally associated with the geometrical acoustics approximation. Under these conditions, the approach is commonly termed “ray theory with corrections.”

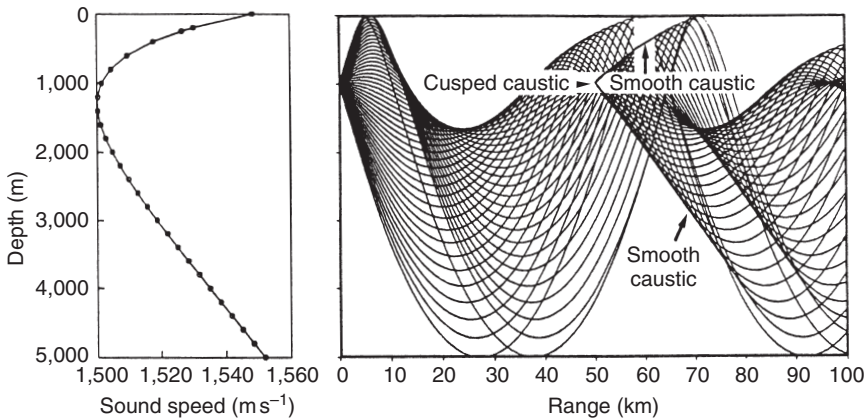


Figure 4.4 Sound-speed profile and associated ray trace showing the formation of smooth and cusped caustics. (Adapted from Jensen, 1988; *IEEE J. Oceanic. Eng.*, 13, 186–97; copyright by IEEE.)

4.3.3 *Gaussian beam tracing*

Another method useful in dealing with caustics is Gaussian beam tracing (e.g. Porter and Bucker, 1987; Bucker, 1994), which has been adapted from seismic applications. This method associates with each ray a beam with a Gaussian intensity profile normal to the ray. A pair of differential equations that govern the beamwidth and curvature are integrated along with the standard ray equations to compute the beam field in the vicinity of the central ray of the beam. This method avoids certain ray-tracing artifacts such as perfect shadows and infinite energy levels at caustics. Furthermore, this technique is attractive for high-frequency, range-dependent applications in which wave-theoretical approaches might not be practical alternatives (see Section 4.4.2).

4.3.4 *Range dependence*

Although ray-tracing techniques are theoretically applicable to fully range-dependent (3D) problems (refer to Figure 4.1), they are rarely implemented as such. The mathematical complexity discourages 3D versions in favor of 1D or 2D versions. The 2D versions can be implemented by one of three methods: (1) by mapping rays over discrete range intervals in which the environment remains constant (Weinberg and Dunderdale, 1972; Weinberg and Zabalgoceazcoa, 1977); (2) by dividing the range-depth plane into triangular regions (Bucker, 1971; Roberts, 1974; Watson and McGirr, 1975); or (3) by allowing the environment to vary smoothly as a function of range, through the use of cubic splines (Foreman, 1983). These methods are explained in the following paragraphs.

A significant problem that confronts range-dependent ray-tracing programs is the proper representation of the transition of sound-speed profiles between adjacent measurement points in the range dimension. Two aspects of this problem are important from a practical standpoint. First, the interpolated intermediate sound-speed profiles should be physically plausible. Second, it is desirable that the resulting ray trajectories be analytically computable (versus numerically integratable) in order to maximize computational efficiency.

In method (1) (Figure 4.5(a)), rays are traced in the first range interval. Selected rays are then mapped into the second interval, and the process continues throughout the remaining intervals. Drawbacks to this approach stem from discontinuities in ray tracing at the boundaries between adjacent intervals, and also from the potential omission of important rays in the selection process at each boundary. In particular, as the water (or duct) depth decreases, rays can properly be eliminated. As the depth increases, however, there is no valid and consistent process for adding new rays into consideration.

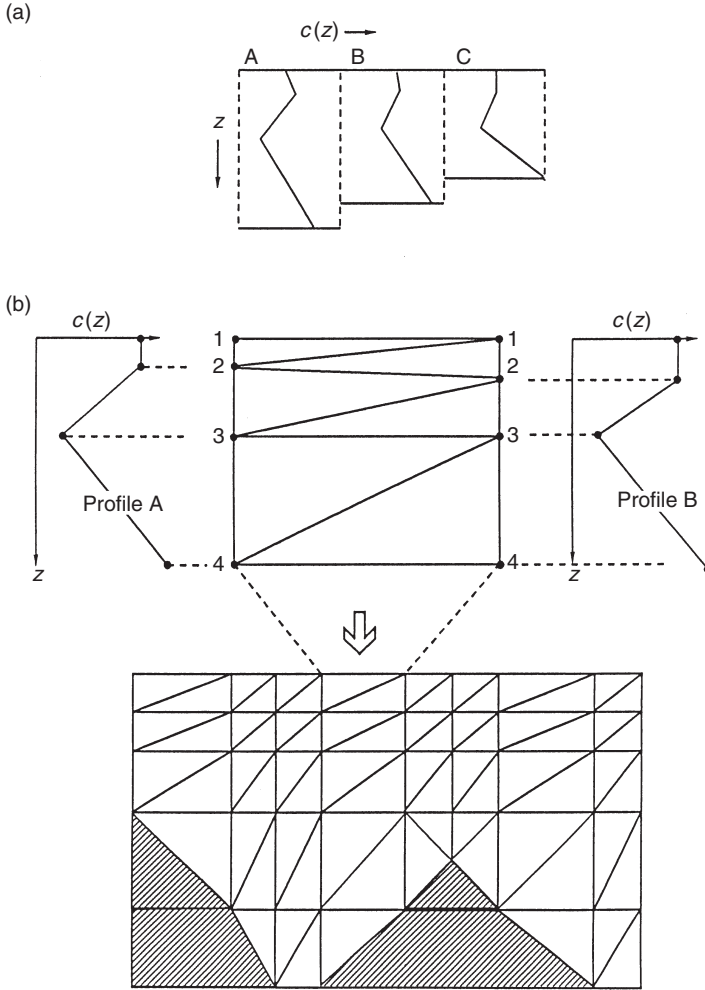


Figure 4.5 Range-partitioning techniques: (a) discrete range intervals and (b) typical network of triangular regions formed by connecting corresponding features between two adjacent sound-speed profiles (Roberts, 1974; Watson and McGirr, 1975).

In method (2) (Figure 4.5(b)), the input sound-speed profiles are represented as piecewise-linear functions of depth. Then, the range–depth plane between specified profiles can be divided into triangular sections within which the sound-speed varies linearly in both range and depth. In each sector, ray trajectories then correspond to arcs of circles for which analytical ray-tracing programs are available (e.g. Urlick, 1983: 124–8). Each triangular

sector is selected to provide a smooth and physically realizable transition between adjacent profiles. The vertexes are commonly selected at those depths representing sound-speed minima. Otherwise, the triangular sides are selected to subtend the gradient that departs least from the gradient of the preceding triangle. These procedures generally require the expertise of an oceanographer to ensure the generation of realistic intermediate sound-speed profiles. One tries to maintain continuity in features such as the SLD and the sound channel axis.

In method (3), the sound-speed profiles and bathymetry are fitted with cubic splines (Solomon *et al.*, 1968) or quadratic functions. The domains thus formed are rectangular, much like that in method (1) above. However, linear interpolations in range are performed between adjacent profiles to obtain continuous range derivatives. The differential ray geometry and amplitude equations [derived from Equations (4.4) and (4.5), respectively] are then solved numerically (Foreman, 1983).

The proper use and application of complex range-dependent models requires a great deal of planning, especially with regard to the selection and spacing of the range-dependent environmental data inputs. Improper spacing of inputs can overlook important ocean frontal systems or bathymetric features (Henrick, 1983).

Limited 3D ray-tracing techniques have been developed to account more properly for the effects of horizontal gradients of oceanic properties, which are manifested as cross-range variations in the TL patterns. Examples include the use of a hybrid approach involving horizontal rays and vertical modes (Weinberg and Burridge, 1974; Burridge and Weinberg, 1977) and the use of 3D Hamiltonian ray tracing (Jones, 1982; Jones *et al.*, 1986). A compact, 3D ray-tracing algorithm suitable for implementation on small computers was developed by Einstein (1975). Bowlin *et al.* (1992) developed a versatile, range-dependent ray-tracing program (RAY) that is available from the Ocean Acoustics Library (OALIB) website (see Appendix C).

4.3.5 *Arrival structure*

A useful property of ray models is their ability to calculate arrival structure. Similar information can be obtained from wave-theoretical models, but only with much additional computation. Arrival-structure contours indicate the horizontal range from source to receiver that will be traversed by a ray leaving the source (or arriving at the receiver) at the specified angle for each propagation path of interest. These contours are not frequency dependent, but they do depend on the source and receiver depths.

These contours are also referred to as θ - r diagrams. An alternative way of viewing these contours is that r represents the range at which a ray leaving the source (arriving at the receiver) at angle θ crosses a horizontal line representing the depth of the receiver (source). To be properly utilized, these contours must indicate a reference to either the source or the receiver angle,

and the sign conventions must be explicitly stated. For example, relative to the receiver, a negative angle (θ) usually, but not always, signifies rays arriving from above the horizontal axis (i.e. rays traveling downward), and a positive angle signifies rays arriving from below (i.e. rays traveling upward).

Arrival structure information is not just an academic curiosity. Fundamentally, it facilitates discrimination of multipath arrivals. This information is essential for the proper computation of the vertical directionality of ambient noise (see Chapter 7) and for the proper evaluation of the performance of vertically oriented hydrophone arrays. Arrival structure information is also important in the calculation of volumetric and boundary reverberations (see Chapter 9).

In practice, arrival structure diagrams are produced in conjunction with ray traces, TL curves and other diagnostic information, as will be demonstrated during discussions of the RAYMODE propagation model later in this chapter. Here, Figure 4.6 is introduced in isolation to illustrate the utility of arrival structure diagrams in identifying particular ray families, which are evidenced by distinctive sets of patterns. For example, the inverted L-shaped trace at very short range in Figure 4.6 is indicative of direct path arrivals, while the more graceful arching contours on either side of the horizontal axis are associated with bottom-bounce paths. The sets of

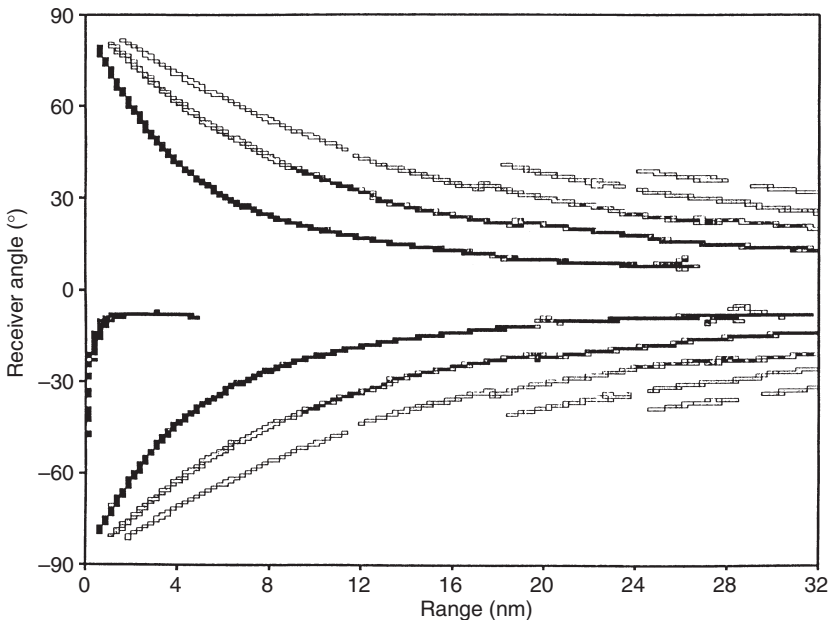


Figure 4.6 Example of a vertical arrival structure diagram.

contours (for both positive and negative arrival angles), which represent bottom-bounce paths, are referred to as order contours. Rays with the same number of bottom reflections belong to the same order. Thus, the first set of contours represents one bottom bounce and is of order 1. The contour associated with the positive angle within this first order has traveled from the source to the receiver over a RBR path and arrives at the receiver from below the horizontal axis. The corresponding contour with the negative angle has traveled from source to receiver over a refracted–bottom–reflected–surface–reflected (RBRSR) path and arrives at the receiver from above the horizontal axis.

These order contours can be used to identify all ray paths connecting the source and receiver that encounter the bottom at any range r . This information is very useful in the calculation of bottom reverberation. For example, only those rays encountering the bottom will contribute to bottom reverberation. The concept of order contours also applies to convergence zone (CZ) paths.

The θ – r contours can also be used to identify caustic formations. An instructive example was provided by Franchi *et al.* (1984). Figure 4.7 illustrates order contours obtained for a typical deep-ocean sound-speed profile. The two rays that just graze the bottom at ranges X_B and $X_{B'}$ determine points B and B' on the contour. The two rays that just graze the surface at ranges X_A and $X_{A'}$ occur at shallower angles and determine points A and A' on the contour. Thus, rays with angles in the interval $(\theta_{B'}, \theta_B)$ and (θ_B, θ_A) hit the surface but not the bottom. Caustics are associated with points C and C' on these contours.

4.3.6 Beam displacement

Propagation models based on ray-tracing techniques generally treat bottom reflection as specular and reduce the intensity through application of a bottom reflection loss. However, acoustic energy can be transmitted into the bottom where it is subsequently refracted, attenuated and even transmitted back into the water column at some distance down range (Figure 4.8). This spatial offset is referred to as “beam displacement.” Time displacements would also be associated with this process while the ray is absent from the water column.

In their initial study of the effects of beam displacement in ray calculations, Tindle and Bold (1981) considered a simple two-fluid Pekeris model as a good first approximation to many shallow-water environments. The Pekeris model (Pekeris, 1948) consists of a fluid (water) layer of depth H , density ρ_1 and sound speed c_1 overlying a semi-infinite fluid (sediment) layer of density ρ_2 and sound speed c_2 , where $c_2 > c_1$. Attenuation was neglected and only rays totally reflected at the interface were considered to propagate to a range (r) greater than the water depth (H). The vertical wavenumbers

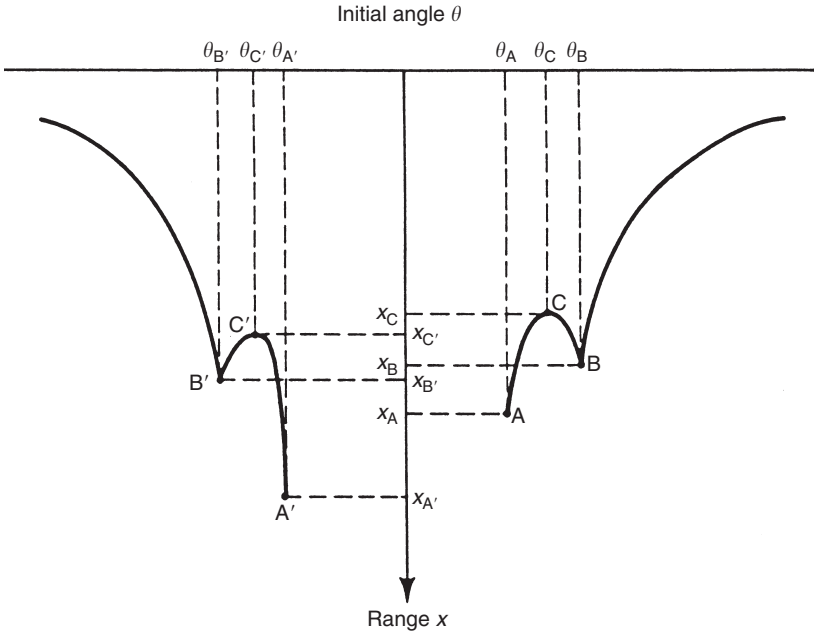


Figure 4.7 Smoothed order contours showing caustic behavior (Franchi *et al.*, 1984).

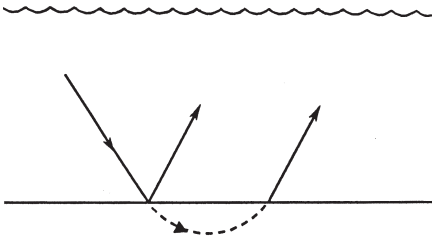


Figure 4.8 Geometry for beam displacement.

(γ_1, γ_2) in the two layers were defined as:

$$\gamma_1 = \left(\frac{\omega}{c_1}\right) \sin \theta, \quad \gamma_2 = \left(\frac{\omega}{c_1}\right) \sqrt{\cos^2 \theta - \frac{c_1^2}{c_2^2}}$$

where θ is the grazing angle and ω the angular frequency of the wave field. The lateral displacement (Δ) of a beam of finite width undergoing reflection

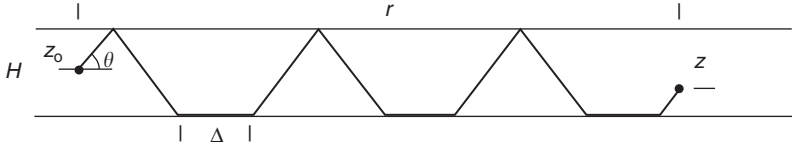


Figure 4.9 A typical ray path with beam displacement included (Tindle and Bold, 1981).

at the water-sediment interface is:

$$\Delta = \frac{2k_h \rho_1 \rho_2 (\gamma_1^2 + \gamma_2^2)}{\gamma_1 \gamma_2 (\rho_1^2 \gamma_2^2 + \rho_2^2 \gamma_1^2)}$$

where k_h is the horizontal wavenumber in the water layer

$$k_h = \left(\frac{\omega}{c_1} \right) \cos \theta$$

A typical ray path for this simple model is presented in Figure 4.9. The source and receiver depths are z_0 and z , respectively. A ray leaving the source at an angle θ relative to the horizontal travels in a straight (unrefracted) path in the water layer. There is no beam displacement at the sea surface and the ray is reflected in the conventional manner. At the bottom, the beam is displaced horizontally by an amount Δ before traveling upward again at angle θ .

Recent efforts to improve ray-theory treatments of bottom attenuation and beam displacement have been conducted by Siegmann *et al.* (1987) and Westwood and Tindle (1987), among others. Modified ray theory with beam and time displacements has advantages over wave theory in that the interaction of the acoustic energy with the bottom can be intuitively visualized. Moreover, Jensen and Schmidt (1987) computed complete wave-theory solutions for a narrow Gaussian beam incident on a water-sediment interface near the critical grazing angle. They observed that the fundamental reflectivity characteristics of narrow beams could be explained entirely within the framework of linear acoustics.

4.4 Normal-mode models

4.4.1 Basic theory

Normal-mode solutions are derived from an integral representation of the wave equation. In order to obtain practical solutions, however, cylindrical symmetry is assumed in a stratified medium (i.e. the environment changes as

a function of depth only). Then, the solution for the potential function ϕ in Equation (4.3b) can be written in cylindrical coordinates as the product of a depth function $F(z)$ and a range function $S(r)$:

$$\phi = F(z) \cdot S(r) \quad (4.10)$$

Next, a separation of variables is performed using ξ^2 as the separation constant. The two resulting equations are:

$$\frac{d^2F}{dz^2} + (k^2 - \xi^2)F = 0 \quad (4.11)$$

$$\frac{d^2S}{dr^2} + \frac{1}{r} \frac{dS}{dr} + \xi^2 S = 0 \quad (4.12)$$

Equation (4.11) is the depth equation, better known as the normal mode equation, which describes the standing wave portion of the solution. Equation (4.12) is the range equation, which describes the traveling wave portion of the solution. Thus, each normal mode can be viewed as a traveling wave in the horizontal (r) direction and as a standing wave in the depth (z) direction.

The normal-mode equation (4.11) poses an eigenvalue problem. Its solution is known as the Green's function. The range Equation (4.12) is the zero-order Bessel equation. Its solution can be written in terms of a zero-order Hankel function ($H_0^{(1)}$). The full solution for ϕ can then be expressed by an infinite integral, assuming a monochromatic (single-frequency) point source:

$$\phi = \int_{-\infty}^{\infty} G(z, z_0; \xi) \cdot H_0^{(1)}(\xi r) \cdot \xi \, d\xi \quad (4.13)$$

where G is Green's function, $H_0^{(1)}$ a zero-order Hankel function of the first kind and z_0 the source depth. Note that ϕ is a function of the source depth (z_0) and the receiver depth (z). The properties of these various functions are described in standard mathematical handbooks such as Abramowitz and Stegun (1964).

4.4.2 Normal-mode solution

To obtain what is known as the normal-mode solution to the wave equation, the Green's function is expanded in terms of normalized mode functions (u_n). The eigenvalues, which are the resulting values of the separation constants, are represented by ξ_n . These eigenvalues (or characteristic values) represent the discrete set of values for which solutions of the mode functions u_n exist. The infinite integral in Equation (4.13) is then evaluated by contour

integration:

$$\phi = \oint \sum \frac{u_n(z) \cdot u_n(z_0)}{\xi^2 - \xi_n^2} H_0^{(1)}(\xi r) \cdot \xi \, d\xi + \text{branch-cut integral} \quad (4.14)$$

The contour integral represents the trapped (or discrete) modes that propagate through the water column. The branch-cut integral is associated with the continuous mode spectrum, which represents those modes propagating through the ocean floor and which are strongly attenuated. The branch-cut integral describes the near-field conditions and corresponds in ray theory to those rays striking the bottom at angles greater than the critical angle. Thus, the contribution from the branch-cut integral is often neglected, particularly when horizontal distances greater than several water depths separate the source and receiver. For acoustic propagation problems using an impedance boundary condition at the bottom, the solution actually comprises three spectral intervals: the continuous, discrete and evanescent. The evanescent spectrum is associated with interface waves that decay exponentially away from the boundary (Jensen *et al.*, 1994). Interface waves that propagate along a fluid–solid boundary (i.e. water–sediment interface) are called Scholte waves. In seismology, interface waves propagating along the boundaries between solid layers are called Stoneley waves.

By neglecting the branch-cut integral, evaluating the contour integral and replacing the Hankel function expression by its asymptotic expansion for large arguments:

$$H_0^{(1)}(\xi r) \approx \sqrt{\frac{2}{\pi \xi r}} e^{i(\xi r - \pi/4)} \quad \text{for } \xi r \gg 1$$

(where $\xi r \gg 1$ is the far-field approximation), a simple solution for the potential function ϕ can be obtained:

$$\phi = g(r, \rho) \sum \frac{u_n(z) \cdot u_n(z_0)}{\sqrt{\xi_n}} \exp[i(\xi_n r - \pi/4)] \exp(-\delta_n r) \quad (4.15)$$

where $g(r, \rho)$ is a general function of range (r) and water density (ρ). Each of the n -terms in Equation (4.15) corresponds to the contribution of a single normal mode of propagation. Each of these modal contributions is propagated independently of the others. Under idealized conditions, there is usually an upper limit on the number of modes to be calculated, and this number increases with increasing frequency.

The attenuation coefficient δ_n can be written in the form (Miller and Wolf, 1980):

$$\delta_n = \varepsilon \gamma_n + \varepsilon_c \gamma_n^{(c)} + \varepsilon_s \gamma_n^{(s)} + S_n^{(0)} + S_n^{(1)} + \alpha_n \quad (4.16)$$

where ε is the plane-wave attenuation coefficient in the sediment layer, $\varepsilon_c, \varepsilon_s$ the compressional and shear plane-wave attenuation coefficients, respectively, of the basement, $\gamma_n, \gamma_n^{(c)}, \gamma_n^{(s)}$ measures of n th mode interactions with sediment, and with basement compressional and shear wave mechanisms, $S_n^{(0)}, S_n^{(1)}$ the attenuation of the modal field due to the interaction of the n th mode with statistically rough boundaries at the pressure release boundary (sea surface) and the water–sediment boundary, respectively, and α_n the attenuation due to absorption by sea water.

One advantage of normal-mode solutions over ray-theoretical methods is that TL can easily be calculated for any given combination of frequency and source depth (z_0) at all receiver depths (z) and ranges (r) [refer to Equation (4.14)]. Ray models, on the other hand, must be executed sequentially for each change in source or receiver depths (compare Figures 3.2 and 3.3).

A disadvantage associated with normal-mode solutions is the degree of information required concerning the structure of the sea floor, as indicated in Equation (4.16). In order to execute effectively, this type of model generally requires knowledge of the density as well as the shear and compressional sound speeds within the various sediment layers. Figure 4.10 shows an ideal three-layer physical model usable in normal-mode solutions. The fluid layer boundaries are defined by duct depths or by other notable features in the sound-speed profile. Accordingly, more layers can be added to the physical model as the complexity of the profile increases. The computational intensity increases in proportion to this complexity. In Figure 4.10, the sediment layer is treated as a second fluid layer (below the water column) and is characterized by a compressional sound speed only, thus ignoring shear effects. The effects of sediment attenuation can be included, as noted above in Equation (4.16).

Some normal-mode models (Stickler, 1975; Bartberger, 1978b) partition the sound-speed profile into N layers such that the square of the index of refraction in each layer can be approximated by a straight line and the density can be assumed constant. Under these conditions, it is then possible to represent the depth-dependent portion of the pressure field in terms of Airy functions and thus improve computational efficiency. The model by Stickler (1975) is noteworthy in that it includes the continuous modes as well as the trapped modes. Fast finite difference methods have been used to accurately determine the real (versus imaginary) eigenvalues (Porter and Reiss, 1984). Errors in these eigenvalues would otherwise appear as phase shifts in the range dependence of the acoustic field.

4.4.3 *Dispersion effects*

Unlike ray-theoretical solutions, wave-theoretical solutions inherently treat dispersion effects. Dispersion is the condition in which the phase velocity is

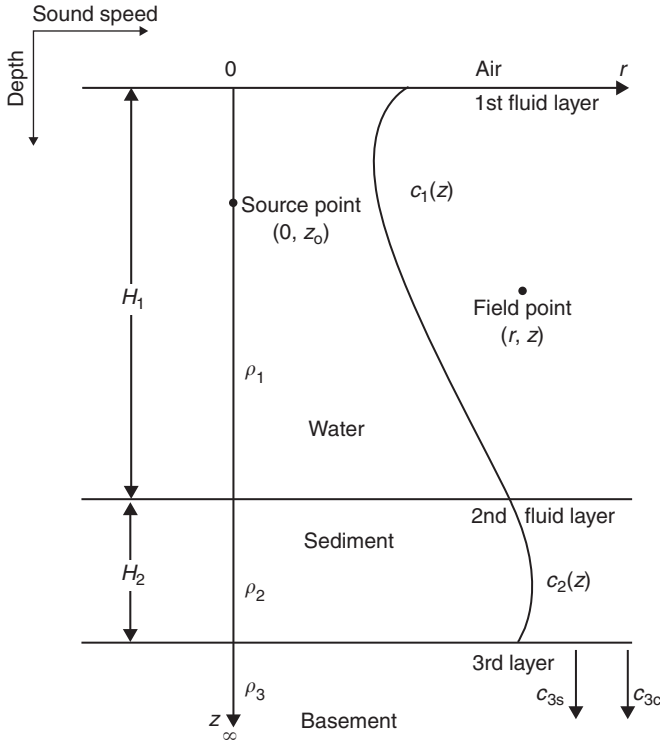


Figure 4.10 Simple physical model depicting an infinite half-space consisting of: two fluid layers with depths H_1, H_2 ; densities ρ_1, ρ_2 ; and sound speeds c_1, c_2 . A semi-infinite third layer (representing the bottom) has density ρ_3 , and compressional (c_{3c}) and shear (c_{3s}) sound speeds (adapted from Miller and Ingenito, 1975).

a function of the acoustic frequency. If present, dispersion effects are most noticeable at low frequencies. In oceanic waveguides, dispersion depends on the characteristics and geometry of the waveguide and is referred to as geometrical dispersion. This is distinguished from intrinsic dispersion as might result from sound propagation through bubbly water layers near the sea surface (Clay and Medwin, 1977: 311–12).

4.4.4 Experimental measurements

Ferris (1972) and Ingenito *et al.* (1978) summarized results from field measurements at a site near Panama City, Florida. The experiments were conducted over tracks having a range-independent water depth and sound-speed profile. The sea floor was composed of hard-packed sand. The modal field distribution was calculated on the basis of Equation (4.14). If all acoustic and environmental parameters except for the receiver depth are held

constant, then the dependence of the pressure amplitude (ϕ_n) of the n th-order mode on receiver depth (z) is directly proportional to the corresponding mode function (u_n):

$$\phi_n(z) \propto u_n(z)$$

If range and receiver depths are held constant, then the dependence of the pressure amplitude (ϕ_n) of the n th-order mode on source depth (z_0) is

$$\phi_n(z_0) \propto u_n(z_0)$$

Comparisons of measured and calculated pressure amplitude distributions at the receiver (using an arbitrary amplitude scale) are presented in Figure 4.11 for the first and second modes. Two frequencies (400 and 750 Hz) were considered, as were three different sound-speed profiles (positive gradient, negative gradient and isospeed). The influence of the sound-speed gradient on the low-order modes is evident. Specifically, the first mode is nearly symmetrically distributed about mid-depth in the isospeed case (Figure 4.11(c)). The sound-speed gradients alter this symmetry and concentrate the energy in the low-speed portion of the water column (Figures 4.11(a), (b)).

Boyles (1984: chapter 6) provided a comprehensive discussion demonstrating that certain groupings of normal modes could be associated with particular ray families propagating in specific oceanic waveguides. This was accomplished by explicitly calculating the TL associated with selected subsets of modes using Equation (4.14). These calculations were then compared to the full TL curve. One example involved a typical North Atlantic Ocean sound-speed profile during the winter season. This profile was characterized by a surface duct, a sound channel and sufficient depth excess to support CZ propagation (refer back to Figure 2.7). The source and receiver were both placed within the surface duct, and a frequency of 30 Hz was selected. Only 27 modes were trapped in the water column at this frequency. Of these, only one mode (mode 11) contributed to the TL in the surface duct. Modes that uniquely contribute to surface duct propagation are referred to as “virtual modes” (Labianca, 1973). Thus, mode 11 is also referred to as virtual mode 1. Modes 13–27 accounted for the TL associated with the CZ paths. The remaining modes contributed very little to the overall TL. The association of certain normal modes with particular ray families will be explored further in discussions of the RAYMODE model later in this chapter.

4.4.5 *Range dependence*

As noted previously in Figure 4.1, normal-mode models assume range independence. Extensions to range dependence can be accommodated either

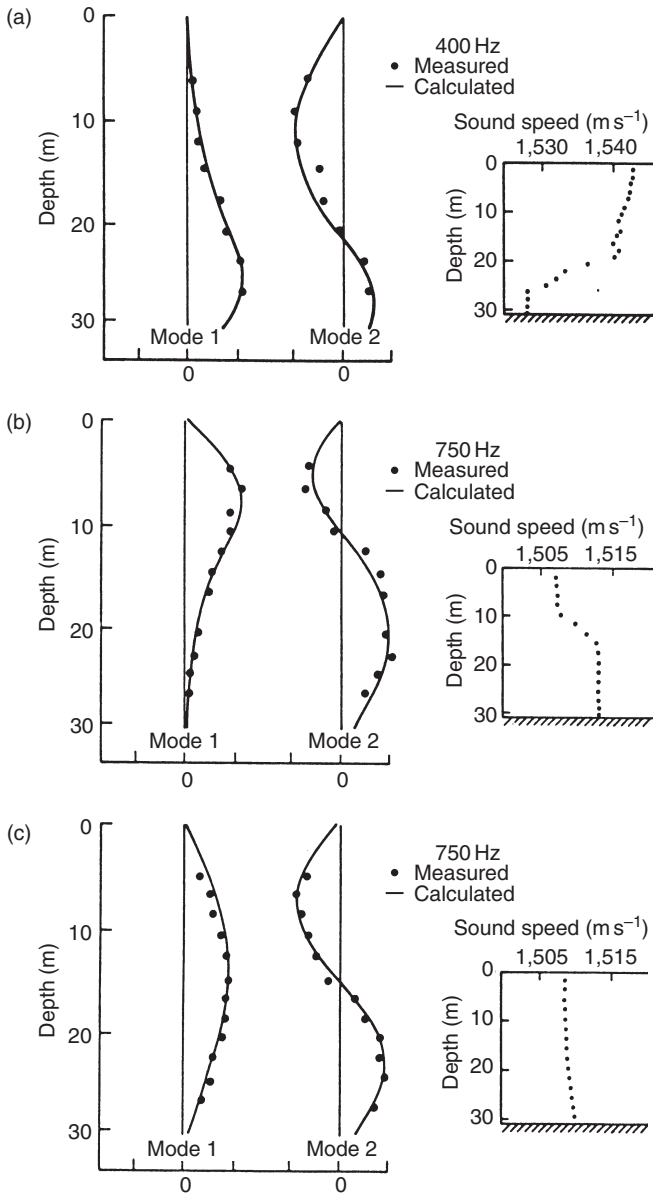


Figure 4.11 Comparison of measured and calculated amplitude functions (using arbitrary scales) for the first and second modes: (a) at 400 Hz with a downward-refracting (negative-gradient) profile; (b) at 750 Hz with an upward-refracting (positive-gradient) profile; and (c) at 750 Hz with a nearly constant sound-speed profile (Ferris, 1972).

by “mode coupling” or by “adiabatic approximation.” Mode coupling considers the energy scattered from a given mode into other modes. Adiabatic approximation assumes that all energy in a given mode transfers to the corresponding mode in the new environment, provided that environmental variations in range are gradual.

Three-dimensional propagation modeling using normal-mode theory has been attempted using two different approaches. The first approach employs the $N \times 2D$ technique in which the 3D problem is solved using N horizontal radials (or sectors) in conjunction with range-dependent (2D) adiabatic mode (or coupled mode) theory along each radial. The resulting quasi-3D propagation fields can then be contoured on polar plots, for example. The second approach directly includes the effects of horizontal refraction through use of the lateral wave equation. One implementation by Kuperman *et al.* (1988) and Porter (1991) employed Gaussian beam tracing (Porter and Bucker, 1987) to solve the lateral wave equation. In essence, the horizontal field of each modal wavenumber is translated into a horizontal sound-speed field that defines the Gaussian beam environment for each mode. In related work, a new development called wide-area rapid acoustic prediction (WRAP) precomputed local acoustic eigenvalues and normal modes for complex 3D ocean environments comprising a number of distinct local environments (Perkins *et al.*, 1990). For mild horizontal variability, the full 3D acoustic field was constructed by adiabatic mode computations. Another 3D model called CMM3D included horizontal refraction and radial mode coupling (Chiu and Ehret, 1990, 1994). Ainslie *et al.* (1998a) demonstrated the importance of leaky modes in range-dependent environments with variable water depth. In this particular investigation, the bottom-interacting field was computed by mode summation. Gabrielson (1982) investigated the application of normal-mode models to leaky ducts.

4.4.6 *High-frequency adaptations*

Normal-mode approaches tend to be limited to acoustic frequencies below about 500 Hz due to computational considerations (and not due to any limitations in the underlying physics). Specifically, the number of modes required to generate a reliable prediction of TL increases in proportion to the acoustic frequency. However, by invoking some simplifying assumptions regarding the complexity of the ocean environment, upper frequency limits in the multi-kilohertz range can be achieved (Ferla *et al.*, 1982).

4.4.7 *Wedge modes*

Primack and Gilbert (1991) investigated so-called “wedge modes,” which are the intrinsic normal modes in a wedge (i.e. sloping-bottom) coordinate

system. Wedge modes are identical to the usual normal modes of a range-invariant waveguide except that the mode functions are referenced to the arc of a circle rather than to a vertical line. This difference derives from use of a polar coordinate system, with its origin at the apex of the wedge, rather than the usual range–depth coordinate system in a wedge domain (Fawcett *et al.*, 1995). For shallow-water acoustic propagation, the acoustic wavelength is commensurate with the water depth, but short compared to the horizontal extent of the problem. Under these conditions, a sloping bottom causes the development of normal modes having wavefronts that are curved in the vertical direction. Using simple slopes, for example, wedge modes were found to propagate with cylindrical wavefronts (Mignerey, 1995).

Fawcett *et al.* (1995) developed an efficient coupled-mode method based on the concept of wedge modes. Leaky modes were also included because of their importance in range-dependent waveguide geometries. In related work, Tindle and Zhang (1997) developed an adiabatic normal-mode solution for a well-known benchmark wedge problem (discussed in Chapter 11) that included both fluid and solid attenuating bottom boundaries. The continuous-mode contribution was treated as a sum of leaky modes, and each trapped mode gradually transitioned into a leaky mode as the water depth decreased.

4.5 Multipath expansion models

Multipath expansion techniques expand the acoustic field integral representation of the wave equation [Equation (4.13)] in terms of an infinite set of integrals, each of which is associated with a particular ray-path family. This method is sometimes referred to as the “WKB method” since a generalized WKB (Wentzel, Kramers and Brillouin) approximation is used to solve the depth-dependent equation derived from the normal-mode solution [Equation (4.11)]. Each normal mode can then be associated with corresponding rays (see the discussion in the latter part of Section 4.4.4). Multipath expansion models do not currently accommodate environmental range dependence.

The WKB approximation (sometimes also referred to as the WKBJ or Liouville–Green approximation) facilitates an asymptotic solution of the normal mode equation by assuming that the speed of sound varies gradually as a function of depth. Advanced versions of the WKB method provide connection formulae to carry the approximation through “turning points” (i.e. depths where an equivalent ray becomes horizontal). Unlike ray-theoretical solutions, however, the WKB method normally accounts for first-order diffraction effects and caustics.

The specific implementation of this approach is accomplished by directly evaluating the infinite integral of Equation (4.13) over a limited interval of the real ξ -axis. Thus, only certain modes are considered. By using a restricted number of modes, an angle-limited source can be simulated. The resulting

acoustic pressure field ϕ in Equation (4.13) is then expressed as a sum of finite integrals, where each integral is associated with a particular ray family. As implemented, this approach is particularly applicable to the modeling of acoustic propagation in deep water at intermediate and high frequencies. Multipath expansion models thus have certain characteristics in common with ray models. Moreover, the pressure field is properly evaluated in caustics and shadow zones. Weinberg (1975) provided a brief summary of the historical development of this technique. This approach is explored in more detail in Section 4.8 where the RAYMODE model (which is based in part on the multipath expansion approach) is described.

4.6 Fast-field models

In underwater acoustics, fast-field theory is also referred to as “wavenumber integration.” In seismology, this approach is commonly referred to as the “reflectivity method” or “discrete-wavenumber method.” In fast-field theory, the wave-equation parameters are first separated according to the normal-mode approach. Then, the Hankel function expression in Equation (4.13) is replaced by the first term in the asymptotic expansion (DiNapoli and Deavenport, 1979):

$$H_0^{(1)}(\xi r) \approx \sqrt{\frac{2}{\pi \xi r}} e^{i(\xi r)} \quad \text{for } \xi r \gg 1$$

Equation (4.13) can now be written as

$$\phi = \int_{-\infty}^{\infty} \sqrt{\frac{2\xi}{\pi r}} G(z, z_0; \xi) e^{i(\xi r)} d\xi \quad (4.17)$$

The infinite integral is then evaluated by means of the fast Fourier transform (FFT), which provides values of the potential function ϕ at n discrete points for a given source–receiver geometry. Evaluation of the Green’s function can be simplified by approximating the sound-speed profile by exponential functions. Such an approximation facilitates the matrizant solution, but complicates specification of the sound-speed profiles.

Historically, models based on fast-field theory did not allow for environmental range dependence. However, two early developments introduced the possibility of range-dependent calculations of TL. First, Gilbert and Evans (1986) derived a generalized Green’s function method for solving the one-way wave equation exactly in an ocean environment that varied discretely with range. They obtained an explicit marching solution in which the source distribution at any given range step was represented by the acoustic field at the end of the previous step. Gilbert and Evans (1986) further noted that their method, which they called the range-dependent fast-field program (RDFFP) model, was computationally intensive. Second, Seong (1990) used

a hybrid combination of wavenumber integration and Galerkin boundary element methods (BEM), referred to as the SAFRAN model, to extend the fast-field theory technique to range-dependent ocean environments (see also Schmidt, 1991). The experimental nature of these early methods imposed uncertain restrictions on their application to system performance modeling in range-dependent ocean environments. As described below, however, further research proved these methods useful in modeling range-dependent wave propagation.

One approach to range-dependent modeling partitioned the ocean environment into a series of range-independent sectors called “super elements” (Schmidt *et al.*, 1995). Goh and Schmidt (1996) extended the spectral super-element approach for acoustic modeling in fluid waveguides to include fluid–elastic stratifications. Their method used a hybridization of finite elements, boundary integrals and wavenumber integration to solve the Helmholtz equation in a range-dependent ocean environment. It provided accurate, two-way solutions to the wave equation using either a global multiple scattering solution or a single-scatter marching solution.

Grilli *et al.* (1998) combined BEM and eigenfunction expansions to solve acoustic wave propagation problems in range-dependent, shallow-water regions. Their hybrid BEM technique (HBEM) was validated by comparing outputs to analytical solutions generated for problems with simple boundary geometries including rectangular, step and sloped domains. Hybrid BEM was then used to investigate the transmission of acoustic energy over bottom bumps while emphasizing evanescent modes and associated “tunneling” effects. Related developments in BEM in shallow water were reported by Santiago and Wrobel (2000).

The FFP approach has been modified to accommodate acoustic pulse propagation in the ocean by directly marching the formulation in the time domain (Porter, 1990). Applications included specification of arbitrary source time series instead of the more conventional time-harmonic sources used in frequency-domain solutions of the wave equation.

4.7 Parabolic equation models

Use of the parabolic approximation in wave propagation problems can be traced back to the mid-1940s when it was first applied to long-range tropospheric radio wave propagation (Keller and Papadakis, 1977: 282–4). Subsequently, the parabolic approximation method was successfully applied to microwave waveguides, laser beam propagating, plasma physics and seismic wave propagation. Hardin and Tappert (1973) reported the first application to problems in underwater acoustic propagation (also see Spofford, 1973b: 14–16). Lee and Pierce (1995) and Lee *et al.* (2000) carefully traced the historical development of the parabolic equation (PE) method in underwater acoustics.

4.7.1 Basic theory

The PE (or parabolic approximation) approach replaces the elliptic reduced equation [Equation (4.3b)] with a PE. The PE is derived by assuming that energy propagates at speeds close to a reference speed – either the shear speed or the compressional speed, as appropriate (Collins, 1991).

The PE method factors an operator to obtain an outgoing wave equation that can be solved efficiently as an initial-value problem in range. This factorization is exact when the environment is range independent. Range-dependent media can be approximated as a sequence of range-independent regions from which backscattered energy is neglected. Transmitted fields can then be generated using energy-conservation and single-scattering corrections. The following derivation is adapted from that presented by Jensen and Krol (1975).

The basic equation for acoustic propagation, Equation (4.3a), can be rewritten as:

$$\nabla^2 \phi + k_0^2 n^2 \phi = 0 \quad (4.18)$$

where k_0 is the reference wavenumber (ω/c_0), $\omega (=2\pi f)$ the source frequency, c_0 the reference sound speed, $c(r, \theta, z)$ the sound speed in range (r), azimuthal angle (θ) and depth (z), n the refraction index (c_0/c), ϕ the velocity potential and ∇^2 the Laplacian operator.

Equation (4.18) can be rewritten in cylindrical coordinates as:

$$\frac{\partial^2 \phi}{\partial r^2} + \frac{1}{r} \frac{\partial \phi}{\partial r} + \frac{\partial^2 \phi}{\partial z^2} + k_0^2 n^2 \phi = 0 \quad (4.19)$$

where azimuthal coupling has been neglected, but the index of refraction retains a dependence on azimuth. Further, assume a solution of the form:

$$\phi = \Psi(r, z) \cdot S(r) \quad (4.20)$$

and obtain:

$$\Psi \left[\frac{\partial^2 S}{\partial r^2} + \frac{1}{r} \frac{\partial S}{\partial r} \right] + S \left[\frac{\partial^2 \Psi}{\partial r^2} + \frac{\partial^2 \Psi}{\partial z^2} + \left(\frac{1}{r} + \frac{2}{S} \frac{\partial S}{\partial r} \right) \frac{\partial \Psi}{\partial r} + k_0^2 n^2 \Psi \right] = 0 \quad (4.21)$$

Using k_0^2 as a separation constant, separate Equation (4.21) into two differential equations as follows:

$$\left[\frac{\partial^2 S}{\partial r^2} + \frac{1}{r} \frac{\partial S}{\partial r} \right] = -S k_0^2 \quad (4.22)$$

and

$$\left[\frac{\partial^2 \Psi}{\partial r^2} + \frac{\partial^2 \Psi}{\partial z^2} + \left(\frac{1}{r} + \frac{2}{S} \frac{\partial S}{\partial r} \right) \frac{\partial \Psi}{\partial r} + k_0^2 n^2 \Psi \right] = \Psi k_0^2 \quad (4.23)$$

Rearrange terms and obtain:

$$\frac{\partial^2 S}{\partial r^2} + \frac{1}{r} \frac{\partial S}{\partial r} + k_0^2 S = 0 \quad (4.24)$$

which is the zero-order Bessel equation, and:

$$\frac{\partial^2 \Psi}{\partial r^2} + \frac{\partial^2 \Psi}{\partial z^2} + \left(\frac{1}{r} + \frac{2}{S} \frac{\partial S}{\partial r} \right) \frac{\partial \Psi}{\partial r} + k_0^2 n^2 \Psi - k_0^2 \Psi = 0 \quad (4.25)$$

The solution of the Bessel equation (4.24) for outgoing waves is given by the zero-order Hankel function of the first kind:

$$S = H_0^{(1)}(k_0 r) \quad (4.26)$$

For $k_0 r \gg 1$ (far-field approximation):

$$S \approx \sqrt{\frac{2}{\pi k_0 r}} \exp \left[i \left(k_0 r - \frac{\pi}{4} \right) \right] \quad (4.27)$$

which is the asymptotic expansion for large arguments. The equation for $\Psi(r, z)$ [Equation (4.25)] can then be simplified to:

$$\frac{\partial^2 \Psi}{\partial r^2} + \frac{\partial^2 \Psi}{\partial z^2} + 2ik_0 \frac{\partial \Psi}{\partial r} + k_0^2 (n^2 - 1) \Psi = 0 \quad (4.28)$$

Further assume that:

$$\frac{\partial^2 \Psi}{\partial r^2} \ll 2k_0 \frac{\partial \Psi}{\partial r} \quad (4.29)$$

which is the paraxial approximation. Then, Equation (4.28) reduces to:

$$\frac{\partial^2 \Psi}{\partial z^2} + 2ik_0 \frac{\partial \Psi}{\partial r} + k_0^2 (n^2 - 1) \Psi = 0 \quad (4.30)$$

which is the parabolic wave equation. In this equation, n depends on depth (z), range (r) and azimuth (θ). This equation can be numerically solved by “marching solutions” when the initial field is known (e.g. Tappert, 1977). The computational advantage of the parabolic approximation lies in the

fact that a parabolic differential equation can be marched in the range dimension whereas the elliptic reduced wave equation must be numerically solved in the entire range–depth region simultaneously. Typically, a Gaussian field or a normal-mode solution is used to generate the initial solution. Additional methods for generating accurate starting fields have been described by Greene (1984) and by Collins (1992). Collins (1999) improved the “self-starter” (a PE technique for generating initial conditions) by removing a stability problem associated with evanescent modes.

4.7.2 *Numerical techniques*

Existing PE models employ one of four basic numerical techniques: (1) split-step Fourier algorithm; (2) implicit finite-difference (IFD); (3) ordinary differential equation (ODE); or (4) finite element (FE). The original split-step algorithm developed by Tappert (1977) solves the parabolic wave equation by imposing an artificial zero bottom-boundary condition and pressure-release surface condition.

At the time Tappert introduced the PE method to the underwater acoustics community, there was a critical need for a capability to predict long-range, low-frequency sound propagation, as would occur in the vicinity of the sound channel axis. Since this type of propagation is characterized by low-angle, non-boundary interacting energy, the PE method was ideally suited to this purpose. Thus, the first introduction of the PE method to naval sonar applications was a celebrated event. Subsequent work focused on making the PE method more robust so that it could be applied to a wider range of problems in underwater acoustics.

While the split-step algorithm is an efficient method for solving a pure initial-value problem (Perkins *et al.*, 1982), several difficulties arise when there is significant interaction with the sea floor (Bucker, 1983). These difficulties are due to density and compressional sound-speed discontinuities at the water–sediment interface, strong gradients of the compressional sound speed in the sediment layers and rigidity in the sediment layers that produces shear waves. Thus, when bottom interaction is strong, a more general-purpose solution is desirable. For this reason, implicit finite-difference (IFD) schemes (Lee *et al.*, 1981; Robertson *et al.*, 1989) and ordinary differential equation (ODE) methods (Lee and Papadakis, 1980) have also been developed to solve the parabolic equation. Lee and McDaniel (1987) provided an in-depth development of the IFD technique. Their development was made more useful by the inclusion of benchmark test examples together with a listing of the computer program (comprising approximately 1,700 lines of FORTRAN code). A microcomputer implementation of the IFD model was reported by Robertson *et al.* (1991), who included a listing of their computer program. Collins (1988a) described an FE solution for the PE.

Recent modeling developments utilizing parabolic approximations have been directed at refining and expanding the capabilities of existing techniques. Useful summaries of this progress are available in the literature (Lee, 1983; Scully-Power and Lee, 1984; Lee and Pierce, 1995; Lee *et al.*, 2000). Actual comparisons of computer model results for a set of four ocean acoustic test cases was documented by Davis *et al.* (1982). A more recent comparison of PE models involving seven test cases was described by Chin-Bing *et al.* (1993b). One of the most interesting test cases described by Chin-Bing *et al.* (1993b) involved a leaky surface duct. So-called “ducted precursors” are generated by modal energy in the surface duct that leaks out and travels as CZ or bottom-bounce paths or both, before coupling back into the surface duct down range. The importance of this problem is that a small phase error in the refracted (leaky) path can produce large changes in the predicted sound level in the duct beyond the first CZ (Porter and Jensen, 1993). This pathology was particularly evident in some wide-angle, split-step PE models. Yevick and Thomson (1994) explored this problem further and formulated a new propagation operator that retained the computational efficiency of the split-step algorithm but which was more accurate.

Traditionally, PE models have been applied to anelastic ocean-bottom regions by treating the shear waves as an additional loss mechanism. This approximation breaks down when anelastic propagation becomes significant, as in shear conversion due to backscattered acoustic fields. In general, PE models propagate the acoustic field only in the forward direction, thus excluding backscatter. A two-way PE model (Collins and Evans, 1992) was developed to improve the computation of backscattered energy for use in reverberation simulations (e.g. Schneider, 1993). A modified version of this two-way PE model (called spectral PE) treats backscattering problems in 3D geometries (Orris and Collins, 1994). Lingeitch and Collins (1998) argued that a poro-acoustic medium is, in fact, the limiting case of a poro-elastic medium in which the shear wave speed vanishes. Collins and Siegmann (1999) extended energy-conservation corrections from the acoustic case to the elastic case.

By using operator formalism, the parabolic equation can be derived in another fashion (Lee and McDaniel, 1987: 314–15). By assuming commutation of operators:

$$\frac{\partial}{\partial r} \frac{\partial}{\partial z} \Psi = \frac{\partial}{\partial z} \frac{\partial}{\partial r} \Psi \quad (4.31)$$

the equation:

$$\frac{\partial^2 \Psi}{\partial r^2} + \frac{\partial^2 \Psi}{\partial z^2} + 2ik_0 \frac{\partial \Psi}{\partial r} + k_0^2 (n^2 - 1) \Psi = 0 \quad (4.32)$$

can be factored as:

$$\left[\frac{\partial}{\partial r} + ik_0 - i\sqrt{k_0^2 + k_0^2(n^2 - 1) + \frac{\partial^2}{\partial z^2}} \right] \times \left[\frac{\partial}{\partial r} + ik_0 + i\sqrt{k_0^2 + k_0^2(n^2 - 1) + \frac{\partial^2}{\partial z^2}} \right] \Psi = 0 \quad (4.33)$$

By considering only the outgoing wave, Equation (4.33) reduces to:

$$\left(\frac{\partial}{\partial r} + ik_0 - i\sqrt{k_0^2 + k_0^2(n^2 - 1) + \frac{\partial^2}{\partial z^2}} \right) \Psi = 0 \quad (4.34)$$

which can be rewritten as:

$$\frac{\partial}{\partial r} \Psi = i(\sqrt{Q} - k_0) \Psi \quad (4.35)$$

where

$$Q = k_0^2 + k_0^2(n^2 - 1) + \frac{\partial^2}{\partial z^2} \quad (4.36)$$

The square-root operator (Q) can be approximated using a rational functional representation:

$$\sqrt{Q} = k_0 \left(\frac{A + Bq}{C + Dq} \right) \quad (4.37)$$

where

$$q = \left(\frac{Q}{k_0^2} \right) - 1 \quad (4.38)$$

Using Equation (4.37), Equation (4.35) can be rewritten as:

$$\frac{\partial}{\partial r} \Psi = ik_0 \left(\frac{A + Bq}{C + Dq} - 1 \right) \Psi \quad (4.39)$$

For $[A \ B \ C \ D] = [1 \ \frac{1}{2} \ 1 \ 0]$, Equation (4.39) reverts back to that of Tappert [Equation (4.30)]. For $[A \ B \ C \ D] = [1 \ \frac{3}{4} \ 1 \ \frac{1}{4}]$, the form attributed to Claerbout (1976) is obtained.

4.7.3 Wide-angle and 3D adaptations

Tappert's (1977) original split-step PE method handled small-angle ($\leq 15^\circ$) propagation paths, a restriction imposed by the basic paraxial assumption. Unless the split-step algorithm is modified for wide angles (e.g. Thomson and Chapman, 1983), large phase errors may be introduced into the solution. In order to extend the maximum angle of half-beamwidth propagation in the PE model, alternate forms of the square-root operator have been explored. For split-step PE formulations, Thomson and Chapman's (1983) wide-angle approximation has been used. The Claerbout (1976: 206) wide-angle approximation is used in some finite-difference PE formulations with values of $[A \ B \ C \ D] = [1 \frac{3}{4} \ 1 \ \frac{1}{4}]$ in Equation (4.39). Other approximations of the square-root operator have been explored including higher-order Padé forms, which have been incorporated in finite-difference and finite-element PE formulations to achieve near 90° half-beamwidth propagation (Chin-Bing *et al.*, 1993b). Thomson and Wood (1987) investigated a post-processing method for correcting phase errors in the parabolic approximation approach. This method was later extended by Thomson and Mayfield (1994) to include an exact, non-local boundary condition at the sea floor. Since strong boundary (surface and bottom) interactions are associated with wide-angle propagation, the accurate treatment of irregular interfaces and rough boundaries assumed greater importance in PE models (Bucker, 1983; Lee and McDaniel, 1983; Dozier, 1984; Collins and Chin-Bing, 1990; Brooke and Thomson, 2000). Adaptations to under-ice environments have also been of interest to sonar modelers.

Extensions to 3Ds are generally implemented in an approximate manner (e.g. $N \times 2D$), although the primary parabolic wave equation is fully 3D (Perkins *et al.*, 1983; Siegmann *et al.*, 1985; Lee and Siegmann, 1986). Such 3D extensions are often coupled with wide-angle modifications to achieve maximum utility from the models (Botseas *et al.*, 1983; Thomson and Chapman, 1983).

4.7.4 Range-refraction corrections

Range-refraction corrections are introduced to accommodate propagation through strong oceanic fronts. The standard parabolic approximation is known to have intrinsic phase errors that will degrade the accuracy of any PE solution for long-range propagation in the ocean (Tappert and Lee, 1984; Jensen and Martinelli, 1985). The accuracy can be improved using updated mean phase speeds as a function of range. Tolstoy *et al.* (1985) suggested a simple transformation of the sound-speed profile to compensate for the inability of the PE approach to correctly locate the range of the signal turning points (e.g. Brock *et al.*, 1977). Schurman *et al.* (1991) developed an energy-conserving PE model that incorporated range refraction. A model called LOGPE (Berman *et al.*, 1989) used a logarithmic expression for the index

of refraction in the standard PE in order to closely approximate solutions of the more exact Helmholtz equation in weakly range-dependent ocean environments.

4.7.5 *High-frequency adaptations*

At frequencies higher than about 500 Hz, PE models become impractical due to excessive execution times. Computational intensity is proportional to the number of range-interval steps. As the frequency increases, the step size decreases and more steps are thus required to achieve the desired prediction range. High-frequency approximations can be obtained by introducing a hybrid approach that combines aspects of parabolic approximations and ray theory (Tappert *et al.*, 1984). A special-purpose microcomputer model (PESOGEN) was developed to compute the acoustic field in a fully range-dependent environment over a wide range of frequencies for both deep-water and shallow-water regions with greatly reduced execution times (Nghiem-Phu *et al.*, 1984).

The so-called calculation frequency method (CFM) can be used to extend PE solutions to high frequencies with execution speeds typically associated with those at low frequencies (Moore-Head *et al.*, 1989). The CFM produces range-averaged TL information by substituting a (low) calculation frequency for a (high) prediction frequency. This substitution is accomplished by sacrificing volume attenuation and boundary-loss phase information under the assumption that diffraction and interference effects are not important at the desired (high) prediction frequency.

4.7.6 *Time-domain applications*

Only frequency-domain applications of the PE have been explored thus far. However, the parabolic approximation has been adapted to consider time-domain applications. Specifically, the acoustic pressure is advanced in time by the so-called progressive wave equation (PWE). However, the PWE is, for practical purposes, limited to narrow-angle propagation paths. Collins (1988b) derived an inverse Fourier transform of the wide-angle parabolic equation referred to as the time-domain PE (TDPE). The TDPE advances the acoustic pressure field in range. Collins (1988b) used the TDPE to investigate the effects of sediment dispersion on pulse (or broadband) propagation in the ocean. Orchard *et al.* (1992) described the development of a TDPE model appropriate for use in 3D ocean acoustic propagation problems.

The progressive wave equation has also been adapted to model the propagation of a non-linear acoustic pulse that is subject to refraction and diffraction. McDonald and Kuperman (1987) examined the problem of acoustic propagation of finite-amplitude pulses and weak shocks in the ocean where refraction can lead to caustic formation. Their result was a first-order non-linear PWE (NPE), which is the non-linear time-domain counterpart

of the linear frequency-domain PE. When the non-linear term is omitted, the NPE reduces to the linear frequency-domain PE. The simplicity of their formulation suggests additional applications to broadband linear acoustic problems in the ocean.

4.8 The RAYMODE model – a specific example

The RAYMODE model, originally developed by Leibiger (1968), numerically solves the wave equation for underwater acoustic propagation using the multipath expansion approach (Section 4.5). RAYMODE is actually a hybrid approach involving elements of both ray theory and wave theory. RAYMODE is a stand-alone propagation model intended for application to passive sonar performance prediction problems in range-independent ocean environments.

Since its original development, the RAYMODE passive acoustic propagation model was widely used in the naval sonar modeling community. The US Navy later brought RAYMODE under configuration management where it was maintained as an interim standard for many years. While use of this model has subsequently been eclipsed by the development of more capable models, RAYMODE continues to provide an instructive example of acoustic model construction. Additional sources of information for RAYMODE are provided in Section 4.9.

The model accommodates beam patterns at both the source and the receiver. Boundary interaction losses are also included. Sea-surface losses are computed by a user-supplied table or by internal algorithms. Surface-scattering losses assume two mechanisms: (1) a high-frequency, large-roughness loss (Beckmann and Spizzichino, 1963: 89; Clay and Medwin, 1964) and (2) a low-frequency loss (Marsh and Schulkin, 1962a). Sea-floor losses are computed either through identification of bottom province types in order to access stored values or by a user-supplied table. The volume attenuation expression of Thorp (1967) is used. Transmission loss is calculated both coherently and incoherently.

The basic assumptions incorporated in RAYMODE are:

- 1 range-independent sound speed and bathymetry;
- 2 sound-speed profile fit with segments such that the index-of-refraction squared is a linear function of depth;
- 3 multiple reflections due to sound-speed discontinuities are ignored except in surface duct situations;
- 4 plane wave reflection coefficients are assumed;
- 5 only a finite number of ray cycles is considered in the multipath evaluation of pressure integrals;
- 6 a harmonic (single-frequency) source is assumed; and
- 7 a water density of unity is assumed.

The specific implementation of the multipath expansion technique is explained as follows. The infinite integral in Equation (4.13) is expressed as a sum of finite integrals, each of which is associated with a particular ray path. In Equation (4.13), ϕ is taken to represent the acoustic field pressure and the integration is performed piecewise over particular ray-path regions defined by the limiting rays (R.L. Deavenport, 1978: unpublished manuscript):

$$\int_{-\infty}^{\infty} \cong \int_{\xi_3}^{\xi_0} = \int_{\xi_1}^{\xi_0} + \int_{\xi_2}^{\xi_1} + \int_{\xi_3}^{\xi_2} \tag{4.40}$$

(SD) (CZ) (BB)

where $\xi_i = \omega/c_i$, c_i is the sound speed at vertexes, SD the surface duct region, CZ the convergence zone region and BB the bottom-bounce region.

Figure 4.12 illustrates a typical geometry. Here, z_s is the source depth, c_0 is the sound speed at the sea surface, c_1 is the sound speed at the sonic layer depth (SLD) and c_2 is the sound speed at the sea floor (at the base of the water column). The particular sound-speed profile and source depth geometry illustrated here would support all three ray-path families described (i.e. surface duct, CZ and bottom bounce). Note that:

$$\xi_3 = \left[\frac{\omega}{c_s} \right] \cos \theta_s$$

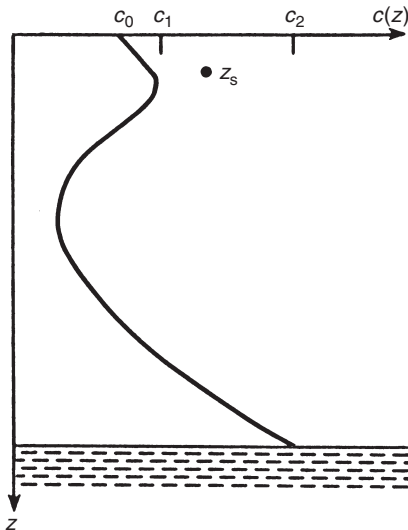


Figure 4.12 Typical environment for the RAYMODE propagation model showing a sound-speed profile with a source located at depth z_s .

where θ_s is the maximum ray angle leaving the source and c_s is the sound speed at the source depth.

The integral for each region is expanded into four parts:

$$\phi = \sum_{i=1}^4 \phi_i$$

Each ϕ_i corresponds to one of the four ray types associated with upgoing and downgoing rays at both the source and the receiver. The path geometries and associated sign conventions are prescribed in the RAYMODE L-path chart illustrated in Figure 4.13. These paths may be compared with those described previously in Figure 4.2. The cycle counter (q) represents the number of bottom reflections.

Each segment is then evaluated by either wave theory or ray theory. A special option is available to the user for surface ducts in order to incorporate the effects of leakage (diffraction effects). This option is exercised only for that wavenumber segment for which it is appropriate. If the special surface duct option is not exercised, then the segment is evaluated using the normal-mode approach. However, if the number of normal modes for a given segment exceeds ten, then a multipath expansion of the four parts of the integral is employed. If the segment contains bottom bounce paths, then ray-theoretical methods are used. At frequencies below 45 Hz, a normal-mode solution is used to evaluate propagation through the sediments. There is also a separate high-frequency routine that is used for frequencies greater than 1 kHz. The key parameters controlling the decision for the method of solution are the acoustic frequency and the physical environment. Consequently, slight variations in the problem statement may possibly result in unexpectedly abrupt changes in TL brought about by changes in the method of solution.

The resulting acoustic pressure field is modified by a beam pattern attenuation factor characterizing the off-axis beam position of an equivalent ray. The real and imaginary pressure components (P_i) are then used to form incoherent and coherent intensities for each range point and each ξ -partition. Transmission loss relative to unit intensity at unit distance from the source is calculated from the incoherent and coherent intensity sums as follows:

Incoherent TL

$$-10 \log_{10} \left\{ \sum_{i=1}^4 \left[(\text{Re } P_i)_{\text{SD}}^2 + (\text{Im } P_i)_{\text{SD}}^2 + (\text{Re } P_i)_{\text{BB}}^2 + (\text{Im } P_i)_{\text{BB}}^2 + (\text{Re } P_i)_{\text{CZ}}^2 + (\text{Im } P_i)_{\text{CZ}}^2 \right] \right\} + \alpha r \quad (4.41)$$

Resolution* of sign of source and receiver angles in RAYMODE:

General range $\bar{R} = qR_C \pm R_S \pm R_d$ or $qR_C + P_2R_S + P_1R_d$ where $q = \text{Cycle } 0, 1, 2, \dots, \lambda$
 R_C = Cycle range
 R_S = Source term
 R_d = Receiver term

Path L	P_2	P_1	Equation \bar{R}	$q=0$ (D.P.)	$q=1$ (EX. BB)	$q=2$	Source angle	Receiver angle
1	-	+	$qR_C - R_S + R_d$				+ Down	- Up
2	+	+	$qR_C + R_S + R_d$				- Up	- Up
3	-	-	$qR_C - R_S - R_d$	(Does not exist)			+ Down	+ Down
4	+	-	$qR_C - R_S - R_d$				- Up	+ Down

* Sign of angle is opposite sign of range adjustment term for both source and receiver

Figure 4.13 RAYMODE L-path chart illustrating the sign convention for source and receiver angles (Yarger, 1982).

Coherent TL

$$-10 \log_{10} \left\{ \left(\sum_{i=1}^4 [(\text{Re } P_i)_{\text{SD}} + (\text{Re } P_i)_{\text{BB}} + (\text{Re } P_i)_{\text{CZ}}] \right)^2 + \left(\sum_{i=1}^4 [(\text{Im } P_i)_{\text{SD}} + (\text{Im } P_i)_{\text{BB}} + (\text{Im } P_i)_{\text{CZ}}] \right)^2 \right\} + \alpha r \quad (4.42)$$

where α is the attenuation coefficient according to Thorp (1967).

In the RAYMODE model, user-supplied input information includes:

- 1 sound-speed profile;
- 2 source and receiver depths;
- 3 frequency;
- 4 horizontal range determinants;
- 5 bottom loss (default values used if inputs not supplied);
- 6 surface loss (default values used if inputs not supplied);
- 7 source and receiver beam patterns (default values used if inputs not supplied);
- 8 program controls (e.g. number of ray cycles to be processed, ray angle limits, mode cutoff values, calculation method options); and
- 9 output options.

Graphical outputs from RAYMODE include:

- 1 sound-speed profile plot and plots of bottom loss, surface loss and beam deviation loss;
- 2 source and receiver angles versus horizontal range (i.e. arrival structure) for selected ray paths (Figure 4.14);
- 3 travel time versus horizontal range for the ray paths in item (2) above (Figure 4.15);
- 4 TL versus horizontal range for coherent or incoherent combination of multipaths with beam pattern attenuation (Figure 4.16); and
- 5 ray trace diagram (Figure 4.17).

4.9 Numerical model summaries

This section summarizes available underwater acoustic propagation models. These models are applicable to work in sonar technology (e.g. sonar design and operation) and in acoustical oceanography (e.g. oceanographic research and data analysis). As is true of any summary of this nature, the information represents a snapshot in time of the present state-of-the-art. While comprehensive in coverage, this summary does not claim to be exhaustive.

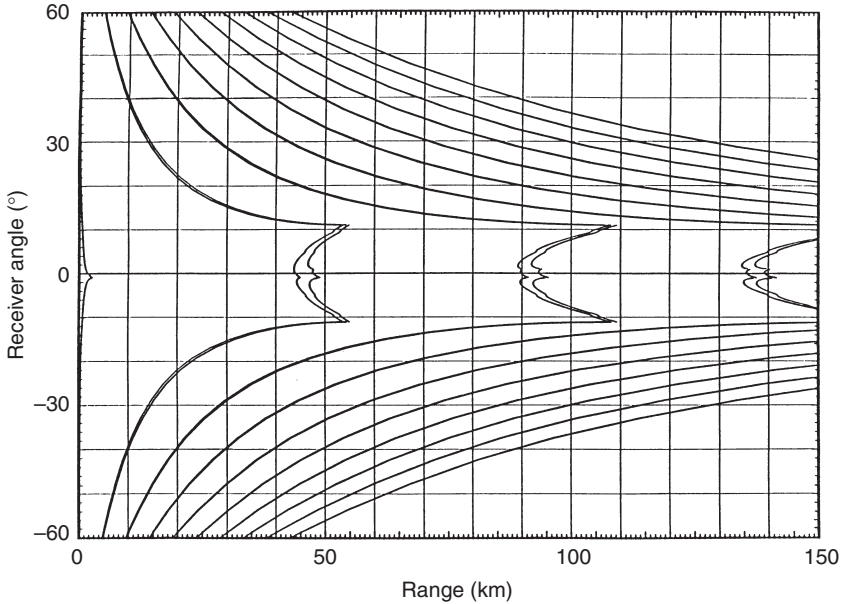


Figure 4.14 RAYMODE arrival structure diagram. This graph displays receiver angle versus horizontal range for selected rays representing bottom bounce (BB) and CZ paths. The CZ paths are associated with the near-axis features at 45, 90 and 135 km (Yarger, 1982).

In order to optimize the utility of this information, the models are arranged in categories reflecting the basic modeling technique employed (i.e. the five canonical approaches) as well as the ability of the model to handle environmental range dependence. Such factors define what is termed “domains of applicability.” Hybrid models occasionally compromise strict categorization, and some arbitrariness has been allowed in the classification process. The environmental range dependence considers variations in sound speed or bathymetry. Other parameters may be considered to be range-dependent by some of the models, although they are not explicitly treated in this summary.

The specific utility of these categories is further explained below. In sonar design and operation problems, for example, the analyst is normally faced with a decision matrix involving water depth (deep versus shallow), frequency (high versus low) and range-dependence (range-independent versus range-dependent ocean environments). Jensen (1982, 1984) developed a very useful classification scheme for optimizing this decision logic against the available modeling approaches and their domains of applicability. Jensen’s scheme is slightly modified here to accommodate the five modeling approaches utilized in this book (Figure 4.18). The following assumptions and conditions were imposed in the construction

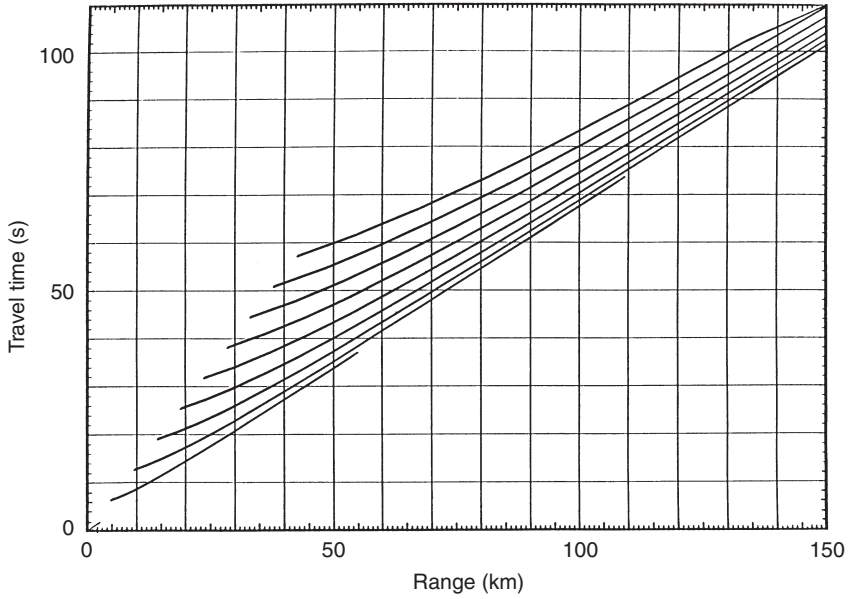


Figure 4.15 RAYMODE travel time versus horizontal range for the ray paths selected in Figure 4.14 (Yarger, 1982).

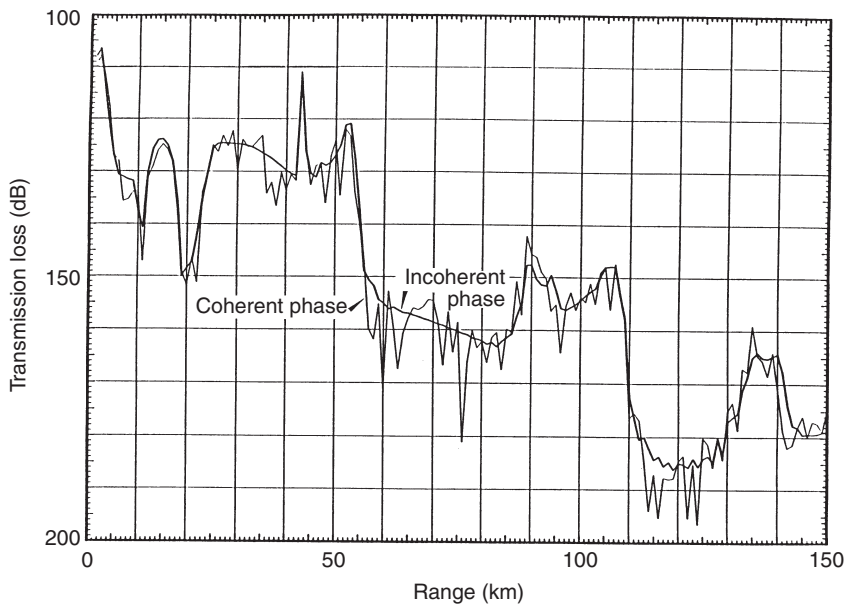


Figure 4.16 RAYMODE TL versus range for both coherent and incoherent phase summations (Yarger, 1982).

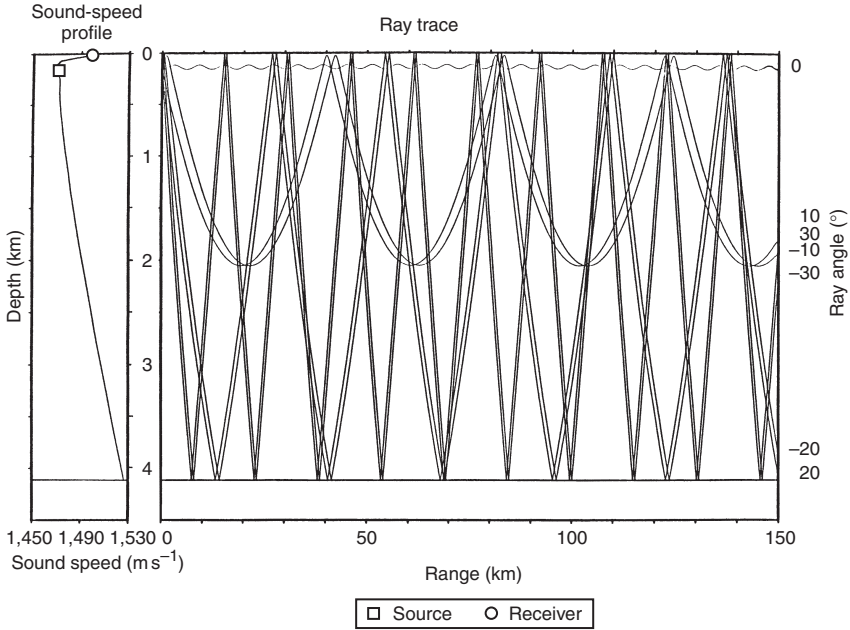


Figure 4.17 RAYMODE ray trace diagram (Yarger, 1982).

of Figure 4.18:

- 1 Shallow water includes those water depths for which the sound can be expected to interact significantly with the sea floor.
- 2 The threshold frequency of 500 Hz is somewhat arbitrary, but it does reflect the fact that above 500 Hz, many wave-theoretical models become computationally intensive. Also, below 500 Hz, the physics of some ray-theoretical models may become questionable due to restrictive assumptions.
- 3 A solid circle indicates that the modeling approach is both applicable (physically) and practical (computationally). Distinctions based on speed of execution may change as progress is made in computational capabilities.
- 4 A partial circle indicates that the modeling approach has some limitations in accuracy or in speed of execution.
- 5 An open circle indicates that the modeling approach is neither applicable nor practical.

Table 4.1 identifies available stand-alone passive propagation models, which are categorized according to the five modeling approaches discussed earlier. (Stand-alone FE models are not included in this summary.) These

Model type	Applications							
	Shallow water				Deep water			
	Low frequency		High frequency		Low frequency		High frequency	
	RI	RD	RI	RD	RI	RD	RI	RD
Ray theory	○	○	◐	●	◐	◐	●	●
Normal mode	●	◐	●	◐	●	◐	◐	○
Multipath expansion	○	○	◐	○	◐	○	●	○
Fast field	●	○	●	○	●	○	◐	○
Parabolic equation	◐	●	○	○	◐	●	◐	◐

Low frequency (<500 Hz) RI: Range-independent environment
 High frequency (> 500 Hz) RD: Range-dependent environment

- Modeling approach is both applicable (physically) and practical (computationally)
- ◐ Limitations in accuracy or in speed of execution
- Neither applicable nor practical

Figure 4.18 Domains of applicability of underwater acoustic propagation models. (Adapted from Jensen, 1982; Proc. MTS/IEEE Oceans 82 Conf., 147–54; copyright by IEEE.)

models are further segregated according to their ability to handle range-dependent environments. Note that range-dependent models can also be used for range-independent environments by inserting a single environmental description to represent the entire horizontal range. Numbers within brackets following each model refer to a brief summary and appropriate documentation. Model documentation can range from informal programming commentaries to journal articles to detailed technical reports containing a listing of the actual computer code. Abbreviations and acronyms are defined in Appendix A.

Taken together, Figure 4.18 and Table 4.1 provide a useful mechanism for selecting a subset of candidate models once some preliminary information is available concerning the intended applications. There are many cases in which two different modeling approaches are suitable (as indicated by a solid circle in Figure 4.18). In such cases, the user is encouraged to select candidates from both categories in order to assess any intermodel differences. Even when only one modeling approach is suitable, more than one candidate model should be tried. In the event of divergences in model predictions (a very likely event), the envelope defining spreads in model outputs can be used to assess the degree of uncertainty in the predictions. Moreover, this envelope may provide diagnostic information that is useful in identifying model pathologies.

Table 4.1 Summary of underwater acoustic propagation models

<i>Technique</i>	<i>Range independent</i>	<i>Range dependent</i>
Ray theory	CAPARAY [1] FACT [2] FLIRT [3] GAMARAY [4] ICERAY [5] PLRAY [6] RANGER [7]	ACCURAY [8] BELLHOP [9] Coherent DELTA [10] FACTEX [11] GRAB [12] GRASS [13] HARORAY [14] HARPO [15] HARVEST [16] LYCH [17]
Normal mode	AP-2/5 [27] BDRM [28] COMODE [29] DODGE [30] FNMSS [31] MODELAB [32] NEMESIS [33] NLNM [34] NORMOD3 [35] NORM2L [36] ORCA [37]	PROTEUS [38] SHEAR2 [39] Strickler [40] ADIAB [41] ASERT [42] ASTRAL [43] CENTRO [44] CMM3D [45] COUPLE [46] CPMS [47] FELMODE [48] Kanabis [49] KRAKEN [50] MOATL [51]
Multipath expansion	FAME [62] MULE [63] NEPBR [64] RAYMODE [65]	MOCYESUMA [52] NAUTILUS [53] PROLOS [54] PROSIM [55] SHAZAM [56] SNAP/C-SNAP [57] WEDGE [58] WKBZ [59] WRAP [60] 3D Ocean [61]
Fast-field or wavenumber integration	FFP [66] Kutschale FFP [67] MSPFFP [68] OASES [69] Pulse FFP [70]	No existing solutions CORE [75] RDEFP [76] RD-OASES [77] RDOASP [78] RDOAST [79]
		SAFRAN [80]

Parabolic
equation

AMPE/CMPE [81]	PAREQ [98]
CCUB/SPLN/CNP1 [82]	PDPE [99]
Corrected PE [83]	PE [100]
DREP [84]	PECan [101]
FDHB3D [85]	PE-FFRAME [102]
FEPE [86]	PESOGEN [103]
FEPE-CM [87]	PE-SSF (UMPE/MMPE) [104]
FEPEs [88]	RAM/RAMS [105]
FOR3D [89]	SNUPE [106]
HAPE [90]	Spectral PE [107]
HYPHER [91]	TDPE [108]
IFD Wide Angle [92]	Two-Way PE [109]
IMP3D [93]	ULETA [110]
LOGPE [94]	UNIMOD [111]
MaCh1 [95]	3DPE (NRL-1) [112]
MOREPE [96]	3DPE (NRL-2) [113]
OS2IFD [97]	3D TDPA [114]

Use single environmental specification

Notes

Ray theory

Range independent

- 1 CAPARAY simulates the effects of layering in the ocean bottom on the propagation of a broadband signal. The ocean bottom is characterized by a geoacoustic profile that includes compressional and shear velocities, density and compressional wave attenuation. Velocity profiles that allow the derivation of analytic expressions for a ray's range, travel time and attenuation are used in the ocean and in the bottom layers. A transfer function representing the total effect of the environment is constructed from the characteristics of each eigenray. The receiver time series is generated using a linear systems approach (Westwood and Vidmar, 1987).
- 2 FACT combines ray theory with higher-order asymptotic corrections near caustics to generate TL in range-independent ocean environments (Baker and Spofford, 1974; Spofford, 1974; Jacobs, 1982; McGirr *et al.*, 1984; Holt, 1985; King and White, 1986a,b).
- 3 FLIRT provides estimates of bottom-bounce and CZ TL using linear ray-tracing methods (McGirr and Hall, 1974).
- 4 GAMARAY is a multi-frequency (broadband) extension to the ray-theoretical approach (Westwood, 1992).

- 5 ICERAY is an extension of CAPARAY that includes layers above the ocean surface to model propagation in the ice. Three types of ray paths are included in the model: (1) compressional rays; (2) shear vertical rays in the upper layer that are converted at the water-ice interface from (or to) compressional rays in the water; and (3) a ray form of the evanescent shear or compressional field in the upper layers (Stotts and Bedford, 1991; Stotts *et al.*, 1994).
- 6 PLRAY is a ray propagation loss program applicable to a horizontally stratified ocean with a flat bottom. It contains a surface duct model based on a simplified approximation to mode theory, which replaces ray computations when the sources and receivers are located in a surface duct (Bartberger, 1978a).
- 7 RANGER is a package of acoustic ray propagation programs used as research tools for bottom-interaction studies. These programs assume an ocean environment that is horizontally stratified with respect to sound speed and water depth (Foreman, 1977).

Range dependent

- 8 ACCURAY uses complex ray methods to find the field due to a point source in the presence of a single plane, penetrable interface (Westwood, 1989b).
- 9 BELLHOP computes acoustic fields in range-dependent environments (Porter, 1991) via Gaussian beam tracing (Porter and Buckner, 1987) [also see the updated summary of SACLANTCEN models by Jensen *et al.* (2001)].
- 10 Coherent DELTA is an extension of a ray-theoretic algorithm developed by A.L. Piskarev, which computes acoustic intensity without calculating eigenrays or focusing factors in caustics. The original algorithm has been modified to sum ray contributions coherently in a range-dependent environment (Dozier and Lallemand, 1995).
- 11 FACTEX extends the FACT model to range-dependent environments by adiabatic mapping of ray families over a sequence of sound-speed profiles with associated bathymetry (Caron, 1975).
- 12 GRAB computes high-frequency (10–100 kHz) TL in range-dependent, shallow-water environments. The model is based on Gaussian ray bundles, which are similar in form (but somewhat simpler) than Gaussian beams (Weinberg and Keenan, 1996; Keenan, 2000; Keenan and Weinberg, 2001). The US Navy standard GRAB model (under OAML configuration management) is a subset of CASS (Keenan *et al.*, 1998).
- 13 GRASS utilizes a ray-tracing technique involving iteration along the ray path to compute TL in range-dependent ocean environments (Cornyn, 1973a,b).
- 14 HARORAY is a 2D broadband propagation model based on ray theory. This code was written to provide synthetic ocean environments to simulate signals used in the Haro Strait coastal-ocean processes experiment (June 1996). The model uses a single point source and a vertical array of receivers. The speed of sound in the water column and bottom layers is homogeneous in depth but variable in range (Pignot and Chapman, 2001).
- 15 HARPO numerically integrates Hamilton's equations in three dimensions. Transmission loss is calculated by computing 3D ray divergence and complex reflection coefficients at the upper and lower boundaries, and by numerically integrating absorption (Jones, 1982; Jones *et al.*, 1982, 1986; Weickmann *et al.*, 1989; Georges *et al.*, 1990; Newhall *et al.*, 1990; Harlan *et al.*, 1991a,b; Jones and Georges, 1991).
- 16 HARVEST is a general hybrid technique that solves the 2D acoustic-viscoelastic equations for bottom-interacting acoustics in water depths exceeding 1 km in the frequency range 100–500 Hz. The model comprises three methods: a Gaussian-beam method is used to propagate the source wave field vertically through the water column; a viscoelastic, finite-difference grid is used to compute the complex acoustic-anelastic interaction of the incident wave field with the rough sea floor; and the backscattered wave field is extrapolated to a distant receiver array using the Kirchhoff integral (Robertsson *et al.*, 1996).
- 17 LYPCH calculates TL on the basis of ray tracing in an environment where both sound speed and bathymetry vary as functions of range (Plotkin, 1996).

- 18 MEDUSA is a ray theoretical model intended for range-dependent, azimuthally symmetric ocean environments. The model uses modified cubic splines to fit the bathymetry and sound-speed profiles with smooth curves, thus eliminating false caustics and shadow zones (Foreman, 1982, 1983).
- 19 MIMIC is a wave-like ray summation model that treats propagation at low frequencies (< 150 Hz) and short ranges ($< CZ$ ranges) in range-dependent ocean environments. The environment is modeled as a water column overlying a sedimentary seabed with an acoustically hard bottom (Ocean Acoustic Developments Ltd, 1999b).
- 20 MPC is a real-time model for engineering applications, particularly training simulators. Surface duct and CZ caustic calculations are performed by the FACT model while the methods of the RAYWAVE model are used to transition across ocean frontal zones (Miller, 1982, 1983).
- 21 MPP is a ray-theoretical model that accommodates range-dependent environments using constant-gradient sound-speed layers with a triangular profile interpolation system (Spofford, 1973a; Jacobs, 1974).
- 22 Pedersen is a ray-theoretical model that uses multiple sound-speed profiles above the sound channel axis, flat bathymetry and bottom loss inputs to compute TL as a function of range. The individual sound-speed profiles are fit by segments with continuous slopes (Pedersen *et al.*, 1962; Gordon, 1964).
- 23 RAYWAVE generates long-range TL values in ocean environments where sound speed, bottom depth and boundary losses may vary significantly along the transmission path. RAYWAVE computes sound speed as a function of depth and range by using triangular regions between adjacent profiles. The prototype RAVE model of Bucker (1971) was the starting point for the development of RAYWAVE (Watson and McGirr, 1975).
- 24 RP-70 is a long-range ray-theoretical model that allows for changing sound-speed profiles and bottom depth over the propagation track. The TL routines utilize an adjacent-ray approach and provide loss values based on incoherent signal addition. An interpolation routine computes intermediate sound speed points, and a linearly segmented bottom-depth profile is used. Absorption can also be made to vary along the propagation path (Colilla, 1970; Harding, 1970).
- 25 SHALFACT is a special version of the FACT model designed for use in shallow-water environments by allowing for a sloping (flat) bottom (Garon, 1976). Contributions from surface-reflected and bottom-reflected paths are made using a rapidly computed analytic expression that represents the average acoustic field.
- 26 TRIMAIN is a ray-theoretical model that divides the range-depth plane into triangular regions (Roberts, 1974). Interpolation of sound speed (c) within each triangle is performed by making $1/c^2$ linear in depth and range. The rays are assumed to be parabolic in each triangle.

Normal mode

Range independent

- 27 AP2 is a normal-mode model based upon the Pekeris branch cut in the complex plane, an infinite sum of normal modes and a branch line integral. AP5 is a normal-mode model similar to AP2 but with a geophysical bottom approximated by up to five sediment layers containing sound-speed and attenuation gradients overlying a homogeneous semi-infinite basement layer characterized by a shear wave speed (Bartberger, 1978b).
- 28 BDRM extends the WKBJ model to include beam-displacement ray-mode theory. These extensions permit calculation of pulse propagation in shallow water as well as extensions to elastic bottom boundaries (Zhang and Li, 1999; Liu *et al.*, 2001).
- 29 COMODE is a normal-mode model that treats bottom attenuation exactly using complex eigenvalues (Gilbert *et al.*, 1983).

- 30 DODGE uses the effective-depth method to determine the normal modes in a shallow-water channel. Using equations developed from simple arguments, the grazing angle and phase speed of each propagating mode are easily determined (Ward, 1989). The effective-depth method (Weston, 1960) replaces the actual seabed (at depth H) with a pressure-release surface at an effective depth (H_e) below the surface.
- 31 FNMSS is a normal-mode model that computes boundary losses due to surface scattering (Gordon and Bucker, 1984). Empirical scattering tables for Arctic pack ice are optional.
- 32 MODELAB is an efficient and numerically robust algorithm for calculating acoustic normal modes in a fluid-layered ocean. Each layer has a sound-speed profile for which the mode functions can be expressed analytically in terms of Airy functions. Attenuation is included as a perturbation. The form of the propagator matrices avoids the numerical instabilities associated with evanescent fields (Levinson *et al.*, 1995).
- 33 NEMESIS is a low-frequency model designed to compute eigenvalues and normal modes in a horizontally stratified deep ocean with single-channel profiles and multiple fluid sediment layers overlying a substrate. Sound speeds in the water and sediment vary with depth, although the density is constant within each layer. The last layer is a homogeneous, semi-infinite fluid or solid substrate in which the compressional and shear speeds (and density) remain constant with depth (Gonzalez and Hawker, 1980; Gonzalez and Payne, 1980).
- 34 NLNM is a normal-mode model for ideal layered media. User-assisted mode selection permits flexibility, but requires user familiarity with mode structures (Gordon, 1979). This model is an extension of the two-layer model of Pedersen and Gordon (1965).
- 35 NORMOD3 is a normal-mode model that uses a finite-difference algorithm (Blatstein, 1974). This model is based on the earlier model by Newman and Ingenito (1972).
- 36 NORM2L calculates the discrete normal modes and acoustic propagation loss for the Pekeris model of the ocean, a simple two-layer model in which the water and seabed have constant acoustic properties (Ellis, 1980). The user interactively enters the frequency, water depth, sound speed and density for the two layers, and the absorption coefficient for the bottom layer.
- 37 ORCA uses a normal-mode method to model propagation in acousto-elastic ocean waveguides. The model assumes horizontally stratified layers in which the sound speed (c) is either constant or varies linearly in $1/c^2$. Multiple-duct environments are handled, and short-range propagation is accurately modeled by including leaky modes in the mode summation. Seismic interface modes such as the Scholte and Stonely modes are also computed. The model uses analytic solutions to the wave equation in each layer: Airy functions for gradient layers and exponentials for isospeed layers (Westwood *et al.*, 1996) [also see the PROSIM model, which is based in part on ORCA. Tolstoy (2001) compared the performance of the ORCA, KRAKEN and PE models against a reference solution generated by the SAFARI model. All three models were highly accurate (mostly within 1 dB of the reference solution) for range-independent environments].
- 38 PROTEUS is a multi-frequency (broadband) extension to the normal-mode approach (Gragg, 1985).
- 39 SHEAR2 extends the standard Pekeris waveguide model (homogeneous layer of fluid overlying an infinite homogeneous fluid half-space of greater sound speed) to handle the case of a fluid overlying an elastic basement in which the shear speed is less than the compressional speed of sound in the fluid. This gives rise to leaky modes in which both the mode eigenfunctions and eigenvalues are complex (Ellis and Chapman, 1985).
- 40 Stickler is a normal-mode model that computes the continuous as well as the discrete modal contributions (Stickler, 1975; Stickler and Ammicht, 1980; Ammicht and Stickler, 1984). The determination of the continuous spectrum to the TL is performed using a uniform asymptotic method that avoids costly numerical evaluation. However, the improper eigenvalues must be found.

Range dependent

- 41 ADIAB is an adiabatic normal-mode program that conserves energy using a consistent boundary-condition approximation (R.A. Koch, unpublished manuscript). Milder's (1969) criterion is used to test the amount of coupling per mode-cycle distance.
- 42 ASFRT uses the ASTRAL model, together with specialized databases, to generate multi-radial portraits of ocean acoustic TL (Lukas *et al.*, 1980a).
- 43 ASTRAL assumes adiabatic invariance in propagating mode-like envelopes through a range-dependent environment (Blumen and Spofford, 1979; Spofford, 1979; Dozier and White, 1988; White *et al.*, 1988; White and Corley, 1992a, b).
- 44 CENTRO is an adiabatic normal-mode model that includes absorptive effects and elastic waves in the ocean floor (Arvelo and Überall, 1990). The source is located in the water column, while the receiver may be located either in the water or in the elastic medium.
- 45 CMM3D is a 3D, coupled-mode model (Chiu and Ehret, 1990, 1994) that is based on the earlier work of Pierce (1965). This model has been interfaced with data generated by an ocean circulation model to examine 3D environmental effects on sound transmission through intense ocean frontal systems.
- 46 COUPLE utilizes a stepwise-coupled-mode method that overcomes the failure of previous coupled-mode techniques to properly conserve energy over sloping bottoms. This method of stepwise-coupled modes avoids problems associated with sloping bottoms by using only horizontal and vertical interfaces. The full solution includes both forward and backscattered energy (Evans, 1983, 1986; Evans and Gilbert, 1985).
- 47 CPMS combines a conventional coupled-mode solution with perturbation theory to provide fast and accurate solutions of TL in range-dependent ocean environments. The efficiency of the coupled-mode solution is improved by removing the need to solve the depth-separated wave equation for the normal modes at each range step. Specifically, the normal modes are found by applying perturbation theory to the modes of the previous step (Tindle *et al.*, 2000).
- 48 FELMODE is a standard normal-mode model that considers an ocean environment consisting of three layers: water column, sediment layer and homogeneous half-space. Density and attenuation in all layers are independent of depth, although attenuation is a function of frequency. The sound speed in the water column and sediment varies with depth while it remains constant in the half-space. Finite-difference discretization is used to solve the modal equation and its boundary conditions. Only discrete modes are calculated, omitting the continuous spectrum. Volume-attenuation losses in the water, sediment and half-space are incorporated by first-order perturbation theory. Shear in the bottom layers is ignored. Range-dependent ocean environments are handled by using the adiabatic approximation. The model was developed in MATLAB with a user-friendly GUI (Simons and Laterveer, 1995; Simons and Snellen, 1998).
- 49 Kanabis is a normal-mode model appropriate for low-frequency, long-range propagation in shallow-water regions (Kanabis, 1975, 1976).
- 50 KRAKEN is a normal-mode model that handles range dependence through either adiabatic coupling or full forward mode coupling between environmental provinces (Porter and Reiss, 1984, 1985; Porter, 1991). KRAKEN is recommended for more experienced modelers or for those requiring a 3D capability [the original KRAKEN algorithm was incorporated into the SNAP model, whereupon SNAP was renamed SUPERSNAP. Since 1984, SUPERSNAP became a standard model at SACLANTCEN and is now simply referred to as SNAP (Porter, 1991)]. Also see the updated summary of SACLANTCEN models by Jensen *et al.* (2001)].
- 51 MOATL computes TL on the basis of the discrete normal modes that propagate in the water column. The sound-speed profile in the water is arbitrary, and the ocean bottom consists of a sediment layer with arbitrary sound-speed profile and an underlying uniform fluid or solid sub-bottom (Miller and Ingenito, 1975; Ingenito *et al.*, 1978; Miller and Wolf, 1980).

- 52 MOCESUMA is a coupled normal-mode model developed by Thomson Sintra, Activités Sous Marines, France (Dr Alain Plaisant). There are two versions: one for 2D environments with fluid-elastic sediments and one for 3D environments with fluid sediments (Noutary and Plaisant, 1996; Papadakis *et al.*, 1998).
- 53 NAUTILUS is a broadband, range-dependent normal-mode model based on the adiabatic formulation. This model is designed for use in shallow water and is currently under review by OAML for designation as a US Navy configuration-managed model. The mode-generating engine is derived from the MODELAB model (Koch and LeMond 2001a-c; Koch and Knobles, 1995).
- 54 PROLOS is a normal-mode propagation loss program that uses the adiabatic approximation to model an environment in which the sound-speed profile, water depth and bottom properties vary slowly with range. PROLOS can handle up to ten layers in the bottom and used up to 500 layers to interpolate the sound-speed profile in the water column. The normal-mode equations are solved using a two-ended shooting technique borrowed from quantum mechanics and generalized to include the effects of density. Shooting from both ends results in a more stable algorithm and gives more accurate eigenfunctions than those obtained from conventional one-ended shooting methods (Ellis, 1985).
- 55 PROSIM is a broadband adiabatic normal-mode propagation model, the kernel of which is based on the range-independent normal-mode propagation model called ORCA. Using PROSIM, the calculation of broadband transfer functions at frequencies up to 10 kHz in shallow water is attainable in a few minutes on a modern workstation (Bini-Verona *et al.*, 2000). [The PROSIM project was partly funded by the European Commission through the Marine Science and Technology programme (MAST3). Recent applications of the PROSIM model were reported by Siderius *et al.* (2001) and by Simons *et al.* (2001). Also see the updated summary of SACLANTCEN models by Jensen *et al.* (2001).]
- 56 SHAZAM is a normal-mode model with both adiabatic and coupled-mode solutions for application to shallow-water environments (Navy Modeling and Simulation Management Office, 1999).
- 57 SNAP is a normal-mode model based on a computer program originally developed at the US Naval Research Laboratory (Miller and Ingenito, 1975; Ingenito *et al.*, 1978). Solutions are found only for the discrete part of the spectrum corresponding to the propagating modes. Losses are introduced in a perturbational manner. Slight range dependence is handled in the adiabatic approximation (Jensen and Ferla, 1979). C-SNAP is a coupled-mode version of SNAP (Ferla *et al.*, 1993). The numerical solution technique for one-way mode coupling was obtained from KRAKEN. When the original KRAKEN algorithm was incorporated into the SNAP model, SNAP was renamed SUPERSNAP. Since 1984, SUPERSNAP became a standard model at SACLANTCEN and is now simply referred to as SNAP (Porter, 1991) [also see the updated summary of SACLANTCEN models by Jensen *et al.* (2001)].
- 58 WEDGE calculates downslope propagation using a 2D representation of the continental slope and realistic environmental parameters (Primaack and Gilbert, 1991). Numerical implementation is divided into two parts: (1) pre-calculation of local modes and (2) mode manipulation. This wedge-mode model is limited to geometries where the propagation can accurately be predicted using only trapped modes. Wedge modes are the intrinsic normal modes in the wedge coordinate system.
- 59 WKBZ is an adiabatic normal-mode model based on a uniform WKB approximation to the modes (Zhang *et al.*, 1995).
- 60 WRAP uses adiabatic and coupled-mode theory for rapid computation of acoustic fields in 3D ocean environments (Perkins *et al.*, 1990; Kuperman *et al.*, 1991).
- 61 3D Ocean expresses the solution of the reduced wave equation for an almost stratified medium in the form of an asymptotic power series. The vertical structure of the solution is expressed as a linear combination of the normal-mode eigenfunctions whose coefficients satisfy 2D eikonal and transport equations (Weinberg and Burridge, 1974).

Multipath expansion

Range independent

- 62 FAME is based upon the multipath expansion for acoustic propagation in a horizontally stratified ocean. The multipaths are expressed in terms of Fresnel integrals and effective range derivatives (Weinberg, 1981).
- 63 MULE is a multi-frequency (broadband) extension to the multipath expansion method (Weinberg, 1985a).
- 64 NEPR modifies the RAYMODE model to account for frequency smearing in the narrowband spectrum (McCammon and Crowder, 1981).
- 65 RAYMODE is a hybrid technique combining elements of ray theory and normal-mode theory to compute TL in range-independent ocean environments (Leibiger, 1968; Yarger, 1976, 1982; Medeiros, 1982a, 1985a; Almeida and Medeiros, 1985; Naval Oceanographic Office, 1991a,c) (the RAYMODE model is discussed in detail in Section 4.8).

Range dependent

- No existing solutions

Fast field or wavenumber integration

Range independent

- 66 FFP applies fast Fourier transform methods to acoustic field theory to obtain TL as a function of range (DiNapoli, 1971; DiNapoli and Deavenport, 1980).
- 67 Kutschale FFP is a rapid and accurate method for calculating TL in the ice-covered Arctic Ocean. Input parameters include source and detector depths, frequency, ice roughness bottom topography and the sound velocity structure as a function of depth in the ice, water and bottom. Computation is performed by direct integration of the wave equation derived from a harmonic point source located in a multilayered, interbedded liquid–solid half-space. The integration method introduced by H.W. Marsh employs the FFT for rapid evaluation of the integral solution (Kutschale, 1973).
- 68 MSPFP, or multiple scattering pulse FFP (Kutschale, 1984), models bottom-interacting pulses corresponding to the coherent summation of many modes over a limited time interval. Specifically, MSPFP decomposes the Kutschale (or pulse) FFP model (Kutschale, 1973; Kutschale and DiNapoli, 1977) into ray-path contributions. Each decomposed term can then be interpreted as the desired path contribution for a corresponding bottom-interacting pulse. The FFP algorithm directly integrates the full-wave solution. Temporal waveforms are computed by Fourier synthesis.
- 69 OASES is a general-purpose computer code for modeling seismo-acoustic propagation in horizontally stratified waveguides using wavenumber integration in combination with the direct global matrix solution technique (Schmidt, 1999). The OASES model is essentially an upgraded version of SAFARI. Compared to SAFARI (version 3.0), OASES provides improved numerical efficiency, and the global matrix mapping has been redefined to ensure unconditional numerical stability. OASES is downward compatible with SAFARI and the preparation of input files follows the format used by SAFARI [also see the updated summary of SACLANTCEN models by Jensen *et al.* (2001)]. (<http://acoustics.mit.edu/arctic0/henrik/www/oases.html>)

- 70 Pulse FFP is a time-marched fast-field program for modeling acoustic pulse propagation in the ocean (Porter, 1990).
- 71 RPRESS uses a high-order, adaptive integration method for efficient computation of the Hankel-transform integral for the wave field in a laterally homogeneous fluid–solid medium (Ivansson and Karasalo, 1992). This model has been used to investigate frequency-dependent propagation losses in shallow water caused by shear losses in the sediment (Ivansson, 1994).
- 72 SAFARI is based on the wavenumber integration technique (or fast field program) to solve the wave equation exactly for strictly range-independent environments (Schmidt and Glatterre, 1985; Schmidt, 1988). The model includes propagation of waves in fluid and solid media by discretizing the environment into layers with different acoustic properties. The Green’s function is evaluated analytically within each layer and the boundary conditions are fulfilled at each layer interface by using a numerically stable direct-global-matrix approach. SAFARI consists of three independent models: FIPR to compute the plane-wave complex reflection coefficient due to an arbitrarily layered medium; FIP for general single frequency wave propagation; and FFP for pulse propagation. An updated version of SAFARI called OASES (discussed above) is available on the Web [also see the updated summary of SACLANTCEN models by Jensen *et al.* (2001)].
- 73 SCOOTER is a finite-element FFP code for computing acoustic fields in range-independent environments. It is recommended for use when the horizontal range is less than ten water depths (Porter, 1990).
- 74 SPARC is a time-marched FFP model that treats problems dealing with broadband or transient sources (i.e. pulses) (Porter, 1990, 1991).

Range dependent

- 75 CORE is a coupled version of OASES for range-dependent environments. It belongs to the new spectral super-element class of propagation models for range-dependent waveguides. This approach is a hybridization of the FE and BEM. The ocean environment is divided into a series of range-independent sectors separated by vertical interfaces (Goh *et al.*, 1997).
- 76 RDPFP utilizes a generalized Green’s function method for solving the one-way wave equation exactly in an ocean environment that varies discretely with range. An explicit marching solution is obtained in which the source distribution at any given range step is represented by the acoustic field at the end of the previous step (Gilbert and Evans, 1986).
- 77 RD-OASES is a range-dependent version of OASES (Schmidt, 1999). RD-OASES extends to fluid–elastic stratifications the development of a spectral super-element approach for acoustic modeling in fluid waveguides using a hybridization of FE, boundary integrals and wave-number integration to solve the Helmholtz equation in a range-dependent ocean environment. The ocean environment is divided into a series of range-independent sectors separated by vertical interfaces. This model provides accurate, full two-way solutions to the wave equation using either a global multiple scattering solution or a single-scatterer, marching solution.
- 78 RDOASP is a pulse version of RD-OASES (Goh and Schmidt, 1996). (http://acoustics.mit.edu/arctic0/henrik/www/rd_oases.html)
- 79 RDOAST refers to the specific combination of RD-OASES and VISA (Goh and Schmidt, 1996). The virtual source algorithm (VISA) uses the marching, local single-scatterer approximation to the transmission and reflection problem at the sector boundaries; thus, a virtual array of sources and receivers is introduced on each sector boundary, (http://acoustics.mit.edu/arctic0/henrik/www/rd_oases.html).

80 SAFRAN uses a hybrid combination of wavenumber integration and Galerkin BEM to extend the fast-field theory technique to range-dependent ocean environments (Seong, 1990).

Parabolic equation

Range independent

Use single environmental specification with range-dependent model.

Range dependent

- 81 AMPE was developed to solve global-scale ocean acoustic problems that are too large to solve with other existing 3D codes. The PE method was used to solve 2D wave equations for the adiabatic mode coefficients over latitude and longitude (Collins, 1993d). CMPE is a generalization of AMPE that includes mode-coupling terms. It is practical to apply this approach to large-scale problems involving coupling of energy between both modes and azimuths (Abawi *et al.*, 1997).
- 82 CCUB/SPLN/CNP1 represent a family of higher-order, finite-element PE methods developed by the Foundation for Research and Technology – Hellas, Institute of Applied and Computational Mathematics, Greece (Papadakis *et al.*, 1998).
- 83 Corrected PE solves the PE using the split-step algorithm. (Perkins and Baer, 1978; Perkins *et al.*, 1982). By assuming cylindrical propagation symmetry, it is possible to simulate a tilted acoustic array placed in the calculated complex-valued acoustic field.
- 84 DREP is a wide-angle PE based on an operator-splitting that permits the use of a marching type Fourier transform solution method (Thomson and Chapman, 1983; Thomson, 1990).
- 85 FDB3D is a hybrid 3D, two-way propagation model for solving 3D backscattering problems. It is based on the IFD PE approach (Zhu and Bjørnø, 1999).
- 86 FEPE computes the complex acoustic pressure in range-dependent ocean environments. The model solves higher-order parabolic equations using a numerical solution based on Galerkin's method, alternating directions and Crank-Nicolson integration (Collins, 1988a). The model allows arbitrary sound-speed, density and attenuation profiles. FEPE provides several options for the initial starting field including the Gaussian PE starter (Tappert, 1977) and Greene's (1984) PE starter.
- 87 FEPE-CM combines the FEPE code with the PERUSE surface scattering formulation to model the forward scattering from both periodic and single realizations of randomly rough sea surfaces. A conformal mapping technique converts the rough-surface scattering problem into a succession of locally flat-surface problems (Norton *et al.*, 1995). Norton and Novarini (1996) used FEFE-CM to investigate the effect of sea-surface roughness on shallow-water waveguide propagation.
- 88 FEPEs extends the FEPE model to handle range-dependent elastic media (Collins, 1993b,c). This energy-conserving, elastic PE model is applicable to a large class of problems involving waveguides consisting of both fluid and solid layers.
- 89 FOR3D implements the Lee-Saad-Schultz (LSS) method for solving the 3D, wide-angle wave equation (Botseas *et al.*, 1987; Lee *et al.*, 1988, 1992). The model is designed to predict TL in ocean environments that vary as functions of range, depth and azimuth.

- 90 HAPE implements the rational-linear approximation in a finite-difference formulation to provide accurate treatment of high-angle propagation to angles of about 40° with respect to the horizontal (Greene, 1984). A rational approximation to the square-root operator was first suggested by Claerbout (1976; 206). This approximation reduced the phase error problem inherent in the original, narrow-angle PE models that had been limited to about 15° [note: more recent, higher-order PE implementations have virtually eliminated the phase error problem and are accurate for propagation angles of nearly 90°].
- 91 HYPEP is a hybrid parabolic equation-ray model intended for high-frequency applications (Tappert *et al.*, 1984).
- 92 IFD wide angle implements an implicit finite-difference scheme for solution of the PE (Lee and Botseas, 1982; Botseas *et al.*, 1983). This model can handle arbitrary surface boundary conditions and an irregular bottom with arbitrary bottom boundary conditions.
- 93 IMP3D extends the FOR3D model by including a simplified elastic impedance bottom boundary condition (Papadakis *et al.*, 1998).
- 94 LOGPE uses a logarithmic expression for the index of refraction in the standard PE in order to closely approximate solutions of the more exact Helmholtz equation in weakly range-dependent ocean environments (Berman *et al.*, 1989).
- 95 MaCh1 is a broadband, range-dependent acoustic propagation model based on the one-way form of the Maslov integral representation of the wave field. The one-way propagation assumption may be combined with a parabolic approximation (Brown, 1994).
- 96 MOREPE is an energy-conserving parabolic equation that can handle relatively large variations in the index of refraction (Schurman *et al.*, 1991).
- 97 OS2IFD is a full-featured version of IFD parabolic equation that runs on personal computers (PCs) under the OS/2 operating system (Robertson *et al.*, 1991).
- 98 PAREQ is a PE model based on the split-step algorithm (Jensen and Krol, 1975). This model is a modified version of the one developed by AESD (Brocks, 1978) [also see the updated summary of SACLANTCEN models by Jensen *et al.* (2001)].
- 99 PDPE is a pseudodifferential PE model. The documentation contains a numerical algorithm for its implementation (Avilov, 1995).
- 100 PE is based on the original algorithm developed by Hardin and Tappert (1973) and Tappert (1977). The original US Navy version was implemented by Brock (1978). Upgrades have been reported by Holmes (1988) and by Holmes and Gainey (1992a–c). A version of this model can accommodate ice-covered regions.
- 101 PECAN is an $N \times 2D/3D$ parabolic equation model for underwater sound propagation that was developed for matched-field processing applications (Brooke *et al.*, 2001).
- 102 PE-FRAME applies the FE method to produce a full-wave, range-dependent, scalar, ocean acoustic propagation model (Chin-Bing and Murphy, 1988; Murphy and Chin-Bing, 1988). The term “full wave” includes the continuous and discrete spectra, forward propagation and backscatter. The model can be given a long-range capability through super elements or marching frames.
- 103 PESOGEN is a special-purpose microcomputer model used to compute the acoustic field in a fully range-dependent environment over a wide range of frequencies for both deep-water and shallow-water regions with greatly reduced execution times (Nghiem-Phu *et al.*, 1984).
- 104 PE-SSF (UMPE/MIMPE): MMPE and its predecessors, UMPE (Smith and Tappert, 1993) and MIMPE, are now collectively referred to as PE-SSF (parabolic equation-split-step Fourier algorithm). PE-SSF thus represents a wide class of PE models (Tappert, 1998).
- 105 RAM incorporates an improved elastic PE (Collins, 1998) together with a stable self-starter (Cederberg and Collins, 1997). A companion version called RAMS is available for acousto-elastic problems. Both RAM and RAMS use the split-step Padé solution, which is approximately two orders of magnitude faster than the Crank-Nicolson solution of the wide-angle PE (Collins, 1993a).
- 106 SNUPE achieves linearization of the depth-direction operator by expansion into a multiplicative Padé approximation. Galerkin’s method is used for computational efficiency to approximate the depth-direction equation. Crank-Nicolson’s method is used to approximate the range-direction equation. A numerical self-starter initiates the near-field solution (Seong and Choi, 2001).

107 Spectral PE extends the two-way PE to 3D problems involving a point source in a waveguide in which the acoustic properties vary with depth and range
(Orris and Collins, 1994). This model presents an efficient approach for solving backscattering problems that are separable in one of the horizontal
Cartesian coordinates, including backscattering from extended features such as ridges.

108 TDPE is the inverse Fourier transform of the wide-angle PE (Collins, 1988b).

109 Two-way PE generalizes the PE to handle backscattered acoustic energy in the ocean (Collins and Evans, 1992). The two-way PE is based on the single-
scattering approximation and the approach of the two-way coupled modes in which range-dependent environments are approximated by a sequence of
range-independent regions. The outgoing and incoming fields are propagated by two-way range marching.

110 ULETA is based on Tappert's (1977) PE model. ULETA generates transmission losses for single frequency (CW) or pulse sources in range-dependent
ocean environments (Palmer *et al.*, 1988b).

111 UNIMOD is a hybrid combination of PE (for waterborne energy) and FACT or MPP for bottom-interacting energy (R.B. Lauer, unpublished).

112 3DPE (NRL-1) solves the 3D PE using the split-step algorithm (Perkins and Baer, 1982; Perkins *et al.*, 1983). The input sound-speed profiles and
bathymetry need not be specified on a regular grid. However, interpolation schemes based on user-supplied triangularizations of the region are employed.
Three graphic outputs can be produced: (1) TL versus range (with depth and azimuthal angle held fixed); (2) TL versus depth (with range and azimuthal
angle held fixed); and (3) TL versus azimuthal angle (with range and depth held fixed). An additional program can simulate the performance of a horizontal
acoustic array at given ranges.

113 3DPE (NRL-2) handles wide propagation angles in depth, narrow propagation angles in azimuth and rough boundaries (Collins and Chin-Bing, 1990).

114 3D TDPA uses one-way narrow-angle and wide-angle, 3D, time domain paraxial approximations to simulate pulse propagation in 3D ocean geometries
characterized by volume attenuation and variable density (Orchard *et al.*, 1992).

5 Propagation II

Mathematical models (Part Two)

5.1 Background

Mathematical models of underwater acoustic propagation include both numerical models and empirical models. Chapter 4 addressed the theoretical development of numerical models and summarized their availability. This chapter addresses the development of empirical models applicable to special propagation paths such as surface ducts, shallow water and Arctic half-channels. Where appropriate, comparisons are made with predictions generated by numerical models. Data support requirements for mathematical models of propagation are discussed and a select number of special applications are described in order to highlight promising areas for future research and development.

5.2 Surface duct models

Properties of the surface duct were discussed previously in Chapter 3. Both ray- and wave-theoretical solutions can be applied to propagation in the surface duct.

5.2.1 Ray-theory models

An expression for transmission loss (TL) in a surface duct may be obtained through simple ray-theoretical considerations (Urlick, 1983). In Figure 5.1, let a nondirectional source of sound be located at P in a surface duct (or mixed layer). Also, let c_0 denote the reference sound speed in the duct. Of all the rays leaving the source, only those within a certain limiting angle 2θ remain in the duct. At a distance of 1 m, the power contained in this ray bundle is distributed over a portion of the spherical surface A_1 . At a long distance r , this same amount of power (in the absence of leakage and absorption) is distributed over a cylindrical surface A_2 . Because the power crossing areas A_1 and A_2 is conserved, the TL to range r , averaged over the duct thickness H , is

$$TL = 10 \log_{10} \frac{A_2}{A_1}$$

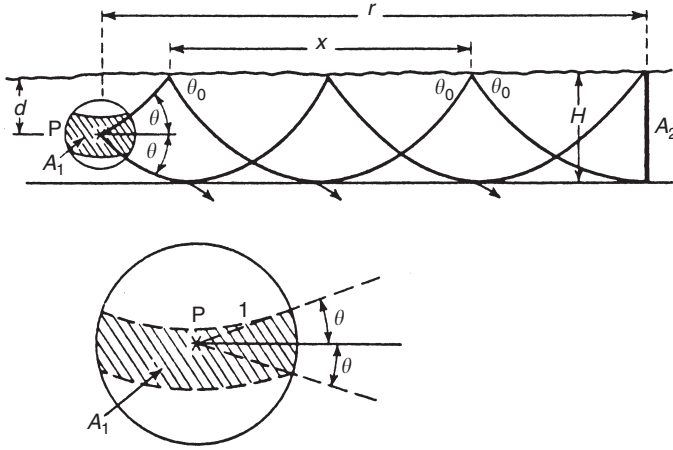


Figure 5.1 Propagation geometry in a surface duct. (Urlick, 1983; *Principles of Underwater Sound*, 3rd edn; reproduced with permission of McGraw-Hill Publishing Company.)

By geometry

$$A_2 = 2\pi rH \quad \text{and} \quad A_1 = 2\pi \int_{-\theta}^{\theta} \cos \theta \, d\theta = 4\pi \sin \theta$$

Therefore, for the surface duct

$$TL = 10 \log_{10} \frac{rH}{2 \sin \theta} = 10 \log_{10} r r_0 = 10 \log_{10} r_0^2 \frac{r}{r_0}$$

where $r_0 = H/(2 \sin \theta)$ and θ is the inclination angle at the source of the maximum trapped ray. The quantity $r_0^2 r/r_0$ indicates that the propagation to range r may be viewed as the result of spherical spreading out to a transition range r_0 , followed by cylindrical spreading from r_0 to r . The range r_0 also corresponds to the condition in which the vertical extent of the beam subtended by the angle 2θ equals the duct thickness H . Ranges greater than r_0 are generally considered to represent far-field conditions. When the attenuation due to absorption and leakage is added, the duct TL expression becomes

$$TL = 10 \log_{10} r_0 + 10 \log_{10} r + (\alpha + \alpha_L)r \times 10^{-3} \tag{5.1}$$

where α is the absorption coefficient (dB km^{-1}), α_L is the leakage coefficient (dB km^{-1}) that expresses the rate at which acoustic energy leaks out of the duct and r is the range (m). This expression is applicable to all ducts.

154 Propagation II: mathematical models (Part Two)

For a duct with a constant sound-speed gradient (g), in which the rays are arcs of circles with radius of curvature $R = c_0/g$, the following relationships result from geometry when $R \gg H$ and when $\sin \theta_0 \ll 1$ at source depth d (refer to Figure 5.1):

$$R = \frac{c_0}{g} = \text{radius of curvature of rays}$$

$$x = \sqrt{8RH} = \text{skip distance of limiting ray}$$

$$\theta_0 = \sqrt{\frac{2H}{R}} = \text{maximum angle of limiting ray (rad)}$$

$$\theta = \sqrt{\frac{2(H-d)}{R}} = \text{angle of limiting ray at source depth (rad)}$$

$$r_0 = \sqrt{\frac{RH}{8}} \sqrt{\frac{H}{H-d}} = \frac{x}{8} \sqrt{\frac{H}{H-d}} = \text{transition range}$$

Kinsler *et al.* (1982: 402–6) also presented an insightful development of these relationships.

Marsh and Schulkin (1955) developed empirical surface duct equations based on an extensive set of data collected during Project AMOS in 1953–54. These equations have been incorporated into many ray-theoretical models to handle the special case of surface duct propagation. Graphical summaries of the AMOS data were presented in Chapter 3. Other empirically derived formulae have been reviewed by Urick (1982: chapter 6).

5.2.2 Wave-theory models

Pedersen and Gordon (1965) adapted Marsh's (1950) normal-mode approach to short ranges for a bilinear gradient (positive gradient overlying a negative gradient) model of a surface duct (Figure 5.2). This now classic bilinear surface duct model has been incorporated into some ray-theoretical models to augment their capabilities.

Assuming that leakage due to surface roughness can be neglected, TL is given as a function of range by

$$\text{TL} = -10 \log_{10} \left| \sum_1^N H_0^{(2)}(\lambda_n r) u_n(t) u_n(t_0) \right|^2 - 20 \log_{10} \pi + \alpha r \quad (5.2)$$

where N is the number of modes included in the computation, $H_0^{(2)}$ the zero-order Hankel function of the second kind, λ_n the complex wavenumber, n the mode counter index ($n = 1, 2, \dots, N$), r the range, $u_n(\cdot)$ the depth function, t the ratio of receiver depth to depth of channel, t_0 the ratio of source depth to depth of channel and α the absorption coefficient.

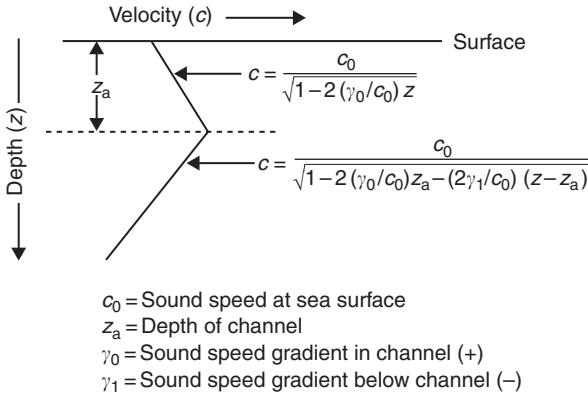


Figure 5.2 Geometry of bilinear-gradient model (Pedersen and Gordon, 1965).

Qualitatively, the relationship in Equation (5.2) predicts cylindrical spreading as a function of range combined with the effects of modal interactions. These modes may be thought of as damped sinusoidal waves. There are two basic factors that determine the degree to which a particular mode contributes to the result. First, the product $|u_n(t)u_n(t_0)|$ depends on the source and receiver depths, but not on range. Specifically, an exponential damping factor implicit in the formulation causes the relative contributions of a mode to decrease with increasing range and with increasing mode number.

By invoking simplifying approximations, Pedersen and Gordon (1965) were able to generate analytical solutions using a variation of Equation (5.2) that agreed favorably with both ray-theoretical solutions and with experimental data. There are three important aspects of this approach that differ from other normal mode solutions: (1) the solution is valid for short ranges because the branch-cut integral is zero for this model; (2) the modes are damped since the wavenumbers are complex; and (3) there are no cutoffs in the frequency domain. Thus, higher-order modes are highly damped and only the lower-order modes need be considered for most practical problems.

5.2.3 Oceanographic mixed-layer models

New developments in numerical modeling in oceanography now permit the depth of the mixed layer to be forecast in both time and location. These predicted values can then be incorporated into surface duct models to predict the corresponding acoustic transmission loss. Such interfacing of models is referred to as “coupled ocean acoustic modeling” (Mooers *et al.*, 1982). Models of the mixed layer have largely been restricted to the treatment of 1D approximations, which have proved useful when horizontal advection

can be neglected. In many ocean areas, however, the 1D approximations appear to be inappropriate for estimating mixed layer depths (Garwood, 1979).

Mixed-layer models are of two basic types: differential and bulk. Differential models use the equations for conservation of momentum, heat, salt and turbulent kinetic energy (TKE) in their primitive form, and are not integrated over the mixed layer. The region where the local TKE is large enough to provide a certain minimum level of vertical mixing defines the mixed layer for these models. Bulk, or integrated, models assume that the mixed layer is a well-defined layer that is uniform in temperature and salinity. The governing equations for these models are obtained by integrating the primitive equations over the depth of the mixed layer.

Mixed-layer models respond to three basic types of forcing conditions: wind deepening, heating and cooling. Wind deepening is defined to occur when the mixed layer deepens due to the erosion of the stably stratified region at its base by wind-generated turbulence. The depth of mixing is governed by a balance between the stabilizing effect of surface heating, or a positive surface buoyancy flux, and the effect of mixing due to wind-generated turbulence. This balance governs the mixed layer depth during periods when the mixed layer is shallowing. Under conditions of cooling, a net surface heat loss, or negative surface buoyancy flux, causes the mixed layer to deepen due to convection. Convection usually occurs at night and is the dominant mechanism for deepening the mixed layer in fall and winter, especially under conditions of reduced solar heating and increased evaporative cooling due to increased wind speeds.

A number of mixed-layer models have been developed and some have been coupled with underwater acoustic transmission loss models to provide input (and feedback) for the parameters important for prediction of sound propagation in the surface duct. One system that is operational for fleet applications is the thermodynamical ocean prediction system, or TOPS (Clancy and Martin, 1979). TOPS is categorized as a differential mixed-layer model. Forecasts appear to agree well with measurements in those ocean area where the layer depth is dependent primarily on local conditions and not on advection from neighboring regions. A comparison of observations and predictions generated by TOPS (Figure 5.3) shows reasonable agreement. The top panel illustrates the observed wind speed. The middle panel compares the observed and predicted mixed layer temperatures while the bottom panel compares the observed and predicted depths over the same period.

Clancy and Pollak (1983) advocated coupling the TOPS synoptic mixed-layer model to an objective ocean thermal analysis system in order to produce a continuously updating, real-time, analysis–forecast–analysis system. The forecast component (TOPS) employs the Mellor and Yamada (1974) level-2 turbulence parameterization scheme. It includes advection by instantaneous wind drift and climatologically averaged geostrophic currents, and is forced by surface fluxes supplied by atmospheric models.

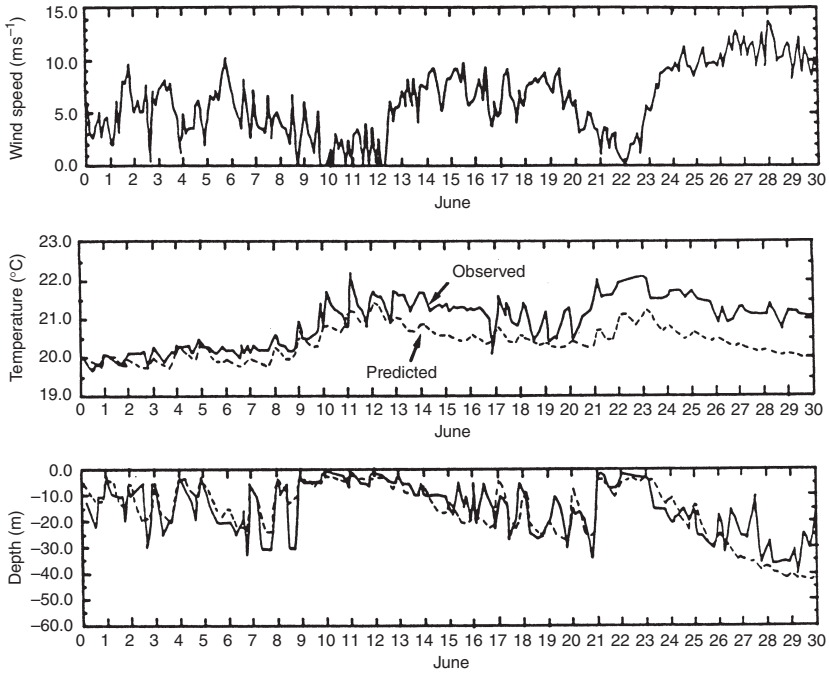


Figure 5.3 Observations and predictions at Ocean Station November (in the North Pacific Ocean) during June 1961. Upper panel: observed wind speed. Middle panel: observed (solid line) and predicted (dashed line) sea-surface temperatures. Bottom panel: observed (solid line) and predicted (dashed line) mixed layer depths (Clancy *et al.*, 1981).

The diurnal ocean surface layer (DOSL) model, which predicts diurnal patterns of the sea-surface temperature (SST) field, has been developed to support high-frequency sonar operations against shallow targets (Clancy *et al.*, 1991b; Hawkins *et al.*, 1993). Diurnal variability in the mixed layer dominates short-term changes in the acoustic behavior of the surface duct. The well-known ‘afternoon effect’ discovered during Second World War denotes the loss of a surface duct due to the creation of a shallow, transient thermocline by local heating. Diurnal SST changes also affect the use and interpretation of satellite data. Specifically, satellites measure the skin temperature of the ocean, and these surface measurements may or may not be characteristic of the bulk mixed-layer temperature (the desired parameter for naval operations) depending on the amplitude and phase of the SST cycle at the time of measurement. Since the diurnal SST response is a strongly nonlinear function of the wind speed, smooth variations in the synoptic wind field can produce sharp horizontal SST gradients that might be misinterpreted as the thermal signature of ocean frontal features.

5.3 Shallow-water duct models

5.3.1 *Shallow-water propagation characteristics*

Acoustic propagation in shallow water is dominated by repeated interactions with the sea floor. Generally, shallow water is restricted to consideration of the continental shelves with depths less than 200 m. Detection ranges in shallow water are severely limited both by the high attenuation that results from interaction with the bottom and by the limited water depth, which will not support the long-range propagation paths available in deep water. In a recent book, Katsnelson and Petnikov (2002) discussed results from acoustical measurements made over the continental shelves of the Barents Sea and the Black Sea.

Determination of source location (bearing, range and depth) can be affected by the horizontal refraction caused by repeated boundary reflections over a sloping bottom. Doolittle *et al.* (1988) experimentally confirmed the horizontal refraction of CW acoustic radiation from a point source in a wedge-shaped ocean environment. A striking graphical presentation of a 3D ray trace in a complicated wedge-shaped ocean environment is illustrated in Figure 5.4 (Bucker, 1994). This ray trace vividly displays the effects of horizontal refraction caused by a sloping bottom boundary. The source (denoted by an asterisk) appears in the background. Such horizontal refractive effects complicate the determination of bearing angles between sources and receivers. Consequently, sonar detections made against targets in shallow water may need to be corrected for horizontal refraction.

It is convenient to categorize sound-speed profiles into generic groupings to facilitate subsequent discussions of shallow-water propagation. Assuming

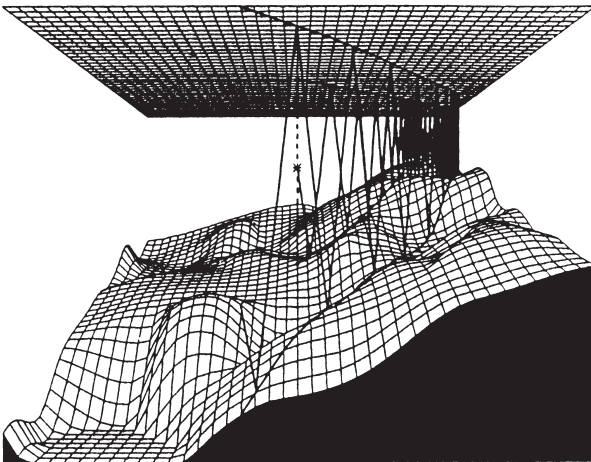


Figure 5.4 Typical beam trace in a shallow-water region (Bucker, 1994).

linearly segmented profiles, three groupings of profiles can be distinguished by the degree of segmentation: Category I – linear, Category II – bilinear and Category III – multiply segmented. Subgroupings (labeled A, B, . . .) can be formed to further distinguish these profiles according to the sound-speed gradient.

Linear profiles consist of single segments that can be further distinguished according to their gradient as: I-A – positive-gradient ($\partial c/\partial z > 0$), I-B – negative-gradient ($\partial c/\partial z < 0$) or I-C – isovelocity ($\partial c/\partial z = 0$), where c is the speed of sound and z is the depth (measured positive downward).

Bilinear profiles consist of two segments and can be formed in two ways in the ocean. If a positive-gradient overlies a negative-gradient (II-A), then a surface duct is formed in the upper layer above the sound-speed maximum. If a negative-gradient overlies a positive-gradient (II-B), then a sound channel is formed at the juncture of the two segments (i.e. at the sound-speed minimum).

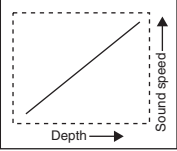
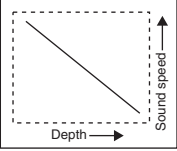
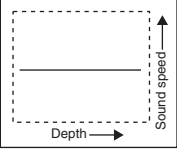
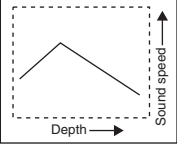
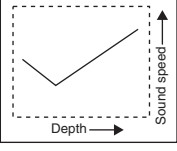
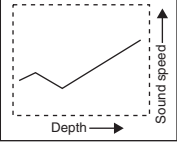
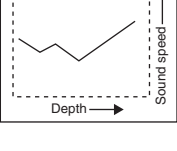
Multiply segmented profiles consist of three or more segments and can assume a variety of forms. However, the most common manifestation of this type occurs when a surface duct overlies a channel (III-A). Other manifestations typically involve multiple channels (III-B).

This classification system provides a convenient method for describing the general distribution of sound-speed profiles in shallow-water environments (with depths ≤ 200 m). For example, Reise and Etter (1997) used this classification system in a sonar trade study that examined representative shallow-water profiles from the Pacific and Atlantic oceans, and the Mediterranean and Arabian seas (Table 5.1). Based on this small but representative sampling, the most common occurrence (42 percent of all profiles examined) was the bilinear profile with a surface duct (II-A). This form was almost twice as likely to occur in summer as in winter (64 versus 36 percent, respectively). The next most common occurrence (23 percent of all profiles examined) was the linear positive-gradient profile (I-A). This form occurred exclusively in winter (100 percent). No isovelocity cases (I-C) were encountered in the study. Multiply segmented forms (III-A and III-B) represented 15 percent of the profiles examined and were three times more frequent in summer than in winter (75 versus 25 percent). The linear negative-gradient profile (I-B) represented 12 percent of the profiles examined and occurred exclusively in summer (100 percent). Finally, the bilinear sound channel (II-B) represented 8 percent of the profiles examined and occurred as frequently in summer as in winter (50 percent each). It should be noted that these results might not be representative of every shallow-water region in every season.

5.3.2 Optimum frequency of propagation

Understanding and predicting acoustic sensor performance in shallow water is complicated by the relatively high temporal and spatial variability of the

Table 5.1 Categorization of shallow-water sound-speed profiles. Also shown are the probabilities of occurrence as determined by Reise and Etter (1997)

Group designation/ subgroup	Linear		Bilinear		Multiply segmented		
	I-A, positive gradient (%)	I-B, negative gradient (%)	I-C, isovelocity	II-A, surface duct (%)	II-B, sound channel (%)	III-A, duct over channel (%)	III-B, multiple channels (%)
Relative occurrence	23	12	-	42	8	15	
Summer	-	100	-	64	50	75	
Winter	100	-	-	36	50	25	
							

ocean environment. Improper optimization of the frequency or the depth of operation at a particular location and time of year can degrade sonar performance.

In shallow-water environments, the optimum frequency of propagation is often the result of competing propagation and attenuation mechanisms at either end of the frequency spectrum. Jensen and Kuperman (1979, 1983) investigated this problem and concluded that the optimum frequency is strongly dependent on water depth, is somewhat dependent on the particular sound-speed profile, and is only weakly dependent on the bottom type. Jensen and Kuperman (1983) also noted that shear waves in the bottom were important in determining the optimum frequency of propagation and the actual transmission loss levels at lower frequencies. A major loss mechanism for low-frequency acoustic propagation in shallow water is the attenuation in ocean sediments. Research results (e.g. Focke, 1984) indicate that variations in attenuation as a function of sediment depth have a significant impact on propagation.

An important analytical tool used by Jensen and Kuperman (1979, 1983) was a frequency-range representation of transmission loss, as illustrated in Figures 5.5 and 5.6. This type of representation has been used to characterize acoustic propagation in different waveguides (e.g. Milne, 1967). For the particular environment studied (Figure 5.5), a normal mode model was used to generate repeated TL runs versus frequency. In Figure 5.6(b), the

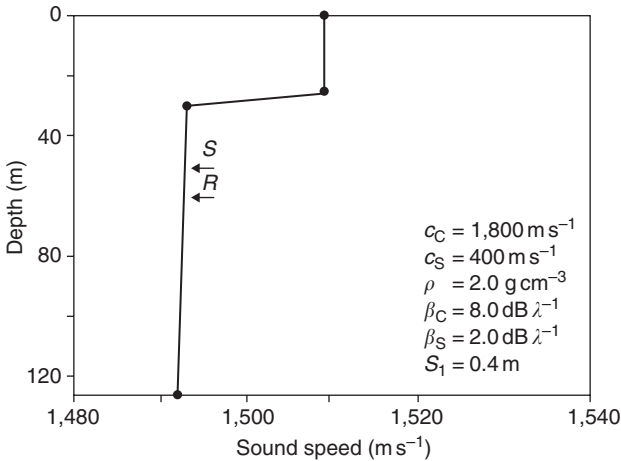


Figure 5.5 Sound-speed profile and bottom properties for a shallow-water area located in the eastern North Atlantic Ocean: c = sound speed, ρ = density, β = attenuation, S_1 = rms bottom roughness. Subscripts “C” and “S” refer to compressional and shear waves, respectively. Source (S) and receiver (R) depths are indicated on the sound-speed profile (Jensen and Kuperman, 1979).

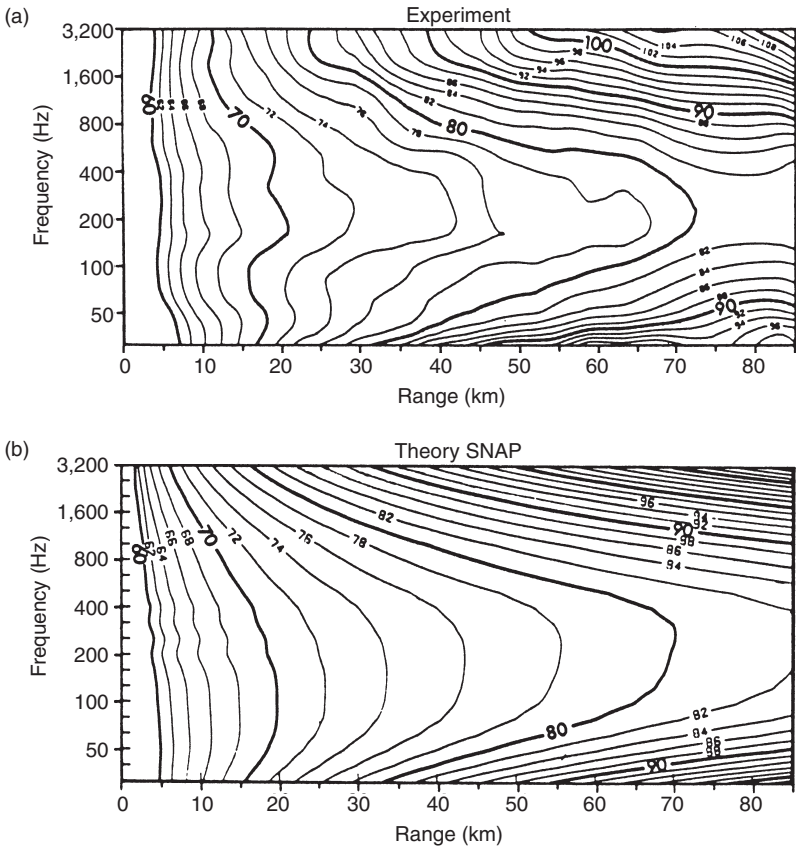


Figure 5.6 Transmission loss contours (in 2-dB intervals) for the environment presented in Figure 5.5: (a) experimental measurements and (b) predictions generated by the SNAP propagation model (Jensen and Kuperman, 1979).

optimum frequency predicted by the model is about 200 Hz, as evidenced by the elongated axis of low-loss values. These predicted results compared favorably with experimental results (Figure 5.6(a)).

Shallow-water modeling techniques include both numerical models and empirical models. Eller (1984b, 1986) summarized important development in shallow-water acoustic modeling. Katsnelson and Petnikov (2002) reviewed experimental results in shallow-water acoustics together with approximate approaches for modeling such phenomena.

5.3.3 *Numerical models*

Both ray- and wave-theoretical approaches have been used to numerically model sound propagation in shallow water. Since shallow water

environments are best approximated by range-dependent geometries (e.g. sloping bottom and high spatial variability of water-column and sediment properties), attention will be focused on the range-dependent modeling approaches. Moreover, the high-angle boundary interactions encountered in shallow water have traditionally limited consideration to two basic approaches: ray theory and normal-mode solutions (with either adiabatic approximations or mode coupling). More recently, appropriately modified PE models have also been utilized successfully in shallow-water environments (Jensen, 1984; Jensen and Schmidt, 1984). Approximately 18 percent of the numerical modeling inventory is specifically tailored for shallow-water applications (Eter, 2001c).

Much emphasis has been placed on modeling sound propagation over a sloping bottom. This geometry is commonly referred to as a “wedge problem” and involves both upslope and downslope propagation. The direction of propagation (i.e. upslope or downslope) considerably alters the observed propagation characteristics. Consequently, this problem is of great practical interest to sonar operations in shallow water. This geometry has also been used as a benchmark problem in model evaluation (see Chapter 11).

The basic mechanisms involved in acoustic propagation in a horizontally stratified (i.e. range-invariable) waveguide are spreading loss, attenuation due to bottom-interaction effects, and intermode phasing effects. In a range-variable waveguide, an additional mechanism must be considered. This mechanism is related to changes in the acoustic energy density that occur with bathymetric changes and is often referred to a renormalization loss, or megaphone effect. The term renormalization is used because the so-called megaphone effect is manifested as a change in the normalization of the normal mode depth function due to changes in the waveguide depth (Koch *et al.*, 1983). The megaphone effect produces a gain in upslope propagation and a loss in downslope propagation.

The processes involved in upslope propagation can be better understood by using the ray-mode analogy. This analogy is a heuristic concept which states that any given mode trapped in the water column can be associated with upgoing and downing rays corresponding to specific grazing angles at the bottom (e.g. Urick, 1983: 174–6; Boyles, 1984: 197–204). As sound propagates upslope, the horizontal wavenumber associated with each mode decreases. In the ray analogy, the grazing angle at the bottom increases. For each mode, then, a point on the slope will be reached at which the grazing angles of the analogous rays will approach the critical angle at the bottom. At this point, the energy essentially leaves the water column and enters the bottom. In the ray analogy, the bottom-reflection losses associated with those rays become very large. In the wave analogy, the modes transition from the trapped (waterborne) to the continuous (bottom propagating) spectrum. This point is called the “cutoff depth” for the equivalent modes. Upslope propagation is then said to exhibit a transition from a trapped to a radiative state (e.g. Arnold and Felsen, 1983; Jensen, 1984).

In the case of downslope propagation, the transition is from a radiative to a trapped state.

Conventional modal formulations fail to adequately explain circumstances in which a mode suddenly disappears from the water column with its energy being radiated into and dissipated within the sea floor (Pierce, 1982). Thus, the particular case of mode coupling where discrete modes (trapped in the water column) couple into continuous modes (which propagate in the bottom) has been further explored as a matter of practical interest (e.g. Miller *et al.*, 1986). Evans and Gilbert (1985) developed a stepwise-coupled-mode method that overcame the failure of previous coupled-mode techniques to properly conserve energy over sloping bottoms. Their method of stepwise-coupled modes avoided problems associated with sloping bottoms by using only horizontal and vertical interfaces. The full solution thus included both forward and backscattered energy (Jensen and Ferla, 1988). Also see the discussion of wedge modes in Chapter 4, Section 4.4.7.

Collins (1990a) suggested using a rotated parabolic equation (PE) in those wedge geometries involving complicated bottom-boundary conditions. Specifically, by rotating the coordinate system, the PE could be marched parallel to the sea floor. The sea surface was then a sloping boundary with simplistic boundary conditions (pressure-release surface) that could be approximated by a sequence of range-independent regions in which the surface was specified as a series of stair steps.

Eigenray formulations can be useful in determining significant propagation paths and propagation mechanisms in a wedge geometry. One particular phenomenon of interest in the upslope problem is that of backscattered eigenrays. These rays have paths that travel up the slope, past the receiver and then back down the slope before arriving at the receiver (Westwood, 1990). The method of images has also been used to construct ray-path solutions in shallow-water environments with a sloping bottom (Macpherson and Daintith, 1967).

The Shallow Water Acoustic Modeling (SWAM) Workshop, held in Monterey, California, in September 1999, provided a forum for the comparison of single-frequency (CW) and broadband (pulse) propagation models in synthetic (i.e. virtual) environments. Test cases included up-sloping, down-sloping, flat and 3D bathymetries. Additional cases considered the effects of internal waves and a shelf break. The goal was to determine which shallow-water environmental factors challenged existing propagation models and what details were important for constructing accurate, yet efficient, solutions. The results of this workshop, designated SWAM '99, were published in a series of papers in the *Journal of Computational Acoustics* (see Tolstoy *et al.*, 2001).

Jensen (1984) examined both upslope and downslope propagation using an appropriately modified PE model. These results will be discussed below. Other researchers have investigated the wedge problem utilizing normal

mode solutions (Evans, 1983; Tindle and Zhang, 1997) and ray theory (Arnold and Felsen, 1983; Westwood, 1989c).

5.3.3.1 *Upslope propagation*

For the wedge problem involving upslope propagation, Jensen (1984) considered the particular environment illustrated in Figure 5.7. [Note that the material presented by Jensen (1984) is also available in a report by Jensen and Schmidt (1984), which contains the papers presented by these two researchers at the same conference.] The water–bottom interface is indicated on the contour plot by the heavy line starting at 350 m depth and then inclining towards the sea surface beyond a range of 10 km. The bottom slope is 0.85° . The frequency is 25 Hz and the source is located at a depth of 150 m. The sound speed is constant at $1,500 \text{ m s}^{-1}$. The bottom has a sound speed of $1,600 \text{ m s}^{-1}$, a density of 1.5 g cm^{-3} and an attenuation coefficient of 0.2 dB per wavelength. Shear waves were not considered.

In Figure 5.7, Jensen displayed transmission loss contours between 70 and 100 dB in 2-dB intervals. Thus, high-intensity regions (where the loss is less than 70 dB) appear as black areas while low-intensity regions (where the loss is greater than 100 dB) appear as white areas. The PE solution was started by a Gaussian initial field, and there are four propagating modes. The high intensity within the bottom at ranges less than 10 km corresponds to the radiation of continuous modes into the bottom. As sound propagates upslope, four well-defined beams (numbered 1–4) are seen, one corresponding to each of the four modes. This phenomenon of energy leaking out of the water column as discrete beams has been confirmed experimentally by Coppens and Sanders (1980). These points correspond to the cutoff depths associated with each mode.

5.3.3.2 *Downslope propagation*

For the wedge problem involving downslope propagation, Jensen (1984) considered the environment illustrated in Figure 5.8. The initial water depth is 50 m and the bottom slope is 5° . The sound speed is constant at $1,500 \text{ m s}^{-1}$. The sound speed in the bottom is $1,600 \text{ m s}^{-1}$ and the attenuation coefficient is 0.5 dB per wavelength. The density ratio between the bottom and the water is 1.5. The contour plot is for a source frequency of 25 Hz. The initial field for the PE calculation was supplied by a normal mode model, and only the first mode was propagated downslope. Shear waves were not considered.

Figure 5.8 shows that some energy propagates straight into the bottom at short ranges. That is, it couples into the continuous spectrum. Beyond the near field, however, propagation within the wedge is adiabatic, with the one mode apparently adapting well to the changing water depth. At a range of 20 km, the energy is entirely contained in the local first mode, even though as many as 21 modes could exist in a water depth of 1,800 m.

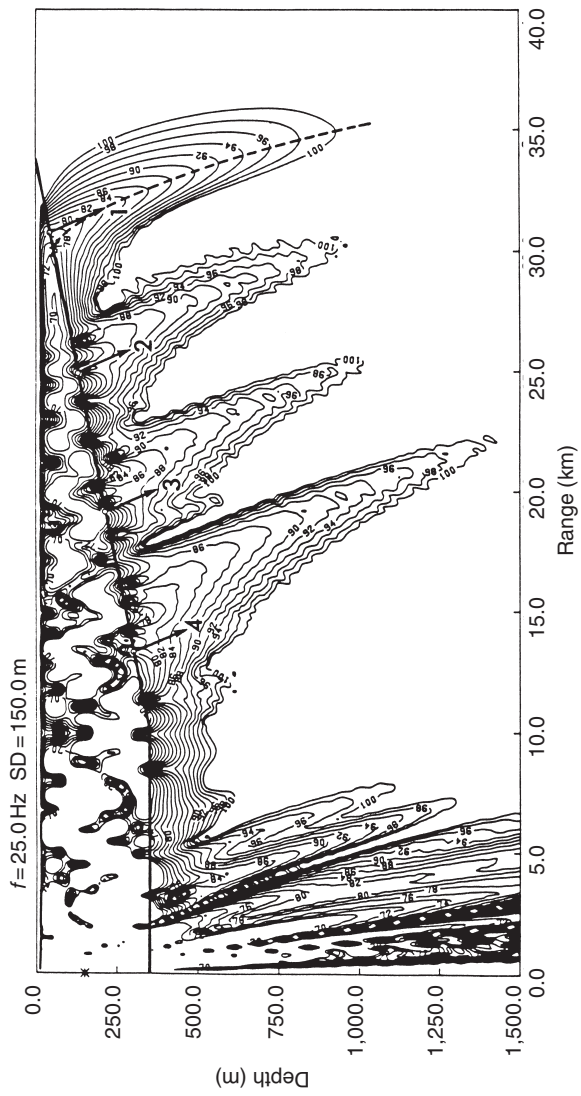


Figure 5.7 Upslope propagation showing discrete mode cutoffs. Results were generated using a PE propagation model (Jensen, 1984).

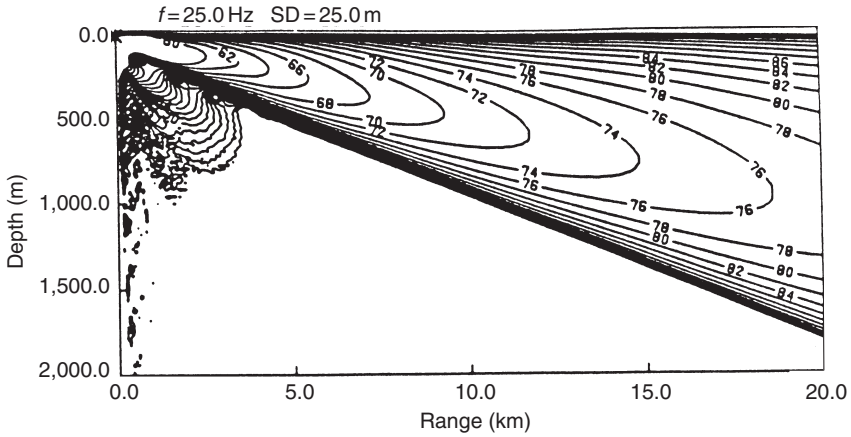


Figure 5.8 Downslope propagation over a constant 5° slope. Results were generated using a PE propagation model (Jensen and Schmidt, 1984).

5.3.4 Empirical models

Two noteworthy empirical algorithms have been developed for use in predicting transmission loss in shallow water, both of which provide depth-averaged estimates for range-independent ocean environments. One model (Rogers, 1981) was derived from theoretical (physics-based) considerations. The second model (Marsh and Schulkin, 1962b; Schulkin and Mercer, 1985), also known as Colossus, was derived from field measurements obtained from a limited number of geographic areas.

5.3.4.1 Rogers model

Rogers (1981) found that virtually all shallow-water TL curves could be described by an equation of the form

$$TL = 15 \log_{10} R + AR + B + CR^2 \tag{5.3}$$

where R is the range, and A , B and C are coefficients.

For the case of a negative sound speed gradient (i.e. sound speed decreases with increasing depth), Rogers obtained the following equation:

$$TL = 15 \log_{10} R + 5 \log_{10}(H\beta) + \frac{\beta R \theta_L^2}{4H} - 7.18 + \alpha_w R \tag{5.4}$$

where R is the range (m), H the water depth (m), β the bottom loss (dB rad⁻¹), θ_L the limiting angle (rad) and α_w the absorption coefficient of sea water.

The term $15 \log_{10} R$ represents the spreading loss for the mode-stripping regions. Thereafter, the spreading loss corresponds to cylindrical spreading ($10 \log_{10} R$). The limiting angle (θ_L) is the larger of θ_g or θ_c , where θ_g is the maximum grazing angle for a skip distance (i.e. the maximum-RBR ray) and θ_c is the effective plane-wave angle corresponding to the lowest propagating mode:

$$\theta_g = \sqrt{\frac{2Hg}{c_w}} \text{ (rad)} \quad (5.5)$$

$$\theta_c = \frac{c_w}{2fH} \text{ (rad)} \quad (5.6)$$

where g is the magnitude of the negative sound-speed gradient (s^{-1}), c_w the maximum (sea surface) sound speed (m s^{-1}), and f the frequency (Hz).

The bottom loss (β) was derived from the theoretical expression for the Rayleigh reflection coefficient for a two-fluid lossy interface, for small grazing angles. For most cases of interest (small values of θ_L), the bottom loss can be approximated as

$$\beta \approx \frac{0.477M_0N_0K_s}{[1 - N_0^2]^{3/2}} \text{ (dB rad}^{-1}\text{)} \quad (5.7)$$

where $N_0 = c_w/c_s$, $M_0 = \rho_s/\rho_w$, ρ_w is the density of sea water, ρ_s the sediment density and K_s the sediment attenuation coefficient ($\text{dB m}^{-1} \text{ kHz}^{-1}$).

For example, at a fixed frequency of 200 Hz, Rogers (1981) considered eight different sound-speed profiles for which sound speed decreased monotonically with depth (Figure 5.9). Using Equation (5.3), the coefficients A , B and C were determined for a number of test cases between 5 and 100 km. The maximum deviation between Equation (5.3) and the actual transmission loss curves generated by a normal mode model was also reported (Table 5.2). The sediment properties were based on Hamilton (1980). The intent was to demonstrate the importance of the sound-speed profile (versus the average gradient in the duct) in determining depth-averaged transmission loss. The eight TL curves generated using the coefficients presented in Table 5.2 are plotted in Figure 5.10 to demonstrate the spread in values. At a range of 100 km, the minimum and maximum TL values differ by more than 20 dB even though the overall gradients of all eight sound-speed profiles were the same. These results demonstrate the importance of the shape of the sound-speed profile, and not just the overall gradient, in determining transmission loss in a shallow-water waveguide.

5.3.4.2 *Marsh-Schulkin model*

The model by Marsh and Schulkin (1962b), also referred to as Colossus, is an empirical model for predicting TL in shallow water (e.g. Podeszwa, 1969).

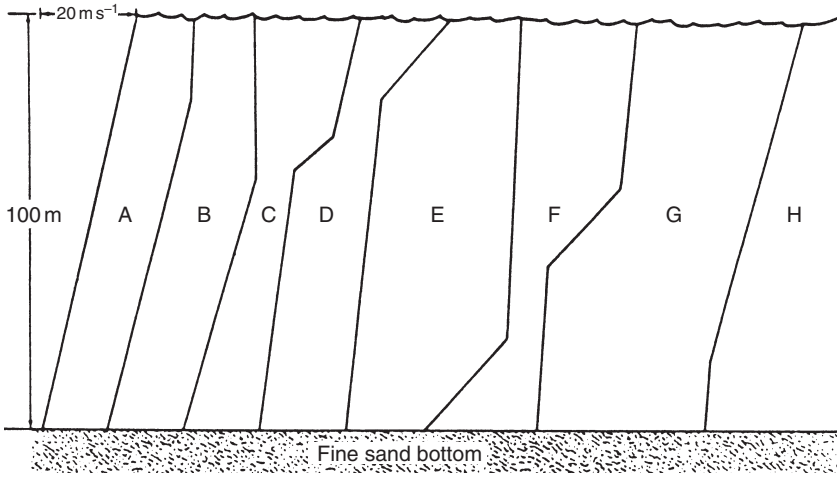


Figure 5.9 Eight different sound-speed profiles in which the sound speed decreases with an average gradient is 0.2 s⁻¹ (Rogers, 1981).

Table 5.2 Coefficients for the empirical shallow-water transmission loss formula: $TL = 15 \log_{10}(R) + AR + B + CR^2$ (dB). Range (R) is measured in km, and the coefficients A , B and C are valid for a frequency of 200 Hz for the sound-speed profiles (A–H) illustrated in Figure 5.9 over a fine-sand bottom

Sediment	Profile type	Three-parameter fit			Maximum deviation
		A	B	$C \times 10^4$	
Fine sand	A	0.18	49.18	+1.098	0.017
Fine sand	B	0.22	49.04	+1.772	0.043
Fine sand	C	0.27	49.02	+0.461	0.042
Fine sand	D	0.149	49.04	+0.020	0.047
Fine sand	E	0.0729	49.61	-0.801	0.042
Fine sand	F	0.146	49.76	-0.587	0.051
Fine sand	G	0.252	48.80	-4.360	0.046
Fine sand	H	0.173	49.14	+0.090	0.021

Source: Rogers (1981).

Colossus employs several concepts: (1) refractive cycle, or skip distance; (2) deflection of energy into the bottom at high angles by scattering from the sea surface; and (3) a simplified Rayleigh two-fluid model of the bottom for sand or mud sediments. With a few free parameters (including water depth), about 100,000 measurements spanning the frequency range from 100 Hz to 10 kHz were fitted within stated error bounds.

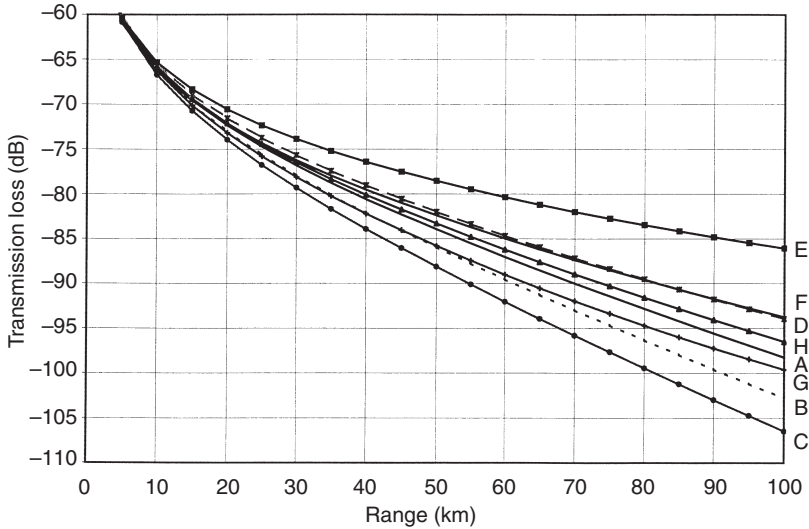


Figure 5.10 Composite illustration of the eight TL curves resulting from the coefficients presented in Table 5.2 (Rogers, 1981).

Along with the concepts of skip distance and bottom loss, the Colossus model used the AMOS results (Marsh and Schulkin, 1955) for a deep-water isothermal surface duct, but with an average thermocline appropriate for shallow water. It also used measurements of actual transmission losses in shallow water off the east coast of the United States as a function of frequency, categorized by bottom type (sand or mud) and by season. Two other mechanisms characteristic of shallow-water processes were also included in the Colossus model. The first mechanism was a “near-field anomaly” correction in the direct radiation zone that included the gain due to multiple bottom and surface bounces. The second was an energy-conservation rule that was used to establish the effective shallow-water attenuation coefficient (α_t), which included the additional loss due to the coupling of energy from the wind-roughened sea surface to the bottom.

The bilinear gradient used in the Colossus model is composed of two constant, linear segments drawn toward the surface and toward the bottom from the depth of maximum sound speed (or temperature). This profile corresponds to the bilinear gradient with a surface duct (Category II-A) that was illustrated previously in Table 5.1. By placing the layer depth (maximum sound speed) at the sea surface, a linear negative-gradient profile (Category I-B) is obtained. Alternatively, placing the layer depth at the sea floor produces a linear positive-gradient sound-speed profile (Category I-A). As noted in Table 5.1, profiles from Categories I-A, I-B and II-A collectively

comprised about 77 percent of all sound-speed profiles encountered in shallow-water regions.

In Colossus, the sound ray cycles have one upward radius of curvature (positive sound-speed gradient) for surface bounces and one downward radius of curvature (negative gradient) for bottom bounces. Based on the depth of the surface layer and the water depth, a single effective skip distance (H) is formulated. Multiples of this effective skip distance are used to define a zone of direct ray paths ($20 \log_{10} R$, where R is the range), a zone of mode stripping ($15 \log_{10} R$), and a zone of single-mode control ($10 \log_{10} R$). The mode-stripping process was found to be complete at a range equal to $8H$, where H is the skip distance.

In the Marsh–Schulkin (or Colossus) model, TL is a function of sea state (or wave height), bottom type, water depth, frequency and the depth of the positive-gradient layer. The skip distance (H) is used as a reference to define regions where wavefront spreading follows square, three-halves and first-power laws as a function of range (R). Accordingly, three equations were developed to provide for the gradual transition from spherical spreading in the near field to cylindrical spreading in the far field:

Short range ($R < H$)

$$TL = 20 \log_{10} R + \alpha R + 60 - K_L \quad (5.8)$$

Intermediate range ($H < R < 8H$)

$$TL = 15 \log_{10} R + \alpha R + \alpha_t[(R/H) - 1] + 5 \log_{10} H + 60 - K_L \quad (5.9)$$

Long range ($R > 8H$)

$$TL = 10 \log_{10} R + \alpha R + \alpha_t[(R/H) - 1] + 10 \log_{10} H + 64.5 - K_L \quad (5.10)$$

where $H = [(L+D)/3]^{1/2}$ is the skip distance (km), L the mixed layer depth (m), D the water depth (m), R the range (km), α the absorption coefficient (dB km^{-1}), α_t the effective shallow-water attenuation coefficient (dB per bounce) and K_L the near-field anomaly (dB).

The absorption coefficient (α) can be estimated from Figure 3.14. The effective shallow-water attenuation coefficient (α_t) and the near-field anomaly (K_L) are functions of frequency, sea state and bottom composition. Values of α_t range from about 1 to 8 dB per bounce. Typical values of K_L range from about 1 to 7 dB. Complete tables of α_t and K_L are contained in the paper by Marsh and Schulkin (1962b).

According to Schulkin and Mercer (1985), the model's chief criticisms have been that it could not be adjusted for arbitrary negative sound-speed gradients (it uses the same constant gradient in all cases), and that it uses empirical bottom loss values. Consequently, the Colossus model has been

extended to accommodate arbitrary gradients in both negative and bilinear sound-speed profiles. These extensions use new general expressions for the skip distance, the near-field anomaly, and the reflection coefficients. The extended model (Schulkin and Mercer, 1985) and the model by Rogers (1981) were found to give about the same predictions when the same inputs were used.

5.4 Arctic models

5.4.1 Arctic environmental models

Basic descriptors of the Arctic marine environment that require specialized algorithms for use in propagation models are limited to absorption and surface (under-ice) scattering (Etter, 1987c; Ramsdale and Posey, 1987). The generation of other parameters, such as sound speed and bottom scattering, appear to be adequately supported by existing algorithms that are valid over a wide range of oceanic conditions.

Absorption is regionally dependent mainly due to the pH dependence of the boric acid relaxation. In the Arctic, the pH range is roughly 8.0–8.3 (versus 7.7–8.3 for nominal sea water), but the greatest variability occurs much closer to the sea surface than in other ocean areas. Absorption formulae appropriate for use in the Arctic regions were presented by Mellen *et al.* (1987c).

Existing under-ice scattering loss models appropriate for inclusion in mathematical models of acoustic propagation were reviewed and evaluated by Eller (1985). Chapter 3 described physical models of under-ice roughness. Many under-ice scattering loss models can be incorporated directly into existing propagation models that were constructed using a modular architecture.

5.4.2 Arctic propagation models

Developments in acoustic propagation modeling for the Arctic Ocean have been very limited. Much of the past effort on characterizing propagation in the Arctic has been devoted to gathering acoustical data and developing empirical models based on that data. While these models tend to be site and season specific with little generality, they do provide basic information on the frequency and range dependence of acoustic propagation in ice-covered regions.

In general, there are four factors peculiar to the Arctic environment that complicate the modeling of acoustic propagation: (1) the ice keels present a rapidly varying surface; (2) the reflection, transmission and scattering properties at the water–ice interface are not well known; (3) the measurement of under-ice contours is difficult; and (4) the diffraction of sound around ice obstacles may be important. In the Arctic half-channel, ray theory may

provide a useful predictive method, whereas its utility in temperate-water surface ducts may actually be quite limited. The utility of ray theory in the Arctic derives from the fact that the Arctic half-channel is between one and two orders of magnitude greater in gradient (and much greater in depth) than the temperate-water surface ducts. The strong positive thermocline and halocline produce an exceptionally strong positive sound-speed gradient in the subsurface layer. This markedly shortens the ray-loop length, causing many surface reflections for rays with small grazing angles (Mobile Sonar Technology, 1983, unpublished manuscript).

The open ocean region in the Arctic environment also poses potential problems as far as existing propagation models are concerned. Surface reflection losses, which may not be significant in deep-ocean propagation, become more important in the upward-refracting environment of the Arctic since multiple surface reflections now play a dominant role. Moreover, multiple ducts are prevalent in this region and many propagation models do not adequately treat them.

Two basic modeling approaches are currently being pursued: the application of ice-scattering coefficients to existing numerical models of acoustic propagation and the development of empirical models. These two approaches are discussed in more detail below.

5.4.3 Numerical models

Numerical models of underwater acoustic propagation specifically designed for ice-covered regions are limited. Since the Arctic half-channel acts as a low-pass filter (discriminating against higher-frequency components), and since bottom interaction is not as important as in other ocean regions (because of the upward-refracting sound-speed profile), most modeling applications in the Arctic have employed either normal mode (Gordon and Bucker, 1984) or fast-field (Kutschale, 1973, 1984) approaches. These models are considered most appropriate for prediction of low-frequency (<350 Hz) propagation at long ranges (>25 nm). Other modeling techniques (e.g. ray theory and parabolic equation) have also proved suitable for calculation of transmission losses once the required ice-scattering algorithms were incorporated (e.g. Chin-Bing and Murphy, 1987). For example, Stotts *et al.* (1994) developed a ray-theoretical propagation model called ICERAY that is valid for under-ice environments, and at least one implementation of the PE technique has been modified to include the effects of ice scattering (refer back to Table 4.1).

Shot signals in the Arctic channel propagate via low-order normal modes, a result of the constructive interference of RSR rays traveling in the upper few hundred meters of the water column. Due to scattering at the rough boundaries of the ice, only low frequencies (typically less than 40 Hz) can propagate to long distances in the Arctic channel. If the channel is sufficiently deep along the entire propagation path, as over an abyssal plain, then the received wave trains display an impulsive character corresponding

to arrivals of deep-penetrating RSR rays while the latter part of the wave trains retain the nearly sinusoidal character typical of low-order modes traveling in the upper layers of the water column (Kutschale, 1984). Using the normal-mode theory of Pekeris (1948), the measured frequency dispersion of low-order modes has often been used to infer acoustic properties of sediments in shallow-water waveguides. Kutschale and Lee (1983) and Kutschale (1984) utilized a similar approach to infer acoustic properties of bottom sediments in the Arctic based on the dispersion of high-order normal modes. A normal mode model was used to interpret the frequency dispersion of bottom-interacting wave trains. The MSPFFP model was used to derive a geoacoustic model that predicted synthetic waveforms matching the dispersion profiles of the bottom-interacting signals. More information on MSPFFP can be found in Table 4.1.

5.4.4 *Empirical models*

Empirical models are inherently limited by the databases from which they were derived. Attempts to fit results from a large data set with simplistic curves generally imply large errors in the model results. Comparisons of model results with data are clearly quite limited by a lack of comprehensive data sets. A recent intercomparison of available empirical techniques applicable to the Arctic revealed large unresolved discrepancies in the manner in which under-ice scattering losses were computed (Deavenport and DiNaploi, 1982). Two of the better-known empirical models are described below.

5.4.4.1 *Marsh–Mellen model*

The Marsh–Mellen Arctic transmission loss model (Marsh and Mellen, 1963; Mellen and Marsh, 1965) is based on observations made during the summers of 1958 and 1959 between Arctic drift stations separated by 800–1,200 km. The measured arrivals were found to consist of a dispersive, quasi-sinusoidal wave train in the 10–100 Hz frequency range. A half-channel model in which the higher frequencies were attenuated by under-ice scattering explained these features. Using these and other experimental data, long-range, low-frequency (<400 Hz) TL data in the Arctic were fitted with an equation of the form

$$TL = 10 \log_{10} r_0 + 10 \log_{10} R + \alpha_s N_s \quad (5.11)$$

where r_0 is the skip distance for the limiting ray, N_s is the number of surface reflections, R is the range in meters ($R = r_0 N_s$), and α_s is the loss per bounce. The wind-generated ocean wave spectrum (Marsh, 1963) was taken to approximate the ice roughness.

5.4.4.2 Buck model

The Buck Arctic transmission loss model (Buck, 1981) consists of a short-range (10–100 nm) and a long-range (100–1,000 nm) model for low-frequency (<100 Hz) transmission loss in that part of the Arctic Ocean deeper than 1,000 m. The crossover range at 100 nm is where higher-order, deeper cycling modes begin to dominate the acoustic propagation. These preliminary empirical models represent linear regression fits to winter data collected in the Beaufort Sea in 1970, in the Fram Strait in 1977, and in an intermediate area in 1979 for a source depth of 244 m and a receiver depth of 30 m:

Short range (10–100 nm)

$$TL = 62.4 + 10 \log_{10} R + 0.032 f + 0.065 R + 0.0011 fR \quad (5.12)$$

Long range (100–1,000 nm)

$$TL = 68.5 + 10 \log_{10} R + 0.07 f - 0.0015 sR + 0.000487 fsR \quad (5.13)$$

where f is the frequency (Hz), R the range (nm) and s the standard deviation ice depth (m), also referred to as the under-ice roughness parameter. A chart of the standard deviation ice depth (s) suitable for use in Equation (5.13) is presented in Figure 5.11 (from Buck, 1985).

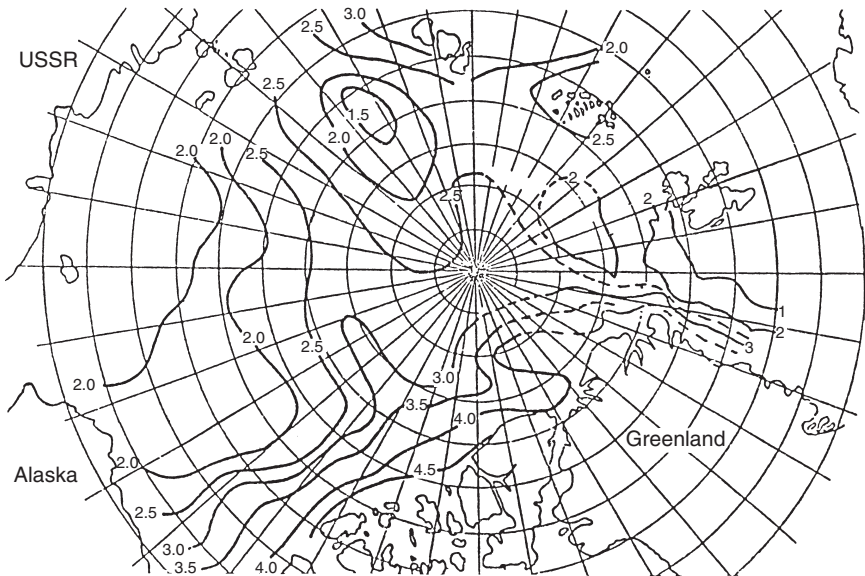


Figure 5.11 Estimates of under-ice roughness in standard deviation (m) about the mean ice depth. These estimates were derived, in part, from nuclear submarine sonar data analyzed by L.A. LeSchack (Buck 1985).

There is some doubt regarding the applicability of Equations (5.12) and (5.13) to summer conditions and to other source–receiver depth combinations. Therefore, these equations should be used with caution. To obtain coarse estimates, refer to Figure 3.29 where average curves of Arctic TL versus frequency have been derived from measured data (Buck, 1968).

5.5 Data support requirements

The development of numerical models requires data with which to support model initialization and model evaluation. Initialization of propagation models requires various descriptors of the ocean environment including the water column, the sea surface and the sea floor. Wave-theoretical models tend to be more demanding of bottom sediment information than do the ray-theoretical models. Evaluation of propagation models requires TL measurements that are keyed to descriptions of the prevailing ocean environment. Such coordinated measurements are necessary to ensure that the model is initialized to the same environment for which the TL data are valid (e.g. Hanna, 1976).

Data support requirements are further complicated by the fact that long-range TL can rarely be considered to occur in a truly range-independent environment. With few exceptions, changes in sound speed or water depth (among other parameters) can be expected not only as a function of range but also as a function of azimuth (or bearing). Consequently, data management in support of model development and operation can be formidable, and is often a limiting factor in the proper employment and evaluation of numerical models.

When working with a variety of propagation models (either different models within one category or models from different categories, as illustrated previously in Figure 4.1), it becomes obvious very quickly (sometimes painfully so) that each model not only requires somewhat different parameters but sometimes requires varying format specifications for any given parameter. In response to this situation, two related developments have occurred. First, gridded databases (i.e. those organized by latitude and longitude) have been established that contain all the required ocean environmental parameters in a standardized format with automated update and retrieval mechanisms. Second, model-operating systems (see Chapter 10) have been created to automatically interface the standard databases with the various models resident in the operating system, and to accommodate the format specifications peculiar to each of the models.

A graphic example of a retrieval from a gridded ocean database is presented in Figure 5.12. This presentation of range-dependent sound speed and bathymetry data is suitable for use in many existing propagation models. Chapter 10 presents a summary of available oceanographic and acoustic databases.

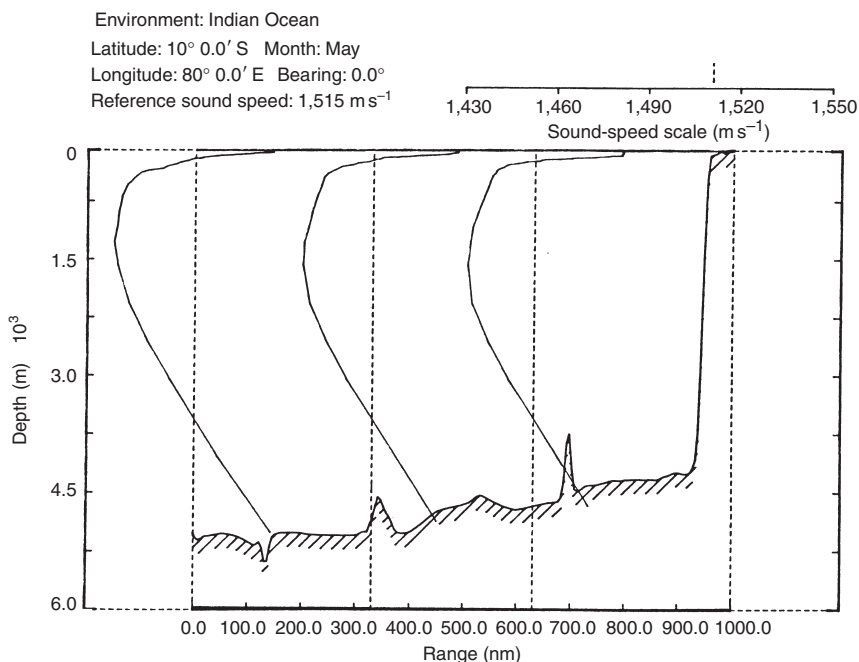


Figure 5.12 Example of a range-dependent ocean environment extracted from a gridded database appropriate for use in many propagation models.

One of the newest automated ocean data products is the generalized digital environmental model (GDEM), developed by Dr Tom Davis at the US Naval Oceanographic Office (Wells and Wargelin, 1985). GDEM uses a digitized database of major oceanic features together with their climatic location to display temperature, salinity and sound-speed profiles on a 30' latitude and longitude grid. A simple parabolic fit is used to describe the deep portion of the sound-speed profile. The more variable near-surface fields of temperature, salinity and sound speed are constructed using orthogonal polynomials between the surface and a depth of 800 m. GDEM has been rigorously compared with reliable climatologies (Teague *et al.*, 1990). Refer to Chapter 10 (specifically Table 10.5) for further details regarding GDEM. The specification of sound-speed profiles for initialization of propagation models is very important, and the following sections will elaborate on this topic.

5.5.1 Sound-speed profile synthesis

In preparation for a typical modeling run, a sound-speed profile is reconstructed (or synthesized) from a tabulation of sound-speed values at discrete

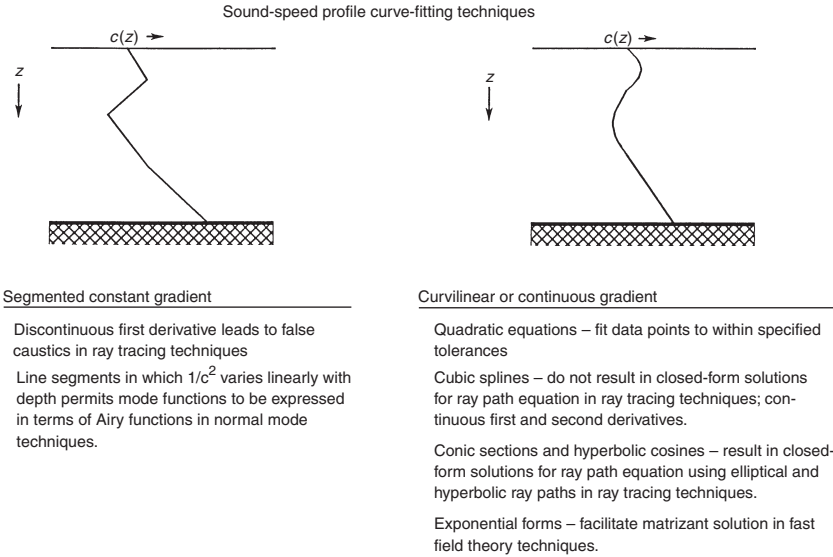


Figure 5.13 Summary of sound-speed profile curve-fitting techniques.

depths. The best functional representation of the synthesized sound-speed profile varies with the type of modeling technique employed. There are basically two different approaches in use, each with its own advantages and disadvantages, as summarized in Figure 5.13.

5.5.1.1 Segmented constant gradient

The sound-speed profile can be constructed by connecting the discrete points with straight-line segments. Because of discontinuities in the first derivative of the resulting function, transmission losses calculated on the basis of ray-tracing techniques are undefined at certain ranges (see Pedersen, 1961). These regions are referred to as false caustics since they are false regions of infinite intensity.

In some propagation models, the sound-speed profile is fitted with segments in which the inverse of the sound-speed squared ($1/c^2$) varies linearly with depth. This often permits a more efficient mathematical solution in which the mode functions are expressed in terms of Airy functions.

5.5.1.2 Curvilinear or continuous gradient

Curvilinear profile approximations that preserve the continuity of slope as well as sound speed have been developed by Pedersen and Gordon (1967).

The sound-speed profile can also be fitted with quadratic equations within specified tolerances (Weinberg, 1969, 1971).

Cubic splines can be used to approximate the sound-speed profile for application to ray-theoretical techniques (Solomon *et al.*, 1968; Moler and Solomon, 1970). However, this method does not result in closed-form solutions for the rays. Approximating profiles with conic sections and hyperbolic cosines results in closed-form solutions for the ray-path equations when using elliptical and hyperbolic ray paths (Flanagan *et al.*, 1974).

Exponential forms are sometimes used in those modeling techniques employing fast-field theory to facilitate a matrizant solution. To simplify the mathematical treatment of long-range sound propagation in the ocean, some investigators (Munk, 1974; Flatté, 1979) have introduced what is termed a “canonical” model of the sound-speed profile. This model has an exponential form that is valid in the vicinity of the deep sound channel axis:

$$\begin{aligned}
 c(z) &= c_1 [1 + \varepsilon(\eta + e^{-\eta} - 1)] \\
 \eta &= \frac{2(z - z_1)}{B} \\
 \varepsilon &= \frac{B\gamma_A}{2}
 \end{aligned}
 \tag{5.14}$$

where $c(z)$ is the sound speed as a function of depth, c_1 the sound speed at channel axis (z_1), η the dimensionless distance beneath channel axis, B the scale depth, ε the perturbation coefficient and γ_A the fractional sound-speed gradient for adiabatic ocean.

Munk (1974) used the following typical values: $c_1 = 1,492 \text{ m s}^{-1}$, $B = 1.3 \text{ km}$, $z_1 = 1.3 \text{ km}$, $\gamma_A = 1.14 \times 10^{-2} \text{ km}^{-1}$ and $\varepsilon = 7.4 \times 10^{-3}$.

5.5.2 Earth curvature corrections

In problems involving acoustic propagation over great distances (greater than 30 nm or 56 km), the fact that the reference plane is situated on a spherical surface can no longer be ignored. The curvature of Earth’s surface is roughly equivalent to a linear sound-speed profile. A linear surface duct is closely analogous to a whispering gallery.

First-order spherical Earth curvature corrections are usually applied to the sound-speed profile before any curve-fitting techniques are employed. These corrections are typically of the form (Watson, 1958; Hoffman, 1976)

$$c_i = c'_i \left(1 + \frac{z'_i}{R_0} \right)
 \tag{5.15}$$

$$z_i = z'_i \left(1 + \frac{z'_i}{2R_0} \right)
 \tag{5.16}$$

where R_0 is the mean radius of Earth (6,370.949 km), c'_i the input sound speed at depth z'_i and c_i the corrected sound speed at corrected depth z_i .

The effect of curvature is more than just a matter of chords versus arcs of great circles. Rather, the important feature is that the contours of constant sound speed (as represented on a range–depth plane) are actually concentric spheres instead of flat, parallel planes. The differences in ray angles as calculated by Snell’s law produce effects of potential importance to sonar performance predictions. A detailed comparison between state-of-the-art ray theory and experimental TL data (Pedersen *et al.*, 1984) revealed that Earth curvature corrections to the sound-speed profile produced model predictions that were in better agreement with the data than would have otherwise been obtained. The effect of curvature was to reduce the range to the leading edge of the first convergence zone by about 1 percent. Errors might be expected to increase with increasing range. Yan (1999) noted that the incorporation of spherical-Earth-curvature corrections into 2D ray equations considerably extended the applicability of these equations in certain classes of 3D problems.

5.5.3 *Merging techniques*

Propagation models generally require sound-speed data from the surface of the ocean to the sea floor. When the local water depth exceeds the limits of available sensing devices such as the XBT, the required surface-to-bottom sound-speed profiles are often derived from a combination of *in situ* data for the near-surface (or shallow) layer together with climatology for the deep layer (Fisher and Pickett, 1973).

A number of algorithms have been developed for automatically merging data from the shallow and deep layers. Statistical relationships based on oceanographic analyses are typically employed to associate the shallow-layer data with the most appropriate deep-layer climatology. This practice is usually satisfactory when the historical databases are characterized by high spatial and temporal resolutions. However, merging algorithms can occasionally introduce errors into the derived surface-to-bottom sound-speed profile as a result of curve-fitting artifacts or incomplete data near the juncture of the two layers. Additional errors may result from the measurement and digitization processes.

5.6 **Special applications and inverse techniques**

This section will review specialized applications of underwater acoustic propagation models. Progress in these particular areas is advancing rapidly and the following sections are intended to identify areas of particular interest at the present time as well as areas that may be appropriate for future research.

5.6.1 *Stochastic modeling*

Methods by which to investigate the stochastic (versus deterministic, or completely predictable) nature of acoustic propagation in the ocean have been refined as part of ongoing, long-term projects. Such efforts are concerned with probabilistic predictions of the environmental limits to sonar aperture designs (Perkins *et al.*, 1984). A workshop conducted at the US Naval Research Laboratory addressed the model and database requirements for current and new highly complex sonar systems (Spofford and Haynes, 1983). Among the topics addressed were estimates of both the first and second moments (variances) or spreads in space, time and frequency required in a variety of ocean environments to support the operation of current sonar systems and the design of advanced sonar systems.

A review of stochastic signal modeling efforts (Wood and Papadakis, 1985) concluded that spread function models are efficient for computing lower-order statistics, although with limited capability. General-purpose Monte Carlo models are desirable for their higher-order capabilities, despite higher computing costs.

In the so-called “model-based” approach to acoustic signal processing in the ocean, mathematical models of physical phenomena and measurement processes are incorporated into the processor. The inclusion of a propagation model in the signal-processing scheme introduces environmental information in a self-consistent manner. Furthermore, stochastic properties of the oceanic medium can be included in the model.

Solutions using state-space techniques employ two sets of equations: the state equation and the measurement equation. The state equation describes the evolution in space of the modal and range functions while the measurement equation relates these states to the hydrophone array measurements. One specific implementation (Candy and Sullivan, 1992) cast the normal-mode propagation model into state-space form, extended the formulation to a Gauss–Markov model, and applied the results to an ocean-acoustic signal-processing problem in the context of a horizontally stratified ocean with a known source position. A related implementation investigated the inverse reconstruction of a sound-speed profile from hydrophone measurements (Candy and Sullivan, 1993).

The use of finite element techniques for computing underwater acoustic propagation has been studied as part of a computationally intensive probabilistic acoustics program, the major objective of which was to develop models for propagation of the moments of the acoustic field in regions where the ocean boundaries are random surfaces (Goldstein, 1984). The possibility of using exact techniques such as the FEM for solving the wave equation have been made more attainable by the augmentation of computers with array processors. Recent developments in finite element modeling include ISVRFEM (Pack, 1986), the FEPE (Collins, 1988a), the finite element ocean acoustic model (FOAM) (Murphy and Chin-Bing, 1989) and

the seismo-acoustic finite element (SAFE) model (Murphy and Chin-Bing, 1991).

5.6.2 *Broadband modeling*

Broadband (also referred to as pulse or wideband) propagation modeling is concerned with simulating the effects associated with the transmission of a signal characterized by a frequency spectrum (versus a single-frequency continuous wave). When considering such signals, the simplest approach has been to first calculate the geometric mean frequency (f_M), defined as $f_M = (f_1 f_2)^{1/2}$, where f_1 and f_2 are the lower and upper limits, respectively, of the frequency band. The propagation of an equivalent signal at frequency f_M is then simulated using one of the available propagation models. When the bandwidth is small, this approach probably generates a reasonable approximation. Otherwise, this approach may lead to substantial errors, particularly when the spectrum is not flat over the bandwidth, and other methods must be tried including Fourier synthesis and time-domain methods.

In Fourier synthesis, multiple executions of an existing propagation model are performed over the frequency range (f_1, f_2) at a number of discrete frequencies at intervals Δf , where Δf might be 1 Hz, for example. The resulting transmission losses for each frequency in the bandwidth are then combined through an appropriate weighting and averaging process (i.e. and interpolation postprocessor) to arrive at the TL corresponding to the bandwidth. Examples of such multi-frequency extensions include the ray-theoretical model GAMARAY (Westwood, 1992), the normal mode model PROTEUS (Gragg, 1985) and the multilayer expansion model MULE (Weinberg, 1985a).

Alternatively, the method developed by McDonald and Kuperman (1987) for modeling the propagation of a broadband linear pulse in a waveguide is one example of a broader class of techniques referred to as time-domain methods (Kuperman, 1985). In principle, the frequency-domain wave equation (valid for a single-frequency CW signal) can treat broadband signals by Fourier synthesis of the individual CW solutions over the frequency spectrum. In the presence of nonlinearities, however, interactions among frequency components invalidate the frequency-domain approach. In the time domain, the wave equation can be formulated using methods that remove such pathological limitations from the numerical solutions.

In related developments, Porter (1990) developed a time-marched FFP (Pulse FFP) for modeling acoustic pulse propagation in the ocean. Collins (1988b) used the TDPE model to investigate the effects of sediment dispersion on pulse propagation. Orchard *et al.* (1992) developed the 3D TDPA (time-domain parabolic approximation) model for simulating pulse propagation in 3D ocean geometries.

Jensen (1988) summarized wave-theoretical techniques suitable for the practical modeling of low-frequency acoustic pulse propagation in the ocean.

Jensen emphasized the computational efficiency of pulse propagation predictions using Fourier synthesis of existing CW propagation models based on normal mode and parabolic equation approaches. Jensen (1993) further explored these issues by placing particular emphasis on propagation in leaky surface ducts.

Futa and Kikuchi (2001) investigated the use of the finite-difference time-domain (FDTD) method for pulse propagation in shallow water. The FDTD method facilitates a direct analysis of the effect of sediment impedance on the time–depth pattern of the received acoustic pulse. The FDTD method was particularly efficient in analyzing the acoustic field in the vicinity of the sound source. By comparison, the normal-mode approach would have required a complicated analysis of both the discrete and continuous modes in the near field.

Advances in the computational efficiency of propagation codes have facilitated the practical analysis of broadband sources using the waveguide invariant approach. The “waveguide invariant” summarizes in a single scalar parameter the dispersive characteristics of the acoustic field in a waveguide. Using a ray (versus normal mode) formulation, the invariant is computed in part by varying the ray launch angle about a mean value and then computing the corresponding changes in the ray-cycle distance and the ray-cycle time. The term “invariant” derives from the fact that the (computed) dispersive character of the propagation in the environment is nearly independent of the particular ray pair selected. This interesting approach was described by Brekhovskikh and Lysanov (1982) (and earlier by S.D. Chuprov). Song *et al.* (1998) and D’Spain *et al.* (1999) described practical applications of the waveguide invariant approach in realistic environments, including matched field processing.

5.6.3 *Matched field processing*

The use of matched field processing techniques in underwater acoustics has been explored by a number of investigators, and comprehensive overviews are available (Tolstoy, 1992, 1993; Baggeroer *et al.*, 1993). This technique correlates the acoustic pressure field from a submerged source, as detected at each receiver in a hydrophone array, with the field modeled at the array by assuming a particular source position and ocean environment. Consequently, a high degree of correlation between the experimental and modeled pressure fields indicates a high probability that the source is located at the estimated position in the range–depth plane. The basic components of matched field processing are illustrated in Figure 5.14 (Tolstoy, 1993). Accordingly, this technique shows promise as a high-resolution localization tool. This technique can also be used to reconstruct prevailing oceanic conditions when the source and receiver positions are known *a priori*.

A variety of mathematical estimator functions have been utilized to perform the comparisons between the experimental and modeled pressure fields.

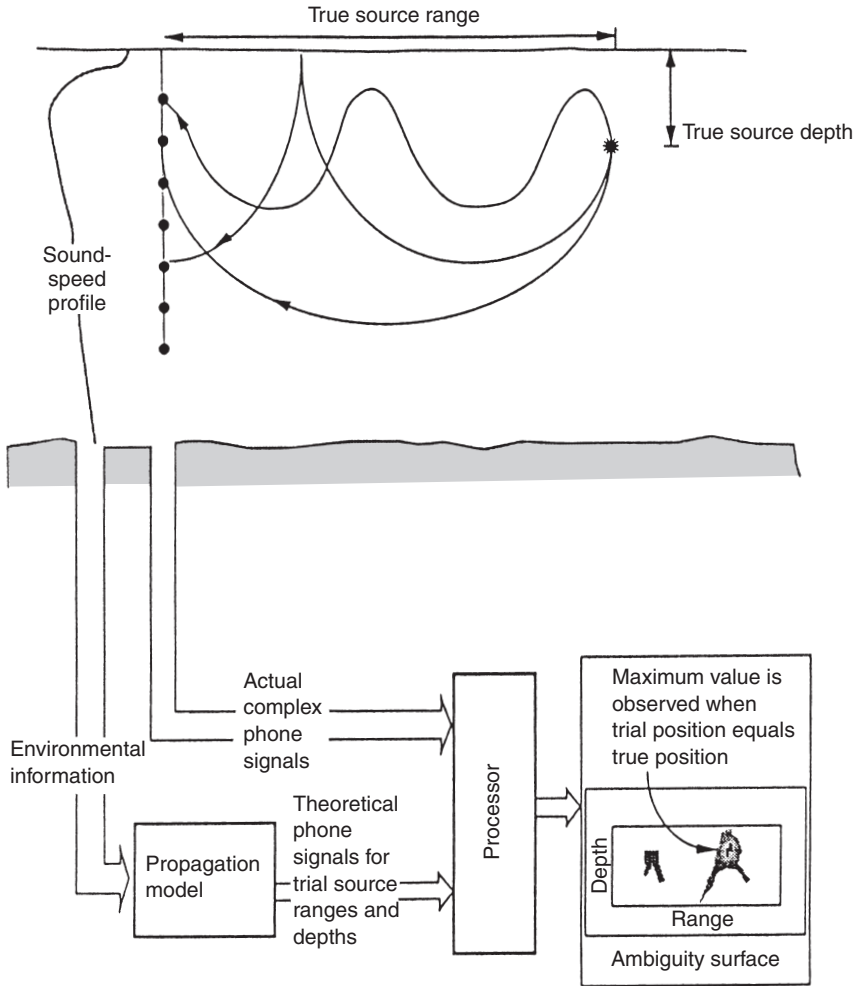


Figure 5.14 Illustration of the basic components of matched field processing. (Tolstoy, 1993; *Matched Field Processing for Underwater Acoustics*; reproduced with permission of World Scientific Publishing.)

These include linear, minimum variance, multiple constraint, matched mode, eigenvector, maximum entropy, approximate orthogonal, variable coefficient likelihood and optimum uncertain field processors (Fizell, 1987; Tolstoy, 1993). The outputs of these processors are often presented graphically on so-called “performance surfaces” to facilitate identification of probable source positions. The ambiguity surface illustrated in Figure 5.14 is one example. The matched field technique has been found attractive for

application to shallow-water geometries. For example, Bucker (1976) used a conventional cross correlation of the experimental and modeled pressure fields while Del Balzo *et al.* (1988) used a maximum-likelihood estimator. The maximum-likelihood estimator has also been applied to deep-water Arctic environments by Fizell and Wales (1985). Dosso *et al.* (1993) used matched field inversion to estimate properties of the ocean bottom. In as yet unpublished work, M. Snellen and D.G. Simons applied the downhill simplex algorithm to reduce the uncertainty in matched field inversion results.

Westwood (1992) explored the use of broadband signals in matched field processing. In addition, D'Spain *et al.* (1999) developed an adiabatic normal-mode model to analyze broadband, matched-field-processing data collected in shallow water. The model incorporated the concept of "effective depth," which was first introduced by Weston (1960) for a Pekeris waveguide and later extended by Chapman *et al.* (1989) to include shear waves. In essence, the phase change associated with the reflection of a plane wave from a fluid-elastic interface at the sea floor is equal to that from a pressure-release boundary that is offset a distance below the true bottom. This offset, which is virtually independent of the grazing angle, can be calculated from available waveguide parameters. Thus, the normal-mode wave numbers can be provided by a closed-form expression rather than by more cumbersome numerical complex-root-finding techniques.

Bogart and Yang (1992) used matched mode localization as an alternative to matched field processing and found that the matched mode ambiguity surface showed equal or improved (i.e. lower) sidelobes compared to that of matched field processing; moreover, it was easier to compute. Collison and Dosso (2000) documented a useful comparison of modal decomposition algorithms for matched-mode processing.

5.6.4 *Transmutation approaches*

A transmutation approach has been applied to underwater acoustic propagation by Duston *et al.* (1986). As described by Gilbert and Wood (1986), who also provided historical references to the literature, transmutation theory allows one to find an integral operator that transforms the solutions of a simpler partial differential equation into solutions of another, more complicated, partial differential equation. A third partial differential equation exists that the kernel of the integral operator must then satisfy. The advantage gained is that more freedom exists in assigning useful initial boundary conditions to the kernel. Thus, instead of separating the Helmholtz equation into two ordinary differential equations, it is separated into two related partial differential equations, one of which is solved analytically and the other by a hybrid of symbolic and numerical computations.

5.6.5 *Chaos*

Chaos in underwater acoustic modeling has been explored by Tappert *et al.* (1988) and by Palmer *et al.* (1988a). They observed that ray path solutions exhibit “classical chaos,” that is, unpredictable and stochastic behavior. The phenomenon of chaos in underwater acoustics is presumed to be caused by the exponential proliferation of catastrophes (in the form of caustics) due to the loss of control implied by the nonseparability of variables in the eikonal equation. Consequently, there exists a prediction horizon that cannot be exceeded even when the ocean environment is known exactly.

The application of chaotic concepts to underwater acoustic propagation modeling has been further investigated by Brown *et al.* (1991a,b), Tappert *et al.* (1991) and Smith *et al.* (1992a,b). These studies have emphasized the practical importance of chaotic ray trajectories as limiting factors in generating deterministic predictions of acoustic propagation, particularly in the presence of mesoscale ocean structure. Collins and Kuperman (1994a) suggested that the computational difficulties associated with chaos may be overcome by solving eigenray problems with boundary-value techniques as opposed to initial-value techniques.

The deliberate use of chaotic waveforms as sonar signals has also been investigated. One theoretical study (Alapati *et al.*, 1993) used chaotic metrics (e.g. Rasband, 1990) and conventional ambiguity functions to evaluate the performance of several nonlinear waveforms after convolution with realistic ocean impulse-response functions. These impulse-response (or Green’s) functions were generated using the generic sonar model (GSM) (Chapter 10, Section 10.4.4). Ziomek (1985: 4–5) discussed the mathematical formalism of impulse-response functions in a signal-processing context. Because of their amenability to signal enhancement (or noise-reduction) techniques, chaotic waveforms have been suggested for use in bistatic active sonar systems operating in shallow-water regions (Chapter 10, Section 10.2).

Time-domain analysis of ocean ambient-background pressure fluctuations collected at the Atlantic undersea test and evaluation center (AUTEK) during a mine-deployment exercise (MINEX) revealed a positive Lyapunov exponent, which identified the system as chaotic. The prediction horizon was confined to a few samples. Determination of the degrees of freedom was important for the construction of physical models and nonlinear noise-reduction filters, which were based on characteristics of the observed degrees of freedom (in this case, 9) from the background acoustic source. The magnitude of the largest Lyapunov exponent provided a measure of confidence for signal-state prediction (Frison *et al.*, 1996).

In nonseparable, range-dependent environments, ray paths can be chaotic, thus placing a fundamental limit on tracing rays by the classical *shooting* approach in which the launch angles of rays from a source point are varied until the rays intersect the receiver endpoint within specified tolerances. To circumvent this problem, Mazur and Gilbert (1997a,b) used Rayleigh–Ritz

and simulated-annealing methods rather than minimizing the travel-time integral indirectly.

The effects of ocean internal waves on long-range acoustic pulse propagation were analyzed from the geometrical-optics viewpoint by Simmen *et al.* (1997), who also investigated the chaotic behavior of rays and the micro-folding of timefronts. The extent of the region of the timefront in which strongly chaotic rays appear, and the strength of the rays' sensitivity to initial conditions, were found to depend on the average sound-speed profile, the source-to-receiver range and the internal-wave spectral model.

Tappert and Tang (1996) found that groups of chaotic eigenrays tended to form *clusters* having stable envelopes. Sundaram and Zaslavsky (1999) studied the dispersion of wave packets using a parabolic approximation to the wave equation. They noted that, in a manner similar to that observed in quantum chaos, enhanced dispersion due to chaotic ray dynamics was counterbalanced by wave coherence effects.

5.6.6 *Three-dimensional modeling*

Modeling underwater acoustic propagation in three dimensions, sometimes referred to a volume acoustic field modeling (Chin-Bing *et al.*, 1986), has assumed greater importance as sonar systems have become more complex (Jones, 1983). Ray theory and PEs can theoretically treat 3D propagation, although such implementations are rarely accomplished in practice due to computational complexity (e.g. Johnson, 1984). Therefore, such modeling is generally, but not always, accomplished by extending the capabilities of existing range-dependent (2D) techniques such as PE, normal mode and ray theory models to form composite 3D pictures. Such approaches are commonly termed $N \times 2D$ since the models are sequentially executed for N adjacent range-dependent (2D) radials (or sectors). Tolstoy (1996) stressed the point that $N \times 2D$ (sometimes referred to as 2.5D) approximations to full 3D modeling will fail whenever the out-of-plane energy is significant, as in the case of bottom topography (wedges, ridges and seamounts), eddies and fronts.

Three-dimensional propagation modeling has been used to simulate acoustic interactions with seamounts (Medwin *et al.*, 1984) and with mesoscale oceanographic features (Kuperman *et al.*, 1987; Tsuchiya *et al.*, 1999). Coupled with appropriate color graphic displays, 3D modeling promises to be a powerful analytical and predictive tool. In the case involving seamounts, Medwin *et al.* (1984) were able to show that: (1) depending on the roughness of the sea surface, diffraction over the crest of the seamount can be the strongest contributor to the sound field in the shadow region; (2) the diffracted signal always arrives before the multiply reflected sound; (3) the diffraction loss is proportional to the square root of the acoustic frequency; and (4) a 2D model produces excessive diffraction and excessive multiple reflection signal compared to a more realistic 3D model. The 3D

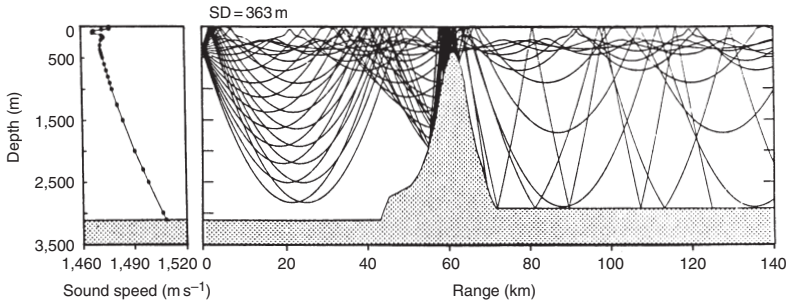


Figure 5.15 Ray-trace representation of sound propagation across a seamount based on data from Chapman and Ebbeson (1983). (Jensen, 1988; *IEEE J. Oceanic Eng.*, 13, 186–97; copyright by IEEE.)

model used by Medwin *et al.* (1984) is a hybrid solution formed by combining the range-independent FACT model (to calculate acoustic propagation to and from the seamount) with 3D physical models of the frequency-dependent wave interaction at the seamount. Comparisons with experimental data obtained from the Dickens Seamount in the northeastern Pacific Ocean (Chapman and Ebbeson, 1983; Ebbeson and Turner, 1983) verified the accuracy of this model in the frequency range 50–500 Hz. A ray trace illustrating interaction with a seamount is presented in Figure 5.15.

The 3D Hamiltonian ray-tracing model, HARPO, has been used in tomographic studies of the ocean (Newhall *et al.*, 1990; Jones *et al.*, 1991). Both HARPO (Lynch *et al.*, 1994) and the 3D coupled-mode model CMM3D (Chiu and Ehret, 1994) have been interfaced with sound-speed fields generated by the Harvard open ocean model (HOOM). Lee and Schultz (1995) described a stand-alone 3D ocean acoustic propagation model. In related work, Perkins *et al.* (1993) modeled the ambient noise field in 3D ocean environments.

5.6.7 Ocean fronts, eddies and internal waves

Ocean fronts, eddies (or rings) and internal waves were discussed in Chapter 2 (Section 2.5.2) where they were classified as mesoscale oceanic features. This section will examine their acoustic impacts.

5.6.7.1 Fronts and eddies

The distribution of ocean fronts and eddies was discussed previously in Chapter 2. The impacts of fronts and eddies on acoustic propagation have been intensely studied and modeled principally because of their importance to naval operations. Heathershaw *et al.* (1991) demonstrated the feasibility of coupling the range-dependent propagation model GRASS with a 3D

eddy-resolving ocean model to study acoustic propagation through frontal systems. The effects of eddies on acoustic propagation were investigated by Vastano and Owens (1973) using ray-theoretical models. More sophisticated wave-theoretical models have since been employed in more comprehensive studies. For example, Baer (1981) utilized a primary 3D version of the parabolic equation to study propagation through an eddy, and Hall and Irving (1989) used an adiabatic normal mode technique to investigate propagation through Baer's example of an eddy. All investigators indicated that eddies significantly modify major characteristics of the acoustic field relative to those obtained in the absence of eddies. Such effects include the shifting of convergence zones, altered multipath arrival sequences and horizontal refraction, among others (Munk, 1980). In a comprehensive study of warm-core eddies, Browning *et al.* (1994) found that the greatest acoustic impact was obtained for a shallow source and receiver configuration. Tsuchiya *et al.*, 1999 used a 3D wide-angle PE model to analyze acoustic propagation through an ocean populated by warm- and cold-water masses approximating the characteristics of eddies in the Pacific Ocean. The 3D model computed horizontal and vertical refraction for comparison with 2D results. Relative to the 3D model, the 2D results underestimated the effects of eddies on acoustic propagation. Shang *et al.* (2001) proposed a new, less restrictive, criterion for adiabaticity in the presence of ocean fronts or internal solitary waves in shallow water.

As an illustration, the results of Vastano and Owens (1973) are used to quantify the effects of a cold-core eddy (surrounded by warmer Sargasso Sea water) on acoustic propagation. Assuming a frequency of 100 Hz, a source depth (S) of 200 m, a receiver depth (R) of 300 m, and a FOM of 90 dB (see Chapter 10), the resulting TL curves in Figure 5.16(a) would result in the detection zones in Figure 5.16(b) for a sonar located both inside and outside the eddy. The shaded areas denote detection opportunities under the stated conditions. The shifts of the convergence zones are readily apparent as one effect of the eddy. The particular situation illustrated in Figure 5.16 could arise, for example, if a sonar were located on the outer edge of an eddy, with the eddy on the left and the Sargasso Sea on the right.

To further explore the effects of eddies (or rings, as they are sometimes called) on sonar detection, the case of a surface ship located in the Sargasso Sea trying to detect a submarine located inside an eddy will be examined. Figure 5.17 shows contours of constant sound speed through a typical Gulf Stream eddy situated within the Sargasso Sea (Gemmill and Khedouri, 1974). Since sound speed is proportional to water temperature in the upper layers of the ocean, this figure also demonstrates this to be a cold-core eddy since the low sound speed values in the center reflect lower water temperatures relative to the surrounding waters. Also shown (by a dashed line) is the SOFAR channel axis, which indicates the depth of minimum sound speed. Next, consider Figure 5.18, which schematically portrays the corresponding isotherms. A surface ship located within the warmer Sargasso Sea is frustrated in its attempts to passively detect the sound energy emitted by the

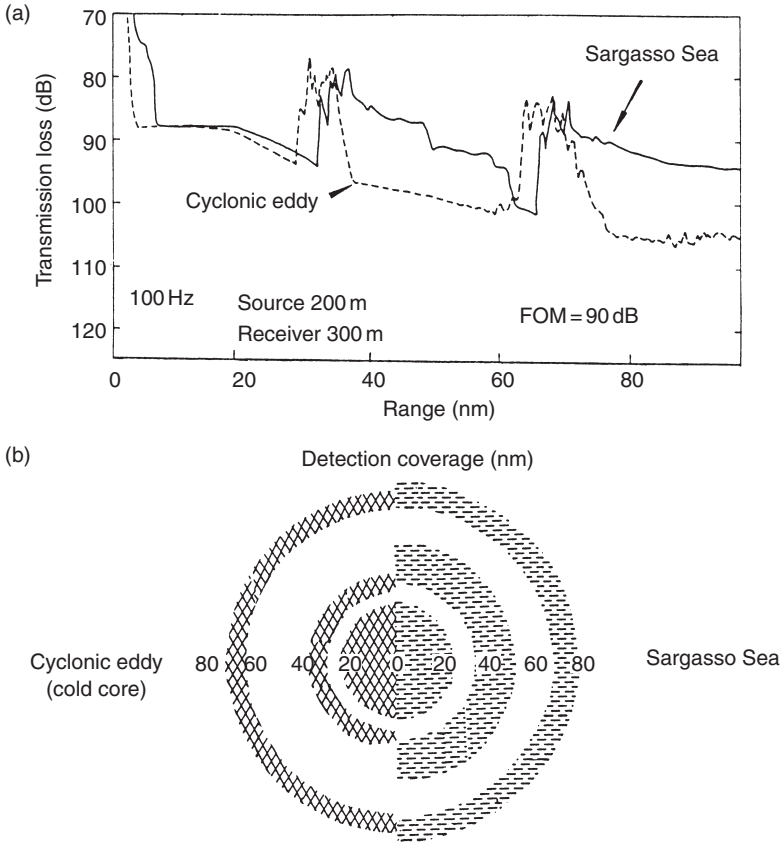


Figure 5.16 Effect of a cold-core eddy on acoustic propagation: (a) TL versus range; and (b) corresponding detection zones assuming an FOM of 90 dB. (Transmission loss curves are from Vastano and Owens, 1973; *J. Phys. Oceanogr.*, 3, 470–8; copyright by the American Meteorological Society.)

submarine located in the colder interior of the eddy since the sound waves are refracted downward (away from the higher temperatures and higher sound speeds) and away from the ship’s passive listening device. The submarine thus can successfully avoid detection by positioning itself inside known eddy locations.

5.6.7.2 Internal waves

Zhou *et al.* (1991) investigated the interaction of underwater sound with internal gravity waves (specifically solitons) in an attempt to explain the

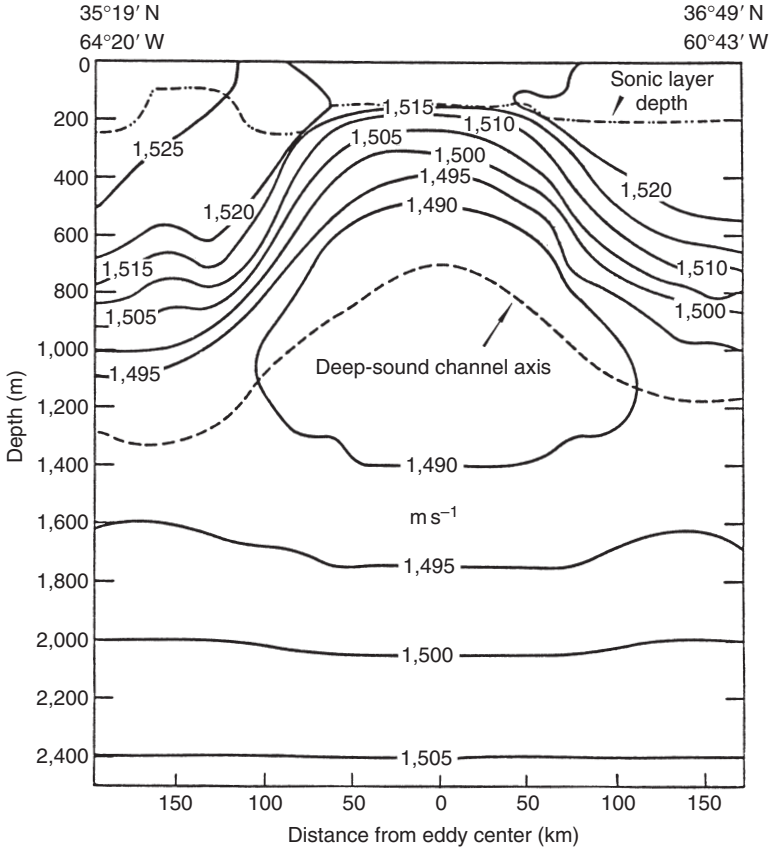


Figure 5.17 Sound-speed contours through a cold-core eddy (Gemmill and Khedouri, 1974).

anomalous behavior of low-frequency ($\sim 300\text{--}1,100\text{ Hz}$) acoustic propagation conditions observed in some shallow-water areas. As a result of this investigation, it was noted that acoustic measurements could be employed in an inverse fashion to remotely sense internal wave activity in the coastal zone. Rodríguez *et al.* (2000) used a range-dependent normal-mode model (C-SNAP) to simulate the propagation of acoustic signals through soliton-like fields of temperature and sound speed. The simulation reproduced experimental observations of signal enhancement attributed to focusing effects correlated with peaks in current, temperature and surface tides. Chin-Bing *et al.* (1993a) numerically simulated the effects of a solitary internal wave on the low-frequency acoustic field in a shallow-water waveguide using two-way, range-dependent, finite-element models (FOAM, FFRAME and SAFE). These simulations focused on the refractive and backscatter effects

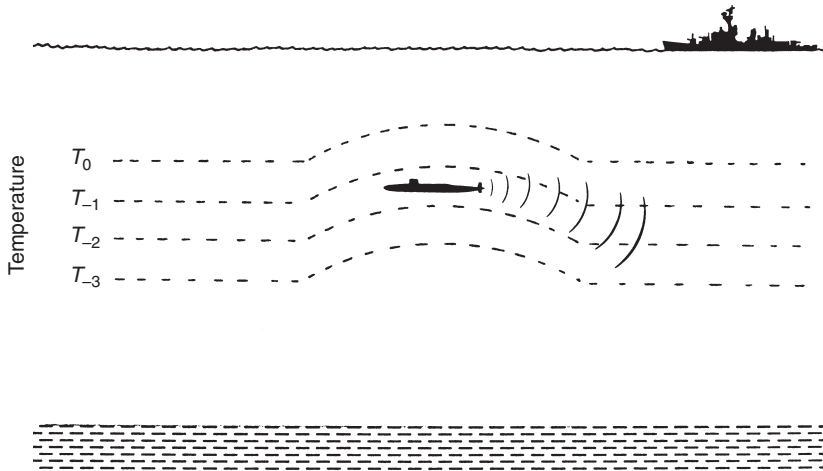


Figure 5.18 Schematic illustration of a submarine in a cold-core eddy avoiding detection by a surface ship equipped with passive sonar. Sound is refracted downward away from the ship by the effects of the colder water in the interior of the eddy.

of a single soliton wave packet in an effort to understand the cumulative effects of multiple resonances on acoustic propagation.

Oba and Finette (2002) simulated acoustic propagation in a shallow-water, anisotropic ocean environment at frequencies of 200 and 400 Hz for horizontal ranges extending to 10 km. Their simulation employed a 3D PE code based on differential operators representing wide-angle coverage in elevation and narrow-angle coverage in azimuth. The water column was characterized by random volumetric fluctuations in the sound-speed field induced by internal gravity waves superimposed on a thermocline. There was a localized contribution from a solitary wave packet (undular bore or solibore). The resulting simulation showed azimuthal filtering of the propagated field, with the strongest variations appearing when the propagation was parallel to the solitary wave depressions of the thermocline. The solitary wave packet was interpreted as a nonstationary oceanographic waveguide within the water column that preferentially funneled acoustic energy between the thermocline depressions.

Tang and Tappert (1997) used a broadband model (UMPE) to explain the lack of multipath replicas of a transmitted pulse in broadband acoustic experiments in the Straits of Florida. The observed single broad cluster was attributed to the effects of internal waves, which produced moving acoustic “footprints” on a rough sea floor. Tielbürger *et al.* (1997) investigated the acoustic field properties in a shallow-water waveguide where the

sound speed had a deterministic, time-independent component and two stochastic components induced by internal-wave activity. Simons *et al.* (2001) used a broadband normal mode model (PROSIM) to simulate variability in a shallow-water channel resulting from fluctuations in oceanographic parameters. The acoustic band of interest was 1–8 kHz.

5.6.8 *Coupled ocean–acoustic modeling*

Oceanographers have recently developed synoptic forecasting techniques appropriate for predicting the locations of frontal features such as currents and eddies (Mooers *et al.*, 1982; Robinson *et al.*, 1984; Robinson, 1987; Peloquin, 1992). These forecasts can be used by forces afloat to facilitate the efficient allocation of naval resources during ASW operations.

These same dynamical ocean models can be used in conjunction with underwater acoustic propagation models to generate timely forecasts of sonar performance in the vicinity of highly variable frontal features. When used in this fashion, the ocean models generate input variables necessary for initialization of the acoustic models. This synergistic arrangement is referred to as coupled ocean–acoustic modeling. Such coupling has been successfully demonstrated, for example, by Botseas *et al.* (1989), who interfaced an implicit-finite-difference PE model with ocean forecasts generated by the HOOM.

Coupled ocean–acoustic forecast systems comprise three basic components: an oceanic forecast scheme, a coupling scheme and an ocean acoustic propagation scheme (Robinson *et al.*, 1994). These systems can also be used to generate nowcasts and hindcasts. Nowcasts are estimates of the present state of a system. They are based on a combination of observations and dynamical modeling. Hindcasts are *a posteriori* forecasts. They are useful in evaluating modeling capabilities based on historical benchmark data (e.g. Martin, 1993).

Requirements for oceanographic data to support coupled ocean–acoustic forecast systems often exceed observational capabilities. Therefore, data assimilation, which introduces data generated by feature models, is used to achieve accurate synoptic realizations. Feature models are statistical representations of common synoptic structures in the ocean such as fronts and eddies (Robinson *et al.*, 1994).

The optimum thermal interpolation system (OTIS) (Clancy *et al.*, 1991a) forms the basis for an upgraded tactical ocean thermal structure (TOTS) system (Hawkins, 1992) designed for use aboard ships equipped with the tactical environmental support system (TESS). OTIS assimilates real-time observations from multiple sources into a complete 3D representation of the oceanic thermal field. A corresponding 3D representation of the salinity field is derived using empirical techniques. To compensate for sparse subsurface measurements, OTIS supplements actual observations with synthetic data derived from an empirical orthogonal function (EOF) representation of

water masses, from ocean feature models, and from subjective interpretation of satellite imagery. The resulting product provides an accurate 3D representation of the temperature and salinity fields together with a realistic depiction of fronts and eddies. Such information is useful in organizing naval assets as well as in planning oceanographic field work. OTIS has also been used to generate high-quality data for the evaluation of oceanographic forecasting models (Lai *et al.*, 1994).

The coupling of oceanographic mixed layer models with surface duct propagation models was discussed earlier in this chapter (Section 5.2.3). The subject of marine modeling, which properly embraces the numerical modeling of ocean physics, geology, chemistry and biology, has been summarized by Goldberg *et al.* (1977) and by Kraus (1977).

5.6.9 Acoustic tomography

Ocean-acoustic tomography (Munk and Wunsch, 1979) is an inverse technique that measures perturbations in travel times between fixed acoustic sources and receivers (see Figure 5.19). This technique is analogous to the medical procedure called tomography (from the Greek word for “slice” or “cut”), and also has elements in common with conventional seismology (Menke, 1989). A recent book by Munk *et al.* (1995) provided

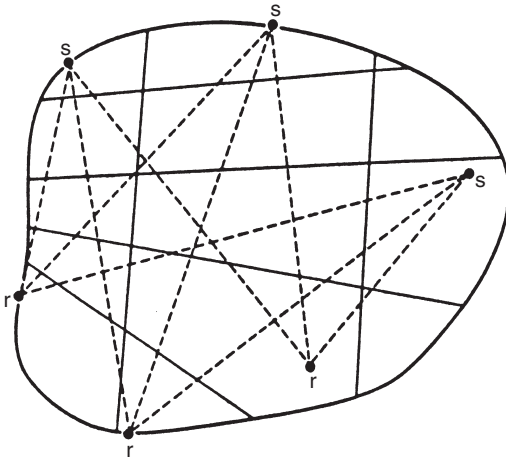


Figure 5.19 Schematic illustration of an ocean tomographic geometry. Perturbations in acoustic travel time from any source *s* to any receiver *r* (dashed paths) are used to estimate sound speed perturbations in an arbitrary grid area formed by the solid lines. (Munk and Wunsch, 1979; *Deep-Sea Res.*, 26, 123–61; copyright by Pergamon Press Plc.)

a comprehensive review of the oceanography and mathematics necessary to understand and develop ocean–acoustic tomographic systems.

This technique has been proposed for large-scale monitoring of ocean basins. Specifically, the perturbations in travel times between sources and receivers can be used to deduce sound-speed (and thus water density) fluctuations in the interior of the oceans. Moreover, if reciprocal transmissions are used between sources and receivers, the differences in travel times can be used to compute the mean ocean currents along the acoustic path (Spiesberger, 1989). Sea surface spectra can also be estimated using acoustic tomography (Miller *et al.*, 1989).

The temporal resolution required to distinguish multipath arrivals has been estimated at 50 ms. Existing low-frequency (<200 Hz) broadband sources appear to satisfy these requirements. The real limiting factor will probably be the lack of spatial resolution owing to practical limitations on the number of sources and receivers. Consequently, there will usually be insufficient information from which to determine a unique solution to the inverse problem.

A field test of ocean–acoustic tomography was conducted in the North Atlantic Ocean in 1981 (Cornuelle *et al.*, 1985). The test was conducted over a 2-month period in a 300 km² area centered at 26° N, 70° W using nine acoustic deep-sea moorings with sea floor transponders. The acoustic sources operated at a center frequency of 224 Hz, with a 5.4 Hz rms bandwidth. The 3D sound-speed field obtained by inversion techniques compared favorably with direct observations of sound-speed profiles. Tomographic maps constructed at 3-day intervals over the test period revealed a pattern of eddy structure in general agreement with that deduced from direct observations. Mapping errors were attributed to noise variance in travel-time measurements.

Acoustic tomography experiments have been conducted to detect climatic trends of temperature in the oceans with basin-scale resolution (Munk and Forbes, 1989; Spindel and Worcester, 1990a,b, 1991; Spiesberger and Metzger, 1991a; Spiesberger *et al.*, 1992; Forbes, 1994). Since acoustic travel times are inversely related to water temperature, tomography provides a method for ascertaining the bulk temperature of the oceans. This bulk temperature is potentially a more reliable metric for global warming than are conventional atmospheric measurements which, for example, can be influenced by the heat island effect that is often associated with urban temperature records. Moreover, basin-scale averages of water temperature suppress the intense mesoscale eddies that would otherwise dominate the climatic variations.

The Heard Island feasibility test (HIFT) established the limits of phase-coded, electrically driven sound sources (instead of explosive sources) in tomographic experiments (Munk, 1994). Figure 5.20 illustrates the ability of an acoustic source situated at Heard Island to sample vast volumes of the oceans over ray paths unimpeded by bathymetric obstructions. These ray

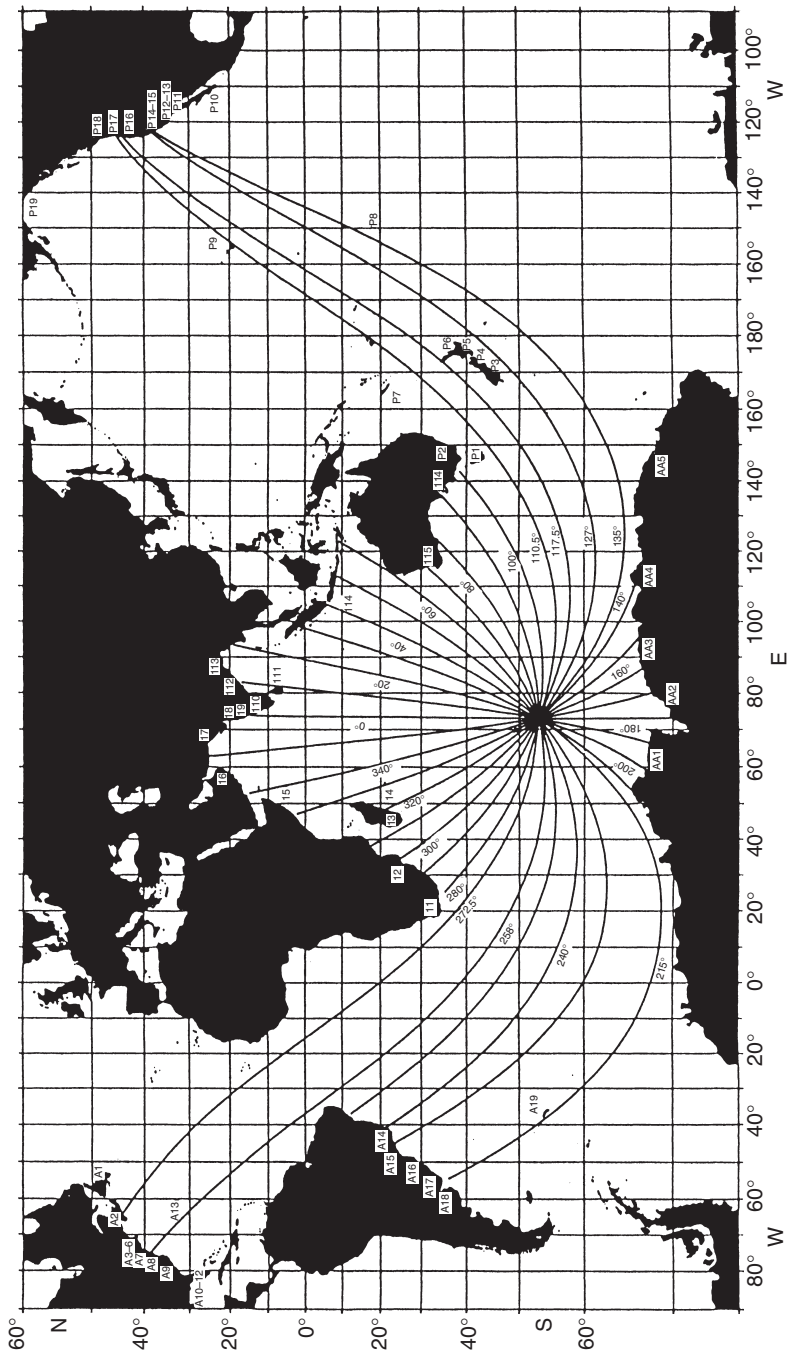


Figure 5.20 Illustration of bathymetrically unimpeded ray paths emanating from Heard Island with the indicated launch angles. All rays are refracted geodesics along the surface containing the sound channel axis (see Figure 2.8). White boxes indicate locations of oceanographic research stations capable of receiving acoustic signals. (Munk and Forbes, 1989; *J. Phys. Oceanogr.*, 19, 1765–78; copyright by the American Meteorological Society.)

paths represent refracted geodesics along the surface containing the sound channel axis (see Figure 2.8). A geodesic path is the shortest distance between two points on the surface of an elliptical (versus spherical) Earth. Geodesics would be the proper ray paths in a uniform sound-speed field; however, the refractive effects of lateral sound-speed gradients alter these paths.

HIFT is a prerequisite to a program for ATOC. The goals of ATOC are: (1) to verify the acoustically measured changes in travel time by comparison with those inferred from traditional oceanographic measurements along the transmission path in the North Pacific Ocean; (2) to study the coherence of climatic scale variability in the North Pacific gyre; (3) to test long-range acoustic transmission characteristics using 40-element vertical receiver arrays; and (4) to test specially designed ATOC sound sources. The potential effects of acoustic transmissions on marine mammals have also been investigated in related efforts (Green, 1994; National Research Council, 1994). A series of 17 technical papers addressing various aspects of HIFT was recently published. These papers were introduced by Munk and Baggeroer (1994).

Long-range acoustic propagation issues relevant to tomographic investigations include bathymetric interactions. These aspects have been investigated by Munk (1991), Munk and Zachariasen (1991) and Heaney *et al.* (1991). Forward scatter by islands and seamounts was found to produce significant scattered arrivals (Munk and Zachariasen, 1991). Such arrivals can complicate interpretation of the recorded acoustic travel times if they are not properly differentiated from the direct arrivals.

Gaillard (1985) demonstrated that mobile sources or receivers can also be used in tomographic experiments, but that this mobility increases the sensitivity to noise. More efficient use of *a priori* knowledge of the ocean reduces this sensitivity by decreasing the number of degrees of freedom. Moving ship tomography (MST) is a method for obtaining high-resolution, quasi-synoptic, 3-D maps of the oceanic temperature field over large areas (The Acoustic Mid-Ocean Dynamics Experiment Group, 1994). All previous work in ocean acoustic tomography has been performed with fixed or moored instruments. MST is part of the larger acoustic mid-ocean dynamics experiment (AMODE), which has the goal of determining the measurement limits of moving ship tomography. The larger number of acoustic ray paths generated by a moving receiver will improve measurements of advecting fronts and interacting eddies. This increased volumetric resolution will enable more rigorous testing of the predictive capabilities of dynamical ocean circulation models.

Methods for computing and plotting tomographic inversions in ocean environments have been described by Nesbitt and Jones (1994a–c). In related work, Weickmann and Jones (1994) described computer programs used to perform ocean–acoustic tomography inversions based on a nonperturbative-inversion method. Harrison *et al.* (1998) described a localization technique that was an efficient approximation to the maximum *a posteriori* probability

(MAP) estimator intended for use in matched-field source-localization methods. Yaremchuk and Yaremchuk (2001) developed a nonlinear method for inverting ocean–acoustic tomography data. This method accounts for the quadratic term of the travel-time expansion in the powers of the reciprocal sound-speed perturbations. The higher-order correction to the travel-time model can be essential in regions of large spatial variability. This method was tested against data acquired in the Kuroshio extension region (near 32° N, 148° E). While this method does improve the quality of data processing, it increases the associated computational requirements. Dzieciuch *et al.* (2001) introduced a technique referred to as a “turning point filter” that permits a uniform treatment of long-range acoustic transmissions from the early ray-like arrivals to the late mode-like arrivals. This method may also be applicable to source localization problems.

As summarized by Spindel (1985), acoustic tomography is particularly attractive for application to the ocean for a number of reasons: (1) images of the ocean interior can be obtained from periphery measurements; (2) large ocean areas can be measured with relatively few instruments; (3) a single source–receiver pair samples the ocean vertically due to multipath propagation effects; and (4) the integrating properties of acoustic propagation produce average quantities not obtainable with point measurements.

5.6.10 *Phase conjugation and time-reversal mirrors*

Kuperman *et al.* (1998) experimentally demonstrated that a time-reversal mirror (or phase-conjugate array) could spatially and temporally refocus an incident acoustic field back to its origin. This work was extended by Song *et al.* (1998) to refocus an incident acoustic field at ranges other than that of the probe source. The basic idea of the approach was that the sound field maxima could be shifted to different ranges by appropriately increasing or decreasing the source frequency for a specific propagation environment.

Time-reversal acoustics can be applied in shallow water to focus energy back to a source location. This refocusing produces spatial intensification of the field (through removal of multipath spreading) as well as temporal convergence of the signal. These properties suggested potential applications in underwater acoustic communication systems (Abrantes *et al.*, 1999).

5.6.11 *Deductive geoacoustic inversion*

Since direct measurements of seabed parameters are practical only over short distances, considerable attention has been devoted to the inversion of acoustic propagation measurements as a cost-effective alternative to measurements over large ocean areas (e.g. Diachok *et al.*, 1995; Siderius *et al.*, 2000). Using inverse techniques, the desired geoacoustic seabed parameters are extracted from the forward measurements of acoustic propagation in the oceanic waveguide.

Deductive geoacoustic inversion derives the desired sediment and substrate parameters from direct measurements of acoustic propagation. The desired parameters are deduced from the propagation measurements using, for example, simulated annealing or genetic algorithms (Gerstoft, 1994; Snellen *et al.*, 2001). The resulting geoacoustic parameters represent averages over long ranges. Direct measurements over comparably long ranges are frustrated by sparse sampling (Hamson and Ainslie, 1998; Ainslie *et al.*, 2001). Deductive geoacoustic inversion assumes that acoustic data are sensitive to different geoacoustic parameters at different frequencies. Sediment parameters of interest include sediment thickness, sound speed (and gradient), density, attenuation and shear speed. Substrate parameters of interest include density, attenuation, compressional sound speed and shear speed (Ainslie *et al.*, 2000).

Siderius *et al.* (2001) used experimental data collected at a shallow-water site to demonstrate the impact of ocean sound-speed fluctuations on the quality of seabed properties deduced from geoacoustic inversion. The experimental TL, when averaged over frequency (0.2–3.8 kHz) and time (3 days), was modeled with sufficient accuracy. In fact, the mean modeled TL was within one standard deviation of the data for both short- (2 km) and long-range (10 km) propagation. However, the modeled standard deviation of the TL was in poor agreement with that of the data due to insufficient knowledge of the changing ocean environment. Fluctuations in the sound speed destroyed coherent processing beyond a few kilometers. Without reliable predictions of acoustic propagation, the inverted geoacoustic parameters showed erroneous time variability (erroneous since the seabed properties being deduced are expected to remain fixed over time). At ranges of 2 km, the temporal stability of the geoacoustic inversion indicated that the method was indeed sound. This demonstrated that, without sufficient temporal and spatial knowledge of the volumetric properties of the ocean, geoacoustic inversion at long ranges is subject to degradation.

Ainslie *et al.* (2001) compared results deduced from three different methods, all of which used a Bartlett processor: (1) the evolutionary search algorithm (ESA) used a PE forward model; (2) the genetic algorithm (GA) used a normal mode forward model; and (3) the deductive rapid environmental assessment model (DREAM) used a normal mode forward model. The results showed good agreement among the three methods, although differences in the computational procedures complicated definitive numerical assessments.

Recently, geoacoustic inversion of ambient noise has also been explored (see Chapter 6, Section 6.7). In particular, Harrison and Simons (2001) noted that inversion of the noise field could complement active-acoustic propagation inversion techniques in which sound-speed fluctuations might impede model matching.

6 Noise I

Observations and physical models

6.1 Background

Ambient noise is the prevailing, unwanted background of sound at a particular location in the ocean at a given time of the year. It does not include transient sounds such as the noise of nearby ships and marine organisms, or of passing rain showers. It is the background of noise, typical of the time, location and depth against which a signal must be detected. Ambient noise also excludes all forms of self-noise, such as the noise of current flow around the sonar. Thus, ambient noise is the residual sound level remaining after all identifiable, transient-noise sources have been removed (Urick, 1983: chapter 7). Levels of noise sources are commonly specified as the root-mean-square (rms) sound pressure level in a 1-Hz band (referred to as “spectrum level”). Different units indicate how the noise levels were derived (see Pierce, 1989: chapter 2, for an in-depth discussion). Units commonly encountered in the technical literature include: spectrum level, dB re $1 \mu\text{Pa}$; dB re $1 \mu\text{Pa}^2 \text{Hz}^{-1}$; and dB re $\mu\text{Pa Hz}^{1/2}$ (where “re” is an abbreviation for “relative to”). The discussion by Carey (1995) regarding the potential for confusion when using decibels to estimate spectral quantities is relevant here.

6.2 Noise sources and spectra

Figure 6.1 is a hypothetical example of the spectrum of ambient noise in the open ocean (Urick, 1983: chapter 7). This spectrum is composed of segments of different slope, each exhibiting a different behavior. A number of frequency bands in the spectrum can be associated with readily identifiable noise sources. Five such frequency bands are indicated in Figure 6.1. Band I, lying below 1 Hz, is associated with noise of hydrostatic origin (tides and waves) or with seismic activity (Kibblewhite and Ewans, 1985). Valid measurements in this band (and in Band II) are extremely difficult to make because of the self-noise of the hydrophone and its supporting structure caused by currents (e.g. cable strumming). Band II is characterized by a spectral slope of -8 to -10 dB octave $^{-1}$ (about -30 dB decade $^{-1}$). The most probable source of noise in deep water appears to be oceanic turbulence.

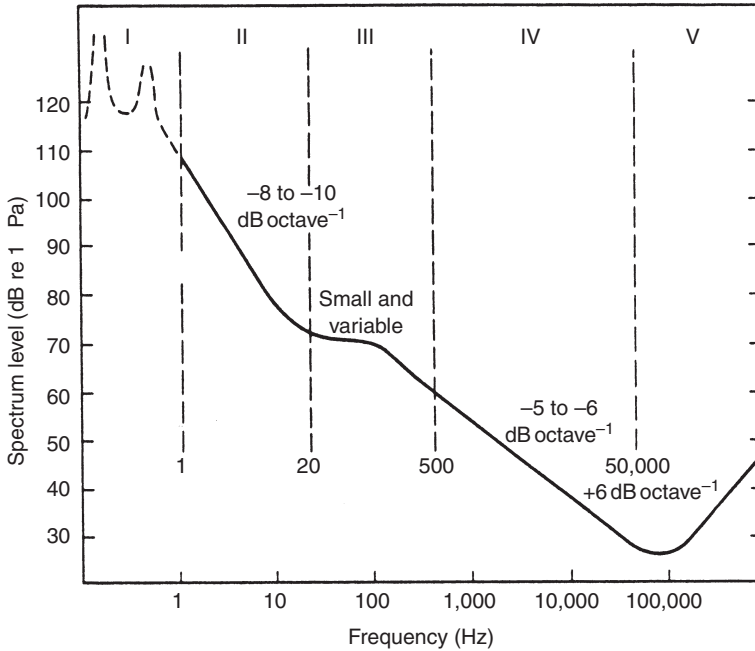


Figure 6.1 General spectrum of deep-sea noise showing five frequency bands of differing spectral slopes. The slopes are given in decibels (dB) per octave of frequency. (Urick, 1983; *Principles of Underwater Sound*, 3rd edn; reproduced with permission of McGraw-Hill Publishing Company.)

In Band III, the ambient noise spectrum flattens out and the noise appears to be dominated by distant shipping traffic. Band IV contains the Knudsen spectra (Knudsen *et al.*, 1948) having a slope of -5 to -6 dB octave $^{-1}$ (about -17 dB decade $^{-1}$) in which the noise originates at the sea surface near the point of measurement. Band V is dominated by thermal noise originating in the molecular motion of the sea and is uniquely characterized by a positive spectrum having a slope of $+6$ dB octave $^{-1}$.

For some prediction purposes, average representative ambient-noise spectra for different conditions are adequate. Such average working curves are shown in Figure 6.2 for different conditions of shipping and wind speed. These curves are adapted from Wenz (1962); consequently, they are often referred to as Wenz curves. In the infrasonic region below 20 Hz, only a single line is drawn. The ambient-noise spectrum at any location and time is approximated by selecting the appropriate shipping and wind curves and connecting them at intermediate frequencies. When more than one source of noise is present (e.g. shipping and wind noise), the effective noise background is obtained by summing the intensities of the contributing sources. When

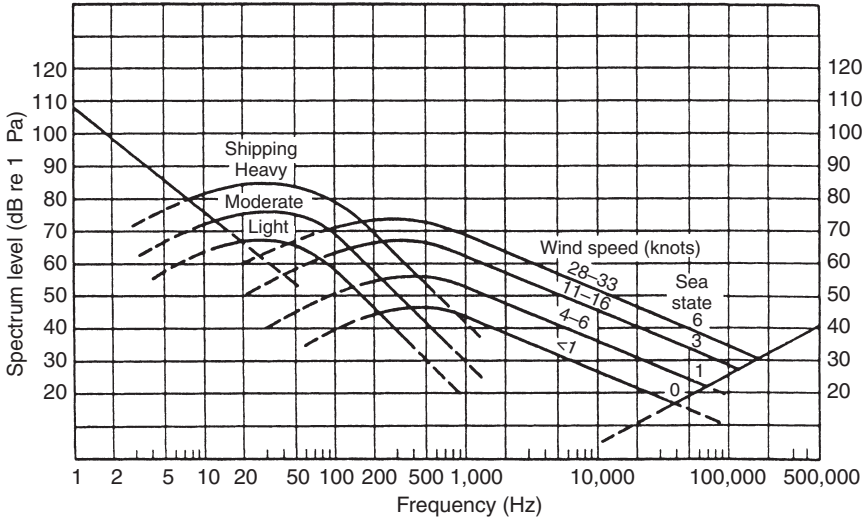


Figure 6.2 Average deep-sea ambient-noise spectra. (Urlick, 1983; *Principles of Underwater Sound*, 3rd edn; reproduced with permission of McGraw-Hill Publishing Company.)

using noise levels (specified in units of spectrum level, dB re 1 μPa), this summation process is easily accomplished using the “power summation” operator, denoted by the symbol \oplus , and defined as:

$$\oplus = 10 \log_{10} \sum_{i=1}^n 10^{L_i/10} \tag{6.1}$$

where L_i is the level of the i th noise source (dB) and n the number of contributing noise sources. This operation effectively converts the noise levels (L_i) to units of intensity, sums the intensities, and then converts the sum back to units of decibels.

For example, in Figure 6.2 at a frequency of 100 Hz under conditions of moderate shipping and sea state 6, the individual noise levels are about 69 and 71 dB, respectively. In effect, however, the noise level obtained using Equation (6.1) is:

$$69 \text{ dB} \oplus 71 \text{ dB} = 10 \log_{10}[10^{6.9} + 10^{7.1}] = 73 \text{ dB}$$

or 2 dB higher than the level due to surface weather alone.

6.2.1 *Seismo-acoustic noise*

The term seismo-acoustics is used broadly in reference to low-frequency noise signals originating in Earth’s interior and the oceans. In the frequency

range below 3 Hz, Orcutt (1988) defined three specific frequency bands distinguished by the physics of the noise sources:

- 1 Microseism band (80 mHz–3 Hz) contains high-level microseism noise resulting from nonlinear wave–wave interactions.
- 2 Noise-notch band (20–80 mHz) contains noise controlled by currents and turbulence in the boundary layer near the sea floor.
- 3 Ultralow-frequency (ULF) band (<20 mHz) contains noise resulting from surface gravity waves.

6.2.2 Shipping noise

Shipping noise can exhibit both spatial and temporal variabilities. The spatial variability is largely governed by the distribution of shipping routes in the oceans. Temporal variability can be introduced, for example, by the seasonal activities of fishing fleets.

The noise generated by coastal shipping and by high-latitude shipping can contribute to the noise field in the deep sound channel in tropical and subtropical ocean areas. Specifically, coastal shipping noise is introduced into the deep sound channel through the process of downslope conversion. High-latitude shipping noise is introduced through the latitudinal dependence of the depth of the sound channel axis. These mechanisms are explained below.

Wagstaff (1981) used ray-theoretical considerations to illustrate the mechanisms involved in the downslope conversion process. The following hypothetical arrangement was assumed (Figure 6.3): (1) the continental shelf extends from the coastline to the shelf break (approximately 11.4 km from shore), with an inclination angle of about 1° from the horizontal; (2) the continental slope extends from the shelf break seaward to a depth in excess of 1,000 m, with an inclination of about 5° ; and (3) the deep sound channel axis is located at a depth of 1,000 m. Then, in an 11-km band extending seaward from the shelf break, downward-directed radiated noise from surface ships can enter the sound channel by direct reflection off the sea floor.

Kibblewhite *et al.* (1976) demonstrated the importance of the latitudinal dependence of the sound channel axis depth in introducing high-latitude shipping noise into the deep sound channel. In Figure 6.4, the sound-speed structure in the north Pacific Ocean is related to the local water masses. Also shown are the critical depth and the bathymetry. Figure 6.4 vividly illustrates the shoaling of the sound channel axis as it approaches the Arctic region. Thus, low-frequency noise from shipping sources near latitude 50°N will be refracted into the (relatively) shallow sound channel and then propagate with little attenuation to lower latitudes.

Tappert *et al.* (2002) used the UMPE propagation model to simulate a range-dependent phenomenon that occurs over a sloping bottom when a source is located on the sea floor in shallow water with

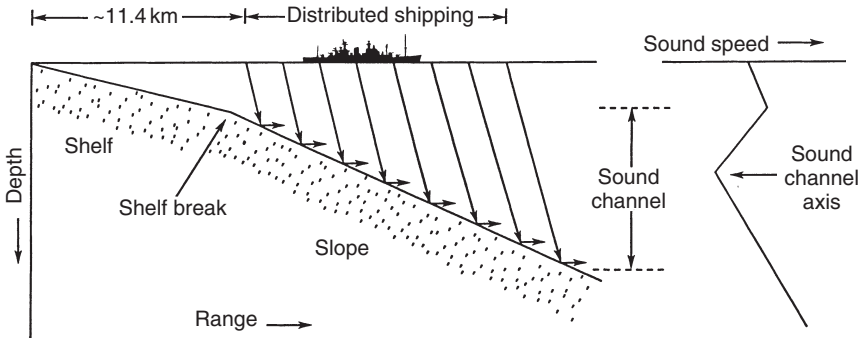


Figure 6.3 Illustration of the conversion of coastal shipping noise, represented by high-angle rays, to noise in the deep sound channel, represented by horizontal rays (adapted from Wagstaff, 1981).

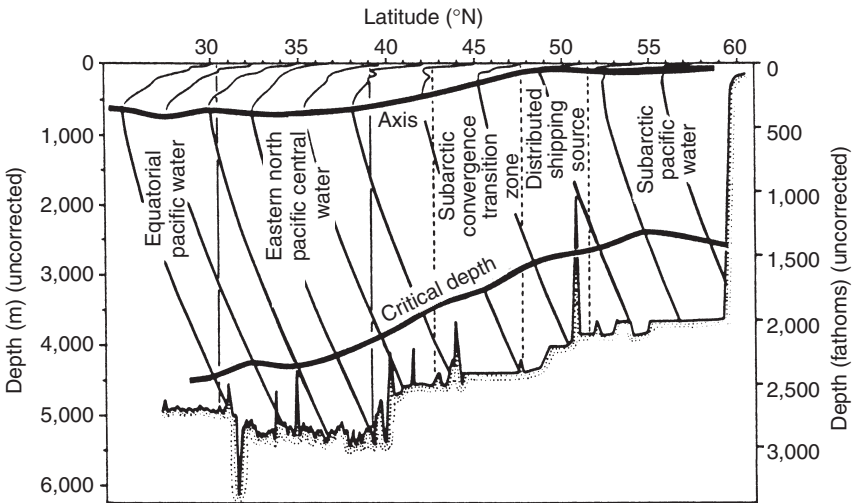


Figure 6.4 Bathymetric and sound-speed structure in the north Pacific Ocean. The noise from distributed shipping sources at high latitudes can enter the sound channel and propagate with little attenuation to lower latitudes. Relationships between the sound speed structure and the prevailing water masses are also illustrated (Kibblewhite *et al.*, 1976).

a downward-refracting (negative-gradient) sound-speed profile. Sound waves propagate downslope with small grazing angles until they reach the depth of the sound channel axis in deep water where they then detach from the bottom and propagate within the sound channel. Tappert *et al.* (2002)

refer to this as the “mudslide” effect, which they characterize as one of a few robust and predictable acoustic propagation effects that occur in range-dependent ocean environments.

6.2.3 Bioacoustic noise

Marine bioacoustic signal sources are typically transient in nature and exhibit diverse temporal, spatial and spectral distributions. The main contributors to bioacoustic signals include certain shellfish, fish and marine mammals. Of the marine mammals, whales are the most notable contributors. Au *et al.* (1987), Cummings and Holliday (1987) and Watkins *et al.* (1987) described whale signal characteristics and distributions. A paper by Watkins and Schevill (1977) included a phonograph recording of actual whale codas.

Richardson *et al.* (1995: chapter 7) provided comprehensive summaries of marine mammal sounds in the form of tabulations that included frequency ranges and associated source levels for each species. Specifically included were the sounds produced by baleen whales (bowhead, right, gray, humpback, fin, blue, Bryde’s, sei and minke), toothed whales [Physeteridae (sperm whale), Ziphiidae (bottlenose whale), Monodontidae (beluga and narwhal), Delphinidae (killer whale and dolphin), Phocoenidae (porpoise) and river dolphins], phocid (hair) seals, eared seals (sea lions and fur seals), walruses, sea otters and sirenian (manatees and dugongs).

As discussed by Richardson *et al.* (1995: chapters 8–11) and the National Research Council (2000), understanding of both the sensitivity of marine mammals’ hearing and the reactions of marine mammals to various noise sources has advanced through additional fieldwork. This work provides relevant guidance to the design and operation of high-intensity sources, especially in multistatic and tomographic experiments.

Furthermore, this research aids in the development of meaningful acoustical regulations to ensure the health and safety of marine mammals.

6.2.4 Wind and rain noise

Kerman (1988, 1993) and Buckingham and Potter (1996) provided updated summaries of sea-surface sound. The established relationships between surface weather phenomena and noise levels have been used to advantage by oceanographers. Shaw *et al.* (1978) demonstrated that surface wind speeds derived from measured noise spectra could be used to calculate the wind stress over the oceans. Synoptic wind stress information is required for the dynamic modeling of wind-driven ocean currents. Scrimger *et al.* (1987) and Lemon and Duddridge (1987) described the development and operation of WOTAN (weather observation through ambient noise) systems. These systems operate over the frequency range 0.5–30 kHz and have been successfully used to infer wind speeds that were highly correlated with

buoy-mounted anemometer measurements. Vagle *et al.* (1990) made further measurements in support of WOTAN.

Zedel *et al.* (1999) modified an acoustic Doppler current profiler (ADCP) to record ambient sound in the frequency range 1–75 kHz. The resulting instrument package, called OASIS (ocean ambient sound instrument system), inferred wind speeds and directions from these acoustic measurements that were determined to be in good agreement with direct observations made at Ocean Weather Station Mike in the Norwegian Sea.

Felizardo and Melville (1995) concluded that ambient noise correlated well with wind speed (in the Knudsen range) but correlated poorly with significant wave height. The poor correlation with wave height was attributed to the disproportionate effect of swell on the frequency of breaking waves, which are considered the primary source of wind-dependent noise in the ocean.

The noise attributable to rainfall over the oceans has also been used in an inverse fashion to provide estimates of oceanic precipitation (Nystuen, 1986). The underwater noise spectrum generated by rain has a unique spectral shape that is distinguishable from other noise sources by a broad peak at about 15 kHz. Moreover, the relationship between spectral level and rate of rainfall is quantifiable. Scrimger *et al.* (1987) made measurements of the underwater noise generated by rain in a lake located on Vancouver Island, British Columbia (Figure 6.5). These data illustrate the peak in noise levels at 15 kHz. Pumphrey and Crum (1990) determined that the major cause of

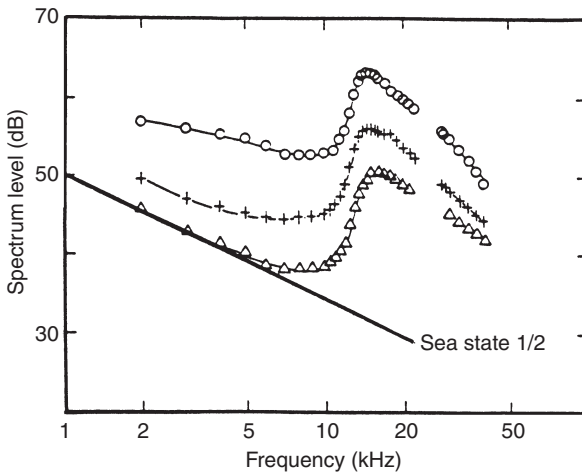


Figure 6.5 Rain noise spectra observed at moderate wind speeds for rain rates of 0.5 mm h^{-1} (Δ), 0.8 mm h^{-1} (+) and 1.3 mm h^{-1} (O) compared to the Knudsen curve for sea state 1/2 (Scrimger *et al.*, 1987).

rain-generated sound is the production of bubbles upon water-drop impact at the surface. These bubbles then oscillate with small amplitude and radiate as a dipole.

The effects of bubbles and rain as noise-generating mechanisms have been investigated further by Buckingham (1991) and Laville *et al.* (1991), respectively. As previously noted, there are two sources of rainfall sound: raindrop impacts on the water surface and air bubble resonances. Bubble resonances were found to be responsible for the spectral peak near 13–15 kHz, while raindrop impacts were associated with a broadband spectrum having a negative slope (Laville *et al.*, 1991). The underwater sound due to rainfall can be distinguished further according to raindrop diameters (Medwin *et al.*, 1992): small drops (0.8–1.1 mm) radiate primarily from bubble resonances near 15 kHz; mid-size drops (1.1–2.2 mm) radiate only broadband impact sound; and large drops (>2.2 mm) radiate both impact and resonance sounds. Nystuen and Medwin (1995) proposed a new bubble-entrapment mechanism to account for a missing component in the modeling of underwater sound levels produced by raindrops. In related investigations, Rohr and Detsch (1992) attributed the effect of films on suppressing high-frequency ambient noise to the opposition of bubble-producing events by these films. Crum *et al.* (1992) and Pumphrey (1994) reviewed the nature of precipitation sounds underwater, while Prosperetti and Oğuz (1993) reviewed the physics of drop impacts on liquid surfaces. Collectively, these studies have improved upon earlier investigations such as those reported by Heindsmann *et al.* (1955), Franz (1959) and Bom (1969).

Indirect measurements of rainfall are important since roughly 80 per cent of Earth's precipitation occurs over the oceans and lakes where only about 10 per cent of the weather stations are located (e.g. islands and buoys). This information allows oceanographers and meteorologists to improve their understanding of the oceanic heat and fresh-water budgets (e.g. Etter *et al.*, 1987) that, in turn, can provide measures of both short-term and long-term fluctuations in the global climate.

Nystuen (1994) developed an acoustic rainfall analysis (ARA) algorithm consisting of: detection of rainfall in the presence of other underwater noise sources, classification of rainfall type based on drop-size distribution and acoustic quantification of rainfall rate. The classification of rainfall type (e.g. according to stratiform or convective) will permit meteorologists to infer the vertical distribution of atmospheric latent-heat release in support of global climate studies.

Oğuz (1994) developed a theoretical model to predict the ambient noise levels arising from bubble clouds generated by breaking waves and resultant whitecap formation. Cloud geometries were modeled by inverted hemispherical shapes within which solutions to the wave equation could be obtained analytically. Empirical relationships between wind speed and whitecap occurrence permitted calculation of noise levels as a function of frequency and wind speed.

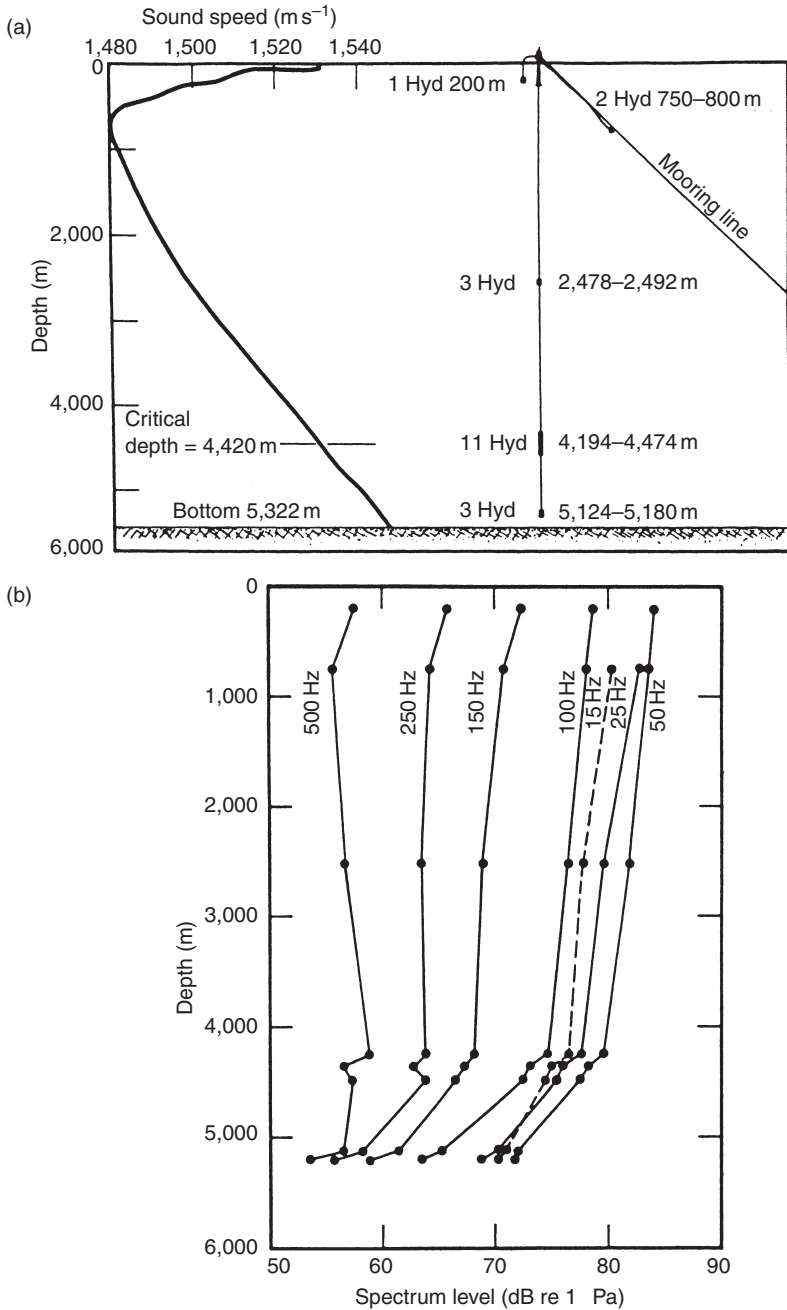


Figure 6.6 Northeast Pacific Ocean ambient noise measurements: (a) sound-speed profile and hydrophone depths and (b) measured noise profiles in one-third-octave bands (Morris, 1978).

6.3 Depth dependence

Measurements of the depth dependence of low-frequency ambient noise were made by Morris (1978) in the northeastern Pacific Ocean. Hydrophones were suspended from the research platform FLIP (floating instrument platform). Figure 6.6 shows the sound-speed profile, hydrophone depths and average noise profiles in one-third-octave bands for this experiment. There is a decrease of noise with increasing depth at low frequencies, with a smaller decrease with depth at 500 Hz as wind noise overcomes the dominance of shipping noise. Below the critical depth, the fall-off with depth is steeper as the bottom is approached. This is the result of the loss of refracted sound energy through the effects of bottom interaction.

Urlick (1984: chapter 4) demonstrated that ambient noise at frequencies greater than 10 kHz is rapidly attenuated with increasing depth due to the effects of absorption.

6.4 Directionality

As a first-order approximation, the noise field in the ocean might be considered to be isotropic in nature, that is, uniform in all directions, both horizontal and vertical. Measurements have shown that this is not the case.

Axelrod *et al.* (1965) made measurements of the vertical directionality of ambient noise at frequencies of 112 and 1,414 Hz. Figure 6.7 presents polar plots of the ambient noise intensity per unit solid angle $N(\theta)$ arriving at a bottomed hydrophone as a function of the vertical angle θ . At 112 Hz, more noise arrives at the hydrophone from the horizontal than from the vertical. This effect diminishes with increasing wind speed. At 1,414 Hz, the opposite is true in that more noise arrives from overhead than horizontally. This effect increases with increasing wind speed.

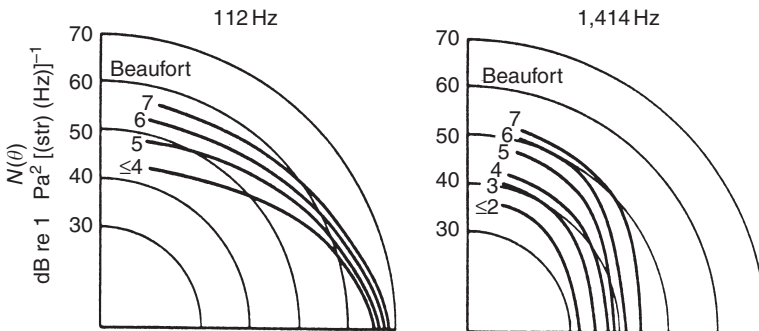


Figure 6.7 Distribution of ambient noise in the vertical plane at a bottomed hydrophone at two frequencies (Axelrod *et al.*, 1965).

This directional behavior is consistent with the view that low-frequency noise originates at great distances and arrives at the measurement hydrophone principally via horizontal paths, suffering little attenuation. Alternatively, high-frequency noise originates locally at the sea-surface overhead (Urlick, 1984: chapter 5).

The horizontal (or azimuthal) directionality of ambient noise can be highly variable, particularly at low frequencies. Shipping traffic is the dominant source of noise at low frequencies, and the temporal and spatial variations in shipping densities explain much of the observed azimuthal variation.

6.5 Arctic ambient noise

The noise environment under the Arctic ice is different from that of any other ocean area. Shipping noise is extremely low due to the lack of surface traffic. The ice cover itself affects the ambient noise field significantly. It can decouple the water from the effects of the wind and produce ambient noise conditions that are much quieter than a corresponding sea state zero in the open ocean. The ice itself may produce noises as wind, waves and thermal effects act on it (e.g. Milne, 1967). Other sources of noise in the Arctic include seismic and biological activities.

The character of the ice cover is different in areas of shore-fast pack ice, moving pack ice and the marginal ice zone (MIZ). The under-ice noise levels, directionality, spectrum shape and temporal character are very different in each of these regions. Noise originating within the ice stems principally from its state of stress, which gives rise to fracturing. Noise measurements under the pack ice span the frequency range from 3 Hz to more than 1,000 Hz (Dyer, 1984, 1988).

Pack ice is very dynamic and its characteristics are highly variable in space and time (Makris and Dyer, 1986). Nevertheless, the lack of wind-wave interaction and the absence of local shipping can lead to noise levels 10 dB lower than those encountered in the open ocean.

Noise levels in the MIZ are typically higher than those in either the pack ice regions or the open ocean regions (Diachok and Winokur, 1974; Diachok, 1980). Figure 6.8 illustrates the variations in median ambient-noise levels that occur across a compact ice-water MIZ area. The relative magnitudes of the noise levels generated at the ice-water boundary are a function of the rate of change of ice concentration with distance. Thus, the relative maximum noise level measured at a diffuse ice-water boundary would be smaller than that measured at a compact ice edge. Ambient noise levels in the MIZ also depend on such variables as sea state, water depth and dominant ocean-wave period. The last variable is hypothesized as being related to the efficiency of coupling ocean-wave energy into the ice. Makris and Dyer (1991) demonstrated that surface gravity wave forcing was the primary correlate of ice-edge noise in the MIZ.

Pritchard (1990) developed an ambient noise model to simulate the time history of under-ice noise generated by dynamical ice movement, stress

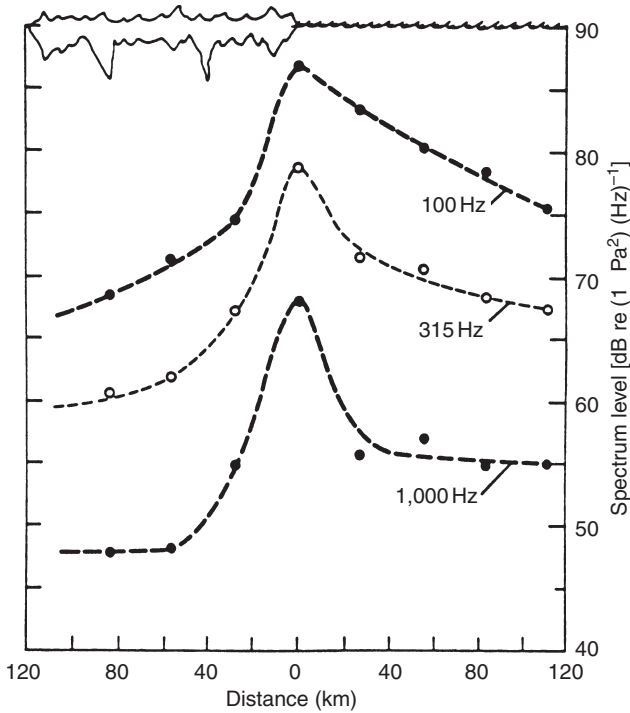


Figure 6.8 Variation of median-ambient noise sound-pressure spectrum levels with distance from a compact ice edge for frequencies of 100, 315 and 1,000 Hz in sea state 2 (Diachok, 1980).

and deformation. The model included noise contributions from local and distant sources as well as a transmission loss (TL) module appropriate for the Arctic environment. Time series data were simulated for a frequency of 31.5 Hz.

Lewis and Denner (1988) reported observations of higher-frequency (1,000 Hz) ambient noise data in the Arctic Ocean. These noises were attributed to the thermal fracturing of ice. Related aspects of ice-generated noise have been reviewed by Sagen *et al.* (1990).

6.6 Acoustic daylight

Ambient noise in the ocean can be used to form pictorial images of underwater objects. An analogy can be drawn between the natural optical (daylight) field in the atmosphere and the radiating ambient noise field in the ocean: both fields consist of random, incoherent radiation propagating in all directions. Thus, the concept of imaging with ambient noise has been referred to as “acoustic daylight” (Buckingham *et al.*, 1992). A reasonable operating frequency range for the acoustic daylight system is 5–50 kHz; the lower limit

is determined by angular resolution considerations while the upper limit is determined by the onset of thermal noise. A general introduction to imaging underwater objects with ambient noise was presented by Buckingham *et al.* (1996b).

Buckingham (1993) analyzed the incoherent acoustic imaging of a spherical target in order to quantify the contrast ratio (acoustic contrast) under various degrees of anisotropy. In the case of isotropic noise, the contrast (acoustic visibility) was found to have a maximum value of about 4 dB. This result was consistent with field measurements when the angle of view of the acoustic lens matched the angle subtended by the target at the phase center of the measurement array.

An acoustic daylight ocean noise imaging system (ADONIS) was constructed. The system was designed to operate over the frequency range 15–75 kHz with a corresponding minimum wavelength of 20 mm, formed 126 individual beams of nominal width of 0.76° (at the upper frequency), and operated over the spatial range 10–200 m. Simulations developed to predict the performance of ADONIS (Potter, 1994) demonstrated that near perfectly reflecting objects were unlikely to be imaged in volume isotropic noise, except perhaps in the near field. However, the ocean was expected to exhibit considerable anisotropy, if only in the vertical direction, thus improving performance over the conjectured isotropic baseline. Buckingham *et al.* (1996a) described the results of an experiment with ADONIS, which in practice operated in the frequency range 8–80 kHz and relied on ambient noise to provide the acoustic contrast between look angles on-target and off-target. Epifanio *et al.* (1999) described results from the ORB experiments, which were conducted with targets at ranges between 20 and 40 m using ADONIS' 126 receive-only beams spanning the vertical and horizontal. Makris *et al.* (1994) conducted a careful analysis of this noise-imaging concept and concluded that it pressed the limits of current technology. Furthermore, they traced similar approaches back to 1985 when the possibility of detecting submarines solely by their noise absorbing and scattering properties (*acoustic contrast versus acoustic glow*) had been investigated by S. Flatté and W. Munk.

Potter and Chitre (1999) extended the concept of *acoustic daylight* (which uses the mean intensity of backscattered ambient-noise energy to produce images of submerged objects, and is thus analogous to *vision*) by exploring the information contained in higher moments. Specifically, information embodied in the second temporal and spatial moments of intensity, for which there are no visual analogs like *acoustic daylight*, was referred to as ambient-noise imaging (ANI), a broader imaging approach.

6.7 Geoacoustic inversion

In shallow water, the spatial structure of the ambient-noise field is strongly influenced by multiple interactions with the sea floor. Consequently, both

the vertical directionality and coherence of the shallow-water noise field are determined primarily by the geoacoustic properties of the seabed rather than by any temporal variations in source distributions. Several investigators have deduced geoacoustic parameters through inversion of the ambient noise field in range- and azimuth-independent shallow-water environments in which the noise sources were uniformly distributed. For example, Buckingham and Jones (1987) determined critical angles, Carbone *et al.* (1998) determined compressional and shear wave speeds and Aredov and Furduev (1994) determined reflection losses.

For non-uniformly distributed noise sources in range-dependent environments, sophisticated vertical hydrophone arrays are required to resolve the arrival structure of the noise field. Furthermore, the experimental data must be analyzed using detailed noise models. For simpler geoacoustic parameters such as reflection loss, however, Harrison and Simons (2001) argued that detailed models are not required in the inversion analysis, although a densely populated vertical array is required to resolve the arrival structure. Harrison and Simons (2002) report additional experimental results.

7 Noise II

Mathematical models

7.1 Background

Chapter 6 discussed aspects of ambient-noise measurements in the ocean. In particular, Figure 6.2 portrayed the average deep-sea ambient-noise spectra as originating from shipping traffic at low frequencies (~ 5 Hz to ~ 200 Hz) and from surface weather at high frequencies (~ 200 Hz to ~ 50 kHz). In the range 50–500 Hz, both mechanisms (shipping and weather) contribute to the observed noise levels. The significance of these dual mechanisms has influenced the course of noise model developments.

Mathematical models of noise in the ocean can be segregated into two categories: ambient-noise models and beam-noise statistics models. Ambient-noise models predict the mean levels sensed by an acoustical receiver when the noise sources include surface weather, biologics and such commercial activities as shipping and oil drilling. Beam-noise statistics models are more specialized in that they predict the properties of low-frequency shipping noise for application to large-aperture, narrow-beam passive sonar systems. The latter models use either analytic (deductive) or simulation (inductive) techniques to generate statistical descriptions of the beam noise. In this context, beam noise is defined as the convolution of the receiver beam pattern with the sum of the intensities from the various noise sources. The analytic models calculate statistical properties directly from the components (e.g. source level, propagation loss) while the simulation models use Monte Carlo techniques.

7.2 Theoretical basis for noise modeling

Mathematical models of noise in the ocean predict both the level and directionality (vertical and horizontal) of noise as a function of frequency, depth, geographic location and time of year. Both categories of noise models (ambient-noise and beam-noise statistics) consist of two components: a transmission loss (TL) component and a noise level and directionality component. In principle, the TL can be computed internal to the noise model or it can be input externally from other (stand-alone) model predictions or from field measurements.

Ambient-noise models treat noise sources as variable densities distributed over large areas. This approximates the generation of wind noise and distant shipping noise. Consequently, the TL calculations in ambient-noise models can be range-averaged (as opposed to point-to-point). This greatly relaxes the accuracy to which TL must be known. Alternatively, beam-noise statistics models treat noise sources (individual ships) as discrete sources, and thus require point-to-point representations of TL.

Empirical regression formulae can sometimes satisfy low-fidelity modeling requirements. The loss of fidelity stems principally from a lack of directionality information (vertical and horizontal) and also from a lack of temporal and spatial resolutions. Moreover, the use of regression formulae to estimate the ambient-noise levels (but not directionality) presumes that the noise levels can be considered independently of the sonar system characteristics. Rigorous noise modeling convolves the system beam pattern (i.e. receiver response) with the calculated noise field levels and directionalities (Wagstaff, 1982).

Sadowski *et al.* (1984) reviewed regression formulae appropriate for the estimation of average ambient-noise spectra below 100 kHz, including noise sources arising from ocean turbulence, shipping traffic, surface weather (both wind and rain) and molecular agitation. Wagstaff (1973) also presented regression formulae that were incorporated into an ambient-noise model that was valid over the frequency range 10–500 Hz. Ross (1976: chapter 8) reviewed regression formulae appropriate for shipping noise levels. For a brief history of such work, see Ross (1993). Bjørnø (1998) summarized the general characteristics of ambient-noise in littoral waters.

Using radiated-noise measurements collected from 272 ships over the period 1986–92, Wales and Heitmeyer (2002) updated the classical merchant ship radiated-noise regression formulae utilized by Ross (1976). These classical regression formulae postulated that the source spectrum for an individual ship was proportional to a baseline spectrum whose constant of proportionality was determined by power-law exponents for the ship speed (sixth power) and ship length (second power). The reanalysis by Wales and Heitmeyer (2002) over the frequency range 30–1,200 Hz now represented the individual ship spectra by a modified rational spectrum. At high frequencies (400–1,200 Hz), most of the individual spectra showed a simple power-law dependence on frequency with exponents concentrated around a mean value of about 2. At low frequencies (30–400 Hz), many of the source spectra exhibited a more complex dependence on frequency with greater spectral variability across the ensemble.

Bradley and Bradley (1984) developed an elaborate empirical model called the geophysics ambient-noise model. This model provided estimates of seasonal deep-water ambient-noise levels and azimuthal directionalities over the frequency range 25 Hz–15 kHz. This model was based on a comprehensive empirical database of shipping and wind noise, but not noise due to biologics or industrial activity. The model further assumed a nominal receiver depth of 100 m, thus ignoring any depth dependence. Hamson (1997) reviewed

techniques for modeling shipping and wind noise over the frequency range 50–3,000 Hz, concentrating mainly on work performed after 1980. Noise level, horizontal and vertical directionalities, and the noise responses of arrays were used to characterize the ambient-noise field. Harrison (1996) used a simple ray approach to approximate the full-wave treatment of noise levels and coherence in range-independent ocean environments. Alvarez *et al.* (2001) used an approach based on genetic algorithms to study the physical characteristics of measured underwater ambient noise in the frequency range 10–2,000 Hz. The resulting predictability of the recorded signals was attributed, in part, to the contributions of shipping noise.

7.3 Ambient-noise models

A simple model of ambient noise in the ocean would consist of an infinite layer of uniform water with a plane surface over which the sources of noise (shipping and weather) were uniformly distributed. In this model, the ambient-noise level would be independent of depth (Urlick, 1983: chapter 7). Of course, a more realistic model would include volume absorption in addition to the effects of refraction and boundary reflections over long-range paths (Talham, 1964).

To compute the low-frequency component of noise due to distant shipping, three inputs are required: (1) the density of shipping as a function of azimuth and range from the receiver; (2) the source level of the radiated noise for each generic type of merchant ship; and (3) the TL as a function of range between the near-surface sources (ships) and the depth of the receiver. Then, contributions from successive range rings centered about the receiver can be summed to obtain the level of shipping noise as a function of azimuth at the receiver. The theory behind this kind of modeling, in addition to some observational data on the density of shipping traffic in the North Atlantic, has been described by Dyer (1973), among others.

The high-frequency component of noise due to surface weather is usually computed on the assumption that it is locally generated and isotropic. Thus, only the weather conditions (sea state or wind speed) prevailing in the immediate vicinity of the receiver need be considered, in addition to any localized rain shower or biologic activity.

Modeling the vertical directionality of deep-water ambient-noise can be approached by means of the simple model mentioned earlier. Consider a bottomless, uniform ocean, without refraction or attenuation, having a surface covered with a dense, uniform distribution of noise sources. Furthermore, let each unit area of the surface radiate with an intensity $I(\theta)$ at a distance of 1 m. Then, at point P (the receiver) in Figure 7.1(a) the incremental intensity dI produced by a small circular annulus of area dA at horizontal range r is (Urlick, 1983: chapter 7):

$$dI = \frac{I(\theta) dA}{l^2} = \frac{I(\theta) 2\pi r dr}{l^2} \quad (7.1)$$

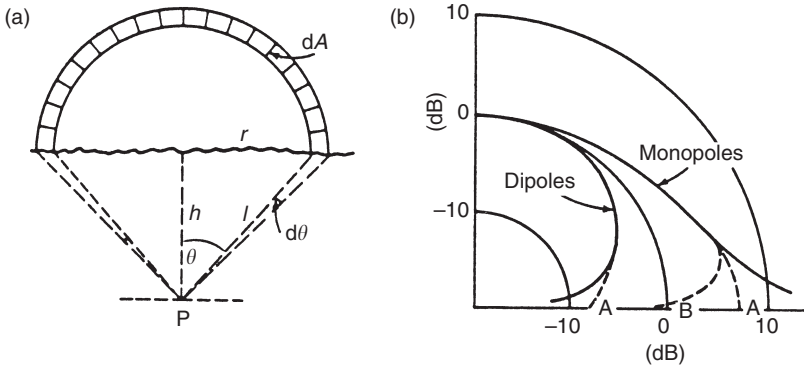


Figure 7.1 Simple model for the vertical directionality of ambient-noise: (a) geometry with straight-line propagation paths and (b) directional patterns for surface distribution of monopoles and dipoles. The dashed segments near the horizontal show the effect of attenuation and refraction near the sea floor (A) and near the deep-sound channel axis (B). (Urlick, 1983; *Principles of Underwater Sound*, 3rd edn; reproduced with permission of McGraw-Hill Publishing Company.)

But $r = h \tan \theta$, so that $dr = h \sec^2 \theta d\theta$. Also, $l = h \sec \theta$. On substituting and rearranging terms, Equation (7.1) reduces to:

$$dI = 2\pi I(\theta) \tan \theta d\theta \tag{7.2}$$

If ψ is a solid angle, then $d\psi = 2\pi \sin \theta d\theta$, so that the noise intensity per unit solid angle, $N(\theta)$, becomes

$$N(\theta) = \frac{dI}{d\psi} = I(\theta) \sec \theta \tag{7.3}$$

When $I(\theta) = I_0$, which represents a nondirectional source, Equation (7.3) yields

$$N(\theta) = I_0 \sec \theta \tag{7.4a}$$

which is the ambient noise intensity per unit solid angle for a surface distribution of monopole sources. Using a distribution of dipole sources for which the intensity radiated at an angle θ is $I(\theta) = I_0 \cos^2 \theta$, the beam pattern of the noise received at a depth below the surface is:

$$N(\theta) = I_0 \cos \theta \tag{7.4b}$$

Equations (7.4a) and (7.4b) are plotted in polar coordinates in Figure 7.1(b). At angles near the horizontal (where $\theta = 90^\circ$), the effects of attenuation, refraction and boundary multipaths prevent the curves from

going to either zero or infinity. Using this simple model, a receiver located within the deep-sound channel would not be expected to receive noise arriving along paths near the horizontal since range-independent ray tracing would show that such ray paths do not exist. The beam pattern of the noise from monopole sources would therefore have a maximum at an oblique angle above and below the horizontal (typically $\pm 10^\circ$ to $\pm 15^\circ$ off the horizontal axis in temperate, deep-sea regions), with a minimum at $\theta = 90^\circ$. This simple conceptual picture is not always valid in realistic (range-dependent) environments. Specifically, more sophisticated models would consider the effects of range-dependent refraction, bottom reflection and multipath arrivals. This aspect will be discussed further under the topic of the noise notch (Section 7.5).

For high-frequency noise sources ($>1,000$ Hz), many investigators (e.g. Anderson, 1958; Becken, 1961; Von Winkle, 1963) have suggested a function of the form $I(\theta) = I_0 \cos^m \theta$, where I_0 is the intensity radiated by a small area of the sea surface in the downward direction ($\theta = 0^\circ$) and where m is an integer. Values of $m = 1, 2$ or 3 have been obtained, depending upon conditions and methods of measurement. Most measurements center roughly about $m = 2$, a value consistent with the hypothesis of a dipole source formed by the actual source and its image in the sea surface.

For low-frequency noise sources (<500 Hz), the agreement between available observations (see Figure 6.7) and the findings of this simple model (Figure 7.1) further suggests that a distribution of monopoles [$m = 0$; thus, $I(\theta) = I_0$] adequately models distant shipping noise.

Pertinent examples from the ANDES noise model (Renner, 1995b) will illustrate how the horizontal and vertical noise directionalities are computed. The fundamental output from ANDES is the directional noise intensity per unit solid angle [$N_S(\theta, \phi)$]. The horizontal noise directionality [$N(\phi)$] is calculated from [$N_S(\theta, \phi)$] as:

$$N(\phi) = \int_{-\pi/2}^{\pi/2} N_S(\theta, \phi) \cos \theta \, d\theta \quad (7.5)$$

The vertical noise directionality [$N(\theta)$] is calculated from [$N_S(\theta, \phi)$] as:

$$N(\theta) = \frac{1}{2\pi} \int_0^{2\pi} N_S(\theta, \phi) \, d\phi \quad (7.6)$$

The omnidirectional noise level (N) is then calculated as:

$$N = \int_0^{2\pi} \int_{-\pi/2}^{\pi/2} N_S(\theta, \phi) \cos \theta \, d\theta \, d\phi \quad (7.7a)$$

By noting the relationship with Equation (7.5), Equation (7.7a) can be simplified as

$$N = \int_0^{2\pi} N(\phi) \, d\phi \quad (7.7b)$$

The horizontal angle (ϕ) is measured positive clockwise from true North while the vertical angle (θ) is measured positive upward from the horizontal plane. Note that no receiver beam patterns were convolved with the noise levels in Equations (7.5) and (7.6).

7.4 The RANDI model – a specific example

The research ambient-noise directionality (RANDI) model is an instructive example of an ambient-noise model. RANDI calculates the vertical and horizontal directionalities of low-frequency (10–500 Hz) ambient noise for a selected ocean environment (Wagstaff, 1973).

7.4.1 *Transmission loss*

RANDI utilizes one of three sources of TL inputs:

- 1 self-contained linear ray-trace routine;
- 2 input data consisting of TL versus range in addition to arrival angle arrays; and
- 3 deep-sound channel propagation algorithm.

7.4.2 *Noise sources and spectra*

RANDI considers six sources of isotropic and anisotropic surface and volumetric noise: (1) shipping; (2) wind-wave; (3) biological; (4) sea state zero; (5) rain; and (6) distant sources. A seventh source, that of a target, is also included as an option (Figure 7.2). Figure 7.3 illustrates the modeled noise field. The surface noise is generated by an infinite number of point sources distributed along a horizontal noise source plane located at a depth of about 6 m, corresponding to the nominal drafts of surface vessels. Empirical algorithms are used to calculate squared pressure spectrum levels for each of the seven noise-generation mechanisms. All of the noise (and target) squared pressure spectrum levels are then integrated over a user-specified bandwidth using an input frequency-response function. Noise level in this context refers to the mean squared spectrum level.

7.4.3 *Directionality*

To determine the horizontal directionality of the noise field, the ocean is divided into n wedge-shaped regions (called sectors) with the receiver at the center. The vertical thickness of the sectors is equal to the ocean depth at the receiver location. Noise calculations are performed independently in each sector defined by the user. The total squared noise pressure, as measured by an omnidirectional hydrophone, is obtained by summing the squared noise pressures for the n sectors. An example of horizontal directionality of the

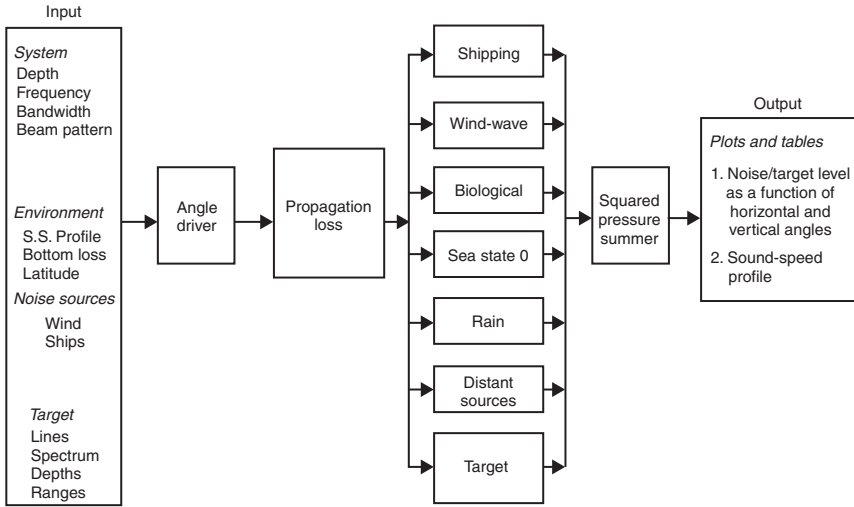


Figure 7.2 Block diagram of the RANDI noise model (Wagstaff, 1973).

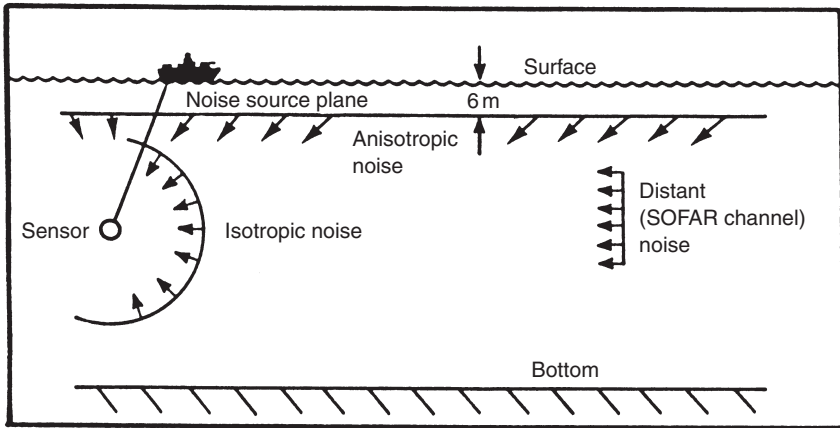


Figure 7.3 The noise field used in the RANDI model (Wagstaff, 1973).

noise field is presented in Figure 7.4 (note that the units for noise level are referenced to degrees).

The vertical directionality of the noise field is determined for a differential vertical angle by first calculating the area defined by the intersections of the corresponding ray bundles with the anisotropic noise field plane (i.e. shipping noise). Next, these areal extents are multiplied by the local effective squared noise pressure levels. The resulting levels are reduced by the

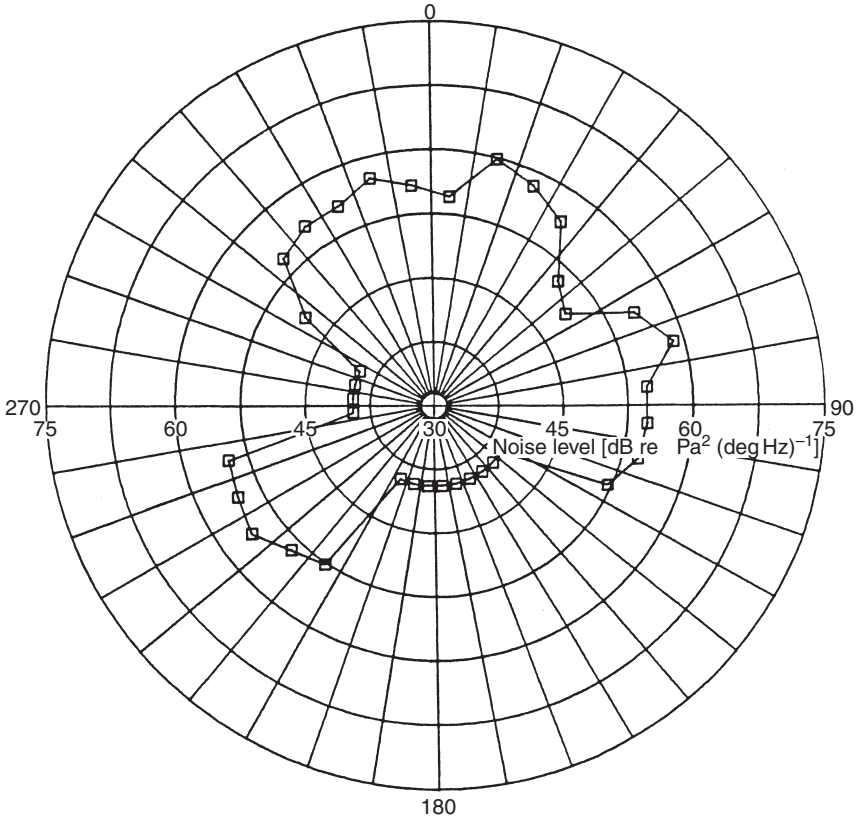


Figure 7.4 Per-degree horizontal directionality of ambient noise in 10° sectors generated by the RANDI noise model for a frequency of 100 Hz at a depth of 91 m in the North Pacific Ocean (Wagstaff, 1973).

appropriate TL and then summed. At this point, the contribution of the isotropic noise sources (i.e. weather noise) is considered. These new levels are then convolved with the vertical response of the receiver array. This whole process is then repeated for each new differential angle. An example of vertical directionality of the noise field is presented in Figure 7.5. Note that the units for noise level in Figure 7.5 are referenced to steradians.

7.4.4 Recent developments

The latest version of this model (RANDI III) was developed for application to shallow-water and coastal areas in the low-to-mid frequency range (~ 10 – 300 Hz). The receiver can be either a horizontal or a vertical line array (Breeding, 1993). The dominant sources of noise are assumed to be shipping,

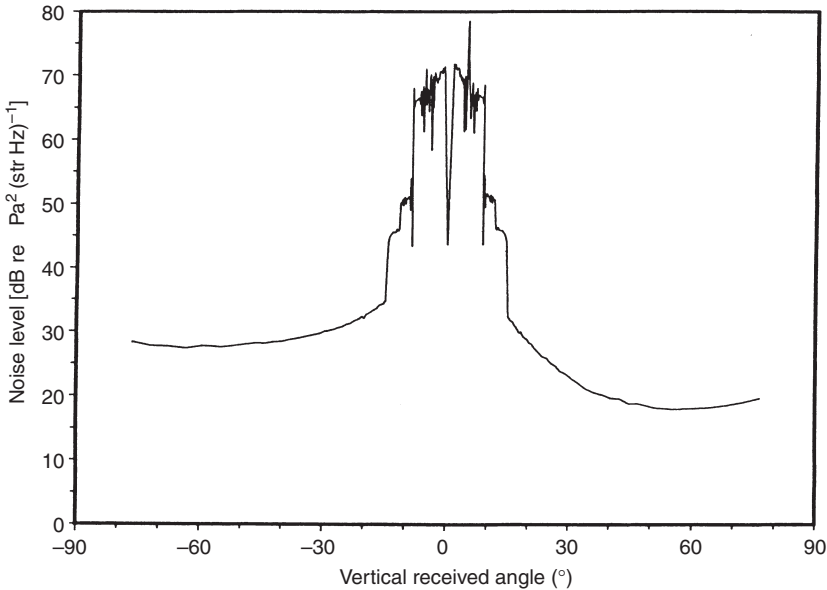


Figure 7.5 Ambient-noise vertical directionality for the 10° horizontal sector centered at 15° in Figure 7.4. Rays with positive angles arrive at the receiver from below the horizontal plane. A ray with an angle of -90° arrives from the surface directly over the receiver (Wagstaff, 1973).

distant storms and local winds. The ships are treated as discrete sources, and the shipping noise is propagated over great-circle routes to the receiver elements using a wide-angle, finite-element parabolic equation (FEPE) model. The arriving contributions from all ships are added coherently at the receiver, and the array response is determined by beamforming with various shading schemes. Environmental and shipping information is automatically extracted from US Navy standard databases: HITS for determination of shipping densities; DBDB for bathymetry; GDEM for sound-speed profiles; and LFBF for bottom-interaction parameters (refer to Chapter 10, specifically Table 10.5).

7.5 The noise notch

The so-called noise notch is often manifested in the vertical directionality of low-frequency noise fields generated by those noise models utilizing range-independent TL inputs. Figure 7.6 presents a vertical noise directionality diagram generated by the fast ambient-noise model (FANM). This particular example is for a low-frequency (50 Hz) case under the assumption of a range-independent ocean environment. Consistent with the conceptual picture discussed in Chapter 6 and earlier in this chapter, most of the low-frequency noise arrives near the horizontal. Furthermore, slightly higher

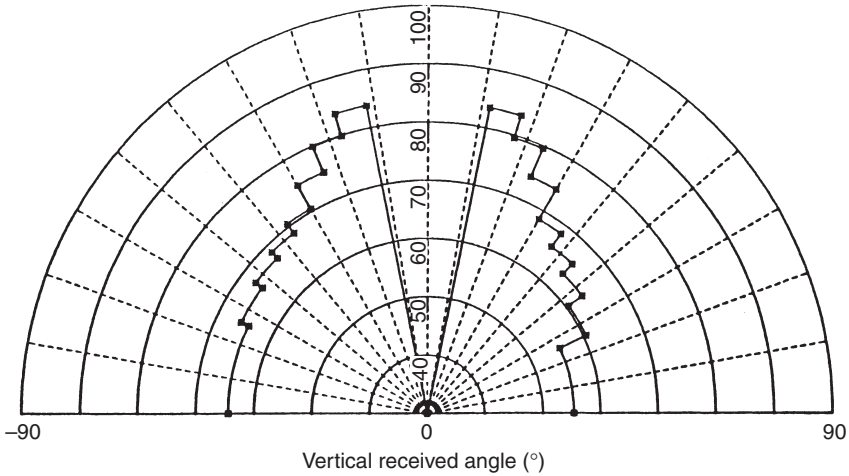


Figure 7.6 Vertical noise directionality [$\text{dBre } \mu\text{Pa}^2(\text{Hz str}^{-1})$] computed by the FANM noise model at a frequency of 50 Hz. Rays with positive angles arrive at the receiver from below the horizontal plane.

levels are observed in the direction of the sea surface than in the direction of the sea floor. This result is also expected in that the bottom-reflected rays are attenuated more than the corresponding surface-interacting rays are. Figures 7.5 and 7.6 both show this effect. The feature of real interest, however, is the horizontal notch (or null) that is predicted by range-independent ray theory. Since the notch feature is not always observed in measurements at sea, this situation presents a paradox. The generation of notch features is not limited to range-independent ray-tracing techniques. Carey *et al.* (1987), for example, were able to produce similar notch features using a PE model under similar range-independent environmental assumptions.

Anderson (1979) made measurements of the vertical directionality of noise in the North Pacific Ocean in September 1973. He did not observe the horizontal null (notch) in the directional spectrum of the noise that is predicted by ray theory for a horizontally homogeneous (range-independent) ocean.

This aspect can be explored further by examining basic ray-theoretical considerations in typical deep-ocean, range-independent environments. Specifically, this notch (or null) is the result of ray arrivals being excluded from a region that is centered on the horizontal axis of the receiver and limited in angular width to $\pm\theta_R$, where θ_R defines the limiting ray as:

$$\theta_R = \cos^{-1} \frac{c_R}{c_S} \quad (7.8)$$

where θ_R is the limiting ray angle at the receiver, c_R the sound speed at the receiver position and c_S the sound speed at the source position.

This corresponds to those rays leaving the source horizontally ($\theta_S = 0^\circ$). Equation (7.8) then follows directly from Snell's law. Figure 7.7 illustrates the geometry for defining the limiting ray. The sound-speed profile is based on measured data presented by Anderson (1979). Assuming that the noise source plane is near the surface, and that the receiver is located at 1,200 m (just below the deep-sound channel axis), then Equation (7.8) yields

$$\theta_R = \cos^{-1} \left[\frac{1,485 \text{ m s}^{-1}}{1,530 \text{ m s}^{-1}} \right] = \cos^{-1}(0.971) \approx 14^\circ$$

Thus, ray-theoretical considerations indicate that noise from the surface cannot arrive within about 14° of the horizontal axis of the receiver, at least under the environmental and geometrical conditions assumed here. These conditions, however, are typical of many deep-ocean environments that support deep-sound channel propagation.

The apparent paradox created by the discrepancy between range-independent ray theory and observations can be explained in terms of range-dependent propagation effects. In particular, two effects can

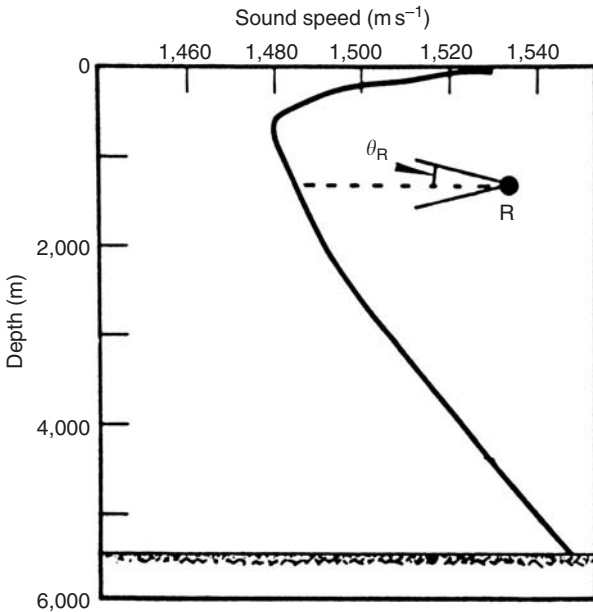


Figure 7.7 Geometry for calculation of limiting rays. Noise source plane is located near the sea surface. Receiver (R) is located at a depth of 1,200 m. In this example, limiting ray angles (θ_R) are $\pm 14^\circ$ off the horizontal axis of the receiver (sound profile is from Anderson, 1979).

contribute to filling the noise notch through conversion of near-surface shipping and weather noise into shallow-angle propagation paths near the sound channel axis. These mechanisms are slope conversion and horizontal sound-speed variations (e.g. Anderson, 1979). These mechanisms were addressed previously in Chapter 6. Slope conversion considers the reflection and scattering of sound into the deep-sound channel from ships transiting the continental shelves and slopes of the ocean basins. Horizontal sound-speed variations versus latitude cause the axis of the sound channel to shoal at high latitudes, thus allowing far northern (Kibblewhite *et al.*, 1976) or far southern (Bannister, 1986) shipping and weather noise to enter the deep-sound channel and to propagate for long distances. Dashen and Munk (1984) examined this problem and suggested that diffusion may also play a role.

Carey and Wagstaff (1986) reviewed low-frequency (<500 Hz) physical-noise models and measurements. They confirmed that coherent signals from surface ships were a dominant characteristic of the horizontal ambient-noise field. The vertical directionality of the noise showed a broad angular distribution centered about the horizontal axis at lower frequencies (<200 Hz), and a dual-peaked ($\pm 10^\circ$ to $\pm 15^\circ$ off the horizontal) distribution at frequencies between 300 and 500 Hz. In the frequency range 20–200 Hz, the data exhibited a smooth variation with frequency. However, the tonal nature of surface ship radiated-noise spectra would suggest a spiky spectral variation. Smooth spectral variations in the vertical directionality of the noise field are also characteristic of low-traffic areas. Carey and Wagstaff (1986) thus suggested that environmental noise sources such as wind-driven noise, in addition to shipping, might be required to explain the broad angular and frequency characteristics observed in the data. Carey *et al.* (1990) conducted additional simulations using a parabolic equation (PE) model. These simulations confirmed the role of downslope conversion as a low-pass filter in determining the vertical noise field at mid-basin.

Hodgkiss and Fisher (1990) made a series of direct measurements that confirmed the contribution of the downslope conversion mechanism to the near-horizontal noise distribution. They noted that the effects of absorption appeared to diminish the near-horizontal energy with increasing distance from the coast, and that these effects were more pronounced at higher frequencies.

7.6 Beam-noise statistics models

Models of beam noise statistics use a statistical approach to model the low-frequency ambient-noise field in the ocean. To be of practical use to large-aperture, narrow-beam passive sonar systems, these models must include sonar-specific beam pattern characteristics in addition to point-to-point representations of TL.

The probability measures of beam noise depend on array configuration, orientation, location and season. For detection predictions, the measure

of interest is the total power in selected frequency bands. For prediction of false alarm rates, the desired measure is a characterization of the narrowband components of shipping noise (Moll *et al.*, 1979). Only detection predictions will be addressed here.

Using the formalism developed by Moll *et al.* (1979), an expression for the total noise power in a specified band at the beamformer output can be presented. As a consequence of the principle of superposition of the instantaneous pressures of sound from multiple point sources, the averaged noise power at the beamformer output (Y) can be expressed as:

$$Y = \sum_{i=1}^m \sum_{j=1}^n \sum_{k=1}^{A_{ij}} S_{ijk} Z_{ijk} B_{ijk} \quad (7.9)$$

where m is the number of routes in the basin, n the number of ship types, A_{ij} the number of ships of type j on route i (a random variable), S_{ijk} the source intensity of the k th ship of type j on route i (a random variable that is statistically independent of the source intensity of any other ship), Z_{ijk} the intensity transmission ratio from ship ijk to the receiving point and B_{ijk} the gain for a plane wave arriving at the array from ship ijk .

The probability density function for Y can then be obtained from its characteristic function.

7.7 Data support requirements

The utilization of noise models requires a specialized database containing information on shipping routes, shipping density by merchant vessel type and radiated noise levels by vessel type. Vessel types are usually differentiated according to freighters, tankers and fishing craft. Further distinctions can be made according to gross tonnage. A ship-count database that can be automatically accessed by ambient-noise models is the historical temporal shipping (HITS) database, which is incorporated in AUTOSHIPS (see Chapter 10). The resolution of HITS is 1° latitude–longitude squares by ship type. Spatial coverage is essentially worldwide (Estalote *et al.*, 1986).

The complexity of the databasing task can be better appreciated by examining Figure 7.8, which shows generalized shipping routes from Solomon *et al.* (1977). The routes are generalized in the sense that the lines connecting the various ports are not necessarily indicative of the exact paths followed by the merchant traffic. (The numbering of the various routes in Figure 7.8 served as a bookkeeping mechanism for tracking port destinations.) Factors such as seasonal climates and severe weather patterns can alter the exact routes followed by the ships at any particular time.

Mapping transformations between rectangular (for the ship positions and routes) and polar (for noise model sector geometry applications) further complicate model implementation. Figure 7.9 illustrates one particular implementation that relates polar sector geometries to Cartesian latitude and

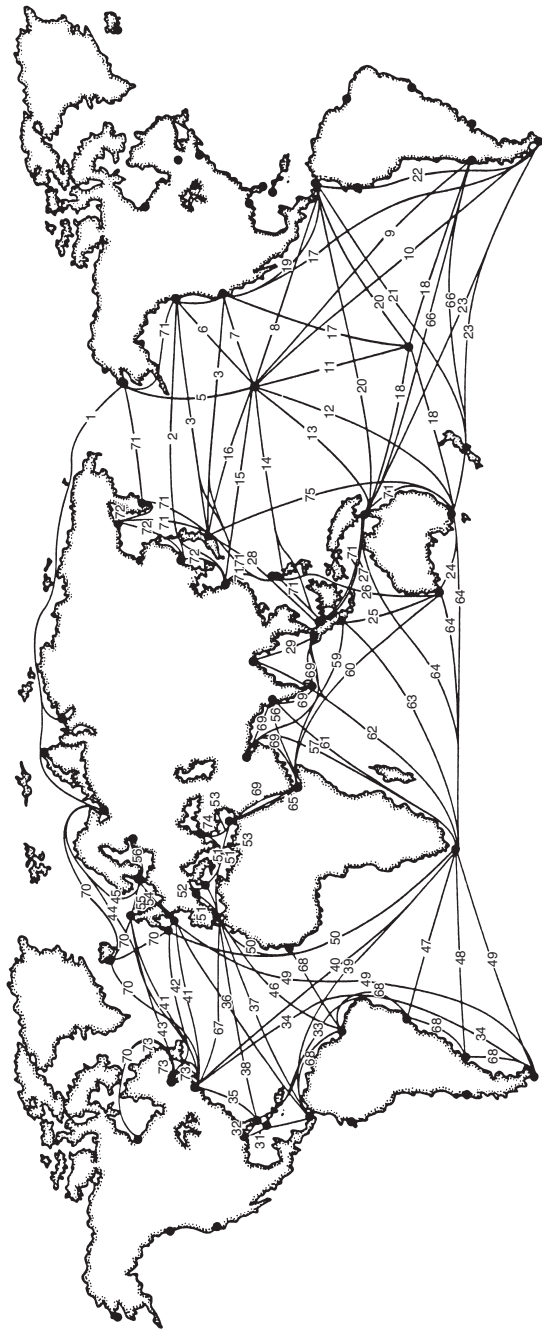


Figure 7.8 Generalized shipping routes (Solomon *et al.*, 1977).

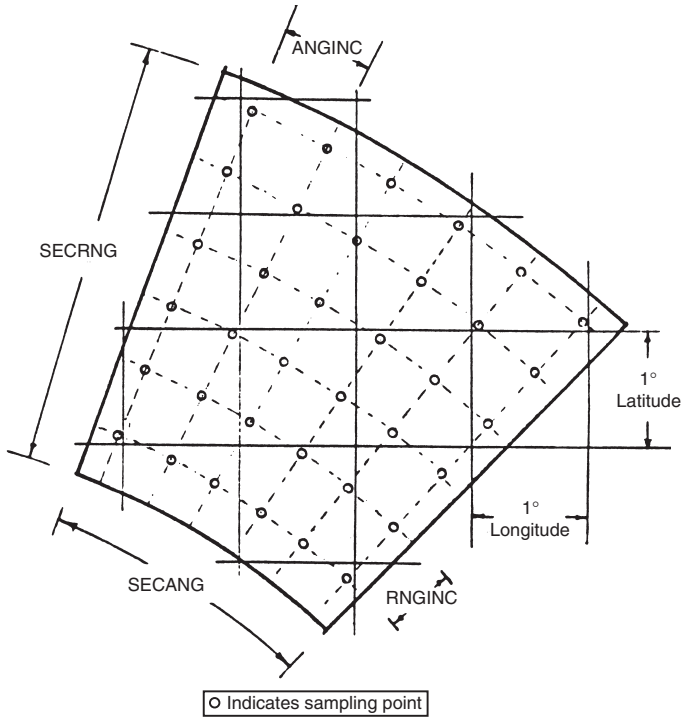


Figure 7.9 Mapping transformation from a rectangular to a polar coordinate system. Shipping density data are usually represented on a Cartesian coordinate system while noise models utilize a polar (sector) reference frame. This particular example is from the FANM noise model (Baker, 1976).

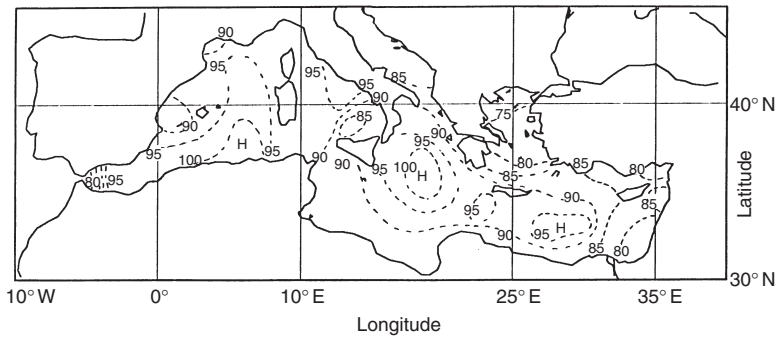


Figure 7.10 Ambient noise level (spectrum level, dB re $1 \mu\text{Pa}$) variations in the Mediterranean Sea as simulated by a noise model. Simulation is valid for low frequency (<100 Hz) noise for a shallow receiver depth during the winter season. The contour interval is 5 dB and H signifies areas of high noise levels.

longitude divisions. Here, a sector is defined in terms of sector angle (SECANG), sector range (SECRNG), angle increment (ANGINC) and range increment (RNGINC).

An example of the spatial variability of ambient-noise levels generated by a noise model is presented in Figure 7.10 for the Mediterranean Sea. At low frequencies (<100 Hz), most noise is due to shipping traffic. The regions of high noise levels (denoted by H) coincide with established shipping routes (compare with Figure 7.8). Noise variations of as much as 20 dB can occur over relatively short distances.

7.8 Numerical model summaries

A summary of available noise models is presented in Table 7.1. This summary segregates the models according to the categories of ambient-noise and beam-noise statistics. Models in the category of beam-noise statistics are further segregated according to analytic and simulation approaches. Numbers within brackets following each model refer to a brief summary and appropriate documentation. Model documentation can range from informal programming commentaries to journal articles to detailed technical reports containing a listing of the actual computer code. Abbreviations and acronyms are defined in Appendix A. This summary does not claim to be exhaustive.

Table 7.1 Summary of underwater acoustic-noise models

<i>Ambient noise</i>	<i>Beam-noise statistics</i>	
	<i>Analytic</i>	<i>Simulation</i>
AMBENT [1]	BBN shipping noise [11]	BEAMPL [15]
ANDES [2]	BTL [12]	DSBN [16]
CANARY [3]	USI array noise [13]	NABTAM [17]
CNOISE [4]	Sonobuoy noise [14]	
DANES [5]		
DINAMO [6]		
DUNES [7]		
FANM [8]		
Normal mode ambient noise [9]		
RANDI - I / II / III [10]		

Notes

Ambient noise

- 1 AMBENT calculates the ambient-noise level for a cylindrically symmetric beam generated by a uniform distribution of surface radiators. Propagation effects are computed by NISSM (McConnell, 1983; Robinson and McConnell, 1983). AMBENT is intended to determine the noise level due to wind, or rain or both.

- 2 ANDES (Version 4.2) addresses issues related to shallow-water ambient-noise modeling including upgrades to the shipping-density and sound-speed databases, in addition to a new capability to model fluctuations in noise directionality due to changes in wind speed and the movement of discrete sources through the TL field (Renner, 1986a,b, 1988, 1995a,b).
- 3 CANARY is a ray-based model of ambient noise and noise coherence that is used to estimate the performance of sonars in range-dependent and azimuth-dependent environments. CANARY treats noise sources as surface distributions rather than as points (Harrison, 1997a,b; Harrison *et al.*, 1999, 2001). (Also see the DINAMO model.)
- 4 CNOISE predicts ambient noise due to shipping. TL versus range files must be generated externally (Estalote, 1984).
- 5 DANES generates noise levels and horizontal directionality estimates for shipping traffic and wind noise (Osborne, 1979; Lukas *et al.*, 1980b).
- 6 DINAMO models three-dimensional noise directionality and array performance for operational applications (Harrison, 1998). DINAMO is closely related to CANARY, which was designed for research use. While CANARY first calculates the correlation matrix for the array and then sums these terms to form the array response, DINAMO performs a straight-forward integral over all solid angles of the calculated noise directionality multiplied by the array's beam pattern.
- 7 DUNES provides estimates of omnidirectional, vertical, horizontal and three-dimensional directional noise versus frequency. The model includes high-latitude and slope-enhanced wind noise effects. The model emphasizes calculation of noise due to the natural environment. Therefore, shipping contributions are entered explicitly and not via extensive shipping databases (Bannister *et al.*, 1989).
- 8 FANM uses a simplified (range-independent) ocean environment together with shipping and wind speed databases to predict ambient noise at a fixed receiver location (Lasky and Colilla, 1974; Cavanagh, 1974a,b; Baker, 1976; Long, 1979).
- 9 Normal mode ambient noise calculates the relative noise level versus depth in addition to the coherence of the noise field at any two points. This calculation is performed using a normal-mode representation of the acoustic field (Kuperman and Ingenito, 1980).
- 10 RANDI-I/II/III – The original version, RANDI-I (Wagstaff, 1973) calculates and displays the vertical and horizontal directionalities of ambient noise in the frequency range 10 Hz–10 kHz. RANDI-II (Hamson and Wagstaff, 1983) was constructed at the SACLANTCEN to account for the special nature of ambient noise in shallow-water environments. RANDI-III (Version 3.1) predicts ambient-noise levels and directionalities at low-to-mid frequencies in both shallow and deep waters. Shipping noise can be calculated for highly variable environments using either the finite-element or the split-step PE method. Local wind noise is computed using the range-independent theory of Kuperman–Ingenito, including both discrete normal modes and continuous spectra. US Navy standard and historical databases are used to describe the environment (Schreiner, 1990; Breeding, 1993; Breeding *et al.*, 1994, 1996). Version 3.3 is a modified version of RANDI 3.1 for use in shallow water. This version provides the user with the option to supply the model with measured or estimated environmental information in areas where the US Navy standard databases may not provide coverage (Pflug, 1996). (The RANDI model is discussed in detail in Section 7.4.)

Beam-noise statistics

Analytic

- 11 BBN shipping noise calculates probability density functions of the beam noise power envelope using acoustic source-level data for classes of surface ships, shipping routes and traffic density along those routes (Mahler *et al.*, 1975; Moll *et al.*, 1977, 1979).
- 12 BTL provides statistical descriptions of shipping noise for low-frequency, horizontally beamed systems (Goldman, 1974).
- 13 USI array noise numerically estimates the ensemble and time-averaged, one-dimensional statistical probability density function of beam noise (Jennette *et al.*, 1978).
- 14 Sonobuoy noise was developed for sonobuoy applications (McCabe, 1976). It considers both the temporal correlation of ship-generated noise and the spatial correlation of average intensities for distributed sensors.

Simulation

- 15 BEAMPL computes random ambient noise time series within a user-specified beam by statistically taking into account the motion of ships along user-specified routes (Estalote, 1984).
- 16 DSBN generates beam-noise time series from component submodels for surface ships, TL and receiver (Cavanagh, 1978a,b).
- 17 NABTAM computes the response of a linear array of hydrophones to wind–sea interactions, surface ships and designated target vessels (W. Galati, E. Moses and R. Jennette, unpublished manuscript).

8 Reverberation I

Observations and physical models

8.1 Background

Reverberation is defined as that portion of the sound received at a hydrophone that is scattered by the ocean boundaries or by volumetric inhomogeneities. Accordingly, reverberation-producing scatterers in the sea can be grouped into three classes: sea surface, sea floor and ocean volume. Surface and bottom reverberation both involve a 2D distribution of scatterers and therefore can be considered jointly as boundary reverberation. Volume reverberation is produced by the marine life and inanimate matter distributed within the sea, and also by fine-scale features of the ocean itself. Useful reviews of oceanic scattering and reverberation have been provided by Farquhar (1970), Andersen and Zahuranec (1977), Ellis *et al.* (1993) and Pierce and Thurston (1993). A collection of papers dealing with high-frequency acoustics in shallow water (Pace *et al.*, 1997) addressed issues relating to scattering and reverberation in shallow water. Love *et al.* (1996) noted that variability is the principal feature of volume reverberation in littoral waters.

Reverberation has several features that distinguish it from noise (Bartberger, 1965; Moritz, 1982). Principal among these is the fact that reverberation is produced by the sonar itself. Thus, the spectral characteristics of reverberation are essentially the same as the transmitted signal. The intensity of reverberation varies with the range of the scatterers and also with the intensity of the transmitted signal.

Based on its characteristic temporal and spatial correlation properties, oceanic reverberation can be segregated according to diffuse and facet components (Gerstoft and Schmidt, 1991). Diffuse reverberation results from scattering by the small-scale, stochastic structure of the oceanic waveguide (e.g. surface and bottom roughness and bottom inhomogeneity). Facet reverberation results from abrupt changes in the bathymetric and subbottom features of the ocean (e.g. seamounts and faults). Due to its stochastic nature, diffuse reverberation is characterized by a relatively low correlation. Alternatively, the deterministic nature of oceanic facets gives rise to “signal-like” reverberation from seamounts and faults.

The fundamental ratio upon which reverberation depends is called the scattering (or backscattering) strength (Urick, 1983: chapter 8). It is the ratio (in dB) of the intensity of sound scattered by a unit area (for boundary reverberation) or volume (for volume reverberation), referred to a distance of 1 m, to the incident plane-wave intensity:

$$S_{b,v} = 10 \log_{10} \frac{I_s}{I_i} \quad (8.1)$$

where $S_{b,v}$ is the scattering strength for boundary (b) or volume (v) reverberation, I_s the intensity of sound scattered by a unit area or unit volume of water and I_i the intensity of incident plane wave.

The computation of volume and boundary reverberation levels based on scattering strengths is discussed in Chapter 9.

8.2 Volume reverberation

The major source of volume reverberation in the sea has been established as biological (e.g. Johnson *et al.*, 1956). Different marine organisms affect different bands of the active sonar spectrum. At frequencies in excess of 30 kHz, the scatterers are zooplankton. At frequencies between 2 and 10 kHz, the dominant scatterers are the various types of fish that possess a swim bladder (an air-filled sac that enables fish to maintain and adjust their buoyancy). Acoustically, the bladder amounts to an internal air bubble that becomes resonant at a frequency depending on the size and depth of the fish. Love (1978) reviewed the current understanding and modeling of swim bladder resonant acoustic scattering.

Saenger (1984) developed a volume-scattering strength model that is valid over the frequency range 1–15 kHz. The depth variability is a function of seasonal bioacoustic constants (organized by ocean province), the mean water density profile and its gradient, and the acoustic frequency. The absolute level of the volume-scattering strength depends upon the seasonal standing crop of scatterers, which may exhibit interannual variability.

Love (1975) developed a volume reverberation model based on fish distribution data. The use of fishery data to predict volume reverberation was explored further by Love (1993). In 1988 and 1989, volume-reverberation measurements were made in the Norwegian Sea and North Atlantic Ocean in the frequency range of 800 Hz to 5 kHz. Below 5 kHz, volume reverberation is usually caused by scattering from the swimbladders of relatively large fish. The scattering strength (S_L) of a layer of dispersed, nonacoustically interacting fish is

$$S_L = 10 \log_{10} \sum_{i=1}^n \sigma_i(f) \times 10^{-4}$$

where n is the number of fish in the layer and σ the acoustic cross-section of an individual fish (cm^2) at any given frequency (f).

The parameter σ represents a swimbladder-bearing fish as a spherical shell enclosing an air cavity in water. Love (1993) concluded that a possible pitfall of relying solely on fishery data to predict low-frequency volume reverberation is that fishery research concentrates on species of present or potential commercial value. Species of no commercial value could be ignored in such data, despite their potential contribution to low-frequency volume reverberation.

8.2.1 *Deep scattering layer*

Measurements of the depth variation of volume-scattering strengths show an overall decrease with increasing depth. This is consistent with the general distribution of biological organisms within the sea. However, there is often a well-marked increase at certain depths. The depth of such increased volume scattering is called the DSL.

The DSL generally exhibits a diurnal migration in depth, being at greater depth by day than by night, and with a rapid change near sunrise and sunset. The depth of the DSL can be expected to lie between 180 and 900 m by day in mid-latitudes, and to be shallower by night. In the Arctic, the DSL lies just below the ice cover.

Greene and Wiebe (1988) reported on the use of high-frequency (420 kHz), dual-beam acoustics to measure target strength distributions of zooplankton and micronekton. Their results are consistent with the present picture of the diel vertical migration of sound-scattering layers in the ocean. At this frequency, the most abundant targets (off the northeast coast of the United States) corresponded to animals the size of mature krill with target strengths between -71 and -62 dB. The use of acoustic techniques to estimate biomass has also been explored (e.g. Penrose *et al.*, 1993; Wiebe *et al.*, 1995).

8.2.2 *Column or integrated scattering strength*

Some kinds of scatterers in the sea, such as the DSL or a layer of air bubbles just below the sea surface, lie in layers of finite thickness instead of being diffusely distributed throughout an irregular volume. The resultant layered reverberation is more easily considered as a form of boundary reverberation. When the layer is made infinitely great, the quantity S_b in Equation (8.1) becomes the scattering strength of the entire water column and is called the column, or integrated, scattering strength. It can be readily measured in the field by means of explosive sound signals and sonobuoys, and it is a convenient single number to characterize the total amount of volume reverberation existing at the time and location the data were obtained.

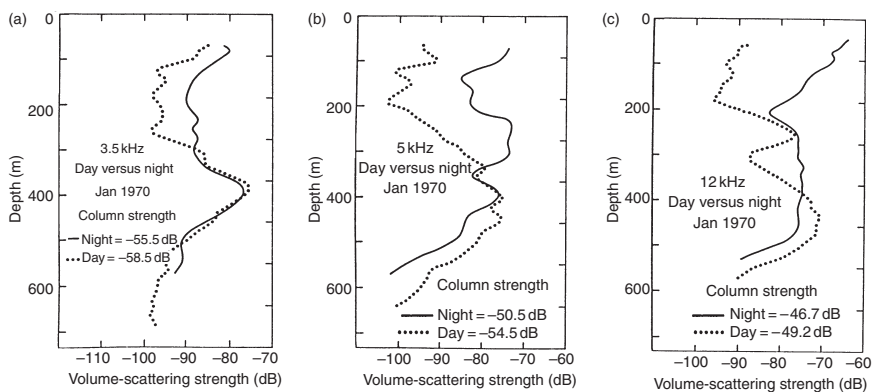


Figure 8.1 Comparison of day and night profiles of volume-scattering strength versus depth during January 1970 in the eastern Pacific Ocean: (a) 3.5 kHz, (b) 5 kHz and (c) 12 kHz. Column strengths are calculated by integrating the volume scattering strengths over the entire profile (Vent, 1972).

Measurements of volume reverberation have been obtained, for example, by Vent (1972) and by Gold and Renshaw (1978). Figure 8.1 compares day and night profiles of volume scattering versus depth during January 1970 in the eastern North Pacific Ocean at three frequencies: 3.5, 5 and 12 kHz (Vent, 1972). The corresponding column strengths are also indicated. Note the large differences in scattering strengths between night and day. It is important to note that different reverberation models require different characterizations of volume-scattering strengths: some require input as a profile versus depth while others require input as a column-scattering strength.

8.2.3 Vertical-scattering plumes

Pelagic organisms tend to favor horizontal orientations, thus forming what are termed scattering layers. In certain areas of the oceans, the seepage of gas or liquids from the seabed produces vertical-scattering plumes that are detectable over the frequency range 10–1,000 kHz (Hovland, 1988). A special case of particular interest to underwater acousticians concerns the plumes formed over some seamounts. A scattering plume over the Hancock Seamount in the Hawaiian chain was investigated using an echo sounder operating at 38 kHz. This plume was detectable over a vertical extent of approximately 300 m directly above the seamount. These seepages appear to attract various marine organisms that might further complicate the scattering dynamics in the water column overlying seamounts.

8.3 Boundary reverberation

8.3.1 Sea-surface reverberation

The roughness of the sea surface and the presence of trapped air bubbles make the sea surface an effective but complex scatterer of sound. Scattering can occur out-of-plane as well as within the vertical plane containing the source and receiver.

Sea-surface scattering strengths have typically been measured using nondirectional (mostly explosive) sources and receivers as well as directional sonars in which a sound beam is formed so as to intercept the sea surface at a desired angle. The scattering strength of the sea surface has been found to vary with grazing angle, acoustic frequency and the roughness of the surface. Sea-surface roughness is usually characterized either by the near-surface wind speed or by wave heights. The measured scattering strengths show a strong variation with frequency at low frequencies and low grazing angles, and little variation with frequency at high frequencies and high grazing angles.

A series of measurements conducted by Chapman and Harris (1962) were analyzed in octave bands between 0.4 and 6.4 kHz, and the results were fitted by the empirical expressions:

$$S_s = 3.3\beta \log_{10} \frac{\theta}{30} - 42.2 \log_{10} \beta + 2.6 \quad (8.2)$$

$$\beta = 158 \left[\nu f^{1/3} \right]^{-0.58}$$

where S_s is the surface scattering strength (dB), θ the grazing angle (degrees), ν the wind speed (knots) and f the frequency (Hz).

Chapman and Scott (1964) later validated these results over the frequency range 0.1–6.4 kHz for grazing angle below 80°. Figure 8.2 presents curves computed using Equation (8.2) at several frequencies with wind speed as a parameter.

McDaniel (1993) reviewed recent advances in the physical modeling of monostatic sea-surface reverberation in the frequency range 200 Hz–60 kHz (also see the extensive review by Fortuin, 1970). Three sources of surface reverberation were considered: rough-surface scattering, scattering from resonant bubbles and scattering from bubble clouds (or plumes).

In the absence of subsurface bubbles, rough-surface scattering is adequately explained by the composite-roughness model (e.g. Thorsos, 1990). This model partitions treatment of surface scattering into two regimes according to the wind-wave spectrum: large-scale waves (using the Kirchhoff approximation) and small-scale waves (using a modified Rayleigh

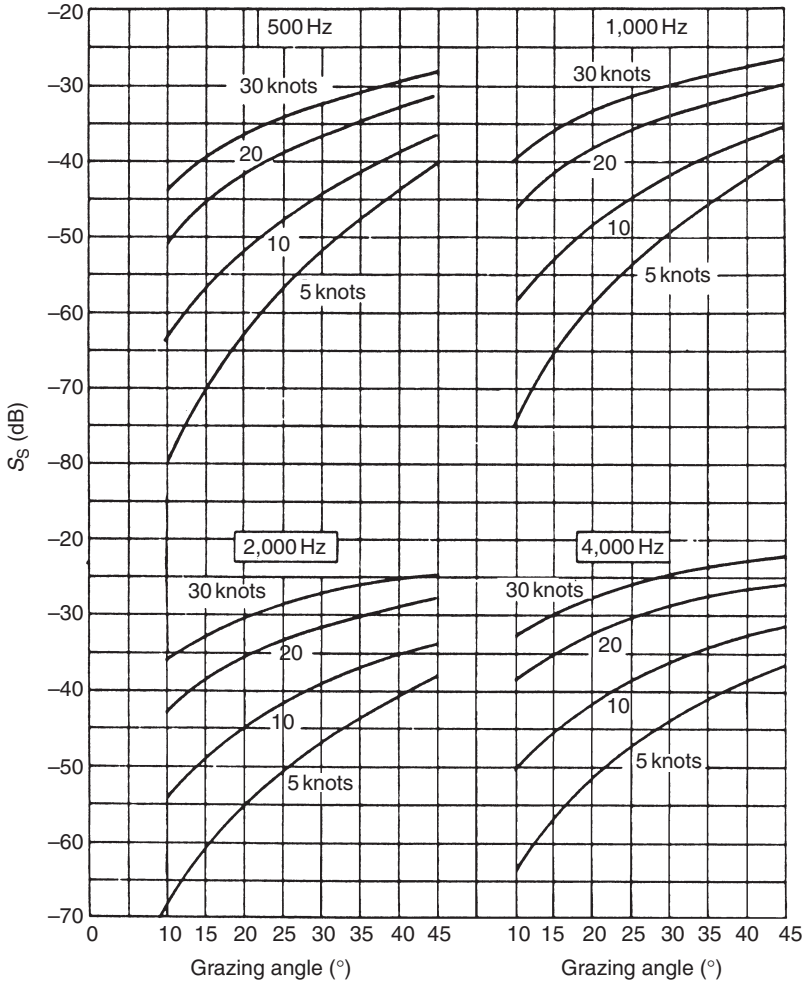


Figure 8.2 Low-frequency scattering strengths of the sea surface (S_s) computed from the empirical expressions given by Chapman and Harris (1962). (Urlick, 1983; *Principles of Underwater Sound*, 3rd edn; reproduced with permission of McGraw-Hill Publishing Company.)

approximation). McDaniel (1993) summarized recent advances in surface reverberation modeling according to acoustic frequency:

High-frequency reverberation (3–25 kHz). Backscattering at grazing angles above 30° is in agreement with rough-surface scattering theories. At lower grazing angles, anomalously higher backscattering strengths are assumed due to scatter from resonant microbubbles. Backscattering

in coastal waters is higher (by an order of magnitude) than in the open ocean under similar wind conditions. This effect is attributed, in part, to the greater generation of microbubbles in coastal waters. McDaniel (1993) also observed that many recent backscattering-strength measurements are lower than would be predicted using the Chapman and Harris (1962) empirical model.

Low-frequency reverberation (<1 kHz). Anomalous scatter similar to that observed at higher frequencies is evident, apparently due to entrained air. However, the nature of the physical processes governing the scattering at these lower frequencies is not evident from an examination of the available data.

Extensive measurements of low-frequency (70–950 Hz) sea-surface backscattering strengths were made during the critical sea test (CST) experiments for grazing angles ranging from 5° to 30°, and for wind speeds ranging from 1.5 to 13.5 m s⁻¹ (Ogden and Erskine, 1994a). Analyses of these measurements revealed several regimes in the frequency-versus-wind speed (f - U) domain corresponding to at least two different scattering mechanisms. Perturbation theory (Thorsos, 1990) was found to provide adequate descriptions of the data at high frequencies for calm seas, and at lower frequencies for all wind speeds, where air-water interface scattering is the dominant mechanism. The Chapman-Harris empirical relationship adequately described surface backscattering for rougher seas at higher frequencies where scattering from bubble clouds is presumed to dominate the scattering process. In the transition region where these two effects are competing, the scattering strengths depended upon the details of the surface and wind characteristics.

Ogden and Erskine (1994a) proposed a formula for computing the total scattering strength at the sea surface (S_{total}) as a combination of perturbation theory (S_{pert}) and the Chapman-Harris empirical relationship (S_{CH}):

$$S_{\text{total}} = \alpha S_{\text{CH}} + (1 - \alpha) S_{\text{pert}} \quad (8.3)$$

$$S_{\text{pert}} = 10 \log_{10} \left[1.61 \times 10^{-4} \tan^4 \theta \exp \left(-\frac{1.01 \times 10^6}{f^2 U^4 \cos^2 \theta} \right) \right] \quad (8.4)$$

where S_{CH} is the Chapman-Harris empirical formula (Equation (8.2))

$$\alpha = \frac{U - U_{\text{pert}}}{U_{\text{CH}} - U_{\text{pert}}} \quad (8.5)$$

This formula is valid for grazing angles (θ) less than 40° for wind speeds (U) less than 20 m s⁻¹ (measured at a height of 19.5 m above the sea surface) over the frequency range (f) 50–1,000 Hz.

For practical applications, the algorithm used a minimum wind speed of 2.5 m s⁻¹ since, at lower wind speeds, swell is likely to dominate the scattering process. Also, an arbitrary cutoff of 1° has been specified for the

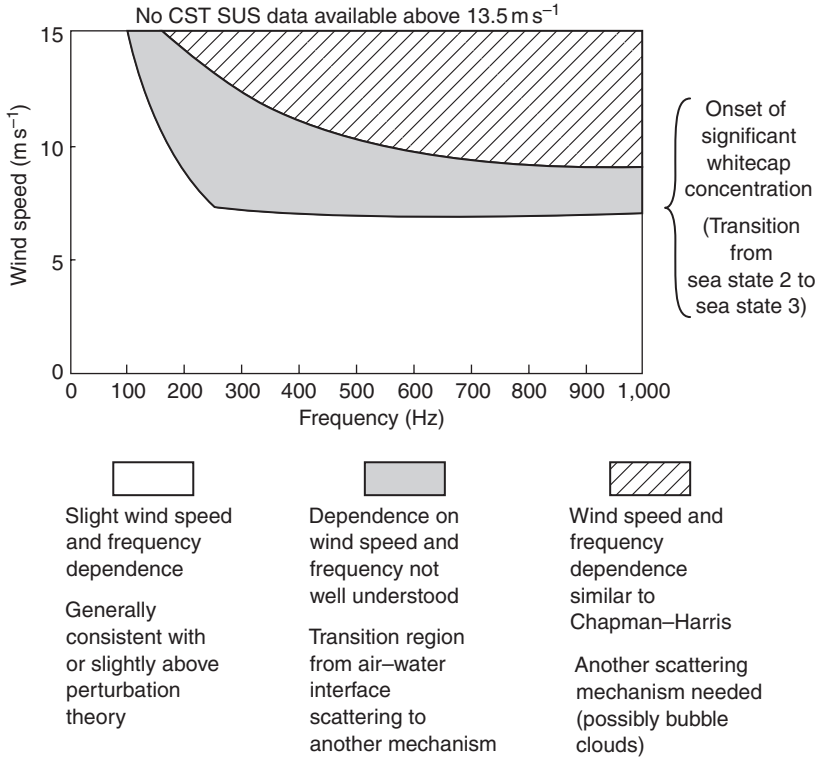


Figure 8.3 Frequency–wind speed ($f-U$) domain for sea-surface scattering strengths (Ogden and Erskine, 1994a).

grazing angle. In the hatched area of the $f-U$ domain of Figure 8.3, *only* the Chapman–Harris formula (S_{CH}) should be used (i.e. $\alpha = 1$). In the blank area of the $f-U$ domain, *only* the perturbation theory formula (S_{pert}) should be used (i.e. $\alpha = 0$). In the stippled area corresponding to the transition region, the full equation (S_{total}) should be used where α is evaluated at the input frequency (f) and input wind speed (U). Figure 8.3 can be used to determine the wind speeds at the perturbation theory (lower) boundary (U_{pert}) and at the Chapman–Harris (upper) boundary (U_{CH}). For convenience, Ogden and Erskine (1994a) put these boundaries into analytical form. The lower boundary was approximated by two line segments: from 240 to 1,000 Hz, the segment was defined by $y = 7.22$, while from 50 to 240 Hz the segment was given by $y = 21.5 - 0.0595x$. The upper boundary was approximated by the cubic equation:

$$y = 20.14 - 0.0340x + 3.64 \times 10^{-5}x^2 - 1.330 \times 10^{-8}x^3$$

Ogden and Erskine (1994b) extended the range of environmental parameters (principally wind speed) used in modeling sea-surface backscattering strengths in the CST experiments. Related work (with minimal analysis) summarized bottom-backscattering strengths that had been measured during the CST program over the frequency range 70–1,500 Hz for grazing angles ranging from 25° to 50° (Ogden and Erskine, 1997). Nicholas *et al.* (1998) extended the analysis of surface-scattering strengths that were measured during the CST experiments over the approximate frequency range 60–1,000 Hz. Unexplained variations between measured and modeled scattering strengths were attributed to an incomplete parameterization of subsurface bubble clouds.

8.3.2 *Under-ice reverberation*

The detection, localization and classification of targets with active sonars under an ice canopy is limited by reverberation from the rough under-ice surface and by the false targets presented by large ice features such as ice keels. Sea ice is the dominant cause of reverberation in Arctic regions. For undeformed first-year ice, reverberation levels at frequencies above about 3 kHz are approximately equivalent to that expected from an ice-free sea surface with a 30-knot wind.

Because of the variation in the under-ice surface, scattering strength measurements as a function of grazing angle reveal different characteristics. When the under-ice surface is relatively smooth, the scattering strength increases with grazing angle as in the open ocean. When ridge keels are present, low-grazing-angle sound waves strike them at a near-normal incidence and substantial reflection occurs. Measurements of the scattering strength of the ice-covered sea for two Arctic locations at different times of the year have been summarized by Brown (1964) and by Milne (1964). Both sets of data show an increase of scattering strength with increasing frequency and grazing angle. Using highly directional sources and receivers to exploit optimum ray paths can minimize reverberation under the ice. Such paths could provide time discrimination between target echoes and reverberation for those targets spatially separated from the sea surface (Hodgkiss and Alexandrou, 1985).

8.3.3 *Sea-floor reverberation*

The sea floor, like the sea surface, is an effective reflector and scatterer of sound. Scattering can occur out-of-plane as well as within the vertical plane containing the source and receiver. A correlation of scattering strength with the size of the particles in a sedimentary bottom has consistently been observed (e.g. McKinney and Anderson, 1964). The sea floor can then be classified according to sediment composition (sand, clay, silt) and correlated with the scattering strength. For example, mud bottoms tend to be smooth

and have a low impedance contrast to water, while coarse sand bottoms tend to be rough, with a high impedance contrast. There can be large spreads in the measured data for apparently the same bottom type. This may be due, in part, to the refraction and reflection of sound within the subbottom sediment layers.

A Lambert's law relationship (Urlick, 1983: chapter 8) between scattering strength and grazing angle appears to provide a good approximation to the observed data for many deep-water bottoms at grazing angles below about 45° . Lambert's law refers to a type of angular variation that many rough surfaces appear to satisfy for both the scattering of sound and light. According to Lambert's law, the scattering strength varies as the square of the sine of the grazing angle. Mackenzie (1961) analyzed limited reverberation measurements at two frequencies (530 and 1,030 Hz) in deep water. The scattered sound responsible for reverberation was assumed to consist of nonspecular reflections obeying Lambert's law:

$$S_B = 10 \log_{10} \mu + 10 \log_{10} \sin^2 \theta \quad (8.6)$$

where S_B is the bottom scattering strength (dB), μ the bottom scattering constant and θ the grazing angle (degrees). The term $10 \log_{10} \mu$ was found to be constant at -27 dB for both frequencies. This value has been largely substantiated by other measurements over a broad range of frequencies. The bottom-scattering strength (S_B) has been graphed in Figure 8.4 according to Equation (8.6), using a value of -27 dB for $10 \log_{10} \mu$.

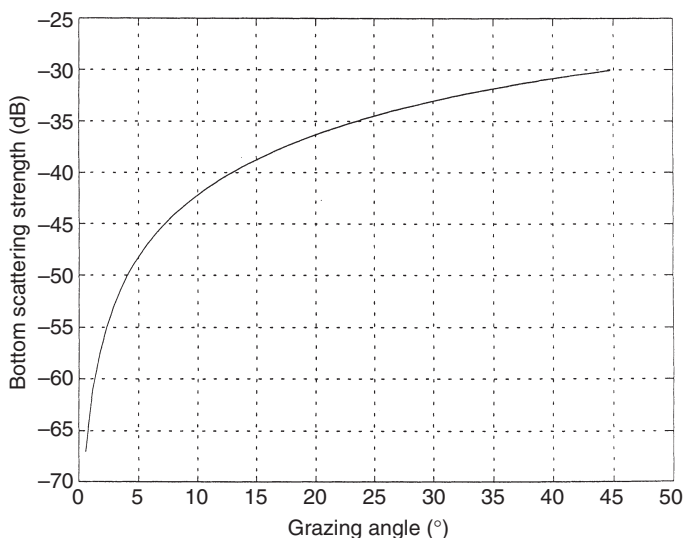


Figure 8.4 Bottom-scattering strengths (S_B) calculated according to Equation (8.6) using a value of -27 dB for the term $10 \log_{10} \mu$.

As part of the US Navy's acoustic reverberation special research program (ARSRP), sponsored by the Office of Naval Research (ONR), an area on the northern Mid-Atlantic Ridge has been designated as a natural laboratory. This area is a natural reverberation site because its steep rock inclines, deep subsurface structures and sediment structure provide opportunities to study many aspects of bottom reverberation. The resulting data have permitted detailed comparisons with numerical codes of bistatic reverberation (e.g. Smith *et al.*, 1993).

Ellis and Crowe (1991) combined Lambert's law scattering with a surface-scattering function based on the Kirchhoff approximation to obtain a new functional form that allowed a reasonable extension from backscattering to a general, 3D scattering function useful in bistatic-reverberation calculations. This new functional form was tested in a bistatic version of the GSM and was shown to be an improvement over two other commonly used methods, neither of which included azimuthal dependence: the separable approximation and the half-angle approximation.

In long-range acoustic propagation problems in the deep ocean, interactions with the sea floor generally occur at subcritical grazing angles. Under conditions of smooth basaltic surfaces and low grazing angles, most waterborne energy should be internally reflected. Furthermore, the scattering functions should be monotonic with respect to grazing angle, as would be predicted by Lambert's law. However, in ocean areas characterized by a flat, basaltic sea floor, the observed scattering functions are not always monotonic with respect to angle. Rather, peaks in the scattering functions sometimes occur at angles corresponding to compressional and shear head (or interface) wave propagation. In order to investigate this seemingly anomalous behavior, Swift and Stephen (1994) generated scattering functions using a model that also included volumetric heterogeneities below a flat, basaltic sea floor. They executed the model over a wide range of length scales for the embedded scatterers when ensonified by a Gaussian pulse beam at a grazing angle of 15° . At this angle, a truly homogeneous sea floor composed of basaltic rocks would produce total internal reflection. However, they found that bottom models containing 10 percent velocity perturbations (representing the volumetric heterogeneities) produced significant levels of upward-scattered energy. In reality, energy leaks below the sea floor as an evanescent phase existing only when the incident energy is subcritical, and this energy only penetrates to depths of a few wavelengths. Interactions between this energy and those volumetric heterogeneities just below the surface excite interface waves (as well as compressional and shear waves in the bottom), in agreement with the observed scattering functions. Swift and Stephen (1994) also found that the scattering functions were influenced by the presence of velocity gradients (both compressional and shear) below the sea floor. Specifically, in the absence of velocity gradients, bottom-propagated energy is not refracted upward. Thus, it interacts with yet deeper velocity anomalies and produces greater scattering.

Greaves and Stephen (1997) determined that a sea-floor dip on the scale of a few hundred meters influenced, but did not determine, scattering strength. This suggested that other characteristics of steeply dipping areas, such as subsurface properties or smaller-scale surface features, strongly affected the level of backscattered signals. Greaves and Stephen (2000) advanced this work in an extended analysis of ARSRP data to examine reverberation at low-grazing angles from rough and heterogeneous seafloors.

The presence of plant life on the sea floor can complicate the scattering processes at the bottom boundary of the ocean. In a theoretical study, Shenderov (1998) treated acoustical scattering by algae as the diffraction of sound waves on a random system of 3D, bent, elastic bodies. This approach considered the statistical properties of algae. McCarthy and Sabol (2000) characterized submerged aquatic vegetation in terms of military and environmental monitoring applications.

8.4 Inversion techniques

The utility of the reverberation field as an inverse sensing technique is analogous to that of the ambient noise field (Chapter 6, Section 6.6). Makris (1993), for example, inverted the reverberation field to image the sea floor. This was accomplished by using simultaneous inversions of multiple reverberation measurements made at different locations. The outputs of the inversion can include optimally resolved reverberation, scattering coefficients or physical properties of the sea floor. Through simulation, Makris (1993) demonstrated the utility of this method for determining bottom-scattering strengths using a monostatic-observation geometry together with operational parameters obtained from bottom-reverberation experiments sponsored by the ONR special research program. First, a synthetic ocean basin was created using a representation of scattering coefficients. Next, the true scattering coefficients were estimated from the observed reverberation maps using a global inversion method. This method is applicable to many monostatic and bistatic experimental geometries, although it cannot be used arbitrarily since a series of separate inversions is necessary to determine the angular dependence of the bottom reverberation. Specifically, for each inversion the separation between observations must be small enough to maintain a similar orientation relative to the imaged region. It may be possible to plan an optimal set of experimental observations by considering measurement-resolution constraints, platform maneuverability, time and observation sites by solving what W.A. Kuperman referred to as the “traveling acoustician problem” (Makris, 1993: 992).

9 Reverberation II

Mathematical models

9.1 Background

Mathematical models of reverberation generate predictions of boundary and volumetric reverberation using the physical models of boundary and volumetric scattering strengths developed in Chapter 8. The development of reverberation models has proved to be formidable for two reasons (e.g. Moritz, 1982; Goddard, 1993). First, there are theoretical difficulties in solving complex boundary value problems for which analytical tools are poorly developed. Second, there are practical difficulties in identifying and measuring all the parameters affecting the reverberation process.

9.2 Theoretical basis for reverberation modeling

9.2.1 *Basic approaches*

The scattering of sound by volumetric inhomogeneities in the ocean can be described either by Rayleigh's law or by geometrical acoustic scattering (Albers, 1965: 121). Rayleigh's law applies when the size (d) of the scattering particle is much smaller than the wavelength (λ) of the incident sound. Geometrical acoustic scattering is valid when d is much larger than λ . An intermediate condition applies when d is approximately equal to λ . Specifically, the following relationships hold:

- 1 If $d \ll \lambda$, the pressure of the scattered sound is proportional to f^2 (where f is the acoustic frequency) and to the volume of the scatterer, regardless of its shape (Rayleigh's law).
- 2 If $d \approx \lambda$, the pressure is a complicated function of frequency and also varies with the acoustic properties of the scatterer together with the characteristics of the ocean medium or boundaries.
- 3 If $d \gg \lambda$, the scattering is independent of frequency and depends only on the acoustic properties of the scatterer and its cross-section (geometrical acoustic scattering).

This situation has, in part, encouraged the development of two different approaches to the modeling of reverberation in the ocean: cell-scattering models and point-scattering models.

Cell-scattering models assume that the scatterers are uniformly distributed throughout the ocean. Thus, the ocean can be divided into cells, each containing a large number of scatterers. Summing the contribution of each cell yields the total average reverberation level as a function of time after transmission. A scattering strength is used per unit area or volume, as appropriate. This approach is the one most commonly used in sonar modeling.

Point-scattering models are based on a statistical approach in which the scatterers are assumed to be randomly distributed throughout the ocean. The reverberation level is then computed by summing the echoes from each individual scatterer. This approach is particularly well suited, for example, to under-ice modeling.

Reverberation is a time-domain problem. Reverberation levels can be represented as a function of range from the receiver by identifying the reverberation level corresponding to the time after transmission that the leading edge of the backscattered signal arrives at the receiver.

The TL component of many reverberation models is based on ray-theoretical considerations. Models based on wave-theoretical considerations are usually not well suited to calculations at the high frequencies associated with traditional sonar applications because of the required computational time (Chapter 4, Section 4.9). However, for modern low-frequency applications, wave-theoretical techniques have been used with some success. For example, normal-mode techniques have been used to model reverberation in oceanic waveguides (Bucker and Morris, 1968; Zhang and Jin, 1987; Ellis, 1993), and a two-way parabolic equation model that computes backscattered energy (Collins and Evans, 1992; Orris and Collins, 1994) has been used in reverberation simulations (e.g. Schneider, 1993). LeMond and Koch (1997) developed a normal-mode scattering formulation that was useful in computing single-frequency bottom reverberation for bistatic and monostatic scattering geometries in both shallow- and deep-water environments.

Reverberation models are typically combined with environmental, propagation, noise and signal-processing models to form a new class of models referred to as active sonar models (see Chapter 10). In the analysis of sonar performance, reverberation and ambient noise are jointly considered as the background masking level against which a signal must be detected. In many situations, it is useful to understand which contributor (noise or reverberation) is most responsible for creating the interfering background. Such diagnostic information can be used to improve new sonar designs or to optimize the performance of existing sonars.

Figure 9.1 illustrates a graphic product generated by a long-range reverberation model based on the cell-scattering approach. The reverberation level corresponds to the time the leading edge of the signal arrives at the receiving

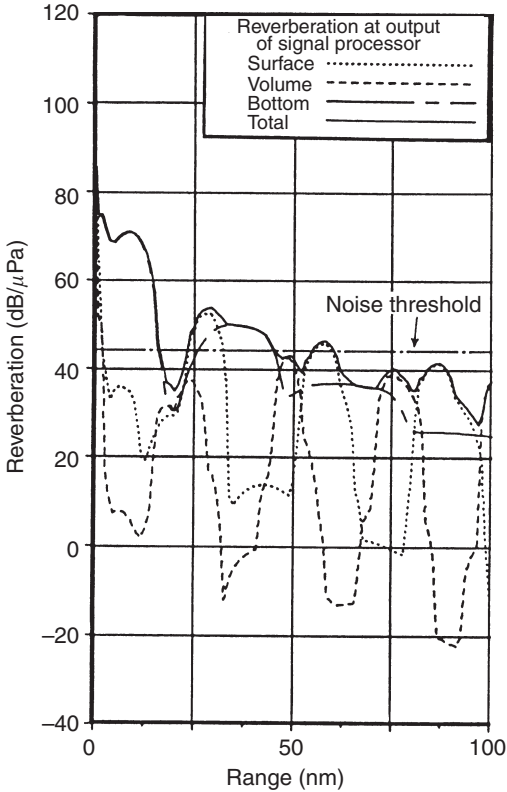


Figure 9.1 Averaged reverberation (surface, bottom, volume and total) levels versus range as predicted by a reverberation model. The noise threshold is also plotted for comparison (adapted from Hoffman, 1979).

array after bouncing off the target at the specified range. The plotted reverberation level is averaged over pulse length and corrected for processing gain. This corresponds to reverberation in the receiver bandwidth at the output of the signal processor before the thresholding device. Each of the bottom, surface and volume components of reverberation is the incoherent sum of the respective intensities derived from ray tracing. The noise threshold displayed on the reverberation plot is the combined ambient noise and self-noise in the receiver bandwidth at the output of the signal processor. In this example, the noise threshold is calculated by correcting spectrum-level noise for array gain, bandwidth and processing gain. Thus, the range (time) at which the background-masking level changes from reverberation-limited to noise-limited can be determined.

9.2.2 Advanced developments

A numerical method known as transmission-line modeling (TLM) has been used to model the scattering of acoustic waves off underwater targets. This method models the target and propagation space using meshes, rendering the problem discrete in both space and time. The mesh method models target features in considerable detail, operates readily in both two and three dimensions, and is capable of dealing with complicated scattering processes (Orme *et al.*, 1988). The method has already found use in volume-scattering modeling, and in modeling time-varying propagation phenomena in multipath channels. It is now also being applied to transducer structure modeling (Coates *et al.*, 1990).

A combination of the boundary element method (BEM) and wavenumber integration (WI), referred to as the hybrid BEM–WI approach, has been used extensively in the seismic community to model elastic-scattering problems. Wavenumber integration reduces the 2D Helmholtz equation to a 1D ordinary differential equation in a range-independent environment. BEM combines an integral representation of the wave field in a volume with a point representation of stresses and displacements on the boundary between fluid and elastic media (Schmidt, 1991).

Keiffer and Novarini (1990) demonstrated that the wedge assemblage (or facet ensemble) method offers a unique description of sea-surface scattering processes in the time domain by allowing for separation of the reflected and scattered components. Jackson *et al.* (1986) applied the composite-roughness model (Chapter 8, Section 8.3.1) to high-frequency bottom backscattering. Lyons *et al.* (1994) enhanced this model by incorporating the effects of volume scattering and scattering from subbottom interfaces. A new bottom-scatter modeling approach was proposed by Holland and Neumann (1998) to account for artifacts observed in field data when the subbottom plays a role in the scattering process.

Gostev and Shvachko (2000) considered kinematic models of volume reverberation caused by scattering from different types of inhomogeneities in the caustic zones of a surface waveguide. This reverberation component is important because the scattered field contains information on the statistical parameters of the inhomogeneities, including the location of caustics in the insonified zones.

Ellis (1995) built upon the method of Bucker and Morris (1968) for computing shallow-water boundary reverberation using normal modes to calculate the acoustic energy propagating from the source to the scattering area and back to the receiver. Ray-mode analogies and empirical scattering functions were used to compute the scattered energy at the scattering area. Continuing along this line of investigation, Desharnais and Ellis (1997) developed the bistatic normal-mode reverberation model OGO-POGO, which is a further extension of the method of Bucker and Morris (1968). The propagation was described in terms of normal modes computed

by the normal-mode model PROLOS. Travel times of the reverberation signals were derived from the modal-group velocities. Volume reverberation from either the water column or the subbottom is not currently included, but boundary reverberation is computed using empirical scattering functions and ray-mode analogies. The OGOPOGO model was used to interpret reverberation measurements from shallow-water sites in the frequency range 25–1,000 Hz.

9.3 Cell-scattering models

Simplifying assumptions are often necessary in order to make reverberation modeling feasible. These assumptions may seem to restrict the results to purely idealized situations. However, the resulting expressions for reverberation have been found to be practical for many sonar design and prediction purposes. The assumptions necessary are the following (Urick, 1983: chapter 8):

- 1 Straight-line propagation paths, with all sources of attenuation other than spherical spreading neglected. The effect of absorption on the reverberation level can be accommodated.
- 2 A homogeneous distribution of scatterers throughout the area or volume producing reverberation at any given time.
- 3 A sufficiently high density of scatterers to ensure that a large number of scatterers occurs in an elemental volume (dV) or area (dA).
- 4 A pulse length short enough for propagation effects over the range extension of the elemental volume or area to be neglected.
- 5 An absence of multiple scattering (i.e. the reverberation produced by reverberation is negligible).

In the following sections, basic theoretical relationships will be developed for volume and boundary reverberation, as adapted from Urick (1983: chapter 8).

9.3.1 Volume-reverberation theory

Let a directional projector in an ideal medium (as implied by the above assumptions) insonify a volume of water containing a large number of uniformly distributed scatterers. The beam pattern of the projector can be denoted by $b(\theta, \phi)$, and the axial intensity at unit distance will be I_0 . The source level (SL) is then given by $SL = 10 \log_{10} I_0$. The intensity at 1 m in the (θ, ϕ) direction is $I_0 b(\theta, \phi)$ by the definition of the beam-pattern function. Let there be a small volume dV of scatterers at range r . The incident intensity at dV will be $I_0 b(\theta, \phi)/r^2$. The intensity of the sound scattered by dV at a point P distant 1 m back toward the source will be $(I_0 b(\theta, \phi)/r^2) s_v dV$, where s_v is the ratio of the intensity of the scattering produced by a unit volume, at a distance of 1 m from the volume, to the intensity of the incident sound

wave. The quantity $10 \log_{10} s_v$ is the scattering strength for volume reverberation and is denoted by the symbol S_v . In the region near the source, the reverberation contributed by dV will have the intensity $(I_0/r^4)b(\theta, \phi)s_v dV$ and will produce a mean-squared voltage output of

$$R^2(I_0/r^4)b(\theta, \phi)b'(\theta, \phi)s_v dV$$

at the terminals of a hydrophone having a receiving beam pattern $b'(\theta, \phi)$ and voltage response R . By assumption, the elemental volumes dV can be made sufficiently small that their total contribution can be summed up by integration, and the coefficient s_v is then a constant. Furthermore, the equivalent plane-wave volume reverberation level (RL_v) can be defined as the intensity (in dB) of an axially incident plane wave producing the same hydrophone output as the observed reverberation, in which case the following relationship is obtained:

$$RL_v = 10 \log_{10} \left[\frac{I_0}{r^4} s_v \int_v b(\theta, \phi)b'(\theta, \phi) dV \right] \tag{9.1}$$

In order to proceed further, the elemental volumes dV must be examined more closely. As shown in Figure 9.2, take dV to be an infinitesimal cylinder of finite length with ends normal to the incident direction. The area of the end-face of this cylinder dV may be written $r^2 d\Omega$, where $d\Omega$ is the elemental solid angle subtended by dV at the source. Using a pulsed sonar, the extension in range of dV is such that the scattering produced by all portions of dV arrive back near the source at the same instant of time. Another way of viewing this is that the scattering of the front end of the pulse by the rear scatterers in dV will arrive back at the source at the same instant as the scattering of the rear of the pulse by the front scatterers in dV . The extension

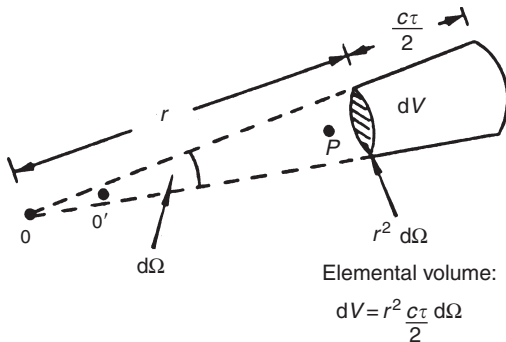


Figure 9.2 Geometry for volume scattering.

250 *Reverberation II: mathematical models*

in range is thus $c\tau/2$, where τ is the pulse length and c the speed of sound (Urlick, 1983: 241–2). The elemental volume can then be expressed as

$$dV = r^2 \frac{c\tau}{2} d\Omega \quad (9.2)$$

and the volume reverberation level (RL_v) is

$$\begin{aligned} RL_v &= 10 \log_{10} \left[\frac{I_0}{r^4} r^2 \frac{c\tau}{2} s_v \int_0^{4\pi} b(\theta, \phi) b'(\theta, \phi) d\Omega \right] \\ &= SL - 40 \log_{10} r + S_v + 10 \log_{10} \left[r^2 \frac{c\tau}{2} \int_0^{4\pi} b(\theta, \phi) b'(\theta, \phi) d\Omega \right] \end{aligned} \quad (9.3)$$

where the range extension ($c\tau/2$) is small compared to the range r .

9.3.2 *Boundary-reverberation theory*

Boundary reverberation pertains to the reverberation produced by scatterers distributed over the sea surface or the sea floor. The derivation of an expression for the equivalent plane-wave level of boundary reverberation proceeds in a manner similar to that for volume reverberation. The result is

$$RL_b = 10 \log_{10} \left[\frac{I_0}{r^4} s_b \int b(\theta, \phi) b'(\theta, \phi) dA \right] \quad (9.4)$$

where dA is an elemental area of the scattering surface and $10 \log s_b$ is the scattering strength (S_b) for boundary reverberation. If dA is taken as a portion of a circular annulus in the plane of the scatterers with the center directly above or below the transducer, then

$$dA = \frac{c\tau}{2} r d\phi \quad (9.5)$$

where $d\phi$ is the subtended plane angle of dA at the center of the annulus. The reverberation level then becomes

$$\begin{aligned} RL_b &= 10 \log_{10} \left[\frac{I_0}{r^4} r \frac{c\tau}{2} s_b \int_0^{2\pi} b(\theta, \phi) b'(\theta, \phi) d\phi \right] \\ &= SL - 40 \log_{10} r + S_b + 10 \log_{10} \left[r \frac{c\tau}{2} \int_0^{2\pi} b(\theta, \phi) b'(\theta, \phi) d\phi \right] \end{aligned} \quad (9.6)$$

9.4 The REVMOD model – a specific example

The reverberation spectrum model (REVMOD), originally developed by C.L. Ackerman and R.L. Kesser at the Applied Research Laboratory, The Pennsylvania State University, has been expanded and further documented by Hodgkiss (1980, 1984). REVMOD is a set of computer programs that models surface, bottom and volume reverberations. It is based on the cell-scattering approach.

REVMOD considers the effects of motion of the sonar platform, transmit signal windowing, transmit and receive beam patterns, scatterer velocity distributions and sound absorption. Model constraints include specification of a constant sound-speed profile and nonreflection of sound at the surface and bottom boundaries.

Geometrically, REVMOD divides the ensonified volume of the ocean into cells and evaluates scatterer motion relative to the sonar platform for a measure of the spectral shifting and spreading due to the environment. Acoustically, REVMOD determines the backscattering level for each cell. The contributions from each cell are then summed to compute the total reverberation power spectra received at the sonar.

REVMOD is composed of three major software modules:

- 1 RVMS – computes the scattering function resulting from the combined effects of the environment, vehicle dynamics, and transmit and receive beam patterns.
- 2 RVMDT – convolves the scattering function with the transmit-signal energy spectrum to yield the reverberation power spectrum.
- 3 RVMDR – convolves the reverberation power spectrum with the receiver-impulse response-energy spectrum.

Module RVMS computes the scattering function for reverberation and describes the effects of the ocean medium on a transmit signal with carrier frequency ω_c . Module RVMDT completes the reverberation model by combining a detailed description of the transmit signal (pulse length, envelope shape and source level) with the environmental characterization provided by module RVMS. Module RVMDR creates a model of a receiver operating in a reverberant ocean environment. A matched filter envelope detector uses the reverberation spectra generated by module RVMDT. Optional software can also be included to model a matched filter envelope detection receiver appropriate for post-processing the reverberation spectra. Thus, the effects of utilizing a receiver impulse response window, which differs from that of the transmitter waveform, can be investigated.

A mathematical description of the scattering function (RVMS) will be provided here. Calculations of the reverberation power spectrum (RVMDT) and subsequent convolution with the receiver impulse response energy spectrum (RVMDR) were discussed by Hodgkiss (1980, 1984). REVMOD generates a scattering-function description of the ocean medium that does

not require a detailed description of the transmit signal. Thus, the model is appropriate for investigations of the influence of the medium on various transmit-signal types.

Acoustic backscatter can be modeled as the passage of a transmit waveform through a linear, time-varying filter:

$$\tilde{s}_r = \sqrt{E_t} \int_{-\infty}^{\infty} \tilde{f}(t - \lambda) \tilde{b}\left(t - \frac{\lambda}{2}, \lambda\right) d\lambda \quad (9.7)$$

where $\tilde{s}_r(t)$ is the received backscattered signal, E_t the transmit-signal energy, $\tilde{f}(t - \lambda)$ the transmit waveform, t the time, λ the time delay and $\tilde{b}(t - \lambda/2, \lambda)$ the time-varying impulse function of the filter.

The basic geometry of REVMOD consists of a spherical shell representing that portion of the ocean medium ensounded by the signal wavefront corresponding to a range (R) after transmittance (refer to Figure 9.3). The shell thickness is governed by the variables D_S, D_B and ΔR for surface, bottom and volume scattering, respectively. The spherical shell is further subdivided into a grid of cells, each of which contributes to surface, bottom or volume backscatter. The location of each cell is specified in terms of an azimuth-elevation angle pair (θ_j, ϕ_i) . Using this geometry, REVMOD calculates the scattering functions corresponding to the surface, bottom and volume backscatter of a transmit waveform at specified ranges of interest. Specifically, the normalized attenuation ($\hat{A}_{i,j}$) of the transmitted signal (including propagation and beam pattern effects) is calculated for each surface, bottom

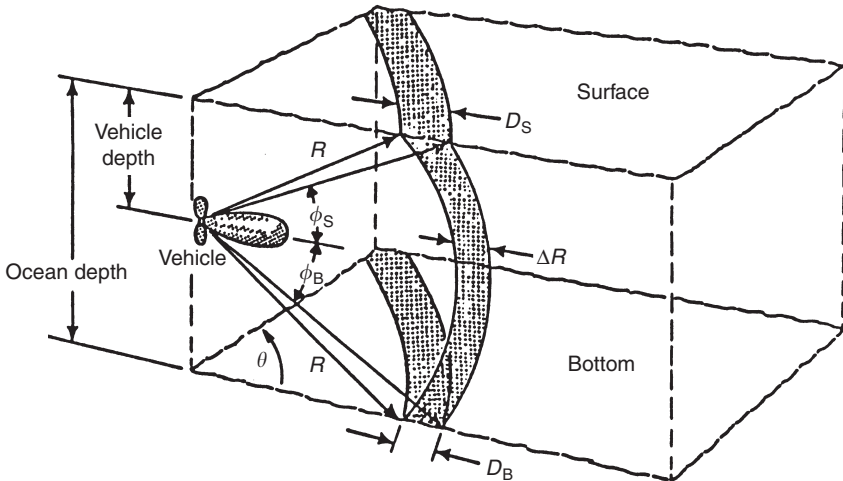


Figure 9.3 REVMOD reverberation model geometry. (Hodgkiss, 1984, *IEEE J. Oceanic Eng.*, 10, 285-9; copyright by IEEE.)

and volume grid cell as follows:

Surface scattering

$$\begin{aligned}
 10 \log_{10} (\hat{A}_{i,j}) &= 10 \log_{10} [D_S(R\Delta\theta)] + S_S - 40 \log_{10}(R) - (2\alpha R) \\
 &\quad + 10 \log_{10} \left[\hat{P}_T(\theta_j, \phi_S) \hat{P}_R(\theta_j, \phi_S) \right] + 10 \log_{10}[c/2\Delta R]
 \end{aligned}
 \tag{9.8}$$

Volume scattering

$$\begin{aligned}
 10 \log_{10} (\hat{A}_{i,j}) &= 10 \log_{10}[\Delta R(R\Delta\theta)(R\Delta\phi)] + S_V - 40 \log_{10}(R) - (2\alpha R) \\
 &\quad + 10 \log_{10} \left[\hat{P}_T(\theta_j, \phi_i) \hat{P}_R(\theta_j, \phi_i) \right] + 10 \log_{10}[c/2\Delta R]
 \end{aligned}
 \tag{9.9}$$

Bottom scattering

$$\begin{aligned}
 10 \log_{10} (\hat{A}_{i,j}) &= 10 \log_{10}[D_B(R\Delta\theta)] + S_B - 40 \log_{10}(R) - (2\alpha R) \\
 &\quad + 10 \log_{10} \left[\hat{P}_T(\theta_j, \phi_B) \hat{P}_R(\theta_j, \phi_B) \right] + 10 \log_{10}[c/2\Delta R]
 \end{aligned}
 \tag{9.10}$$

where $\hat{A}_{i,j}$ is the scattering level (normalized to 1 s in range) from the (i, j) -th grid cell (s^{-1}), D_S the lateral dimension of surface-scattering patch (m), D_B the lateral dimension of bottom-scattering patch (m), R the range (m), ΔR the increment in range over which scattering is averaged (m), $\Delta\theta$ the angular grid cell width in azimuth (rad), $\Delta\phi$ the angular grid cell height in elevation (rad), S_S the surface-scattering coefficient (dB m^{-2}), S_V the volume-scattering coefficient (dB m^{-3}), S_B the bottom-scattering coefficient (dB m^{-2}), α the sound absorption coefficient (dB m^{-1}), $\hat{P}_T(\theta_j, \phi_i)$ the transmit beam pattern (normalized to 1 at $\theta_j = \theta_T$ and $\phi_i = \phi_T$), $\hat{P}_R(\theta_j, \phi_i)$ the receive beam pattern (normalized to 1 at $\theta_j = \theta_R$ and $\phi_i = \phi_R$), θ_j the azimuth to center of j th grid column (rad), ϕ_i the elevation to center of i th grid row (rad), (θ_T, ϕ_T) the transmit beam vector, (θ_R, ϕ_R) the receive beam vector, ϕ_S the elevation angle to surface (rad), ϕ_B the elevation angle to bottom (rad) and c the sound speed (m s^{-1}).

Hodgkiss (1984) provided sample results from REVMOD for the case of a bottom-mounted transducer with a steerable, axially symmetric beam pattern (Figure 9.4). Wind-driven surface waves and a surface current both contributed to spectral broadening and Doppler shifting of the transmit spectrum upon backscattering from the sea surface. The volume-backscattering

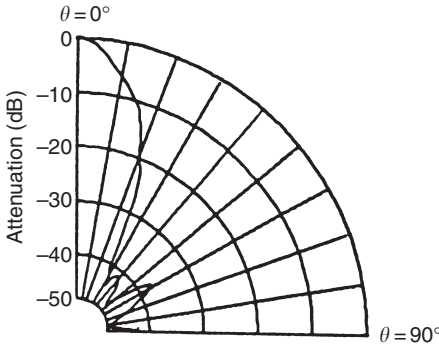


Figure 9.4 Transmit and receive beam pattern used in an example from the REVMOD reverberation model. (Hodgkiss, 1984; *IEEE J. Oceanic Eng.*, 10, 285–9; copyright by IEEE.)

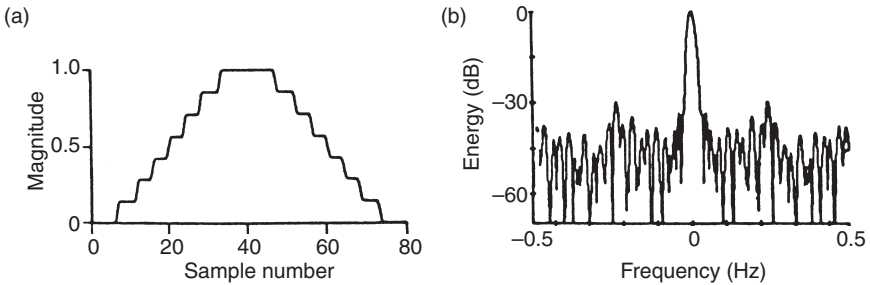


Figure 9.5 Sampled envelope function (a) and energy spectra (b) for quantized Hanning transmit envelope used in an example from the REVMOD reverberation model. (Hodgkiss, 1984; *IEEE J. Oceanic Eng.*, 10, 285–9; copyright by IEEE.)

component contributed only to spectral broadening of the transmit spectrum since the water column was assumed motionless on average. In this particular example, bottom backscattering was not a factor owing to the bottom-mounted transducer geometry.

For the purposes of discussion here, only a downwind transducer orientation is considered, although Hodgkiss (1984) also addressed upwind and crosswind orientations. This downwind case considers only the reverberation received at a range of 400 m. A quantized Hanning transmit envelope (Figure 9.5) and a Hanning receive envelope (Figure 9.6) are used in conjunction with the beam pattern shown previously in Figure 9.4. The transmit beam vector is horizontal and the receive beam vector is inclined towards the surface 25° off the horizontal. The transmit and receive envelope durations

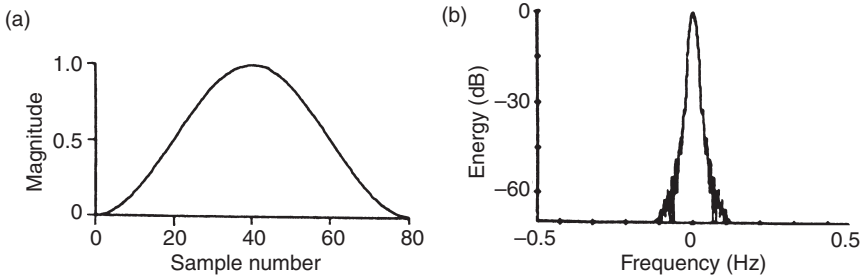


Figure 9.6 Sampled envelope function (a) and energy spectra (b) for Hanning receive envelope used in an example from the REVMOD reverberation model. (Hodgkiss, 1984; *IEEE J. Oceanic Eng.*, 10, 285–9; copyright by IEEE.)

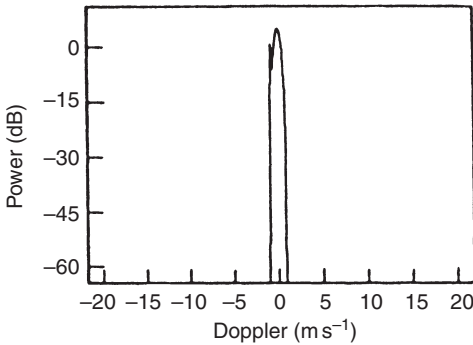


Figure 9.7 Example from the REVMOD reverberation model showing the surface-scattering function for a downwind case. (Hodgkiss, 1984; *IEEE J. Oceanic Eng.*, 10, 285–9; copyright by IEEE.)

were 102 and 86 ms, respectively. See Ziomek (1985: chapters 3 and 4) for a discussion of complex apertures and directivity functions.

The Doppler of the surface component of the scattering function reflects a complex interaction with this moving boundary (specifically, a negative Doppler ridge), as shown in Figure 9.7. This ridge corresponds to the Doppler-shifting effects of the surface wave and current velocity vectors.

9.5 Bistatic reverberation

9.5.1 Computational considerations

Most traditional active sonars are configured in what is termed a monostatic geometry, meaning that the source and receiver are at the same position.

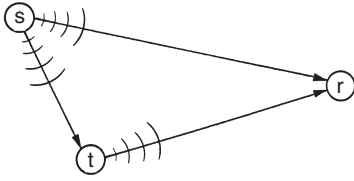


Figure 9.8 Geometry for bistatic reverberation showing relative positions of the source (s), target (t) and receiver (r) in either the vertical or the horizontal plane.

In some sonar systems, however, the source and receiver are separated in range or depth, or both, in what is termed a bistatic configuration. Bistatic geometries are characterized by a triangle of source, target and receiver positions, and by their respective velocities (Cox, 1989). Such geometries are commonly employed in sonobuoy applications (Bartberger, 1985) and also in active surveillance applications (Franchi *et al.*, 1984). Geometries involving multiple sources and receivers are termed multistatic.

A bistatic sonar must detect the target signal against the background noise level that is the intensity sum of the ambient noise, the surface, bottom and volume reverberation, and the energy propagating directly from the source to the receiver over a set of one-way paths referred to as direct arrivals (Figure 9.8). These direct arrivals represent a significant difference between bistatic and monostatic sonars. Since the direct (one-way) paths are very intense, they must be carefully considered in predicting the performance of bistatic sonars (Bartberger, 1985). Each different propagation path may require separate predictions of transmission loss. Bistatic reverberation models are commonly confronted with substantial bookkeeping requirements associated with sorting the various reverberation and noise contributions. In the monostatic situation, reverberation is due to backscatter. In bistatics, forward and out-of-plane scattering are important (Cox, 1989).

The bistatic problem is further complicated by the presence of certain bathymetric features, particularly seamounts, which can introduce a discrimination problem between acoustic returns from these geologic features and from potential targets of interest. Eller and Haines (1987) described seamount statistics as well as the characteristics of acoustic reverberation from seamounts. A real-time bathymetric reflection and scattering prediction system was developed to support at-sea acoustical surveys (Haines *et al.*, 1988). The system utilized gridded databases to generate 3D environmental scenarios in conjunction with the ASTRAL propagation model and the ANDES noise model. As configured, the system operated on a HP-9020 desktop computer and provided color graphic displays of predicted ocean bottom reverberation as well as echoes from seamounts.

A computer model called ocean refraction and bathymetric scattering (ORBS) was developed to calculate the directional distribution of bottom-scattered acoustic energy received at an array (Baer *et al.*, 1985; Wright *et al.*, 1988). ORBS incorporated the refractive effects of a varying sound speed structure in the ocean volume as well as the effects of out-of-plane scattering caused by rough bathymetry. A seamount could be considered where it made sense to consider only a single encounter with the sea floor. The numerical techniques used included the split-step solution to the parabolic equation away from the boundary, propagation of the coherence function near the boundary, and a modified Kirchhoff formulation to incorporate scattering. Smith *et al.* (1996) used field measurements and model results to correlate reverberation events with bathymetric features.

9.5.2 *The bistatic acoustic model – a specific example*

The bistatic acoustic model (BAM) predicts the performance of a sonar system consisting of a sound source and a receiver separated in both range and depth (Bartberger, 1991a; Vendetti *et al.*, 1993a). BAM computes the echo-to-background ratios for targets located at a set of bipolar grid locations in a horizontal plane containing a specific target. The bipolar grid points are defined by the intersections of circles of constant range about the source and receiver. There are three separate versions of BAM corresponding to three different sonar system configurations: vertical line array, horizontal line array or volumetric array. BAM consists of four computer programs:

- 1 BISON computes the ray arrival structure, the surface, bottom and volume reverberation time histories, and the vertical distribution of ambient noise.
- 2 BISTAT computes the echo-to-background ratios on a bipolar grid within a specified circle about the receiver.
- 3 CTEST generates the time series of the direct arrivals, the surface, bottom and volume reverberation, and the combined interference of all of these components.
- 4 PLOSS calculates the source-to-target transmission loss and the target-to-receiver transmission loss as a function of range.

A sample output product from BAM is illustrated in Figure 9.9, which shows computed echo-to-background levels. These levels are numerically coded to facilitate printer output. The digital pattern in Figure 9.9 indicates the potential for target detection under the hypothetical problem geometry and acoustic conditions:

- frequency = 2 kHz;
- source depth = 300 m (four-element omni source array);
- receiver depth = 500 m (six-element omni receiver array);
- target depth = 350 m (no Doppler);

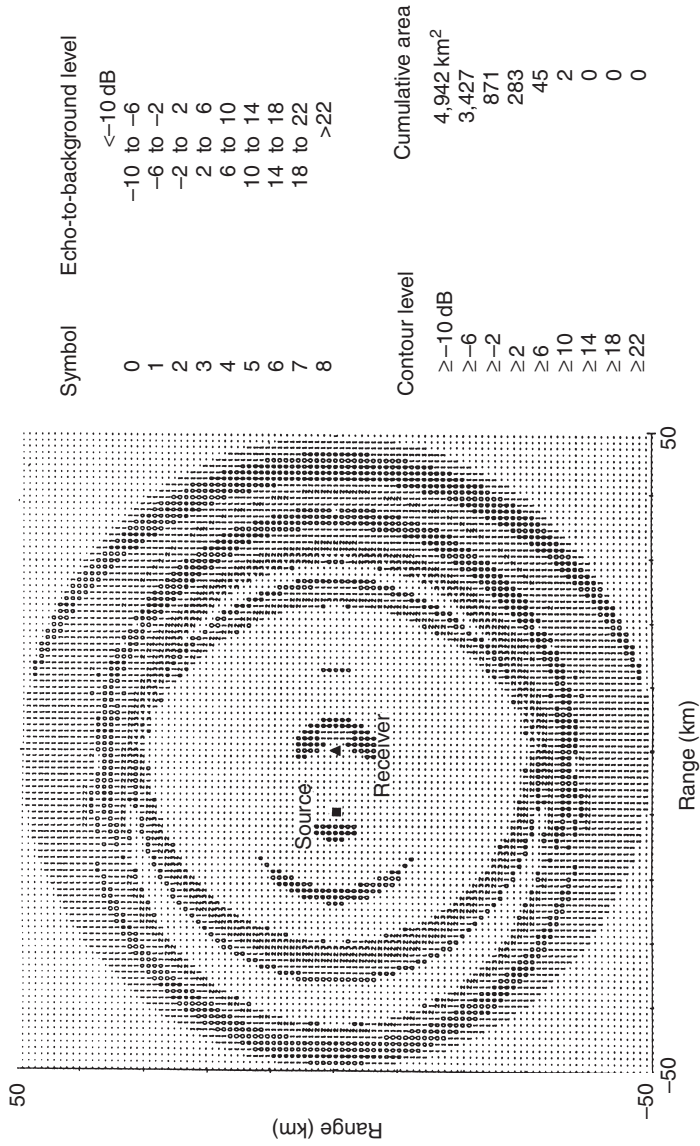


Figure 9.9 Sample output from the BAM showing echo-to-background levels. Also shown is the cumulative area coverage contained within specified contours of echo-to-background level.

- source–receiver range = 10 km;
- maximum target–receiver range = 50 km;
- pulse length = 5 s.

The problem area is delimited by a circle centered about the receiver with a radius equal to the maximum target–receiver range. Also shown is the cumulative area coverage (km^2) contained within specified contours of echo-to-background level. In this example, the maximum area coverage possible would be $\pi \times (50 \text{ km})^2 \approx 7,854 \text{ km}^2$. Thus, for echo-to-background levels greater than or equal to -10 dB , only 63 percent ($4,942 \text{ km}^2/7,854 \text{ km}^2$) of the specified search area would be covered effectively. Clearly, this information is useful in assessing the effectiveness of candidate sensors and search tactics. For example, optimum search tactics could be developed by varying selected parameters and then assessing the resulting changes in area coverage.

The elliptically shaped region of poor detection (less than -10 dB) located immediately between the source and receiver is a consequence of the direct arrivals, which represent the transmission of energy directly from the source to the receiver. These direct arrivals, also referred to as the direct blast, consist of a number of multipath arrivals extending over a time interval that is determined by geometry, environment and system characteristics. The direct blast often masks target echoes of interest. The extent of this masking region is approximately determined by the inequality (Cox, 1989):

$$\tau_1 + \tau_2 < \tau_3 + \tau_b$$

where τ_1 is the travel time, source to target; τ_2 the travel time, target to receiver; τ_3 the travel time, source to receiver and τ_b the effective masking time of direct blast.

The effects of the direct blast can be mitigated to some extent in one of three ways: (1) by controlling the vertical beam pattern of the receiver or source, or both, to minimize the contribution of steep-angle (boundary-interacting) arrivals; (2) by nulling the receiver in the direction of the source; or (3) by using Doppler to discriminate between direct-blast energy and target echoes.

9.6 Point-scattering models

9.6.1 Computational considerations

Point-scattering models are based on a statistical approach that assumes the scatterers are randomly distributed throughout the ocean. The echoes from each individual scatterer are then summed to compute the reverberation level. This approach is not as widely used as the cell-scattering technique. When dealing with scatterers whose dimensions are comparable to the acoustic wavelength, the point-scattering approach may be the preferred alternative.

This situation arises in two common problems: high-frequency sonars and under-ice scattering. A point-scattering model suitable for high-frequency applications was described by Princehouse (1977). A model appropriate for under-ice scattering is briefly described below.

9.6.2 *The under-ice reverberation simulation model – a specific example*

Bishop (1987, 1989a,b) and Bishop *et al.* (1986, 1987) developed a bistatic, high-frequency (≥ 2 kHz), under-ice acoustic-scattering model to evaluate the scatter produced by a pulse, originating from an arbitrarily located source, as detected by an arbitrarily located receiver. This model, referred to as “under-ice reverberation simulation,” uses measured 2D under-ice acoustic profile data and empirical results relating geometric parameters of the large-scale under-ice relief features (such as ice keels) to construct a 3D bimodal under-ice surface consisting of first-year ice keels and sloping flat-ice regions. A first-year keel is modeled as an ensemble of randomly oriented ice blocks on a planar surface inclined at some slope angle with respect to a horizontal plane at sea level. The keel is characterized by length, draft, width, ice thickness and aspect angle. A region of flat ice is modeled as a smooth planar surface whose slope angle is less than some critical angle that serves to distinguish a flat-ice feature from an ice keel. The Kirchhoff approximation is used to evaluate the target strength of a facet of an ice block. This approximation assumes that reflection coefficients appropriate for an infinite plane wave at an infinite plane interface can be used in the local scattering geometry of a rough surface (in some texts, this approximation is referred to as the tangent-plane method). The target strength of a keel is calculated in range increments as the coherent sum of the backscatter from all scattering facets contained within one-half the pulse length projected onto the keel. The model has been used to show the effects of various ice and acoustic parameters on reverberation and target-strength frequency distributions.

The under-ice reverberation simulation model was used to calculate monostatic backscattering and reverberation for one realization at a site near the North Pole, a site in the Chuckchi Sea and a site in the Beaufort Sea (Bishop, 1989a,b). To parameterize the large-scale surface roughness at these sites, the keel frequency and mean keel relief were calculated. The Chuckchi Sea site was the roughest of the three sites with a keel frequency of $16.0 \text{ keels km}^{-1}$ and an average keel relief of 4.1 m. The North Pole site had a keel frequency of $13.7 \text{ keels km}^{-1}$ and an average keel relief of 4.0 m. The Beaufort Sea site was the least rough of the sites with a keel frequency of $4.5 \text{ keels km}^{-1}$ and an average keel relief of 3.4 m.

Figure 9.10 illustrates the results obtained for these three sites. The under-ice profiles for 1.15-km transects at each site are indicated by a heavy solid line. The measured and modeled under-ice monostatic reverberation levels

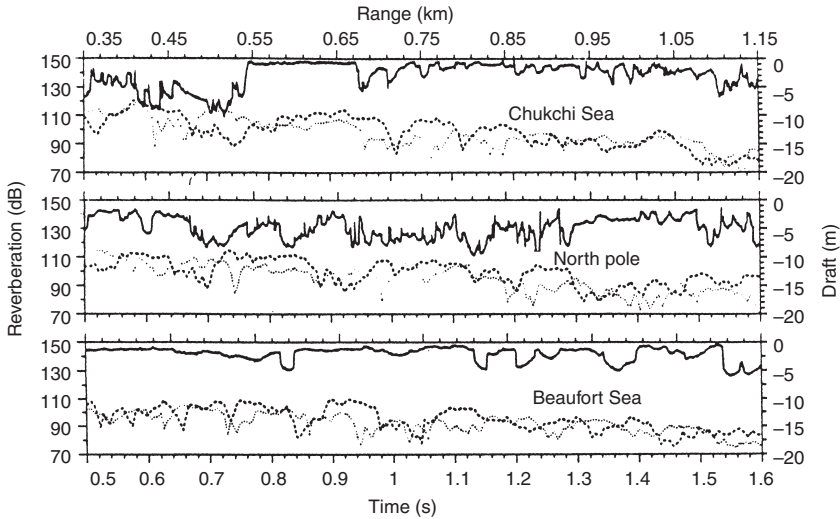


Figure 9.10 Under-ice profiles (solid line), and measured (dashed line) and modeled (dotted line) under-ice monostatic reverberation time series for three Arctic sites (Bishop, 1989b).

are indicated by the dashed and dotted lines, respectively. The time scale (in seconds) is indicated at the bottom of the figure. These results support the intuitive notion that relatively high reverberation levels are associated with areas of high ice roughness. More specifically, average keel draft determines the average scattering facet surface area (which determines the average amplitude of a specular return) and the keel frequency determines the total number of scattering facets (which determines the probability of scatter occurrence). Differences between measured and modeled results are thought to be due to significant scatterers present in the under-ice surface but not present in either the measured or modeled data.

9.7 Numerical model summaries

A summary of stand-alone underwater acoustic reverberation models is presented in Table 9.1. The models are segregated according to cell-or point-scattering approaches. Numbers within brackets following each model refer to a brief summary and appropriate documentation. Model documentation can range from informal programming commentaries to journal articles to detailed technical reports containing a listing of the actual computer code. Abbreviations and acronyms are defined in Appendix A. This summary does not claim to be exhaustive.

Table 9.1 Summary of underwater acoustic reverberation models

<i>Cell scattering</i>		<i>Point scattering</i>	
<i>Monostatic</i>	<i>Bistatic</i>	<i>Monostatic</i>	<i>Bistatic</i>
DOP [1]	BAM [8]	REVGGEN [16]	Under-ice reverberation simulation [17]
EIGEN/REVERB [2]	BiKR [9]		
MAM [3]	BiRASP [10]		
PEREV [4]	BISAPP [11]		
REVMOD [5]	BISSM [12]		
REVSIM [6]	OGOPOGO [13]		
TENAR [7]	RASP [14]		
	RUMBLE [15]		

Notes

Cell scattering

Monostatic

- 1 DOP divides the ocean into time-Doppler cells, sums the received energy incoherently, and produces a spectrum for the surface, volume or bottom reverberation at a given time after transmission (Marsh, 1976).
- 2 EIGEN/REVERB is a series of programs used to calculate ambient noise, reverberation-versus-time signals, and transmission-loss values (Sienkiewicz *et al.*, 1975). These programs are based on NISSM.
- 3 MAM was designed as a monostatic companion to the bistatic BAM model. For monostatic operation, it is required that the source and receiver be located at the same horizontal location, although they may differ in depth (Bartberger, 1991b; Vendetti *et al.*, 1993b).
- 4 PEREV (Tappert's PE reverberation model), together with the UMPE propagation model, are described by Smith *et al.* (1993, 1996).
- 5 REVMOD calculates reverberation power spectra (C.L. Ackerman and R.L. Kesser, 1973, unpublished manuscript; Hodgkiss, 1980, 1984). [The REVMOD model is discussed in detail in Section 9.4.]
- 6 REVSIM generates coherent, multi-beam, non-stationary reverberation time series (Chamberlain and Galli, 1983).
- 7 TENAR is a subroutine that uses the sonar equation to calculate underwater target echoes, reverberation and noise (Luby and Lytle, 1987).

Bistatic

- 8 BAM predicts the performance of a sonar system consisting of a sound source and a receiver separated in both range and depth (Bartberger, 1985, 1991a; Vendetti *et al.*, 1993a). The model computes the echo-to-background ratios for targets located at a set of bipolar grid locations in a horizontal plane at a specified target depth. The bipolar grid points are defined at the intersections of circles of constant range about the source and receiver. [BAM is discussed in detail in Section 9.5.2.]
- 9 BiKR is a bistatic reverberation model (Fromm, 1999) based on the KRAKEN propagation model.
- 10 BiRASP extended the RASP model to handle arbitrary (bistatic) source and receiver configurations in a 3D, range-dependent environment (Fromm *et al.*, 1996). RASP had been previously modified to predict range-dependent, monostatic reverberation at higher frequencies (up to 10 kHz) and in water shallower than originally intended. This modification was referred to as the *Shallow Water RASP Upgrade* (Fulford, 1991).
- 11 BISAPP uses an integral fast eigenray model to calculate point-by-point echo levels to facilitate analysis of bistatic and multistatic scenarios (Pomerenk and Novick, 1987).

- 12 BISSM computes bistatic bottom-scattering strengths (Caruthers *et al.*, 1990; Caruthers and Novarini, 1993; Caruthers and Yoerger, 1993).
- 13 OGOPOGO is based on the Bucker–Morris method for computing shallow-water boundary reverberation using normal modes to calculate the acoustic energy propagating from the source to the scattering area and back to the receiver. Ray-mode analogies and empirical scattering functions are used to compute the scattered energy at the scattering area (Ellis, 1995). The normal-mode model PROLOS computes the propagation loss. Travel times of the reverberation signals are derived from the modal-group velocities. Volume reverberation from either the water column or the subbottom is not currently included, but boundary reverberation is computed using empirical scattering functions and ray-mode analogies. Both monostatic and bistatic geometries can be handled, and horizontal or vertical arrays can be specified for the source and receiver. OGOPOGO was used to interpret reverberation measurements from shallow-water sites in the frequency range 25–1,000 Hz (Desharnais and Ellis, 1997).
- 14 RASP is a sequence of computer programs using multipath propagation and scattering processes to predict the long-range, low-frequency boundary reverberation and target returns that would be received in real ocean environments (Franchi *et al.*, 1984; Palmer and Fromm, 1992).
- 15 RUMBLE calculates reverberation as a function of time for bistatic sonars (Bucker, 1986; Kewley and Bucker, 1987).

Point scattering

Monostatic

- 16 REVGEM produces digital baseband samples of transducer or beamformer signals for use by active or passive sonars (Princehouse, 1977).

Bistatic

- 17 Under-Ice Reverberation Simulation is a bistatic, high-frequency (≥ 2 kHz), under-ice acoustic-scattering model to evaluate the scatter produced by a pulse, originating from an arbitrarily located source, as detected by an arbitrarily located receiver (Bishop *et al.*, 1986, 1987; Bishop, 1987, 1989a,b). [This model is discussed in detail in Section 9.6.2.]

10 Sonar performance models

10.1 Background

The ultimate purpose of sonar performance modeling is two-fold. First, advanced sonar concepts can be optimally designed to exploit the ocean environment of interest. Second, existing sonars can be optimized for operation in any given ocean environment.

In the case of naval sonars, performance prediction products can be tailored to individual sonar systems by providing the sonar operators with on-scene equipment mode selection guidance. When combined with current tactical doctrine, this information product is commonly referred to as a tactical decision aid (TDA). These decision aids are used by the force commanders to optimize the employment of naval assets in any particular tactical environment at sea. Performance prediction products help both the force commanders and sonar operators to better understand and thus exploit the ocean environment from a tactical standpoint. Sonar performance models also support various naval underwater acoustic surveillance activities.

Tactical decision aids are in the realm of engagement modeling, which will be discussed more fully in Chapter 12. In essence, engagement models use sonar detection performance data (either measured or predicted by sonar performance models) to simulate integrated system performance. These simulations are usually conducted in the context of a naval force that is set in opposition to a hypothetical threat force. The output data typically include exchange ratios, which are useful in determining force level requirements and in developing new tactics.

Sonar performance models use active and passive sonar equations to generate performance predictions. Mathematical models of propagation, noise and reverberation generate the input variables required for solution of these equations. This hierarchy of models was previously illustrated in Figure 1.1. Sonar performance models can logically be separated into active sonar models and passive sonar models, as would be suggested by the distinction between active and passive sonar equations.

The complexity of the sonar performance-modeling problem is a natural consequence of the naval operations that these models support. In modern

naval battle group operations, for example, TL must be calculated along a multiplicity of paths connecting widely separated sources and receivers. Noise interference from nearby consort vessels must be factored into sonar performance calculations together with distant merchant shipping and local weather noises. Furthermore, scattering and reverberation from bathymetric features and volumetric false targets must be efficiently and realistically modeled. The demands placed on computational efficiency and database management are enormous. Underwater acoustic modelers face challenges that severely tax existing mathematical methods. Moreover, with the advent of multistatic scenarios involving multiple sets of separated sources and receivers, true 3D modeling is no longer a theoretical luxury but rather a practical necessity.

This situation has become even more complex with the heightened interest in shallow-water sonar operations. Acoustic interactions with highly variable sea floor topographies and compositions further compound already intensive scattering and reverberation calculations. In addition, the sound-speed field in shallow-water areas is often characterized by high spatial and temporal variability. As a result, statistical approaches have been explored in order to obtain meaningful predictions of active sonar performance in shallow-water environments. In the MOCASSIN model, for example, Schneider (1990) provided the option to specify a stochastic sound speed field in order to approximate the horizontal variability typical of coastal regions.

10.2 Sonar equations

The sonar equations are simple algebraic expressions used to quantify various aspects of sonar performance. These equations vary according to active or passive sonars, and within active sonars they further differentiate according to noise or reverberation limited conditions. The various system and environmental parameters that make up the sonar equations are listed in Table 10.1 together with reference locations and brief descriptions. A condensed statement of the equations is presented below (Urick, 1983: chapter 2):

Active sonars (monostatic)

Noise background

$$SL - 2TL + TS = NL - DI + RD_N \quad (10.1)$$

Reverberation background

$$SL - 2TL + TS = RL + RD_R \quad (10.2)$$

Passive sonars

$$SL - TL = NL - DI + RD \quad (10.3)$$

Table 10.1 Sonar parameter definitions and reference locations

<i>Parameter</i>	<i>Symbol</i>	<i>Reference</i>	<i>Definition</i>
Source level	SL	1 m from source on its acoustic axis	$10 \log_{10} \frac{\text{intensity of source}}{\text{reference intensity}^a}$
Transmission loss	TL	1 m from source and at target or receiver	$10 \log_{10} \frac{\text{signal intensity at target or receiver}}{\text{signal intensity at 1 m}}$
Target strength	TS	1 m from acoustic center of target	$10 \log_{10} \frac{\text{echo intensity at 1 m from target}}{\text{incident intensity}}$
Noise level	NL	At hydrophone location	$10 \log_{10} \frac{\text{noise intensity}}{\text{reference intensity}^a}$
Receiving directivity index	DI	At hydrophone terminals	$10 \log_{10} \frac{\text{noise power generated by an equivalent nondirectional hydrophone}}{\text{noise power generated by actual hydrophone}}$
Reverberation level	RL	At hydrophone terminals	$10 \log_{10} \frac{\text{reverberation power at hydrophone terminals}}{\text{power generated by signal of reference intensity}^a}$
Recognition differential	RD	At display	$10 \log_{10} \frac{\text{signal power to just perform a certain function}}{\text{noise power at display}}$

Source: Adapted from Urlick, 1983; *Principles of Underwater Sound*, 3rd edn; reproduced with permission of McGraw-Hill Publishing Company.

Note

a The reference intensity is that of a plane wave of rms pressure $1 \mu\text{Pa}$.

In this application, recognition differential (RD) replaces detection threshold (DT) as used by Urick (1983, chapter 12). Dawe (1997) distinguished the modern usage of RD in sonar modeling from its obsolescent usage in relation to auditory detection. The concepts of DT and RD are related to each other through the level at which a signal can be detected for a given combination of probability of detection (P_D) and probability of false alarm (P_F). The difference between DT and RD relates to the location in the information-processing chain at which the threshold signal-to-noise ratio (SNR) is effectively measured. For DT, the SNR is measured at the receiver input terminals. For RD, the SNR is measured at the display.

Furthermore, RD has been subscribed in the case of active sonars to make it clear that this parameter is quantitatively different for noise (N) and reverberation (R) backgrounds. The sonar equations are valid for the condition in which the signal excess is zero. Beam pattern functions are implicitly included in the TL term. The apparent simplicity of the individual components of the sonar equations can be misleading. The complexity of these parameters will be better appreciated through the discussions to be presented in Sections 10.3 and 10.4. These equations are valid for sound levels in a 1-Hz wide frequency band (referred to as spectrum level). For frequency bands greater than 1 Hz, the sound levels in Equations (10.1), (10.2) and (10.3) must be corrected for bandwidth (e.g. Kinsler *et al.*, 1982: 409–17).

It is convenient in practical work to assign separate names to different combinations of terms in the sonar equations. A summary of commonly used terms is presented in Table 10.2. The combination of terms labeled FOM is the most useful because it combines environmental, sonar and target parameters into one convenient quantitative measure of sonar performance. Since the FOM quantitatively equals the TL under the conditions specified in the sonar equation, the FOM can give an immediate indication of the range at which active or passive sonars can detect targets provided that corresponding TL curves are available. When using the FOM in this manner, it should be stressed that the TL curves must match the ocean environment, acoustic frequency, sonar depth, target depth and other sonar parameters used in computing the FOM value. In the case of active sonars that are reverberation (versus noise) limited, the FOM is not constant but varies with range (time) and thus fails to be a useful indicator of active sonar performance.

The parameters listed in Table 10.1 can be related to the functions of basic acoustic models. Specifically, propagation models generate estimates of TL, noise models predict noise levels (NL) and reverberation models provide estimates of the RL. For passive sonars, the sonar equipment will define directivity index (DI) and RD while the target will define SL; TS is not considered in purely passive sonar models. For active sonars, the sonar equipment will define SL, DI and RD and the target will define TS.

Useful overviews of sonar signal processing have been assembled by Knight *et al.* (1981) and by Nielsen (1991). Vaccaro (1998) edited a collection

Table 10.2 Terminology of various combinations of the sonar parameters

<i>Name</i>	<i>Parameters</i>	<i>Remarks</i>
Echo signal level	$SL - 2TL + TS$	The intensity of the echo as measured in the water at the hydrophone
Noise-masking level	$NL - DI + RD_N$	Another name for these two combinations (noise-masking level and reverberation-masking level) is minimum detectable echo level
Reverberation-masking level	$RL + RD_R$	
Signal excess	$SL - 2TL + TS - (NL - DI) - RD_N$	Detection just occurs, under the probability conditions implied in RD_N , when the signal excess is zero. This expression pertains to a noise-limited active sonar
Performance figure	$SL - (NL - DI)$	Difference between the source level and the noise level measured at the hydrophone terminals
Figure of merit (FOM)	$SL - (NL - DI) - RD$	Equals the maximum allowable one-way TL in passive sonars, or the maximum allowable two-way TL in active sonars when $TS = 0$

Source: Adapted from Urick, 1983; *Principles of Underwater Sound*, 3rd edn; reproduced with permission of McGraw-Hill Publishing Company.

of papers that reviewed past progress and future challenges in underwater acoustic signal processing. Specific applications included sonar signal processing, time-delay estimation and underwater acoustic communications.

Bistatic geometries are characterized by a triangle of source, target and receiver positions. Bistatic sonar equations, which differ from their monostatic counterparts, are required. Cox (1989) carefully developed a set of bistatic sonar equations using energy forms to anticipate the wide variety of waveforms likely to be used in such bistatic systems. The following nomenclature is introduced to facilitate subsequent discussions (also refer to Figure 10.1):

c	speed of sound
R_M	monostatic range from target (T) to collocated source-receiver (S-R)
TL_M	monostatic transmission loss from target (T) to collocated source-receiver (S-R)
R_1	range from source (S) to target (T)
R_2	range from target (T) to receiver (R)
R_3	range from source (S) to receiver (R)
TL_1	transmission loss from source (S) to target (T)

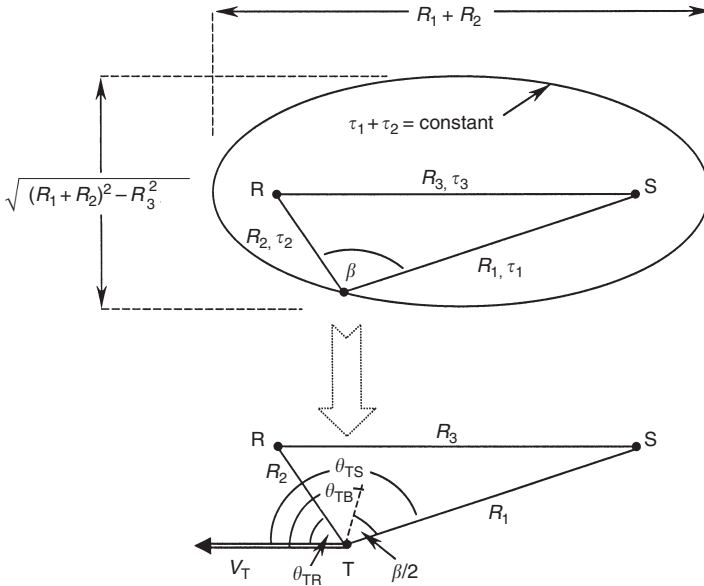


Figure 10.1 Bistatic geometry (adapted from Cox, 1989).

- TL₂ transmission loss from target (T) to receiver (R)
- TL₃ transmission loss from source (S) to receiver (R)
- τ₁ travel time from source (S) to target (T)
- τ₂ travel time from target (T) to receiver (R)
- τ₃ travel time from source (S) to receiver (R)
- V_T target velocity
- β bistatic angle (∠STR)
- θ monostatic aspect angle
- θ_E equivalent (bistatic) aspect angle
- θ_{TS} relative bearing of source (S) from target (T)
- θ_{TR} relative bearing of receiver (R) from target (T)
- θ_{TB} angle from target heading to bisector of β

By reference to Figure 10.1, the equivalent bistatic aspect angle (θ_E) is defined as

$$\cos \theta_E = \frac{\cos \theta_{TS} + \cos \theta_{TR}}{2} = \cos \theta_{TB} \cos \left(\frac{\beta}{2} \right) \tag{10.4}$$

The energy source level (ESL) is related to the intensity source level (SL) as

$$\text{ESL} = \text{SL} + 10 \log_{10} T \tag{10.5}$$

Table 10.3 Comparison of monostatic and bistatic sonar parameters (Cox, 1989)

<i>Parameter</i>	<i>Monostatic</i>	<i>Bistatic</i>
Time of arrival	circle: $2R_M/c$	ellipse: $(R_1 + R_2)/c$
Bistatic angle	0	β
Aspect angle	θ	θ_E
Doppler	$2(V_T/c) \cos \theta$	$2(V_T/c) \cos \theta_E$
Target strength	$f(\cos \theta)$	$f(\cos \theta_E)$
Transmission loss	$2TL_M$	$TL_1 + TL_2$

where T is the duration of the transmitted pulse. The echo energy level (EEL) received from the target at a hydrophone on the receiver array is then

$$EEL = ESL - TL_1 - TL_2 + TS \tag{10.6}$$

where TS is the target strength. The noise-limited signal excess (SE_N) can be defined as

$$SE_N = ESL - TL_1 - TL_2 + TS - N_0 + AG_N - \Lambda - L \tag{10.7}$$

where N_0 is the noise spectral level, AG_N the array gain against noise, Λ is the threshold on the SNR required for detection, and L is a loss term to account for time spreading and system losses.

Cox (1989) noted that the problem of estimating reverberation-limited bistatic sonar performance is more complicated than the monostatic case since it involves summing the contributions of a large number of scatterers ensonified by numerous propagation paths that differ in angle of incidence and position on the beam patterns of the source and receiver. Let R_0 represent the reverberation spectral level, then the signal excess can be written to anticipate both noise- and reverberation-limited cases as

$$SE = ESL - TL_1 - TL_2 - [(N_0 - AG_N) \oplus R_0] + TS - \Lambda - L \tag{10.8}$$

where \oplus represents power summation (Chapter 6, see Equation (6.1)).

Equations (10.7) and (10.8) do not include the effects of the direct blast. Analogies to the direct blast in monostatic sonars are the fathometer returns, which are the multiple surface- and bottom-reflected arrivals following each transmission. Comparisons of selected monostatic and bistatic parameters are presented in Table 10.3.

10.3 The NISSM model – a specific example

The Navy interim surface ship model (NISSM) II, developed by Weinberg (1973), is a computer program designed to predict the performance of active

monostatic sonar systems using ray-theoretical techniques. The measure of performance is expressed in terms of probability of detection versus target range for a given false-alarm rate. Selected intermediate results can also be displayed, including ray traces, TL, and boundary and volume reverberation. This model is applicable to range-independent ocean environments.

Navy interim surface ship model uses a cell-scattering model for reverberation. The most time-consuming phase in the execution of NISSM is the volume reverberation computation. The volume scattering strength is expressed in terms of a column (or integrated) scattering strength, and a careful integration of the volume reverberation integral is performed, which considers multipath structure.

Because the NISSM II model encompasses all the modeling categories addressed thus far, and because it has been widely used in the sonar-modeling community, it is considered to be representative of the more general class of active sonar models. Examples of selected NISSM outputs are also presented in this section.

10.3.1 Propagation

The depth-dependent sound speed $c(z)$ and the inclination angle (θ) at a point on a ray in the x - z plane can be related by Snell's law (see Figure 10.2) as

$$\frac{c(z)}{\cos \theta} = c_v$$

where $c(z)$ is the sound speed as a function of depth (z), θ the inclination angle and c_v the vertex sound speed. Snell's law implies that the range (x)

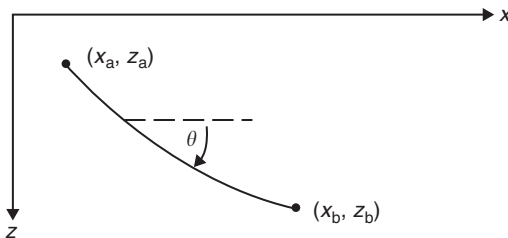


Figure 10.2 Ray geometry showing inclination angle along a ray, as used in the NISSM active sonar model (Weinberg, 1973).

and travel time (T) along the ray can be calculated as

$$x = x_a + \int_{z_a}^z \frac{c(z)|dz|}{\sqrt{c_v^2 - c(z)^2}} \quad (10.9)$$

$$T = T_a + \int_{z_a}^z \frac{c_v|dz|}{c(z)\sqrt{c_v^2 - c(z)^2}} \quad (10.10)$$

Officer (1958, chapter 2) provided a rigorous development of these equations.

The range derivative ($\partial x/\partial c_v$) is given by

$$\left. \frac{\partial x}{\partial c_v} \right|_{z=\text{const}} = \left. \frac{\partial x_a}{\partial c_v} \right|_{z=z_a} - \int_{z_a}^z \frac{c(z) c_v |dz|}{[c_v^2 - c(z)^2]^{3/2}} \quad (10.11)$$

(which equals zero at caustics) and is used in computing the geometrical spreading loss factor (η_{sp}):

$$\eta_{\text{sp}} = |p| = \left| c_v \tan \theta \tan \theta_0 x \frac{\partial x}{\partial c_v} \right|^{-1/2} \quad (10.12)$$

where θ_0 is the inclination angle of the ray at a point source of unit magnitude situated at $x_a = 0$, $z_a = z_0$.

The relative geometrical acoustic pressure field at field point (x, y) at time (t) is

$$p = \eta_{\text{sp}} e^{-i\omega(t-T)} \quad (10.13)$$

where $\omega = 2\pi f$ and f is the frequency.

Since the range, travel time and range-derivative integrals are symmetric with respect to the initial and final depths, it follows that the pressure satisfies the law of reciprocity. This law states that the acoustic pressure will remain unchanged if the source and receiver positions are interchanged. The sound-speed profile is approximated by a continuous function of depth (Weinberg, 1971) using Leroy's (1969) sound-speed formula. Earth curvature corrections are also applied.

The relative acoustic pressure along a ray is found by multiplying the relative geometrical acoustic pressure (p) by the surface, bottom and absorption loss factors:

$$p = \eta_{\text{sp}} (\eta_{\text{sur}})^{n_{\text{sur}}} (\eta_{\text{bot}})^{n_{\text{bot}}} e^{-i\omega t + i\omega T + i\Phi + \alpha S} \quad (10.14)$$

and the TL is given by

$$\text{TL} = -20 \log_{10} |p| \quad (10.15)$$

where $N_{\text{sp}} = -20 \log_{10} \eta_{\text{sp}}$ is the geometrical spreading loss (dB), $N_{\text{sur}} = -20 \log_{10} \eta_{\text{sur}}$ the surface loss per bounce (dB/bounce), n_{sur} the number

of surface bounces, $N_{\text{bot}} = -20 \log_{10} \eta_{\text{bot}}$ the bottom loss per bounce (dB / bounce), n_{bot} the number of bottom bounces, $A = -20 \log_{10}(\alpha) / \log_e$ (10) the absorption coefficient (dB km⁻¹), α the absorption in nepers per unit distance, t the elapsed time (s), T the travel time (s), Φ the accumulated phase shift (rad), S the arc length (km), $\omega = 2\pi f$ the radian frequency (rad s⁻¹) and f the acoustic frequency (Hz).

The surface loss may be input as a table of surface loss per bounce versus angle of incidence. The bottom loss may either be input as a table of bottom loss per bounce versus angle of incidence, or internally computed either by marine geophysical survey (MGS) data or by an empirical equation.

The absorption coefficient can be represented in one of three ways: (1) input as a table of absorption per unit distance versus frequency; (2) calculated by Thorp's (1967) equation; or (3) calculated by the equation attributed to H.R. Hall and W.H. Watson (1967, unpublished manuscript).

Eigenrays are found by tracing a preselected fan of test rays to the target depth. When two adjacent rays of the same type bracket a target range, a cubic spline interpolation is performed to determine the eigenray. The principal ray types were defined previously in Figure 4.2.

Shadow zone propagation is characterized according to Pekeris (1946) as

$$\left| p^2 \right| = \left| p_b^2 \right| \frac{x_b}{x} \exp[-\alpha(x - x_b)] \tag{10.16}$$

$$\alpha = \frac{5.93}{c_{\text{sur}}} g_{\text{sur}}^{2/3} f^{1/3}$$

where p is the pressure in the shadow zone at (x, z) , p_b the pressure on the shadow boundary at (x_b, z) , c_{sur} the surface sound speed (km s⁻¹), g_{sur} the surface sound speed gradient (s⁻¹) and f the frequency (Hz).

A uniform asymptotic expansion at a caustic is used to calculate the pressure in the vicinity of a caustic (Ludwig, 1966). Phase shifts are accumulated as follows: π radians decrease in Φ at the (pressure-release) surface; $\pi/2$ radians decrease in Φ at caustics; and zero phase shift at the (rigid) bottom. The computation of surface-duct propagation by ray theory does not allow for leakage from the surface layer into the underlying medium. Therefore, the AMOS equations are used (Marsh and Schulkin, 1955).

10.3.2 Reverberation

The basic theory for reverberation modeling was described in Chapter 9. Referring to Figure 10.3, the reverberation pressure at the end of the closed path is determined in NISSM as

$$\left| p_{\text{rev}} \right|^2 = \int_R \left| d_{\text{tra}} \eta_{\text{tra}}(\theta_{a,1}) p_1 p_2 \eta_{\text{rec}}(\theta_{a,2}) \right|^2 \mu \, dR \tag{10.17}$$

where $D_{\text{tra}} = 20 \log_{10} d_{\text{tra}}$ is the reference level of the transmitting array, $p_1 = -20 \log_{10} |p_1|$ the transmission loss of the incident ray,

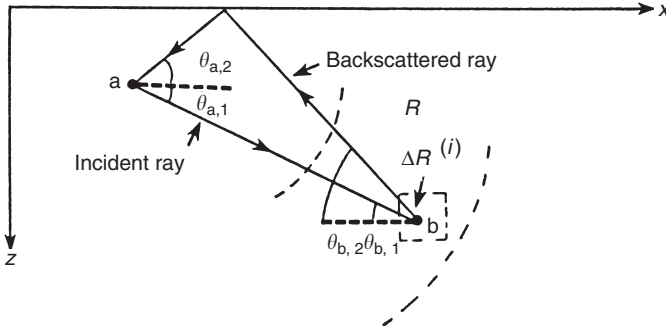


Figure 10.3 Closed ray path used in reverberation calculations in the NISSM active sonar model (Weinberg, 1973).

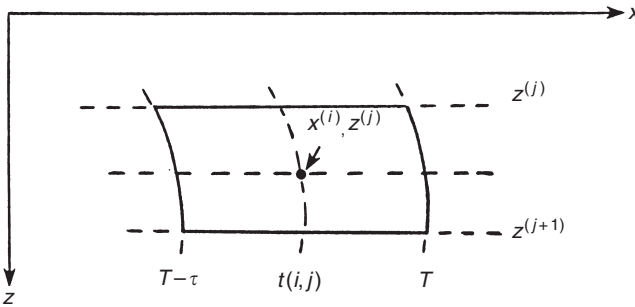


Figure 10.4 Ensonified region used in reverberation calculations in the NISSM active sonar model (Weinberg, 1973).

$P_2 = -20 \log_{10} |p_2|$ the transmission loss of the backscattered ray, $N_{tra} = -20 \log_{10} \eta_{tra}$ the transmitter response (dB), $N_{rec} = -20 \log_{10} \eta_{rec}$ the receiver response (dB), R the region containing the scatterers corresponding to rays with travel time (t): $T - \tau \leq t \leq T$, τ the pulse length (s), $T = t_0 + t_1 + t_2$; $0 \leq t_0 \leq \tau$, t_0 the initial time, t_1 the travel time of incident ray, t_2 the travel time of backscattered ray and μ the backscattering strength (volume, surface or bottom).

Navy interim surface ship model usually computes eight paths to each representative scatterer $[\Delta R^{(i)}]$. Thus, there may be as many as 56 (i.e. $8^2 - 8$) differently oriented closed paths per scatterer.

For volume reverberation, the expression for p_{rev} is replaced by the double summation (refer to Figure 10.4 for an illustration of the ensonified

region)

$$|p_{\text{vol}}|^2 = \sum_{i,j} \left| d_{\text{tra}} \eta_{\text{tra}} \left(\theta_{\text{a},1}^{(i,j)} \right) p_1^{(i,j)} p_2^{(i,j)} \eta_{\text{rec}} \left(\theta_{\text{a},2}^{(i,j)} \right) \right|^2 \mu_{\text{vol}}^{(i)} x^{(i)} \Delta x^{(i,j)} \Delta z^{(j)} \Delta \phi \quad (10.18)$$

where $\Delta \phi$ is the horizontal beamwidth (rad), $x^{(i)}$ the range of the (i, j) -th scatterer (km), $z^{(j)}$ the depth of the (i, j) -th scatterer (km) and $U_{\text{vol}}^{(i)} = 10 \log_{10} \mu_{\text{vol}}^{(i)}$ the volume scattering strength per unit volume of ocean.

The surface reverberation is calculated using an expression similar to that for p_{rev} (Equation (10.17)), except now $U_{\text{sur}} = 10 \log_{10} \mu_{\text{sur}}$ is the surface scattering constant per unit area of sea surface (dB) (Chapman and Harris, 1962).

Bottom reverberation is calculated in a manner analogous to that for surface reverberation, but where $U_{\text{bot}} = 10 \log_{10} \mu_{\text{bot}}$ is the bottom scattering constant per unit area of sea floor (dB) (Mackenzie, 1961).

The total reverberation is assumed to be the random-phase addition of surface and bottom echoes from directly above and beneath the sonar (also referred to as fathometer returns), together with volume, surface and bottom reverberation.

10.3.3 Target echo

Target echo (or echo signal level) at a particular time is determined by

$$|p_{\text{echo}}|^2 = \sum_i \left| d_{\text{tra}} \eta_{\text{tra}} \left(\theta_{\text{a},1}^{(i)} \right) p_1^{(i)} p_2^{(i)} \eta_{\text{rec}} \left(\theta_{\text{a},2}^{(i)} \right) \right|^2 \mu_{\text{tar}}^{(i)} \quad (10.19)$$

where $U_{\text{tar}} = 10 \log_{10} \mu_{\text{tar}}$ is the target strength. The summation is taken over all closed paths with round-trip travel times between $T - \tau$ and T .

10.3.4 Noise

Noise is separated into two components: self-noise and ambient noise. Assuming isotropic noise fields:

$$P_{\text{noise}} = 10 \log_{10} \left[\eta_{\text{DI}} \left(p_{\text{self}}^2 + p_{\text{amb}}^2 \right) \right] \quad (10.20)$$

where $\text{DI} = -10 \log_{10} \eta_{\text{DI}}$ is the directivity index (dB), $P_{\text{self}} = 20 \log_{10} p_{\text{self}}$ the self-noise spectrum density and $P_{\text{amb}} = 20 \log_{10} p_{\text{amb}}$ the ambient noise spectrum density.

10.3.5 *Signal-to-noise ratio*

Target echo to masking background, for a narrowband process, may be approximated by the signal-to-noise ratio (s/n):

$$s/n = \frac{\Delta f_{\text{echo}} p_{\text{echo}}^2}{\Delta f_{\text{noise}} p_{\text{noise}}^2 + \Delta f_{\text{rev}} p_{\text{rev}}^2} \quad (10.21)$$

where $P_{\text{echo}} = 20 \log_{10} p_{\text{echo}}$ is the target spectrum density at time T (dB), $P_{\text{rev}} = 20 \log_{10} p_{\text{rev}}$ the reverberation spectrum density at time T (dB), $P_{\text{noise}} = 20 \log_{10} p_{\text{noise}}$ the noise spectrum density at the beamformer output (dB), Δf_{echo} the equivalent bandwidth for the received echo (Hz), Δf_{rev} the equivalent bandwidth for the received reverberation (Hz) and Δf_{noise} the equivalent bandwidth for the received noise (Hz).

Assuming that the target echo is Gaussian distributed and centered about the receiving (Doppler shifted) frequency with a standard deviation of $\tau/2$, then

$$\Delta f_{\text{echo}} = \phi(\tau \Delta f) - \phi(-\tau \Delta f) \quad (10.22)$$

where Δf is the receiving bandwidth (Hz), τ the pulse length (s) and where the function $\phi(x)$ is defined as

$$\phi(x) = \frac{1}{\sqrt{2\pi}} \int_{-\infty}^x e^{-y^2/2} dy \quad (10.23)$$

is the normal probability function (e.g. Hassab, 1989; Burdic, 1991; Ziomek, 1995).

Reverberation is also assumed to be Gaussian with a standard deviation of $\tau/2$, but is centered about the transmitting frequency. Therefore, reverberation energy falling outside the echo band is $\Delta f_{\text{rev}} p_{\text{rev}}^2$, where

$$\Delta f_{\text{rev}} = \phi(2\tau \Delta f_{\text{Dop}} + \tau \Delta f) - \phi(2\tau \Delta f_{\text{Dop}} - \tau \Delta f) \quad (10.24)$$

and where

$$\Delta f_{\text{Dop}} = 2f \frac{V_{\text{cl}}}{c_s} \quad (10.25)$$

where Δf_{Dop} is the Doppler shift (Hz), f the frequency (Hz), V_{cl} the closing speed (km s^{-1}) and c_s the sound speed (km s^{-1}).

[Note that for passive systems, the factor of 2 in Equation (10.25) is removed.] If the noise-spectrum density can be considered constant over the receiving band, then

$$\Delta f_{\text{noise}} = \Delta f \quad (10.26)$$

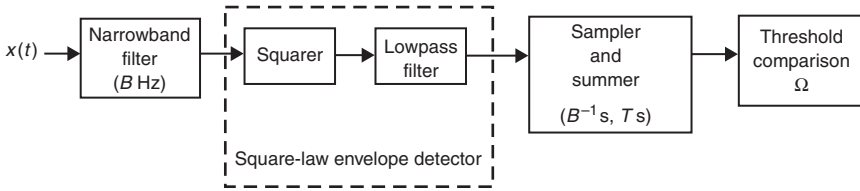


Figure 10.5 Narrowband detector employed in the NISSM active sonar model (Weinberg, 1973).

10.3.6 Probability of detection

Probability of detection is modeled using a narrowband, square-law envelope detector (Figure 10.5). The input $x(t)$ is assumed to be either a stationary zero-mean Gaussian signal, $s(t)$ and noise, $n(t)$, or noise alone. It is assumed that the signal spectrum has the same bandwidth as the narrowband filter and is centered on it, and that the noise is flat over the frequency interval. Samples of the squared-envelope, which are taken every $1/B$ seconds, are accumulated for an observation time of T seconds. The threshold (Ω) is fixed.

If P_F is a given probability of a false alarm, a quantity A is determined by inverting the following expression:

$$P_F = e^{-A} \sum_{m=0}^{M-1} \frac{1}{m!} A^m \tag{10.27}$$

where $M = BT + 1$. Once A is known, the probability of detection (P_D) is given by

$$P_D = e^{-A/(1+S/N)} \sum_{m=0}^{M-1} \frac{1}{m!} \left(\frac{A}{1+S/N} \right)^m \tag{10.28}$$

where S/N is the maximum value with respect to time of s/n at a particular target.

10.3.7 Model outputs

Navy interim surface ship model II can generate data appropriate for graphical presentation of ray diagrams, TL versus range reverberation (surface, bottom, volume and total) versus time, SNR versus range and probability of detection versus range. Sample outputs are illustrated for reverberation (Figure 10.6), SNR (Figure 10.7) and probability of detection

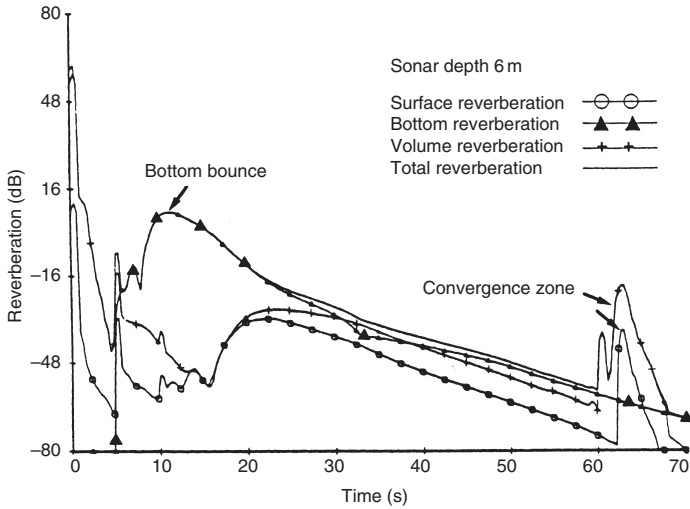


Figure 10.6 Sample reverberation versus time plot generated by the NISSM active sonar model. The bottom bounce contribution is readily visible in the bottom reverberation curve. The convergence zone contribution is evident in both the surface and volume reverberation curves (Weinberg, 1973). (The reverberation levels are reported here in dB re: 1 dyn cm^{-2} . To convert to levels in dB re: $1 \mu\text{Pa}$, add 100 dB to the levels shown in the figure.)

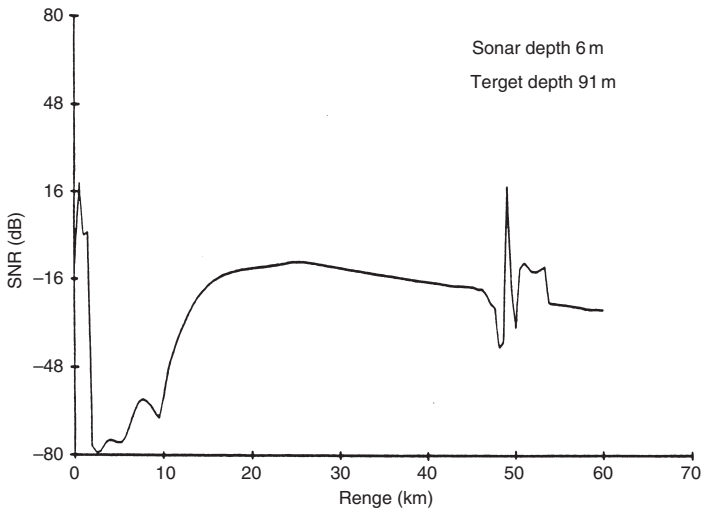


Figure 10.7 Sample signal-to-noise ratio (SNR) plot generated by the NISSM active sonar model based in part on the data presented in Figure 10.6 (Weinberg, 1973).

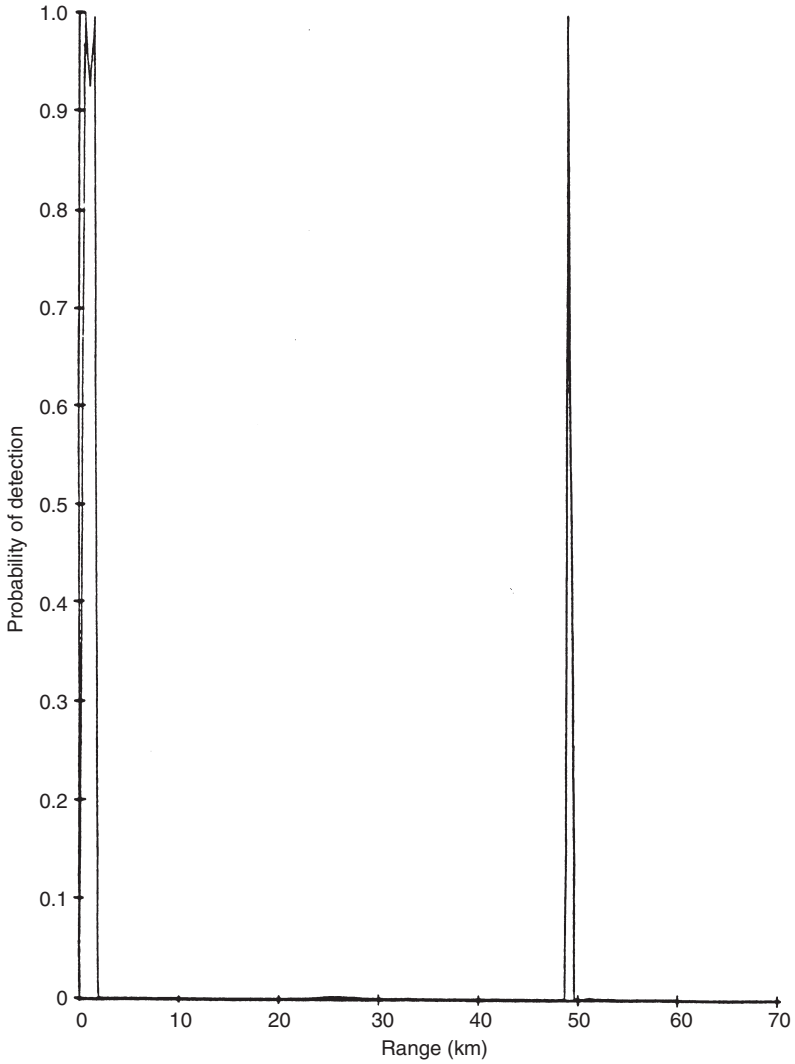


Figure 10.8 Sample probability of detection plot generated by the NISSM active sonar model based in part on the data presented in Figure 10.7 (Weinberg, 1973).

(Figure 10.8). Representative illustrations of ray diagrams and TL have already been presented elsewhere in this book. These examples are presented for illustrative purposes only and are not intended to portray a complete model run.

The reverberation versus time plots illustrated in Figure 10.6 are valid for a deep-water environment with a shallow sonic layer depth, a critical depth and sufficient depth excess to support convergence zone propagation, as well as surface duct and bottom bounce paths. At about 11 s, a strong bottom bounce return is evident in the bottom reverberation curve. At about 63 s, a strong CZ return is evident in both the volume and surface reverberation curves (but not in the bottom reverberation curve).

The SNR plot in Figure 10.7 indicates a high (positive) ratio at ranges corresponding to direct path (0–2 km) and convergence zone (near 50 km) detections. These sonar detection opportunities are vividly demonstrated in Figure 10.8. Here, high probabilities of detection are associated with direct-path and CZ ranges.

It is sometimes useful to plot different combinations of active sonar parameters on the same graph. From Table 10.2, for example, echo signal level can be plotted together with the noise and reverberation masking levels, as in Figure 10.9. With such information, signal excess as a function of range can be computed, as in Figure 10.10, which provides a direct indication of sonar detection performance. Specifically, all areas under the signal excess curve, but above the horizontal zero signal excess line, are associated

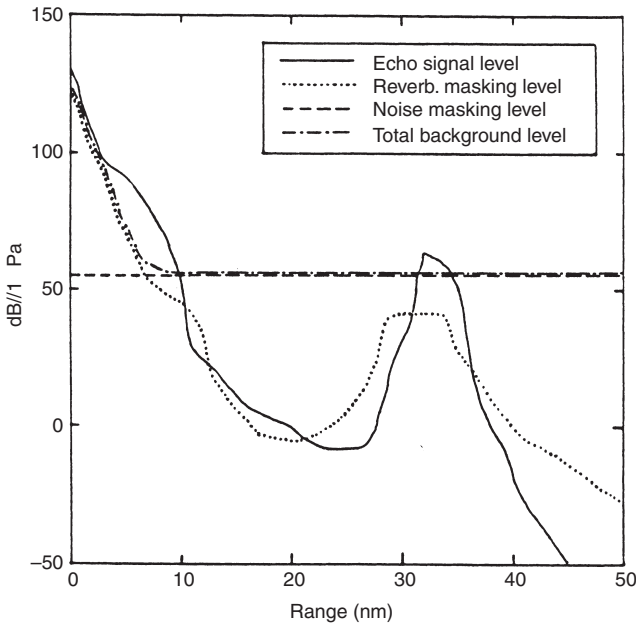


Figure 10.9 Sample graphical combination of selected sonar parameters. See Table 10.2 for an explanation of terms.

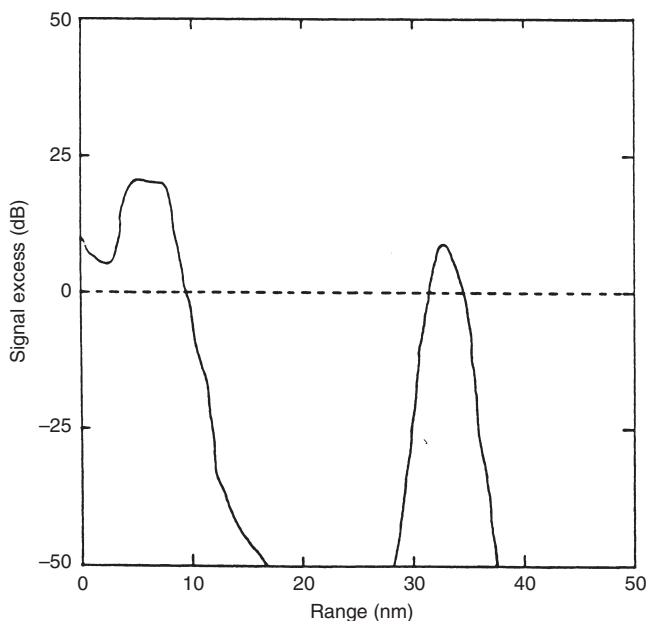


Figure 10.10 Signal excess as a function of range based on the data presented in Figure 10.9. Active sonar detection ranges are indicated by regions of positive signal excess.

with detection opportunities. That is, detection is accomplished when the signal excess is greater than, or equal to, zero. Thus, NISSM and similar models can provide graphic assessments of active sonar performance under the stated environmental and system-specific conditions. The intermediate quantities provide diagnostic tools for analyzing particular aspects of active sonar design and operation problems.

10.4 Model operating systems

The trend toward modular designs in the programming of underwater acoustic models is evidenced by continued interest in what are here termed model operating systems (MOS) (e.g. Eller, 1990; Holmes *et al.*, 1990). These systems provide a framework for the direct linkage of data-management software with computer-implemented codes of acoustic models. Such systems relieve model operators of much of the tedium associated with data entry operations.

Model operating systems facilitate comparative model evaluations (see Chapter 11) by standardizing the hardware and software configurations of different modeling techniques. The resulting uniformity also encourages

a higher degree of configuration management and thus assists in the process of model evaluation. Sonar trainers now commonly utilize sophisticated range-dependent acoustic models to generate realistic training environments for the operators of sonar equipment (Miller, 1982, 1983). Requirements for near-real-time program execution are frequently satisfied by using modular approaches similar to those employed in the construction of MOS.

In general, the development of sonar model operating systems is based on several considerations (Locklin and Webster, 1980): (1) it is assumed that the complex sonar performance modeling problem can be decomposed into a set of generic functions, each of which solves a well-defined and bounded portion of the overall problem (decomposition is a powerful technique to break down large problems into manageable units); (2) it is assumed that the problem can be solved on a computer through the use of an automated data system and that the development of this system can be accomplished such that its computational structure bears a precise relationship to the problem's decomposed functions; and (3) it is assumed that the functions implemented on a computer have the means to communicate with each other in a prescribed manner.

10.4.1 *System architecture*

Model operating systems fall into two general classes of software architecture: bundled and executive. The principal distinction between these two architectures concerns the packaging of the software and databases to meet specific modeling requirements. Bundled systems are tailored to a narrow range of modeling applications and, in general, have only one method implemented to perform a generic modeling function. Executive systems are tailored to respond to a broader range of modeling applications by allowing the user to interactively control the hierarchical selection of functions. Furthermore, executive systems allow for several methods of performing a single generic function, thus providing a dynamic formulation of a modeling application.

Two different modeling environments can be addressed by the MOS: research and production. These two environments are not different with respect to what computing functions are performed, but rather how the analyst uses the computing functions. This difference in usage should be reflected in the MOS architecture in order to provide the analyst with an optimized capability to perform both types of activities, if necessary. These environments are briefly discussed below to provide potential users with a perspective and a choice of the appropriate style of computing suitable to their specific needs.

The research environment entails activities such as experimentation, iterative problem solutions, computation of intermediate model results and model input sensitivity studies, among others. Practical applications include

sonar system design and environmental-acoustics research. This implies that the MOS must be highly interactive with respect to the interface between the analyst and the MOS, and usually suggests an executive architecture.

The production environment is typified by operations that are definable, structurally organized and ordered. To a large extent, these activities, once defined, have specific end products, solve a complete problem and are performed repetitively using the same (or slightly modified) functions. Practical applications include routine sonar performance predictions and sonar operational trainers. This implies that the computing tools can be organized and structured beforehand, and then used repetitively thereafter. It further indicates that a more optimal composition of functions may be needed, with less user interactive capability and less flexibility with respect to the computing function composition. This usually suggests a bundled architecture.

The functional organization of the MOS features a uniform way of viewing the system structure for solution of both the passive and active sonar equations. While these two problems are distinctly different, this need not imply that the active MOS and passive MOS must be constructed as two independent systems. Rather, the redundancy in system control software and in certain lower level functions common to both the active and passive sonar problems makes separate approaches less attractive. For illustrative purposes, a hypothetical functional decomposition of both the passive and active sonar equations will be described below.

10.4.2 Sonar modeling functions

A representative decomposition of the sonar equations into generic modeling functions is shown in the system data flows in Figure 10.11 for the passive sonar equation (Locklin and Webster, 1980) and in Figure 10.12 for the active sonar equation (Locklin and Etter, 1988). These particular decompositions are appropriate for incorporation into an executive architecture.

Although no decisionary logic options or looping controls are shown in these figures, a prerequisite processing sequence is nonetheless established. This sequence starts with an extraction process operating on databases that results in the generation of data sets specific to the analyst's application. In the case of passive sonars (Figure 10.11), subsequent calculations use the extracted data to develop the data sets required by either the beam noise (BN) or beam signal (BS) functions, which contribute to the final sonar performance (SP) function. This particular conceptual picture identifies three methods for generating BN, and two methods for generating BS, although a greater or lesser number of methods could be accommodated. This reflects the various levels of complexity possible in noise modeling and passive sonar system parameterization, respectively.

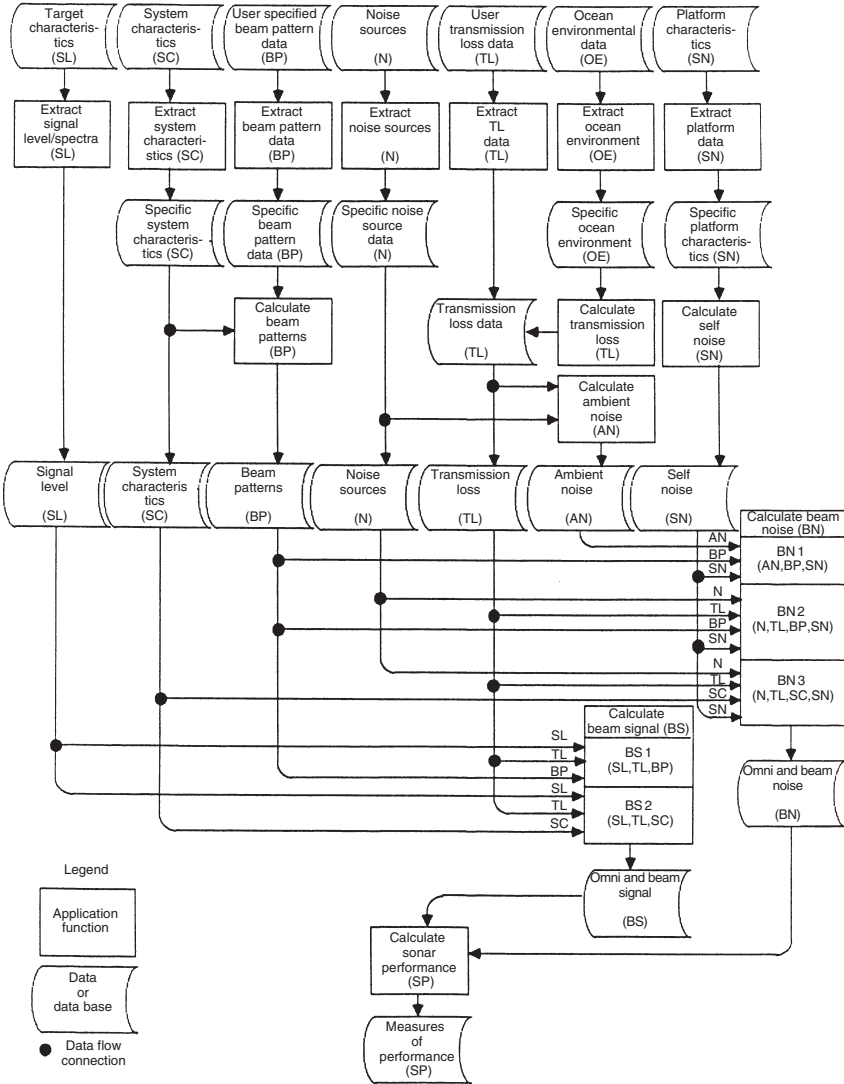


Figure 10.11 Sample acoustic modeling data flow concept showing model operating system application functions for the passive sonar equation (Locklin and Webster, 1980).

In the case of active sonars (Figure 10.12), the three key processes involve calculation of the echo signal level (ESL), the reverberation masking level (RML) and the noise-masking level (NML) for a specific active sonar configuration. The signal level/spectra (SL) function for target characteristics

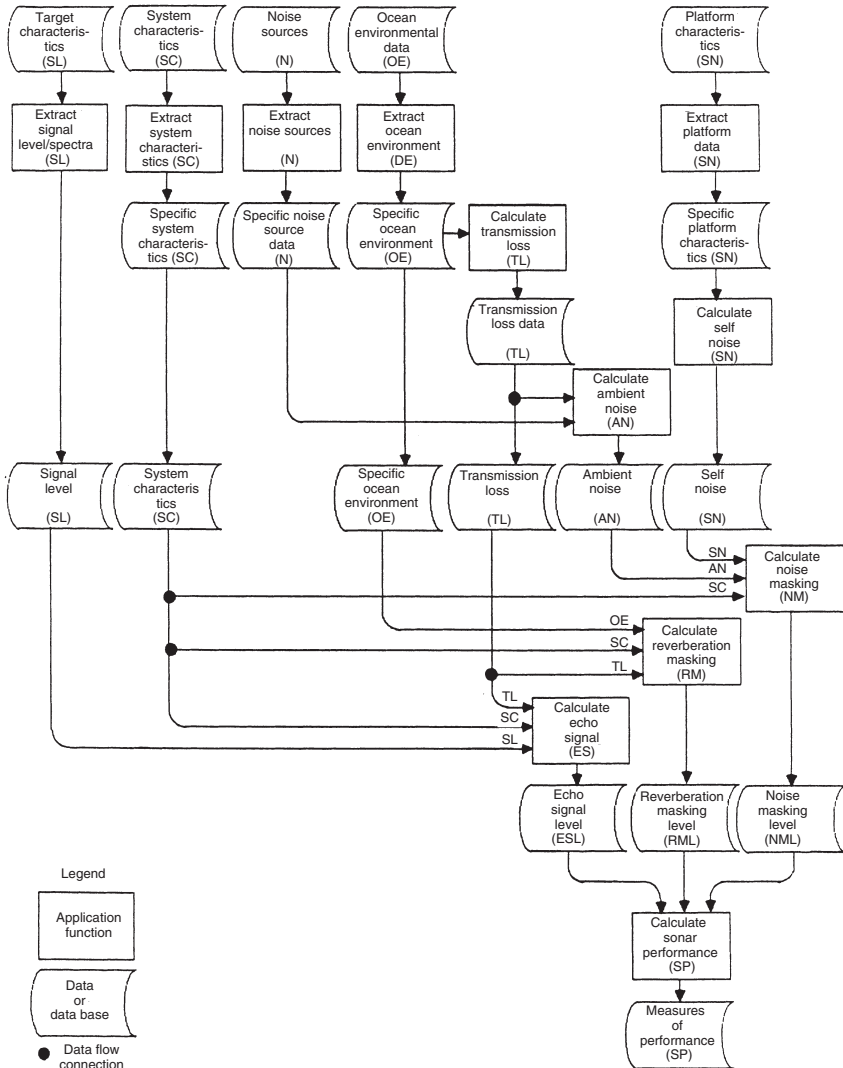


Figure 10.12 Sample acoustic modeling data flow concept showing model operating system application functions for the active sonar equation (Locklin and Etter, 1988).

describes the nature of the signal reflected from the target and considers the effects of target strength (TS), as specified in the active sonar equation. Furthermore, the beam pattern (BP) function is implicit in the system characteristics (SC) function. The final SP function would then contain the algorithms necessary to generate signal excess and probability of detection outputs.

An important consideration for Figures 10.11 and 10.12 involves the usage of “EXTRACT” and “CALCULATE,” and the symbols denoting application functions and data. “EXTRACT” implies such operations as database access, retrieval, reformatting and output in a standard form and includes the computational algorithms necessary to prepare the required data. “CALCULATE” implies that the primary emphasis is placed on some computational model or algorithm, with all input and output handled by standardized file interface utilities. The application functions shown in Figures 10.11 and 10.12 are the highest level of modularization envisioned in these particular representations. A further decomposition may be possible depending upon the particular requirements of the MOS. Each identified function would be associated with families of software application programs and associated data storage facilities.

10.4.3 *System usage*

Model operating systems, by design, facilitate and thus encourage the generation of multiple solutions for any given sonar performance problem. Divergent answers obtained from different models can alert the user to potential problems in either the problem specification or in the underlying physics of the model (i.e. a violation of the domains of applicability or an unexpected modeling pathology). Unexplained divergences can be graphically represented by envelopes illustrating the spread in predictions.

Many criteria drive the design of any particular MOS. Design decisions will likely entail tradeoffs between cost and ease of use, and between accuracy and understanding. Some degree of compromise will be involved. There is always the danger of “creeping elegance” in which product embellishments not contained in the original design specifications add to the life-cycle costs and delay the implementation schedule. There is also a common desire expressed by potential MOS users to obtain “all the information” generated by the models. While noble in principle, what is usually more important in practice is how the information is presented. Creative visualization techniques that logically combine essential information on a very few charts are highly desirable. The generation of high data volumes in 3D modeling, for example, necessitates the development of data fusion and animation techniques that permit the rapid assimilation and comprehension of complex acoustic interactions with dynamically changing ocean environments. Finally, documentation of MOS design and operation is essential for system maintenance and operator training.

10.4.4 *The generic sonar model – a specific example*

The GSM was designed to provide sonar system developers and technologists with a comprehensive modeling capability for evaluating the performance of (monostatic and bistatic) sonar systems and for investigating the ocean

environment in which these systems operate (Weinberg, 1981, 1985b). The development approach used a modular design, adhered to a strict programming standard, and implemented off-the-shelf software when practical. The generic sonar model is presently restricted to an ocean environment that is independent of range and time. In particular, the oceanic sound speed profile is layered, the surface and bottom are assumed to be horizontal reflecting boundaries, and sonar beam patterns are assumed constant over all azimuthal angles.

From a sonar system design standpoint, the significant capabilities of GSM include the modeling of passive signal excess versus range or frequency, active signal excess versus range, range and bearing errors versus range, low-frequency analysis and recording (LOFAR) diagrams, and autocorrelation and cross-correlation functions.

The next lower level of investigation involves computation of the signal, noise, reverberation, target echo and detection threshold. These, in turn, require inputs of ambient noise, self-noise, scattering strength profiles, scattering spectra, sonar system responses, SL, DI, filter equalizers and eigenrays.

10.4.5 *The comprehensive acoustic system simulation – a specific example*

A range-dependent (3D) version of GSM was developed by Dr Henry Weinberg, formerly with the Naval Undersea Warfare Center in Newport, Rhode Island (USA). This new system is designated CASS (comprehensive acoustic system simulation) (Weinberg *et al.*, 1997; Weinberg, 2000).

The CASS model simulates the performance of active sonar systems operating in the frequency range 600 Hz to 100 kHz. Weinberg (2000) traced the evolution of CASS from its genesis in CONGRATS, through NISSM, to GSM. The generic sonar modal used integral (or multipath-expansion) approaches such as FAME instead of the range-derivative and divided-difference algorithms that had been used in the earlier CONGRATS and NISSM models. Like CONGRATS and NISSM before it, GSM assumed a range-independent ocean environment.

In CASS, all environmental parameters can vary as functions of range, azimuth and frequency. Weinberg (2000) tabulated the 30 environmental-acoustics submodels, the 26 system submodels and the 22 sonar analysis submodels comprising CASS. The CASS model computes reverberation in the time domain by accounting for the leading and trailing scattering-cell reverberation times for all possible combinations of eigenrays. Signal excess is computed at each range step by first mapping the signal into the time domain and then selecting the peak signal-to-masking level, where the masking level represents the power summation of noise and reverberation. This approach implies that the selected signal level may not always represent the time-integrated pressure level (Keenan, 2000).

The propagation component of CASS is GRAB, which computes high-frequency (10–100 kHz) transmission loss in range-dependent, shallow-water environments. Favorable modeling results have been obtained for frequencies as low as 600 Hz. The GRAB model is based on Gaussian ray bundles, which are similar in form (but somewhat simpler) than Gaussian beams (Weinberg and Keenan, 1996; Keenan, 2000; Keenan and Weinberg, 2001). Eigenrays are found by power averaging test rays having the same path history (Keenan, 2000). The GRAB model is under configuration management by OAML (Keenan *et al.*, 1998).

10.5 Data sources and availability

Databases with which to support model development, evaluation and operation are available in a variety of formats. Many have automated data-retrieval features that make them attractive for application to model operating systems. Available automated oceanographic and acoustic databases have been identified and summarized by Etter *et al.* (1984). Two categories of data banks were described: primary data banks and modified data banks. Primary data banks contain original or modestly processed data (e.g. National Oceanographic Data Center, 1992). Modified data banks are distinguished by the fact that they modify or extrapolate data derived from primary data banks in order to satisfy operational requirements for compactness or for ease of handling (e.g. Naval Oceanographic Office, 1999). Parameter summaries for primary data banks are provided in Table 10.4. Not all of these data banks are fully documented, and some may not be available for use outside the custodian's facilities. This summary does not claim to be exhaustive.

The US Navy has established sets of databases as standards for use in sonar modeling. These databases are maintained in the oceanographic and atmospheric master library (OAML), which is chartered to provide fleet users with standard models and databases (Willis, 1992; Naval Oceanographic Office, 1999). A subset of these databases is available through the tactical oceanography wide area network (TOWAN). Selected TOWAN databases are summarized in Table 10.5 together with brief descriptions of their contents, temporal resolution, and spatial coverage and resolution. Related information on websites is provided in Appendix C. It should be noted that the US Navy strictly controls dissemination of the OAML databases.

The accessibility of many of these databases has been facilitated by the US Navy's technology transfer program. One such example is NEONS (naval environmental operational nowcasting system) developed by the Naval Research Laboratory (NRL). NEONS manages three types of environmental data: observations, images and gridded data (Schramm, 1993). The Naval Research Laboratory designed NEONS for compatibility with computer-industry and international data-exchange standards. NEONS supports civilian distribution of FNMOC data products via the Navy-NOAA oceanographic data distribution system (NODDS).

Table 10.4 Summary of primary data banks. Abbreviations and acronyms are defined in Appendix A

<i>Data bank</i>	<i>Custodian</i>	<i>Representative database parameters</i>
FNMOC data files http://www.fnmoc.navy.mil/	FNMOC <i>Marine meteorology</i> <ul style="list-style-type: none"> • Solar radiation • Clouds • Surface pressure 	<ul style="list-style-type: none"> • Precipitation • Surface air temperature • Surface marine winds • Total heat flux • Sensible and evaporative heat fluxes
	<i>Oceanography</i> <ul style="list-style-type: none"> • Wave direction, period and height • Combined sea height direction and period • Significant wave height • Swell direction, period and height • White caps 	<ul style="list-style-type: none"> • Insolation, reflected radiation • Sensible and evaporative heat flux • Total heat flux • Bathymetry • Shipping density • Operational bathy-thermograph observations • MBT, XBT, STD, hydrocasts • Sea-surface temperature • Sea-surface temperature anomaly • Potential mixed layer depth • Primary layer depth • Temperature at the top of the thermocline • Thermocline gradient
DoD Bathymetric Data Library http://www.nima.mil/	NIMA <ul style="list-style-type: none"> • Ocean floor depth 	

(Continued)

Table 10.4 (Continued)

<i>Data bank</i>	<i>Custodian</i>	<i>Representative database parameters</i>
NAVOCEANO data files http://www.navy.mil	NAVOCEANO	<ul style="list-style-type: none"> • Bathymetry • Climatology • Temperature/salinity/oxygen versus depth • Computed sound speed, sigma-t, specific volume • Conductivity • Transmission loss • Ambient noise • Volume reverberation • Bottom loss • Surface currents • Subsurface currents • Ice type/thickness • Core samples • Sediment samples • Geomagnetics • Seismic profiles • Gravity • Dangerous marine animals • Boring / fouling organisms • Plankton • Bioluminescence
NCDC Marine Climatic data files http://hwf.ncdc.noaa.gov/oa/ncdc.html	NOAA / NCDC	<ul style="list-style-type: none"> • Air temperature • Pressure • Waves • Dew point temperature • Sea-surface temperature • Low clouds • Total Clouds • wind • Visibility
NGDC Marine Geology and Geophysics data files http://www.ngdc.noaa.gov/	NOAA/NGDC	<ul style="list-style-type: none"> • Airborne magnetic survey (elements D, I, F) • Marine magnetic survey (total intensity F only) • Megascopic core description, marine geological sample index, grain size analysis • Digital hydrographic survey • Summary bathymetric and topographic files • Marine bathymetry • Seismic profiles • Marine gravity
NODC data files http://www.nodc.noaa.gov/	NOAA/NODC	<ul style="list-style-type: none"> • Marine meteorological parameters • Temperature • Salinity • Computed sound speed • Marine chemical parameters • Surface currents

Table 10.5 Databases from the US Navy TOWAN. Abbreviations and acronyms are defined in Appendix A

<i>Database</i>	<i>Contents</i>	<i>Temporal resolution</i>	<i>Spatial coverage/resolution</i>
High-frequency bottom loss (HFBL)	Bottom loss versus grazing angle ($1.5 \text{ kHz} < f < 4 \text{ kHz}$)	Fixed	Global / 5' latitude and longitude
Low-frequency bottom loss (LFBL)	Reflective and refractive characteristics of ocean bottom (bottom loss versus grazing angle) ($f < 1 \text{ kHz}$)	Fixed	Global / 5' latitude and longitude
Generalized digital environmental model (GDEM)	Steady-state digital model of ocean temperat. Gridded sets of coefficients are used with 1D linear or cubic spline interpolation in time to generate vertical profiles from the surface to the bottom where $z_B \geq 100 \text{ m}$	Seasonal	Global / 30' latitude and longitude
Historical wind speed (HWS)	Ocean surface wind-speed and direction statistics based on analysis of historical data collected from 1946 to 1986. Data derived from NCDC Historical / Marine data. Data prior to 1980 derived from COADS	Monthly	Global / 1° latitude and longitude
Digital bathymetric data base – variable resolution (DBDB-V)	Combination of different resolution gridded bathymetric databases	Fixed	Global / variable resolution (0.5, 1, 2 or 5' latitude and longitude)
Volume scattering strength (VSS)	Column scattering strengths at selected frequencies.	Fixed	Northern hemisphere / 0.75° latitude and longitude
Shipping Noise – High Resolution (SNHR)	Estimated omnidirectional shipping noise and spectra for a receiver depth of 100 m at a nominal frequency of 50 Hz. Spectral range is 10–1,000 Hz for predominantly under-ice areas and 25–15,000 Hz for predominantly open-water areas	Seasonal	Northern hemisphere / 5' latitude and longitude
Shipping Noise – Low Resolution (SNLR)	Estimated omni/horizontal directional shipping noise, spectra and statistics for receiver at 100 m at a nominal frequency of 50 Hz Ambient noise below 300 Hz is derived from industrial and natural sources (e.g. oil rigs, ice)	Seasonal	Northern hemisphere / 5° latitude and longitude
Historical Temporal Shipping (HITS)	Shipping densities (fishing vessels, merchants, tankers, large tankers, and super tankers)	Monthly	Global / 1° latitude and longitude
ICECAP	Ice thickness characteristics and ice keel distribution	Seasonal (spring / fall)	Arctic / 60-nm grid cells

Source: Tactical oceanography wide area network (TOWAN) <http://www7180.nrlssc.navy.mil/homepages/TOWAN/towanpgs/TOWANDataIndex.html>.

Note

f = frequency; z_B = bottom depth; nm = nautical mile.

Ocean Acoustic Developments Ltd (1999a) created the WADER global ocean information system, which is based on DBDB5 bathymetry (an OAML database) and the Levitus temperature-salinity data (a NOAA dataset discussed previously in Chapter 2).

Clancy (1999) and Clancy and Johnson (1997) provided useful overviews of naval operational ocean data products. In particular, Clancy and Johnson (1997) identified and briefly described meteorological models (NOGAPS, NORAPS, LABL), ocean thermal models (OTIS, MODAS), ocean thermodynamics and circulation models (TOPS, SWAFS), ocean waves and surf models (WAM, SWAPS), a sea-ice model (PIPS) and a tide and surge model (TSPS). The meteorological models drive the ocean models, which, in turn, synthesize useful operational products from disparate and spatially sparse oceanographic data. The oceanographic models can then drive underwater acoustic models to simulate sonar performance.

10.6 Numerical model summaries

Available sonar performance models (subcategorized as active sonar models, MOS and tactical decision aids) are summarized in Table 10.6. Numbers within brackets following each model refer to a brief summary and appropriate documentation. Model documentation can range from informal programming commentaries to journal articles to detailed technical reports containing a listing of the actual computer code. Abbreviations and acronyms are defined in Appendix A. This summary does not claim to be exhaustive.

The majority of the active sonar models listed in Table 10.6 are intended for use in ASW scenarios, although four of these models (CASTAR, MINERAY, SEARAY and SWAT) were designed for use in mine-hunting scenarios.

Model-operating systems provide a framework for the direct linkage of data-management software with computer-implemented codes of acoustic models, thus facilitating the construction of versatile simulation capabilities. Model-operating systems are further distinguished from stand-alone active sonar performance models by virtue of their ability to conduct sensitivity analyses by computing components of the active-sonar equation using alternative solution techniques. Since sonar model operating systems normally utilize existing underwater acoustic models and standard oceanographic databases, these systems are unique only in the sense of the number and types of models and databases included, and the particular architectures, GUIs and other features employed.

Tactical decision aids, a newly introduced subcategory, represent a form of engagement-level simulation that blends environmental information with tactical rules. These decision aids guide system operators and scene commanders in planning missions and allocating resources by exploiting knowledge of the operating environment.

Table 10.6 Summary of sonar performance models including active sonar models, model-operating systems and tactical decision aids

<i>Active sonar models</i>		<i>Model operating systems</i>	<i>Tactical decision aids</i>
Active RAYMODE [1]	LORA [11]	CAAM [20]	IMAT [25]
ALMOST [2]	MINERAY [12]	CASS [21]	NECTA [26]
ASPM [3]	MOCASSIN [13]	GSM – Bistatic [22]	
CASTAR [4]	MSASM [14]	HydroCAM [23]	
CONGRATS [5]	NISSM-II [15]	PRISM [24]	
GASS [6]	SEARAY [16]		
HODGSON [7]	SONAR [17]		
INSIGHT [8]	SST [18]		
INSTANT [9]	SWAT [19]		
LIRA [10]			

Notes

Sonar performance – active sonar models

- 1 Active RAYMODE, which is based on the passive RAYMODE propagation model, also considers surface, bottom and column scattering strengths to calculate reverberation (Medeiros, 1982b, 1985b; Smith, 1982; Naval Oceanographic Office, 1991b,d).
- 2 ALMOST, which was developed for the Royal Netherlands Navy, is a complete sonar performance prediction model for active and passive systems. ALMOST contains three modules: PROPLOSS for transmission loss; REPAS for passive sonar range predictions; and REACT for active sonar range predictions. The transmission-loss component is based on range-dependent ray tracing (Schippers, 1995). As part of the European MAST III project, an ambient noise time signal model was implemented in the ALMOST software package. The ambient noise is assumed to be generated at the surface by wind, rain or shipping. Biological sources are not included (Schippers, 1998). When sediment conditions warrant, bottom propagation (versus bottom-reflection loss) can be incorporated by using the MULTIPAD model (Schippers, 1996). Further enhancements to ALMOST include bistatic calculations of reverberation and echo level. Doppler receiver-band and target-structure highlights are also available as inputs to monostatic and bistatic calculations (P. Schippers, 2002, private communication). [Dreini *et al.* (1995) compared the TL component of ALMOST with similar models.]
- 3 ASPM is a system of prediction tools used to predict the performance of active and passive acoustic systems over a wide range of environmental conditions, including littoral regions, in support of system concept evaluation, advance deployment planning, and at-sea operational or exercise support (Berger *et al.*, 1994).
- 4 CASTAR predicts the performance of mine-hunting sonars (Naval Oceanographic Office, 1999).
- 5 CONGRATS is an active sonar model constructed in several segments: I – ray plotting and eigenray generation (Weinberg, 1969); II – eigenray processing (Cohen and Einstein, 1970); and III – boundary and volume reverberation (Cohen and Weinberg, 1971).
- 6 GASS is a simulator/stimulator for air ASW systems trainers. GASS contains an environmental–acoustics (EVA) server that provides underwater acoustic propagation, noise and reverberation characteristics based on US Navy standard acoustic models (ASTRAL and ANDES) and environmental databases from OAML. These characteristics are provided in the form of parameters that control the generation and propagation of time-series signals in other parts of GASS. The models used are range-dependent, and seamlessly support a wide operating envelope in frequency, range and water depth. The EVA server was designed to be responsive to real-time systems and therefore should be suitable for a wide range of other acoustic prediction, simulation and modeling applications (US Navy Air ASW Project Office, 1996a,b).

- 7 HODGSON, which was originally developed by Lt Cdr J. M. Hodgson of the Royal Navy, treats a fully range-dependent (sound speed and bathymetry) ocean environment. The TL component is based on range-dependent ray tracing (UK Ministry of Defence, 1995). The UK Ministry of Defence has formally validated the propagation model for both shallow and deep water. HODGSON also contains a reverberation module that computes surface and bottom reverberation. This model is available commercially from Ocean Acoustic Developments Ltd. [Dreini *et al.* (1995) compared the TL component of HODGSON with similar models.]
- 8 INSIGHT is a PC-based model with a GUI interface. It computes signal excess for both active and passive sonars in range-independent ocean environments. INSIGHT incorporates a full ambient noise model for wind, shipping and rain noise, including propagation effects. The model has recently been upgraded with improved calculations of reverberation for both monostatic and bistatic sonar configurations. INSIGHT does not compute echo level and reverberation in the time domain. Rather, it calculates the associated energy flux density levels and displays signal excess versus target position or other user-selected parameter (Harrison *et al.*, 1990; Packman *et al.*, 1992; Ainslie *et al.*, 1994, 1996; Ainslie, 2000).
- 9 INSTANT computes transmission loss in range-dependent ocean environments using a hybrid of ray and mode concepts. The formulation is based on the conservation of energy flux and the exploitation of the ray invariant to model weak range dependence (Packman *et al.*, 1996). INSTANT calculates echo and reverberation levels for monostatic and bistatic sonar configurations, although the bistatic option is restricted to range-independent environments. Volume reverberation is not computed in INSTANT. A version of the CANARY noise model (referred to as CANARD) is used to estimate range-dependent noise (Ainslie, 2000).
- 10 LIRA is an extension of LORA to predict the performance low-, mid- and high-frequency active sonars (Hoffman, 1979). The source and receiver may be separated in depth.
- 11 LORA is an extension of FAST NISSM, the utility version of the NISSM model. LORA predicts the performance of monostatic active sonar systems, either hull-mounted or towed (Hoffman, 1976).
- 12 MINERAY was initially developed in the 1970s to predict the performance of submarine minehunting sonars. There are three distinct generations of the MINERAY model. The first generation (1970s) was appropriate for modeling high-frequency sonars in deep-water environments. The second generation (mid-1980s) was extended to allow multipath sound propagation via bottom and surface bounces (Jaster and Boehme, 1984). The third generation (mid-1990s) has been extended to support modeling in littoral environments (Bailey *et al.*, 1997).
- 13 MOCASSIN predicts the performance of active sonars operating in range-dependent shallow waters that are characterized by highly variable sound-speed conditions (Schneider, 1990). Stochastic sound-speed variability in the horizontal is modeled by a diffusion approximation. Reverberation is computed and stored separately for the sea surface and ocean bottom.
- 14 MSASM assesses the effectiveness of air-deployed, multistatic-acoustic sonobuoy fields (Navy Modeling and Simulation Management Office, 1999).
- 15 NISSM – II computes propagation and reverberation (Weinberg, 1973). [The NISSM model is discussed in detail in Section 10.3.]
- 16 SEARAY models the acoustic environment by using ray-tracing techniques to determine sound paths in a horizontally stratified water column. The SNR along each path is determined by calculating directivity, absorption, spherical spreading loss and the effects of various noise sources, and then applying the active sonar equation (Tuovila, 1989). SEARAY is derived from the MINERAY model.
- 17 SONAR is designed to compute eigenrays in ocean environments where the bottom profiles consists of a series of plane segments with slopes entirely in the vertical plane (Marsh and Poynter, 1969; Bertuccelli, 1975). Reverberation is computed using the cell scattering formulation.
- 18 SST is a set of object-oriented software components and software-development tools for building sonar simulators (virtual oceans) that “sound” like a real ocean to an existing or proposed sonar system. SST-based simulators produce a digital representation of the predicted signal, which includes random fluctuations with controlled statistical properties (Goddard, 1989, 1994).

- 19 SWAT was developed to support mine-countermeasure (MCM) sonars (Sammelmann, 1998). SWAT actually comprises two models: one for detection sonars and one for classification sonars. The detection model is hosted on a personal computer and is designated PC SWAT. The classification model is designed to run on a workstation and is referred to as SWAT. Inputs and commands are menu driven in PC SWAT. Surface and bottom reverberation are computed by considering the multipath contributions, which are important in shallow and very shallow littoral environments. A three-dimensional, coherent acoustic scattering model of mines is also incorporated. Both PC SWAT and SWAT include the latest high-frequency environmental models (Applied Physics Laboratory, University of Washington, 1994).

Model operating systems

- 20 CAAM is a flexible R&D tool for sonar technologists (Navy Modeling and Simulation Management Office, 1999). It integrates the OAML environmental databases (Naval Oceanographic Office, 1999) together with selected propagation models including PE, ASTRAL and RAYMODE.
- 21 CASS is a model architecture developed to support passive and active sonars with moderate fidelity in wide frequency bands (Weinberg, 2000). (CASS is discussed in Section 10.4.4.)
- 22 GSM is a modularized computer program that calculates passive and active sonar system performance in range-independent ocean environments (Weinberg, 1982, 1985b). GSM has been extended to include a bistatic active signal excess model (Powers, 1987). Version G (updated through December 1996) removed unsupported propagation models (RAYMODE, FACT and MULE) and added bistatic scattering strength tables, among other features. (GSM is discussed in Section 10.4.4.)
- 23 HydroCAM was developed to predict the detection and localization performance of hydroacoustic monitoring networks in support of the international monitoring system (Farrell and LePage, 1996).
- 24 PRISM is an interactive sonar performance model used to evaluate the acoustic performance of mobile sonar systems in various ocean environments. (Chaika *et al.*, 1979). The original version of PRISM contained range-independent transmission loss models including the FACT, RAYMODE, Normal Mode (Newman and Ingenito, 1972) and LORA models.

Tactical decision aids

- 25 IMAT was developed to integrate training, operational preparation, tactical execution and postmission analysis into a seamless support system (Ellis and Parchman, 1994; Wetzel-Smith *et al.*, 1995; Wetzel-Smith and Czech, 1996; Foret *et al.*, 1997; US Department of the Navy, 1999; Beatty, 1999).
- 26 NECTA supports oceanographic and environmental data analysis as well as sensor performance predictions. The open and modular design of the system allows the ready inclusion of additional environmental data and tactical guidance to meet changing demands (BAeSEMA Ltd, 1998).

11 Model evaluation

11.1 Background

Model evaluation is defined as the systematic gathering and promulgation of information about models in order to determine model limitations and domains of applicability. Model evaluation should be viewed as a process rather than a specific result.

The intent of this chapter is not to furnish a compendium of evaluation results but rather to describe the evaluation process itself. Such a description can provide useful insights into the benefits and shortcomings of model evaluation. The fundamental steps involved in the evaluation process will be described and only a select number of examples will be used to further illustrate the process.

At first glance, the process of model evaluation might appear to be very straightforward. When examined more closely, however, a number of factors are seen to complicate and frustrate the process. To be credible, the evaluations must be based on statistically comprehensive comparisons with benchmark data. Such benchmark data can include field measurements, outputs from other models or closed-form analytical solutions. Each of these data sources has limitations. Field measurements are quite limited with regard to temporal, spatial and spectral coverage. Furthermore, these data sets are sometimes classified on the basis of national security concerns. Outputs from other models are useful only when those models themselves have been properly evaluated. Analytical solutions can provide very accurate, albeit idealistic, comparisons for a relatively small number of useful problems.

Model development is an evolving process. Any particular version of a model quickly becomes outdated and the attendant evaluation results become obsolete. Therefore, comparisons of model accuracy are valid only for the particular model version tested. To ignore progress in model developments gained through previous evaluation experiences is to do an injustice to those models. Accordingly, only the most recent and authoritative evaluation results should be considered when assessing models.

Rivalries among different governmental, academic and industrial laboratories frequently add a political dimension to the model evaluation process.

Many of the well-known models have gained their notoriety, in part, through the zealous advocacy of their developers and sponsors.

Clearly what is needed then is an autonomous clearinghouse to provide for both the unbiased evaluation of models and the timely promulgation of the results. An intermediate step in this direction was taken by the naval sonar modeling community through the establishment of configuration management procedures. These procedures provided a disciplined method for controlling model changes and for distributing the models (together with selected test cases) to qualified users. Configuration management comprises four major activities: (1) configuration identification and use of a product baseline; (2) configuration change control; (3) status accounting and documentation of all product changes; and (4) reviews, audits and inspections to promote access to information and decision-making throughout the software life cycle.

The US Chief of Naval Operations established the oceanographic and atmospheric master (OAML) in 1984. The OAML is chartered to provide fleet users with standard models and databases while ensuring consistent, commonly based environmental service products (Willis, 1992).

11.2 Past evaluation efforts

Comprehensive model evaluation efforts in the past have been very limited. Notable efforts have been sponsored by the US Navy, but these efforts have focused largely on propagation models. None of these efforts is presently active and their results are therefore only of limited academic interest. All of these efforts were successful in addressing the immediate concerns at the time, but were unsuccessful in the longer term due to the evolutionary nature of model developments and the lack of widely accepted evaluation criteria. It is instructive, nonetheless, to review these past efforts.

The model evaluation program (MEP) was administered by the (now defunct) acoustic environmental support detachment (AESD) under Office of Naval Research (ONR) sponsorship. Emphasis was placed on model-to-model comparisons and the evaluation results were not widely disseminated.

A methodology for comparing acoustic-propagation models against both other models and measured data was developed by the panel on sonar system models (POSSM). POSSM was administered by the Naval Underwater Systems Center (NUSC) and was sponsored by the US Naval Sea Systems Command (Lauer and Sussman, 1976, 1979). Some of these results will be discussed later in this chapter. Among the many observations made by POSSM was the lack of documentation standards for acoustic models (Lauer, 1979).

In an effort to promote standardization, the US Navy established the acoustic model evaluation committee (AMEC) in 1987. The specific charter of AMEC was to develop a management structure and administrative procedures for the evaluation of acoustic models of propagation, noise

and reverberation, although initial attention was restricted to propagation models. Specific evaluation factors included model accuracy, running time, core storage, ease of effecting slight program alterations and available ancillary information. The activities of AMEC culminated in evaluation reports for two propagation models: FACT and RAYMODE. As a result of AMEC's activities, RAYMODE was designated the (interim) Navy standard model for predicting acoustic propagation in the ocean. Subsequently, AMEC was disbanded.

More recent publications have proposed various theoretical and practical procedures for model evaluation (McGirr, 1979, 1980; Hawker, 1980; Pedersen and McGirr, 1982). Additional evaluation studies have been described for both propagation models (Hanna, 1976; Eller and Venne, 1981; Hanna and Rost, 1981) and reverberation models (Eller *et al.*, 1982). Spofford (1973b), Davis *et al.* (1982) and Chin-Bing *et al.* (1993b) reported practical test cases suitable for all types of propagation models. In May 1994, the ONR conducted a reverberation workshop in Gulfport, Mississippi (USA). The purpose of this workshop was to assess the fidelity of low-frequency (30–400 Hz) scattering and reverberation models. Six test cases comprising either field-measurement data sets or analytic problems with known reference solutions were used to establish the accuracy and state of current reverberation model development. Uniform plot standards facilitated intercomparison of test-case results. The results of this workshop are to be published in a proceedings volume.

11.3 Analytical benchmark solutions

In the absence of comprehensive experimental data, underwater acousticians have explored the use of analytical benchmark solutions to assess the quality of numerical models (Felsen, 1986; Jensen, 1986; Jensen and Ferla, 1988; Robertson, 1989). Such benchmarks emphasize idealized but exactly solvable problems. In the case of propagation models, two benchmark problems have been investigated in detail: (1) upslope propagation in a wedge-shaped channel and (2) propagation in a plane-parallel waveguide with range-dependent sound-speed profile (Felsen, 1987). These two problems are illustrated in Figures 11.1 and 11.2, respectively (Jensen and Ferla, 1988, 1990).

A special series of papers coordinated by the Acoustical Society of America described the results of a concerted effort to apply standard benchmark problems (with closed-form solutions) to the evaluation of propagation models. The propagation models selected for evaluation were based on different formulations of the wave equation (Buckingham and Tolstoy, 1990; Collins, 1990b; Felsen, 1990; Jensen and Ferla, 1990; Stephen, 1990; Thomson, 1990; Thomson *et al.*, 1990; Westwood, 1990). The results of this evaluation provided several important insights (Jensen and

Parameters common to all three cases

- Wedge angle: $\theta_0 = \arctan 0.05 \approx 2.86^\circ$
- Frequency: $f = 25 \text{ Hz}$
- Isovelocity sound speed in water column: $c_1 = 1,500 \text{ m s}^{-1}$
- Source depth: 100 m
- Source range from the wedge apex: 4 km
- Water depth at source position: 200 m

Pressure-release surface

- Case 1: *Pressure-release bottom.* This problem should be done for a line source parallel to the apex, i.e. 2D geometry.
- Case 2: *Penetrable bottom with zero loss.*
 Sound speed in the bottom: $c_2 = 1,700 \text{ m s}^{-1}$
 Density ratio: $\rho_2/\rho_1 = 1.5$
 Bottom attenuation: $0 \text{ dB } \lambda^{-1}$
 This problem should be done for a point source in cylindrical geometry.
- Case 3: *Penetrable lossy bottom.* As in Case 2 except with a bottom loss of $0.5 \text{ dB } \lambda^{-1}$

Receiver depths

- Case 1: 30 m
- Cases 2 and 3: 30 m and 150 m

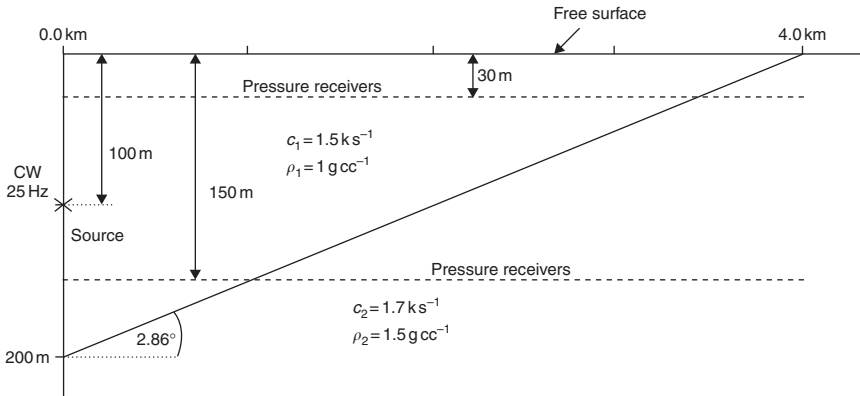


Figure 11.1 Analytical benchmark problem: wedge geometry for cases 1–3 (Jensen and Ferla, 1988).

Ferla,1990):

- 1 One-way (versus two-way) wave equation solutions do not provide accurate results for propagation over sloping bottoms.
- 2 The COUPLE model provides a full-spectrum, two-way solution of the elliptic-wave equation based on stepwise-coupled normal modes. This code is ideally suited for providing benchmark results in general range-dependent ocean environments. However, the solution technique

is computationally intensive and is therefore impractical at higher frequencies.

- 3 IFDPE provides a limited-spectrum, one-way solution of the parabolic approximation to the full wave equation. The implicit finite-difference solution technique is computationally efficient, and accurate one-way results are provided for energy propagating within $\pm 40^\circ$ of the horizontal axis.
- 4 PAREQ provides a narrow-angle, one-way solution of the parabolic approximation to the full wave equation. The split-step Fourier solution technique is computationally efficient, and accurate one-way results are provided for energy propagating within $\pm 20^\circ$ of the horizontal axis.

The term ‘pathological’ is sometimes used in reference to those test cases that prove to be particularly troublesome to models. In the evaluation of propagation models, for example, ocean environments exhibiting double sound-speed channels near the surface make especially good pathological test cases. Ainslie and Harrison (1990) proposed using simple analytic algorithms as diagnostic tools for identifying model pathologies. They developed simple analytic expressions for computing the intensity contributions from standard

$$\frac{c(r, z)}{c_0} = \left\{ 1 + \left(\frac{\pi l_1}{L} \right)^2 e^{-2\pi r/L} + \left(\frac{2\pi l_2}{L} \right)^2 e^{-4\pi r/L} \right. \\ \left. - \frac{2\pi l_1}{L} \left[1 - \left(\frac{2\pi l_2}{L} \right) e^{-2\pi r/L} \right] \cos \left(\frac{\pi z}{L} \right) e^{-\pi r/L} \right. \\ \left. - \left(\frac{4\pi l_2}{L} \right) \cos \left(\frac{2\pi z}{L} \right) e^{-2\pi r/L} \right\}^{-1/2}$$

where $c_0 = 1,500 \text{ m s}^{-1}$ is a reference sound speed, z the depth below the pressure-release surface, L the channel depth, and r the range from the source; l_1 and l_2 are parameters with the values $l_1 = 0.032L$ and $l_2 = 0.016L$.

Consider two cases:

Case 4: *Low-frequency, shallow water*
 $f = 25 \text{ Hz}$ (frequency),
 $L = 500 \text{ km}$ (channel depth),
 $R = 4 \text{ km}$ (range coverage).

Case 5: *High-frequency, deep water*
 $f = 100 \text{ Hz}$ (frequency),
 $L = 3 \text{ km}$ (channel depth),
 $R = 20 \text{ km}$ (range coverage).

Figure 11.2 Analytical benchmark problem: plane-parallel waveguide for cases 4 and 5 (Jensen and Ferla, 1988).

Note

The field should be computed for both source and receiver at depth $z = L/2$.

propagation paths such as bottom-reflected paths, bottom-refracted paths and Lloyd's Mirror interference. Ainslie and Harrison (1990) further demonstrated the utility of these analytical tools in assessing the performance of numerical models of acoustic propagation. They accomplished this by combining the intensity contributions from the individual propagation paths appropriate for any particular ocean environment and sonar system geometry. This approach allowed a path-by-path analysis of numerical model performance and illuminated any modeling pathologies in an instructive fashion. These tools were subsequently organized into a highly interactive sonar model called INSIGHT (Packman *et al.*, 1992). (INSIGHT is described in more detail in Chapter 10, specifically Table 10.6.) The ability to alter a variety of environmental or sonar system parameters interactively and then rapidly visualize the resulting impacts on system performance makes INSIGHT especially attractive for instructional purposes.

11.4 Quantitative accuracy assessments

Quantitative accuracy assessments of propagation models can be accommodated according to two procedures: difference techniques and figure of merit (FOM) techniques (McGirr, 1979).

Difference techniques measure the distance between the model prediction and a standard (which can comprise field measurements or outputs from other models) in terms of decibel differences at a given range, or over a set

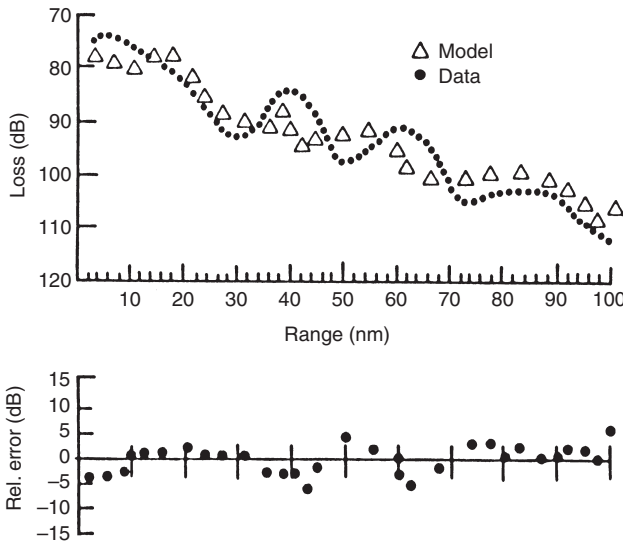


Figure 11.3 Sample outputs from the AESD model evaluation program (MEP) described by R.C. Cavanagh (1974, unpublished) (adapted from McGirr, 1979).

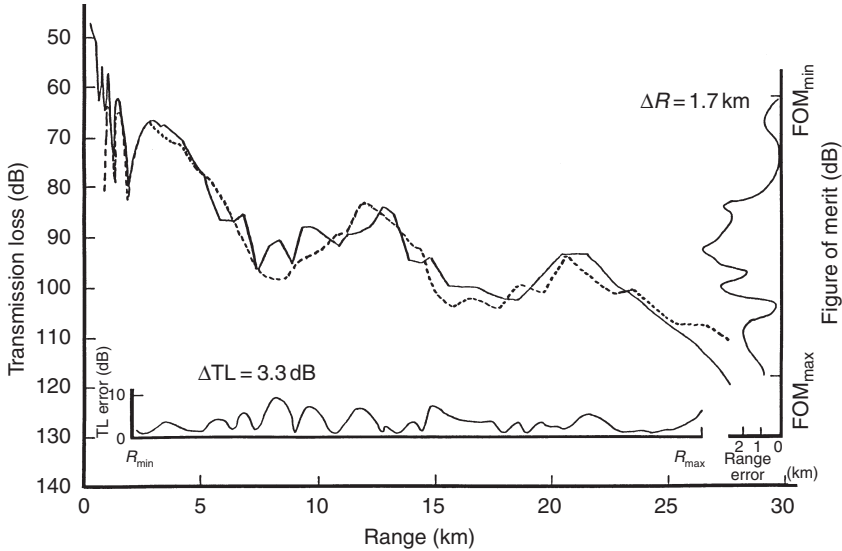


Figure 11.4 Transmission loss comparison concept that combines elements of both the difference technique and the FOM technique. This schematic only illustrates the concept and is not meant to be numerically exact (Leibiger, 1977).

range interval (Figure 11.3). These techniques are best suited to comparative model evaluations conducted in research environments.

Figure-of-merit techniques are essentially an inverted distance measure wherein a specified decibel level (or FOM) is selected and the corresponding ranges (or sonar detection zones) are determined and compared with a standard. The FOM equation was previously discussed in Chapter 10. These techniques are best suited to sensitivity analyses that have as their objective a determination of the operational (versus scientific) impacts of model prediction errors. Such techniques place importance on the location of sonar detection zones relative to a standard. These techniques thus recognize the ultimate application of the model predictions to naval operations. A hypothetical example of this technique, used in combination with the difference technique, is illustrated in Figure 11.4 (Leibiger, 1977).

11.5 The POSSM experience – a specific example

The deliberations of the POSSM are considered to be representative of past evaluation efforts, and aspects of these results will be discussed. The methodology developed and implemented by POSSM is summarized in Figure 11.5 (DiNapoli and Deavenport, 1979; Lauer, 1979). Only propagation models

mean and standard deviation were expressed as (Lauer and Sussman, 1979)

$$\text{CAM}_\mu = \frac{1}{\sum_{i=1}^{N_C} N_{R_i}} \sum_{i=1}^{N_C} \sum_{j=1}^{N_{R_i}} |\mu_{ij}| W_{ij} \quad (11.1)$$

$$\text{CAM}_\sigma = \frac{1}{\sum_{i=1}^{N_C} N_{R_i}} \sum_{i=1}^{N_C} \sum_{j=1}^{N_{R_i}} \sigma_{ij} W'_{ij} \quad (11.2)$$

where i is the case index, j the range interval index, N_C the total number of cases, N_{R_i} the total number of range intervals for the i th case, W_{ij} the weights in each case and range interval bin $(\Delta R)_{ij}$ to be applied to mean values of transmission loss (TL) differences, and W'_{ij} the weights applied to standard deviations of TL differences.

In the event that all values of W_{ij} and W'_{ij} were chosen to be unity, CAM_μ became the “grand” mean taken over all cases and range intervals, and CAM_σ became the “grand” standard deviation taken over all cases and range intervals. The weighting functions (W_{ij}, W'_{ij}) were functions of the acoustic frequency (f), source depth (Z_S), receiver depth (Z_R) and range interval (ΔR).

For the present discussions, only four specific versions of propagation models have been selected. These models represent four of the five different modeling approaches described earlier in Chapter 4. The only modeling approach not investigated by POSSM was the parabolic equation (PE) approach. At the time of POSSM’s activities, PE models were not yet widely used. Moreover, fast-field program (FFP) models were considered to be the most accurate available and were commonly used as standards for comparison. The four approaches and corresponding models represented are:

<i>Approach</i>	<i>Model</i>
Ray theory (with corrections)	FACT
Multipath expansion (hybrid)	RAYMODE
Normal mode	NLNM
Fast-field program	FFP

In the comparisons described by Lauer and Sussman (1979), and by DiNapoli and Deavenport (1979), the FFP model was used as the standard. Table 11.1 summarizes the computer program sizes and execution times for each model in the context of the standard problem selected by POSSM. A quantitative comparison of model accuracies was reported by Lauer and Sussman (1979) based on the methodology summarized in Figure 11.5. Only the four particular models identified above will be discussed here. Representative results from one test case are summarized in Table 11.2. It must be

Table 11.1 Example program sizes and execution times for selected propagation models. The standard problem consists of a single sound-speed profile overlying a flat bottom executed at a low frequency (≤ 200 Hz) on a UNIVAC 1108 computer

<i>Model</i>	<i>Program size (decimal words)</i>	<i>Execution time (s)</i>
FACT	21,855	2.5
RAYMODE	14,115	19.2
NLNM	53,000	30.6
FFP	51,572	373.0

Source: Adapted from Lauer and Sussman (1979).

stressed that these results pertain only to the configuration of these models as they existed at the time of the tests, and these results are only valid for the particular test case run. Different results might be obtained using more recent configurations of the same models or with other test scenarios and geometries, or even with other measurement standards or host computers.

The cumulative accuracy measures were also computed (Table 11.3). These results support the intuitive notion that model accuracy improves with increasing model complexity and computational intensity. Accuracy alone, however, should not be the sole evaluation criterion. A broader view of the model evaluation process is presented in Section 11.6.

11.6 Evaluation guidelines

Model evaluation entails the systematic gathering and promulgation of information about models to determine model limitations and domains of applicability. There is no evaluation procedure appropriate for all models. The procedures must be tailored on the basis of model structure, documentation and other information available to the evaluators. Criteria for model evaluation can be segregated into five basic categories (US General Accounting Office, 1979): documentation, verification, validation, maintainability and usability.

11.6.1 Documentation

Documentation of computer models is important for two reasons: (1) to ensure that the model is thoroughly understood and can be operated and maintained in the present as well as in the future; and (2) to facilitate independent evaluation of the model, particularly by someone other than the model developer or initial user.

Table 11.2 Means (μ) and standard deviations (σ) of the differences between the FFP propagation model and candidate model results for one particular case over direct path (DP), bottom bounce (BB) and convergence zone (CZ) regions

Model	Range interval													
	DP		BB1		CZ		BB2		to 100 km		to 150 km		to 200 km	
	μ	σ	μ	σ	μ	σ	μ	σ	μ	σ	μ	σ	μ	σ
FACT	-	-	1.4	3.6	0.9	2.2	0.1	3.0	-2.2	2.0	-2.0	1.3	-1.9	1.5
RAYMODE	-	-	1.3	3.7	0.5	2.0	-0.4	2.7	-0.3	1.1	-0.4	1.0	-0.8	1.6
NLNM	-	-	0.6	2.0	0.4	2.2	-0.8	1.9	0.7	1.9	-0.3	2.6	-1.0	2.5
FFP	-	-	-	-	-	-	-	-	-	-	-	-	-	-

Source: Adapted from Lauer and Sussman (1979).

Table 11.3 Cumulative accuracy measures: averages of means (μ) and standard deviations (σ) over all cases and range intervals using FFP propagation model results as the standard

<i>Model</i>	$ \mu $	σ
FACT	1.3	2.5
RAYMODE	0.9	2.4
NLNM	0.6	2.3
FFP	—	—

Source: Adapted from Lauer and Sussman (1979).

Elements that should be included in model documentation are (Gass, 1979):

- 1 a precise statement of what the model is supposed to do;
- 2 the mathematical and logical definitions, assumptions and formulation of the problem being modeled;
- 3 a complete set of current input and output, and test cases that have been run;
- 4 a complete set of flow charts of the computer program;
- 5 a set of operating instructions for the computer operator;
- 6 an explanation of the various options available in using the model;
- 7 the computer program itself (listing), with comments about various operations in the program.

Further guidelines for documentation are provided later in this chapter.

11.6.2 Verification

Verification entails an examination of the model to ensure that the computer program accurately describes the model and that the program runs as expected. In order to do this, the following factors must be examined: (1) consistency of mathematical and logical relationships; (2) accuracy of intermediate numerical results; (3) inclusion of important variables and relationships; and (4) proper mechanization and debugging of the program.

Computer hardware selections will sometimes impact model accuracy due to word length and double-precision considerations, among others. Thus, the same model implemented on two different computer systems may produce significantly different results. Related problems concern artifacts, which are false features that arise from some quirk of the computer, and which disappear when the software is written differently.

11.6.3 *Validity*

Validation and critical assessment are required of all theoretical conjectures, hypotheses and models. One of the most difficult but important tasks in model construction is the specification of its limitations: what are its limits, and in what way is it an approximation? The consensus principle in science implies that the evaluation of models must be open, and cannot be accepted on the authority of the model developer alone. The model should not contain adjustable parameters or any hidden variables that have to be invoked to explain discrepancies between theory and experiment. The theoretical properties of the model should be sharply defined, and derived with sufficient mathematical rigor to be compared objectively with the observed phenomena. Elementary errors and misunderstandings will be detected by the independent repetition of experiments and by comparisons of calculations with experimental data, or by theoretical criticism (Ziman, 1978). Even when models are wrong, they can assist in structuring discussions.

The category of validity comprises three factors: theoretical validity, data validity and operational validity. Theoretical validity entails review of the physics underlying the model and the major stated and implied assumptions. The applicability and restrictiveness of these assumptions must also be examined. In addition, the internal logic of the model should be reviewed.

For empirically based models, data validity is concerned with the accuracy and completeness of the original data and the manner in which the empirical model deals with the transformation of the original data.

Operational validity is concerned with assessing the impact of model errors (i.e. divergences between model predictions and reality) on decision processes. This aspect of model evaluation addresses accuracy. When evaluating model accuracy, it is important to examine the error budget. Errors in model predictions (e_p) are assumed to be the sum of two independent, random variables:

$$e_p = e_d + e_m \quad (11.3)$$

where e_d represents errors related to model input data and e_m represents model errors.

11.6.4 *Maintainability*

Maintainability considers the ease of incorporating new data and formulae as well as provisions for reviewing the accuracy of the model as more experimental data become available. A training program must be formalized to ensure that the operators understand how the model should be used and also to make revisions known to the computer-systems personnel.

11.6.5 Usability

Usability addresses the appropriateness of the model for the intended applications. In essence, the model should satisfy the user's specific requirements. This, of course, requires that users articulate their needs very precisely.

It is instructive to distinguish between research and operational models when discussing usability. Specifically, research models are intended to address a wide variety of often ill-posed scientific questions. In order to be responsive to such ambiguous issues, the research models are structured to allow (and often require) a high degree of operator intervention during execution. This allows the researcher to adjust parameters as the problem solution evolves. Alternatively, operational models are structured to minimize (if not eliminate) the need for operator intervention. Indeed, such intervention is viewed as a nuisance to the operator. The parallel between executive-versus-bundled system architectures and research-versus-operational models is valid (refer to Chapter 10, Section 10.4.1).

Model usability is heavily influenced by the model's inherent domains of applicability. Factors such as frequency coverage and problem geometry are implicit in these domains. For example, the use of normal-mode models in the calculation of high-frequency bistatic reverberation is not practical at present due to excessive computation times. Model output options are also important. For example, wave-theoretical propagation models more easily generate TL values in the range-depth plane while arrival structure information is more easily generated by ray-theoretical propagation models.

11.7 Documentation standards

Documentation standards for computer models were reviewed by Gass (1979). Both the US Department of Defense and the National Institute of Standards and Technology (formerly the National Bureau of Standards, or NBS) have issued formal guidelines:

- DOD-STD-7935A – Department of Defense standard: Automated data systems (ADS) documentation.
- DOD-STD-2167A – Military standard: Defense system software development.
- FIPS PUB 38 – Guidelines for documentation of computer programs and automated data systems.
- DOD-STD-2168 – Military standard: Defense system software quality program.

According to the federal information processing standards (FIPS), model documentation is keyed to the various phases and stages of the software life

Table 11.4 Software life cycle and documentation types according to the federal information processing standards (Gass, 1979)

Development phase		Operation phase	
Initiation phase	Definition stage	Design stage	Test stage
	Functional requirements document	System/subsystem specification	User's manual
	Data requirements document	Program specification Database specification	Operations manual Program maintenance manual
		Test plan	Test analysis report

Notes

Functional requirements document – provides a basis for the mutual understanding between users and designers of the initial definition of the software, including the requirements, operating environment and development plan.

Data requirements document – provides data descriptions and technical information about the data collection requirements.

System/subsystem specification – specifies for analysts and programmers the requirements, operating environment, design characteristics and program specifications for a system or subsystem.

Program specification – specifies for programmers the requirements, operating environment and design characteristics of a computer program.

Database specification – specifies the identification, logical characteristics and physical characteristics of a particular database.

User's manual – sufficiently describes the functions performed by the software in non-ADP terminology such that the user organization can determine its applicability, and when and how to use it; moreover, it should serve as a reference document for preparation of input data and parameters, and for interpretation of results.

Operations manual – provides computer operation personnel with a description of the software and of the operational environment so that the software can be run.

Program maintenance manual – provides the maintenance programmer with the information necessary to understand the programs, their operating environment and their maintenance procedures.

Test plan – provides a plan for testing the software; provides detailed specifications, descriptions and procedures for all tests; and provides test data reduction and evaluation criteria.

Test analysis report – documents the test analysis results and findings; presents the demonstrated capabilities and deficiencies for review; and provides a basis for preparing a statement of software readiness for implementation.

cycle (Table 11.4). The major phases are:

Initiation phase – During this phase, the objectives and general definition of the requirements for the software are established. Feasibility studies, cost–benefit analyses and the documentation prepared within this phase are determined by agency procedures and practices.

Development phase – During this phase, the requirements for the software are determined, and software is then defined, specified, programmed and tested. Ten major documents are prepared in this phase to provide an adequate record of the technical information developed (Table 11.4).

Operation phase – During this phase, the software is maintained, evaluated and changed as additional requirements are identified. The documentation is maintained and updated accordingly.

The development phase of the software life cycle is further subdivided into four main stages as follows:

Definition stage – when the requirements for the software and documentation are determined.

Design stage – when the design alternatives, specific requirements and functions to be performed are analyzed and a design is specified.

Programming stage – when the software is coded and debugged.

Test stage – when the software is tested and related documentation is reviewed. The software and documentation are then evaluated in terms of readiness for implementation.

Formal documentation guidelines are frequently amended or even superseded by newer guidelines. Care should be taken to consult the latest governing instructions. For example, DOD-STD-7935A and DOD-STD-2167A (which were noted earlier) were later consolidated into MIL-STD-498 in an effort to implement governing ISO/IEC standards (DIS 12207 – Software Life-Cycle Processes). MIL-STD-498 (Software development and documentation) was issued on 5 December 1994. However, this standard was subsequently canceled on 27 May 1998. In its place, IEEE/EIA 12207 (issued in three parts) is now to be used:

- IEEE/EIA 12207.0: “Industry implementation of international standard ISO/IEC 12207, Standard for information technology – *Software life-cycle processes*” (March 1998), contains concepts and guidelines to foster better understanding and application of the standard. This standard thus provides industry with a basis for software practices usable for both national and international business.
- IEEE/EIA 12207.1: “Guide for ISO/IEC 12207, Standard for information technology – Software life-cycle processes – *Life-cycle data*,” was

adopted on 27 May 1998 for use by the US Department of Defense. This document provides guidance on life-cycle data resulting from the processes of IEEE/EIA 12207.0 including relationships among content of life-cycle data information items, references to documentation of life-cycle data, and sources of detailed software product information.

- IEEE/EIA 12207.2: “Guide for ISO/IEC 12207, Standard for information technology – Software life-cycle processes – *Implementation considerations*,” was adopted on 27 May 1998 for use by the US Department of Defense. This document provides implementation guidance based on software industry experience with the life-cycle processes.

The transfer of modeling and simulation (M&S) technologies among members of the international community continues to stimulate new initiatives for improved international standards in simulation architecture. Such efforts seek to promote the large-scale interoperability of simulation software and hardware.

12 Simulation

12.1 Background

This chapter discusses the structure and applications of simulation in underwater acoustics. Since simulation refers to a method for implementing a model over time, it is fitting that this topic is addressed after a firm foundation of modeling and evaluation has been established in the previous chapters. In the present context, the term “modeling and simulation” refers to those techniques that can predict or diagnose the performance of complex acoustic systems operating in the dynamic undersea environment.

A widely used taxonomic scheme for classifying various types of simulation is based on the degree of human involvement and the realness of the system. This scheme distinguishes three categories of simulation: live, virtual and constructive. Live simulation involves real people operating real systems. Virtual simulation involves real people operating simulated systems. Constructive simulation involves simulated people operating simulated systems. To complete the symmetry of this taxonomic scheme, a fourth category termed “smart systems” is added. In essence, smart systems involve simulated people operating real systems. The resulting taxonomic scheme comprising these four categories of simulation is summarized in Table 12.1.

Another term frequently encountered in discussions of simulation is “stimulation.” Stimulation is the use of simulation to provide external stimuli to a system or subsystem. Stimulation often entails hardware-in-the-loop or software-in-the-loop configurations, which are commonly referred to as “constrained simulation” since the simulated time-advances have a specific relationship to wallclock time.

Table 12.1 Four categories of simulation based on the degree of human involvement

	<i>Real systems</i>	<i>Simulated systems</i>
<i>Real people</i>	Live simulation	Virtual simulation
<i>Simulated people</i>	Smart systems	Constructive simulation

When simulating a complex assemblage of independent, but interconnected, systems, it is common to refer to such an assemblage as a “system-of-systems.” Simulating the performance of such an assemblage is often referred to as “end-to-end” simulation. The “state” of a system is defined by the collection of variables necessary to describe that system at any given time.

Simulations are differentiated at three levels of system representations: static versus dynamic; deterministic versus stochastic; and continuous versus discrete. A static simulation represents a system state in which time is not a variable. Conversely, a dynamic simulation varies as a function of time. A deterministic simulation produces completely predictable values whereas a stochastic simulation produces values that must be represented by statistical variables (e.g. means and variances). A continuous simulation produces state variables that change continuously with changes in time while a discrete simulation produces values that change in a stepwise fashion as a function of time (Law and Kelton, 1991).

Different mathematical approaches are used depending on the type of simulation employed. For example, continuous-system simulations are modeled using differential equations while time-stepped simulations are modeled using discrete-time approaches. Event-based simulations are modeled as discrete events.

Law and Kelton (1991: chapter 12) provide a comprehensive introduction to the use of statistical experimental design and optimization techniques in simulation. Specifically, experimental design provides a way of deciding before any runs are made which particular configurations should be simulated so that the desired information can be obtained with the least amount of simulation. The term “design of experiment” (DOE) is sometimes used in the literature in reference to this process. Design of experiment is particularly important when simulation is used to evaluate (or trade) alternative system configurations.

To structure subsequent discussions, the four hierarchical levels of simulation (engineering, engagement, mission and theater) are first reviewed in Section 12.2. Next, simulation infrastructure is discussed in Section 12.3 using examples drawn from defense-related activities. Section 12.4 discusses the high-level architecture (HLA), currently the highest priority effort within the defense modeling and simulation community. The role of testbeds is described in Section 12.5. Finally, a survey of current applications in Section 12.6 provides specific examples of generally accepted approaches and common practices.

12.2 Hierarchical levels

As previously mentioned in Chapter 1, simulation in support of naval applications can be decomposed into four fundamental levels: engineering, engagement, mission and theater. Table 12.2 summarizes the outputs and

Table 12.2 Four principal levels of simulation for naval applications

<i>Level</i>	<i>Output</i>	<i>General applications</i>
Theater	Force dynamics	Evaluate force structures Evaluate strategies
Mission	Mission effectiveness	Evaluate force employment concepts
Engagement	System effectiveness	Evaluate system alternatives Train system operators Evaluate tactics
Engineering	System performance	Design and evaluate systems/subsystems Support system testing

Source: National Research Council (1997).

applications associated with each of these four levels. Each level is discussed below in greater detail.

12.2.1 *Engineering*

Engineering-level simulation comprises the categories of environmental, propagation, noise, reverberation and sonar performance models. This level of simulation generates measures of system performance that are used to design and evaluate systems and subsystems and also to support system testing. Representative measures of performance include probability of detection and median detection ranges. Sonar technologists and acoustical oceanographers routinely use this level of simulation for prognostic or diagnostic applications. These performance metrics are also useful in system design, cost, manufacturing and supportability trade studies.

12.2.2 *Engagement*

Engagement-level simulation executes engineering-level models to generate measures of system effectiveness in a particular spatial and temporal realization of an ocean environment when operating against (engaging) a particular target. This level of simulation is used to evaluate system alternatives, train system operators and evaluate tactics. Engagement outputs can be used to estimate exchange ratios, which are useful in evaluating tactical effectiveness against known and postulated targets.

Tactical decision aids represent a form of engagement-level simulation products that blend environmental information with tactical rules garnered from higher-level, aggregate simulations. These decision aids guide system operators and scene commanders alike in planning missions and allocating resources by exploiting knowledge of the operating environment. While TDAs are usually associated with naval applications, the conceptual approach is valid in research and commercial applications as well.

12.2.3 *Mission*

Mission-level simulation aggregates multiple engagements to generate statistics useful in evaluating mission effectiveness. At this level, system concepts are evaluated within the context of well-defined mission scenarios. The outputs of this level of simulation are used to evaluate force employment concepts. The effectiveness of multiple platforms performing specific missions can be assessed using this level of simulation.

12.2.4 *Theater*

Theater-level simulation aggregates mission-level components to generate measures of force dynamics and analyze alternative system-employment strategies. This type of simulation is used in planning, budgeting and operational analysis. Planning includes decisions regarding force structure, modernization, readiness and sustainability. Budgeting includes decisions regarding specific line items in the defense budget. Operational analysis considers issues such as developing contingency plans, estimating logistics demands and analyzing specific combat plans (Bracken *et al.*, 1995). This level of simulation is useful in wargaming with joint or combined forces.

12.3 **Simulation infrastructure**

The National Research Council (1997) portrayed modeling and simulation as a foundation technology for many developments that will be central to the US Navy over the next several decades. Representative applications of simulation in the defense industry were summarized by Bracken *et al.* (1995), who edited a useful collection of papers coordinated by the Military Operations Research Society (MORS).

The DMSO was established in 1991 to provide a focal point for information concerning US DOD M&S activities. The DMSO is leading an effort to establish a common technical framework (CTF) to facilitate the interoperability and reuse of all types of models and simulations. The foundation for this effort is the HLA (see Section 12.4). Two other elements of the common technical framework include conceptual models of the mission space (CMMS) and data standards. When completed, CMMS will provide simulation-independent descriptions of real-world processes, entities, environments and relationships. The data standards program will provide the M&S community with certified data to promote interoperability of models and simulations, thus improving the credibility of simulation results. Planned representations of the natural environment will include terrain, oceans, atmosphere and space.

The DMSO also provides services to complement the common technical framework including VV&A procedures and environmental databases. The US Department of Defense (1994) officially adopted definitions for VV&A that originated from the efforts of the MORS. These definitions are useful

for applications in naval operations, offshore industries and oceanographic research:

- *Verification* – The process of determining that a model implementation accurately represents the developer’s conceptual description and specifications.
- *Validation* – The process of determining the degree to which a model is an accurate representation of the real world from the perspective of the intended uses of the model.
- *Accreditation* – The official certification that a model or simulation is acceptable for a specific purpose.

The US Department of Defense (1996) assembled a very useful compendium of VV&A techniques from sources in government, industry and academia. This evolving document provides practical guidelines for formulating VV&A procedures in a wide range of modeling and simulation environments.

12.4 High-level architecture

The HLA (Kuhl *et al.*, 1999) is the highest-priority effort within the DOD modeling and simulation community. The HLA has been adopted as IEEE Standard 1516 and has also been proposed for acceptance by the North Atlantic Treaty Organization (NATO) as the standard for simulations used within the alliance. The HLA is composed of three parts: the HLA rules, the HLA interface specification and the object model template (OMT). The HLA rules describe the general principles defining the HLA and also delineate 10 basic rules that apply to HLA federations and their participating applications (called federates). The HLA interface specification defines the functional interface between federates and the runtime infrastructure (RTI). The OMT provides specifications for documenting key information about simulations and federations. Use of the OMT to describe simulation and federation object models (called SOMs and FOMs, respectively) is a key part of the HLA (North Atlantic Treaty Organization, 1998; Kuhl *et al.*, 1999).

The NATO Alliance is generally dependent upon the modeling and simulation contributions of the member nations. These contributions include the cooperative development of technical capabilities such as the defence modeling and simulation technologies research program in the European Cooperation for the Long-term in Defense (EUCLID). In this environment, required simulations must either be specified and then developed anew, or else legacy simulations must be adapted to meet the specified requirements.

The development of individual models and simulations has been occurring for decades and is therefore relatively well understood by NATO. The alliance, however, only has limited experience with the cooperative development of federations of diverse simulations. To be prudent, therefore,

NATO has opted to demonstrate the viability of this innovative development approach by conducting a pathfinder development of an HLA-based federation of national simulations. This federation would be planned and centrally integrated and tested, but the individual national simulation developments would be executed by the involved nations. Ideally, such a pathfinder effort would be built on the experience base established during NATO's Distributed Multi-National Defence Simulation (DiMuNDS) project. Selected legacy simulations will have to fulfill the specified criteria and will, therefore, require some modifications (North Atlantic Treaty Organization, 1998, 2000).

12.5 Testbeds

Testbeds allow the simultaneous use of high- and low-detail system representations (i.e. variable resolution) in a single simulation. This flexibility enables an analyst to simulate a key system in high detail while simulating the less-critical contextual environment in lower detail.

In integrated hierarchical variable resolution (IHVR) simulations, high-level variables are expressed as functions of lower-level (but higher-resolution) variables. Here, hierarchies of variables can relate models at different resolutions (Davis, 1995). Complications may arise from so-called configural effects, which consider the influences of temporal and spatial correlations on simulated outcomes (National Research Council, 1997: 90 and 233). Specifically, the configuration of the simulated assets is inseparable from the outcome of the particular simulation. Consequently, if the assets were configured differently at the outset, the simulated outcome would likely be different.

An integrated testbed includes the processor on which the simulation software will run together with all other units that will interface with the processor. This arrangement affords the opportunity to perform early interface testing using the actual hardware. For example, the tactical oceanography simulation laboratory (TOSL) provides a testbed for the development, testing and validation of high-fidelity underwater acoustic models and supporting databases (Ellis *et al.*, 1996).

From a broader perspective, simulation testing can be accomplished either in laboratory-based testbeds or in at-sea tests. At-sea tests provide engineers the opportunity to validate sonar-system performance in real (versus synthetic) ocean environments. For example, the littoral warfare advanced development (LWAD) project provides at-sea tests (including platforms and coordination) to identify and resolve technical issues that arise from operating undersea systems in littoral environments (Spikes *et al.*, 1997). Sea tests can range from simple focused technology experiments (FTE) to more complex system-concept validations (SCV). The penalty paid for testing in a real (versus synthetic) environment is the loss of experimental control and repeatability.

Situating testbeds at a fixed site in the field can create an interesting hybrid testbed configuration. Such arrangements, sometimes referred to as “natural laboratories,” have attractive features over laboratory-based testbeds. For example, field sites permit sustained modeling and observing systems to be deployed so that models can be continually tested and refined in real (versus synthetic) environments. Moreover, operational training can be collocated with fielded testbeds so that realistic experience can be obtained. The loss of experimental control and repeatability is limited by selecting a fixed location in an ocean area that is well understood environmentally. An example of a fielded testbed is the northern Gulf of Mexico littoral initiative, or NGLI (Carroll and Szczechowski, 2001). The NGLI is a multi-agency program established through a partnership between the Commander, Naval Meteorology and Oceanography Command and the Environmental Protection Agency’s Gulf of Mexico Program Office. The goal of NGLI is to become a sustained comprehensive nowcasting/forecasting system for the coastal areas of Mississippi, Louisiana and Alabama that will use model forecasts and observational data for training and coastal resource management. The program integrates a reliable and timely meteorological and oceanographic modeling scheme, combining 3D circulation, sediment transport, and atmosphere and wave models with *in situ* and remotely sensed observations via an extensive data distribution network that is available to a wide range of users in near-real time through an interactive website. The Naval Oceanographic Office, who manages the program, chose the Mississippi Bight as an ideal testbed to examine new modeling and observational technologies before they are applied to other littoral areas of interest. The NGLI directly addresses the US Navy’s requirement to project oceanographic information from deep-water environments shoreward into littoral areas. Model nowcasts and forecasts are being applied to the ocean littoral environment by cascading information from large ocean basin models to shallow-water models. Lessons learned within this “natural laboratory” provide civil authorities with metrics by which to evaluate environmental stresses (e.g. sediment transport modifications and increased pollution) caused by growth in population and industry.

12.6 Applications

Simulations are used in diverse scientific and engineering disciplines. Although the following discussions will highlight many naval applications, the basic approaches and practices surveyed here are applicable to offshore industries and oceanographic research as well. Specific attention will be given to those activities relating to engineering- and engagement-level simulations. It may be useful at this point to again refer to the discussions in Section 12.2 (especially Table 12.2).

Discussions will start with engineering-level simulations that generate system-performance outputs. As indicated in Table 12.2, general applications include design and evaluation of systems (or subsystems) and system-testing support. As specific examples, Section 12.6.1 will discuss applications in systems engineering and Section 12.6.2 will discuss applications in SBA.

The next level above engineering is engagement-level simulations, which generate system-effectiveness outputs. As indicated in Table 12.2, general applications include the evaluation of system alternatives, training of system operators and evaluation of tactics. As specific examples, Section 12.6.3 will discuss applications in operations analysis and Section 12.6.4 will discuss applications in training.

These discussions emphasize *processes* as opposed to *specific implementations* of simulation packages. The intent is to familiarize the reader with generally accepted approaches to simulation as practiced in government (both civil and military) and in industry (both offshore and defense related). Research applications may utilize variations of these approaches.

12.6.1 *Systems engineering*

An objective of systems engineering is to gain visibility in the early stages of a system's development. The intent is to explore all feasible approaches to system design, identify and eliminate potential problems, select a preferred design configuration and thus reduce risks and costs (Blanchard, 1998). The use of simulation allows designers to investigate alternative design solutions prior to committing to any particular design. In a systems-engineering context, simulation is used to understand the behavior of a system or to evaluate alternative system-design considerations in tradeoff studies. The use of simulation is most effective in the early stages of system development before any physical elements comprising the system are available for evaluation.

The systems-engineering process is often represented by the so-called “V” diagram, as illustrated in Figure 12.1. The decomposition-and-definition process flows downward along the left leg of the “V” while the integration-and-verification process flows upward along the right leg of the “V.” In the decomposition-and-definition process (on the left side of Figure 12.1), the utilization of simulation during the preliminary design phase would have the greatest impact on the final system configuration.

An important asset in the systems engineering process is the software engineering environment (SEE), which supports the software development process. The SEE comprises the facilities, integration methods, tools, procedures and management information system (MIS) necessary to maintain productivity, simulation product quality and software reuse.

12.6.2 *Simulation-based acquisition*

Simulation-based acquisition is an acquisition process in which both the US Department of Defense (DOD) and industry collaborate in the use of

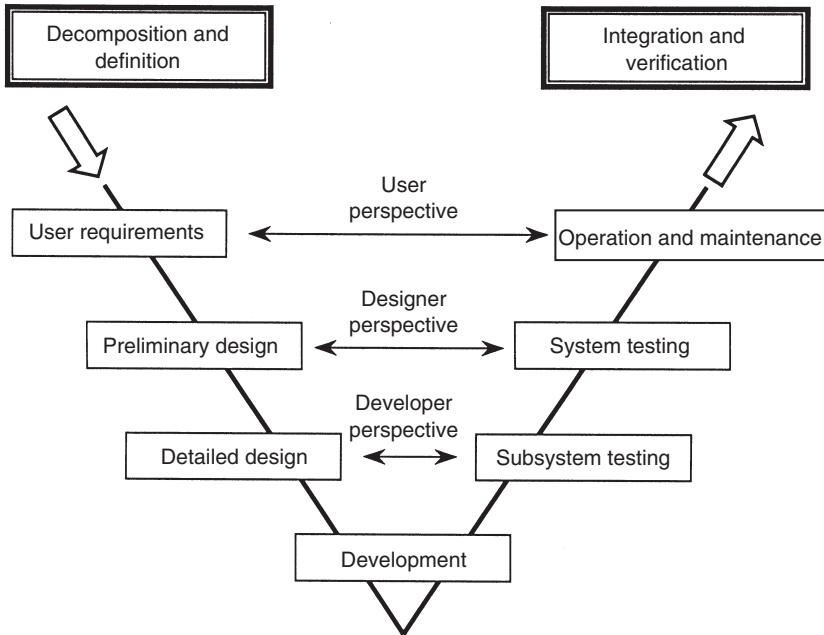


Figure 12.1 Systems engineering decomposition and definition process flow. (Blanchard, 1998; *System Engineering Management*, 2nd edn; this material is used by permission of John Wiley & Sons, Inc.)

simulation technologies that are integrated across acquisition phases and programs (US Department of the Navy, 2000a). Specifically, SBA entails the optimization of system performance versus total ownership cost (TOC) through exploration of the largest possible trade space. Total ownership cost comprises the cost to research, develop, acquire, own, operate, and dispose of primary and support systems, other equipment and real property, the costs to recruit, train, retain, separate and otherwise support military and civilian personnel, and other costs of business operations in the DOD. Johnson *et al.* (1998) provided a very useful introduction to the concepts underpinning SBA.

It is helpful to revisit the modeling and simulation hierarchy pyramid introduced previously in Chapter 1 (see Figure 1.3) in the context of system-design applications. In Figure 12.2 (US Department of the Navy, 2000a), the four categories of simulation (engineering, engagement, mission and theater) are related to their principal outputs: engineering-level simulations output system or component performance; engagement-level simulations output system effectiveness; mission-level simulations output mission effectiveness; and theater-level simulations output the overall outcomes. Requirements are generally developed in a top-down approach as indicated by the

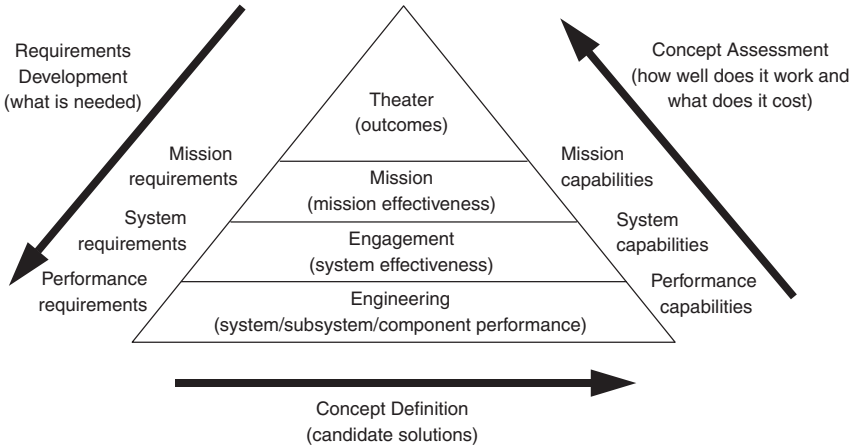


Figure 12.2 Modeling and simulation in system design (US Department of Navy, 2000a).

downward-directed arrow (labeled “requirements development”) on the left side of the pyramid in Figure 12.2. Specifically, mission requirements (derived from theater-level simulations) flow down to system requirements which, in turn, flow down to performance requirements. These performance requirements are then allocated among the various subsystems and components using engineering-level simulations. Alternatively, a bottom-up approach may be used as indicated by the upward-directed arrow (labeled “concept assessment”) on the right side of the pyramid. In this approach, performance capabilities (generated by engineering-level simulations) are translated into system capabilities which, in turn, are translated into mission capabilities whereafter the outcomes are evaluated in theater-level simulations. The arrow at the base of the pyramid in Figure 12.2 (labeled “concept definition”) suggests a connection with the “V” diagram presented in Figure 12.1. Specifically, adhering to the discipline of the decomposition-and-definition process ensures that the perspectives of users, designers and developers are reflected in the concept definition.

The US DOD divides the system-acquisition process into three principal phases: concept and technology development; system development and demonstration; and production and deployment. A fourth phase (operations and support) covers life-cycle sustainment (refer to Table 12.3). In each phase, it is possible to identify the generic functions performed by each of the four levels of simulation (engineering, engagement, mission and theater). In Table 12.3, each phase of acquisition or sustainment is identified in the first column. In the second column, the relationship to notable requirements documents is indicated. The third through sixth columns identify the generic

Table 12.3 Functions of the four levels of simulation corresponding to each phase of the acquisition process

Phase	Level of simulation			Metrics/tools		
	Requirements	Engineering	Engagement		Mission	Theater
Concept and technology development	Mission needs statement (MNS)	Generate system/subsystem performance parameters Conduct performance tradeoffs	Evaluate effectiveness Conduct cost and performance tradeoffs	Evaluate mission effectiveness	Examine outcomes of new system capabilities, technologies and tactics	Key performance parameters (KPP) Cost as an independent variable (CAIV)
System development and demonstration	Operational requirements document (ORD)	Develop design specifications	Evaluate mission effectiveness		Examine how well proposed system meets identified needs	Measures of effectiveness (MOE)
Production and deployment		Plan prototype tests Reduce risk Support reliability and maintainability (R&M)	Define interoperability requirements			Measures of performance (MOP)
Operations and support		Support pre-test planning and post-test analysis Verify compliance with specifications Evaluate and verify design changes	Evaluate mission effectiveness		Evaluate consistency of measures of effectiveness (MOE)	Hardware-in-the-loop (HWIL)/software-in-the-loop (SWIL)
			Conduct training on tactics and concepts of operation			Training systems

functions appropriate at each level of simulation to support that phase. The last column lists the metrics or tools associated with those simulations. Further guidance on US DOD acquisition policy (sometimes referred to as “the 5000 model”) can be found in DOD Directive 5000.1 (*Defense Acquisition System*), DOD Instruction 5000.2 (*Operations of the Defense Acquisition System*) and DOD Regulation 5000.2-R [*Mandatory Procedures for Major Defense Acquisition Programs (MDAPs) and Major Automated Information System (MAIS) Acquisition Programs*]. DOD Regulation 5000.2-R (US Department of Defense, 2001) mandates that every defense acquisition program establish performance, schedule and cost goals that can be defined by the least number of parameters necessary to characterize the program over its life cycle. Each parameter has a *threshold* value and an *objective* value.

For performance, the *threshold* is the minimum acceptable value necessary to satisfy the users’ needs. For schedule and cost, the threshold is the maximum allowable value. The *objective* value is what the user desires and what the program manager tries to obtain. The objective value thus represents an incremental, operationally meaningful, time-critical and cost-effective improvement to the threshold value of each program parameter.

Performance-threshold values represent true minima, with requirements stated in terms of capabilities rather than as technical solutions or specifications. If the performance-threshold values are not achieved, program performance may be seriously degraded and the utility of the system may become questionable. If schedule-threshold values are not achieved, the program may no longer be timely. Cost-threshold values represent true maxima. If cost-threshold values are not achieved, the program may be too costly and the affordability of the system may become questionable.

In establishing realistic objectives, cost is now treated as a requirement. The cost-as-an-independent-variable (CAIV) process is therefore used to develop TOC, schedule, performance thresholds and objectives. Cost is addressed in the operational requirements document (ORD). The CAIV trades consider the cost of delays as well as the potential for an early operational capability. The CAIV process relies heavily on modeling and simulation to perform trades in the multi-dimensional parameter space of threshold and objective values. Cost, schedule and performance may be traded within the “trade space” between the objective and the threshold values. However, validated key performance parameters (KPPs) may not be traded-off without proper authorization. The KPPs are a critical subset of the performance parameters found in the ORD. Each KPP has a threshold and an objective value. The significance of a KPP is that failure to meet the threshold value can cause the concept or system to be re-evaluated, or the program to be reassessed or terminated.

The best time to reduce TOC and shorten the program schedule is early in the acquisition process. Continuous cost–schedule–performance trade-off analyses can greatly facilitate cost and schedule reductions. When appropriate, COTS equipment may be considered. For example, Veenstra

(1998) demonstrated the feasibility of using COTS hardware and software to build advanced sonar simulation–stimulation systems at costs that were significantly lower than traditional approaches.

12.6.3 Operations analysis

Operations analysis is a scientific method for providing executives with a quantitative basis for making decisions regarding the operations under their control (Wagner *et al.*, 1999). Operations research (or operational research, as it is sometimes called) is closely related to operations analysis. Modern operations analysis, which is a discipline that matured rapidly during Second World War, has found application in a wide variety of military and civilian endeavors. The present focus is on naval operations analysis and those decisions that are useful to naval personnel in the conduct of naval operations. Wagner *et al.* (1999) presented instructive discussions concerning the role of modeling and simulation in sonar detection, search and patrol.

The basis for decision-making entails predicting and describing the expected results of alternative courses of action. These results are presented in terms of appropriate measures of effectiveness (MOE). The MOE has four important attributes: (1) it is quantitative; (2) it is measurable from data or calculable from models; (3) it is highly correlated with an outcome gain or loss; and (4) it reflects the benefits and penalties of a given course of action (Wagner *et al.*, 1999).

Many of the problems addressed in modern naval operations analysis have become so complex that simple analytical models can no longer be used to solve them. Recourse is, therefore, made to more sophisticated numerical models and Monte Carlo simulations. Typical problems to be solved in naval operations analysis include, for example, the determination of optimal deployment patterns for mobile or stationary sensor systems. Sonar performance models are used to generate appropriate MOE values such as median detection ranges for a stated probability of detection. Typically, Monte Carlo simulations are executed to create statistically meaningful data for subsequent analysis. Ultimately, sensor system performance may have to be traded against other metrics such as cost or asset availability (e.g. delivery platforms) to arrive at the best decision. Such approaches are commonly used in developing tactics for new sensor systems, or in comparing the merits of two or more candidate systems vying for the same acquisition funding. In the latter case, the process is often referred to formally as an analysis of alternatives (AOA) or a cost and operational effectiveness analysis (COEA).

Methods commonly associated with operations research – linear and dynamic programming, optimization techniques, queuing analysis and control theory – are also used as design tools in systems engineering (Blanchard, 1998).

Recent developments worthy of further exploration by serious students of naval operations analysis include effects-based (versus attrition-based) operations and capability-based (versus threat-based) analysis. Following Davis (2001), effects-based operations can be defined as those naval operations that are planned with full consideration of all possible direct, indirect and cascading effects. The application of effects-based naval operations poses challenges to modeling and simulation since different degrees of probability must be assigned to each constituent (but interacting) effect. Capability-based analysis considers *how* (versus *where* and *with whom*) naval operations will be conducted. This approach leads to the development of generic (versus context-specific) systems and tactics. Here, the challenge to modeling and simulation is to develop analytical approaches that will provide usable products and guidance in specific (but as yet unrealized) contexts.

12.6.4 *Training*

Reductions in at-sea training opportunities have particularly encouraged (even necessitated) increased reliance on simulations for sonar-related training. For example, the use of CBT has grown extensively, and sonar models have become common elements of simulations used in such learning environments. Two problems continue to plague advances in this area, however. First, the cost of developing quality courseware often becomes a limiting factor. Consequently, even the best-intentioned training products can quickly degenerate into page-turner programs that are useful for drill and practice among students of dissimilar educational backgrounds, but do not challenge students of more advanced topics. Second, the rapid evolution in computer technology often renders training systems prematurely obsolete by outpacing the financial capacity of educational centers to update their equipment. Moreover, installing upgraded software on aging equipment aggravates student-computer interactions by slowing computer response times, thereby frustrating students' experiences with CBT. An important consideration in the design of effective training environments is the creation of a standardized interface between the real-time host simulation devices and the image generator that provides realistic visualization of the simulated physics-based effects.

A notable development in underwater modeling and simulation is the IMAT system. The IMAT system was originally developed to enhance the training of naval-aviation ASW operators (Ellis and Parchman, 1994; Wetzel-Smith *et al.*, 1995; Wetzel-Smith and Czech, 1996), but has since expanded to include surface-ship and submarine ASW operators as well. Useful IMAT products include classroom multimedia systems and integrated curricula, PC-based learning systems, operator-console and tactical simulations (US Department of the Navy, 1999). While primarily used to teach the physics of underwater acoustics, IMAT also has modules for optics, magnetics and radar (Beatty, 1999).

The IMAT system couples scientific visualization with standard US Navy physics-based models and high-resolution databases to illustrate complex physical interactions. This combination of modeling and simulation creates a highly visual cause-and-effect-training tool. Variables characterizing targets, sensors and environments can be manipulated to enable students to observe the overall impact of the changes. Many IMAT displays permit the creation of animations that illustrate how acoustic and oceanographic phenomena vary over a range of parameters. The US Navy air, surface and submarine communities use the IMAT system to train officer and enlisted personnel in acoustics and oceanography (Beatty, 1999). In teaching acoustical oceanography (e.g. Foret *et al.*, 1997), IMAT enables students to display temperature, salinity and sound-speed profiles worldwide during any month of the year. This information can be combined with tactical displays showing 3D representations of the ocean environment (Beatty, 1999).

Passive sonars detect the sounds emitted by surface or submerged targets. The IMAT system can display 3D graphics of various platforms to illustrate the source and operation of various sound-generating mechanisms aboard these vessels. It can turn the external hull transparent, enabling students to see the internal components of the platform. Sonar displays can be generated from either a real-time acoustic simulator or from actual recordings of *in-situ* data. Additionally, an audio playback feature allows the student to listen to the time-series data represented by the display. A variety of processing options are available to emulate the various sonar systems and modes used by the naval air, surface and submarine communities (Beatty, 1999).

The IMAT system contains standard US Navy range-dependent acoustic and electromagnetic propagation models. Passive acoustic propagation models include PE, GRAB and ASTRAL. Passive sonar outputs can be combined with 3D tactical displays to visualize the environment along with the predicted propagation loss in that environment. Directional background noise can be incorporated into the display to illustrate the impact on signal excess. Active sonar predictions can be generated using ASPM or CASS. Active sonar outputs include echo, noise and reverberation components (Beatty, 1999).

Instructors can also use IMAT to build tactical scenarios. The 3D tactical displays can be populated with objects such as sonobuoy fields, submarines, aircraft and surface ships. The instructor can then use the scenario to analyze a contact's motion and solve for its range, course and speed by designating one animated object as the search platform and another as the target. It is also possible to match scenarios with specific sonar data and thus evaluate alternative tactics (Beatty, 1999).

Appendix A Abbreviations and acronyms

AAIW	Antarctic Intermediate Water
ACCURAY	Range-Dependent Shallow-Water Ray Propagation Model
ADCIRC	Advanced Circulation Model (US Army)
ADCP	Acoustic Doppler Current Profiler
ADIAB	Adiabatic Normal Mode
ADONIS	Acoustic Daylight Ocean Noise Imaging System
ADP	Automated Data Processing
ADS	Automated Data Systems
AEAS	Advanced Environmental Acoustic Support
AESD	Acoustic Environmental Support Detachment
AIAA	American Institute of Aeronautics and Astronautics
ALMOST	Acoustic Loss Model for Operational Studies and Tasks
AMBENT	Ambient-Noise Model
AMEC	Acoustic Model Evaluation Committee
AMODE	Acoustic Mid-Ocean Dynamics Experiment
AMOS	Acoustic, Meteorological and Oceanographic Survey
AMPE	Adiabatic-Mode Parabolic Equation
AN	Ambient Noise
ANDES	Ambient Noise Directionality Estimation System
ANI	Ambient-Noise Imaging
AOA	Analysis of Alternatives
AP	Arbitrary Profile Model
APL	Applied Physics Laboratory
APP	Acoustic Performance Prediction
ARA	Acoustic Rainfall Analysis

ARL	Applied Research Laboratory
ARSRP	Acoustic Reverberation Special Research Program
ASEPS	Automated Signal Excess Prediction System
ASERT	ASTRAL System for Estimation of Radial Transmission
ASPM	Acoustic System Performance Model
ASTRAL	ASEPS Transmission Loss
ASW	Anti-Submarine Warfare
ATOC	Acoustic Thermometry of Ocean Climate
AUAMP	Advanced Underwater Acoustic Modeling Program
AUTEC	Atlantic Undersea Test and Evaluation Center
AUTO OCEAN	Automated Oceanographic Database
AUTO SHIPS	Automated Shipping Density Database
AUV	Autonomous Underwater Vehicle
AVHRR	Advanced Very High Resolution Radiometer
AW	Acoustic Mode Generation Program using Chebyshev Polynomials as Basis Functions
BAM	Bistatic Acoustic Model
BB	Bottom Bounce
BBN	Bolt, Beranek and Newman, Inc.
BDRM	Beam-Displacement Ray-Mode Propagation Model
BEAMPL	Beam Program Library
BELLHOP	Gaussian Beam, Finite-Element, Range-Dependent Propagation Model
BEM	Boundary Element Method
BiKR	Bistatic Shallow-Water Reverberation Model Based on KRAKEN
BiRASP	Bistatic Range-Dependent Active System Prediction Model
BISAPP	Bistatic Acoustic Performance Prediction
BISSM	Bistatic Scattering Strength Model
BLUG	Bottom Loss Upgrade
BN	Beam Noise
BP	Beam Pattern
BS	Beam Signal
BT	Bathythermograph
BTL	Bell Telephone Laboratories
CAAM	Composite Area Analysis Model
CAIV	Cost As an Independent Variable
CAM	Cumulative Accuracy Measure
CANARD	CANARY (Version 6)
CANARY	Coherence and Ambient Noise for Arrays

330 *Abbreviations and acronyms*

CAPARAY	Broadband Eigenray Model
CASP	Canadian Atlantic Storms Program
CASS	Comprehensive Acoustic System Simulation
CASTAR	Computer Aided Sonar Tactical Recommendations
CBT	Computer-Based Training
CCUB	Finite-Element Parabolic Equation Model
CENTRO	Normal-Mode Model with Shear-Wave Effects
CFM	Calculation Frequency Method
C-MAN	Coastal-Marine Automated Network
CMMS	Conceptual Models of the Mission Space
CMM3D	Three-Dimensional Coupled Normal Mode Model
CMPE	Coupled Mode Parabolic Equation
CNOISE	Noise Model
CNP1	Finite-Element PE Model
COADS	Comprehensive Ocean-Atmosphere Data Set
COAMPS	Coupled Ocean-Atmosphere Mesoscale Prediction System
COEA	Cost and Operational Effectiveness Analysis
Coherent DELTA	3D Range-Dependent Ray Model
COMODE	Normal-Mode Model
CONGRATS	Continuous Gradient Ray-Tracing System
CORE	Coupled OASES for Range-Dependent Environments
COTS	Commercial Off-the-Shelf
COUPLE	Coupled-Mode Model
CPMS	Coupled Perturbed Mode Solution
C-SALT	Caribbean Sheets and Layers Transects Program
C-SNAP	Coupled SNAP
CST	Critical Sea Test
CTBT	Comprehensive Test-Ban Treaty
CTD	Conductivity, Temperature, Depth Sensor
CTF	Common Technical Framework
CW	Continuous Wave
CZ	Convergence Zone
DANES	Directional Ambient Noise Estimation System
dB	Decibel
DBDB	Digital Bathymetric Database
DCDB	Data Center for Digital Bathymetry (IHO)
DI	Directivity Index
DiMuNDS	Distributed Multi-National Defence Simulation
DINAMO	Directional Noise Array Model
DIS	Draft International Standard

DMA	Defense Mapping Agency (now NIMA)
DMSO	Defense Modeling and Simulation Office
DMSP	Defense Meteorological Satellite Program
DOD	Department of Defense
DODGE	Normal-Mode Model
DOE	Design of Experiment
DOP	Doppler Content of Reverberation Model
DOSL	Diurnal Ocean Surface Layer Model
DP	Direct Path
DREA	Defense Research Establishment Atlantic (Canada)
DREAM	Deductive Rapid Environmental Assessment Model
DREP	Defense Research Establishment Pacific (Canada)
DSBN	Discrete Shipping Beam Noise Model
DSC	Deep-Sound Channel
DSL	Deep Scattering Layer
DSMC	Defense Systems Management College
DT	Detection Threshold
DUNES	Directional Underwater Noise Estimates Model
EAST	Environmentally Adaptive Sonar Technology
EIA	Electronic Industries Association
EIGEN/REVERB	Eigenray/Reverberation Model
EFEPE	Exponential FEPE (superseded by RAM)
EOF	Empirical Orthogonal Function
E&P	Exploration and Production
ERL	Environmental Research Laboratory
ESA	Evolutionary Search Algorithm
ESL	Echo Signal Level, Energy Source Level
EUCLID	European Co-operation for the Long-term in Defence
EVA	Environmental Acoustics
FACT	Fast Asymptotic Coherent Transmission
FACTEX	FACT Extended to Range-Dependent Environments
FAME	Fast Multipath Expansion Model
FANM	Fast Ambient Noise Model
FDHB3D	Hybrid 3D, Two-Way IFD PE Model for Computing 3D Backscattering
FDTD	Finite-Difference Time-Domain
FE	Finite Element
FELMODE	TNO Fysisch en Elektronisch Laboratorium (FEL) Normal Mode Model
FEPE	Finite-Element Parabolic Equation Model

332 *Abbreviations and acronyms*

FEPE-CM	FEPE with Conformal Mapping
FEPEs	Finite-Element Parabolic Equation Model with Shear-Wave Effects
FFP	Fast-Field Program
FFRAME	Finite-Element, Full-Wave Range-Dependent, Acoustic Marching Element Model
FFT	Fast Fourier Transform
FIPS	Federal Information Processing Standards
FLIP	Floating Instrument Platform
FLIRT	Fast Linear Intermediate Range Transmission Model
FNMOc	Fleet Numerical Meteorology and Oceanography Center (formerly FNOC)
FNMSs	Fast Normal Mode with Surface Scattering Integrals Model
FNOC	Fleet Numerical Oceanography Center (now FNMOc)
FOAM	Finite-Element Ocean Acoustic Model
FOM	Figure of Merit; Federation Object Model
FOR3D	Finite Difference Methods, Ordinary Differential Equations, and Rational Function Approximations to Solve the LSS 3D Wave Equation
FPSO	Floating Production, Storage and Off-loading
FTE	Focused Technology Experiments
GA	Genetic Algorithm
GAMARAY	Broadband Ray Propagation Model
GASS	Generic Acoustic Stimulator System
GDEM	Generalized Digital Environmental Model
GEOSECS	Geochemical Ocean Section Study
GFMPPL	Geophysics Fleet Mission Program Library
GRAB	Gaussian Ray Bundles (Propagation Model in CASS)
GRASS	Germinating Ray-Acoustics Simulation
GSM	Generic Sonar Model
GUI	Graphical User Interface
HAPE	High-Angle PE Model
HARORAY	(Haro Strait) 2D Broadband Propagation Model Based on Ray Theory
HARPO	Hamiltonian Acoustic Raytracing Program – Ocean
HARVEST	Hybrid Adaptive Regime Visco-Elastic Simulation Technique
HBEM	Hybrid BEM
HFBL	High-Frequency Bottom Loss

HIE	Historical Ice Edge
HIFT	Heard Island Feasibility Test
HITS	Historical Temporal Shipping
HLA	High-Level Architecture
HODGSON	Range-Dependent Ray Theoretical Propagation Model
HOOM	Harvard Open Ocean Model
HWIL	Hardware in the Loop
HWS	Historical Wind Speed
HydroCAM	Hydroacoustic Coverage Assessment Model
HYPER	Hybrid Parabolic Equation-Ray Model
IAPSO	International Association for the Physical Sciences of the Ocean
ICAPS	Integrated Command ASW Prediction System
ICECAP	Interactive Computer Environment for Comprehensive Arctic Predictions
ICERAY	Under-Ice Ray Propagation Model
IEC	International Electrotechnical Commission
IEEE	Institute of Electrical and Electronics Engineers
IFD	Implicit Finite Difference
IHO	International Hydrographic Organization
Im	Imaginary
IMACS	International Association for Mathematics and Computers in Simulation
IMAT	Interactive Multisensor Analysis Training
IMP3D	Finite-Difference Parabolic Equation Model with Elastic Impedance Bottom Boundary
IMR	Inspection, Maintenance and Repair
IMS	International Monitoring System
INSACT	Analytical Active / Passive Sonar Model
INSIGHT	Analytical Range-Independent Propagation Model
INSTANT	Analytical Range-Dependent Propagation Model
IOA	Institute of Acoustics
IOC	Intergovernmental Oceanographic Commission
ISO	International Organization for Standardization
ISVRFEM	Institute of Sound and Vibration Research Finite Element Model
IUSS	Integrated Undersea Surveillance System
IHVR	Integrated Hierarchical Variable Resolution
KPP	Key Performance Parameters
KRAKEN	Adiabatic/Coupled Normal-Mode Model
LABL	Littoral Atmospheric Boundary Layer
LFBL	Low-Frequency Bottom Loss (formerly BLUG)

LIRA	Low-Frequency Intermediate-Surveillance-Range Active Model
LOFAR	Low-Frequency Analysis and Recording
LOGPE	Parabolic Equation Model Using Logarithmic Expression for Index of Refraction
LORA	Long Range Active Model
LRAPP	Long Range Acoustic Propagation Project
LSS	Lee-Saad-Schultz Method
LWAD	Littoral Warfare Advanced Development
LYCH	Range-Dependent, Ray-Theoretical Propagation Model
MaCh1	Broadband, Range-Dependent Propagation Model
MAIS	Major Automated Information System
MAM	Monostatic Acoustic Model
MAP	Maximum <i>a posteriori</i> Probability
MAST	Marine Science and Technology (European Commission Program)
MATE	Mid-Ocean Acoustic Transmission Experiment
MBT	Mechanical Bathythermograph
MCM	Mine Countermeasures
MDAP	Major Defense Acquisition Program
MEDUSA	Propagation Model
MEP	Model Evaluation Program
MGS	Marine Geophysical Survey
MIL	Military
MIMIC	Low-Frequency, Range-Dependent, Ray-Theoretical Propagation Model
MINERAY	Active Sonar Model used in Mine-Hunting Scenarios
MINEX	Mine Deployment Exercise
MIPE	(University of) Miami Parabolic Equation Model
MIS	Management Information System
MIW	Mediterranean Intermediate Water
MIZ	Marginal Ice Zone
MLD	Mixed Layer Depth
MMPE	Monterey-Miami Parabolic Equation (formerly UMPE, now PE-SSF)
MNS	Mission Needs Statement
MOATL	Modal Acoustic Transmission Loss Model
MOCASSIN	Monte Carlo Schall-Strahlen Intensitäten (Monte Carlo Sound Ray Intensities)
MOCTESUMA	Coupled Normal-Mode Model

MODAS	Modular Ocean Data Analysis System
MODELAB	Normal-Mode Model
MOE	Measures of Effectiveness
MOODS	Master Oceanographic Observation Data Set
MOP	Measures of Performance
MOREPE	Modified Refraction Parabolic Equation Model
MORS	Military Operations Research Society
MOS	Model Operating System
MOST	Mobile Sonar Technology
MPC	Multiple Profile Configuration Model
MPP	Multiple Profile Program
M&S	Modeling and Simulation
MSASM	Multistatic Active System Model; Multistatic Anti-Submarine Model
MSPFFP	Multiple Scattering Pulse FFP Model
MST	Moving Ship Tomography
MTS	Marine Technology Society
MULE	Multilayer Expansion Model
N	Noise Sources
NABTAM	Narrow Beam Towed Array Model
NADC	Naval Air Development Center (now NAWC)
NATO	North Atlantic Treaty Organization
NAUTILUS	Broadband Adiabatic Normal-Mode Model for Shallow-Water Areas
NAVDAB	Navy Ocean Environmental Acoustic Data Bank
NAVMSMO	Navy Modeling and Simulation Management Office
NAVOCEANO	Naval Oceanographic Office
NAWC	Naval Air Warfare Center
NBS	National Bureau of Standards (now NIST)
NCCOSC	Naval Command Control and Ocean Surveillance Center
NCDC	National Climatic Data Center
NDRC	National Defense Research Committee
NECTA	Naval Environmental Command Tactical Aid
NEMESIS/PLMODE	Propagation Model
NEONS	Naval Environmental Operational Nowcasting System
NEPBR	Numerable Energy Paths by RAYMODE
NGDC	National Geophysical Data Center
NGLI	Northern Gulf of Mexico Littoral Initiative
NIAG	NATO Industrial Advisory Group
NIMA	National Imagery and Mapping Agency (formerly DMA)

336 *Abbreviations and acronyms*

NISSM	Navy Interim Surface Ship Model
NL	Noise Level
NLAYER	N-Layer Normal-Mode Model
NLBC	Non-Local Boundary Condition
NLNM	N-Layer Normal-Mode Model
NML	Noise-Masking Level
NMSG	NATO Modelling and Simulation Group
NOAA	National Oceanographic and Atmospheric Administration
NOARL	Naval Oceanographic and Atmospheric Research Laboratory (now part of NRL)
NODC	National Oceanographic Data Center
NODDS	Navy/NOAA Oceanographic Data Distribution System
NOGAPS	Navy Operational Global Atmospheric Prediction System
NORAPS	Navy Operational Regional Atmospheric Prediction System
NORDA	Naval Ocean Research and Development Activity (now part of NRL)
NORM2L	Normal-Mode 2-Layer Model
NORMOD3	Normal-Mode Model
NOSC	Naval Ocean Systems Center
NPE	Non-linear Progressive-Wave Equation
NRL	Naval Research Laboratory
NSIDC	National Snow and Ice Data Center
NUSC	Naval Underwater Systems Center (now NUWC)
NUWC	Naval Undersea Warfare Center
OAML	Oceanographic and Atmospheric Master Library
OASES	Ocean Acoustics and Seismic Exploration Synthesis
OASIS	Ocean Ambient Sound Instrument System
ODE	Ordinary Differential Equation
OE	Ocean Environment
OGOPOGO	Normal-Mode Reverberation Model
OI	Optimum Interpolation
OMS	Optimum Mode Selection
OMT	Object Model Template
ONR	Office of Naval Research
ORB	Research Platform
ORBS	Ocean Refraction and Bathymetric Scattering Model

ORCA	Normal-Mode Model for Acousto-Elastic Ocean Environments
ORD	Operational Requirements Document
OS2IFD	Implicit Finite-Difference Parabolic Equation Model
OTIS	Optimum Thermal Interpolation System
PAREQ	Parabolic Equation Model
PARSIFAL	Plane Wave Acoustic Reflection from a Sediment of Inhomogeneous Fluid
PDPE	Pseudo-Differential PE
PE	Parabolic Equation
PECan	Canadian Parabolic Equation
PE-SSF	Parabolic Equation-Split-Step Fourier
PEREV	Parabolic Equation Reverberation Model
PERUSE	Parabolic Equation Rough Surface
PESOGEN	Parabolic Equation Solution Generator
PIPS	Polar Ice Prediction System
PLRAY	Ray Propagation Loss Model
POM	Princeton Ocean Model
POSSM	Panel on Sonar System Models
PRISM	Program for Integrated Sonar Modeling
PROLOS	Propagation Loss Model
PROPLOSS	Transmission Loss Module in ALMOST
PROSIM	Propagation Channel Simulator (Broadband Adiabatic Normal-Mode Propagation Model)
PROTEUS	Propagation Model
psu	Practical Salinity Unit
PWE	Progressive Wave Equation
RAM	Range-Dependent Acoustic Model
RAMS	RAM for Acousto-Elastic Problems
RANDI	Research Ambient Noise Directionality Model
RANGER	Range-Invariant Ray Model
RAP	Reliable Acoustic Path
RASP	Range-Dependent Active System Performance Model
RAY	Range-Dependent Raytracing Program
RAYMODE	Ray/Normal-Mode Model
RAYWAVE	Ray/Wave Propagation Model
RBR	Refracted-Bottom-Reflected
RBRSR	Refracted-Bottom-Reflected-Surface Reflected
RD	Recognition Differential; Range-Dependent
R&D	Research and Development
RDFFP	Range-Dependent FFP Model

RD-OASES	Range-Dependent OASES
RDOASP	Pulse Version of RD-OASES
RDOAST	RD-OASES with VISA
Re	Real
re	Relative to
REACT	Active Sonar Range Prediction Module in ALMOST
REPAS	Passive Sonar Range Prediction Module in ALMOST
REVGEN	Reverberation Generator
REVMOD	Reverberation Spectrum Model
REVSIM	Reverberation Simulation
RI	Range-Independent
RL	Reverberation Level
R&M	Reliability and Maintainability
RML	Reverberation-Masking Level
rms	Root Mean Square
RP-70	Ray-Tracing Program – 1970
RPG	Recommended Practices Guide
RPRESS	Model for Computing Seismoacoustic Wavefields
RR	Refracted–Refracted
RSR	Refracted–Surface-Reflected
RSRBR	Refracted–Surface-Reflected–Bottom-Reflected
RTI	Runtime Infrastructure
RUMBLE	Reverberation Underwater Model, Bistatic Level Estimation; Reverberation Undersea Model for Bottom-Limited Environments
SACLANTCEN	Supreme Allied Commander, Atlantic (SACLANT) Undersea Research Centre
SAFARI	Seismo-Acoustic Fast-Field Algorithm for Range-Independent Environments
SAFE	Seismo-Acoustic Finite-Element Model
SAFRAN	Hybrid BEM and WI Model
SALT	Sound Angle, Level and Travel Time
SBA	Simulation-Based Acquisition
SC	System Characteristics
SCOOTER	FFP, Finite-Element, Range-Independent Propagation Model
SCV	System Concept Validation
SDD	Software Design Document; Software Development and Documentation
SEARAY	Mine-Hunting Sonar Performance Model
SEE	Software Engineering Environment
SHALFACT	Shallow-Water FACT

SHAZAM	Shallow-Water Model
SHEAR2	Normal-Mode Model with Shear-Wave Effects
SI	Système International [d'Unités] (International System [of Units])
SIAM	Simulated Ambient Noise Model; Society for Industrial and Applied Mathematics
SIMAS	Sonar <i>In Situ</i> Mode Assessment System
SIO	Scripps Institution of Oceanography
SL	Source Level; Signal Level
SLD	Sonic Layer Depth
SN	Self-Noise; Shipping Noise
SNAP	SACLANTCEN Normal-Mode Acoustic Propagation Model
SNHR	Shipping Noise – High Resolution
SNLR	Shipping Noise – Low Resolution
SNR	Signal-to-Noise Ratio
SNUPE	Seoul National University Parabolic Equation
SOFAR	Sound Fixing and Ranging
SOM	Simulation Object Model
SONAR	Sound Navigation and Ranging
SP	Sonar Performance
SPARC	SACLANTCEN Pulse Acoustic Research Code
SPAWAR	US Navy Space and Naval Warfare Systems Command
Spectral PE	Parabolic Equation Model with 3D Backscattered Energy
SPLN	Finite Element PE Model
SRS	Software Requirements Specification
SSM / I	Special Sensor Microwave/Imager
SST	Sonar Simulation Toolset; Sea-Surface Temperature
STD	Salinity, Temperature, Depth Sensor; Software Test Description; Standard
SuperSNAP	Enhanced SNAP
SWAFS	Shallow Water Analysis and Forecasting System
SWAM	Shallow Water Acoustic Model Workshop
SWAPS	Spectral Wave Prediction System
SWAT	Shallow Water Acoustics Toolset
SWIL	Software in the Loop
SYNBAPS	Synthetic Bathymetric Profiling System
TA	Transmission Anomaly
TAMU	Texas A&M University
TDA	Tactical Decision Aid
TDPA	Time-Domain Parabolic Approximation Model

TDPE	Time-Domain Parabolic Equation
TENAR	Target Echo, Noise and Reverberation
TESS	Tactical Environmental Support System
TKE	Turbulent Kinetic Energy
TL	Transmission Loss
TLM	Transmission Line Matrix Modeling
TNO	Netherlands Organization for Applied Scientific Research
TOC	Total Ownership Cost
TOPEX	Topography Experiment for Ocean Circulation (unflown NASA precursor mission to TOPEX/Poseidon)
TOPEX / Poseidon	Joint US-French orbital mission launched in 1992 to track changes in sea-level height using radar altimeters
TOPS	Thermodynamical Ocean Prediction System
TOSL	Tactical Oceanography Simulation Laboratory
TOTS	Tactical Ocean Thermal Structure
TOWAN	Tactical Oceanography Wide Area Network
TRIMAIN	Range-Dependent Acoustic Propagation Model Based on Triangular Segmentation of the Range-Depth Plane
TRM	Time-Reversal Mirror
TS	Target Strength
TSPS	Tide and Surge Prediction System
TTCP	The Technical Cooperation Program
Two-Way PE	PE Model with Backscattered Energy
UK	United Kingdom
ULETA	Propagation Model
ULF	Ultra-low Frequency
UMPE	University of Miami PE (now MMPE)
UNIMOD	Propagation Model
US	United States
USI	Underwater Systems, Inc.
UUV	Unmanned Undersea Vehicle
VISA	Virtual Source Algorithm
VLA	Vertical Line Array
VLF	Very-Low Frequency
VSS	Volume Scattering Strength
VV&A	Verification, Validation and Accreditation
WADER	Global Ocean Information System
WAM	Wave Model
WDC	World Data Center
WEDGE	Range-Dependent Shallow-Water Normal Mode Model

WHOI	Woods Hole Oceanographic Institution
WI	Wavenumber Integration
WKB	Wentzel, Kramers and Brillouin
WKBJ	Wentzel, Kramers, Brillouin and Jeffreys
WOTAN	Weather Observation Through Ambient Noise
WRAP	Wide-Area Rapid Acoustic Prediction
WRN	Wind and Residual Noise
XBT	Expendable Bathythermograph
XSV	Expendable Sound Velocimeter

Appendix B Glossary of terms

- Absorption** – loss of acoustic energy due to conversion to heat.
- Accreditation** – the official certification that a model or simulation is acceptable for a specific purpose.
- Acoustic daylight** – imaging of underwater objects using the ambient noise field.
- Acoustic impedance** – characteristic acoustic impedance is quantitatively equal to the product of the density and sound speed of the medium.
- Acoustic tomography** – inverse technique that uses acoustic signals to sample the interior of a water body.
- Adiabatic process** – thermodynamic change in which there is no transfer of heat or mass across the system boundaries.
- Advection** – movement of oceanic properties by currents.
- Ambient noise** – background level of unwanted sound in the sea, exclusive of occasional (transient) noise sources.
- Ambient noise models** – mathematical models that predict the levels and directionality of noise in the ocean due to surface weather and shipping sources.
- Analog models** – controlled acoustic experiments in water tanks using appropriate scaling factors.
- Analytical models** – same as physical (physics-based) models.
- Anticyclonic** – gyral pattern of motion, induced by Earth's rotation, that is clockwise in the northern hemisphere but counterclockwise in the southern hemisphere.
- Archipelagic apron** – a gentle slope with a smooth surface on the sea floor.
- Attenuation** – loss of acoustic energy due to the combined effects of absorption and scattering.
- Backscattering** – scattering of sound in the direction of the source.
- Bank** – an elevation of the sea floor located on a shelf.
- Baroclinic** – state of stratification in the ocean in which surfaces of constant pressure intersect surfaces of constant density.
- Barotropic** – state of stratification in the ocean in which surfaces of constant pressure and surfaces of constant density are parallel.

- Basic acoustic models** – category of models containing underwater acoustic propagation, noise and reverberation models.
- Basin** – a depression of variable extent, generally in a circular or oval form.
- Bathymograph** – instrument used to measure water temperature versus depth.
- Beam displacement** – lateral displacement of an acoustic beam, of finite width, undergoing reflection at a water–sediment interface.
- Beam noise statistics models** – mathematical models that predict the levels and directionality of low-frequency shipping noise for application to large-aperture, narrow-beam passive sonar systems.
- Bistatic** – geometry in which the acoustic source and receiver are not at the same position.
- Borderland** – a region adjacent to a continent that is highly irregular with depths in excess of those typical of a shelf.
- Bottom bounce** – ray paths that have reflected off the sea floor.
- Bottom limited** – ocean environment characterized by a water-depth and sound-speed profile that will not support long-range refracted paths.
- Bottom loss** – reflection loss at the sea floor.
- Boundary conditions** – constraints imposed on possible solutions of the wave equation by adjacent surfaces.
- Buoyancy frequency** – frequency at which a water parcel displaced from equilibrium will oscillate.
- Canonical sound-speed profile** – standard sound-speed profile applicable to ocean areas having a deep sound channel; the profile normally assumes an exponential form in the region of the sound channel axis.
- Canyon** – a narrow, deep depression with steep slopes.
- Caustics** – envelopes formed by sets of tangential rays.
- Cell scattering models** – mathematical models of reverberation based on the assumption that the scatterers are uniformly distributed throughout the ocean.
- Chaotic** – a deterministic process for which certain ranges of parameters are unpredictable.
- Composite roughness model** – model that partitions treatment of boundary scattering into two regimes according to large-scale and small-scale surface roughness.
- Conjugate depth** – depth below the sound channel axis at which the value of sound speed equals that at a shallower depth above the axis.
- Constructive simulation** – models and simulations involving simulated people operating simulated systems.
- Continental margin** – a zone separating the continent from the deeper sea bottom, generally consisting of the rise, slope and shelf.
- Continental rise** – a gentle slope rising toward the foot of the continental slope.
- Continental shelf** – zone adjacent to a continent or island from the waterline to the depth at which there is usually a marked increase of slope to greater depth (shelf break).

- Continental slope** – zone between the continental shelf and the continental rise.
- Convergence zone** – ray paths formed by long-range refraction in deep-water environments having both a critical depth and sufficient depth excess.
- Cordillera** – an entire underwater mountain system including all the subordinate ranges, interior plateaus and basins.
- Coriolis force** – an apparent force acting on moving particles resulting from Earth's rotation; the force is proportional to the speed and latitude of the particle, and results in a deflection to the right of motion in the northern hemisphere, or to the left of motion in the southern hemisphere.
- Crank-Nicolson method** – method for numerically solving partial differential equations of the parabolic type (can be considered integration by the trapezoidal rule).
- Critical angle** – angle in the vertical plane separating the angular region of total reflection from that of partial reflection and partial transmission at a boundary.
- Critical depth** – depth at which the value of sound speed equals that of the near-surface maximum sound speed.
- Cusped caustic** – intersection of two (smooth) caustics.
- Cyclonic** – gyral pattern of motion, induced by Earth's rotation, that is counterclockwise in the northern hemisphere but clockwise in the southern hemisphere.
- Cylindrical spreading** – form of geometrical spreading that is confined between two parallel planes.
- Decibel** – unit of measure of acoustic intensity based on a logarithmic scale.
- Deep scattering layer** – layer of biological organisms associated with an increased scattering of sound.
- Deep sound channel axis** – location of the deep-sound speed minimum in the ocean.
- Deterministic** – state of being completely predictable (as distinguished from stochastic or chaotic).
- Diagnostic information** – information used to analyze the past or present state of a system, particularly with reference to identifying sonar system pathologies.
- Diel** – characterized by a 24-h period.
- Diffraction** – frequency-dependent interference effects.
- Direct path** – ray paths directly connecting source and receiver over short ranges without boundary interaction.
- Dispersion** – separation of sound into component frequencies; condition in which the phase velocity is frequency dependent.
- Diurnal** – having a daily cycle.
- Domains of applicability** – the spatial, temporal or spectral ranges over which a model's output can be considered valid; in general, such limitations are imposed by the model's physical or mathematical basis.

- Doppler** – frequency shift resulting from relative motion of source and receiver.
- Downwelling** – downward-directed water motion in the ocean.
- Ducted precursors** – acoustic energy that leaks out of a surface duct, travels via a convergence zone or bottom bounce path or both, before coupling back into the surface duct down range.
- Earth curvature correction** – correction applied to the sound-speed profile to adjust for propagation of sound over the curved Earth surface rather than over a flat surface.
- Eddies** – isolated patterns of gyral motion in the ocean.
- Eigenray** – ray that connects the source and the receiver.
- Eigenvalue** – solution to the normal-mode equation.
- Eikonal** – acoustic path length as a function of the endpoints.
- Ekman drift current** – surface current produced by the wind, but directed perpendicular to the wind direction.
- Empirical models** – mathematical models based on observations.
- Environmental models** – empirical algorithms used to quantify the boundary conditions and volumetric effects of the ocean environment.
- Escarpment** – an elongated and comparatively steep slope of the sea floor separating flat or gently sloping areas.
- Fan** – a gently sloping, fan-shaped feature normally located near the lower termination of a canyon.
- Fast-field models** – mathematical models of acoustic propagation based on a variation of the normal-mode technique.
- Fathometer returns** – multiply reflected echoes arriving from the sea surface directly above or from the sea floor directly below a monostatic sonar.
- Feature model** – statistical representation of a common synoptic structure in the ocean such as a front or an eddy.
- Fidelity** – the accuracy of a simulation representation when compared to the real world.
- Figure of merit** – quantitative measure of sonar performance; value equals allowable one-way transmission loss in passive sonars or two-way transmission loss in noise-limited active sonars.
- Finite difference** – mathematical technique for solving differential equations.
- Finite element** – mathematical technique for solving complex problems; in underwater acoustics, this method is implemented by dividing the range-depth plane into a gridded pattern of small elements.
- Fracture zone** – an extensive linear zone of unusually irregular topography of the sea floor characterized by large seamounts, steep-sided ridges, troughs or escarpments.
- Front** – boundary between two different water masses.
- Galerkin's method** – a member of the class of so-called weighted-residual methods and a variational formulation that has been the generally accepted basis of finite-element discretizations.

- Gap** – a depression cutting transversely across a ridge or rise.
- Gaussian beam tracing** – method that associates each acoustic ray with a beam having a Gaussian intensity profile normal to the ray.
- Geodesic path** – shortest distance between two points on the surface of an elliptical Earth; the shortest distance between two points on the surface of a spherical Earth is referred to as a great-circle path.
- Grazing angle** – angle in the range–depth plane measured from the horizontal.
- Half channel** – ducted environment defined by the equivalent sound-speed profile either above or below the deep-sound channel axis (the deep-sound channel is considered to be a full channel).
- Harmonic solution** – solution to the wave equation based on a single frequency.
- Hidden depths** – concept that regards as unimportant the deep ocean sediment structure below the ray turning point.
- Hill** – a small elevation rising less than about 200 m above the sea floor.
- Hindcast** – estimate of a previous state of a system.
- Hole** – a small depression on the sea floor.
- Hybrid models** – models based on multiple physical or mathematical approaches in order to broaden the domains of applicability.
- Incidence angle** – angle in the range–depth plane measured from the vertical.
- Inertial motion** – periodic, quasi-circular oceanic motions influenced by Earth’s rotation.
- Isotherm** – line connecting values of equal temperature.
- Knoll** – an elevation rising less than about 1 km above the sea floor and of limited extent across the summit.
- Levee** – an embankment bordering either one of both sides of a sea channel, or the low-gradient seaward part of a canyon or valley.
- Limiting angle** – angle of ray measured relative to a horizontal surface that leaves the source tangent to the horizontal plane.
- Littoral zone** – region between the shore and water depths of approximately 200 m. (The usage and interpretation of this term can vary widely.)
- Live simulation** – simulation involving real people operating real systems.
- Lloyd mirror effect** – near-field interference patterns associated with a shallow acoustic source and receiver.
- Marginal ice zone** – area of ice cover separating pack ice from the open ocean.
- Mathematical models** – category of models containing empirical models and numerical models.
- Mesoscale features** – dynamic features of the ocean with characteristic length scales on the order of 100 m to 100 km; examples include eddies and internal waves.
- Mixed layer** – surface layer of uniform temperature that is well mixed by wind or wave action or by thermohaline convection.

- Moat** – a depression located at the base of many seamounts or islands.
- Modified data banks** – data banks containing modified or extrapolated data derived from a primary data bank.
- Monostatic** – geometry in which the acoustic source and receiver are at the same position.
- Mountains** – a well-delineated subdivision of a large and complex feature, generally part of a cordillera.
- Multipath** – propagation conditions characterized by a combination of different types of paths.
- Multipath expansion models** – mathematical models of acoustic propagation based on a variation of the normal mode technique.
- Noise models** – mathematical models of noise levels and directionality in the ocean consisting of two categories: ambient-noise and beam-noise statistics models.
- Normal-mode models** – mathematical models of acoustic propagation based on the normal-mode technique.
- Normal modes** – natural frequencies at which a medium vibrates in response to an excitation.
- Nowcast** – estimate of the present state of a system.
- Numerical models** – mathematical models based on the governing physics.
- Ocean impulse response function** – time-variant and space-variant Green's function that describes the response of the ocean medium to a unit impulse.
- Parabolic equation models** – mathematical models of acoustic propagation based on a solution of the parabolic versus the elliptic-reduced wave equation.
- Pathological test case** – specification of inputs to a model that prove to be particularly troublesome; a test case that produces disorders in an otherwise well-functioning model.
- Physical models** – theoretical or conceptual (physics-based) representations of the physical and acoustical processes occurring within the ocean.
- Plain** – a flat, gently sloping or nearly level region of the sea floor.
- Plateau** – a comparatively flat-topped elevation of the sea floor of considerable extent across the summit and usually rising more than 200 m above the sea floor.
- Point-scattering models** – mathematical models of reverberation based on the assumption that the scatterers are randomly distributed throughout the ocean.
- Primary data banks** – data banks containing original or modestly processed environmental acoustic data.
- Prognostic information** – information used to forecast the future state of a system, particularly with reference to predicting sonar system performance.
- Propagation** – transmission of acoustic energy through the ocean medium.

Propagation models – mathematical models of underwater acoustic transmission loss consisting of five categories: ray-theory, normal-mode, multipath expansion, fast-field and parabolic equation models.

Province – a region composed of a group of similar bathymetric features whose characteristics are markedly in contrast with the surrounding areas.

Range – a series of generally parallel ridges or seamounts.

Rayleigh parameter – measure of the acoustic roughness of a surface.

Ray-theory models – mathematical models of acoustic propagation based on ray-tracing techniques.

Reef – an offshore consolidation with a depth below the sea surface of less than about 20 m.

Reflection – return of a portion of the incident energy in the forward direction after an encounter with a boundary.

Refraction – directional changes in acoustic propagation caused by density discontinuities.

Reliable acoustic path – ray paths formed when a source or receiver is located at the critical depth.

Reverberation – backscattered sound.

Reverberation models – mathematical models of reverberation based on boundary and volumetric scattering processes consisting of two categories: cell- and point-scattering models.

Ridge – a long, narrow elevation of the sea floor with steep sides.

Saddle – a low part on a ridge or between seamounts.

Salinity – a measure of the quantity of dissolved salts in sea water.

Scattering – random dispersal of sound after encounters with boundaries or with volumetric inhomogeneities.

Seachannel – a long, narrow, shallow depression of the sea floor, usually occurring on a gently sloping plain or fan, with either a U-shaped or V-shaped cross-section.

Seamount – an elevation rising 1 km or more above the sea floor, and of limited extent across the summit.

Self-noise – noise background originating from own ship or sonar structure.

Shadow zone – region of the range-depth plane into which little, if any, acoustic energy penetrates owing to the refractive properties of the water column.

Shoal – an offshore hazard to navigation with a depth below the sea surface of 20 m or less, usually composed of unconsolidated material.

Signal processing models – mathematical models of signal detection processes.

Significant wave height – the average height of the one-third highest waves of a given wave group.

Sill – the low part of a ridge or rise separating ocean basins from one another or from the adjacent sea floor.

- Simulation** – dynamic execution of models to generate prognostic or diagnostic information.
- Skip distance** – distance traveled by a ray that just grazes the sea surface, the sea floor or some intermediate layer in the ocean such as the sonic layer depth.
- Smart systems** – simulated people operating real systems.
- Soliton** – Internal solitary waves in the ocean, often generated by the non-linear deformation of internal tides.
- Sonar performance models** – mathematical models organized to solve specific sonar applications problems; contain environmental models, basic acoustic models and signal processing models.
- Sonic layer** – acoustic equivalent of mixed layer; surface layer characterized by near isovelocity conditions.
- Spherical spreading** – form of geometrical spreading that is unbounded.
- Spur** – a subordinate elevation, ridge or rise projecting from a larger feature.
- Stochastic** – state of being random; describable in probabilistic terms.
- Surface duct** – propagation channel bounded by the sea surface and the base of the sonic layer.
- Surface loss** – reflection loss at the sea surface.
- Tablemount** – a seamount having a comparatively smooth, flat top (also called a bench).
- Thermocline** – region of the water column characterized by a strong negative temperature gradient.
- Thermohaline** – of or relating to the effects of water temperature (thermo) and salinity (haline).
- Transmission anomaly** – difference between the observed transmission loss and the loss expected from spherical spreading alone.
- Trench** – a long, narrow and deep depression of the sea floor, with relatively steep sides.
- Trough** – a long depression of the sea floor, normally wider and shallower than a trench.
- Turning point** – position in the range-depth plane at which an upgoing or a downgoing ray reverses direction.
- Upwelling** – upward-directed motion in the ocean.
- Validation** – the process of determining the degree to which a model is an accurate representation of the real world from the perspective of the intended uses of the model.
- Valley** – a relatively shallow, wide depression with gentle slopes, the bottom of which grades continually downward (as opposed to a canyon).
- Verification** – The process of determining that a model implementation accurately represents the developer's conceptual description and specifications.

Virtual mode – mode associated with acoustic propagation in the surface duct.

Virtual simulation – simulation involving real people operating simulated systems (human-in-the-loop).

Water mass – body of water characterized by a unique temperature-salinity relationship.

Wave equation – equation describing motion of acoustic waves in the ocean.

Whispering gallery – phenomenon relating to the propagation of sound along the curved walls of a gallery, especially those of a hemispherical dome.

Appendix C Websites

The Internet has become a data-access “bus” for work in modeling and simulation. This appendix contains references to selected sites of practical use to sonar technologists and acoustical oceanographers. Addresses for these websites sometimes change or disappear entirely. In such cases, web searches using appropriate key words may help in locating new addresses or alternate sites. Many of these websites themselves contain helpful directories that refer readers to related websites.

OALIB (<http://oalib.saic.com>)

The Ocean Acoustics Library provides access to some of the stand-alone propagation models reviewed in this book. This access is provided directly to downloadable software or indirectly by reference to other authoritative websites. The Ocean Acoustics library contains acoustic modeling software and data. It is supported by the US Office of Naval Research (Ocean Acoustics Program) as a means of publishing software of general use to the international ocean acoustics community. Table C.1 summarizes the propagation models and other information currently available from the Ocean Acoustics Library. The contents of this site are subject to change.

Table C.1 Contents of the ocean acoustics library (OALIB) website

<i>Category</i>	<i>Contents</i>
Rays	BELLHOP, HARPO, RAY, TRIMAIN
Normal Modes	AW, COUPLE, KRAKEN, MOATL, NLayer, WKBZ
Wavenumber integration	OASES, RPRESS, SCOOTER, SPARC
Parabolic equation	FOR3D, MMPE, PDPE, PECAN, RAM / RAMS, UMPE
Other	Related modeling software and datasets to support oceanographic and acoustic analyses

DMSO (<http://www.dmsomil/>)

The Defense Modeling and Simulation Office (DMSO) promulgates M&S policy, initiatives and guidance to promote cooperation among DOD components to maximize efficiency and effectiveness. The DMSO assembled the *DOD Modeling and Simulation (M&S) Glossary* (DOD 5000.59-M), which prescribes a uniform M&S terminology, particularly for use throughout the DOD.

NAVMSMO (<http://navmsmo.hq.navy.mil>)

The US Navy Modeling and Simulation Management Office (NAVMSMO) maintains the Navy Modeling and Simulation Catalog, which allows users to find and obtain M&S resources in support of analyses and training. The NAVMSMO web site serves as the web-enabled single point of public access to the Navy's M&S Information Service (NMSIS). The NMSIS collects, maintains and distributes information about Navy modeling and simulation for the use of program managers, engineers, M&S builders and others throughout the M&S community.

TOWAN (<http://www7180.nrlssc.navy.mil/homepages/TOWAN/towanpgs/TOWANDataIndex.html>)

The US Navy Tactical Oceanography Wide Area Network (TOWAN) is a data server dedicated to supplying the DOD and supporting contractors with environmental data for simulation, modeling and other analyses. The purpose of TOWAN is to provide rapid sub-setting and data extractions from existing databases, and to deliver the extracted data using a consistent and documented output format. It is not the intent of TOWAN to merge datasets or do any interpolation on the data extracted. The contents of TOWAN are organized by the generic parameter groupings of ambient noise, bathymetry, geoacoustics, gravity, ice, oceanography, observational, physical parameters and reverberation.

NESDIS (<http://www.nesdis.noaa.gov/>)

Under NESDIS (National Environmental Satellite, Data, and Information Service), the National Oceanic and Atmospheric Administration (NOAA) maintains three data centers: climatic, geophysical and oceanographic.

NCDC (<http://lwf.ncdc.noaa.gov/oa/ncdc.html>)

The National Climatic Data Center (NCDC) archives surface marine data from around the world. Surface marine observations contain various meteorological elements, which, over time, can describe the nature of the climate of a location or region. These elements include temperature, dew point, relative

humidity, precipitation, snowfall, snow depth on ground, wind speed, wind direction, cloudiness, visibility, atmospheric pressure, evaporation, soil temperatures and various types of weather occurrences such as hail, fog, thunder and glaze. NCDC receives and archives meteorological data from ships at sea as well as from buoys, both fixed and free floating. The weather observations are normally hourly (although they can be more frequent) and there are daily and monthly summaries. Many of the summaries are published on paper, electronically and via CD-ROM.

NGDC (<http://www.ngdc.noaa.gov/>)

The National Geophysical Data Center (NGDC) Marine Geology & Geophysics Division (and the collocated World Data Center for Marine Geology & Geophysics) compiles and maintains extensive databases in both coastal and open ocean areas. Key data types include bathymetry and gridded relief, trackline geophysics (gravity, magnetics and seismic reflection), sediment thickness, data from ocean drilling and sea floor sediment and rock samples, digital coastlines and data from the Great Lakes. The NGDC also operates the International Hydrographic Organization Data Center for Digital Bathymetry (IHO DCDB), and is an active participant in international ocean mapping projects sponsored by the IHO and the Intergovernmental Oceanographic Commission (IOC). The National Snow and Ice Data Center (NSIDC) (<http://nsidc.org/>) monitors sea ice concentrations and snow extent using near-real-time satellite imagery. The NSIDC is part of the University of Colorado Cooperative Institute for Research in Environmental Sciences, and is affiliated with the National Oceanic and Atmospheric Administration National Geophysical Data Center through a cooperative agreement.

NODC (<http://www.nodc.noaa.gov/>)

The National Oceanographic Data Center (NODC) archives physical, chemical and biological oceanographic data collected by US federal agencies (including the DOD – primarily the US Navy), state and local government agencies, universities and research institutions and private industry. The NODC serves as a repository and dissemination facility for data collected by other organizations.

References

- Abawi, A.T., Kuperman, W.A. and Collins, M.D. (1997) The coupled mode parabolic equation. *J. Acoust. Soc. Amer.*, **102**, 233–8.
- Abramowitz, M. and Stegun, I.A. (eds) (1964) *Handbook of Mathematical Functions with Formulas, Graphs and Mathematical Tables*. National Bureau of Standards Applied Mathematics Series 55. US Government Printing Office, Washington, DC.
- Abrantes, A.A.M., Smith, K.B. and Larraza, A. (1999) Examination of time-reversal acoustics and applications to underwater communications. *J. Acoust. Soc. Amer.*, **105**, 1364 (abstract).
- Ainslie, M.A. (1999) Interface waves in a thin sediment layer: review and conditions for high loss. *Proc. Inst. Acoust.*, **21** (Part 9), 33–47.
- Ainslie, M.A. (2000) Bistatic sonar performance assessment. Proc. Undersea Defence Technology Conf. (UDT Europe), paper 2A.1.
- Ainslie, M.A. and Harrison, C.H. (1990) Diagnostic tools for the ocean acoustic modeller. In *Computational Acoustics. Vol. 3: Seismo-Ocean Acoustics and Modelling*, eds, D. Lee, A. Cakmak and R. Vichnevetsky. North-Holland, Amsterdam, pp. 107–30.
- Ainslie, M.A. and McColm, J.G. (1998) A simplified formula for viscous and chemical absorption in sea water. *J. Acoust. Soc. Amer.*, **103**, 1671–2.
- Ainslie, M.A., Harrison, C.H. and Burns, P.W. (1994) Reverberation modelling with INSIGHT. *Proc. Inst. Acoust.*, **16** (Part 6), 105–12.
- Ainslie, M.A., Harrison, C.H. and Burns, P.W. (1996) Signal and reverberation prediction for active sonar by adding acoustic components. *IEE Proc. (Radar, Sonar and Navigation)* **143** (3), 190–5.
- Ainslie, M.A., Packman, M.N. and Harrison, C.H. (1998a) Fast and explicit Wentzel–Kramers–Brillouin mode sum for the bottom-interacting field, including leaky modes. *J. Acoust. Soc. Amer.*, **103**, 1804–12.
- Ainslie, M.A., Robins, A.J. and Prior, M.K. (1998b) Benchmark solutions of plane wave reflection loss. *J. Acoust. Soc. Amer.*, **104**, 3305–12.
- Ainslie, M.A., Hamson, R.M., Horsley, G.D., James, A.R., Laker, R.A., Lee, M.A., Miles, D.A. and Richards, S.D. (2000) Deductive multi-tone inversion of seabed parameters. *J. Comput. Acoust.*, **8**, 271–84.
- Ainslie, M.A., Laker, R.A. and Hamson, R.M. (2001) Deductive geoacoustic inversion: application to measurements in the Strait of Sicily. In *Acoustical Oceanography*, eds, T.G. Leighton, G.J. Heald, H.D. Griffiths and G. Griffiths. *Proc. Inst. Acoust.*, **23** (Part 2), 66–73.

- Akal, T. and Berkson, J.M. (eds) (1986) *Ocean Seismo-Acoustics: Low-Frequency Underwater Acoustics*. NATO Conf. Series IV, Marine Sciences, Vol. 16. Plenum, New York.
- Alapati, N.K., Kirklin, R.H. and Etter, P.C. (1993) Analysis of chaotic waveforms for application to active sonar systems. Radix Systems, Inc., TR-93-081.
- Albers, V.M. (1965) *Underwater Acoustics Handbook – II*. The Pennsylvania State Univ. Press, University Park, USA.
- Almeida, R.J. Jr and Medeiros, R.C. (1985) RAYMODE accuracy, limitations and transportability. Nav. Underwater Syst. Ctr, Tech. Memo. 841032.
- Alvarez, A., Harrison, C. and Siderius, M. (2001) Predicting underwater ocean noise with genetic algorithms. *Phys. Lett. A*, **280**, 215–20.
- Amato, I. (1993) A sub surveillance network becomes a window on whales. *Science*, **261**, 549–50.
- Amnicht, E. and Stickler, D.C. (1984) Uniform asymptotic evaluation of the continuous spectrum contribution for a stratified ocean. *J. Acoust. Soc. Amer.*, **76**, 186–91.
- Andersen, N.R. and Zahuranec, B.J. (eds) (1977). *Oceanic Sound Scattering Prediction*. Plenum, New York.
- Anderson, V.C. (1958) Arrays for the investigation of ambient noise in the ocean. *J. Acoust. Soc. Amer.*, **30**, 470–7.
- Anderson, V.C. (1979) Variation of the vertical directionality of noise with depth in the North Pacific. *J. Acoust. Soc. Amer.*, **66**, 1446–52.
- Anderson, A.L. and Hampton, L.D. (1980a) Acoustics of gas-bearing sediments I. Background. *J. Acoust. Soc. Amer.*, **67**, 1865–89.
- Anderson, A.L. and Hampton, L.D. (1980b) Acoustics of gas-bearing sediments II. Measurements and models. *J. Acoust. Soc. Amer.*, **67**, 1890–903.
- Apel, J.R. (1987) *Principles of Ocean Physics*. International Geophysics Series, Vol. 38. Academic Press, San Diego.
- Applied Physics Laboratory, University of Washington (1994) APL-UW high-frequency ocean environmental acoustic models handbook. APL-UW TR 9407 (also, Office of Naval Research Tech. Rept AEAS 9501).
- Aredov, A.A. and Furduev, A.V. (1994) Angular and frequency dependencies of the bottom reflection coefficient from the anisotropic characteristics of a noise field. *Acoust. Phys.*, **40**, 176–80.
- Arnold, J.M. and Felsen, L.B. (1983) Rays and local modes in a wedge-shaped ocean. *J. Acoust. Soc. Amer.*, **73**, 1105–19.
- Arrhenius, G. (1963) Pelagic sediments. In *The Sea. Vol. 3, The Earth Beneath the Sea, History*, ed., M.N. Hill. Interscience Publishers, New York, pp. 655–727.
- Arvelo, J.I. and Überall, H. (1990) Adiabatic normal-mode theory of sound propagation including shear waves in a range-dependent ocean floor. *J. Acoust. Soc. Amer.*, **88**, 2316–25.
- Au, W.W.L., Penner, R.H. and Turl, C.W. (1987) Propagation of Beluga echolocation signals. *J. Acoust. Soc. Amer.*, **82**, 807–13.
- Auer, S.J. (1987) Five-year climatological survey of the Gulf Stream system and its associated rings. *J. Geophys. Res.*, **92**, 11709–26.
- Avilov, K.V. (1995) Pseudodifferential parabolic equations of sound propagation in the slowly range-dependent ocean and their numerical solutions. *Acoust. Phys.*, **41**, 1–7.

356 *References*

- Axelrod, E.H., Schoomer, B.A. and VonWinkle, W.A. (1965) Vertical directionality of ambient noise in the deep ocean at a site near Bermuda. *J. Acoust. Soc. Amer.*, **37**, 77–83.
- Baer, R.N. (1981) Propagation through a three-dimensional eddy including effects on an array. *J. Acoust. Soc. Amer.*, **69**, 70–5.
- Baer, R.N., Berman, D.H., Perkins, J.S. and Wright, E.B. (1985). A three-dimensional model for acoustic scattering from rough ocean bathymetry. *Comp. Math. Applic.*, **11**, 863–71.
- BAeSEMA Ltd (1998) Tactical support systems. Product description literature.
- Baggeroer, A.B., Kuperman, W.A. and Mikhalevsky, P.N. (1993) An overview of matched field methods in ocean acoustics. *IEEE J. Oceanic Eng.*, **18**, 401–24.
- Bailey, R.S., Beck, M.A., Fink, I.M., Garcia, M.L., Kaduchak, G. and Lawrence, M.Z. (1997) Installation and user's guide for Mineray 3 sonar performance prediction model, X-Windows version (XMineray). Appl. Res. Labs., Univ. Texas at Austin, USA.
- Baker, C.L. (1976) FANIN preprocessor for the FANM-I ambient noise model. Ocean Data Syst., Inc.
- Baker, C.L. and Spofford, C.W. (1974) The FACT model, Vol II. Acoustic Environmental Support Detachment, Off. Nav. Res., Tech. Note TN-74-04.
- Bannister, R.W. (1986) Deep sound channel noise from high-latitude winds. *J. Acoust. Soc. Amer.*, **79**, 41–8.
- Bannister, R.W., Kewley, D.J. and Burgess, A.S. (1989) Directional underwater noise estimates – The DUNES model. Australia Department of Defence, Defence Science and Technology Organisation, Maritime Systems Division, Weapons Systems Research Laboratory, WSRL-TN-34/89.
- Barkhatov, A.N. (1968) *Modeling of Sound Propagation in the Sea. Gidrometeorologicheskoe Izdatel'stvo*. (Translated from Russian by J.S. Wood, Consultants Bureau, a Division of Plenum Publishing Corp., New York, 1971.)
- Bartberger, C.L. (1965) Lecture notes on underwater acoustics. Nav. Air Devel. Ctr, Rept NADC-WR-6509.
- Bartberger, C.L. (1978a) PLRAY: a ray propagation loss program. Nav. Air Devel. Ctr, Rept NADC-77296-30.
- Bartberger, C.L. (1978b) AP-2 normal mode program. Nav. Air Devel. Ctr, Rept.
- Bartberger, C.L. (1985) The NADC bistatic active sonar model. Nav. Air Devel. Ctr, Rept.
- Bartberger, C.L. (1991a) The physics of the bistatic acoustic model. Nav. Air Devel. Ctr, Rept NADC-91020-50.
- Bartberger, C.L. (1991b) The NADC monostatic sonar model (version 1.0). Nav. Air Devel. Ctr, TN-5044-7-91.
- Bathen, K.H. (1972) On the seasonal changes in the depth of the mixed layer in the North Pacific Ocean. *J. Geophys. Res.*, **77**, 7138–50.
- Beatty, W.F. (1999) Interactive multisensor analysis training. *Wavelengths*, January/February, pp. 14–15. Published by Naval Surface Warfare Center, Carderock Division, West Bethesda, Maryland, USA.
- Becken, B.A. (1961) The directional distribution of ambient noise in the ocean. Scripps Inst. Oceanogr., Rept 61-4.
- Beckmann, P. and Spizzichino, A. (1963) *The Scattering of Electromagnetic Waves from Rough Surfaces*. International Series of Monographs on Electromagnetic Waves, Vol. 4. Pergamon Press, New York.

- Bedard, A.J. Jr and Georges, T.M. (2000) Atmospheric infrasound. *Physics Today*, 53 (3), 32–7.
- Beebe, J.H., McDaniel, S.T. and Rubano, L.A. (1982) Shallow-water transmission loss prediction using the Biot sediment model. *J. Acoust. Soc. Amer.*, 71, 1417–26.
- Bennett, A.F. (1992) *Inverse Methods in Physical Oceanography*. Cambridge University Press, New York.
- Berger, M.D., Boucher, C.E., Daley, E.M., Renner, W.W., Pastor, V.L., Haines, L.C. and Eller, A.I. (1994) Acoustic system performance model (ASPM) 4.0A: user's guide. Sci. Appl. Inter. Corp., SAIC-94/1000.
- Berman, D.H., Wright, E.B. and Baer, R.N. (1989) An optimal PE-type wave equation. *J. Acoust. Soc. Amer.*, 86, 228–33.
- Bertucelli, H.C. (1975) Digital computer programs for analyzing acoustic search performance in refractive waters, Vol. 3. Nav. Undersea Ctr, Tech. Pub. 164.
- Bialek, E.L. (1966) *Handbook of Oceanographic Tables*. Nav. Oceanogr. Off., Special Pub. SP-68. US Government Printing Office, Washington, DC.
- Bini-Verona, F., Nielsen, P.L. and Jensen, F.B. (2000) PROSIM broadband normal-mode model: a users' guide. SAACLANT Undersea Res. Ctr, Memo SM-358.
- Biot, M.A. (1956a) Theory of propagation of elastic waves in a fluid-saturated porous solid. I. Low-frequency range. *J. Acoust. Soc. Amer.*, 28, 168–78.
- Biot, M.A. (1956b) Theory of propagation of elastic waves in a fluid-saturated porous solid. II. Higher frequency range. *J. Acoust. Soc. Amer.*, 28, 179–91.
- Bishop, G.C. (1987) A bistatic, high-frequency, under-ice, acoustic scattering model. *J. Acoust. Soc. Amer.*, 82 (Suppl. 1), S30 (abstract).
- Bishop, G.C. (1989a) A bistatic, high-frequency, under-ice, acoustic scattering model. I: theory. *J. Acoust. Soc. Amer.*, 85, 1903–11.
- Bishop, G.C. (1989b) A bistatic, high-frequency, under-ice, acoustic scattering model. II: applications. *J. Acoust. Soc. Amer.*, 85, 1912–24.
- Bishop, G.C., Ellison, W.T. and Mellberg, L.E. (1987) A simulation model for high-frequency under-ice reverberation. *J. Acoust. Soc. Amer.*, 82, 275–86.
- Bishop, G.C., Mellberg, L.E. and Ellison, W.T. (1986) A simulation model for high-frequency, under-ice reverberation. Nav. Underwater Syst. Ctr, Tech. Rept 6268.
- Bjørnø, L. (1998) Sources of ambient noise in littoral waters. *Arch. Acoust.*, 23, 211–25.
- Blanchard, B.S. (1998) *System Engineering Management*, 2nd edn. John Wiley & Sons, New York.
- Blatstein, I.M. (1974) Comparisons of normal mode theory, ray theory, and modified ray theory for arbitrary sound velocity profiles resulting in convergence zones. Nav. Ordnance Lab., NOLTR 74-95.
- Blumen, L.S. and Spofford, C.W. (1979) The ASTRAL model, Vol. II: software implementation. Sci. Appl., Inc., SAI-79-743-WA.
- Bogart, C.W. and Yang, T.C. (1992) Comparative performance of matched-mode and matched-field localization in a range-dependent environment. *J. Acoust. Soc. Amer.*, 92, 2051–68.
- Bom, N. (1969) Effect of rain on underwater noise level. *J. Acoust. Soc. Amer.*, 45, 150–6.
- Botseas, G., Lee, D. and Gilbert, K.E. (1983) IFD: wide angle capability. Nav. Underwater Syst. Ctr, Tech. Rept 6905.

- Botseas, G., Lee, D. and King, D. (1987) FOR3D: a computer model for solving the LSS three-dimensional, wide angle wave equation. Nav. Underwater Syst. Ctr, Tech. Rept 7943.
- Botseas, G., Lee, D. and Siegmann, W.L. (1989) IFD: interfaced with Harvard open ocean model forecasts. Nav. Underwater Syst. Ctr, Tech. Rept 8367.
- Bowditch, N. (1977) *American Practical Navigator*. Vol. I. Defense Mapping Agency Hydrographic Center, Pub. No. 9, Washington, DC. (Continuously maintained since first published in 1802.)
- Bowlin, J.B., Spiesberger, J.L., Duda, T.F. and Freitag, L.F. (1992) Ocean acoustical ray-tracing software RAY. Woods Hole Oceanogr. Inst., Tech. Rept WHOI-93-10.
- Boyles, C.A. (1984) *Acoustic Waveguides. Applications to Oceanic Science*. John Wiley & Sons, New York.
- Bracken, J., Kress, M. and Rosenthal, R.E. (eds) (1995) *Warfare Modeling*. John Wiley & Sons, New York.
- Bradley, M.R. and Bradley, B.W. (1984) Computer program performance specification for the geophysics ambient noise model. Planning Syst., Inc., Tech. Rept TR-S310018.
- Breeding, J.E. Jr (1993) Description of a noise model for shallow water: RANDI-III. *J. Acoust. Soc. Amer.*, **94**, 1820 (abstract).
- Breeding, J.E., Pflug, L.A., Bradley, M., Hebert, M. and Wooten, M. (1994) RANDI 3.1 user's guide. Nav. Res. Lab., Rept NRL/MR/7176-94-7552.
- Breeding, J.E. Jr, Pflug, L.A., Bradley, M., Walrod, M.H. and McBride, W. (1996) Research ambient noise directionality (RANDI) 3.1 physics description. Nav. Res. Lab., Rept NRL/FR/7176-95-9628.
- Brekhovskikh, L. and Lysanov, Yu. (1982) *Fundamentals of Ocean Acoustics*. Springer-Verlag, New York.
- Brock, H.K. (1978) The AESD parabolic equation model. Nav. Ocean Res. Devel. Activity, Tech. Note 12.
- Brock, H.K., Buchal, R.N. and Spofford, C.W. (1977) Modifying the sound-speed profile to improve the accuracy of the parabolic-equation technique. *J. Acoust. Soc. Amer.*, **62**, 543–52.
- Brooke, G.H. and Thomson, D.J. (2000) Non-local boundary conditions for high-order parabolic equation algorithms. *Wave Motion* **31**, 117–29.
- Brooke, G.H., Thomson, D.J. and Ebbeson, G.R. (2001) PECAN: a Canadian parabolic equation model for underwater sound propagation. *J. Comput. Acoust.*, **9**, 69–100.
- Brown, J.R. (1964) Reverberation under Arctic ice. *J. Acoust. Soc. Amer.*, **36**, 601–3.
- Brown, M.G. (1994) Global acoustic propagation modeling using MaCh1. *J. Acoust. Soc. Amer.*, **95**, 2880 (abstract).
- Brown, M.G., Tappert, F.D. and Goni, G. (1991a) An investigation of sound ray dynamics in the ocean volume using an area preserving mapping. *Wave Motion*, **14**, 93–9.
- Brown, M.G., Tappert, F.D., Goni, G.J. and Smith, K.B. (1991b) Chaos in underwater acoustics. In *Ocean Variability and Acoustic Propagation*, eds, J. Potter and A. Warn-Varnas. Kluwer Academic Publishers, Dordrecht, The Netherlands, pp. 139–60.
- Brown, N.R., Leighton, T.G., Richards, S.D. and Heathershaw, A.D. (1998) Measurement of viscous sound absorption at 50–150 kHz in a model turbid environment. *J. Acoust. Soc. Amer.*, **104**, 2114–20.

- Browning, D.G., Christian, R.J. and Petitpas, L.S. (1994) A global survey of the impact on acoustic propagation of deep water warm core ocean eddies. *J. Acoust. Soc. Amer.*, **95**, 2880 (abstract).
- Brutzman, D.P., Kanayama, Y. and Zyda, M.J. (1992) Integrated simulation for rapid development of autonomous underwater vehicles. Proc. 1992 IEEE Symposium on Autonomous Underwater Vehicle Technology, pp. 3–10.
- Bryan, G.M. (1967) Underwater sound in marine geology. In *Underwater Acoustics*, Vol. 2, ed., V.M. Albers. Plenum, New York, pp. 351–61.
- Buck, B.M. (1968) Arctic acoustic transmission loss and ambient noise. In *Arctic Drifting Stations*, ed., J.E. Sater. Arctic Inst. of North Amer., Calgary, Canada, pp. 427–38.
- Buck, B.M. (1981) Preliminary underice propagation models based on synoptic ice roughness. Polar Res. Lab., TR-30.
- Buck, B.M. (1985) Long term statistical measurements of environmental acoustics parameters in the Arctic (AEAS Report No. 2 – low frequency transmission loss measurements in the central Arctic Ocean). Polar Res. Lab., TR-55.
- Bucker, H.P. (1971) Some comments on ray theory with examples from current NUC ray trace models. SACLANT ASW Res. Ctr, Conf. Proc. No. 5, Part I, pp. 32–6.
- Bucker, H.P. (1976) Use of calculated sound fields and matched-field detection to locate sound sources in shallow water. *J. Acoust. Soc. Amer.*, **59**, 368–73.
- Bucker, H.P. (1983) An equivalent bottom for use with the split-step algorithm. *J. Acoust. Soc. Amer.*, **73**, 486–91.
- Bucker, H.P. (1986) Use of SALT tables for rapid calculation of sound angle, level and travel time. *J. Acoust. Soc. Amer.*, **80** (Suppl. 1), S63 (abstract).
- Bucker, H.P. (1994) A simple 3-D Gaussian beam sound propagation model for shallow water. *J. Acoust. Soc. Amer.*, **95**, 2437–40.
- Bucker, H.P. and Morris, H.E. (1968) Normal-mode reverberation in channels or ducts. *J. Acoust. Soc. Amer.*, **44**, 827–8.
- Buckingham, M.J. (1991) On acoustic transmission in ocean-surface waveguides. *Philos. Trans. R. Soc. Lond. (A)*, **335**, 513–55.
- Buckingham, M.J. (1992) Ocean-acoustic propagation models. *J. Acoust.*, **3**, 223–87.
- Buckingham, M.J. (1993) Theory of acoustic imaging in the ocean with ambient noise. *J. Comput. Acoust.*, **1**, 117–40.
- Buckingham, M.J. and Jones, S.A.S. (1987) A new shallow-ocean technique for determining the critical angle of the seabed from the vertical directionality of the ambient noise in the water column. *J. Acoust. Soc. Amer.*, **81**, 938–46.
- Buckingham, M.J. and Potter, J.R. (eds) (1996) *Sea Surface Sound '94*. World Scientific Publishing, Singapore.
- Buckingham, M.J. and Tolstoy, A. (1990) An analytical solution for benchmark problem 1: the “ideal” wedge. *J. Acoust. Soc. Amer.*, **87**, 1511–13.
- Buckingham, M.J., Berkhout, B.V. and Glegg, S.A.L. (1992) Imaging the ocean with ambient noise. *Nature*, **356**, 327–9.
- Buckingham, M.J., Epifanio, C.L. and Readhead, M.L. (1996a) Passive imaging of targets with ambient noise: experimental results. *J. Acoust. Soc. Amer.*, **100**, 2736 (abstract).
- Buckingham, M.J., Potter, J.R. and Epifanio, C.L. (1996b) Seeing underwater with background noise. *Sci. Amer.*, **274** (2), 86–90.

- Burdic, W.S. (1991) *Underwater Acoustic System Analysis*, 2nd edn. PTR Prentice Hall, Englewood Cliffs, USA.
- Burridge, R. and Weinberg, H. (1977) Horizontal rays and vertical modes. In *Wave Propagation and Underwater Acoustics*, eds, J.B. Keller and J.S. Papadakis. Lecture Notes in Physics, Vol. 70. Springer-Verlag, New York, pp. 86–152.
- Caiti, A., Hermand, J.-P., Jesus, S. and Porter, M. (eds) (2000) *Experimental Acoustic Inversion Methods for Exploration of the Shallow Water Environment*. Kluwer Academic Publishers, Dordrecht, The Netherlands.
- Candy, J.V. and Sullivan, E.J. (1992) Ocean acoustic signal processing: a model-based approach. *J. Acoust. Soc. Amer.*, **92**, 3185–201.
- Candy, J.V. and Sullivan, E.J. (1993) Sound velocity profile estimation: a system theoretic approach. *IEEE J. Oceanic Eng.*, **18**, 240–52.
- Carbone, N.M., Deane, G.B. and Buckingham, M.J. (1998) Estimating the compressional and shear wave speeds of a shallow water seabed from the vertical coherence of ambient noise in the water column. *J. Acoust. Soc. Amer.*, **103**, 801–13.
- Carey, W.M. (1995) Standard definitions for sound levels in the ocean. *IEEE J. Oceanic Eng.*, **20**, 109–13.
- Carey, W.M. and Wagstaff, R.A. (1986) Low-frequency noise fields. *J. Acoust. Soc. Amer.*, **80**, 1523–6.
- Carey, W.M., Evans, R.B. and Davis, J.A. (1987) Downslope propagation and vertical directionality of wind noise. *J. Acoust. Soc. Amer.*, **82** (Suppl. 1), S63 (abstract).
- Carey, W.M., Evans, R.B., Davis, J.A. and Botseas, G. (1990) Deep-ocean vertical noise directionality. *IEEE J. Oceanic Eng.*, **15**, 324–34.
- Carlson, J.T. (1994) IUSS community adopts collateral uses. *Sea Technol.*, **35** (5), 25–8.
- Carroll, S.N. and Szczechowski, C. (2001) The northern Gulf of Mexico littoral initiative. Proc. MTS/IEEE Oceans 2001 Conf., pp. 1311–17.
- Caruthers, J.W. and Novarini, J.C. (1993) Modeling bistatic bottom scattering strength including a forward scatter lobe. *IEEE J. Oceanic Eng.*, **18**, 100–7.
- Caruthers, J.W. and Yoerger, E.J. (1993) ARSRP reconn results and BISSM modeling of direct path backscatter. In *Ocean Reverberation*, eds, D.D. Ellis, J.R. Preston and H.G. Urban. Kluwer Academic Publishers, Dordrecht, The Netherlands, pp. 203–8.
- Caruthers, J.W., Sandy, R.J. and Novarini, J.C. (1990) Modified bistatic scattering strength model (BISSM2). Nav. Oceanogr. Atmos. Res. Lab., SP 023:200:90.
- Cavanagh, R.C. (1974a) Fast ambient noise model I (FANM I). Acoustic Environmental Support Detachment, Off. Nav. Res.
- Cavanagh, R.C. (1974b) Fast ambient noise model II (FANM II). Acoustic Environmental Support Detachment, Off. Nav. Res.
- Cavanagh, R.C. (1978a) Acoustic fluctuation modeling and system performance estimation, Vol. I. Sci. Appl., Inc., SAI-79-737-WA.
- Cavanagh, R.C. (1978b) Acoustic fluctuation modeling and system performance estimation, Vol. II. Sci. Appl., Inc., SAI-79-738-WA.
- Cederberg, R.J. and Collins, M.D. (1997) Application of an improved self-starter to geoacoustic inversion. *IEEE J. Oceanic Eng.*, **22**, 102–9.
- Chaika, E.D., Granum, R.M. and Marusich, R.B. (1979) Program for integrated sonar modeling (PRISM) user's guide. Nav. Ocean Syst. Ctr, Tech. Note 851.

- Chamberlain, S.G. and Galli, J.C. (1983) A model for numerical simulation of nonstationary sonar reverberation using linear spectral prediction. *IEEE J. Oceanic Eng.*, OE-8, 21–36.
- Chapman, D.M.F. (2000) Decibels, SI units, and standards. *J. Acoust. Soc. Amer.*, 108, 480.
- Chapman, D.M.F., Ward, P.D. and Ellis, D.D. (1989) The effective depth of a Pekeris ocean waveguide, including shear wave effects. *J. Acoust. Soc. Amer.*, 85, 648–53.
- Chapman, N.R. and Ebbeson, G.R. (1983) Acoustic shadowing by an isolated seamount. *J. Acoust. Soc. Amer.*, 73, 1979–84.
- Chapman, R.P. and Harris, J.H. (1962) Surface backscattering strengths measured with explosive sound sources. *J. Acoust. Soc. Amer.*, 34, 1592–7.
- Chapman, R.P. and Scott, H.D. (1964) Surface backscattering strengths measured over an extended range of frequencies and grazing angles. *J. Acoust. Soc. Amer.*, 36, 1735–7.
- Chen, C.-T. and Millero, F.J. (1977) Speed of sound in seawater at high pressures. *J. Acoust. Soc. Amer.*, 62, 1129–35.
- Cheney, R.E. and Winfrey, D.E. (1976) Distribution and classification of ocean fronts. Nav. Oceanogr. Off., Tech. Note 3700-56-76.
- Chin-Bing, S.A. and Murphy, J.E. (1987) Two numerical models – one simplistic, the other sophisticated – applied to under-ice acoustic propagation and scattering. *J. Acoust. Soc. Amer.*, 82 (Suppl. 1), S31 (abstract).
- Chin-Bing, S.A. and Murphy, J.E. (1988) Long-range, range-dependent, acoustic propagation simulation using a full-wave, finite-element model coupled with a one-way parabolic equation model. *J. Acoust. Soc. Amer.*, 84 (Suppl. 1), S90 (abstract).
- Chin-Bing, S.A., Davis, J.A. and Evans, R.B. (1982) Nature of the lateral wave effect on bottom loss measurements. *J. Acoust. Soc. Amer.*, 71, 1433–7.
- Chin-Bing, S.A., Gilbert, K.E., Evans, R.B., Werby, M.F. and Tango, G.J. (1986) Research and development of acoustic models at NORDA. In *The NORDA Review* (March 31, 1976–March 31, 1986). Stennis Space Center, Mississippi, pp. 39–44.
- Chin-Bing, S.A., King, D.B. and Murphy, J.E. (1993a) Numerical simulations of lower-frequency acoustic propagation and backscatter from solitary internal waves in a shallow water environment. In *Ocean Reverberation*, eds, D.D. Ellis, J.R. Preston and H.G. Urban. Kluwer Academic Publishers, Dordrecht, The Netherlands, pp. 113–18.
- Chin-Bing, S.A., King, D.B., Davis, J.A. and Evans, R.B. (eds) (1993b) PE workshop II. Proceedings of the Second Parabolic Equation Workshop. Nav. Res. Lab., Rept NRL/BE/7181-93-0001.
- Chin-Bing, S.A., King, D.B. and Boyd, J.D. (1994) The effects of ocean environmental variability on underwater acoustic propagation forecasting. In *Oceanography and Acoustics: Prediction and Propagation Models*, eds, A.R. Robinson and D. Lee. American Institute of Physics, New York, Chapter 2, pp. 7–49.
- Chiu, C.-S. and Ehret, L.L. (1990) Computation of sound propagation in a three-dimensionally varying ocean: a coupled normal mode approach. In *Computational Acoustics. Vol. 1: Ocean-Acoustic Models and Supercomputing*, eds, D. Lee, A. Cakmak and R. Vichnevetsky. North-Holland, Amsterdam, pp. 187–202.
- Chiu, C.-S. and Ehret, L.L. (1994) Three-dimensional acoustic normal mode propagation in the Gulf Stream. In *Oceanography and Acoustics: Prediction and*

- Propagation Models*, eds, A.R. Robinson and D. Lee. American Institute of Physics, New York, Chapter 8, pp. 179–97.
- Claerbout, J.F. (1976) *Fundamentals of Geophysical Data Processing with Applications to Petroleum Prospecting*. International Series in the Earth and Planetary Sciences. McGraw-Hill, New York.
- Clancy, R.M. (1999) Operational systems, products, and applications today and tomorrow: the Navy perspective. In *Coastal Ocean Prediction, Vol. 56: Coastal and Estuarine Studies*, ed., C.N.K. Mooers. American Geophysical Union, Washington, DC, pp. 501–11.
- Clancy, R.M. and Johnson, A. (1997) An overview of naval operational ocean modeling. *Mar. Tech. Soc. J.*, **31** (1), 54–62.
- Clancy, R.M. and Martin, P.J. (1979) The NORDA/FLENUMOCEANCEN thermodynamical ocean prediction system (TOPS): a technical description. Nav. Ocean Res. Devel. Activity, Tech. Note 54.
- Clancy, R.M. and Pollak, K.D. (1983) A real-time synoptic ocean thermal analysis/forecast system. *Prog. Oceanogr.*, **12**, 383–424.
- Clancy, R.M., Martin, P.J., Piacsek, S.A. and Pollak, K.D. (1981) Test and evaluation of an operationally capable synoptic upper-ocean forecast system. Nav. Ocean Res. Devel. Activity, Tech. Note 92.
- Clancy, R.M., Cummings, J.A. and Ignaszewski, M.J. (1991a) New ocean thermal structure model operational at FNOC. *Naval Oceanography Command News*, **11** (5 and 6), 1–5.
- Clancy, R.M., Price, J.F. and Hawkins, J.D. (1991b) The FNOC diurnal ocean surface layer (DOSL) model. *Naval Oceanography Command News*, **11** (7), 8–10.
- Clay, C.S. (1999) Underwater sound transmission and SI units. *J. Acoust. Soc. Amer.*, **106**, 3047.
- Clay, C.S. and Medwin, H. (1964) High-frequency acoustical reverberation from a rough-sea surface. *J. Acoust. Soc. Amer.*, **36**, 2131–4.
- Clay, C.S. and Medwin, H. (1977) *Acoustical Oceanography: Principles and Applications*. Wiley-Interscience, New York.
- Coates, R., de Cogan, D. and Willison, P.A. (1990) Transmission line matrix modeling applied to problems in underwater acoustics. Proc. IEEE Oceans 90 Conf., pp. 216–20.
- Cohen, J.S. and Einstein, L.T. (1970) Continuous gradient ray tracing system (CONGRATS) II: eigenray processing programs. Navy Underwater Sound Lab., Rept 1069.
- Cohen, J.S. and Weinberg, H. (1971) Continuous gradient ray-tracing system (CONGRATS) III: Boundary and volume reverberation. Nav. Underwater Syst. Ctr, Rept 4071.
- Colilla, R.A. (1970) Improvement in the efficiency of the present model and documentation of the program RP-70. Ocean Data Syst., Inc.
- Collins, M.D. (1988a) FEPE user's guide. Nav. Ocean Res. and Devel. Activity, Tech. Note 365.
- Collins, M.D. (1988b) The time-domain solution of the wide-angle parabolic equation including the effects of sediment dispersion. *J. Acoust. Soc. Amer.*, **84**, 2114–25.
- Collins, M.D. (1990a) The rotated parabolic equation and sloping ocean bottoms. *J. Acoust. Soc. Amer.*, **87**, 1035–7.

- Collins, M.D. (1990b) Benchmark calculations for higher-order parabolic equations. *J. Acoust. Soc. Amer.*, **87**, 1535–8.
- Collins, M.D. (1991) Higher-order Padé approximations for accurate and stable elastic parabolic equations with application to interface wave propagation. *J. Acoust. Soc. Amer.*, **89**, 1050–7.
- Collins, M.D. (1992) A self-starter for the parabolic equation method. *J. Acoust. Soc. Amer.*, **92**, 2069–74.
- Collins, M.D. (1993a) A split-step Padé solution for the parabolic equation method. *J. Acoust. Soc. Amer.*, **93**, 1736–42.
- Collins, M.D. (1993b) A two-way parabolic equation for elastic media. *J. Acoust. Soc. Amer.*, **93**, 1815–25.
- Collins, M.D. (1993c) An energy-conserving parabolic equation for elastic media. *J. Acoust. Soc. Amer.*, **94**, 975–82.
- Collins, M.D. (1993d) The adiabatic mode parabolic equation. *J. Acoust. Soc. Amer.*, **94**, 2269–78.
- Collins, M.D. (1998) New and improved parabolic equation models. *J. Acoust. Soc. Amer.*, **104**, 1808 (abstract).
- Collins, M.D. (1999) The stabilized self-starter. *J. Acoust. Soc. Amer.*, **106**, 1724–6.
- Collins, M.D. and Chin-Bing, S.A. (1990) A three-dimensional parabolic equation model that includes the effects of rough boundaries. *J. Acoust. Soc. Amer.*, **87**, 1104–9.
- Collins, M.D. and Evans, R.B. (1992) A two-way parabolic equation for acoustic backscattering in the ocean. *J. Acoust. Soc. Amer.*, **91**, 1357–68.
- Collins, M.D. and Kuperman, W.A. (1994a) Overcoming ray chaos. *J. Acoust. Soc. Amer.*, **95**, 3167–70.
- Collins, M.D. and Kuperman, W.A. (1994b) Inverse problems in ocean acoustics. *Inverse Problems*, **10**, 1023–40.
- Collins, M.D. and Siegmann, W.L. (1999) A complete energy conservation correction for the elastic parabolic equation. *J. Acoust. Soc. Amer.*, **105**, 687–92.
- Collison, N. and Dosso, S. (2000) A comparison of modal decomposition algorithms for matched-mode processing. *Can. Acoust.*, **28** (4), 15–27.
- Condron, T.P., Onyx, P.M. and Dickson, K.R. (1955) Contours of propagation loss and plots of propagation loss vs range for standard conditions at 2, 5, and 8 kc. Navy Underwater Sound Lab., Tech. Memo. 1110-14-55.
- Coppens, A.B. (1981) Simple equations for the speed of sound in Neptunian waters. *J. Acoust. Soc. Amer.*, **69**, 862–3.
- Coppens, A.B. and Sanders, J.V. (1980) Propagation of sound from a fluid wedge into a fast fluid bottom. In *Bottom-Interacting Ocean Acoustics*, eds W.A. Kuperman and F.B. Jensen. Plenum, New York, pp. 439–50.
- Cornuelle, B., Wunsch, C., Behringer, D., Birdsall, T., Brown, M., Heinmiller, R., Knox, R., Metzger, K., Munk, W., Spiesberger, J., Spindel, R., Webb, D. and Worcester, P. (1985) Tomographic maps of the ocean mesoscale, Part 1: pure acoustics. *J. Phys. Oceanogr.*, **15**, 133–52.
- Cornyn, J.J. (1973a) GRASS: a digital-computer ray-tracing and transmission-loss-prediction system. Vol. I – Overall description. Nav. Res. Lab., Rept 7621.
- Cornyn, J.J. (1973b) GRASS: a digital-computer ray-tracing and transmission-loss-prediction system. Vol. II – User’s manual. Nav. Res. Lab., Rept 7642.

- Coulter, R.L. and Kallistratova, M.A. (1999) The role of acoustic sounding in a high-technology era. *Meteorol. Atmos. Phys.*, **71**, 3–13.
- Cox, H. (1989) Fundamentals of bistatic active sonar. In *Underwater Acoustic Data Processing*. NATO Advanced Science Institutes Series E: Applied Sciences, Vol. 161, ed., Y.T. Chan. Kluwer Academic Publishers, Dordrecht, The Netherlands, pp. 3–24.
- Crum, L.A., Roy, R.A. and Prosperetti, A. (1992) The underwater sounds of precipitation. *Nav. Res. Rev.*, **44** (2), 2–12.
- Culkin, F. and Ridout, P. (1989) Salinity: definitions, determinations, and standards. *Sea Technol.*, **30** (10), 47–9.
- Cummings, W.C. and Holliday, D.V. (1987) Sounds and source levels from Bowhead whales off Pt Barrow, Alaska. *J. Acoust. Soc. Amer.*, **82**, 814–21.
- Dantzler, H.L. Jr, Sides, D.J. and Neal, J.C. (1993) An automated tactical oceanographic monitoring system. *Johns Hopkins APL Tech. Dig.*, **14** (3), 281–92.
- Dashen, R. and Munk, W. (1984) Three models of global ocean noise. *J. Acoust. Soc. Amer.*, **76**, 540–54.
- Davis, J.A., White, D. and Cavanagh, R.C. (1982) NORDA parabolic equation workshop (31 March–3 April 1981). Nav. Ocean Res. Dev. Activity, Tech. Note 143.
- Davis, P.K. (1995) An introduction to variable-resolution modeling. In *Warfare Modeling*, eds, J. Bracken, M. Kress and R.E. Rosenthal. John Wiley & Sons, New York, pp. 5–35.
- Davis, P.K. (2001) Effects-based operations (EBO): a grand challenge for the analytical community. MR-1477-USJFCOM/AF. RAND, Santa Monica, California.
- Dawe, R.L. (1997) Detection threshold modelling explained. Australia Department of Defence, Defence Science and Technology Organisation, Maritime Operations Division, Aeronautical and Maritime Research Laboratory, DSTO-TR-0586.
- Deavenport, R.L. and DiNapoli, F.R. (1982) Evaluation of Arctic transmission loss models. Nav. Underwater Syst. Ctr, Tech. Memo. 82-1160.
- Del Balzo, D.R., Feuillade, C. and Rowe, M.M. (1988) Effects of water-depth mismatch on matched-field localization in shallow water. *J. Acoust. Soc. Amer.*, **83**, 2180–5.
- Del Grosso, V.A. (1974) New equation for the speed of sound in natural waters (with comparisons to other equations). *J. Acoust. Soc. Amer.*, **56**, 1084–91.
- DeSanto, J.A. (1979) Derivation of the acoustic wave equation in the presence of gravitational and rotational effects. *J. Acoust. Soc. Amer.*, **66**, 827–30.
- Desharnais, F. and Ellis, D.D. (1997) Data-model comparisons of reverberation at three shallow-water sites. *IEEE J. Oceanic Eng.*, **22**, 309–16.
- Diachok, O.I. (1976) Effects of sea-ice ridges on sound propagation in the Arctic Ocean. *J. Acoust. Soc. Amer.*, **59**, 1110–20.
- Diachok, O. (1980) Arctic hydroacoustics. *Cold Regions Sci. Technol.*, **2**, 185–201.
- Diachok, O.I. and Winokur, R.S. (1974) Spatial variability of underwater ambient noise at the Arctic ice-water boundary. *J. Acoust. Soc. Amer.*, **55**, 750–3.
- Diachok, O., Caiti, A., Gerstoft, P. and Schmidt, H. (eds) (1995) *Full Field Inversion Methods in Ocean and Seismo-Acoustics*. Modern Approaches in Geophysics, Vol. 12. Kluwer Academic Publishers, Dordrecht, The Netherlands.
- DiNapoli, F.R. (1971) Fast field program for multi-layered media. Nav. Underwater Syst. Ctr, Rept 4103.

- DiNapoli, F.R. and Deavenport, R.L. (1979) Numerical models of underwater acoustic propagation. In *Ocean Acoustics*. Topics in Current Physics, Vol. 8, ed., J.A. DeSanto. Springer-Verlag, New York, pp. 79–157.
- DiNapoli, F.R. and Deavenport, R.L. (1980) Theoretical and numerical Green's function field solution in a plane multilayered medium. *J. Acoust. Soc. Amer.*, **67**, 92–105.
- Donn, W.L. and Rind, D. (1971) Natural infrasound as an atmospheric probe. *Geophys. J. Roy. Astron. Soc.*, **26**, 111–33.
- Doolittle, R., Tolstoy, A. and Buckingham, M. (1988) Experimental confirmation of horizontal refraction of cw acoustic radiation from a point source in a wedge-shaped ocean environment. *J. Acoust. Soc. Amer.*, **83**, 2117–25.
- Dosso, S.E., Yeremy, M.L., Ozard, J.M. and Chapman, N.R. (1993) Estimation of ocean-bottom properties by matched-field inversion of acoustic field data. *IEEE J. Oceanic Eng.*, **18**, 232–9.
- Dozier, L.B. (1984) PERUSE: a numerical treatment of rough surface scattering for the parabolic wave equation. *J. Acoust. Soc. Amer.*, **75**, 1415–32.
- Dozier, L.B. and Cavanagh, R.C. (1993) Overview of selected underwater acoustic propagation models. Office of Naval Research, Advanced Environmental Acoustic Support Program, AEAS Rept 93-101.
- Dozier, L. and Lallement, P. (1995) Parallel implementation of a 3-D range-dependent ray model for replica field generation. In *Full Field Inversion Methods in Ocean and Seismo-Acoustics*, eds, O. Diachok, A. Caiti, P. Gerstoft and H. Schmidt. Kluwer Academic Publishers, Dordrecht, The Netherlands, pp. 45–50.
- Dozier, L.B. and White, D. (1988) Software requirements specification for the ASTRAL model. Sci. Appl. Inter. Corp., OAML-SRS-23.
- Dreini, G., Isoppo, C. and Jensen, F.B. (1995) PC-based propagation and sonar prediction models. SAACLANT Undersea Res. Ctr, Rept SR-240.
- D'Spain, G.L., Murray, J.J., Hodgkiss, W.S., Booth, N.O. and Schey, P.W. (1999) Mirages in shallow water matched field processing. *J. Acoust. Soc. Amer.*, **105**, 3245–65.
- Dushaw, B.D., Worcester, P.F., Cornuelle, B.D. and Howe, B.M. (1993) On equations for the speed of sound in seawater. *J. Acoust. Soc. Amer.*, **93**, 255–75.
- Duston, M.D., Gilbert, R.P. and Wood, D.H. (1986) A wave propagation computation technique using function theoretic representation. In *Numerical Mathematics and Applications*, eds, R. Vichnevetsky and J. Vignes. North-Holland, Amsterdam, pp. 281–8.
- Dyer, I. (1973) Statistics of distant shipping noise. *J. Acoust. Soc. Amer.*, **53**, 564–70.
- Dyer, I. (1984) The song of sea ice and other Arctic melodies. In *Arctic Technology and Policy*, eds, I. Dyer and C. Chryssostomidis. Hemisphere Publishing Corp., Philadelphia, pp. 11–37.
- Dyer, I. (1988) Arctic ambient noise: ice source mechanisms. Physics news in 1987 – Acoustics. *Physics Today*, **41** (1), S5–6.
- Dziedziuch, M., Worcester, P. and Munk, W. (2001) Turning point filters: analysis of sound propagation on a gyre-scale. *J. Acoust. Soc. Amer.*, **110**, 135–49.
- Earle, M.D. and Bishop, J.M. (1984) *A Practical Guide to Ocean Wave Measurement and Analysis*. ENDECO, Inc., Marion, Massachusetts, USA.
- Ebbeson, G.R. and Turner, R.G. (1983) Sound propagation over Dickins Seamount in the northeast Pacific Ocean. *J. Acoust. Soc. Amer.*, **73**, 143–52.

- Eckart, C. (1953) The scattering of sound from the sea surface. *J. Acoust. Soc. Amer.*, **25**, 566–70.
- Einstein, P.A. (1975) Underwater sonic ray tracing in three dimensions. *J. Sound Vib.*, **42**, 503–8.
- Eller, A.I. (1984a) Findings and recommendations of the surface loss model working group: final report, 1984. Nav. Ocean Res. Devel. Activity, Tech. Note 279.
- Eller, A.I. (1984b) Acoustics of shallow water: a status report. Nav. Res. Lab., Memo. Rept 5405.
- Eller, A.I. (1985) Findings and recommendations of the under-ice scattering loss model working group. Nav. Ocean Res. Devel. Activity, Tech. Note 255.
- Eller, A.I. (1986) Shallow water sonar performance prediction assessment. Nav. Ocean Res. Devel. Activity, Tech. Note 330.
- Eller, A.I. (1990) Automated long range acoustic modeling. Proc. IEEE Oceans 90 Conf., pp. 205–8.
- Eller, A.I. and Haines, L. (1987) Identification and acoustic characterization of seamounts. Sci. Appl. Inter. Corp., SAIC-87/1722.
- Eller, A.I. and Venne, H.J. Jr (1981) Evaluation procedure for environmental acoustic models. IEEE Int. Conf. Acoust. Speech Signal Process., pp. 1026–9.
- Eller, A.I., Venne, H.J. Jr and Hoffman, D.W. (1982) Evaluation of ocean acoustic reverberation models. Proc. MTS/IEEE Oceans 82 Conf., pp. 206–10.
- Ellis, D.D. (1980) NORM2L: an interactive computer program for acoustic normal mode calculations for the Pekeris model. Defence Research Establishment Atlantic (Canada), Tech. Memo. 80/K.
- Ellis, D.D. (1985) Two-ended shooting technique for calculating normal modes in underwater acoustic propagation. Defence Research Establishment Atlantic (Canada), DREA Rept 85/105.
- Ellis, D.D. (1993) Shallow water reverberation: normal-mode model predictions compared with bistatic towed-array measurements. *IEEE J. Oceanic Eng.*, **18**, 474–82.
- Ellis, D.D. (1995) A shallow-water normal-mode reverberation model. *J. Acoust. Soc. Amer.*, **97**, 2804–14.
- Ellis, D.D. and Chapman, D.M.F. (1985) A simple shallow water propagation model including shear wave effects. *J. Acoust. Soc. Amer.*, **78**, 2087–95.
- Ellis, D.D. and Crowe, D.V. (1991) Bistatic reverberation calculations using a three-dimensional scattering function. *J. Acoust. Soc. Amer.*, **89**, 2207–14.
- Ellis, D.D., Preston, J.R. and Urban, H.G. (eds) (1993) *Ocean Reverberation*. Kluwer Academic Publishers, Dordrecht, The Netherlands.
- Ellis, J.A. and Parchman, S. (1994) The interactive multisensor analysis training (IMAT) system: a formative evaluation in the aviation antisubmarine warfare operator (AW) class “A” school. NPRDC TN-94-20. Navy Personnel Research and Development Center, San Diego, California, USA.
- Ellis, J.W., Miller, J.E. and Fernandez, M.R. (1996) NRL’s tactical oceanography simulation lab. *Sea Technol.*, **37** (5), 31–7.
- Emery, W.J. and Meincke, J. (1986) Global water masses: summary and review. *Oceanol. Acta*, **9**, 383–91.
- Epifanio, C.L., Potter, J.R., Deane, G.B., Readhead, M.L. and Buckingham, M.J. (1999) Imaging in the ocean with ambient noise: the ORB experiments. *J. Acoust. Soc. Amer.*, **106**, 3211–25.

- Estalote, E. (1984) NORDA acoustic models and data bases. Nav. Ocean Res. Devel. Activity, Tech. Note 293.
- Estalote, E.A., Kerr, G.A. and King, D.B. (1986) Recent advances in application of acoustic models. In *The NORDA Review* (March 31, 1976–March 31, 1986). Stennis Space Center, Mississippi, pp. 45–50.
- Etter, P.C. (1981) Underwater acoustic modeling techniques. *The Shock and Vibration Digest*, **13** (2), 11–20.
- Etter, P.C. (1984) Underwater acoustic modeling techniques. *The Shock and Vibration Digest*, **16** (1), 17–23.
- Etter, P.C. (1987a) Underwater acoustic modeling techniques. *The Shock and Vibration Digest*, **19** (2), 3–10.
- Etter, P.C. (1987b) Numerical modeling techniques in underwater acoustics. *J. Acoust. Soc. Amer.*, **82** (Suppl. 1), S102 (abstract).
- Etter, P.C. (1987c) Arctic oceanography and meteorology review. Nav. Training Syst. Ctr, NTSC-TR-87-032.
- Etter, P.C. (1989) Underwater acoustic modeling for antisubmarine warfare. *Sea Technol.*, **30** (5), 35–7.
- Etter, P.C. (1990) Underwater acoustic modeling techniques. *The Shock and Vibration Digest* **22** (5), 3–12.
- Etter, P.C. (1991) *Underwater Acoustic Modeling: Principles, Techniques and Applications*. Elsevier Applied Science, London.
- Etter, P.C. (1993) Recent developments in computational ocean acoustics. Radix Systems, Inc., Tech. Rept TR-93-082.
- Etter, P.C. (1995) The status of Naval underwater acoustic modeling. *J. Acoust. Soc. Amer.*, **97**, 3312 (abstract).
- Etter, P.C. (1996) *Underwater Acoustic Modeling: Principles, Techniques and Applications*, 2nd edn. E & FN Spon, London.
- Etter, P.C. (1999) Updated technology baseline in underwater acoustic modeling, simulation, and analysis. *J. Acoust. Soc. Amer.*, **106**, 2298 (abstract).
- Etter, P.C. (2000) Challenges in environmental acoustics. Proc. MTS/IEEE Oceans 2000 Conf., pp. 877–85.
- Etter, P.C. (2001a) Recent advances in underwater acoustic modelling and simulation. *J. Sound Vib.*, **240**, 351–83.
- Etter, P.C. (2001b) Progress in underwater acoustic modeling. In *Acoustic Interactions with Submerged Elastic Structures. Part II: Propagation, Ocean Acoustics and Scattering*, eds, A. Guran, G. Maugin, J. Engelbrecht and M. Werby. World Scientific Publishing, Singapore, pp. 112–23.
- Etter, P.C. (2001c) Models for the analysis and prediction of acoustic phenomena in the coastal ocean. Proc. Fourth Conf. Coastal Atmospheric Oceanic Prediction and Processes, American Meteorological Society, pp. 76–83.
- Etter, P.C. and Cochrane, J.D. (1975) Water temperature on the Texas–Louisiana shelf. Texas A & M Univ., TAMU-SG-75-604.
- Etter, P.C. and Flum, R.S. Sr (1978) A survey of marine environmental/acoustic data banks and basic acoustic models with potential application to the acoustic performance prediction (APP) program. ASW Syst. Proj. Off., ASWR-78-117.
- Etter, P.C. and Flum, R.S. Sr (1979) An overview of the state-of-the-art in naval underwater acoustic modeling. *J. Acoust. Soc. Amer.*, **65** (Suppl. 1), S42 (abstract).
- Etter, P.C. and Flum, R.S. Sr (1980) A survey of underwater acoustic models and environmental-acoustic data banks. ASW Syst. Proj. Off., ASWR-80-115.

- Etter, P.C., Deffenbaugh, R.M. and Flum, R.S. Sr (1984) A survey of underwater acoustic models and environmental-acoustic data banks. ASW Syst. Prog. Off., ASWR-84-001.
- Etter, P.C., Lamb, P.J. and Portis, D.H. (1987) Heat and freshwater budgets of the Caribbean Sea with revised estimates for the Central American Seas. *J. Phys. Oceanogr.*, **17**, 1232–48.
- Evans, R.B. (1983) A coupled mode solution for acoustic propagation in a waveguide with stepwise depth variations of a penetrable bottom. *J. Acoust. Soc. Amer.*, **74**, 188–95.
- Evans, R.B. (1986) COUPLE: a user's manual. Nav. Ocean Res. Devel. Activity. Tech. Note 332.
- Evans, R.B. and Gilbert, K.E. (1985) Acoustic propagation in a refracting ocean waveguide with an irregular interface. *Comp. Math. Applic.*, **11**, 795–805.
- Ewart, T.E. and Reynolds, S.A. (1984) The mid-ocean acoustic transmission experiment, MATE. *J. Acoust. Soc. Amer.*, **75**, 785–802.
- Ewing, M. and Worzel, J.L. (1948) Long-range sound transmission. *Geol. Soc. Amer. Mem.*, **27** (Part III), 1–35.
- Farquhar, G.B. (ed.) (1970) *Proceedings of an International Symposium on Biological Sound Scattering in the Ocean*. US Government Printing Office, Washington, DC.
- Farrell, T. and LePage, K. (1996) Development of a comprehensive hydroacoustic coverage assessment model. BBN Systems and Technologies, Tech. Memo W1278. Formally released as Phillips Lab. Tech. Rept PL-TR-96-2248, Air Force Materiel Command, Hanscom Air Force Base, Massachusetts, USA.
- Fawcett, J.A., Westwood, E.K. and Tindle, C.T. (1995) A simple coupled wedge mode propagation method. *J. Acoust. Soc. Amer.*, **98**, 1673–81.
- Felizardo, F.C. and Melville, W.K. (1995) Correlations between ambient noise and the ocean surface wave field. *J. Phys. Oceanogr.*, **25**, 513–32.
- Felsen, L.B. (1986) Benchmarks: are they helpful, diversionary, or irrelevant? *J. Acoust. Soc. Amer.*, **80** (Suppl. 1), S36 (abstract).
- Felsen, L.B. (1987) Chairman's introduction to session on numerical solutions of two benchmark problems. *J. Acoust. Soc. Amer.*, **81** (Suppl. 1), S39 (abstract).
- Felsen, L.B. (1990) Benchmarks: an option for quality assessment. *J. Acoust. Soc. Amer.*, **87**, 1497–8.
- Ferla, C.M., Porter, M.B. and Jensen, F.B. (1993) C-SNAP: coupled SACLANT-CEN normal mode propagation loss model. SACLANT Undersea Res. Ctr, Memo. SM-274.
- Ferla, M.C., Jensen, F.B. and Kuperman, W.A. (1982) High-frequency normal-mode calculations in deep water. *J. Acoust. Soc. Amer.*, **72**, 505–9.
- Ferris, R.H. (1972) Comparison of measured and calculated normal-mode amplitude functions for acoustic waves in shallow water. *J. Acoust. Soc. Amer.*, **52**, 981–8.
- Fisher, A. Jr and Pickett, R. (1973) Evaluation of methods for merging BT-derived and deep climatological sound speeds. Nav. Oceanogr. Off., Tech. Note 7700-12-73.
- Fisher, F.H. and Simmons, V.P. (1977) Sound absorption in sea water. *J. Acoust. Soc. Amer.*, **62**, 558–64.
- Fizell, R.G. (1987) Application of high-resolution processing to range and depth estimation using ambiguity function methods. *J. Acoust. Soc. Amer.*, **82**, 606–13.

- Fizell, R.G. and Wales, S.C. (1985) Source localization in range and depth in an Arctic environment. *J. Acoust. Soc. Amer.*, **78** (Suppl. 1) S57–8 (abstract).
- Flanagan, R.P., Weinberg, N.L. and Clark, J.G. (1974) Coherent analysis of ray propagation with moving source and fixed receiver. *J. Acoust. Soc. Amer.*, **56**, 1673–80.
- Flatté, S.M. (ed.) (1979) *Sound Transmission through a Fluctuating Ocean*. Cambridge Univ. Press, New York.
- Focke, K.C. (1984) Acoustic attenuation in ocean sediments found in shallow water regions. Appl. Res. Labs., Univ. Texas at Austin, USA, ARL-TR-84-6.
- Fofonoff, N.P. (1985) Physical properties of seawater: a new salinity scale and equation of state for seawater. *J. Geophys. Res.*, **90**, 3332–42.
- Forbes, A. (1994) Acoustic monitoring of global ocean climate. *Sea Technol.*, **35** (5), 65–7.
- Foreman, T.L. (1977) Acoustic ray models based on eigenrays. Appl. Res. Labs., Univ. Texas at Austin, USA, ARL-TR-77-1.
- Foreman, T.L. (1982) The ARL:UT range-dependent ray model MEDUSA. Appl. Res. Labs., Univ. Texas at Austin, USA, ARL-TR-82-64.
- Foreman, T.L. (1983) Ray modeling methods for range dependent ocean environments. Appl. Res. Labs., Univ. Texas at Austin, USA, ARL-TR-83-41.
- Foret, J.A., Korman, M.S., Schuler, J.W. and Holmes, E. (1997) Design and development of PC-IMAT: teaching strategies for acoustical oceanography. *J. Acoust. Soc. Amer.*, **101**, 3097 (abstract).
- Fortuin, L. (1970) Survey of literature on reflection and scattering of sound waves at the sea surface. *J. Acoust. Soc. Amer.*, **47**, 1209–28.
- Franchi, E.R., Griffin, J.M. and King, B.J. (1984) NRL reverberation model: a computer program for the prediction and analysis of medium-to-long-range boundary reverberation. Nav. Res. Lab., Rept 8721.
- Francois, R.E. and Garrison, G.R. (1982a) Sound absorption based on ocean measurements: Part I: pure water and magnesium sulfate contributions. *J. Acoust. Soc. Amer.*, **72**, 896–907.
- Francois, R.E. and Garrison, G.R. (1982b) Sound absorption based on ocean measurements. Part II: boric acid contribution and equation for total absorption. *J. Acoust. Soc. Amer.*, **72**, 1879–90.
- Franz, G.J. (1959) Splashes as sources of sound in liquids. *J. Acoust. Soc. Amer.*, **31**, 1080–96.
- Frisk, G.V. (1994) *Ocean and Seabed Acoustics: A Theory of Wave Propagation*. PTR Prentice-Hall, Englewood Cliffs, USA.
- Frison, T.W., Abarbanel, H.D.I., Cembrola, J. and Neales, B. (1996) Chaos in ocean ambient “noise.” *J. Acoust. Soc. Amer.*, **99**, 1527–39.
- Fromm, D.M. (1999) Multistatic active system performance modeling in littoral waters. Proc. 28th Meeting of the Technical Cooperation Program, Technical Panel MAR TP-9, Nav. Res. Lab., Washington, DC.
- Fromm, D.M., Crockett, J.P. and Palmer, L.B. (1996) BiRASP – The bistatic range-dependent active system prediction model. Nav. Res. Lab., Rept NRL/FR/7140-95-9723.
- Frye, H.W. and Pugh, J.D. (1971) A new equation for the speed of sound in seawater. *J. Acoust. Soc. Amer.*, **50**, 384–6.
- Fulford, J.K. (1991) Shallow water RASP upgrade. Nav. Oceanogr. Atmos. Res. Lab., Tech. Note 135.

- Futa, K. and Kikuchi, T. (2001) Finite difference time domain analysis of bottom effect on sound propagation in shallow water. *Acoust. Sci. Technol.*, **22**, 303–5.
- Gabrielson, T.B. (1982) Mathematical foundations for normal mode modelling in waveguides. Nav. Air Devel. Ctr, Rept NADC-81284-30.
- Gaillard, F. (1985) Ocean acoustic tomography with moving sources or receivers. *J. Geophys. Res.*, **90**, 11891–8.
- Garon, H.M. (1975) FACTEX: FACT extended to range-dependent environments. Acoustic Environmental Support Detachment, Off. Nav. Res.
- Garon, H.M. (1976) SHALFACT: a shallow water transmission loss model. Acoustic Environmental Support Detachment, Off. Nav. Res.
- Garrett, C. and Munk, W. (1979) Internal waves in the ocean. *Ann. Rev. Fluid Mech.*, **11**, 339–69.
- Garwood, R.W. Jr (1979) Air–sea interaction and dynamics of the surface mixed layer. *Rev. Geophys. Space Phys.*, **17**, 1507–24.
- Gass, S.I. (1979) Computer model documentation: a review and an approach. National Bureau of Standards Special Pub. 500-39.
- Gemmill, W. and Khedouri, E. (1974) A note on sound ray tracing through a Gulf Stream eddy in the Sargasso Sea. Nav. Oceanogr. Off., Tech. Note 6150-21-74.
- Georges, T.M., Jones, R.M. and Lawrence, R.S. (1990) A PC version of the HARPO ocean acoustic ray-tracing program. Wave Propagation Lab., NOAA Tech. Memo. ERL WPL-180.
- Gerstoft, P. (1994) Inversion of seismoacoustic data using genetic algorithms and a *posteriori* probability distributions. *J. Acoust. Soc. Amer.*, **95**, 770–82.
- Gerstoft, P. and Schmidt, H. (1991) A boundary element approach to ocean seismoacoustic facet reverberation. *J. Acoust. Soc. Amer.*, **89**, 1629–42.
- Gilbert, K.E. and Evans, R.B. (1986) A Green's function method for one-way wave propagation in a range-dependent ocean environment. In *Ocean Seismo-Acoustics*, eds, T. Akal and J.M. Berkson. Plenum, New York, pp. 21–8.
- Gilbert, K.E., Evans, R.B., Chin-Bing, S.A., White, D. and Kuperman, W.A. (1983) Some new models for sound propagation in bottom-limited ocean environments. *Conf. Proc., Acoustics and the Sea Bed*. Bath Univ. Press, England, pp. 243–50.
- Gilbert, R.P. and Wood, D.H. (1986) A transmutation approach to underwater sound propagation. *Wave Motion*, **8**, 383–97.
- Gill, A.E. (1982) *Atmosphere–Ocean Dynamics*. International Geophysics Series, Vol. 30. Academic Press, San Diego.
- Goddard, R.P. (1989) The sonar simulation toolset. Proc. IEEE Oceans 89 Conf., pp. 1217–22.
- Goddard, R.P. (1993) Simulating ocean reverberation: a review of methods and issues. Appl. Phys. Lab., Univ. Washington, APL-UW TR 9313.
- Goddard, R.P. (1994) Sonar simulation toolset software description. Release 2.5. Appl. Phys. Lab., Univ. Washington, APL-UW TR 9211.
- Goh, J.T. and Schmidt, H. (1996) A hybrid coupled wave-number integration approach to range-dependent seismoacoustic modeling. *J. Acoust. Soc. Amer.*, **100**, 1409–20.
- Goh, J.T., Schmidt, H., Gerstoft, P. and Seong, W. (1997) Benchmarks for validating range-dependent seismo-acoustic propagation codes. *IEEE J. Oceanic Eng.*, **22**, 226–36.

- Gold, B.A. and Renshaw, W.E. (1978) Joint volume reverberation and biological measurements in the tropical Western Atlantic. *J. Acoust. Soc. Amer.*, **63**, 1809–19.
- Goldberg, E.D., McCave, I.N., O'Brien, J.J. and Steele, J.H. (eds) (1977) *The Sea, Vol. 6: Marine Modeling*. Wiley Interscience, New York.
- Goldman, J. (1974) A model of broadband ambient noise fluctuations due to shipping. Bell Telephone Labs. Rept OSTP-31 JG.
- Goldstein, C.I. (1984) The numerical solution of underwater acoustic propagation problems using finite difference and finite element methods. Nav. Res. Lab., Rept 8820.
- Goni, G.J. and Johns, W.E. (2001) A census of North Brazil Current rings observed from TOPEX/POSEIDON altimetry: 1992–1998. *Geophys. Res. Lett.*, **28**, 1–4.
- Gonzalez, R. and Hawker, K.E. (1980) The acoustic normal mode model NEMESIS. Appl. Res. Labs., Univ. Texas at Austin, USA, ARL-TR-80-13.
- Gonzalez, R. and Payne, S.G. (1980) User's manual for NEMESIS and PLMODE. Appl. Res. Labs., Univ. Texas at Austin, USA, ARL-TM-80-6.
- Goodman, R.R. and Farwell, R.W. (1979) A note on the derivation of the wave equation in an inhomogeneous ocean. *J. Acoust. Soc. Amer.*, **66**, 1895–6.
- Gordon, D.F. (1964) Extension of the ray intensity procedure for underwater sound based on a profile consisting of curvilinear segments. Nav. Electron. Lab., Res. Rept 1217.
- Gordon, D.F. (1979) Underwater sound propagation-loss program. Computation by normal modes for layered oceans and sediments. Nav. Ocean Syst. Ctr, Tech. Rept 393.
- Gordon, D.F. and Buckner, H.P. (1984) Arctic acoustic propagation model with ice scattering. Nav. Ocean Syst. Ctr, Tech. Rept 985.
- Gostev, V.S. and Shvachko, R.F. (2000) Caustics and volume prereverberation in a surface oceanic waveguide. *Acoust. Phys.*, **46**, 559–62.
- Gragg, R.F. (1985) The broadband normal mode model PROTEUS. Appl. Res. Labs., Univ. Texas at Austin, USA, ARL-TM-85-6.
- Greaves, R.J. and Stephen, R.A. (1997) Seafloor acoustic backscattering from different geological provinces in the Atlantic natural laboratory. *J. Acoust. Soc. Amer.*, **101**, 193–208.
- Greaves, R.J. and Stephen, R.A. (2000) Low-grazing-angle monostatic acoustic reverberation from rough and heterogeneous seafloors. *J. Acoust. Soc. Amer.*, **108**, 1013–25.
- Green, D.M. (1994) Sound's effects on marine mammals need investigation. *EOS, Trans. Amer. Geophys. Union*, **75**, 305–6.
- Greene, C.H. and Wiebe, P.H. (1988) New developments in bioacoustical oceanography. *Sea Technol.*, **29** (8), 27–9.
- Greene, R.R. (1984) The rational approximation to the acoustic wave equation with bottom interaction. *J. Acoust. Soc. Amer.*, **76**, 1764–73.
- Grilli, S., Pedersen, T. and Stepanishen, P. (1998) A hybrid boundary element method for shallow water acoustic propagation over an irregular bottom. *Eng. Anal. Bound. Elem.*, **21**, 131–45.
- Haines, L.C., Renner, W.W. and Eller, A.I. (1988) Prediction system for acoustic returns from ocean bathymetry. Proc. MTS/IEEE Oceans 88 Conf., pp. 295–7.
- Hall, H.R. and Watson, W.H. (1967) An empirical bottom reflection loss expression for use in sonar range prediction. Nav. Undersea Warfare Ctr, Tech. Note 10.

- Hall, M.V. (1989) A comprehensive model of wind-generated bubbles in the ocean and predictions of the effects on sound propagation at frequencies up to 40 kHz. *J. Acoust. Soc. Amer.*, **86**, 1103–17.
- Hall, M.V. (1995) Dimensions and units of underwater acoustic parameters. *J. Acoust. Soc. Amer.*, **97**, 3887–9.
- Hall, M.V. and Irving, M.A. (1989) Application of adiabatic mode theory to the calculation of horizontal refraction through a mesoscale eddy. *J. Acoust. Soc. Amer.*, **86**, 1465–77.
- Hamilton, E.L. (1980) Geoacoustic modeling of the sea floor. *J. Acoust. Soc. Amer.*, **68**, 1313–40.
- Hamson, R.M. (1997) The modelling of ambient noise due to shipping and wind sources in complex environments. *Appl. Acoust.*, **51**, 251–87.
- Hamson, R.M. and Ainslie, M.A. (1998) Broadband geoacoustic deduction. *J. Comput. Acoust.*, **6**, 45–59.
- Hamson, R.M. and Wagstaff, R.A. (1983) An ambient-noise model that includes coherent hydrophone summation for sonar system performance in shallow water. SACLANT ASW Res. Ctr, Rept SR-70.
- Hanna, J.S. (1976) Example of acoustic model evaluation and data interpretation. *J. Acoust. Soc. Amer.*, **60**, 1024–31.
- Hanna, J.S. and Rost, P.V. (1981) Parabolic equation calculations versus North Pacific measurement data. *J. Acoust. Soc. Amer.*, **70**, 504–15.
- Hardin, R.H. and Tappert, F.D. (1973) Applications of the split-step Fourier method to the numerical solution of nonlinear and variable coefficient wave equations. *SIAM Rev.*, **15**, 423.
- Harding, E.T. (1970) Geometry of wave-front propagation by integration of rays. Meteorology International, Inc.
- Harlan, J.A., Georges, T.M. and Jones, R.M. (1991a) PROFILE – a program to generate profiles from HARPO/HARPA environmental models. Wave Propagation Lab., NOAA Tech. Memo. ERL WPL-198.
- Harlan, J.A., Jones, R.M. and Georges, T.M. (1991b) PSGRAPH – a plotting program for PC-HARPO, PROFILE, CONPLT, and EIGEN. Wave Propagation Lab., NOAA Tech. Memo. ERL WPL-203.
- Harrison, B.F., Vaccaro, R.J. and Tufts, D.W. (1998) Robust matched-field localization in uncertain ocean environments. *J. Acoust. Soc. Amer.*, **103**, 3721–4.
- Harrison, C.H. (1989) Ocean propagation models. *Appl. Acoust.*, **27**, 163–201.
- Harrison, C.H. (1996) Formulas for ambient noise level and coherence. *J. Acoust. Soc. Amer.*, **99**, 2055–66.
- Harrison, C.H. (1997a) CANARY: a simple model of ambient noise and coherence. *Appl. Acoust.*, **51**, 289–315.
- Harrison, C.H. (1997b) Noise directionality for surface sources in range-dependent environments. *J. Acoust. Soc. Amer.*, **102**, 2655–62.
- Harrison, C.H. (1998) DINAMO: a noise directionality model suitable for operational use. Proc. Undersea Defence Technology Conf. (UDT Europe), pp. 11–15.
- Harrison, C.H. and Simons, D.G. (2001) Geoacoustic inversion of ambient noise: a simple method. In *Acoustical Oceanography*, eds, T.G. Leighton, G.J. Heald, H.D. Griffiths and G. Griffiths. *Proc. Inst. Acoust.*, **23** (Part 2), 91–8.
- Harrison, C.H. and Simons, D.G. (2002) Geoacoustic inversion of ambient noise: a simple method. *J. Acoust. Soc. Amer.*, **112**, 1377–89.

- Harrison, C.H., Ainslie, M.A. and Packman, M.N. (1990) INSIGHT: a fast, robust propagation loss model providing clear understanding. Proc. Undersea Defence Technology Conf. (UDT Europe), pp. 317–22.
- Harrison, C.H., Brind, R. and Cowley, A. (1999) Computation of noise directionality and array response in range dependent media with CANARY. In *Theoretical and Computational Acoustics '97*, eds, Y.-C. Teng, E.-C. Shang, Y.-H. Pao, M.H. Schultz and A.D. Pierce. World Scientific Publishing, Singapore, pp. 527–51.
- Harrison, C.H., Brind, R. and Cowley, A. (2001) Computation of noise directionality, coherence and array response in range dependent media with CANARY. *J. Comput. Acoust.*, **9**, 327–45.
- Hassab, J.C. (1989) *Underwater Signal and Data Processing*. CRC Press, Boca Raton, Florida, USA.
- Hawker, K.E. (1980) The use and evaluation of acoustic transmission loss models. Appl. Res. Labs., Univ. Texas at Austin, USA, ARL-TR-80-1.
- Hawkins, J.D. (1992) TOTS: three dimensional ocean thermal structure analysis. *Sea Technol.*, **33** (1), 62–3.
- Hawkins, J.D., Clancy, R.M. and Price, J.F. (1993) Use of AVHRR data to verify a system for forecasting diurnal sea surface temperature variability. *Int. J. Remote Sensing*, **14**, 1347–57.
- Heaney, K.D., Kuperman, W.A. and McDonald, B.E. (1991) Perth–Bermuda sound propagation (1960): adiabatic mode interpretation. *J. Acoust. Soc. Amer.*, **90**, 2586–94.
- Heathershaw, A.D., Stretch, C.E. and Maskell, S.J. (1991) Coupled ocean-acoustic model studies of sound propagation through a front. *J. Acoust. Soc. Amer.*, **89**, 145–55.
- Heindsmann, T.E., Smith, R.H. and Arneson, A.D. (1955) Effect of rain upon underwater noise levels. *J. Acoust. Soc. Amer.*, **27**, 378–9.
- Henrick, R.F. (1983) A cautionary note on the use of range-dependent propagation models in underwater acoustics. *J. Acoust. Soc. Amer.*, **73**, 810–12.
- Hickling, R. (1999) Noise control and SI units. *J. Acoust. Soc. Amer.*, **106**, 3048.
- Hodges, P. (1987) Three decades by the numbers. *Datamation*, **33** (18), 77–87.
- Hodgkiss, W.S. (1980) Reverberation model: I. Technical description and user's guide. Marine Physical Lab., Scripps Inst. Oceanogr., Tech. Memo. 319.
- Hodgkiss, W.S. Jr (1984) An oceanic reverberation model. *IEEE J. Oceanic Eng.*, **OE-9**, 63–72.
- Hodgkiss, W.S. Jr and Alexandrou, D. (1985) Under-ice reverberation rejection. *IEEE J. Oceanic Eng.*, **OE-10**, 285–9.
- Hodgkiss, W.S. Jr and Fisher, F.H. (1990) Vertical directionality of ambient noise at 32°N as a function of longitude and wind speed. *IEEE J. Oceanic Eng.*, **15**, 335–9.
- Hoffman, D.W. (1976) LORA: a model for predicting the performance of long-range active sonar systems. Nav. Undersea Ctr, Tech. Pub. 541.
- Hoffman, D.W. (1979) LIRA: a model for predicting the performance of low-frequency active-sonar systems for intermediate surveillance ranges. Nav. Ocean Syst. Ctr, Tech. Doc. 259.
- Holland, C.W. and Brunson, B.A. (1988) The Biot–Stoll sediment model: an experimental assessment. *J. Acoust. Soc. Amer.*, **84**, 1437–43.

- Holland, C.W. and Neumann, P. (1998) Sub-bottom scattering: a modeling approach. *J. Acoust. Soc. Amer.*, **104**, 1363–73.
- Holmes, E.S. (1988) Software requirements specification for the parabolic equation model. Sci. Appl. Inter. Corp., OAML-SRS-22.
- Holmes, E.S. and Gainey, L.A. (1992a) Software requirements specification for the parabolic equation model version 3.4. Anal. & Technol., Inc. and Sci. Appl. Inter. Corp., OAML-SRS-22.
- Holmes, E.S. and Gainey, L.A. (1992b) Software test description for the parabolic equation model version 3.4. Anal. & Technol., Inc. and Sci. Appl. Inter. Corp., OAML-STD-22.
- Holmes, E.S. and Gainey, L.A. (1992c) Software design document for the parabolic equation model version 3.4. Anal. & Technol., Inc. and Sci. Appl. Inter. Corp., OAML-SDD-22.
- Holmes, E.S., Miller, E.C. and Stephens, R.H. (1990) A PC-based acoustic model operating system. Proc. IEEE Oceans 90 Conf., pp. 227–31.
- Holt, R.M. (1985) FACT-10B version description document. ODSI Defense Syst., Inc., DSIR-PU-85-0124.
- Hovem, J.M. (1993) Mechanisms of bottom loss in underwater acoustics. In *Acoustic Signal Processing for Ocean Exploration*, eds, J.M.F. Moura and I.M.G. Lourtie. Kluwer Academic Publishers, Dordrecht, The Netherlands, pp. 21–40.
- Hovem, J.M., Richardson, M.D. and Stoll, R.D. (eds) (1991) *Shear Waves in Marine Sediments*. Kluwer Academic Publishers, Dordrecht, The Netherlands.
- Hovland, M. (1988) Organisms: the only cause of scattering layers? *EOS, Trans. Amer. Geophys. Union*, **69**, 760.
- Ingenito, F., Ferris, R.H., Kuperman, W.A. and Wolf, S.N. (1978) Shallow water acoustics summary report (first phase). Nav. Res. Lab., Rept 8179.
- Institute of Electrical and Electronics Engineers, Inc. (1989) IEEE standard glossary of modeling and simulation terminology. IEEE Std 610.3-1989.
- International Energy Agency (1996) *Global Offshore Oil Prospects to 2000*. Organisation for Economic Co-operation and Development, Paris.
- Ivansson, S. (1994) Shear-wave induced transmission loss in a fluid-solid medium. *J. Acoust. Soc. Amer.*, **96**, 2870–5.
- Ivansson, S. and Karasalo, I. (1992) A high-order adaptive integration method for wave propagation in range-independent fluid–solid media. *J. Acoust. Soc. Amer.*, **92**, 1569–77.
- Jackson, D.R., Winebrenner, D.P. and Ishimaru, A. (1986) Application of the composite roughness model to high-frequency bottom backscattering. *J. Acoust. Soc. Amer.*, **79**, 1410–22.
- Jacobs, G. (1974) Multiple profile restructuring and supplemental plot programs. Ocean Data Syst., Inc.
- Jacobs, G. (1982) FACT 9-H: version description document. Nav. Ocean Res. Dev. Activity, Tech. Note 133T.
- Jaster, C.E. and Boehme, H. (1984) The MINERAY sonar performance prediction computer model baseline description. Appl. Res. Labs., Univ. Texas at Austin, USA, ARL-TR-84-9.
- Jennette, R.L., Sander, E.L. and Pitts, L.E. (1978) The USI array noise model, Version I documentation. Underwater Syst., Inc. USI-APL-R-8.
- Jensen, F.B. (1982) Numerical models of sound propagation in real oceans. Proc. MTS/IEEE Oceans 82 Conf., pp. 147–54.

- Jensen, F.B. (1984) Numerical models in underwater acoustics. In *Hybrid Formulation of Wave Propagation and Scattering*, ed., L.B. Felsen. Martinus Nijhoff, Dordrecht, The Netherlands, pp. 295–335.
- Jensen, F.B. (1986) The art of generating meaningful results with numerical codes. *J. Acoust. Soc. Amer.*, **80** (Suppl. 1), S20–1 (abstract).
- Jensen, F.B. (1988) Wave theory modeling: a convenient approach to CW and pulse propagation modeling in low-frequency acoustics. *IEEE J. Oceanic Eng.*, **13**, 186–97.
- Jensen, F. (1993) CW and pulse propagation modeling in ocean acoustics. In *Acoustic Signal Processing for Ocean Exploration*, eds, J.M.F. Moura and I.M.G. Lourtie. Kluwer Academic Publishers, Dordrecht, The Netherlands, pp. 3–20.
- Jensen, F.B. and Ferla, M.C. (1979) SNAP: the SACLANTCEN normal-mode acoustic propagation model. SACLANT ASW Res. Ctr, Memo. SM-121.
- Jensen, F.B. and Ferla, C.M. (1988) Numerical solutions of range-dependent benchmark problems in ocean acoustics. SACLANT Undersea Res. Ctr, Rept SR-141.
- Jensen, F.B. and Ferla, C.M. (1990) Numerical solutions of range-dependent benchmark problems in ocean acoustics. *J. Acoust. Soc. Amer.*, **87**, 1499–1510.
- Jensen, F.B. and Krol, H. (1975) The use of the parabolic equation method in sound propagation modelling. SACLANT ASW Res. Ctr, Memo. SM-72.
- Jensen, F.B. and Kuperman, W.A. (1979) Environmental acoustical modelling at SACLANTCEN. SACLANT ASW Res. Ctr, Rept SR-34.
- Jensen, F.B. and Kuperman, W.A. (1983) Optimum frequency of propagation in shallow water environments. *J. Acoust. Soc. Amer.*, **73**, 813–19.
- Jensen, F.B. and Martinelli, G. (1985) Accurate PE calculations for range-dependent environments based on c_0 updates. *J. Acoust. Soc. Amer.*, **78** (Suppl. 1), S23 (abstract).
- Jensen, F.B. and Schmidt, H. (1984) Review of numerical models in underwater acoustics, including recently developed fast-field program. SACLANT ASW Res. Ctr, Rept SR-83.
- Jensen, F.B. and Schmidt, H. (1987) Subcritical penetration of narrow Gaussian beams into sediments. *J. Acoust. Soc. Amer.*, **82**, 574–9.
- Jensen, F.B., Kuperman, W.A., Porter, M.B. and Schmidt, H. (1994) *Computational Ocean Acoustics*. American Institute of Physics, New York (reprinted 1997 by Springer-Verlag).
- Jensen, F.B., Ferla, C.M., LePage, K.D. and Nielsen, P.L. (2001) Acoustic models at SACLANTCEN: an update. SACLANT Undersea Res. Ctr, Rept SR-354.
- Johnson, H.R., Backus, R.H., Hersey, J.B. and Owen, D.M. (1956) Suspended echo-sounder and camera studies of midwater sound scatterers. *Deep-Sea Res.*, **3**, 266–72.
- Johnson, M.V.R. Sr, McKeon, M.F. and Szanto, T.R. (1998) *Simulation Based Acquisition: A New Approach*. Report of the Military Research Fellows DSMC 1997–1998. Defense Systems Management College Press, Fort Belvoir, Virginia, USA. [Available from the US Government Printing Office (GPO 008-020-01461-3).]
- Johnson, O.G. (1984) Three-dimensional wave equation computations on vector computers. *Proc. IEEE*, **72**, 90–5.

- Jones, R.M. (1982) Algorithms for reflecting rays from general topographic surfaces in a ray tracing program. Wave Propagation Lab., NOAA Tech. Memo. ERL WPL-98.
- Jones, R.M. (1983) A survey of underwater-acoustic ray tracing techniques. Wave Propagation Lab., NOAA Tech. Memo. ERL WPL-111.
- Jones, R.M. and Georges, T.M. (1991) HARPX – a program to extend HARPO or HARPA ray paths in horizontally uniform media. Wave Propagation Lab., NOAA Tech. Memo. ERL WPL-201.
- Jones, R.M., Riley, J.P. and Georges, T.M. (1982) A versatile three-dimensional Hamiltonian ray-tracing computer program for acoustic waves in the atmosphere. Wave Propagation Lab., NOAA Tech. Memo. ERL WPL-103.
- Jones, R.M., Riley, J.P. and Georges, T.M. (1986) HARPO: a versatile three-dimensional Hamiltonian ray-tracing program for acoustic waves in an ocean with irregular bottom. Wave Propagation Lab., NOAA Tech. Rept.
- Jones, R.M., Georges, T.M., Nesbitt, L. and Weickmann, A. (1991) Ocean acoustic tomography inversion in the adiabatic-invariant approximation. Wave Propagation Lab., NOAA Tech. Memo. ERL WPL-217.
- Kalinowski, A.J. (1979) A survey of finite element-related techniques as applied to acoustic propagation in the ocean. Part I: finite element method and related techniques. *The Shock and Vibration Digest*, **11** (3), 9–16.
- Kanabis, W.G. (1975) A shallow water acoustic model for an ocean stratified in range and depth, Vol. I. Nav. Underwater Syst. Ctr, Tech. Rept 4887-I.
- Kanabis, W.G. (1976) A shallow water acoustic model for an ocean stratified in range and depth, Vol. II. Nav. Underwater Syst. Ctr, Tech. Rept 4887-II.
- Kapoor, T.K. and Schmidt, H. (1997) Acoustic scattering from a three-dimensional protuberance on a thin, infinite, submerged elastic plate. *J. Acoust. Soc. Amer.*, **102**, 256–65.
- Katsnelson, B.G. and Petnikov, V.G. (2002) *Shallow-Water Acoustics*. Springer Praxis, New York.
- Keenan, R.E. (2000) An introduction to GRAB eigenrays and CASS reverberation and signal excess. Proc. MTS/IEEE Oceans 2000 Conf., pp. 1065–70.
- Keenan, R.E. and Weinberg, H. (2001) Gaussian ray bundle (GRAB) model shallow water acoustic workshop implementation. *J. Comput. Acoust.*, **9**, 133–48.
- Keenan, R.E., Weinberg, H. and Aidala, F.E. Jr (1998) GRAB: Gaussian ray bundle (GRAB) eigenray propagation model version 2.0. Software Test Description. Naval Oceanographic Office, Stennis Space Center, Mississippi.
- Keiffer, R.S. and Novarini, J.C. (1990) A wedge assemblage method for 3-D acoustic scattering from sea surfaces: comparison with a Helmholtz–Kirchhoff method. In *Computational Acoustics. Vol. 1: Ocean-Acoustic Models and Supercomputing*, eds, D. Lee, A. Cakmak and R. Vichnevetsky. North-Holland, Amsterdam, pp. 67–81.
- Keller, J.B. and Papadakis, J.S. (eds) (1977) *Wave Propagation and Underwater Acoustics*. Lecture Notes in Physics, Vol. 70. Springer-Verlag, New York.
- Kerman, B.R. (ed.) (1988) *Sea Surface Sound. Natural Mechanisms of Surface Generated Noise in the Ocean*. NATO Advanced Science Institutes Series C: Mathematical and Physical Sciences 238. Kluwer Academic Publishers, Dordrecht, The Netherlands.
- Kerman, B.R. (ed.) (1993) *Natural Physical Sources of Underwater Sound, Sea Surface Sound* (2). Kluwer Academic Publishers, Dordrecht, The Netherlands.

- Kerr, D.E. (ed.) (1951) *Propagation of Short Radio Waves*. MIT Radiation Laboratory Series, Vol. 13. McGraw-Hill, New York.
- Kerr, R.A. (1977) Oceanography: a closer look at Gulf Stream rings. *Science*, **198**, 387–430.
- Kewley, D.J. and Bucker, H.P. (1987) A fast bistatic reverberation and systems model. *J. Acoust. Soc. Amer.*, **82** (Suppl. 1), S75 (abstract).
- Kibblewhite, A.C. and Ewans, K.C. (1985) Wave-wave interactions, microseisms and infrasonic ambient noise in the ocean. *J. Acoust. Soc. Amer.*, **78**, 981–94.
- Kibblewhite, A.C., Shooter, J.A. and Watkins, S.L. (1976) Examination of attenuation at very low frequencies using the deep-water ambient noise field. *J. Acoust. Soc. Amer.*, **60**, 1040–7.
- King, D. and White, D. (1986a) FACT version 10B. Volume 1: physics description. Nav. Ocean Res. Dev. Activity, Tech. Note 319.
- King, D. and White, D. (1986b) FACT version 10B. Volume 2: software description. Nav. Ocean Res. Dev. Activity, Tech. Note 320.
- Kinsler, L.E., Frey, A.R., Coppens, A.B. and Sanders, J.V. (1982) *Fundamentals of Acoustics*, 3rd edn. John Wiley & Sons, New York.
- Knight, W.C., Pridham, R.G. and Kay, S.M. (1981) Digital signal processing for sonar. *Proc. IEEE*, **69**, 1451–506.
- Knobles, D.P. and Vidmar, P.J. (1986) Simulation of bottom interacting waveforms. *J. Acoust. Soc. Amer.*, **79**, 1760–6.
- Knudsen, V.O., Alford, R.S. and Emling, J.W. (1948) Underwater ambient noise. *J. Mar. Res.*, **7**, 410–29.
- Koch, R.A. and Knobles, D.P. (1995) A practical application of the Galerkin method to the broadband calculation of normal modes for underwater acoustics. *J. Acoust. Soc. Amer.*, **98**, 1682–98.
- Koch, R.A. and LeMond, J.E. (2001a) Software design description (SDD) for the NAUTILUS model (version 1.0). Appl. Res. Labs., Univ. Texas at Austin, USA, ARL-TL-EV-01-17.
- Koch, R.A. and LeMond, J.E. (2001b) Software requirements specification for the NAUTILUS model (version 1.0). Appl. Res. Labs., Univ. Texas at Austin, USA, ARL-TL-EV-01-18.
- Koch, R.A. and LeMond, J.E. (2001c) Software test description for the NAUTILUS model (version 1.0). Appl. Res. Labs., Univ. Texas at Austin, USA, ARL-TL-EV-01-19.
- Koch, R.A., Rutherford, S.R. and Payne, S.G. (1983) Slope propagation: mechanisms and parameter sensitivities. *J. Acoust. Soc. Amer.*, **74**, 210–18.
- Kraus, E.B. (ed.) (1977) *Modelling and Prediction of the Upper Layers of the Ocean*. Pergamon Press, New York.
- Kuhl, F., Weatherly, R. and Dahmann, J. (1999) *Creating Computer Simulation Systems. An Introduction to the High Level Architecture*. Prentice Hall PTR, Upper Saddle River, New Jersey.
- Kuo, E.Y.T. (1988) Sea surface scattering and propagation loss: review, update, and new predictions. *IEEE J. Oceanic Eng.*, **13**, 229–34.
- Kuperman, W.A. (1985) Models of sound propagation in the ocean. *Nav. Res. Rev.*, **37** (3), 32–41.
- Kuperman, W.A. and Ingenito, F. (1980) Spatial correlation of surface generated noise in a stratified ocean. *J. Acoust. Soc. Amer.*, **67**, 1988–96.

- Kuperman, W.A., Porter, M.B. and Perkins, J.S. (1987) Three-dimensional oceanographic acoustic modeling of complex environments. *J. Acoust. Soc. Amer.*, **82** (Suppl. 1), S42 (abstract).
- Kuperman, W.A., Porter, M.B., Perkins, J.S. and Piacsek, A.A. (1988) Rapid three-dimensional ocean acoustic modeling of complex environments. In *Proceedings of the IMACS 12th World Congress on Scientific Computation*, eds, R. Vichnevetsky, P. Borne and J. Vignes. GERFIDN – Cite Scientifique, Villeneuve d'Ascq, France, pp. 231–3.
- Kuperman, W.A., Porter, M.B., Perkins, J.S. and Evans, R.B. (1991) Rapid computation of acoustic fields in three-dimensional ocean environments. *J. Acoust. Soc. Amer.*, **89**, 125–33.
- Kuperman, W.A., Hodgkiss, W.S., Song, H.C., Akal, T., Ferla, C. and Jackson, D.R. (1998) Phase conjugation in the ocean: experimental demonstration of an acoustic time-reversal mirror. *J. Acoust. Soc. Amer.*, **103**, 25–40.
- Kutschale, H.W. (1973) Rapid computation by wave theory of propagation loss in the Arctic Ocean. Lamont-Doherty Geol. Obs., CU-8-73.
- Kutschale, H.W. (1984) Arctic marine acoustics. Lamont-Doherty Geol. Obs., Final Rept, ONR Contr, N00014-80-C-0021.
- Kutschale, H.W. and DiNapoli, F.R. (1977) Pulse propagation in the ocean. II: the fast field program method. *J. Acoust. Soc. Amer.*, **62** (Suppl. 1), S18 (abstract).
- Kutschale, H.W. and Lee, T. (1983) Bottom-interacting acoustic signals in the Arctic channel: long-range propagation. *J. Acoust. Soc. Amer.*, **74** (Suppl. 1), S1 (abstract).
- Labianca, F.M. (1973) Normal modes, virtual modes, and alternative representations in the theory of surface-duct sound propagation. *J. Acoust. Soc. Amer.*, **53**, 1137–47.
- LaFond, E.C. (1962) Internal waves. Part I. In *The Sea, Vol. 1: Physical Oceanography*, ed., M.N. Hill. Interscience Publishers, New York, pp. 731–51.
- Lai, C.-C.A., Qian, W. and Glenn, S.M. (1994) Data assimilation and model evaluation experiment datasets. *Bull. Amer. Meteor. Soc.*, **75**, 793–809.
- Lai, D.Y. and Richardson, P.L. (1977) Distribution and movement of Gulf Stream rings. *J. Phys. Oceanogr.*, **7**, 670–83.
- Lamb, P.J. (1984) On the mixed-layer climatology of the north and tropical Atlantic. *Tellus*, **36A**, 292–305.
- Lasky, M. and Colilla, R. (1974) FANM-I fast ambient noise model. Program documentation and user's guide. Ocean Data Syst., Inc.
- Lau, R.L., Lee, D. and Robinson, A.R. (eds) (1993) *Computational Acoustics, Vol. 1: Scattering, Supercomputing and Propagation*. North-Holland, Amsterdam.
- Lauer, R.B. (1979) Acoustic model evaluation: issues and recommendations incorporating the experience of the panel on sonar system models (POSSM). Nav. Underwater Syst. Ctr, Tech. Rept 6025.
- Lauer, R.B. and Sussman, B. (1976) A methodology for the comparison of models for sonar system applications, Vol. I. Nav. Sea Syst. Command, SEA 06H1/036-EVA/MOST-10.
- Lauer, R.B. and Sussman, B. (1979) A methodology for the comparison of models for sonar system applications – results for low frequency propagation loss in the Mediterranean Sea, Vol. II. Nav. Sea Syst. Command, SEA 06H1/036-EVA/MOST-11.

- Laville, F., Abbott, G.D. and Miller, M.J. (1991) Underwater sound generation by rainfall. *J. Acoust. Soc. Amer.*, **89**, 715–21.
- Law, A.M. and Kelton, W.D. (1991) *Simulation Modeling and Analysis*, 2nd edn. McGraw-Hill, New York.
- Lee, D. (1983) Effective methods for predicting underwater acoustic wave propagation. Proc. AIAA 8th Aeroacoustics Conf. Paper No. 83–0683.
- Lee, D. and Botseas, G. (1982) IFD: an implicit finite-difference computer model for solving the parabolic equation. Nav. Underwater Syst. Ctr, Tech. Rept 6659.
- Lee, D. and McDaniel, S.T. (1983) Wave field computations on the interface: an ocean acoustic model. *Math. Modelling*, **4**, 473–88.
- Lee, D. and McDaniel, S.T. (1987) Ocean acoustic propagation by finite difference methods. *Comp. Math. Applic.*, **14** (5), 305–423.
- Lee, D. and Papadakis, J.S. (1980) Numerical solutions of the parabolic wave equation: an ordinary-differential-equation approach. *J. Acoust. Soc. Amer.*, **68**, 1482–8.
- Lee, D. and Pierce, A.D. (1995) Parabolic equation development in recent decade. *J. Comput. Acoust.*, **3**, 95–173.
- Lee, D. and Schultz, M.H. (1995) *Numerical Ocean Acoustic Propagation in Three Dimensions*. World Scientific Publishing, Singapore.
- Lee, D. and Siegmann, W.L. (1986) A mathematical model for the 3-dimensional ocean sound propagation. *Math. Modelling*, **7**, 143–62.
- Lee, D., Botseas, G. and Papadakis, J.S. (1981) Finite-difference solution to the parabolic wave equation. *J. Acoust. Soc. Amer.*, **70**, 795–800.
- Lee, D., Saad, Y. and Schultz, M.H. (1988) An efficient method for solving the three-dimensional wide angle wave equation. In *Computational Acoustics, Vol. 1: Wave Propagation*, eds, D. Lee, R.L. Sternberg and M.H. Schultz. North-Holland, Amsterdam, pp. 75–89.
- Lee, D., Cakmak, A. and Vichnevetsky, R. (eds) (1990a) *Computational Acoustics, Vol. 1: Ocean-Acoustic Models and Supercomputing*. North-Holland, Amsterdam.
- Lee, D., Cakmak, A. and Vichnevetsky, R. (eds) (1990b) *Computational Acoustics, Vol. 2: Scattering, Gaussian Beams, and Aeroacoustics*. North-Holland, Amsterdam.
- Lee, D., Cakmak, A. and Vichnevetsky, R. (eds) (1990c) *Computational Acoustics, Vol. 3: Seismo-Ocean Acoustics and Modeling*. North-Holland, Amsterdam.
- Lee, D., Botseas, G. and Siegmann, W.L. (1992) Examination of three-dimensional effects using a propagation model with azimuth-coupling capability (FOR3D). *J. Acoust. Soc. Amer.*, **91**, 3192–202.
- Lee, D., Vichnevetsky, R. and Robinson, A.R. (eds) (1993) *Computational Acoustics, Vol. 2: Acoustic Propagation*. North-Holland, Amsterdam.
- Lee, D., Pierce, A.D. and Shang, E.-C. (2000) Parabolic equation development in the twentieth century. *J. Comput. Acoust.*, **8**, 527–637.
- Leibiger, G.A. (1968) Wave propagation in an inhomogeneous medium with slow spatial variation. PhD Dissertation, Stevens Institute of Technology.
- Leibiger, G.A. (1977) Criteria for propagation loss model assessment for APP application. Nav. Underwater Syst. Ctr, Tech. Memo. 771245.
- Leighton, T.G. (1994) *The Acoustic Bubble*. Academic Press, San Diego.
- Lemon, D.D. and Duddridge, G. (1987) A numerical model for the calibration of CASP WOTAN wind data. Proc. MTS/IEEE Oceans 87 Conf., pp. 167–71.

- LeMond, J.E. and Koch, R.A. (1997) Finite correlation and coherent propagation effects in the normal-mode description of bottom reverberation. *J. Acoust. Soc. Amer.*, **102**, 266–77.
- LePage, K. and Schmidt, H. (1994) Modeling of low-frequency transmission loss in the central Arctic. *J. Acoust. Soc. Amer.*, **96**, 1783–95.
- Leroy, C.C. (1969) Development of simple equations for accurate and more realistic calculation of the speed of sound in seawater. *J. Acoust. Soc. Amer.*, **46**, 216–26.
- Leroy, C.C. and Parthiot, F. (1998) Depth-pressure relationships in the oceans and seas. *J. Acoust. Soc. Amer.*, **103**, 1346–52.
- Levinson, S.J., Westwood, E.K., Koch, R.A., Mitchell, S.K. and Sheppard, C.V. (1995) An efficient and robust method for underwater acoustic normal-mode computations. *J. Acoust. Soc. Amer.*, **97**, 1576–85.
- Levitus, S. (1982) Climatological atlas of the world ocean. NOAA Professional Paper 13.
- Lewis, E.L. (1980) The practical salinity scale 1978 and its antecedents. *IEEE J. Oceanic Eng.*, **OE-5**, 3–8.
- Lewis, J.K. and Denner, W.W. (1988) Higher frequency ambient noise in the Arctic Ocean. *J. Acoust. Soc. Amer.*, **84**, 1444–55.
- Lingevitch, J.F. and Collins, M.D. (1998) Wave propagation in range-dependent poro-acoustic waveguides. *J. Acoust. Soc. Amer.*, **104**, 783–90.
- Liu, Q., Li, F., Guo, L., Gong, Z. and Li, X. (2001) Applications of BDRM theory to numerical predictions of acoustic transmission losses in shallow water. *Acta Acust.* **26**, 410–16 (in Chinese).
- Locklin, J.H. and Etter, P.C. (1988) Sonar model operating system functional requirement. SYNTEK Engr. Comp. Syst., Inc.
- Locklin, J. and Webster, J. (1980) NORDA model operating system functional description and FY 80 implementation plan. Ocean Data Syst., Inc.
- Long, D. (1979) FANM/SIAM noise plot program. Ocean Data Syst., Inc.
- Love, R.H. (1975) Predictions of volume scattering strengths from biological trawl data. *J. Acoust. Soc. Amer.*, **57**, 300–6.
- Love, R.H. (1978) Resonant acoustic scattering by swimbladder-bearing fish. *J. Acoust. Soc. Amer.*, **64**, 571–80.
- Love, R.H. (1993) A comparison of volume scattering strength data with model calculations based on quasisynoptically collected fishery data. *J. Acoust. Soc. Amer.*, **94**, 2255–68.
- Love, R.H., Thompson, C.H. and Nero, R.W. (1996) Volume reverberation in littoral waters. *J. Acoust. Soc. Amer.*, **100**, 2799 (abstract).
- Lovett, J.R. (1978) Merged seawater sound-speed equations. *J. Acoust. Soc. Amer.*, **63**, 1713–18.
- Luby, J.C. and Lytle, D.W. (1987) Autoregressive modeling of nonstationary multibeam sonar reverberation. *IEEE J. Oceanic Eng.*, **OE-12**, 116–29.
- Ludwig, D. (1966) Uniform asymptotic expansions at a caustic. *Commun. Pure Appl. Math.*, **19**, 215–50.
- Lukas, I.J., Hess, C.A. and Osborne, K.R. (1980a) ASERT/ASEPS version 4.1 FNOC user's manual. Ocean Data Syst., Inc.
- Lukas, I.J., Hess, C.A. and Osborne, K.R. (1980b) DANES/ASEPS version 4.1 FNOC user's manual. Ocean Data Syst., Inc.
- Lynch, J.F., Newhall, A.E., Chiu, C.-S. and Miller, J.H. (1994) Three-dimensional ray acoustics in a realistic ocean. In *Oceanography and Acoustics: Prediction*

- and Propagation Models, eds, A.R. Robinson and D. Lee. American Institute of Physics, New York, Chapter 9, pp. 198–232.
- Lyons, A.P., Anderson, A.L. and Dwan, F.S. (1994) Acoustic scattering from the seafloor: modeling and data comparison. *J. Acoust. Soc. Amer.*, **95**, 2441–51.
- Macaskill, C. and Ewart, T.E. (1996) Numerical solution of the fourth moment equation for acoustic intensity correlations and comparison with the mid-ocean acoustic transmission experiment. *J. Acoust. Soc. Amer.*, **99**, 1419–29.
- Mackenzie, K.V. (1961) Bottom reverberation for 530- and 1030-cps sound in deep water. *J. Acoust. Soc. Amer.*, **33**, 1498–504.
- Mackenzie, K.V. (1981) Nine-term equation for sound speed in the oceans. *J. Acoust. Soc. Amer.*, **70**, 807–12.
- Macpherson, J.D. and Daintith, M.J. (1967) Practical model of shallow-water acoustic propagation. *J. Acoust. Soc. Amer.*, **41**, 850–4.
- Mahler, J.I., Sullivan, F.J.M. and Moll, M. (1975) Statistical methodology for the estimation of noise due to shipping in small sectors and narrow bands. Bolt, Beranek and Newman, Inc., Tech. Memo. W273.
- Makris, N.C. (1993) Imaging ocean-basin reverberation via inversion. *J. Acoust. Soc. Amer.*, **94**, 983–93.
- Makris, N.C. and Dyer, I. (1986) Environmental correlates of pack ice noise. *J. Acoust. Soc. Amer.*, **79**, 1434–40.
- Makris, N.C. and Dyer, I. (1991) Environmental correlates of Arctic ice-edge noise. *J. Acoust. Soc. Amer.*, **90**, 3288–98.
- Makris, N.C., Ingenito, F. and Kuperman, W.A. (1994) Detection of a submerged object insonified by surface noise in an ocean waveguide. *J. Acoust. Soc. Amer.*, **96**, 1703–24.
- Marsh, H.W. (1950) Theory of the anomalous propagation of acoustic waves in the ocean. Navy Underwater Sound Lab., Rept 111.
- Marsh, H.W. (1963) Sound reflection and scattering from the sea surface. *J. Acoust. Soc. Amer.*, **35**, 240–4.
- Marsh, H.W. and Mellen, R.H. (1963) Underwater sound propagation in the Arctic Ocean. *J. Acoust. Soc. Amer.*, **35**, 552–63.
- Marsh, H.W. Jr and Schulkin, M. (1955) Report on the status of Project AMOS (Acoustic, Meteorological, and Oceanographic Survey) (1 January 1953–31 December 1954). Navy Underwater Sound Lab., Res. Rept 255.
- Marsh, H.W. and Schulkin, M. (1962a) Underwater sound transmission. AVCO Corp. Marine Electronics Office Rept.
- Marsh, H.W. and Schulkin, M. (1962b) Shallow-water transmission. *J. Acoust. Soc. Amer.*, **34**, 863–4.
- Marsh, H.W., Schulkin, M. and Kneale, S.G. (1961) Scattering of underwater sound by the sea surface. *J. Acoust. Soc. Amer.*, **33**, 334–40.
- Marsh, P. (1976) A computer program for studying the Doppler content of reverberation. Nav. Sea Syst. Command, OD 52258.
- Marsh, P. and Poynter, A.B. (1969) Digital computer programs for analyzing acoustic search performance in refractive waters, Vols 1 and 2. Nav. Undersea Ctr, Tech. Pub. 164.
- Martin, P.J. (1993) Sensitivity of acoustic transmission loss prediction to mixed-layer hindcasts calculated with data from Ocean Weather Station Papa. Nav. Res. Lab., Rept NRL/FR/7322-93-9426.

- Mazur, M.A. and Gilbert, K.E. (1997a) Direct optimization methods, ray propagation, and chaos. I. Continuous media. *J. Acoust. Soc. Amer.*, **101**, 174–83.
- Mazur, M.A. and Gilbert, K.E. (1997b) Direct optimization methods, ray propagation, and chaos. II. Propagation with discrete transitions. *J. Acoust. Soc. Amer.*, **101**, 184–92.
- McCabe, B.J. (1976) Ambient noise effects in the modeling of detection by a field of sensors. Daniel H. Wagner Assoc.
- McCammon, D.F. (1988) Fundamental relationships between geoacoustic parameters and predicted bottom loss using a thin layer model. *J. Geophys. Res.*, **93**, 2363–9.
- McCammon, D.F. (1991) Underwater acoustic modeling. *Sea Technol.*, **32** (8), 53–5.
- McCammon, D.F. and Crowder, D.C. (1981) NEPBR – numerable energy paths by RAYMODE computer program. Appl. Res. Lab., Pennsylvania State Univ., Tech. Memo. TM 81-50.
- McCammon, D.F. and McDaniel, S.T. (1985) The influence of the physical properties of ice on reflectivity. *J. Acoust. Soc. Amer.*, **77**, 499–507.
- McCarthy, E.M. and Sabol, B. (2000) Acoustic characterization of submerged aquatic vegetation: military and environmental monitoring applications. Proc. MTS/IEEE Oceans 2000 Conf., pp. 1957–61.
- McConnell, S.O. (1983) Remote sensing of the air-sea interface using microwave acoustics. Proc. MTS/IEEE Oceans 83 Conf., pp. 85–92.
- McDaniel, S.T. (1993) Sea surface reverberation: a review. *J. Acoust. Soc. Amer.*, **94**, 1905–22.
- McDonald, B.E. and Kuperman, W.A. (1987) Time domain formulation for pulse propagation including nonlinear behavior at a caustic. *J. Acoust. Soc. Amer.*, **81**, 1406–17.
- McGirr, R.W. (1979) Acoustic model evaluation procedures: a review. Nav. Ocean Syst. Ctr, Tech. Doc. 287.
- McGirr, R.W. (1980) Applications of statistical distributions in acoustic model evaluation. Nav. Ocean Syst. Ctr, Tech. Doc. 387.
- McGirr, R.W. and Hall, J.C. (1974) FLIRT: a fast linear intermediate-range transmission loss model. Nav. Undersea Ctr, Tech. Note 1282.
- McGirr, R., White, D. and Bartberger, C. (1984) Technical evaluation of FACT 10A. Nav. Ocean Res. Devel. Activity, Rept 70.
- McKinney, C.M. and Anderson, C.D. (1964) Measurements of backscattering of sound from the ocean bottom. *J. Acoust. Soc. Amer.*, **36**, 158–63.
- Medeiros, R.C. (1982a) RAYMODE passive propagation loss program performance specification. New England Tech. Services, Doc. 8205.
- Medeiros, R.C. (1982b) Active acoustic performance prediction using RAYMODE integration. New England Tech. Services, Doc. 8203.
- Medeiros, R.C. (1985a) 1985 baseline RAYMODE passive propagation loss program performance specification. New England Tech. Services, Doc. 8501 Rev. 1.
- Medeiros, R.C. (1985b) 1985 baseline active RAYMODE propagation loss prediction computer program performance specification. New England Tech. Services, Doc. 8502 Rev. 1.
- Medwin, H. (1975) Speed of sound in water: a simple equation for realistic parameters. *J. Acoust. Soc. Amer.*, **58**, 1318–19.
- Medwin, H. and Clay, C.S. (1998) *Fundamentals of Acoustical Oceanography*. Academic Press, San Diego.

- Medwin, H., Childs, E., Jordan, E.A. and Spaulding, R.A. Jr (1984) Sound scatter and shadowing at a seamount: hybrid physical solution in two and three dimensions. *J. Acoust. Soc. Amer.*, **75**, 1478–90.
- Medwin, H., Browne, M.J., Johnson, K.R. and Denny, P.L. (1988) Low-frequency backscatter from Arctic leads. *J. Acoust. Soc. Amer.*, **83**, 1794–803.
- Medwin, H., Nystuen, J.A., Jacobus, P.W., Ostwald, L.H. and Snyder, D.E. (1992) The anatomy of underwater rain noise. *J. Acoust. Soc. Amer.*, **92**, 1613–23.
- Mellen, R.H. and Marsh, H.W. (1965) Underwater sound in the Arctic Ocean. AVCO Marine Electronics Office, Rept MED-65-1002.
- Mellen, R.H., Scheifele, P.M. and Browning, D.G. (1987a) Global model for sound absorption in sea water. Nav. Underwater Syst. Ctr, Tech. Rept 7923.
- Mellen, R.H., Scheifele, P.M. and Browning, D.G. (1987b) Global model for sound absorption in sea water. Part II: GEOSECS pH data analysis. Nav. Underwater Syst. Ctr, Tech. Rept 7925.
- Mellen, R.H., Scheifele, P.M. and Browning, D.G. (1987c) Global model for sound absorption in sea water. Part III: Arctic regions. Nav. Underwater Syst. Ctr, Tech. Rept 7969.
- Mellor, G.L. and Yamada, T. (1974) A hierarchy of turbulence closure models for planetary boundary layers. *J. Atmos. Sci.*, **31**, 1791–806.
- Menke, W. (1989) *Geophysical Data Analysis: Discrete Inverse Theory* (rev. edn). International Geophysics Series, Vol. 45. Academic Press, San Diego.
- Merklinger, H.M. (ed.) (1987) *Progress in Underwater Acoustics*. Proc. 12th International Congress on Acoustics Associated Symposium on Underwater Acoustics, July 16–18, 1986, Halifax, Nova Scotia, Canada. Plenum, New York.
- Mignerey, P.C. (1995) Horizontal refraction of 3-D curvilinear wedge modes. *J. Acoust. Soc. Amer.*, **98**, 2912 (abstract).
- Milder, D.M. (1969) Ray and wave invariants for SOFAR channel propagation. *J. Acoust. Soc. Amer.*, **46**, 1259–63.
- Miller, J.F. (1982) Range-dependent ocean acoustic transmission loss calculations in a real-time framework. 4th Interservice/Industry Training Equip. Conf., pp. 287–99.
- Miller, J.F. (1983) Acoustic propagation loss calculations in a complex ocean environment for simulator-based training. IEE Int. Conf. Simulators (Brighton, England), Conf. Pub. 226, pp. 215–21.
- Miller, J.F. and Ingenito, F. (1975) Normal mode FORTRAN programs for calculating sound propagation in the ocean. Nav. Res. Lab., Memo. Rept 3071.
- Miller, J.F. and Wolf, S.N. (1980) Modal acoustic transmission loss (MOATL): a transmission-loss computer program using a normal-mode model of the acoustic field in the ocean. Nav. Res. Lab., Rept 8429.
- Miller, J.F., Nagl, A. and Überall, H. (1986) Upslope sound propagation through the bottom of a wedge-shaped ocean beyond cutoff. *J. Acoust. Soc. Amer.*, **79**, 562–5.
- Miller, J.H., Lynch, J.F. and Chiu, C.-S. (1989) Estimation of sea surface spectra using acoustic tomography. *J. Acoust. Soc. Amer.*, **86**, 326–45.
- Millero, F.J. and Li, X. (1994) Comments on “On equations for the speed of sound in seawater.” *J. Acoust. Soc. Amer.*, **95**, 2757–9.
- Milne, A.R. (1964) Underwater backscattering strengths of Arctic pack ice. *J. Acoust. Soc. Amer.*, **36**, 1551–6.

- Milne, A.R. (1967) Sound propagation and ambient noise under sea ice. In *Underwater Acoustics*, Vol. 2, ed., V.M. Albers. Plenum, New York, pp. 103–38.
- Moler, C.B. and Solomon, L.P. (1970) Use of splines and numerical integration in geometrical acoustics. *J. Acoust. Soc. Amer.*, **48**, 739–44.
- Moll, M., Zeskind, R.M. and Sullivan, F.J.M. (1977) Statistical measures of ambient noise: algorithms, program, and predictions. Bolt, Beranek and Newman, Inc., Rept 3390.
- Moll, M., Zeskind, R.M. and Scott, W.L. (1979) An algorithm for beam noise prediction. Bolt, Beranek and Newman, Inc., Rept 3653.
- Mooers, C.N.K., Piacsek, S.A. and Robinson, A.R. (eds) (1982) Ocean prediction: the scientific basis and the Navy's needs. A status and prospectus report. Proc. Ocean Prediction Workshop, Monterey, California, USA, May 1981.
- Moore-Head, M.E., Jobst, W. and Showalter, J.A. (1989) The calculation-frequency method for fast parabolic-equation modeling at high frequencies. *J. Acoust. Soc. Amer.*, **85**, 1527–30.
- Morfeý, C.L. (ed.) (2000) *Dictionary of Acoustics*. Academic Press, San Diego.
- Morgan, J.G. Jr (1998) Networking ASW systems: anti-submarine warfare dominance. *Sea Technol.*, **39** (11), 19–22.
- Moritz, E. (1982) Reverberation research overview. Nav. Coastal Syst. Ctr, Tech. Memo. NCSC TM 362-82.
- Morris, G.B. (1978) Depth dependence of ambient noise in the northeastern Pacific Ocean. *J. Acoust. Soc. Amer.*, **64**, 581–90.
- Moskowitz, L. (1964) Estimates of the power spectrums for fully developed seas for wind speeds of 20 to 40 knots. *J. Geophys. Res.*, **69**, 5161–79.
- Munk, W.H. (1974) Sound channel in an exponentially stratified ocean, with application to SOFAR. *J. Acoust. Soc. Amer.*, **55**, 220–6.
- Munk, W.H. (1980) Horizontal deflection of acoustic paths by mesoscale eddies. *J. Phys. Oceanogr.*, **10**, 596–604.
- Munk, W.H. (1991) Bermuda shadow. *Atmos.-Ocean*, **29**, 183–96.
- Munk, W. (1994) Heard Island and beyond. *J. Acoust. Soc. Amer.*, **95**, 567.
- Munk, W. and Baggeroer, A. (1994) The Heard Island papers: a contribution to global acoustics. *J. Acoust. Soc. Amer.*, **96**, 2327–9.
- Munk, W.H. and Forbes, A.M.G. (1989) Global ocean warming: an acoustic measure? *J. Phys. Oceanogr.*, **19**, 1765–78.
- Munk, W. and Wunsch, C. (1979) Ocean acoustic tomography: a scheme for large scale monitoring. *Deep-Sea Res.*, **26**, 123–61.
- Munk, W.H. and Zachariasen, F. (1991) Refraction of sound by islands and seamounts. *J. Atmos. Ocean. Technol.*, **8**, 554–74.
- Munk, W., Worcester, P. and Wunsch, C. (1995) *Ocean Acoustic Tomography*. Cambridge University Press, New York.
- Murphy, J.E. and Chin-Bing, S.A. (1988) A finite element model for ocean acoustic propagation. *Math. Comput. Modelling*, **11**, 70–4.
- Murphy, J.E. and Chin-Bing, S.A. (1989) A finite-element model for ocean acoustic propagation and scattering. *J. Acoust. Soc. Amer.*, **86**, 1478–83.
- Murphy, J.E. and Chin-Bing, S.A. (1991) A seismo-acoustic finite element model for underwater acoustic propagation. In *Shear Waves in Marine Sediments*, eds, J.M. Hovem, M.D. Richardson and R.D. Stoll. Kluwer Academic Publishers, Dordrecht, The Netherlands, pp. 463–70.

- National Defense Research Committee (1946) *Physics of Sound in the Sea*. Summary Technical Report of Division 6, NDRC, Vol. 8. Reprinted by Dept of the Navy, Naval Material Command, 1969, NAVMAT P-9675, Washington, DC.
- National Oceanographic Data Center (1992) *Users Guide*. Key to Oceanographic Records Documentation No. 14, 2nd edn. Washington, DC.
- National Research Council (1994) *Low-Frequency Sound and Marine Mammals: Current Knowledge and Research Needs*. National Academy Press, Washington, DC.
- National Research Council (1996) *Undersea Vehicles and National Needs*. National Academy Press, Washington, DC.
- National Research Council (1997) *Technology for the United States Navy and Marine Corps, 2000–2035. Becoming a 21st-Century Force. Vol. 9: Modeling and Simulation*. National Academy Press, Washington, DC.
- National Research Council (2000) *Marine Mammals and Low-Frequency Sound: Progress Since 1994*. National Academy Press, Washington, DC.
- Naval Oceanographic Office (1967) *Oceanographic Atlas of the North Atlantic Ocean. Section II – Physical Properties*. Pub. No. 700, US Dept of the Navy, Washington, DC.
- Naval Oceanographic Office (1972) *Environmental-Acoustics Atlas of the Caribbean Sea and Gulf of Mexico. Volume II – Marine Environment*. SP-189II, US Dept of the Navy, Washington, DC.
- Naval Oceanographic Office (1991a) Software design document for the 1985 baseline passive RAYMODE computer program. OAML-SDD-01A, US Dept of the Navy, Stennis Space Center, Mississippi.
- Naval Oceanographic Office (1991b) Software design document for the 1985 baseline active RAYMODE computer program. OAML-SDD-02A, US Dept of the Navy, Stennis Space Center, Mississippi.
- Naval Oceanographic Office (1991c) Test specification for the 1985 baseline passive RAYMODE computer program. OAML-TS-01G, US Dept of the Navy, Stennis Space Center, Mississippi.
- Naval Oceanographic Office (1991d) Test specification for the 1985 baseline active RAYMODE computer program. OAML-TS-02F, US Dept of the Navy, Stennis Space Center, Mississippi.
- Naval Oceanographic Office (1999) Oceanographic and atmospheric master library summary. OAML-SUM-21G, US Dept of the Navy, Stennis Space Center, Mississippi.
- Navy Modeling and Simulation Management Office (1999) *Navy M&S Catalog*. NAVMSMO, Washington, DC.
- Nesbitt, L. and Jones, R.M. (1994a) A C program for generating publication-quality plots. NOAA Tech. Memo. ERL ETL-242.
- Nesbitt, L. and Jones, R.M. (1994b) A FORTRAN program for performing non-perturbative ocean acoustic tomography inversion. NOAA Tech. Memo. ERL ETL-243.
- Nesbitt, L. and Jones, R.M. (1994c) A FORTRAN program to generate comparison data to test tomography inversion programs. NOAA Tech. Memo. ERL ETL-245.
- Neumann, G. and Pierson, W.J. Jr (1966) *Principles of Physical Oceanography*. Prentice-Hall, Englewood Cliffs, USA.
- Newhall, A.E., Lynch, J.F., Chiu, C.-S. and Daugherty, J.R. (1990) Improvements in three-dimensional raytracing codes for underwater acoustics. In *Computational*

- Acoustics, Vol. 1: Ocean-Acoustic Models and Supercomputing*, eds, D. Lee, A. Cakmak and R. Vichnevetsky. North-Holland, Amsterdam, pp. 169–85.
- Newman, A.V. and Ingenito, F. (1972) A normal mode computer program for calculating sound propagation in shallow water with an arbitrary velocity profile. *Nav. Res. Lab., Memo. Rept 2381*.
- Newton, J. and Galindo, M. (2001) Hydroacoustic monitoring network. *Sea Technol.*, **42** (9), 41–7.
- Nghiem-Phu, L., Daubin, S.C. and Tappert, F. (1984) A high-speed, compact, and interactive parabolic equation solution generator (PESOGEN) system. *J. Acoust. Soc. Amer.*, **75** (Suppl. 1), S26 (abstract).
- Nicholas, M., Ogden, P.M. and Erskine, F.T. (1998) Improved empirical descriptions for acoustic surface backscatter in the ocean. *IEEE J. Oceanic Eng.*, **23**, 81–95.
- Nielsen, R.O. (1991) *Sonar Signal Processing*. Artech House, Boston.
- North Atlantic Treaty Organization (1998) *NATO Modelling and Simulation Master Plan*. Document AC/323 (SGMS)D/2, Version 1.0. North Atlantic Council, Brussels.
- North Atlantic Treaty Organization (2000) *Follow-On NIAG Prefeasibility Studies on Common Technical Framework and Multi-National Force Rehearsal. PATHFINDER Experiment Definition. Final Report*. NIAG-D(99)6 AC/323 (NMSG).
- Norton, G.V. and Novarini, J.C. (1996) The effect of sea-surface roughness on shallow water waveguide propagation: a coherent approach. *J. Acoust. Soc. Amer.*, **99**, 2013–21.
- Norton, G.V., Novarini, J.C. and Keiffer, R.S. (1995) Coupling scattering from the sea surface to a one-way marching propagation model via conformal mapping: validation. *J. Acoust. Soc. Amer.*, **97**, 2173–80.
- Norton, G.V., Novarini, J.C. and Keiffer, R.S. (1998) Modeling the propagation from a horizontally directed high-frequency source in shallow water in the presence of bubble clouds and sea surface roughness. *J. Acoust. Soc. Amer.*, **103**, 3256–67.
- Noutary, E. and Plaisant, A. (1996) 2D and 3D propagation modelling with coupled modes. In *Theoretical and Computational Acoustics '95*, eds, D. Lee, Y.-H. Pao, M.H. Schultz and Y.-C. Teng. World Scientific Publishing, Singapore, pp. 61–74.
- Nystuen, J.A. (1986) Rainfall measurements using underwater ambient noise. *J. Acoust. Soc. Amer.*, **79**, 972–82.
- Nystuen, J.A. (1994) Acoustical rainfall analysis. *J. Acoust. Soc. Amer.*, **95**, 2882–3 (abstract).
- Nystuen, J.A. and Medwin, H. (1995) Underwater sound produced by rainfall: secondary splashes of aerosols. *J. Acoust. Soc. Amer.*, **97**, 1606–13.
- Oba, R. and Finette, S. (2002) Acoustic propagation through anisotropic internal wave fields: transmission loss, cross-range coherence, and horizontal refraction. *J. Acoust. Soc. Amer.*, **111**, 769–84.
- Ocean Acoustic Developments Ltd (1999a) WADER global ocean information system. Product description literature.
- Ocean Acoustic Developments Ltd (1999b) Global sonar assessment and range prediction system. Product description literature.
- Officer, C.B. (1958) *Introduction to the Theory of Sound Transmission with Application to the Ocean*. McGraw-Hill, New York.

- Ogden, P.M. and Erskine, F.T. (1994a) Surface scattering measurements using broadband explosive charges in the Critical Sea Test experiments. *J. Acoust. Soc. Amer.*, **95**, 746–61.
- Ogden, P.M. and Erskine, F.T. (1994b) Surface and volume scattering measurements using broadband explosive charges in the Critical Sea Test 7 experiment. *J. Acoust. Soc. Amer.*, **96**, 2908–20.
- Ogden, P.M. and Erskine, F.T. (1997) Bottom scattering strengths measured using explosive sources in the Critical Sea Test Program. Nav. Res. Lab., Rept NRL/FR/7140-97-9822.
- Oğuz, H.N. (1994) A theoretical study of low-frequency oceanic ambient noise. *J. Acoust. Soc. Amer.*, **95**, 1895–912.
- Orchard, B.J., Siegmann, W.L. and Jacobson, M.J. (1992) Three-dimensional time-domain paraxial approximations for ocean acoustic wave propagation. *J. Acoust. Soc. Amer.*, **91**, 788–801.
- Orcutt, J.A. (1988) Ultralow- and very-low-frequency seismic and acoustic noise in the Pacific. *J. Acoust. Soc. Amer.*, **84** (Suppl. 1), S194 (abstract).
- Oreskes, N., Shrader-Frechette, K. and Belitz, K. (1994) Verification, validation, and confirmation of numerical models in the Earth sciences. *Science*, **263**, 641–6.
- Orme, E.A., Johns, P.B. and Arnold, J.M. (1988) A hybrid modelling technique for underwater acoustic scattering. *Int. J. Numer. Model.: Electron. Netw., Devices Fields*, **1**, 189–206.
- Orris, G.J. and Collins, M.D. (1994) The spectral parabolic equation and three-dimensional backscattering. *J. Acoust. Soc. Amer.*, **96**, 1725–31.
- Osborne, K.R. (1979) DANES – a directional ambient noise prediction model for FLENUMOCEANCEN. Ocean Data Syst., Inc.
- Pace, N.G., Pouliquen, E., Bergem, O. and Lyons, A.P. (eds) (1997) High frequency acoustics in shallow water. SACLANT Undersea Res. Ctr, Conf. Proc. CP-45.
- Pack, P.M.W. (1986) The finite element method in underwater acoustics. PhD Thesis, Institute of Sound and Vibration Research, Univ. Southampton.
- Packman, M.N., Harrison, C.H. and Ainslie, M.A. (1992) INSIGHT – a fast, robust, propagation loss model with physical intuition. *Acoust. Bull.*, **17** (4), 21–4.
- Packman, M.N., Harrison, C.H. and Ainslie, M.A. (1996) Rapid calculations of acoustic propagation loss in range dependent oceans. *IEE Proc. (Radar, Sonar and Navigation)*, **143** (3), 184–9.
- Palmer, D.R., Brown, M.G., Tappert, F.D. and Bezdek, H.F. (1988a) Classical chaos in nonseparable wave propagation problems. *Geophys. Res. Lett.*, **15**, 569–72.
- Palmer, D.R., Lawson, L.M., Daneshzadeh, Y.-H. and Behringer, D.W. (1988b) Computational studies of the effect of an El Niño/southern oscillation event on underwater sound propagation. In *Computational Acoustics, Vol. 2: Algorithms and Applications*, eds, D. Lee, R.L. Sternberg and M.H. Schultz. North-Holland, Amsterdam, pp. 335–56.
- Palmer, L.B. and Fromm, D.M. (1992) The range-dependent active system performance prediction model (RASP). Nav. Res. Lab., Rept NRL/FR/5160-92-9383.
- Papadakis, J.S., Dougalis, V.A., Kampanis, N.A., Flouri, E.T., Pelloni, B., Plaisant, A., Noutary, E., Bjørnø, L., Nielsen, P. and Zhu, D. (1998) Ocean acoustic models for low frequency propagation in 2D and 3D environments. *ACUSTICA Acta Acustica*, **84**, 1031–41.
- Pedersen, M.A. (1961) Acoustic intensity anomalies introduced by constant velocity gradients. *J. Acoust. Soc. Amer.*, **33**, 465–74.

- Pedersen, M.A. and Gordon, D.F. (1965) Normal-mode theory applied to short-range propagation in an underwater acoustic surface duct. *J. Acoust. Soc. Amer.*, **37**, 105–18.
- Pedersen, M.A. and Gordon, D.F. (1967) Comparison of curvilinear and linear profile approximation in the calculation of underwater sound intensities by ray theory. *J. Acoust. Soc. Amer.*, **41**, 419–38.
- Pedersen, M.A. and McGirr, R.W. (1982) Use of theoretical controls in underwater acoustic model evaluation. Nav. Ocean Syst. Ctr, Tech. Rept 758.
- Pedersen, M.A., Gordon, D.F. and Keith, A.J. (1962) A new ray intensity procedure for underwater sound based on a profile consisting of curvilinear segments. Nav. Electron. Lab., Res. Rept 1105.
- Pedersen, M.A., Gordon, D.F. and Hosmer, R.F. (1984) Comparison of experimental detailed convergence-zone structure with results of uniform asymptotic ray theory. Nav. Ocean Syst. Ctr, Tech. Rept 997.
- Peixoto, J.P. and Oort, A.H. (1992) *Physics of Climate*. American Institute of Physics, New York.
- Pekeris, C.L. (1946) Theory of propagation of sound in a half-space of variable sound velocity under conditions of formation of a shadow zone. *J. Acoust. Soc. Amer.*, **18**, 295–315.
- Pekeris, C.L. (1948) Theory of propagation of explosive sound in shallow water. *Geol. Soc. Amer. Mem.*, **27**, 1–117.
- Peloquin, R.A. (1992) The Navy ocean modeling and prediction program. *Oceanography*, **5** (1), 4–8.
- Penrose, J.D., Pauly, T.J., Arcus, W.R., Duncan, A.J. and Bush, G. (1993) Remote sensing with underwater acoustics. *Acoust. Aust.*, **21** (1), 19–21.
- Perkin, R.G. and Lewis, E.L. (1980) The practical salinity scale 1978: fitting the data. *IEEE J. Oceanic Eng.*, **OE-5**, 9–16.
- Perkins, J.S. and Baer, R.N. (1978) A corrected parabolic-equation program package for acoustic propagation. Nav. Res. Lab., Memo. Rept 3688.
- Perkins, J.S. and Baer, R.N. (1982) An approximation to the three-dimensional parabolic-equation method for acoustic propagation. *J. Acoust. Soc. Amer.*, **72**, 515–22.
- Perkins, J.S., Baer, R.N., Wright, E.B. and Roche, L.F. (1982) Solving the parabolic equation for underwater acoustic propagation by the split-step algorithm. Nav. Res. Lab., Rept 8607.
- Perkins, J.S., Baer, R.N., Roche, L.F. and Palmer, L.B. (1983) Three-dimensional parabolic-equation-based estimation of the ocean acoustic field. Nav. Res. Lab., Rept 8685.
- Perkins, J.S., Adams, B.B. and McCoy, J.J. (1984) Vertical coherence along a macroray path in an inhomogeneous anisotropic ocean. Nav. Res. Lab., Rept 8792.
- Perkins, J.S., Williamson, M., Kuperman, W.A. and Evans, R.B. (1990) Sound propagation through the Gulf Stream: current status of two three-dimensional models. In *Computational Acoustics, Vol. 1: Ocean-Acoustic Models and Supercomputing*, eds, D. Lee, A. Cakmak and R. Vichnevetsky. North-Holland, Amsterdam, pp. 203–15.
- Perkins, J.S., Kuperman, W.A., Ingenito, F., Fialkowski, L.T. and Glattet, J. (1993) Modeling ambient noise in three-dimensional ocean environments. *J. Acoust. Soc. Amer.*, **93**, 739–52.

- Peters, H. and Gregg, M.C. (1987) Equatorial turbulence: mixed layer and thermocline. In *Dynamics of the Oceanic Surface Mixed Layer*, eds, P. Muller and D. Henderson. Hawaii Inst. Geophys. Special Pub., Honolulu, USA, pp. 25–45.
- Pflug, L.A. (1996) Modification of the RANDI model for shallow-water applications. Nav. Res. Lab., Rept NRL/MR/7176-96-8003.
- Pickard, G.L. (1963) *Descriptive Physical Oceanography: An Introduction*. Pergamon Press, New York.
- Pickard, G.L. and Emery, W.J. (1990) *Descriptive Physical Oceanography: An Introduction*, 5th edn. Pergamon Press, New York.
- Pierce, A.D. (1965) Extension of the method of normal modes to sound propagation in an almost-stratified medium. *J. Acoust. Soc. Amer.*, **37**, 19–27.
- Pierce, A.D. (1982) Guided mode disappearance during upslope propagation in variable depth shallow water overlying a fluid bottom. *J. Acoust. Soc. Amer.*, **72**, 523–31.
- Pierce, A.D. (1989) *Acoustics: An Introduction to its Physical Principles and Applications*. Acoustical Society of America, New York.
- Pierce, A.D. and Thurston, R.N. (eds) (1993) *Underwater Scattering and Radiation, Physical Acoustics XXII*. Academic Press, San Diego.
- Pierson, W.J. Jr (1964) The interpretation of wave spectrums in terms of the wind profile instead of the wind measured at a constant height. *J. Geophys. Res.*, **69**, 5191–203.
- Pierson, W.J. Jr (1991) Comment on “Effects of Sea Maturity on Satellite Altimeter Measurements” by Roman E. Glazman and Stuart H. Pilorz. *J. Geophys. Res.*, **96**, 4973–7.
- Pierson, W.J. Jr and Moskowitz, L. (1964) A proposed spectral form for fully developed wind seas based on the similarity theory of S.A. Kitaigorodskii. *J. Geophys. Res.*, **69**, 5181–90.
- Pignot, P. and Chapman, N.R. (2001) Tomographic inversion of geoacoustic properties in a range-dependent shallow-water environment. *J. Acoust. Soc. Amer.*, **110**, 1338–48.
- Piskarev, A.L. (1992) Soviet research in underwater acoustic propagation modeling. EG&G, Tech. Rept 6K1-011A.
- Plotkin, A.M. (1996) LYCH 2-D ray program functional description. ISDCO unpublished manuscript.
- Podeszwa, E.M. (1969) Computer program for Colossus II shallow-water transmission loss equations. Navy Underwater Sound Lab., Tech. Memo. 2040-85-69.
- Pomerenk, K. and Novick, A. (1987) BISAPP user’s manual. Mission Sci. Corp.
- Porter, M.B. (1990) The time-marched fast-field program (FFP) for modeling acoustic pulse propagation. *J. Acoust. Soc. Amer.*, **87**, 2013–23.
- Porter, M. (1991) The KRAKEN normal mode program. SACLANT Undersea Res. Ctr, Memo. SM-245.
- Porter, M.B. (1993) Acoustic models and sonar systems. *IEEE J. Oceanic Eng.*, **18**, 425–37.
- Porter, M.B. and Bucker, H.P. (1987) Gaussian beam tracing for computing ocean acoustic fields. *J. Acoust. Soc. Amer.*, **82**, 1349–59.
- Porter, M.B. and Jensen, F.B. (1993) Anomalous parabolic equation results for propagation in leaky surface ducts. *J. Acoust. Soc. Amer.*, **94**, 1510–16.
- Porter, M. and Reiss, E.L. (1984) A numerical method for ocean-acoustic normal modes. *J. Acoust. Soc. Amer.*, **76**, 244–52.

- Porter, M.B. and Reiss, E.L. (1985) A numerical method for bottom interacting ocean acoustic normal modes. *J. Acoust. Soc. Amer.*, **77**, 1760–7.
- Potter, J.R. (1994) Acoustic imaging using ambient noise: some theory and simulation results. *J. Acoust. Soc. Amer.*, **95**, 21–33.
- Potter, J.R. and Chitre, M. (1999) Ambient noise imaging in warm shallow seas; second-order moment and model-based imaging algorithms. *J. Acoust. Soc. Amer.*, **106**, 3201–10.
- Powers, W.J. (1987) Bistatic active signal excess model – an extension of the Generic Sonar Model. Nav. Underwater Syst. Ctr, Tech. Memo. 871025.
- Primack, H. and Gilbert, K.E. (1991) A two-dimensional downslope propagation model based on coupled wedge modes. *J. Acoust. Soc. Amer.*, **90**, 3254–62.
- Princehouse, D.W. (1977) REVGGEN, a real-time reverberation generator. IEEE Int. Conf. Acoust. Speech Signal Process., pp. 827–35.
- Pritchard, R.S. (1990) Sea ice noise-generating processes. *J. Acoust. Soc. Amer.*, **88**, 2830–42.
- Prosperetti, A. and Oğuz, H.N. (1993) The impact of drops on liquid surfaces and the underwater noise of rain. *Ann. Rev. Fluid Mech.*, **25**, 577–602.
- Pumphrey, H.C. (1994) Underwater rain noise – the initial impact component. *Acoust. Bull.*, **19** (2), 19–28.
- Pumphrey, H.C. and Crum, L.A. (1990) Free oscillations of near-surface bubbles as a source of the underwater noise of rain. *J. Acoust. Soc. Amer.*, **87**, 142–8.
- Rajan, S.D. (1992) Determination of geoacoustic parameters of the ocean bottom – data requirements. *J. Acoust. Soc. Amer.*, **92**, 2126–40.
- Ramsdale, D.J. and Posey, J.W. (1987) Understanding underwater acoustics under the Arctic ice canopy. *Sea Technol.*, **28** (7), 22–8.
- Rasband, S.N. (1990) *Chaotic Dynamics of Nonlinear Systems*. John Wiley & Sons, New York.
- Rayleigh, J.W.S. (1945) *The Theory of Sound*, Vols I and II. Dover Publications, New York. (Republication of the 1894 and 1896 editions of Vols I and II, respectively.)
- Reise, B. and Etter, P.C. (1997) Performance assessment of active sonar configuration options. Proc. Undersea Defence Technology Conf. (UDT Europe), pp. 408–13.
- Renner, W.W. (1986a) Ambient noise directionality estimation system (ANDES) user's guide (HP 9000 installations). Sci. Appl. Inter. Corp., SAIC-86/1705.
- Renner, W.W. (1986b) Ambient noise directionality estimation system (ANDES) technical description. Sci. Appl. Inter. Corp., SAIC-86/1645.
- Renner, W.W. (1988) Ambient noise directionality estimation system (ANDES) II user's guide (VAX 11/78X installations). Sci. Appl. Inter. Corp., SAIC-88/1567.
- Renner, W. (1995a) Software requirements specification for the ANDES model (Version 4.2). Sci. Appl. Inter. Corp. Tech. Rept.
- Renner, W. (1995b) User's guide for the ANDES model (Version 4.2). Sci. Appl. Inter. Corp. Tech. Rept.
- Richards, S.D. (1998) The effect of temperature, pressure, and salinity on sound attenuation in turbid seawater. *J. Acoust. Soc. Amer.*, **103**, 205–11.
- Richards, S.D. and Leighton, T.G. (2001a) Acoustic sensor performance in coastal waters: solid suspensions and bubbles. In *Acoustical Oceanography*, eds, T.G. Leighton, G.J. Heald, H.D. Griffiths and G. Griffiths. *Proc. Inst. Acoust.*, **23** (Part 2), 399–406.
- Richards, S.D. and Leighton, T.G. (2001b) Sonar performance in coastal environments: suspended sediments and microbubbles. *Acoust. Bull.*, **26** (1), 10–17.

- Richards, S.D., Heathershaw, A.D. and Thorne, P.D. (1996) The effect of suspended particulate matter on sound attenuation in seawater. *J. Acoust. Soc. Amer.*, **100**, 1447–50.
- Richardson, W.J., Greene, C.R. Jr, Malme, C.I. and Thomson, D.H. (1995) *Marine Mammals and Noise*. Academic Press, San Diego.
- Roberts, B.G. Jr (1974) Horizontal-gradient acoustical ray-trace program TRIMAIN. Nav. Res. Lab., Rept 7827.
- Robertson, J.S. (1989) A classification scheme for computational ocean acoustic benchmark problems. *Appl. Acoust.*, **27**, 65–8.
- Robertson, J.S., Arney, D.C., Jacobson, M.J. and Siegmann, W.L. (1989) An efficient enhancement of finite-difference implementations for solving parabolic equations. *J. Acoust. Soc. Amer.*, **86**, 252–60.
- Robertson, J.S., Siegmann, W.L. and Jacobson, M.J. (1991) OS2IFD: a microcomputer implementation of the parabolic equation for predicting underwater sound propagation. *Comput. Geosci.*, **17**, 731–57.
- Robertsson, J.O.A., Levander, A. and Holliger, K. (1996) A hybrid wave propagation simulation technique for ocean acoustic problems. *J. Geophys. Res.*, **101**, 11225–41.
- Robins, A.J. (1991) Reflection of a plane wave from a fluid layer with continuously varying density and sound speed. *J. Acoust. Soc. Amer.*, **89**, 1686–96.
- Robinson, A.R. (1987) Predicting open ocean currents, fronts and eddies. In *Three-Dimensional Models of Marine and Estuarine Dynamics*, eds, J.C.J. Nihoul and B.M. Jamart. Elsevier Oceanography Series, **45**, pp. 89–111.
- Robinson, A.R. (1992) Shipboard prediction with a regional forecast model. *Oceanography*, **5** (1), 42–8.
- Robinson, A.R., Carton, J.A., Mooers, C.N.K., Walstad, L.J., Carter, E.F., Rienecker, M.M., Smith, J.A. and Leslie, W.G. (1984) A real-time dynamical forecast of ocean synoptic/mesoscale eddies. *Nature*, **309**, 781–3.
- Robinson, A.R., Carman, J.C. and Glenn, S.M. (1994) A dynamical system for acoustic applications. In *Oceanography and Acoustics: Prediction and Propagation Models*, eds, A.R. Robinson and D. Lee. American Institute of Physics, New York, Chapter 4, pp. 80–117.
- Robinson, E.R. and McConnell, S.O. (1983) Sensitivity of high frequency surface-generated noise to sonar and environmental parameters. Proc. MTS/IEEE Oceans 83 Conf., pp. 11–15.
- Rodríguez, O.C., Jesus, S., Stephan, Y., Demoulin, X., Porter, M. and Coelho, E. (2000) Nonlinear soliton interaction with acoustic signals: focusing effects. *J. Comput. Acoust.*, **8**, 347–63.
- Rogers, P.H. (1981) Onboard prediction of propagation loss in shallow water. Nav. Res. Lab., Rept 8500.
- Rohr, J. and Detsch, R. (1992) A low sea-state study of the quieting effect of monomolecular films on the underlying ambient-noise field. *J. Acoust. Soc. Amer.*, **92**, 365–83.
- Ross, D. (1976) *Mechanics of Underwater Noise*. Pergamon Press, New York.
- Ross, D. (1993) On ocean underwater ambient noise. *Acoust. Bull.*, **18** (1), 5–8.
- Rubenstein, D. and Greene, R. (1991) Modeling the acoustic scattering by under-ice-ridge keels. *J. Acoust. Soc. Amer.*, **89**, 666–72.
- Runyan, L. (1991) 40 years on the frontier. *Datamation*, **37** (6), 34–57.

- Sachs, D.A. and Silbiger, A. (1971) Focusing and refraction of harmonic sound and transient pulses in stratified media. *J. Acoust. Soc. Amer.*, **49**, 824–40.
- Sadowski, W., Katz, R. and McFadden, K. (1984) Ambient noise standards for acoustic modeling and analysis. Nav. Underwater Syst. Ctr, Tech. Doc. 7265.
- Saenger, R.A. (1984) Volume scattering strength algorithm: a first generation model. Nav. Underwater Syst. Ctr, Tech. Memo. 841193.
- Sagen, H., Johannessen, O.M. and Sandven, S. (1990) The influence of sea ice on ocean ambient sound. In *Ice Technology for Polar Operations*, eds, T.K.S. Murthy, J.G. Paren, W.M. Sackinger and P. Wadhams. Second Int. Conf. Ice Technology. Computational Mechanics Publications, Cambridge, England, pp. 415–26.
- Sammelmann, G.S. (1998) SWAT acoustic modeling. Coastal Systems Station, Dahlgren Division, Naval Surface Warfare Center.
- Santiago, J.A.F. and Wrobel, L.C. (2000) A boundary element model for underwater acoustics in shallow water. *Compu. Modeling Eng. Sci.*, **1**, 73–80.
- Schilling, R. (1998) Innovations in remote intervention: pressures for change from the offshore oil industry. *UnderWater Magazine*, **X** (2), 21–4.
- Schippers, P. (1995) The ALMOST PC-model for propagation and reverberation in range dependent environments. Proc. Undersea Defence Technology Conf. (UDT Europe), pp. 430–5.
- Schippers, P. (1996) Modelling of sediment bottom propagation using ray theory. Proc. Undersea Defence Technology Conf. (UDT Europe), pp. 43–7.
- Schippers, P. (1998) First results of a newly developed ambient noise time signal model. Proc. Undersea Defence Technology Conf. (UDT Europe), pp. 6–10.
- Schmidt, H. (1988) SAFARI: seismo-acoustic fast field algorithm for range-independent environments. User's guide. SACLANT Undersea Res. Ctr, Rept SR-113.
- Schmidt, H. (1991) Numerical modeling in ocean seismo-acoustics. Proc. IEEE Oceans 91 Conf., pp. 84–92.
- Schmidt, H. (1999) OASES, Version 2.2 user guide and reference manual. Department of Ocean Engineering, Massachusetts Institute of Technology.
- Schmidt, H. and Glatteire, J. (1985) A fast field model for three-dimensional wave propagation in stratified environments based on the global matrix method. *J. Acoust. Soc. Amer.*, **78**, 2105–14.
- Schmidt, H., Seong, W. and Goh, J.T. (1995) Spectral super-element approach to range-dependent ocean acoustic modeling. *J. Acoust. Soc. Amer.*, **98**, 465–72.
- Schmitt, R.W. (1987) The Caribbean sheets and layers transects (C-SALT) program. *EOS, Trans. Amer. Geophys. Union*, **68**, 57–60.
- Schmitt, R.W., Perkins, H., Boyd, J.D. and Stalcup, M.C. (1987) C-SALT: an investigation of the thermohaline staircase in the western tropical North Atlantic. *Deep-Sea Res.*, **34**, 1655–65.
- Schneider, H.G. (1990) MOCASSIN: sound propagation and sonar range prediction model for shallow water environments. User's guide. Tech. Rept 1990–9, Forschungsanstalt der Bundeswehr für Wasserschall- und Geophysik, Kiel, Germany.
- Schneider, H.G. (1993) Surface loss, scattering, and reverberation with the split-step parabolic wave equation model. *J. Acoust. Soc. Amer.*, **93**, 770–81.
- Schramm, W.G. (1993) NEONS: a database management system for environmental data. *Earth System Monitor*, **3** (4), 7–8. (Published by Dept of Commerce, NOAA, Silver Spring, Maryland, USA.)

- Schreiner, H.F. Jr (1990) The RANDI-PE noise model. Proc. IEEE Oceans 90 Conf., pp. 576–7.
- Schulkin, M. and Mercer, J.A. (1985) Colossus revisited: a review and extension of the Marsh-Schulkin shallow water transmission loss model (1962). Appl. Phys. Lab., Univ. Washington, APL-UW 8508.
- Schurman, I.W., Siegmann, W.L. and Jacobson, M.J. (1991) An energy-conserving parabolic equation incorporating range refraction. *J. Acoust. Soc. Amer.*, **89**, 134–44.
- Scrimger, J.A., Evans, D.J., McBean, G.A., Farmer, D.M. and Kerman, B.R. (1987) Underwater noise due to rain, hail, and snow. *J. Acoust. Soc. Amer.*, **81**, 79–86.
- Scully-Power, P.D. and Lee, D. (eds) (1984) Recent progress in the development and application of the parabolic equation. Nav. Underwater Syst. Ctr, Tech. Doc. 7145.
- Selsor, H.D. (1993) Data from the sea: Navy drifting buoy program. *Sea Technol.*, **34** (12), 53–8.
- Seong, W. (1990) Hybrid Galerkin boundary element – wavenumber integration method for acoustic propagation in laterally inhomogeneous media. PhD Thesis, Massachusetts Institute of Technology.
- Seong, W. and Choi, B. (2001) Multiplicative Padé PE formulation applied to SWAM'99 test cases. *J. Comput. Acoust.*, **9**, 227–41.
- Shang, E.-C., Wang, Y.Y. and Gao, T.F. (2001) On the adiabaticity of acoustic propagation through nongradual ocean structures. *J. Comput. Acoust.*, **9**, 359–65.
- Shaw, P.T., Watts, D.R. and Rossby, H.T. (1978) On the estimation of oceanic wind speed and stress from ambient noise measurements. *Deep-Sea Res.*, **25**, 1225–33.
- Shenderov, E.L. (1998) Some physical models for estimating scattering of underwater sound by algae. *J. Acoust. Soc. Amer.*, **104**, 791–800.
- Siderius, M., Snellen, M., Simons, D.G. and Onken, R. (2000) An environmental assessment in the Strait of Sicily: measurement and analysis techniques for determining bottom and oceanographic properties. *IEEE J. Oceanic Eng.*, **25**, 364–86.
- Siderius, M., Nielsen, P.L., Sellschopp, J., Snellen, M. and Simons, D. (2001) Experimental study of geo-acoustic inversion uncertainty due to ocean sound-speed fluctuations. *J. Acoust. Soc. Amer.*, **110**, 769–81.
- Siegmann, W.L., Kriegsmann, G.A. and Lee, D. (1985) A wide-angle three-dimensional parabolic wave equation. *J. Acoust. Soc. Amer.*, **78**, 659–64.
- Siegmann, W.L., Jacobson, M.J. and Law, L.D. (1987) Effects of bottom attenuation on acoustic propagation with a modified ray theory. *J. Acoust. Soc. Amer.*, **81**, 1741–51.
- Sienkiewicz, C.G., Boyd, M.L., Rosenzweig, J.R. and Pelton, R.M. (1975) Computer-programmed models used at the University of Washington's Applied Physics Laboratory for evaluating torpedo sonar performance. Appl. Phys. Lab., Univ. Washington, APL-UW 7611.
- Simmen, J., Flatté, S.M. and Wang, G.-Y. (1997) Wavefront folding, chaos, and diffraction for sound propagation through ocean internal waves. *J. Acoust. Soc. Amer.*, **102**, 239–55.
- Simons, D.G. and Laterveer, R. (1995) Normal-mode sound propagation modelling for matched-field processing. TNO Physics Electronics Lab., Rept FEL-95-A084.
- Simons, D.G. and Snellen, M. (1998) Multi-frequency matched-field inversion of benchmark data using a genetic algorithm. *J. Comput. Acoust.*, **6**, 135–50.

- Simons, D.G., McHugh, R., Snellen, M., McCormick, N.H. and Lawson, E.A. (2001) Analysis of shallow-water experimental acoustic data including a comparison with a broad-band normal-mode-propagation model. *IEEE J. Oceanic Eng.*, **26**, 308–23.
- Skretting, A. and Leroy, C.C. (1971) Sound attenuation between 200 Hz and 10 kHz. *J. Acoust. Soc. Amer.*, **49**, 276–82.
- Smith, E.M. (1982) Active RAYMODE program user's guide. Nav. Underwater Syst. Ctr, Tech. Memo. 821081.
- Smith, G.B. (1997) "Through the sensor" environmental estimation. *J. Acoust. Soc. Amer.*, **101**, 3046 (abstract).
- Smith, K.B. and Tappert, F.D. (1993) UMPE: The University of Miami parabolic equation model, version 1.0. Marine Physical Lab., Scripps Inst. Oceanogr., Tech. Memo. 432.
- Smith, K.B., Brown, M.G. and Tappert, F.D. (1992a) Ray chaos in underwater acoustics. *J. Acoust. Soc. Amer.*, **91**, 1939–49.
- Smith, K.B., Brown, M.G. and Tappert, F.D. (1992b) Acoustic ray chaos induced by mesoscale ocean structure. *J. Acoust. Soc. Amer.*, **91**, 1950–9.
- Smith, K.B., Tappert, F.D. and Hodgkiss, W.S. (1993) Comparison of UMPE/PEREV bistatic reverberation predictions with observations in the ARSRP natural lab. *J. Acoust. Soc. Amer.*, **94**, 1766 (abstract).
- Smith, K.B., Hodgkiss, W.S. and Tappert, F.D. (1996) Propagation and analysis issues in the prediction of long-range reverberation. *J. Acoust. Soc. Amer.*, **99**, 1387–404.
- Snellen, M., Simons, D.G., Siderius, M., Sellschopp, J. and Nielsen, P.L. (2001) An evaluation of the accuracy of shallow water matched field inversion results. *J. Acoust. Soc. Amer.*, **109**, 514–27.
- Solomon, L.P., Ai, D.K.Y. and Haven, G. (1968) Acoustic propagation in a continuously refracted medium. *J. Acoust. Soc. Amer.*, **44**, 1121–9.
- Solomon, L.P., Barnes, A.E. and Lunsford, C.R. (1977) Ocean route envelopes. Planning Syst., Inc., Tech. Rept TR-036049.
- Song, H.C., Kuperman, W.A. and Hodgkiss, W.S. (1998) A time-reversal mirror with variable range focusing. *J. Acoust. Soc. Amer.*, **103**, 3234–40.
- Spiesberger, J.L. (1989) Remote sensing of western boundary currents using acoustic tomography. *J. Acoust. Soc. Amer.*, **86**, 346–51.
- Spiesberger, J.L. and Metzger, K. (1991a) Basin-scale tomography: a new tool for studying weather and climate. *J. Geophys. Res.*, **96**, 4869–89.
- Spiesberger, J.L. and Metzger, K. (1991b) A new algorithm for sound speed in seawater. *J. Acoust. Soc. Amer.*, **89**, 2677–88.
- Spiesberger, J.L., Metzger, K. and Furgerson, J.A. (1992) Listening for climatic temperature change in the northeast Pacific: 1983–1989. *J. Acoust. Soc. Amer.*, **92**, 384–96.
- Spikes, C.H., Erskine, F.T., McEachern, J.F. and Backes, D.A. (1997) Littoral warfare technology testing. *Sea Technol.*, **38** (6), 71–7.
- Spindel, R.C. (1985) Sound transmission in the ocean. *Ann. Rev. Fluid Mech.*, **17**, 217–37.
- Spindel, R.C. and Worcester, P.F. (1990a) Ocean acoustic tomography programs: accomplishments and plans. Proc. IEEE Oceans 90 Conf., pp. 1–10.
- Spindel, R.C. and Worcester, P.F. (1990b) Ocean acoustic tomography. *Sci. Amer.*, **263** (4), 94–9.

- Spindel, R.C. and Worcester, P.F. (1991) Ocean acoustic tomography: a decade of development. *Sea Technol.*, 32 (7), 47–52.
- Spofford, C.W. (1973a) The Bell Laboratories multiple-profile ray-tracing program. Bell Telephone Labs.
- Spofford, C.W. (1973b) A synopsis of the AESD workshop on acoustic-propagation modeling by non-ray-tracing techniques, 22–25 May 1973, Washington, DC. Acoustic Environmental Support Detachment, Off. Nav. Res., Tech. Note TN-73-05.
- Spofford, C.W. (1974) The FACT model, Vol. I. Acoustic Environmental Support Detachment, Off. Nav. Res., Maury Ctr Rept 109.
- Spofford, C.W. (1979) The ASTRAL model, Vol. I: Technical description. Sci. Appl. Inter., Inc., SAI-79-742-WA.
- Spofford, C.W. and Haynes, J.M. (eds) (1983) Stochastic modeling workshop. Proc. workshop, Nav. Res. Lab., Oct. 26–28, 1982, Washington, DC.
- Stephen, R.A. (1990) Solutions to range-dependent benchmark problems by the finite-difference method. *J. Acoust. Soc. Amer.*, 87, 1527–34.
- Stickler, D.C. (1975) Normal-mode program with both the discrete and branch line contributions. *J. Acoust. Soc. Amer.*, 57, 856–61.
- Stickler, D.C. and Ammicht, E. (1980) Uniform asymptotic evaluation of the continuous spectrum contribution for the Pekeris model. *J. Acoust. Soc. Amer.*, 67, 2018–24.
- Stoll, R.D. (1974) Acoustic waves in saturated sediments. In *Physics of Sound in Marine Sediments*, ed., L. Hampton. Plenum, New York, pp. 19–39.
- Stoll, R.D. (1980) Theoretical aspects of sound transmission in sediments. *J. Acoust. Soc. Amer.*, 68, 1341–50.
- Stoll, R.D. (1989) *Sediment Acoustics*. Lecture Notes in Earth Sciences, Vol. 26. Springer-Verlag, New York.
- Stotts, S.A. and Bedford, N.R. (1991) Development of an Arctic ray model. *J. Acoust. Soc. Amer.*, 90, 2299 (abstract).
- Stotts, S.A., Koch, R.A. and Bedford, N.R. (1994) Development of an Arctic ray model. *J. Acoust. Soc. Amer.*, 95, 1281–98.
- Sundaram, B. and Zaslavsky, G.M. (1999) Wave analysis of ray chaos in underwater acoustics. *Chaos*, 9, 483–92.
- Sverdrup, H.U., Johnson, M.W. and Fleming, R.H. (1942) *The Oceans. Their Physics, Chemistry, and General Biology*. Prentice-Hall, Englewood Cliffs, USA.
- Swift, S.A. and Stephen, R.A. (1994) The scattering of a low-angle pulse beam from seafloor volume heterogeneities. *J. Acoust. Soc. Amer.*, 96, 991–1001.
- Talham, R.J. (1964) Ambient-sea-noise model. *J. Acoust. Soc. Amer.*, 36, 1541–4.
- Tang, X. and Tappert, F.D. (1997) Effects of internal waves on sound pulse propagation in the Straits of Florida. *IEEE J. Oceanic Eng.*, 22, 245–55.
- Tango, G.J. (1988) Numerical models for VLF seismic-acoustic propagation prediction: a review. *IEEE J. Oceanic Eng.*, 13, 198–214.
- Tappert, F.D. (1977) The parabolic approximation method. In *Wave Propagation and Underwater Acoustics*, eds, J.B. Keller and J.S. Papadakis. Lecture Notes in Physics, Vol. 70. Springer-Verlag, New York, pp. 224–87.
- Tappert, F.D. (1998) Parabolic equation modeling with the split-step Fourier algorithm in four dimensions. *J. Acoust. Soc. Amer.*, 103, 2990 (abstract).
- Tappert, F.D. and Lee, D. (1984) A range refraction parabolic equation. *J. Acoust. Soc. Amer.*, 76, 1797–803.

- Tappert, F.D. and Tang, X. (1996) Ray chaos and eigenrays. *J. Acoust. Soc. Amer.*, **99**, 185–95.
- Tappert, F., Lee, D. and Weinberg, H. (1984) High-frequency propagation modeling using HYPER. *J. Acoust. Soc. Amer.*, **75** (Suppl. 1), S30 (abstract).
- Tappert, F.D., Brown, M.G., Palmer, D.R. and Bezdek, H. (1988) Chaos in underwater acoustics. *J. Acoust. Soc. Amer.*, **83** (Suppl. 1), S36 (abstract).
- Tappert, F.D., Brown, M.G. and Goni, G. (1991) Weak chaos in an area-preserving mapping for sound ray propagation. *Phys. Lett. A*, **153**, 181–5.
- Tappert, F.D., Spiesberger, J.L. and Wolfson, M.A. (2002) Study of a novel range-dependent propagation effect with application to the axial injection of signals from the Kaneohe source. *J. Acoust. Soc. Amer.*, **111**, 757–62.
- Taroudakis, M.I. and Makrakis, G.N. (eds) (2001) *Inverse Problems in Underwater Acoustics*. Springer-Verlag, New York.
- Teague, W.J., Carron, M.J. and Hogan, P.J. (1990) A comparison between the generalized digital environmental model and Levitus climatologies. *J. Geophys. Res.*, **95**, 7167–83.
- The Acoustic Mid-Ocean Dynamics Experiment Group (1994) Moving ship tomography in the North Atlantic. *EOS, Trans. Amer. Geophys. Union*, **75**, 17–23.
- The Ring Group (1981) Gulf Stream cold-core rings: their physics, chemistry, and biology. *Science*, **212**, 1091–100.
- Thomson, D.J. (1990) Wide-angle parabolic equation solutions to two range-dependent benchmark problems. *J. Acoust. Soc. Amer.*, **87**, 1514–20.
- Thomson, D.J. and Chapman, N.R. (1983) A wide-angle split-step algorithm for the parabolic equation. *J. Acoust. Soc. Amer.*, **74**, 1848–54.
- Thomson, D.J. and Mayfield, M.E. (1994) An exact radiation condition for use with the *a posteriori* PE method. *J. Comput. Acoust.*, **2**, 113–32.
- Thomson, D.J. and Wood, D.H. (1987) *A posteriori* phase corrections to the parabolic equation. In *Progress in Underwater Acoustics*, ed., H.M. Merklinger. Plenum, New York, pp. 425–31.
- Thomson, D.J., Brooke, G.H. and DeSanto, J.A. (1990) Numerical implementation of a modal solution to a range-dependent benchmark problem. *J. Acoust. Soc. Amer.*, **87**, 1521–6.
- Thorp, W.H. (1967) Analytic description of the low-frequency attenuation coefficient. *J. Acoust. Soc. Amer.*, **42**, 270.
- Thorsos, E.I. (1990) Acoustic scattering from a “Pierson–Moskowitz” sea surface. *J. Acoust. Soc. Amer.*, **88**, 335–49.
- Tielbörger, D., Finette, S. and Wolf, S. (1997) Acoustic propagation through an internal wave field in a shallow water waveguide. *J. Acoust. Soc. Amer.*, **101**, 789–808.
- Tindle, C.T. and Bold, G.E.J. (1981) Improved ray calculations in shallow water. *J. Acoust. Soc. Amer.*, **70**, 813–9.
- Tindle, C.T. and Zhang, Z.Y. (1992) An equivalent fluid approximation for a low shear speed ocean bottom. *J. Acoust. Soc. Amer.*, **91**, 3248–56.
- Tindle, C.T. and Zhang, Z.Y. (1997) An adiabatic normal mode solution for the benchmark wedge. *J. Acoust. Soc. Amer.*, **101**, 606–9.
- Tindle, C.T., O’Driscoll, L.M. and Higham, C.J. (2000) Coupled mode perturbation theory of range dependence. *J. Acoust. Soc. Amer.*, **108**, 76–83.
- Tolstoy, A. (1992) Review of matched field processing for environmental inverse problems. *Inter. J. Modern Phys. C*, **3**, 691–708.

- Tolstoy, A. (1993) *Matched Field Processing for Underwater Acoustics*. World Scientific Publishing, Singapore.
- Tolstoy, A. (1996) 3-D propagation issues and models. *J. Comput. Acoust.*, **4**, 243–71.
- Tolstoy, A. (2001) What about adiabatic normal modes? *J. Comput. Acoust.*, **9**, 287–309.
- Tolstoy, A., Berman, D.H. and Franchi, E.R. (1985) Ray theory versus the parabolic equation in a long-range ducted environment. *J. Acoust. Soc. Amer.*, **78**, 176–89.
- Tolstoy, A., Smith, K. and Maltsev, N. (2001) The SWAM'99 Workshop – an overview. *J. Comput. Acoust.*, **9**, 1–16.
- Tolstoy, I. and Clay, C.S. (1966) *Ocean Acoustics*. McGraw-Hill, New York (reprinted 1987 by the Acoustical Society of America).
- Tsuchiya, T., Okuyama, T., Endoh, N. and Anada, T. (1999) Numerical analysis of acoustical propagation in ocean with warm and cold water mass used by the three-dimensional wide-angle parabolic equation method. *Jpn. J. Appl. Phys.*, **38**, 3351–5.
- Tuovila, S.M. (1989) SEARAY sonar simulation model. Nav. Coastal Syst. Ctr., Tech. Note NCSC TN 946-88.
- Twersky, V. (1957) On scattering and reflection of sound by rough surfaces. *J. Acoust. Soc. Amer.*, **29**, 209–25.
- UK Ministry of Defence, Director Naval Surveying, Oceanography and Meteorology (1995) User Guide. Hodgson propagation loss model version 4.0.
- Untersteiner, N. (1966) Sea ice. In *The Encyclopedia of Oceanography*, ed., R.W. Fairbridge. Van Nostrand Reinhold Co., New York, pp. 777–81.
- Urick, R.J. (1979) *Sound Propagation in the Sea*. US Government Printing Office, Washington, DC.
- Urick, R.J. (1982) *Sound Propagation in the Sea*. Peninsula Publishing, Los Altos, California, USA.
- Urick, R.J. (1983) *Principles of Underwater Sound*, 3rd edn. McGraw-Hill, New York.
- Urick, R.J. (1984) *Ambient Noise in the Sea*. Nav. Sea Syst. Command, Washington, DC.
- US Department of Defense (1994) DoD modeling and simulation (M&S) management. DoD Directive 5000.59 (updated with Change 1 in 1998).
- US Department of Defense (1996) Verification, validation and accreditation (VV&A) recommended practices guide (RPG). Office of the Director of Defense Research and Engineering, Defense Modeling and Simulation Office, Washington, DC.
- US Department of Defense (2001) Mandatory procedures for major defense acquisition programs (MDAPS) and major automated information system (MAIS) acquisition programs. DOD Regulation 5000.2-R. Office of the Secretary of Defense, Washington, DC.
- US Department of the Navy (1999) Interactive multisensor analysis training. Joint publication of the SPAWAR Systems Center and the Naval Surface Warfare Center, Carderock Division.
- US Department of the Navy (2000a) Simulation based acquisition (SBA) status and international implications. Prepared by the Department of the Navy Acquisition Reform Office for The Technical Cooperation Program (TTCP) panel on Systems Engineering for Defence Modernisation.

- US Department of the Navy (2000b) Strategy for research & development: a roadmap to a vision of operational oceanography. Office of the Chief of Naval Operations, Oceanographer of the Navy (CNO N096), Washington, DC.
- US General Accounting Office (1979) Guidelines for model evaluation. PAD-79-17.
- US Navy Air ASW Project Office (1996a) User's guide for the environmental acoustics server software package. Program Executive Office, Air ASW, Assault, and Special Mission Programs (PMA-264).
- US Navy Air ASW Project Office (1996b) Operating system interface description for the environmental acoustics server software package. Program Executive Office, Air ASW, Assault, and Special Mission Programs (PMA-264).
- Vaccaro, R.J. (ed.) (1998) The past, present, and future of underwater acoustic signal processing. *IEEE Signal Process. Mag.*, **15** (4), 21–51.
- Vagle, S., Large, W.G. and Farmer, D.M. (1990) An evaluation of the WOTAN technique of inferring oceanic winds from underwater ambient sound. *J. Atmos. Oceanic Technol.*, **7**, 576–95.
- Vastano, A.C. and Owens, G.E. (1973) On the acoustic characteristics of a Gulf Stream cyclonic ring. *J. Phys. Oceanogr.*, **3**, 470–8.
- Veenstra, D. (1998) A COTS approach to sonar simulation/stimulation. *RTC*, **VII** (12), 135–7.
- Vendetti, A., Zeidler, E. and Bartberger, C. (1993a) The NAWC bistatic acoustic model (version 3.0) software modifications and user's guide. Nav. Air Warfare Ctr Rept.
- Vendetti, A., Zeidler, E. and Bartberger, C. (1993b) The NAWC monostatic acoustic model (version 1.1) software modifications and user's guide. Nav. Air Warfare Ctr Rept.
- Vent, R.J. (1972) Acoustic volume-scattering measurements at 3.5, 5.0, and 12.0 kHz in the eastern Pacific Ocean: diurnal and season variations. *J. Acoust. Soc. Amer.*, **52**, 373–82.
- Von Winkle, W.A. (1963) Vertical directionality of deep ocean noise. Navy Underwater Sound Lab., Rept 600.
- Wagner, D.H., Mylander, W.C. and Sanders, T.J. (eds) (1999) *Naval Operations Analysis*, 3rd edn. Naval Institute Press, Annapolis, Maryland, USA.
- Wagstaff, R.A. (1973) RANDI: research ambient noise directionality model. Nav. Undersea Ctr, Tech. Pub. 349.
- Wagstaff, R.A. (1981) Low-frequency ambient noise in the deep sound channel – the missing component. *J. Acoust. Soc. Amer.*, **69**, 1009–14.
- Wagstaff, R.A. (1982) Noise field calculation or measurement simulation? Some comments on ambient noise modeling. Proc. MTS/IEEE Oceans 82 Conf., pp. 187–91.
- Wales, S.C. and Heitmeyer, R.M. (2002) An ensemble source spectra model for merchant ship-radiated noise. *J. Acoust. Soc. Amer.*, **111**, 1211–31.
- Ward, P.D. (1989) A novel method of finding normal modes in shallow water. *J. Sound Vib.*, **128**, 349–54.
- Watkins, W.A. and Schevill, W.E. (1977) Sperm whale codas. *J. Acoust. Soc. Amer.*, **62**, 1485–90.
- Watkins, W.A., Tyack, P., Moore, K.E. and Bird, J.E. (1987) The 20-Hz signals of finback whales (*Balaenoptera physalus*). *J. Acoust. Soc. Amer.*, **82**, 1901–12.
- Watson, A.G.D. (1958) The effect of the Earth's sphericity in the propagation of sound in the sea. Admiralty Res. Lab., ARL/N29/L.

- Watson, W.H. and McGirr, R. (1975) RAYWAVE II: a propagation loss model for the analysis of complex ocean environments. Nav. Undersea Ctr, Tech. Note 1516.
- Weickmann, A. and Jones, R.M. (1994) A FORTRAN program for performing Abel transforms. NOAA Tech. Memo. ERL ETL-244.
- Weickmann, A.M., Riley, J.P., Georges, T.M. and Jones, R.M. (1989) EIGEN – a program to compute eigenrays from HARPA/HARPO raysets. Wave Propagation Lab., NOAA Tech. Memo. ERL WPL-160.
- Weinberg, H. (1969) CONGRATS I: ray plotting and eigenray generation. Navy Underwater Sound Lab., Rept 1052.
- Weinberg, H. (1971) A continuous-gradient curve-fitting technique for acoustic-ray analysis. *J. Acoust. Soc. Amer.*, **50**, 975–84.
- Weinberg, H. (1973) Navy interim surface ship model (NISSM) II. Nav. Underwater Syst. Ctr, Tech. Rept 4527 (also, Nav. Undersea Ctr, Tech. Pub. 372).
- Weinberg, H. (1975) Application of ray theory to acoustic propagation in horizontally stratified oceans. *J. Acoust. Soc. Amer.*, **58**, 97–109.
- Weinberg, H. (1981) Effective range derivative for acoustic propagation loss in a horizontally stratified ocean. *J. Acoust. Soc. Amer.*, **70**, 1736–42.
- Weinberg, H. (1982) Generic sonar model. Proc. MTS/IEEE Oceans 82 Conf., pp. 201–5.
- Weinberg, H. (1985a) Multilayer expansion for computing acoustic pressure in a horizontally stratified ocean. Proc. 11th IMACS World Congress, System Simulation and Scientific Computation (Oslo, Norway), pp. 135–8.
- Weinberg, H. (1985b) Generic sonar model. Nav. Underwater Syst. Ctr, Tech. Doc. 5971D.
- Weinberg, H. (2000) CASS roots. Proc. MTS/IEEE Oceans 2000 Conf., pp. 1071–6.
- Weinberg, H. and Burrige, R. (1974) Horizontal ray theory for ocean acoustics. *J. Acoust. Soc. Amer.*, **55**, 63–79.
- Weinberg, H. and Keenan, R.E. (1996) Gaussian ray bundles for modeling high-frequency propagation loss under shallow-water conditions. *J. Acoust. Soc. Amer.*, **100**, 1421–31.
- Weinberg, H., Keenan, R.E. and Aidala, F.E. Jr (1997). Uniqueness problems in extracting environmental parameters from high-frequency, shallow-water reverberation measurements. In *High Frequency Acoustics in Shallow Water*, eds, N.G. Pace, E. Pouliquen, O. Bergem and A.P. Lyons. SACLANT Undersea Res. Ctr, Conf. Proc. CP-45, pp. 587–92.
- Weinberg, N.L. and Dunderdale, T. (1972) Shallow water ray tracing with nonlinear velocity profiles. *J. Acoust. Soc. Amer.*, **52**, 1000–10.
- Weinberg, N.L. and Zabalgoceazcoa, X. (1977) Coherent ray propagation through a Gulf Stream ring. *J. Acoust. Soc. Amer.*, **62**, 888–94.
- Wells, D.K. and Wargelin, R.M (1985) Programs and products of the Naval Oceanographic Office. *Mar. Tech. Soc. J.*, **19** (3), 18–25.
- Wenz, G.M. (1962) Acoustic ambient noise in the ocean: spectra and sources. *J. Acoust. Soc. Amer.*, **34**, 1936–56.
- Weston, D.E. (1960) A Moiré fringe analog of sound propagation in shallow water. *J. Acoust. Soc. Amer.*, **32**, 647–54.
- Weston, D.E. and Rowlands, P.B. (1979) Guided acoustic waves in the ocean. *Rep. Prog. Phys.*, **42**, 347–87.
- Westwood, E.K. (1989a) Complex ray methods for acoustic interaction at a fluid–fluid interface. *J. Acoust. Soc. Amer.*, **85**, 1872–84.

400 *References*

- Westwood, E.K. (1989b) Ray methods for flat and sloping shallow-water waveguides. *J. Acoust. Soc. Amer.*, **85**, 1885–94.
- Westwood, E.K. (1989c) Acoustic propagation modeling in shallow water using ray theory. Appl. Res. Labs., Univ. Texas at Austin, USA, ARL-TR-89-6.
- Westwood, E.K. (1990) Ray model solutions to the benchmark wedge problems. *J. Acoust. Soc. Amer.*, **87**, 1539–45.
- Westwood, E.K. (1992) Broadband matched-field source localization. *J. Acoust. Soc. Amer.*, **91**, 2777–89.
- Westwood, E.K. and Tindle, C.T. (1987) Shallow water time-series simulation using ray theory. *J. Acoust. Soc. Amer.*, **81**, 1752–61.
- Westwood, E.K. and Vidmar, P.J. (1987) Eigenray finding and time series simulation in a layered-bottom ocean. *J. Acoust. Soc. Amer.*, **81**, 912–24.
- Westwood, E.K., Tindle, C.T. and Chapman, N.R. (1996) A normal mode model for acousto-elastic ocean environments. *J. Acoust. Soc. Amer.*, **100**, 3631–45.
- Wetzel-Smith, S.K. and Czech, C. (1996) The interactive multisensor analysis training system: using scientific visualization to teach complex cognitive skills. NPRDC TR-96-9. Navy Personnel Research and Development Center, San Diego, California, USA.
- Wetzel-Smith, S.K., Ellis, J.A., Reynolds, A.M. and Wulfeck, W.H. (1995) The interactive multisensor analysis training (IMAT) system: an evaluation in operator and tactician training. NPRDC TR-96-3. Navy Personnel Research and Development Center, San Diego, California, USA.
- White, D. (1992) Software requirements specification for the ASTRAL model (version 4.1). Sci. Appl. Inter. Corp., OAML-SRS-23.
- White, D. and Corley, M. (1992a) Software test description for the ASTRAL model (version 4.1). Sci. Appl. Inter. Corp., OAML-STD-23.
- White, D. and Corley, M. (1992b) Software design document for the ASTRAL model (version 4.1). Sci. Appl. Inter. Corp., OAML-SDD-23.
- White, D., Dozier, L.B. and Pearson, C. (1988) Software product specification for the ASTRAL 2.2 model, Vols I and II. Sci. Appl. Inter. Corp., OAML-SPS-23.
- Whitman, E.C. (1994) Defense conversion in marine technology. *Sea Technol.*, **35** (11), 21–5.
- Wiebe, P.H., Prada, K.E., Austin, T.C., Stanton, T.K. and Dawson, J.J. (1995) New tool for bioacoustical oceanography. *Sea Technol.*, **36** (2), 10–14.
- Williams, A.O. Jr (1976) Hidden depths: acceptable ignorance about ocean bottoms. *J. Acoust. Soc. Amer.*, **59**, 1175–9.
- Willis, C.L. (1992) Oceanographic and atmospheric master library. *Naval Oceanography Command News*, **12** (2), 1–5.
- Wilson, W.D. (1960) Equation for the speed of sound in sea water. *J. Acoust. Soc. Amer.*, **32**, 1357.
- Wood, D.H. and Papadakis, J.S. (1985) An overview of stochastic signal modeling. Nav. Underwater Syst. Ctr, Tech. Rept 7267.
- Wright, E.B., Berman, D.H., Baer, R.N. and Perkins, J.S. (1988) The ocean-refraction bathymetric-scattering (ORBS) model. Nav. Res. Lab., Rept 9123.
- Yan, J. (1999) Effects of earth curvature on two-dimensional ray tracing in underwater acoustics. *Appl. Acoust.*, **57**, 163–77.
- Yaremchuk, M.I. and Yaremchuk, A.I. (2001) Variational inversion of the ocean acoustic tomography data using quadratic approximation to travel times. *Geophys. Res. Lett.*, **28**, 1767–70.

- Yarger, D.F. (1976) The user's guide for the RAYMODE propagation loss program. Nav. Underwater Syst. Ctr, Tech. Memo. 222-10-76.
- Yarger, D.F. (1982) The user's guide for the passive RAYMODE propagation loss program. Nav. Underwater Syst. Ctr, Tech. Memo. 821061.
- Yevick, D. and Thomson, D.J. (1994) Split-step/finite-difference and split-step/Lanczos algorithms for solving alternative higher-order parabolic equations. *J. Acoust. Soc. Amer.*, **96**, 396–405.
- Zabal, X., Brill, M.H. and Collins, J.L. (1986) Frequency and angle spreads of acoustic signals reflecting from a fixed rough boundary. *J. Acoust. Soc. Amer.*, **79**, 673–80.
- Zedel, L., Gordon, L. and Osterhus, S. (1999) Ocean ambient sound instrument system: acoustic estimation of wind speed and direction from a subsurface package. *J. Atmos. Oceanic Technol.*, **16**, 1118–26.
- Zhang, R. and Li, F. (1999) Beam-displacement ray-mode theory of sound propagation in shallow water. *Sci. China (Ser. A)*, **42**, 739–49.
- Zhang, R. and Jin, G. (1987) Normal-mode theory of average reverberation intensity in shallow water. *J. Sound Vib.*, **119**, 215–23.
- Zhang, R., He, Y., Liu, H. and Akulichev, V.A. (1995) Applications of the WKBZ adiabatic mode approach to sound propagation in the Philippine Sea. *J. Sound Vib.*, **184**, 439–51.
- Zhang, Z.Y. and Tindle, C.T. (1995) Improved equivalent fluid approximations for a low shear speed ocean bottom. *J. Acoust. Soc. Amer.*, **98**, 3391–6.
- Zhou, J.-X., Zhang, X.-Z. and Rogers, P.H. (1991) Resonant interaction of sound wave with internal solitons in the coastal zone. *J. Acoust. Soc. Amer.*, **90**, 2042–54.
- Zhu, D. and Bjørnø, L. (1999) A hybrid 3-D, two-way IFD PE model for 3-D acoustic backscattering. *J. Comput. Acoust.*, **7**, 133–45.
- Ziman, J. (1978) *Reliable Knowledge*. Cambridge Univ. Press, New York.
- Ziomek, L.J. (1985) *Underwater Acoustics. A Linear Systems Theory Approach*. Academic Press, San Diego.
- Ziomek, L.J. (1995) *Fundamentals of Acoustic Field Theory and Space-Time Signal Processing*. CRC Press, Boca Raton, Florida.
- Zornig, J.G. (1979) Physical modeling of underwater acoustics. In *Ocean Acoustics*, ed., J.A. DeSanto. Springer-Verlag, New York, pp. 159–86.

Author index

Page numbers appearing in *italic* indicate pages on which references are given in full.

- Abarbanel, H.D.I. 186, 369
Abawi, A.T. 149, 354
Abbott, G.D. 207, 379
Abramowitz, M. 114, 354
Abrantes, A.A.M. 198, 354
Ackerman, C.L. 251, 262
Adams, B.B. 181, 388
Ai, D.K.Y. 109, 179, 394
Aidala, F.E. Jr 142, 287–8, 376, 399
Ainslie, M.A. 75, 80 120, 199, 300–1, 354, 372–3, 387
Akal, T. 57, 198, 355, 378
Akulichev, V.A. 146, 401
Alapati, N.K. 186, 355
Albers, V.M. 68, 244, 355
Alexandrou, D. 240, 373
Alford, R.S. 201, 377
Almeida, R.J., Jr 147, 355
Alvarez, A. 216, 355
Amato, I. 11, 355
Ammicht, E. 144, 355, 395
Anada, T. 189, 397
Andersen, N.R. 232, 355
Anderson, A.L. 76, 247, 355, 381
Anderson, C.D. 240, 382
Anderson, V.C. 218, 223–5, 355
Apel, J.R. 19–20, 52, 77, 355
Applied Physics Laboratory, University of Washington 82, 295, 355
Arcus, W.R. 234, 388
Aredov, A.A. 213, 355
Arneson, A.D. 207, 373
Arney, D.C. 126, 391
Arnold, J.M. 163, 165, 247, 355, 387
Arrhenius, G. 42, 355
Arvelo, J.I. 145, 355
Au, W.W.L. 205, 355
Auer, S.J. 51, 355
Austin, T.C. 234, 400
Avilov, K.V. 150, 355
Axelrod, E.H. 209, 356
Backes, D.A. 318, 394
Backus, R.H. 233, 375
Baer, R.N. 126, 129, 149–51, 189, 257, 356–7, 388, 400
BAeSEMA Ltd 295, 356
Baggeroer, A.B. 183, 197, 356, 384
Bailey, R.S. 294, 356
Baker, C.L. 141, 228, 230, 356
Bannister, R.W. 225, 230, 356
Barkhatov, A.N. 2, 356
Barnes, A.E. 226–7, 394
Bartberger, C.L. 116, 141–3, 232, 256–7, 262, 356, 382, 398
Bathen, K.H. 82, 356
Beatty, W.F. 295, 326–7, 356
Beck, M.A. 294, 356
Becken, B.A. 218, 356
Beckmann, P. 131, 356
Bedard, A.J. Jr 11, 357
Bedford, N.R. 142, 173, 395
Beebe, J.H. 76, 357
Behringer, D.W. 151, 195, 363, 387
Belitz, K. 7, 387
Bennett, A.F. 15, 357
Bergem, O. 232, 387
Berger, M.D. 293, 357
Berkhout, B.V. 211, 359
Berkson, J.M. 57, 355

404 *Author index*

- Berman, D.H. 129, 150, 257, 356–7, 397, 400
 Bertuccelli, H.C. 294, 357
 Bezdek, H.F. 186, 387, 396
 Bialek, E.L. 32, 357
 Bini-Verona, F. 146, 357
 Biot, M.A. 76, 357
 Bird, J.E. 205, 398
 Birdsall, T. 195, 363
 Bishop, G.C. 260–1, 263, 357
 Bishop, J.M. 35, 365
 Bjørnø, L. 146, 149–50, 215, 357, 387, 401
 Blanchard, B.S. 320–1, 325, 357
 Blatstein, I.M. 144, 357
 Blumen, L.S. 145, 357
 Boehme, H. 294, 374
 Bogart, C.W. 185, 357
 Bold, G.E.J. 111, 113, 396
 Bom, N. 207, 357
 Booth, N.O. 183, 185, 365
 Botseas, G. 126, 129, 149–50, 193, 225, 357–8, 360, 379
 Boucher, C.E. 293, 357
 Bowditch, N. 35–6, 41, 358
 Bowlin, J.B. 109, 358
 Boyd, J.D. 54–5, 361, 392
 Boyd, M.L. 262, 393
 Boyles, C.A. 106, 118, 163, 358
 Bracken, J. 316, 358
 Bradley, B.W. 215, 358
 Bradley, M.R. 215, 230, 358
 Breeding, J.E., Jr 221, 230, 358
 Brekhovskikh, L. 8, 183, 358
 Brill, M.H. 78, 401
 Brind, R. 230, 373
 Brock, H.K. 129, 150, 358
 Brooke, G.H. 129, 150, 298, 358, 396
 Brown, J.R. 240, 358
 Brown, M. 195, 363
 Brown, M.G. 150, 186, 358, 387, 394, 396
 Brown, N.R. 69, 358
 Browne, M.J. 70, 383
 Browning, D.G. 82, 172, 189, 359, 383
 Brunson, B.A. 76, 373
 Brutzman, D.P. 6, 13, 359
 Bryan, G.M. 40, 42, 359
 Buchal, R.N. 129, 358
 Buck, B.M. 96–7, 175–6, 359
 Buckner, H.P. 107, 120, 126, 129, 142–3, 158, 173, 185, 245, 247, 263, 359, 371, 377, 389
 Buckingham, M.J. 100, 158, 205, 207, 211–13, 298, 359–60, 365
 Burdic, W.S. 276, 360
 Burgess, A.S. 230, 356
 Burns, P.W. 294, 354
 Burrige, R. 109, 146, 360, 399
 Bush, G. 234, 388
 Caiti, A. 16, 198, 360, 364
 Cakmak, A. 1, 379
 Candy, J.V. 12, 181, 360
 Carbone, N.M. 213, 360
 Carey, W.M. 17, 200, 223, 225, 360
 Carlson, J.T. 11, 360
 Carman, J.C. 193, 391
 Carroll, S.N. 319, 360
 Carron, M.J. 177, 396
 Carter, E.F. 193, 391
 Carton, J.A. 193, 391
 Caruthers, J.W. 263, 360
 Cavanagh, R.C. 100, 127, 230–1, 298, 301, 360, 364–5
 Cederberg, R.J. 150, 360
 Cembrola, J. 186, 369
 Chaika, E.D. 295, 360
 Chamberlain, S.G. 262, 361
 Chapman, D.M.F. 18, 144, 185, 361, 366
 Chapman, N.R. 76, 129, 142, 144, 149, 185, 188, 361, 365, 389, 396, 400
 Chapman, R.P. 236–8, 275, 361
 Chen, C.-T. 25–7, 361
 Cheney, R.E. 45, 47–8, 361
 Childs, E. 187–8, 383
 Chin-Bing, S.A. 55, 75, 127, 129, 143, 150–1, 173, 181–2, 187, 191, 298, 361, 363, 370, 384
 Chitre, M. 212, 390
 Chiu, C.-S. 120, 142, 145, 188, 195, 361, 380, 383, 385
 Choi, B. 150, 393
 Christian, R.J. 189, 359
 Chuprov, S.D. 183
 Claerbout, J.F. 128–9, 150, 362
 Clancy, R.M. 15, 156–7, 193, 292, 362, 373
 Clark, J.G. 179, 369
 Clay, C.S. 18–19, 69, 75, 105, 117, 131, 362, 382, 397
 Coates, R. 247, 362
 Cochran, J.D. 84–7, 367
 Coelho, E. 191, 391

- Cohen, J.S. 293, 362
 Colilla, R.A. 143, 230, 362, 378
 Collins, J.L. 78, 401
 Collins, M.D. 15, 124, 126–7, 129–30, 149–51, 164, 181–2, 186, 245, 298, 354, 360, 363, 380, 387
 Collison, N. 185, 363
 Condron, T.P. 88–90, 363
 Coppens, A.B. 25–6, 66, 68, 101, 154, 165, 267, 363, 377
 Corley, M. 145, 400
 Cornuelle, B.D. 27, 195, 363, 365
 Cornyn, J.J. 142, 363
 Coulter, R.L. 15, 364
 Cowley, A. 230, 373
 Cox, H. 256, 259, 268–70, 364
 Crockett, J.P. 262, 369
 Crowder, D.C. 147, 382
 Crowe, D.V. 242, 366
 Crum, L.A. 206–7, 364, 390
 Culkin, F. 20, 364
 Cummings, J.A. 193, 362
 Cummings, W.C. 205, 364
 Czech, C. 295, 326, 400
- Dahmann, J. 317, 377
 Daintith, M.J. 164, 381
 Daley, E.M. 293, 357
 Daneshzadeh, Y.-H. 151, 387
 Dantzler, H.L., Jr 6, 364
 Dashen, R. 225, 364
 Daubin, S.C. 130, 150, 386
 Daugherty, J.R. 142, 188, 385
 Davis, J.A. 75, 127, 129, 223, 225, 298, 360–1, 364
 Davis, P.K. 318, 326, 364
 Davis, T. 177
 Dawe, R.L. 267, 364
 Dawson, J.J. 234, 400
 Deane, G.B. 212–13, 360, 366
 Deavenport, R.L. 8, 102, 122, 132, 147, 174, 302, 304, 364–5
 de Cogan, D. 247, 362
 Deffenbaugh, R.M. 7, 288, 368
 Del Balzo, D.R. 185, 364
 Del Grosso, V.A. 25–6, 364
 Demoulin, X. 191, 391
 Denner, W.W. 211, 380
 Denny, P.L. 70, 383
 DeSanto, J.A. 101, 298, 364, 396
 Desharnais, F. 247, 263, 364
 Detsch, R. 207, 391
- Diachok, O.I. 16, 71–2, 198, 210–11, 364
 Dickson, K.R. 88–90, 363
 DiNapoli, F.R. 8, 102, 122, 147, 174, 302, 304, 364–5, 378
 Donn, W.L. 15, 365
 Doolittle, R. 158, 365
 Dosso, S.E. 76, 185, 363, 365
 Dougalis, V.A. 146, 149–50, 387
 Dozier, L.B. 100, 129, 142, 145, 365, 400
 Dreini, G. 293–4, 365
 D’Spain, G.L. 183, 185, 365
 Duda, T.F. 109, 358
 Duddridge, G. 205, 379
 Duncan, A.J. 234, 388
 Dunderdale, T. 107, 399
 Dushaw, B.D. 27, 365
 Duston, M.D. 185, 365
 Dwan, F.S. 247, 381
 Dyer, I. 210, 216, 365, 381
 Dzieciuch, M. 198, 365
- Earle, M.D. 35, 365
 Ebbeson, G.R. 150, 188, 358, 361, 365
 Eckart, C. 66, 366
 Ehret, L.L. 120, 145, 188, 361
 Einstein, L.T. 293, 362
 Einstein, P.A. 109, 366
 Eller, A.I. 66, 95, 162, 172, 256, 281, 293, 298, 357, 366, 371
 Ellis, D.D. 144, 146, 185, 232, 242, 245, 247, 263, 361, 364, 366
 Ellis, J.A. 295, 326, 366, 400
 Ellis, J.W. 318, 366
 Ellison, W.T. 260, 357
 Emery, W.J. 19, 25, 366, 389
 Emling, J.W. 201, 377
 Endoh, N. 189, 397
 Epifanio, C.L. 212, 359, 366
 Erskine, F.T. 238–40, 318, 386–7, 394
 Estalote, E.A. 226, 230–1, 367
 Etter, P.C. 6–10, 84–7, 159–60, 163, 172, 186, 207, 283, 285, 355, 367–8, 380, 390
 Evans, D.J. 205–6, 393
 Evans, R.B. 75, 120, 122, 127, 129, 143, 145–6, 148, 151, 164–5, 187, 223, 225, 245, 298, 360–1, 363, 368, 370, 378, 388
 Ewans, K.C. 200, 377
 Ewart, T.E. 53–4, 368, 381
 Ewing, M. 92, 368

406 *Author index*

- Farmer, D.M. 205–6, 393, 398
Farquhar, G.B. 232, 368
Farrell, T. 11, 295, 368
Farwell, R.W. 101, 371
Fawcett, J.A. 121, 368
Felizardo, F.C. 206, 368
Felsen, L.B. 163, 165, 298, 355, 368
Ferla, C.M. 142, 145–8, 150, 164,
198, 298–300, 368, 375, 378
Ferla, M.C. 120, 146, 368, 375
Fernandez, M.R. 318, 366
Ferris, R.H. 59, 117, 119, 145–6,
368, 374
Feuillade, C. 185, 364
Fialkowski, L.T. 188, 388
Finette, S. 192, 386, 396
Fink, I.M. 294, 356
Fisher, A., Jr 180, 368
Fisher, F.H. 80–1, 225, 368, 373
Fizell, R.G. 184, 368–9
Flanagan, R.P. 179, 369
Flatté, S.M. 54, 179, 187, 212,
369, 393
Fleming, R.H. 19, 24, 395
Flouri, E.T. 146, 149–50, 387
Flum, R.S., Sr 7, 288, 367–8
Focke, K.C. 161, 369
Fofonoff, N.P. 20, 369
Forbes, A.M.G. 30–1, 195–6, 369, 384
Foreman, T.L. 107, 109, 142–3, 369
Foret, J.A. 295, 327, 369
Fortuin, L. 236, 369
Franchi, E.R. 111–12, 129, 256, 263,
369, 397
Francois, R.E. 80, 369
Franz, G.J. 207, 369
Freitag, L.F. 109, 358
Frey, A.R. 66, 68, 101, 154, 267,
369, 377
Frisk, G.V. 66, 75–6, 369, 377
Frison, T.W. 186, 369
Fromm, D.M. 262–3, 369, 387
Frye, H.W. 25–6, 369
Fulford, J.K. 262, 369
Furduev, A.V. 213, 355
Furgerson, J.A. 195, 394
Futa, K. 183, 370

Gabrielson, T.B. 120, 370
Gaillard, F. 197, 370
Gainey, L.A. 150, 374
Galati, W. 231
Galindo, M. 11, 386

Galli, J.C. 262, 361
Gao, T.F. 189, 393
Garcia, M.L. 294, 356
Garon, H.M. 142–3, 370
Garrett, C. 53, 370
Garrison, G.R. 80, 369
Garwood, R.W., Jr 156, 370
Gass, S.I. 307, 309–10, 370
Gemmill, W. 189, 191, 370
Georges, T.M. 11, 109, 142, 188, 357,
370, 372, 376, 399
Gerstoft, P. 16, 148, 198–9, 232,
364, 370
Gilbert, K.E. 75, 120, 122, 129, 143,
145–6, 148, 150, 164, 186–7, 357,
361, 368, 370, 382, 390
Gilbert, R.P. 185, 365, 370
Gill, A.E. 19, 370
Glattetre, J. 148, 188, 388, 392
Glegg, S.A.L. 211, 359
Glenn, S.M. 193–4, 378, 391
Goddard, R.P. 244, 294, 370
Goh, J.T. 123, 148, 370, 392
Gold, B.A. 235, 371
Goldberg, E.D. 194, 371
Goldman, J. 230, 371
Goldstein, C.I. 181, 371
Gong, Z. 143, 380
Goni, G.J. 51, 186, 358, 371, 396
Gonzalez, R. 144, 371
Goodman, R.R. 101, 371
Gordon, D.F. 143–4, 154–5, 173, 178,
180, 371, 388
Gordon, L. 206, 401
Gostev, V.S. 247, 371
Gragg, R.F. 144, 182, 371
Granum, R.M. 295, 360
Greaves, R.J. 243, 371
Green, D.M. 197, 371
Greene, C.H. 234, 371
Greene, C.R. Jr 205, 391
Greene, R.R. 71, 126, 149–50,
371, 391
Gregg, M.C. 84, 389
Griffin, J.M. 111–12, 256, 263, 369
Grilli, S. 123, 371
Guo, L. 143, 380

Haines, L.C. 256, 293, 357, 366, 371
Hall, H.R. 75, 273, 371
Hall, J.C. 141, 382
Hall, M.V. 18, 69, 189, 372
Hamilton, E.L. 76, 79, 168, 372

- Hampton, L.D. 76, 355
 Hamson, R.M. 199, 215, 230, 354, 372
 Hanna, J.S. 176, 298, 372
 Hardin, R.H. 123, 150, 372
 Harding, E.T. 123, 143, 372
 Harlan, J.A. 142, 372
 Harris, J.H. 236–8, 275, 361
 Harrison, B.F. 197, 372
 Harrison, C.H. 109, 120, 199, 213, 216, 230, 294, 300–1, 354–5, 372–3, 387
 Hassab, J.C. 276, 373
 Haven, G. 109, 179, 394
 Hawker, K.E. 144, 298, 371, 373
 Hawkins, J.D. 157, 193, 362, 373
 Haynes, J.M. 181, 395
 He, Y. 146, 401
 Heaney, K.D. 197, 373
 Heathershaw, A.D. 70, 188, 373, 391
 Hebert, M. 230, 358
 Heindsmann, T.E. 207, 373
 Heinmiller, R. 195, 363
 Heitmeyer, R.M. 215, 398
 Henrick, R.F. 109, 373
 Hermand, J.-P. 16, 360
 Hersey, J.B. 233, 375
 Hess, C.A. 145, 230, 380
 Hickling, R. 18, 373
 Higham, C.J. 145, 396
 Hodges, P. 7, 373
 Hodgkiss, W.S., Jr 183, 185, 198, 225, 240, 242, 251–5, 257, 262, 365, 373, 378, 394
 Hoffman, D.W. 179, 246, 294, 298, 366, 373
 Hogan, P.J. 177, 396
 Holland, C.W. 76, 247, 373–4
 Holliday, D.V. 205, 364
 Holliger, K. 142, 391
 Holmes, E.S. 150, 281, 295, 327, 369, 374
 Holt, R.M. 141, 374
 Horsley, G.D. 199, 354
 Hosmer, R.F. 180, 388
 Hovem, J.M. 76, 374
 Hovland, M. 235, 374
 Howe, B.M. 27, 365
 Ignaszewski, M.J. 193, 362
 Ingenito, F. 59, 117, 144–6, 188, 212, 230, 295, 374, 377, 381, 383, 386, 388
 Institute of Electrical and Electronics Engineers, Inc. 18, 374
 International Energy Agency 13, 374
 Irving, M.A. 189, 372
 Ishimaru, A. 247, 374
 Isoppo, C. 293–4, 365
 Ivansson, S. 148, 374
 Jackson, D.R. 198, 247, 374, 378
 Jacobs, G. 141, 143, 374
 Jacobson, M.J. 113, 126, 129–30, 150–1, 182, 387, 391, 393
 Jacobus, P.W. 207, 383
 James, A.R. 199, 354
 Jaster, C.E. 294, 374
 Jennette, R.L. 230–1, 374
 Jensen, F.B. 8, 102–3, 113, 115, 120, 124, 127, 129, 136, 139, 142, 145–8, 150, 161–7, 182, 188, 293–4, 298–300, 357, 365, 368, 375, 389
 Jesus, S.M. 16, 191, 360, 391
 Jin, G. 245, 401
 Jobst, W. 130, 384
 Johannessen, O.M. 211, 392
 Johns, P.B. 247, 387
 Johns, W.E. 51, 371
 Johnson, A. 15, 292, 362
 Johnson, H.R. 233, 375
 Johnson, K.R. 70, 383
 Johnson, M.V.R. Sr 321, 375
 Johnson, M.W. 19, 24, 395
 Johnson, O.G. 187, 375
 Jones, R.M. 109, 142, 187–8, 197, 370, 372, 376, 385, 399
 Jones, S.A.S. 213, 359
 Jordan, E.A. 187–8, 383
 Kaduchak, G. 294, 356
 Kalinowski, A.J. 100, 376
 Kallistratova, M.A. 15, 364
 Kampanis, N.A. 146, 149–50, 387
 Kanabis, W.G. 145, 376
 Kanayama, Y. 6, 13, 359
 Kapoor, T.K. 72, 376
 Karasalo, I. 148, 374
 Katsneslon, B.G. 158, 162, 376
 Katz, R. 215, 392
 Kay, S.M. 267, 377
 Keenan, R.E. 142, 287–8, 376, 399
 Keiffer, R.S. 38, 70, 149, 247, 376, 386
 Keith, A.J. 143, 388
 Keller, J.B. 123, 376
 Kelton, W.D. 314, 379
 Kerman, B.R. 205–6, 376, 393

408 *Author index*

- Kerr, D.E. 88, 377
 Kerr, G.A. 226, 367
 Kerr, R.A. 50, 377
 Kesser, R.L. 251, 262
 Kewley, D.J. 230, 263, 356, 377
 Khedouri, E. 189, 191, 370
 Kibblewhite, A.C. 82, 200, 203–4, 225, 377
 Kikuchi, T. 183, 370
 King, B.J. 111–12, 256, 369
 King, D.B. 55, 127, 129, 141, 149, 191, 226, 263, 298, 358, 361, 367, 369, 377
 Kinsler, L.E. 66, 68, 101, 154, 267, 377
 Kirklin, R.H. 186, 355
 Kneale, S.G. 66, 381
 Knight, W.C. 267, 377
 Knobles, D.P. 74, 146, 377
 Knox, R. 195, 363
 Knudsen, V.O. 201, 377
 Koch, R.A. 142–3, 145–6, 163, 173, 245, 377, 380, 395
 Korman, M.S. 295, 327, 369
 Kraus, E.B. 194, 377
 Kress, M. 316, 358
 Kriegsmann, G.A. 129, 393
 Krol, H. 102–3, 124, 150, 375
 Kuhl, F. 317, 377
 Kuo, E.Y.T. 67, 377
 Kuperman, W.A. 8, 15, 59, 115, 117, 120, 130, 143, 145–6, 149, 161–2, 182–3, 186–8, 197–8, 212, 230, 243, 354, 356–7, 363, 368, 370, 373–5, 377–8, 381–2, 388, 394
 Kutschale, H.W. 147, 173–4, 378

 Labianca, F.M. 118, 378
 LaFond, E.C. 53, 88, 378
 Lai, C.-C.A. 194, 378
 Lai, D.Y. 50–1, 378
 Laker, R.A. 199, 354
 Lallement, P. 142, 365
 Lamb, P.J. 82, 207, 368, 378
 Large, W.G. 206, 398
 Larraza, A. 198, 354
 Lasky, M. 230, 378
 Laterveer, R. 145, 393
 Lau, R.L. 1, 378
 Lauer, R.B. 151, 297, 302–7, 378
 Laville, F. 207, 379
 Law, A.M. 314, 379
 Law, L.D. 113, 393
 Lawrence, M.Z. 294, 356
 Lawrence, R.S. 142, 370
 Lawson, E.A. 146, 193, 394
 Lawson, L.M. 151, 387
 Lee, D. 1, 123, 126–7, 129–30, 149–50, 188, 193, 357–8, 378–9, 393, 395–6
 Lee, M.A. 199, 354
 Lee, T. 174, 378
 Leibiger, G.A. 131, 147, 302, 379
 Leighton, T.G. 38, 69–70, 379, 390
 Lemon, D.D. 205, 379
 LeMond, J.E. 146, 245, 377, 380
 LePage, K.D. 11, 72, 142, 145–8, 150, 295, 368, 375, 380
 Leroy, C.C. 25–7, 80, 82, 272, 380, 394
 LeSchack, L.A. 175
 Leslie, W.G. 193, 391
 Levander, A. 142, 391
 Levinson, S.J. 144, 380
 Levitus, S. 21–3, 83–4, 380
 Lewis, E.L. 20, 380, 388
 Lewis, J.K. 211, 380
 Li, F. 143, 380
 Li, Xilu 143, 380
 Li, Xu 26–7, 383
 Lingevitch, J.F. 127, 380
 Liu, H. 146, 401
 Liu, Q. 143, 380
 Locklin, J.H. 282–5, 380
 Long, D. 230, 380
 Love, R.H. 232–4, 380
 Lovett, J.R. 25–6, 380
 Luby, J.C. 262, 380
 Ludwig, D. 273, 380
 Lukas, I.J. 145, 230, 380
 Lunsford, C.R. 226–7, 394
 Lynch, J.F. 142, 188, 195, 380, 383, 385
 Lyons, A.P. 232, 247, 381, 387
 Lysanov, Yu. 8, 183, 358
 Lytle, D.W. 262, 380

 Macaskill, C. 53–4, 381
 Mackenzie, K.V. 25–7, 241, 275, 381
 Macpherson, J.D. 164, 381
 Mahler, J.I. 230, 381
 Makrakis, G.N. 16, 396
 Makris, N.C. 210, 212, 243, 381
 Malme, C.I. 205, 391
 Maltsev, N. 164, 397

- Marsh, H.W., Jr 66, 75, 88, 131,
 147, 154, 167–8, 170–1, 174, 273,
 381, 383
 Marsh, P. 262, 294, 381
 Martin, P.J. 156–7, 193, 362, 381
 Martinelli, G. 129, 375
 Marusich, R.B. 295, 360
 Maskell, S.J. 188, 373
 Mayfield, M.E. 129, 396
 Mazur, M.A. 186, 382
 McBean, G.A. 205–6, 393
 McBride, W. 230, 358
 McCabe, B.J. 230, 382
 McCammon, D.F. 70, 76–7, 100,
 147, 382
 McCarthy, E.M. 243, 382
 McCave, I.N. 194, 371
 McColm, J.G. 80, 354
 McConnell, S.O. 229, 382, 391
 McCormick, N.H. 146, 193, 394
 McCoy, J.J. 181, 388
 McDaniel, S.T. 70, 76, 126–7, 129,
 236–8, 357, 379, 382
 McDonald, B.E. 130, 182, 197,
 373, 382
 McEachern, J.F. 318, 394
 McFadden, K. 215, 392
 McGirr, R.W. 107–8, 141, 143, 298,
 301, 382, 388, 399
 McHugh, R. 146, 193, 394
 McKeon, M.F. 321, 375
 McKinney, C.M. 240, 382
 Medeiros, R.C. 147, 293, 355, 382
 Medwin, H. 19, 25–6, 70, 75, 117,
 131, 187–8, 207, 362, 382–3, 386
 Meincke, J. 25, 366
 Mellberg, L.E. 260, 263, 357
 Mellen, R.H. 82, 172, 174, 381, 383
 Mellor, G.L. 156, 383
 Melville, W.K. 206, 368
 Menke, W. 15, 194, 383
 Mercer, J.A. 167, 172, 393
 Merklinger, H.M. 1, 383
 Metzger, K. 27, 195, 363, 394
 Mignerey, P.C. 121, 383
 Mikhalevsky, P.N. 183, 356
 Milder, D.M. 145, 383
 Miles, D.A. 199, 354
 Miller, E.C. 281, 374
 Miller, J.E. 318, 366
 Miller, J.F. 115, 117, 143, 145–6, 164,
 282, 383
 Miller, J.H. 188, 195, 380, 383
 Miller, M.J. 207, 379
 Millero, F.J. 25–7, 361, 383
 Milne, A.R. 161, 210, 240, 383–4
 Mitchell, S.K. 144, 380
 Mobile Sonar Technology 173
 Moler, C.B. 179, 384
 Moll, M. 226, 230, 381, 384
 Mooers, C.N.K. 155, 193, 384, 391
 Moore, K.E. 205, 398
 Moore-Head, M.E. 130, 384
 Morfey, C.L. 18, 384
 Morgan, J.G. Jr 12, 384
 Moritz, E. 232, 244, 384
 Morris, G.B. 208–9, 384
 Morris, H.E. 245, 247, 359
 Moses, E. 231
 Moskowitz, L. 35, 384, 389
 Munk, W.H. 30–1, 53, 179, 189,
 194–7, 212, 225, 363–4, 370, 384
 Murphy, J.E. 150, 173, 181–2, 191,
 361, 384
 Murray, J.J. 183, 185, 365
 Mylander, W.C. 325, 398

 Nagl, A. 164, 383
 National Defense Research
 Committee 103, 385
 National Oceanographic Data
 Center 288, 385
 National Research Council 7, 9, 197,
 205, 315–16, 318, 385
 Naval Oceanographic Office 24, 28–9,
 34, 44, 47, 147, 288, 293, 295, 385
 Navy Modeling and Simulation
 Management Office 146, 294–5, 385
 Neal, J.C. 6, 364
 Neales, B. 186, 369
 Nero, R.W. 232, 380
 Nesbitt, L. 188, 197, 376, 385
 Neumann, G. 19, 385
 Neumann, P. 247, 374
 Newhall, A.E. 142, 188, 380, 385
 Newman, A.V. 144, 295, 386
 Newton, J. 11, 386
 Nghiem-Phu, L. 130, 150, 386
 Nicholas, M. 240, 386
 Nielsen, P.L. 142, 145–50, 199, 357,
 375, 387, 393–4
 Nielsen, R.O. 267, 386
 North Atlantic Treaty
 Organization 317–18, 386
 Norton, G.V. 38, 70, 149, 386
 Noutary, E. 146, 149–50, 386–7

410 *Author index*

- Novarini, J.C. 38, 70, 149, 247, 263, 360, 376, 386
Novick, A. 262, 389
Nystuen, J.A. 206–7, 383, 386
- Oba, R. 192, 386
O'Brien, J.J. 194, 371
Ocean Acoustic Developments Ltd 143, 292, 386
O'Driscoll, L.M. 145, 396
Officer, C.B. 272, 386
Ogden, P.M. 238–40, 386–7
Oğuz, H.N. 207, 387, 390
Okuyama, T. 187, 189, 397
Onken, R. 198–9, 393
Onyx, P.M. 88–90, 363
Oort, A.H. 19, 388
Orchard, B.J. 130, 151, 182, 387
Orcutt, J.A. 203, 387
Oreskes, N. 7, 387
Orme, E.A. 247, 387
Orris, G.J. 127, 151, 245, 387
Osborne, K.R. 145, 230, 380, 387
Osterhus, S. 206, 401
Ostwald, L.H. 207, 383
Owen, D.M. 233, 375
Owens, G.E. 189–90, 398
Ozard, J.M. 76, 185, 365
- Pace, N.G. 232, 387
Pack, P.M.W. 181, 387
Packman, M.N. 120, 294, 301, 354, 373, 387
Palmer, D.R. 151, 186, 387, 396
Palmer, L.B. 129, 151, 262–3, 369, 387–8
Papadakis, J.S. 123, 126, 146, 149–50, 181, 376, 379, 387, 400
Parchman, S. 295, 326, 366
Parthiot, F. 26–7, 380
Pastor, V.L. 293, 357
Pauly, T.J. 234, 388
Payne, S.G. 144, 163, 371, 377
Pearson, C. 145, 400
Pedersen, M.A. 143–4, 154–5, 178, 180, 298, 388
Pedersen, T. 123, 371
Peixoto, J.P. 19, 388
Pekeris, C.L. 100, 111, 174, 273, 388
Pelloni, B. 146, 149–50, 387
Peloquin, R.A. 193, 388
Pelton, R.M. 262, 393
Penner, R.H. 205, 355
Penrose, J.D. 234, 388
Perkin, R.G. 20, 388
Perkins, H. 54, 392
Perkins, J.S. 120, 126, 129, 146, 149, 151, 181, 187–8, 257, 356, 378, 388, 400
Peters, H. 84, 389
Petitpas, L.S. 189, 359
Petnikov, V.G. 158, 162, 376
Pflug, L.A. 230, 358, 389
Piacsek, A.A. 120, 378
Piacsek, S.A. 155, 193, 384
Pickard, G.L. 19, 43–6, 389
Pickett, R. 180, 368
Pierce, A.D. 123, 127, 145, 164, 200, 232, 379, 389
Pierson, W.J., Jr 19, 35, 385, 389
Pignot, P. 142, 389
Piskarev, A.L. 8, 142, 389
Pitts, L.E. 230, 374
Plaisant, A. 146, 149–50, 386–7
Plotkin, A.M. 142, 389
Podeszwa, E.M. 93, 168, 389
Pollak, K.D. 156, 362
Pomerenk, K. 262, 389
Porter, M.B. 8, 16, 100, 107, 115–16, 120, 123, 127, 142, 145–6, 148, 182, 187, 191, 360, 368, 375, 378, 389–91
Portis, D.H. 207, 368
Posey, J.W. 172, 390
Potter, J.R. 205, 212, 359, 366, 390
Pouliquen, E. 232, 387
Powers, W.J. 295, 390
Poynter, A.B. 294, 381
Prada, K.E. 234, 400
Preston, J.R. 232, 366
Price, J.F. 157, 362, 373
Pridham, R.G. 267, 377
Primack, H. 120, 146, 390
Princehouse, D.W. 260, 263, 390
Prior, M.K. 75, 354
Pritchard, R.S. 210, 390
Prosperetti, A. 207, 364, 390
Pugh, J.D. 25–6, 369
Pumphrey, H.C. 206–7, 390
- Qian, W. 194, 378
- Rajan, S.D. 76, 390
Ramsdale, D.J. 172, 390
Rasband, S.N. 186, 390
Rayleigh, J.W.S. 74, 390
Readhead, M.L. 212, 359, 366

- Reise, B. 159–60, 390
 Reiss, E.L. 116, 145, 389–90
 Renner, W.W. 218, 230, 256, 293, 357, 371, 390
 Renshaw, W.E. 235, 371
 Reynolds, A.M. 295, 326, 400
 Reynolds, S.A. 53, 368
 Richards, S.D. 69–70, 82, 199, 354, 390–1
 Richardson, M.D. 76, 374
 Richardson, P.L. 50–1, 378
 Richardson, W.J. 205, 391
 Ridout, P. 20, 364
 Rienecker, M.M. 193, 391
 Riley, J.P. 109, 142, 376, 399
 Rind, D. 15, 365
 Roberts, B.G. Jr 107–8, 143, 391
 Robertson, J.S. 126, 150, 298, 391
 Robertsson, J.O.A. 142, 391
 Robins, A.J. 75, 354, 391
 Robinson, A.R. 1, 6, 155, 193, 378, 384, 391
 Robinson, E.R. 229, 391
 Roche, L.F. 126, 129, 149, 151, 388
 Rodríguez, O.C. 191, 391
 Rogers, P.H. 167–70, 172, 190, 391, 401
 Rohr, J. 207, 391
 Rosenthal, R.E. 316, 358
 Rosenzweig, J.R. 262, 393
 Ross, D. 215, 391
 Rossby, H.T. 205, 393
 Rost, P.V. 298, 372
 Rowe, M.M. 185, 364
 Rowlands, P.B. 8, 102, 399
 Roy, R.A. 207, 364
 Rubano, L.A. 76, 357
 Rubenstein, D. 71, 391
 Runyan, L. 7, 391
 Rutherford, S.R. 163, 377

 Saad, Y. 149, 379
 Sabol, B. 243, 382
 Sachs, D.A. 106, 392
 Sadowski, W. 215, 392
 Saenger, R.A. 233, 392
 Sagen, H. 211, 392
 Sammelmann, G.S. 295, 392
 Sander, E.L. 230, 374
 Sanders, J.V. 66, 68, 101, 154, 165, 267, 363, 377
 Sanders, T.J. 325, 398
 Sandven, S. 211, 392

 Sandy, R.J. 263, 360
 Santiago, J.A.F. 123, 392
 Scheifele, P.M. 82, 172, 383
 Schevill, W.E. 205, 398
 Schey, P.W. 183, 185, 365
 Schilling, R. 13, 392
 Schippers, P. 293, 392
 Schmidt, H. 8, 16, 61, 72, 100, 113, 115, 123, 147–8, 163, 165, 198, 232, 247, 364, 370, 375–6, 380, 392
 Schmitt, R.W. 54, 392
 Schneider, H.G. 127, 245, 265, 294, 392
 Schoomer, B.A. 209, 356
 Schramm, W.G. 288, 392
 Schreiner, H.F., Jr 230, 393
 Schuler, J.W. 295, 327, 369
 Schulkin, M. 66, 75, 88, 131, 154, 167–8, 170–2, 273, 381, 393
 Schultz, M.H. 149, 188, 379
 Schurman, I.W. 129, 150, 393
 Scott, H.D. 236, 361
 Scott, W.L. 226, 230, 384
 Scrimger, J.A. 205–6, 393
 Scully-Power, P.D. 127, 393
 Sellschopp, J. 146, 199, 393–4
 Selsor, H.D. 6, 393
 Seong, W. 122–3, 148–50, 370, 393
 Shang, E.-C. 123, 127, 189, 379, 393
 Shaw, P.T. 205, 393
 Shenderov, E.L. 243, 393
 Sheppard, C.V. 144, 380
 Shooter, J.A. 82, 203–4, 225, 377
 Showalter, J.A. 130, 384
 Shrader-Frechette, K. 7, 387
 Shvachko, R.F. 247, 371
 Siderius, M. 146, 198–9, 216, 355, 393–4
 Sides, D.J. 6, 364
 Siegmann, W.L. 113, 126–7, 129–30, 149–51, 182, 193, 358, 363, 379, 387, 391, 393
 Sienkiewicz, C.G. 262, 393
 Silbiger, A. 106, 392
 Simmen, J. 187, 393
 Simmons, V.P. 80–1, 368
 Simons, D.G. 145–6, 185, 193, 198–9, 213, 372, 393–4
 Skretting, A. 80, 82, 394
 Smith, E.M. 293, 394
 Smith, G.B. 6, 394
 Smith, J.A. 193, 391

412 *Author index*

- Smith, K.B. 150, 164, 186, 198, 242, 257, 262, 354, 358, 394, 397
Smith, R.H. 207, 373
Snellen, M. 145–6, 185, 193, 198–9, 393–4
Snyder, D.E. 207, 383
Solomon, L.P. 109, 179, 226–7, 384, 394
Sommerfeld, A.N. 74
Song, H.C. 183, 198, 378, 394
Spaulding, R.A., Jr 187–8, 383
Spiesberger, J.L. 27, 109, 195, 203–4, 358, 363, 394, 396
Spikes, C.H. 318, 394
Spindel, R.C. 53, 195, 198, 363, 394–5
Spizzichino, A. 131, 356
Spofford, C.W. 123, 129, 141, 143, 145, 181, 298, 356–8, 395
Stalcup, M.C. 54, 392
Stanton, T.K. 234, 400
Steele, J.H. 194, 371
Stegun, I.A. 114, 354
Stepanishen, P. 123, 371
Stephan, Y. 191, 391
Stephen, R.A. 242–3, 298, 371, 395
Stephens, R.H. 281, 374
Stickler, D.C. 116, 144, 355, 395
Stoll, R.D. 76, 374, 395
Stotts, S.A. 142, 173, 395
Stretch, C.E. 188, 373
Sullivan, E.J. 12, 181, 360
Sullivan, F.J.M. 230, 381, 384
Sundaram, B. 187, 395
Sussman, B. 297, 304–7, 378
Sverdrup, H.U. 19, 24, 395
Swift, S.A. 242, 395
Szanto, T.R. 321, 375
Szczechowski, C. 319, 360

Talham, R.J. 216, 395
Tang, X. 187, 192, 395–6
Tango, G.J. 75, 100, 187, 361, 395
Tappert, F.D. 123, 125–6, 129–30, 149–51, 186–7, 192, 203–4, 242, 257, 262, 358, 372, 386–7, 394–6
Taroudakis, M.I. 16, 396
Teague, W.J. 177, 396
The Acoustic Mid-Ocean Dynamics Experiment Group 197, 396
The Ring Group 50, 396
Thompson, C.H. 232, 380
Thomson, D.H. 205, 391
Thomson, D.J. 127, 129, 149–50, 298, 358, 396, 401
Thorne, P.D. 70, 391
Thorpe, W.H. 80, 131, 273, 396
Thorsos, E.I. 236, 238, 396
Thurston, R.N. 232, 389
Tielbürger, D. 192, 396
Tindle, C.T. 75, 111, 113, 121, 144–5, 165, 368, 396, 400–1
Tolstoy, A. 129, 144, 158, 164, 183–4, 187, 298, 359, 365, 397
Tolstoy, I. 69, 105, 397
Tsuchiya, T. 187, 189, 397
Tufts, D.W. 197, 372
Tuovila, S.M. 294, 397
Turl, C.W. 205, 355
Turner, R.G. 188, 365
Twersky, V. 71, 397
Tyack, P. 205, 398

Überall, H. 145, 164, 355, 383
UK Ministry of Defence 294, 397
Untersteiner, N. 39–40, 70, 397
Urban, H.G. 232, 366
Urick, R.J. 8, 38, 58, 64–5, 68, 73, 77, 80, 86–7, 91–2, 96–7, 108, 152–4, 163, 200–2, 209–10, 216–17, 233, 237, 241, 248, 250, 265–8, 397
US Department of Defense 316–17, 397
US Department of the Navy 15, 295, 321–2, 326, 397–8
US General Accounting Office 305, 398
US Navy Air ASW Project Office 293, 398

Vaccaro, R.J. 197, 267, 372, 398
Vagle, S. 206, 398
Vastano, A.C. 189–90, 398
Veenstra, D. 324, 398
Vendetti, A. 257, 262, 398
Venne, H.J., Jr 298, 366
Vent, R.J. 235, 398
Vichnevetsky, R. 1, 379
Vidmar, P.J. 73–5, 141, 377, 400
Von Winkle, W.A. 209, 218, 356, 398

Wagner, D.H. 325, 398
Wagstaff, R.A. 203–4, 215, 219–22, 225, 230, 360, 372, 398
Wales, S.C. 185, 215, 369, 398
Walrod, M.H. 230, 358
Walstad, L.J. 193, 391

- Wang, G.-Y. 187, 393
 Wang, Y.Y. 189, 393
 Ward, P.D. 144, 185, 361, 398
 Wargelin, R.M. 177, 399
 Watkins, S.L. 82, 203-4, 225, 377
 Watkins, W.A. 205, 398
 Watson, A.G.D. 179, 398
 Watson, W.H. 75, 107-8, 143, 273, 371, 399
 Watts, D.R. 205, 393
 Weatherly, R. 317, 377
 Webb, D. 195, 363
 Webster, J. 282-4, 380
 Weickmann, A.M. 142, 188, 197, 376, 399
 Weinberg, H. 109, 122, 130, 142, 146-7, 150, 179, 182, 270-2, 274, 277-9, 287-8, 293-5, 360, 362, 376, 396, 399
 Weinberg, N.L. 107, 179, 369, 399
 Wells, D.K. 177, 399
 Wenz, G.M. 201, 399
 Werby, M.F. 75, 187, 361
 Weston, D.E. 8, 102, 144, 185, 399
 Westwood, E.K. 73, 75, 113, 121, 141-2, 144, 164-5, 182, 185, 298, 368, 380, 399, 400
 Wetzell-Smith, S.K. 295, 326, 400
 White, D. 127, 141, 143, 145, 298, 364-5, 370, 377, 382, 400
 Whitman, E.C. 11, 400
 Wiebe, P.H. 234, 371, 400
 Williams, A.O., Jr 74, 76, 400
 Williamson, M. 120, 146, 388
 Willis, C.L. 288, 297, 400
 Willison, P.A. 247, 362
 Wilson, W.D. 25-6, 400
 Winebrenner, D.P. 247, 374
 Winfrey, D.E. 45, 47-8, 361
 Winokur, R.S. 210, 364
 Wolf, S.N. 59, 115, 117, 145-6, 192, 374, 383, 396
 Wolfson, M.A. 203-4, 396
 Wood, D.H. 129, 181, 185, 365, 370, 396, 400
 Wooten, M. 230, 358
 Worcester, P.F. 27, 194-5, 363, 365, 384, 394-5
 Worzel, J.L. 92, 368
 Wright, E.B. 126, 129, 149-50, 257, 356-7, 388, 400
 Wrobel, L.C. 123, 392
 Wulfeck, W.H. 295, 326, 400
 Wunsch, C. 194-5, 363, 384
 Yamada, T. 156, 383
 Yan, J. 180, 400
 Yang, T.C. 185, 357
 Yaremchuk, A.I. 198, 400
 Yaremchuk, M.I. 198, 400
 Yarger, D.F. 134, 137-8, 147, 401
 Jeremy, M.L. 76, 185, 365
 Yevick, D. 127, 401
 Yoerger, E.J. 263, 360
 Zabala, X. 78, 401
 Zabalgoatza, X. 107, 399
 Zachariasen, F. 197, 384
 Zahuranec, B.J. 232, 355
 Zaslavsky, G.M. 187, 395
 Zedel, L. 206, 401
 Zeidler, E. 257, 262, 398
 Zeskind, R.M. 226, 230, 384
 Zhang, R. 143, 146, 245, 401
 Zhang, X.-Z. 190, 401
 Zhang, Z.Y. 75, 121, 165, 396, 401
 Zhou, J.-X. 190, 401
 Zhu, D. 146, 149-50, 387, 401
 Ziman, J. 6, 308, 401
 Ziomek, L.J. 97, 186, 255, 276, 401
 Zornig, J.G. 2, 401
 Zyda, M.J. 6, 13, 359

Subject index

- Absorption 80–2, 342; coefficient 80–1; pH dependence 82, 172
Accreditation 317, 342
Acoustic attenuation 80–2; coefficient 79; in turbid and bubbly environments 69–70
Acoustic contrast 212
Acoustic daylight 17, 211–12, 342; acoustic daylight ocean noise imaging system (ADONIS) 212
Acoustic Doppler current profiler (ADCP) 13–14, 206
Acoustic environmental support detachment (AESD) 297
Acoustic impedance 59, 342
Acoustic intensity (I) 59
Acoustic mid-ocean dynamics experiment (AMODE) 197
Acoustic model evaluation committee (AMEC) 297
Acoustic rainfall analysis (ARA) algorithm 207
Acoustic reverberation special research program (ARSRP) 242
Acoustic thermometry of ocean climate (ATOC) 4, 197
Acoustic tomography 17, 194–8, 342
Acoustical oceanography 19–56
Adiabatic: approximation 120; compressibility 20; process 20, 342
Advection 19, 155–6, 342
Afternoon effect 157
Air bubbles 38, 207, 236
Airy function 116
Algae 55; acoustical scattering by 243
Ambient noise 342; Arctic 210–11; depth dependence 209; directionality 209–10; geoacoustic inversion 212–13; models 214, 216–19, 342; spatial variability 229; *see also* Noise
Ambient noise imaging (ANI) 212
Ambiguity surface 184
AMOS (acoustic, meteorological and oceanographic survey) 4, 88, 154, 170, 273
Analog models 2, 342
Analysis of alternatives (AOA) 325
Analytic benchmark solutions 298–301
Analytical models 2, 342
ANDES model 218, 256
Angle of intrusion 80
Antarctic intermediate water (AAIW) 24–5
Anticyclonic 342
Anti-submarine warfare (ASW) 57, 100, 193, 326
Archipelagic apron 41, 342
Arctic: ambient noise 210–11; bottom interaction 79; half-channel 95–7; propagation 172–6
Arrival structure 109–11; RAYMODE model 135–6
ASTRAL model 256
Attenuation 342; coefficient 79; in sediments 78–9; in turbid and bubbly environments 69–70; loss 80
AUTEC 186
Autonomous underwater vehicle (AUV) 6–7, 12–14; *see also* Remotely operated vehicle (ROV)
AUTO SHIPS 226
Background masking level 245
Backscattering 342

- Backscattering strength 233
- Backward-directed (backscattered) energy 66
- Bandwidth correction 267
- Bank 41, 342
- Baroclinic 21, 342
- Barotropic 52, 342
- Bartlett processor 199
- Basic acoustic models 2–3, 343
- Basin 41, 343
- Bathymetric blockage 40
- Bathythermograph 27, 343
- Beam displacement 111–13, 343
- Beam noise (BN) function 283–4
- Beam noise statistics models 214, 225–6, 343; deductive 214, 229; inductive 214, 229
- Beam pattern (BP) function 285
- Beam signal (BS) function 283
- Beaufort wind scale 36–7
- Benthos 55
- Bessel equation 103, 114, 125
- Bioacoustic noise 205
- Biological organisms 55–6
- Biologics 55
- Biomass 234
- Biot–Stoll model 76
- Bistatic 245, 255–9, 268–70, 343; reverberation 255–9; sonar equations 268–70
- Bistatic acoustic model (BAM) 257–9
- Borderland 41, 343
- Bottom bounce 62–3, 343
- Bottom loss 66, 343
- Bottom limited 343
- Bottom loss upgrade (BLUG) model 77
- Bottom-reflected (BR) paths 104
- Boundaries 35
- Boundary conditions 343; rigid (homogeneous Neumann bottom) 75; impedance (Cauchy) 75; pressure-release (Dirichlet) 66
- Boundary element method (BEM) 123, 247
- Boundary reverberation 236–43; scattering strength 233; sea-floor 240–3; sea-surface 236–40; under-ice 240
- Branch cut integral 115
- Broadband modeling 182
- Broken mirror model 78
- Brunt–Väisälä frequency 52
- Bubble layers 69; *see also* Turbidity
- Buck model 175–6
- Buoyancy frequency 52, 343
- CALCULATE function 286
- Calculation-frequency method (CFM) 130
- Canonical sound speed profile 179, 343
- Canyon 343
- Capability-based analysis 326
- CAPARAY model 75
- Cartesian latitude and longitude divisions 226
- Cauchy boundary condition 75
- Caustics 106, 111, 343
- Cell scattering models 248–50, 343
- Chaos 186–7
- Chaotic 186, 343
- Characteristic acoustic impedance 59
- CMM3D model 120, 188
- Coherence 97–8; spatial 97; temporal (fluctuations) 86, 97–8
- Colossus model 167–72
- Column or integrated scattering strength 234
- Commercial-off-the-shelf (COTS) 13, 324–5
- Composite roughness model 236, 247, 343
- Comprehensive acoustic system simulation (CASS) 287–8
- Comprehensive test-ban treaty 10
- Computational ocean acoustics 1
- Computer-based training (CBT) 12, 326
- Configural effects 318
- Configuration management 297
- Conjugate depth 30, 93, 343
- Constrained simulation 313
- Constructive simulation 313, 343
- Continental: margin 343; rise 41, 343; shelf 41, 203–4, 343; slope 41, 204, 344
- Continuous gradient 178–9
- Continuous spectrum 165
- Contour integral 115
- Convergence zone (CZ) 344; paths 93; slide rule (TACAID 6–10) 93
- Cordillera 41, 344
- Coriolis force 344
- Coriolis parameter 52
- Cost and operational effectiveness analysis (COEA) 325

- Cost-as-an-independent-variable (CAIV) 324
- Coupled ocean-acoustic modeling 12, 155, 193
- Crank–Nicolson method 149–50, 344
- Critical angle 75, 344
- Critical depth 30, 93, 344
- Critical sea test (CST) experiments 238
- Cross-layer geometries 88
- C-SNAP model 191
- Cumulative accuracy measures (CAM) 303
- Curvilinear gradient 178–9
- Cusped caustic 106, 344
- Cutoff depth 163, 165
- Cutoff frequency 88–91
- Cyclonic 344
- Cylindrical spreading 65, 344

- Data assimilation 193
- Data limited 7
- Data support requirements 176–80
- Databases: gridded 176; Met / Ocean 12, 14; sources and availability 288–92
- Decibel (dB) 18, 344
- Deductive geoacoustic inversion 17, 198–9
- Deductive rapid assessment model 199
- Deep isothermal layer 30
- Deep scattering layer (DSL) 56, 234, 344
- Deep sound channel 91–3; axis 191, 344
- Defense modeling and simulation office (DMSO) 18, 361
- Depth equation 114
- Depth excess 93
- Design of experiment (DOE) 314
- Detection threshold (DT) 267
- Deterministic 344
- Diagnostic information 9, 344
- Diel 344
- Diffraction 344
- Digital bathymetric database (DBDB) 222
- Dipole 207, 217
- Direct blast 259
- Direct path 104, 344
- Dirichlet boundary condition 66
- Discrete modes 115
- Discrete wavenumber method 122
- Dispersion 116–17, 344

- Diurnal 344
- Diurnal ocean surface layer model (DOSL) 157
- Documentation in model evaluation 305–7; standards 309–12
- DOD-SDD-498 311
- DOD-STD-2167A 309, 311
- DOD-STD-7935A 309, 311
- Domains of applicability 25, 99, 136, 344
- Doppler 255, 345; shift 276; shifted spectrum 69; smeared spectrum 69
- Downhill simplex algorithm 185
- Downslope propagation 165
- Downwelling 44, 345
- Dual-use technologies 11
- Ducted precursors 127, 345
- Ducted propagation 27, 82
- Dynamic ocean features 43

- Earth curvature correction 179, 345
- Echo signal level (ESL) 268, 275, 284–5
- Echo sounder corrections 32
- Eddies 48, 50–2, 188, 345
- Effective depth concept 185
- Effects-based operations 326
- Eigenray 345; formulations 164; paths 104
- Eigenvalue 114, 345
- 18° Water 28
- Eikonal 103, 345; equation 104
- Ekman drift current 43, 345
- Elliptic-reduced wave equation 101
- Empirical models 2, 167–72, 174–6, 345
- Empirical orthogonal function 193
- Engagement modeling 264
- Environmental models 2–3, 172, 345
- EUCLID 317
- Escarpment 345
- European acoustics association 16
- Evanescent spectrum 115
- Evolutionary search algorithm 199
- Expendable bathythermograph (XBT) 27
- Expendable sound velocimeter (XSV) 27
- Experimentation 4–5
- EXTRACT function 286

- Facet ensemble method 247
- FACT model 60, 188, 298, 304–7
- Fan 41, 345

- Farfield approximation 115, 125
 Fast ambient noise model (FANM) 222–3, 228
 Fast field models 122–3, 345; FFP 304–7; MSPFFP 174; Pulse FFP 182; RDIFFP 122
 Fast Fourier transform (FFT) 122
 Fathometer returns 270, 345
 FDTD model 183
 Feature model 193–4, 345
 Federation object model 317
 FEPE model 181, 222
 Fidelity 345
 Field measurements 4
 Figure of merit (FOM) 60, 267–8, 302, 345
 Fine-scale oceanic features 54–5
 Finite difference 116, 345
 Finite-difference time domain (FDTD) method 183
 Finite element 100, 345
 Finite element models: FFRAME 191; FOAM 181, 191; ISVRFEM 181; SAFE 182, 191
 FIPS PUB-38 309
 FLIP research program 209
 Floating production, storage and off-loading (FPSO) vessels 13
 Fluctuations 86, 97–8
 FOAM model 181, 191
 Focal surfaces 106; *see also* Caustics
 Forward reflection loss 66; measurements 72
 Forward scattering 66, 73
 Fouling organisms 55
 Fourier synthesis 182
 Fracture zone 41, 345
 Frequency-domain wave equation 101
 Frequency effect 67
 Front 188, 345
 Full channel 32

 Galerkin's method 345; boundary element method 123
 GAMARAY model 182
 Gap 41, 346
 Gaussian beam tracing 107, 120, 346
 Garrett–Munk internal wave model 53
 Generalized digital environmental model (GDEM) 177, 222
 Generic sonar model (GSM) 186, 242, 286–7
 Genetic algorithm 199, 216

 Geoacoustic: inversion 17, 198–9, 212–13; models of the sea floor 76–8; profile 74
 Geodesic path 197, 346
 Geometric mean frequency 182
 Geometrical acoustic scattering 244
 Geometrical acoustics approximation 104
 Geophysics ambient noise model 215
 Geophysics fleet mission program library (GF MPL) 15
 GRAB model 288
 GRASS model 188
 Grazing angle 64, 346
 Green's function 103, 114, 122
 Gulf Stream 21, 50

 Half channel 32, 346
 Hamiltonian ray tracing 109, 188
 Hankel function 103, 114–15, 122, 125
 Harmonic solution 101, 103, 346
 HARPO model 188
 Harvard open ocean model (HOOM) 188, 193
 Head wave 75
 Heard Island feasibility test (HIFT) 195, 197
 Helmholtz equation 101
 Hidden depths 76, 346
 Hierarchical levels of simulation: engagement 9, 315; engineering 9, 315; mission 9, 316; theater 9, 316
 High-frequency: adaptations 120; domain 105
 High level architecture (HLA) 317–18
 Hill 346
 Hindcast 67, 193, 346
 HITS database 222, 226
 Hole 346
 Homogeneous Neumann bottom boundary condition 75
 Harvard open ocean model (HOOM) 188, 193
 Hybrid models 100, 346; hybrid BEM (HBEM) 123; hybrid BEM-WI approach 247
 Hydrographic cast 28
 Hypsometric shallow water 94

 Ice cover: acoustic interaction with 70–2; marginal ice zone (MIZ) 14, 38; pack ice 38; reverberation 240

- Ice ridge models: continuous
 - statistical 71; discrete 71
- ICERAY model 173
- IEEE/EIA 311–12
- Image generator 326
- Image interference effect 38, 67
- IMAT (interactive multisensor analysis training) 326–7
- Impedance boundary 75, 115
- Implicit finite-difference (IFD) schemes 126
- IMS (international monitoring system) 10
- Incidence angle 64, 346
- Index of refraction (refractive index) 20, 88, 124
- Inertial frequency 52
- Inertial motion 346
- INSIGHT model 301
- Inspection, maintenance and repair (IMR) 13
- Integrated hierarchical variable resolution (IVHR) simulations 318
- Intensity 59
- Interface waves 115
- Interference effects 78
- Internal waves 52, 86, 187, 190;
 - Garrett–Munk model 53
- Internet 351
- Intromission angle 80
- Inverse acoustic sensing 15–16
- Isotherm 21, 346
- Isothermal compressibility 20
- ISVRFEM model 181

- Key performance parameters (KPP) 324
- Kirchhoff approximation 236, 257, 260
- Knoll 346
- Knudsen spectra 201

- Lambert's law 241
- Land masses 43
- Laplacian operator 101
- Large-scale oceanic features 43
- Lateral wave 75
- Lateral wave equation 120
- Law of reciprocity 272
- Leakage coefficient 86, 153
- Leaky ducts 120, 127, 183
- Leaky modes 120–1
- Levee 346
- Limiting angle 152, 167, 346
- Limiting rays 132, 174, 223
- Littoral zone 11, 346
- Live simulation 313, 346
- Lloyd mirror effect 38, 68, 346
- LOFAR diagrams 287
- LOGPE model 129
- Low-frequency bottom loss (LFBL) 78, 222
- Low-frequency cutoff 88
- LRAPP (long range acoustic propagation project) 4

- Marginal ice zone (MIZ) 14, 38, 210, 346
- Marine geophysical survey (MGS) 273
- Marine mammal protection 12, 197, 205
- Marine organisms: algae 55; as false targets 56; benthos 55; nekton 55; plankton 55
- Marsh–Mellen model 174
- Marsh–Schulkin model 168–72
- MAST3 programme 146
- Matched-field processing 17, 183;
 - source localization 198
- Matched mode localization 185
- Mathematical models 2, 346
- Matrizant solution 122
- Maximum-likelihood estimator 185
- Measurements 4–5, 58
- Measures of effectiveness (MOE) 325
- Mediterranean intermediate water (MIW) 24, 28–9
- Megaphone effects 163
- Merging techniques for sound speed profiles 180
- Mesoscale features 44–54, 346
- Met/Ocean data 12, 14
- Method of images 68–9, 164
- Microbaroms 15
- Mid-ocean acoustic transmission experiment (MATE) 53
- Military operations research society (MORS) 316
- Mine-deployment exercise (MINEX) 186
- Mixed layer 346; distribution 82–5; models 155–7
- Mixed layer depth (MLD) 28, 30, 82
- Moat 41, 347
- MOCASSIN model 265
- MODAS 292
- Mode coupling 120

- Model-based approach to signal processing 181
- Model evaluation 296–312; analytical benchmark solutions 298–301; documentation 305–7, 309–12; guidelines 305–9; maintainability 308; past efforts 297–8; quantitative accuracy assessments 301–2; usability 309; validity in 308; verification in 307
- Model evaluation program (MEP) 297
- Model operating systems (MOS) 281–6; design decisions 286; sonar modeling functions 283–6; system architecture 282–3; system usage 286
- Modes: continuous 115; discrete 115; evanescent 115; leaky 120–1; normal 114; trapped 115; virtual 118; wedge 120–1
- Modified data banks 288, 347
- Monopole 217–18
- Monostatic 255, 347
- Monte Carlo 181, 214, 325
- Mountains 347
- Moving ship tomography (MST) 197
- MSPFFP model 174
- Mudslide effect 205
- MULE model 182
- Multipath 61, 347
- Multipath expansion models 121, 347
- Multistatic sonars 11
- $N \times 2D$ technique 120
- National acoustic laboratory 11
- NATO 317–18
- Naval operations 11
- Navy/NOAA oceanographic data distribution system (NODDS) 288
- Near-field condition 115
- Nekton 55
- Nepers 78
- Network-centric data fusion 12
- Neumann boundary condition 75
- NISSM model 270–81; noise 275; outputs 277; probability of detection 277; propagation 271–3; reverberation 273–5; signal-to-noise ratio 276; target echo 275
- NLNM model 304–7
- Noise: ambient 200; Arctic 210; bioacoustic 205; bubbles 207; depth dependence 209; directionality 209; geoacoustic inversion 212; models 214, 216–19, 225–6, 347; NISSM model 270–81; notch 222–5; observations and physical models 200–13; rain 205; seismo-acoustic 202–3; shipping 203; sources and spectra 200–2; summary of numerical models 229; theoretical basis for modeling 214–16; wind 205; *see also* Ambient noise
- Noise levels (NL) 265–8
- Noise masking level (NML) 284
- Noise notch 222–5
- Nonlinear progressive-wave equation (NPE) 130
- Normal mode: adiabatic approximation 120; angle-limited source 121; equation 114; mode coupling 120; models 113–14, 347; range dependence 118; solutions 114–16
- Normal modes 114, 347
- Northern Gulf of Mexico littoral initiative (NGLI) 319
- Nowcast 193, 347
- Numerical models 2, 347; *see also* under specific models and modeling techniques
- OAML databases 288, 297
- OASIS (ocean ambient sound instrument system) 206
- Ocean acoustic tomography, *see* Acoustic tomography
- Ocean acoustics library (OALIB) 109, 351
- Ocean fronts 45; global distribution 48; names 49
- Ocean impulse response 6, 347
- Ocean seismo-acoustics 57
- Oceanic features, dynamic 43
- Oceanic heat and freshwater budgets 207
- Oceanography 19
- Oceanographic and atmospheric master library (OAML) 288, 297
- Oceanographic models 6
- Offshore industries 13
- OGOPGO model 247–8
- Operational models 4
- Operational oceanography 14
- Optimum frequency of propagation 159

- Optimum thermal interpolation system (OTIS) 193–4
- ORB experiments 212
- ORBS model 257
- Ordinary differential equation (ODE) 126
- Organic sediments 43
- Pack ice 38
- Panel on sonar system models (POSSM) 297, 302
- Parabolic equation (PE): basic theory 124; derivation 124–6, 127–8; finite element (FE) 126; high-frequency adaptations 130; implicit finite-difference (IFD) 126; models 123, 347; numerical techniques 126; ordinary differential equation (ODE) 126; Padé forms 129; range-refraction corrections 129; rotated 164; split-step Fourier algorithm 126; square-root operator 128; starting fields 126; time-domain applications 130; two-way 127; wide-angle and 3D adaptations 129
- Paraxial approximation 125
- PARSIFAL model 75
- Pathological test case 300, 347
- Pekeris model 111
- Pelagic sediments 43
- Performance surfaces 184
- Perturbation theory 72, 238
- PERUSE 365
- PESOGEN model 130
- Phase conjugation 198; *see also* Time-reversal mirrors
- Physical (physics-based) models 2, 347
- Pierson–Moskowitz spectrum 35, 38
- Plain 41, 347
- Plankton 55
- Plateau 41, 347
- Plume detection 14
- Point scattering models 245, 259–61, 347
- Polar sector geometries 226
- Pollution studies 13
- Potential function 101, 114–15, 122
- Power summation 202
- Practical salinity scale 20
- Prediction 4–5
- Pressure-release surface 66
- Primary data banks 288–90, 347
- Probability density function 226
- Probability of detection, NISSM model 277
- Prognostic information 9, 347
- Progressive wave equation (PWE) 130
- PROLOS model 248
- Propagation: Arctic 172–6; basic concepts 59–65; bottom bounce 61, 63; classification of modeling techniques 102; convergence zone 61, 63, 93–4; deep sound channel 61, 63, 91–3; definition 347; direct path 61, 63; domains of applicability 99; field measurement programs 4; in shallow water 94–5, 158–72; in surface duct 85–8; in wedge geometry 163–6; initialization of models 176; models 348; observations and physical models 57–98; optimum frequency 90–1, 159–62; reliable acoustic path 61, 63, 94; simple experimental geometry 59; special applications 180–99; summary of numerical models 135–51; surface duct 61, 63, 82; theoretical basis for modeling 100–2; *see also* under specific models and modeling techniques
- PROSIM model 193
- PROTEUS model 182
- Province 41, 348
- Pulse FFP model 182
- Pulse propagation 123; modeling 182
- Rain noise 205–7
- RANDI model 219–22
- Range 348
- Range-depth plane 60
- Range dependence 32, 102, 107, 118, 123
- Range equation 114
- Range partitioning techniques 107–9
- Range-refraction corrections 129–30
- Ray bundle 105
- Ray theory models 103, 348
- Ray theory with corrections 106
- Rayleigh parameter 66, 348
- Rayleigh's law 74, 244
- Rayleigh–Ritz method 186–7
- Ray-mode analogy 163
- RAYMODE model 131–5, 298, 304–7

422 *Subject index*

- RDFFP model 122
- Reciprocity 272
- Reef 41, 348
- Reflection 348; coefficient 66; loss 66, 72
- Reflectivity method 122
- Refracted-bottom-reflected (RBR) 93, 104
- Refracted-bottom-reflected-surface-reflected (RBRSR) 111
- Refracted-surface-reflected (RSR) 104
- Refracted-surface-reflected-bottom-reflected (RSRBR) 104
- Refraction 348
- Reliable acoustic path (RAP) 94, 348
- Remote intervention 13
- Remotely operated vehicle (ROV) 13–14
- Renormalization loss 163
- Research models 4
- Reverberation 232, 348; bistatic 255–7; cell scattering models 245, 248; diffuse 232; facet 232; fundamental ratio 233; models 348; monostatic 255; multistatic 256; NISSM model 273–5; observations and physical models 232–43; point scattering models 245, 259; scattering strength 233; sea-floor 240; sea-surface 236; shallow water 232, 248; summary of numerical models 261; theoretical basis for modeling 244–8; under-ice 240; *see also* Boundary reverberation; Volume reverberation
- Reverberation level (RL) 249, 250, 265–7
- Reverberation masking level (RML) 268
- REVMOD model 251–5
- Ridge 41, 348
- Rigid boundary 75
- Rings 44, 50–2, 189
- Rogers model 167–8
- Rotated PE 164
- ROV (remotely operated vehicle) 13–14
- Runtime infrastructure (RTI) 317
- Saddle 348
- SAFE model 182, 191
- SAFRAN model 123
- Salinity 20, 348; distribution 22; practical salinity scale 20
- Satellites 5, 51
- Scattering 348; algae 243; bottom 233, 241, 275; column or integrated 234; strength 233; surface 233, 236–40, 275; under-ice 240; volume 233, 275
- Scholte waves 115
- Sea floor: boundary 72; topography 40–1; reverberation 240–3
- Sea state codes 36–7
- Sea surface: acoustic roughness 66; boundary 65; circulation 43–6; interference 67–9; loss 66, 349; noise 205–7; reverberation 236–40; roughness 35
- Sea water: binary fluid 20; compressibility 20; density 20
- Seachannel 41, 348
- Seamount 41, 197, 235, 256, 348
- Sediments 42–3; Arctic 79; attenuation 78–9; classification 42–3; pelagic 42; porosity 73; shallow-water 94; terrigenous 42
- Segmented constant gradient 178
- Seismo-acoustic 57, 100, 202; noise 202–3
- Self noise 200, 348
- Self starter 126
- Shadow zone 85, 348
- Shallow water: ambient noise 230; definition 94; ducts 94, 158; empirical models 167; numerical models 162; propagation 158–62; reverberation 232, 248; sound speed profiles 159–60
- Shipping noise 203
- Shoal 41, 348
- Signal level/spectra (SL) function 284
- Signal processing models 2–3, 348
- Signal-to-noise ratio, NISSM model 276
- Significant wave height 35, 348
- Sill 348
- Simulated annealing method 187
- Simulation 9, 313–27, 349; constrained 313; constructive 313; end-to-end 314; engagement 9, 315; engineering 9, 315; hierarchical levels 9, 314; infrastructure 316–17; live 313; mission 9, 316; smart systems 313; system representation

- 314; taxonomic scheme 313;
theater 9, 316; virtual 313
- Simulation based acquisition (SBA) 12,
320–5
- Simulation object model 317
- Skip distance 168–9, 174, 349
- Slope conversion 203, 225
- Smart systems 313, 349
- Smooth caustics 106
- Snell's law 62–3
- SOFAR (sound fixing and ranging)
channel 91, 189
- Software engineering environment
(SEE) 320
- Soliton 52, 190–1, 349
- Sommerfeld model 74
- Sonar equations 265–70
- Sonar modeling functions 283–6
- Sonar parameters 265–70; reference
locations 266
- Sonar performance: data sources and
availability 288–92; models 2–3,
264, 349; summary of numerical
models 292
- Sonar performance (SP) function 283
- Sonar prediction 6
- Sonic layer 28, 30, 349
- Sonic layer depth (SLD) 28, 30, 82
- Sound channel axis 30, 92, 126
- Sound losses 80
- Sound refraction 62
- Sound speed: calculation 25–7;
cross-section 32, 34; distribution
28–34; measurement 25
- Sound speed profiles: canonical 179;
curve-fitting techniques 178;
deep-ocean 30, 33; merging
techniques 180; morphology 31–2;
shallow-water 159–60
- Space scales 43
- Spectral intervals: continuous 115;
discrete 115; evanescent 115
- Spectral PE model 127
- Spectrum level 200, 267
- Speed of sound, *see* Sound speed
- Spherical spreading 64, 349
- Split-step Fourier algorithm 126
- Spreading loss 80
- Spur 41, 349
- Square-root operator 128
- Standard definitions 17–18
- State space techniques 181
- Stepwise-coupled-mode method 164
- Stimulation 313
- Stochastic 7, 349; modeling 181–2
- Stoneley waves 115
- Super elements 123
- SUPERSNAP model 145
- Surface duct 349; bilinear 154; ray
theory models 152–4; wave theory
models 154–5
- Surface expressions 6
- Surface waves: fetch 38; height 35;
hindcasting 67; Pierson–Moskowitz
spectrum 35, 38
- SWAM '99 workshop 164
- Systems engineering 320
- Tablemount 41, 349
- Tactical decision aid (TDA) 264, 315
- Tactical environmental processor 6
- Tactical environmental support system
(TESS) 193
- Tactical ocean thermal structure
(TOTS) 193
- Tactical oceanographic data
collection 6
- Tactical oceanography simulation
laboratory (TOSL) 318
- Tangent plane method 260
- Target echo, NISSM model 275
- Technology transfer 288; dual use 11
- Temperature: distribution 21;
effects 19–20; isotherms 21
- Temperature-salinity (T-S) diagram 24,
28–9
- Terrigenous sediments 43
- Testbeds 12, 318–19; at-sea tests 318;
laboratory-based 318; LWAD 318;
TOSL 318
- Thermal contrast 6
- Thermal noise 201
- Thermocline 28, 30, 349
- Thermodynamical ocean prediction
system (TOPS) 156
- Thermohaline 43, 349; staircase 54–5
- θ -r diagrams 109, 111; *see also* Arrival
structure
- Thin layer model 76–7
- 3-D TDPA model 182
- Three-dimensional (3D) modeling 187;
 $N \times 2D$ (or 2.5 D)
approximations 187
- Time-domain PE (TDPE) 130

424 *Subject index*

- Time-independent (or frequency-domain) wave equation 101
- Time-reversal mirrors 198; *see also* Phase conjugation
- Time scales 43
- Total ownership cost (TOC) 324
- TOWAN (tactical oceanography wide area network) 288
- Transmission anomaly (TA) 68, 349
- Transmission line matrix modeling (TLM) 247
- Transmission loss (TL) 59–60, 102, 349; Arctic 174–6; shallow water 167–72; surface duct 152–4
- Transmutation approaches 185
- Transport equation 104
- Trapped modes 115
- Trench 41, 349
- Trough 41, 349
- Tunneling effects 123
- Turbidity 69–70
- Turbulent kinetic energy 156
- Turning point 121, 349; filter 198
- Two-way PE model 127
- UMPE model 192, 203
- Under-ice reverberation simulation model 260–1
- Underwater acoustic propagation, *see* Propagation
- Unmanned undersea vehicle (UUV) 7, 12; *see also* Remotely operated vehicle (ROV)
- Upslope propagation 163, 165
- Upwelling 44, 349
- Validation 317, 349
- Validity in model evaluation 308
- Valley 41, 349
- Velocimeter 27–8
- Velocity potential 124
- Verification 317, 349; in model evaluation 307
- Vertical scattering plumes 235
- Very low frequency (VLF) band 100
- Virtual mode 118, 350
- Virtual simulation 313, 350
- Volume reverberation: column or integrated scattering strength 234–5; deep scattering layer (DSL) 56, 234; scattering strength 233; theory 248–50; vertical scattering plumes 235
- VV&A (verification, validation and accreditation) 7, 316–17
- WADER global ocean information system 292
- Water column boundaries 35–43
- Water mass 22, 24–5, 350; Antarctic intermediate water (AAIW) 24–5; Mediterranean intermediate water (MIW) 24, 28–9
- Water-sediment velocity ratio 76
- Wave equation 100, 350
- Wave theory models 154–5
- Waveguide invariant 183
- Wavenumber integration (WI) 122, 247
- Waves: fetch 38; height 35; hindcasting 67; internal 52, 86; spectra 35
- Websites 351–3
- Wedge: assemblage (or facet ensemble) method 247; downslope propagation 163, 165; modes 120–1; upslope propagation 163, 165
- Wenz curves 201
- Whispering gallery 179, 350
- Wind: noise 205; speed 36–7
- Wind-driven component of circulation 43
- WKB method 121
- WOTAN systems 205–6
- WRAP model 120
- XBT (expendable bathythermograph) 27
- XSV (expendable sound velocimeter) 27